THE STEADY STATE FORCES AND MOMENTS ON A RAILWAY WHEELSET INCLUDING FLANGE CONTACT CONDITIONS

by

Barrie Vaughan Brickle

A Doctoral Thesis

Submitted in partial fulfilment of the requirements for the award of Ph.D. of the Loughborough University of Technology.

August 1973

Supervisor: Professor F. D. Hales
Department of Transport Technology

SUMMARY

Railway vehicles are fitted with coned wheels to provide a measure of stability, but it can be shown that since the forces between wheel and track are non-conservative, dynamic instability occurs at a certain critical speed. Under these conditions the wheelsets sway from side-to-side of the track with the flanges of the wheels contacting the rails. This can lead to derailment when the wheel climbs up the rail and eventually jumps off.

The forces which exist between wheel and rail are due to the phenomenon known as "creepage", and various theories exist which predict these forces in the plane of the contact area. An investigation has been carried out into these theories with the railway wheelset problem in view, particularly the flange contact case.

It is possible, by assuming small displacements which avoid flange contact, to carry out a linearised study of the lateral dynamics of a wheelset, but the presence of the wheel flanges introduces a non-linearity into the problem.

A mathematical model of a wheelset and track has been defined based on real wheels with a "worn" tyre profile and real track. Computer programs have been written which calculate the contact points when the wheelset is displaced laterally and yawed by various amounts, including flange contact conditions. Up to three contact points can exist between the wheelset and track. Forces in the contact areas have been calculated using the various theories assuming the wheelset to be rolling along the track at a constant velocity in a displaced position. These forces have been manipulated to give the total forces and moments on the wheelset and are presented for various vertical load distributions and for various angular and lateral displacements of the wheelset from its central position.

Although theories exist which predict the forces for flange type contact, i.e. very elongated contact ellipse with a large amount of spin

present, it became apparent during the course of the investigation that very little experimental evidence was available for such conditions. As a result a roller rig was built to provide this data, and measurements were made of the lateral force due to various amounts of lateral creep and spin on elongated contact ellipses. Results from these tests have been compared with the available theories and show reasonable agreement.

CONTENTS

		Page
1.	Introduction	1
2.	Review of Rolling Contact Theories and Experiments	
	2.1 Basic Theory	8
	2.2 Theoretical Review	11
	2.3 Experimental Review	23
3.	Theories used in Present Analysis	
	3.1 The Limiting Case of Infinitesimal Creepage and Spin...	47
	3.2 The Limiting Case of Large Creepage and Spin	54
	3.3 Arbitary Creepage and Spin	57
	3.3.1 Numerical Theory	57
	3.3.2 Simplified Theory	64
4.	Mathematical Model of Wheelset and Track	
	4.1 Introduction	69
	4.2 Rail Geometry	70
	4.3 Wheel Geometry	74
	4.4 Contact Points	79
	4.4.1 Wheelset in Central Position	81
	4.4.2 Wheelset Moved Laterally Only	82
	4.4.3 Wheelset Yawed Only	88
	4.4.4 Wheelset Moved Laterally and Yawed	100
	4.5 Contact Ellipses	105
	4.6 Creepages and Spin	116
	4.7 Forces	121
5.	Comparison of Theories	
	5.1 Introduction	124
	5.2 Results	125

Page

5.3 Discussion 129

5.3.1 Wheelset Displaced Laterally, No Yaw 129

$T_{z_A} = T_{z_B} = -82.29kN$, $T_{z_C} = 0$

5.3.2 Wheelset Displaced Laterally, No Yaw 131

$T_{z_A} = -82.29kN$, $T_{z_B} = 0$, $T_{z_C} = -82.29kN$

5.3.2 Wheelset Displaced Laterally and Yawed 132

$T_{z_A} = -82.29kN$, $T_{z_B} = 0$, $T_{z_C} = -82.29kN$

5.4 Conclusions 134

6. Comparison of Wheelset Forces Using New and Worn Rails

6.1 Introduction 137

6.2 Results 137

6.3 Discussion and Conclusions 138

7. Derailment Ratio

7.1 Introduction 159

7.2 Existing Formulae for Derailment Ratio 160

7.2.1 Nadal's Formula 160

7.2.2 Wagner's Formula 162

7.2.3 Johansen's Formula 163

7.3 Results 164

7.4 Discussion and Conclusions 167

8. Experimental Investigation

8.1 Introduction 170

8.2 Rig Description 171

8.3 Creepages and Forces 185

8.4 Procedure 190

8.5 Results 197

Page

8.6 Discussion 207

8.6.1 Validity, Accuracy and Repeatability of Results 207

8.6.2 Correlation with Theory 219

8.7 Conclusions and Recommendations 229

9. General Discussion and Conclusions 235

10. References 246

11. Acknowledgements 254

12. Appendices

1. Derivation of the Relative Slip Equations for Steady Rolling 255

2. Simplified Theory 257

3. Adaption of Governing Parameters for use in Simplified Theory 263

4. Comparison of Results Obtained Using Subroutine ROL with Kalker's Simplified Theory Program ... 268

5. Program Descriptions 269

6. Coordinate Geometry 361

7. Longitudinal Creep, Lateral Creep and Spin on Roller Rig 363

8. Angle of Yaw, ψ, of Upper Wheel Relative to Lower Wheel 369

9. Contact Ellipse Semi Axes, a,b 370

10. Experimental Data Sheet..... 374

11. Roll Effects on Experimental Rig 376

1. Introduction

In recent years railway technology, and in particular railway dynamics, is a subject which has received renewed interest. This is probably due to the advent of trains which travel in excess of 200 km/h. In the past an empirical approach had been sufficient, but at such high speeds a great number of phenomena need to be thoroughly investigated and a more scientific approach is essential.

When a railway vehicle runs along the track at constant speed there are secondary motions associated with the basic forward motion. These motions can be divided into two parts, the vertical dynamics and the lateral dynamics. The latter comprises all the rocking, rolling and swaying movements of the vehicle body and also the actual stability of the wheelsets and bogies. These depend directly on the interaction phenomena between track and vehicle. (A wheelset comprises two wheels joined by a rigid common axle, while a bogie is a mechanical system formed by the connection of two or three wheelsets).

Railway vehicles are fitted with coned wheels to provide a measure of stability but it can be shown that since the forces are non-conservative, dynamic instability occurs at a certain critical speed. Then motions are characterised by violent swaying movement of the axles on the track called 'hunting'. This motion is caused by the shape of the wheels and rail, and the forces which act in the plane of contact between them.

To study the lateral dynamics of a complete railway vehicle is very difficult since the mechanical system to be considered has a great number of degrees of freedom, and in particular several non-linearities. The most important of these is due to the presence of the wheel flanges, although others may be due to the damping effects of the suspension. It is interesting to note that for a wide range of practical values of the

parameters, the body of a complete vehicle does not strongly participate in the lateral motions of its wheelsets at high speeds.

It is possible by assuming small displacements of the wheelsets from their central positions, i.e. displacements which are small enough to avoid flange contact, to carry out a linearised study of the lateral dynamics, and in fact this is the approach used by several European Railway Administrations, including British Rail. It should be noted that such studies are only possible with the aid of digital or analogue computers.

The results of such an investigation can ensure that guidance is achieved, avoiding contact between wheel flanges and rails, during normal running. At very high speeds the hunting oscillations become more violent and are limited by the flanges striking the rails. The need to know the flange forces becomes more and more necessary so that complete lateral dynamics and curving calculations can be carried out on a wheelset, and eventually on the complete vehicle.

Actual running speeds, which are governed by the lateral dynamics of the vehicle, are usually based on comfort criteria, but to ensure safety standards the limiting case, which is derailment, must also be studied. The start of drailment is considered to be when the wheelset is displaced laterally so that the flange is in contact with the rail. If the wheelset is displaced further in the lateral direction then the flange must climb up the rail until the wheel eventually jumps off the track. Little is known about the derailment phenomena, probably due to the fact that the forces acting between wheel and rail are very complex and are affected by the motion of the vehicle. Furthermore derailment is affected by conditions of vehicle and track and depends on how much wear has taken place on the railhead or wheel tyre. If a large amount of wear takes place at the railhead then a situation is

reached which is so dangerous that the rail must be replaced. Various formulae exist which predict the (lateral force/vertical force) ratio to maintain flange contact for a particular rail/wheel combination. These formulae are only approximate, and in fact British Rail's standards are still based on a graphical study made of flange contact in 1949.

Thus there is an obvious need to be able to predict forces which exist between a wheelset and the track under various operating conditions, including large displacements where the flange of the wheel comes into contact with the rail.

The forces between wheel and rail are due to the phenomena known as "creep" and a knowledge of the relationship between the "creep" and the forces is of fundamental importance. The phenomena of creep exists when two bodies are pressed together with a force and allowed to roll over each other. Under such conditions the circumferential velocities of the two bodies need not be the same and a parameter called the 'creepage' or 'creep' for short, can be defined as the difference in circumferential velocity. The tangential force between the bodies can vary from zero, when the creepage is zero, to equal μN at the onset of gross sliding, where N is the force normal to the contact area and μ the coefficient of friction. Creeps can be defined in the longitudinal and lateral directions and a term called 'spin' can also be defined which is the difference in angular velocity between the bodies about an axis normal to the plane of contact. It can be seen that complete slip of wheel on rail is simply the limiting case of creep and is very important in studies of traction and braking.

Various theories have been proposed for the relationships between the creepages, spin and tangential forces in the contact area. A review of these theories is given in Section 2.2. This review is preceded in 2.1 by a short section showing how the actual equations for creepage and

spin arise in a wheelset using a simple coned wheelset as the model. Apart from the theories, a lot of experimental work has also been carried out in the field of rolling contact, both in connection with railway wheels and on rigs designed specifically for measurements of creep/force relationships. A review of experimental literature is given in Section 2.3.

One of the objectives of the present work is to investigate the various rolling contact theories which have been proposed and to select, compare and recommend those which are most suited for application to railway wheelsets. With this in view, Section 3 discusses, in more detail, the theories most suited to railway contact problems. A computer program has been written for each of these theories and used later in the analysis to calculate forces on a wheelset.

The forces are calculated for a mathematical model of a wheelset and track. This model, described in Section 4, is based on a real wheelset and real track using similar rail and tyre profiles to those found in service. British Rail have found that a standard tyre profile wears very rapidly with use to a "worn" profile, which then remains fairly constant for a long period. Because of this they have designed new tyre profiles based on this 'worn' profile, which, they claim, will then remain stable throughout their life. In the present work this 'worn' profile is incorporated as the tyre profile for the wheel. The rail profile used is a British Standard 110 lb/yd. rail, but the computer program, which calculates the coordinates of the profile, allows simulated wear of the rail to be built-in, and comparisons of the forces on a wheelset can be made between new and worn track. Thus the wheelset and track are developed mathematically as three dimensional equations written to simulate them. By various axes transformations and rotations, the wheelset can be moved relative to the track and the points of contact found between the two. Large displacements and large yaw angles of the wheelset

relative to the track are possible, so that both tread and flange contact conditions can be studied.

A second objective is to give a more accurate value of the forces involved in derailment than has previously been possible. This involves calculating the lateral force on a wheelset needed to keep the flange in contact with the rail, using the most appropriate rolling contact theory. The effects of rail wear on the forces can also be studied using the computer programs developed during the investigation.

These objectives all involve the steady state forces on a wheelset rolling along the track at a constant velocity in a displaced position. Having defined the wheelset and track and found the contact points for a particular lateral displacement and yaw angle, the creepages can be calculated. These are the steady state creepages and do not include time dependent terms, which would have to be included in a dynamic analysis of the wheelset. (This was not one of the objectives of the present work, although it could perhaps be pursued at a later date).

The forces in the planes of the contact areas are calculated from the creepages by using one of the theories mentioned previously. These forces are then resolved and summed to give the total forces on the wheelset.

Section 5 compares results obtained for the creeps and forces using the various theories, for three different contact conditions of the wheelset. Firstly, for tread contact, secondly for flange contact with zero angle of yaw and thirdly for flange contact with a large angle of yaw. The relative merits of each theory are discussed.

The complete results for both new and worn rails are presented in Section 6. These results include forces and creepages for various lateral displacements, angles of yaw and load distributions of the

wheelset. The forces are calculated using the most relative rolling contact theory to suit the conditions.

Section 7 discusses the derailment situation and defines a convenient ratio called the 'derailment ratio' or 'derailment quotient', which is a measure of how easy a particular rail/wheel combination is to derail. Various approximate formulae are described which have been used in the past by railway authorities to calculate this ratio. Values obtained using these formulae for the present rail/wheel combination are compared with the present results.

For tread contact between wheelset and track, the spin component is small because the cone angle of the tread is small, and the contact ellipse is almost circular in shape. For flange contact the opposite is true, the spin component is large and the contact ellipse very elongated in the rolling direction. During the theoretical investigation it became apparent that although theories existed which predicted the forces due to creeps and spin on elongated contact ellipses, there was little experimental evidence available to verify the results. The only experimental work which had been done, was for creep without spin and for contact ellipses with semi-axes ratios, (a/b), of up to three. When the flange is in contact with the rail, the contact ellipse is very elongated, with (a/b) ratios greater than ten, and the spin is large due to the large cone angle of the flange. Under such conditions no experimental work has been done.

As a result an experimental rig was designed and built which simulated flange contact conditions. This is described in Section 8. The object of the rig was to measure the lateral force due to varying amounts of lateral creep and spin on elongated contact ellipses, under conditions similar to those found when the flange is in contact with the rail. In studies of lateral dynamics or derailment, the lateral force is of main

interest, while longitudinal force is used in adhesion and braking studies. The latter was of little interest in the present investigations and was not measured experimentally.

The results of the experimental work are given in Section 8.5 where the lateral force is plotted for various creeps, spins, (a/b) ratios and contact pressures. A discussion of these results follows in 8.6 where they are compared with theoretical results.

Finally, Section 9 is a general discussion of all the work undertaken in the present investigation and brings together the various themes involved.

2. Review of Rolling Contact Theories and Experiments

2.1 Basic Theory

If two bodies of revolution are pressed together with a force N a contact region forms where they touch. According to the theory of Hertz, Ref. 1, this region is elliptical in shape and the ratio of the semiaxes, (a/b), can be calculated from a knowledge of the principal radii of curvature of the bodies of revolution. In order to calculate the actual dimensions of a and b the normal force has also to be known, Ref. 2. If the bodies are spheres, or if one body is a sphere and the other a flat surface, then the shape of the contact area will be circular.

Two such bodies are shown in Fig. 2.1. If the bodies are rotated about their axes so that they roll over each other, tangential forces can be transmitted in the plane of the contact area, due to dry friction. If a couple is applied to one body and taken out on the other, it is found that the circumferential velocities need no longer be the same, without the occurrence of gross sliding. A non-dimensional term called the creepage (or creep) may be defined as the difference in circumferential velocity divided by the mean rolling velocity. If the creepage is zero then the tangential force, or traction as it is often referred to in the literature, is zero and this condition is known as free rolling. If the creepage is increased, a point is reached when the tangential force is equal to μN, where μ is the coefficient of friction, and this is called gross sliding. Thus there exists some relationship between the tangential force and the creepage.

Creepages may be defined in both the longitudinal and lateral directions. Another term, called spin, may also be defined if the bodies rotate about an axis normal to the plane of the contact area, this being the difference in angular velocity of the bodies about an axis normal to the plane of the contact area divided by the mean rolling velocity, and

FIG.2.1 Bodies in Rolling Contact

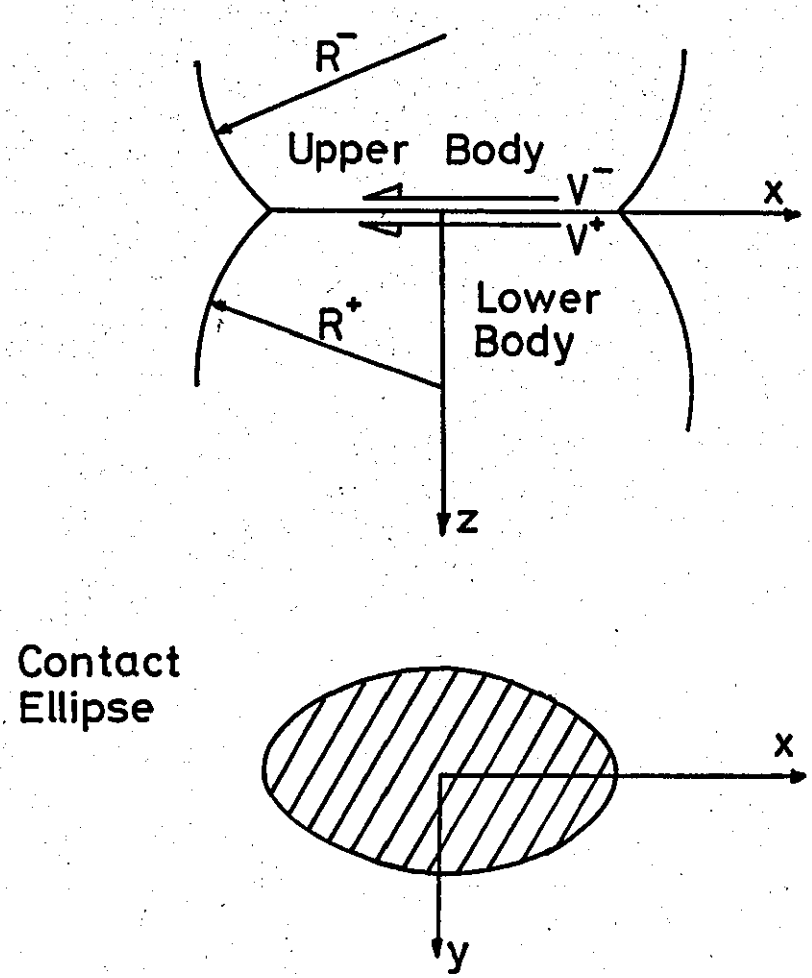

FIG. 2.2 Simple Coned Wheelset in Displaced Position

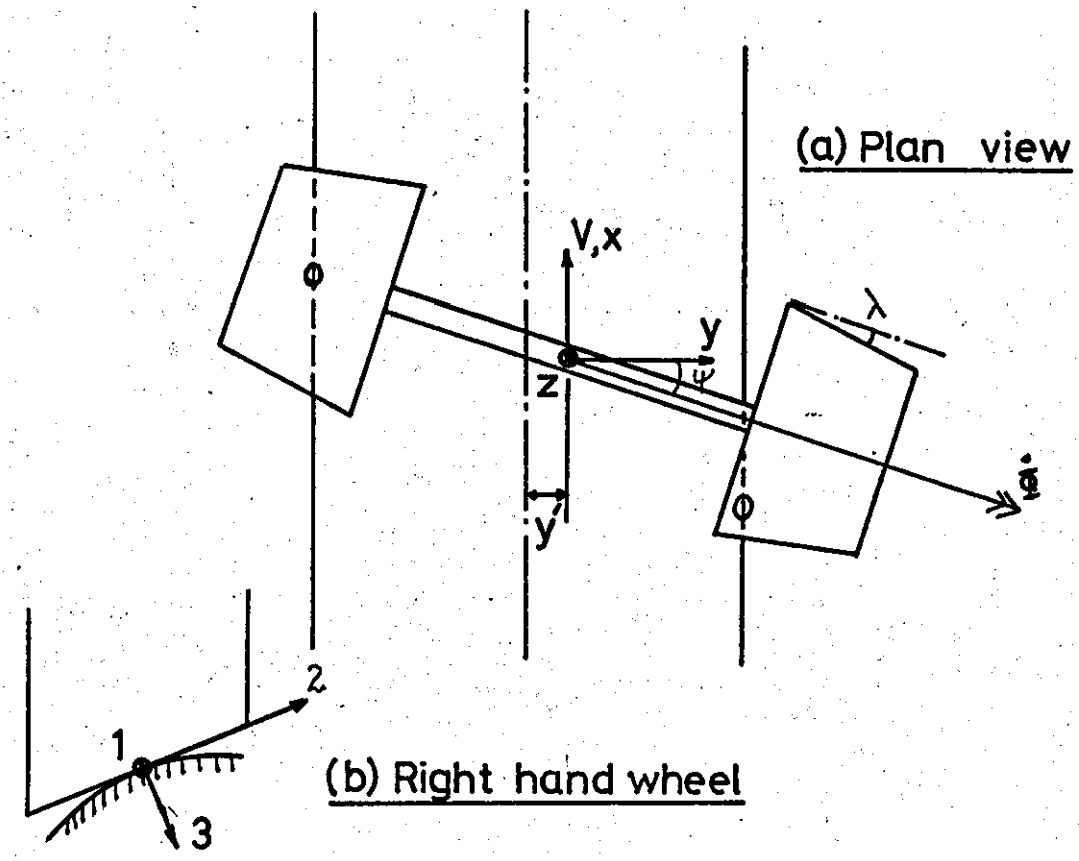

therefore has dimensions $(\text{length})^{-1}$.

The term slip is frequently used and this refers to the local velocity of the bodies relative to each other at a specified point in the contact area. Sliding is used to denote the condition of complete bodily slip.

The way in which creepages and spin arise in a railway wheelset can be seen by referring to Fig. 2.2 where a simple coned wheelset is shown. The wheelset is assumed to be moving freely along perfectly straight track with a constant velocity V in a steady state displaced position with angle of yaw ψ and lateral displacement y. Both these quantities are assumed to be small. If the rolling radius with the wheelset in the central position is r_0, then the angular velocity of rotation is given by

$$\dot{\Phi} = -\frac{V}{r_0} \qquad (1)$$

Track axes (x, y, z) are defined through the centre of the wheelset and moving along with it. Local axes (1, 2, 3) are defined at each contact point, see Fig. 2.2(b). If V_1, V_2 are the velocities of the contact ellipse along the rail in the 01, 02 directions, and V_1', V_2' are the velocities around the wheel, then for the right hand wheel:

$$\begin{aligned} V_1 &= V & V_2 &= 0 \\ V_1' &= V\frac{r_R}{r_0} & V_2' &= \psi V \end{aligned} \qquad (2)$$

where r_R = rolling radius of right hand wheel.

The longitudinal creepage is defined as

$$\gamma_1 = \frac{V_1 - V_1'}{\frac{1}{2}(V_1 + V_1')} \qquad (3)$$

and the lateral creepage as

$$\gamma_2 = \frac{V_2 - V_2'}{\frac{1}{2}(V_1 + V_1')} \qquad (4)$$

If λ = cone angle, then

$$\left.\begin{aligned} r_R &= r_0 + \lambda y \\ r_L &= r_0 - \lambda y \end{aligned}\right\} \qquad (5)$$

Substituting for V_1, V_2, V_1' and V_2' from Equation 2 into Equation 3 and Equation 4 gives

$$\gamma_{1_R} = -\frac{\lambda y}{r_0} \tag{6}$$

and

$$\gamma_{2_R} = -\psi \tag{7}$$

and similarly for the left hand wheel.

If Ω_3 and Ω_3' are the angular velocities of spin of the rail and wheel about the 03 axis, then the spin is defined as

$$\omega_3 = \frac{\Omega_3' - \Omega_3}{\frac{1}{2}(V_1 + V_1')} \tag{8}$$

For the right hand wheel $\Omega_3 = 0$ and $\Omega_3' = \dot{\Phi}\lambda$

Thus

$$\omega_{3_R} = -\frac{\lambda}{r_0} \tag{9}$$

As a generalisation it may be noted that the longitudinal creep is dependant on the lateral displacement of the wheelset, the lateral creep is dependant on the yaw angle and the spin is dependent on the cone angle.

In order to calculate the forces on the wheelset, the problem is to know what takes place in the contact area and to find the relationships between longitudinal creep, lateral creep and spin and hence longitudinal force, lateral force and moment. Various theories have been proposed for these relationships and these are reviewed in Section 2.2. Most of them assume that the bodies are smooth surfaces and that Coulombs law of dry friction holds between the bodies. One theory does not make this assumption and takes into account the roughness of the surfaces.

2.2 Theoretical Review

The earliest theoretical work in rolling contact seems to have been that of Carter, Ref. 3. He gave an exact solution for the relationship between longitudinal creepage and tangential force, from free rolling to gross sliding, for the two dimensional case of two

cylinders with parallel axes rolling together, with creep in the direction of rolling only. In this case the contact area is infinitely long and of width 2a, see Fig. 2.3. Carter assumed that the contact width is divided into an area of adhesion and an area of slip. In the area of adhesion, sometimes called the locked area, the local slip is zero. The resultant traction distribution over the contact width is the difference of two semicircular distributions, one acting over the whole width, equal to μZ, and the other over the area of adhesion. The resultant traction is therefore less than μZ.

Carter assumed, without proof, that the area of adhesion was at the leading edge. Later work by Poritsky, Ref. 4, produced the same result but in greater detail and showed that other results were possible, i.e. with the area of adhesion not at the leading edge. In a discussion of Poritsky's work by Cain, Ref. 5, he showed from the laws of simple friction that the area of adhesion could be only adjoining the leading edge. This important conclusion was in contrast to the static problem where the adhesion zone is centrally placed. Poritsky's work, like Carter's, only applied to the two dimensional case of contact between infinitely long cylinders. Their derived relationship between longitudinal force and longitudinal creep is plotted in Fig. 2.4.

The three dimensional case of an elastic sphere rolling on an elastic plane without spin present, was studied by Johnson, Ref. 6. In this case the contact area is circular and the area of adhesion was also assumed to be circular. The total traction was assumed to be the difference between a spherical traction distribution acting over the whole contact area and another which acts over the adhesion area only. This assumption was similar to that made by Carter, but in this case it is not strictly true, since the slip and the tangential traction do not oppose each other in an area near the leading edge of the contact area. In fact any assumption of slip between contacting points before they have passed through the locked region can be shown to contradict the law of

FIG. 2·3 Contact of Infinitely Long Cylinders

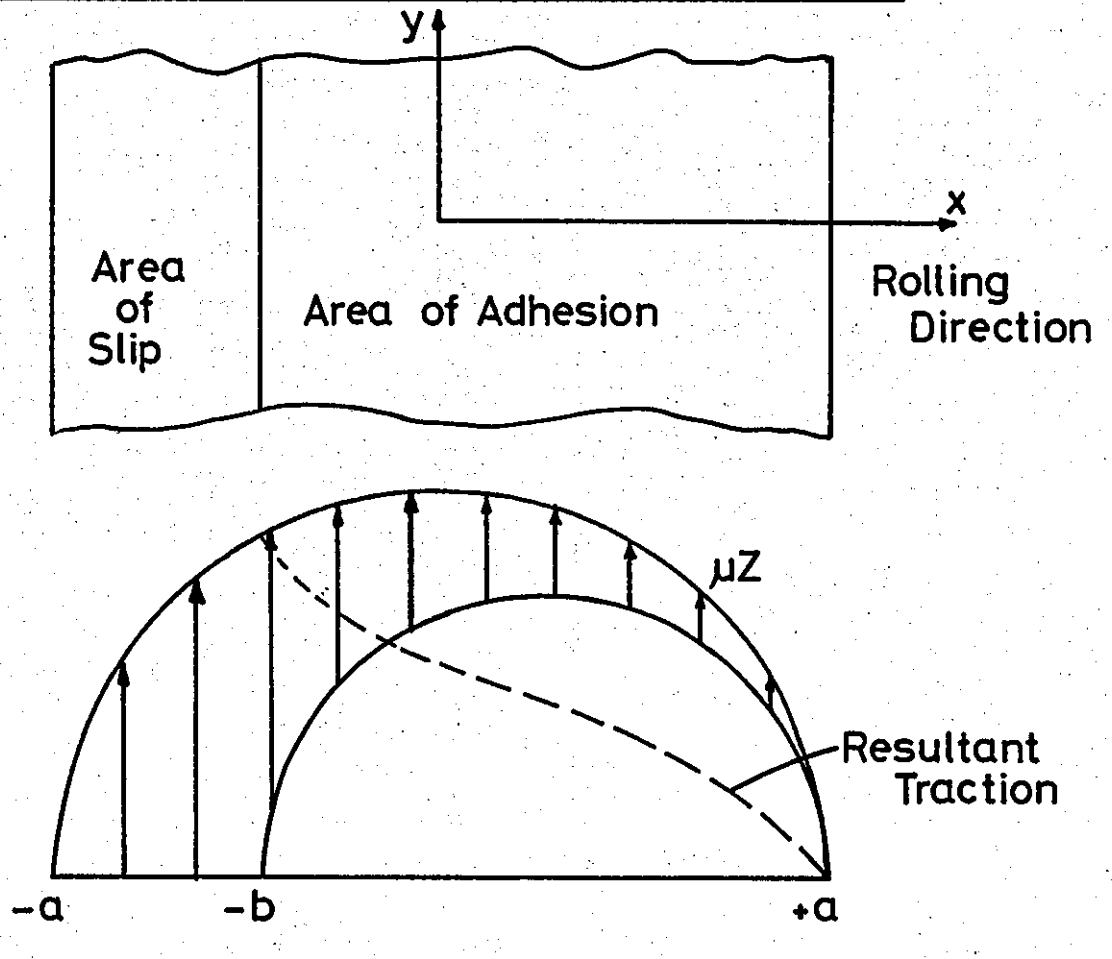

FIG. 2·4 Total Tangential Force for Contact of Cylinders

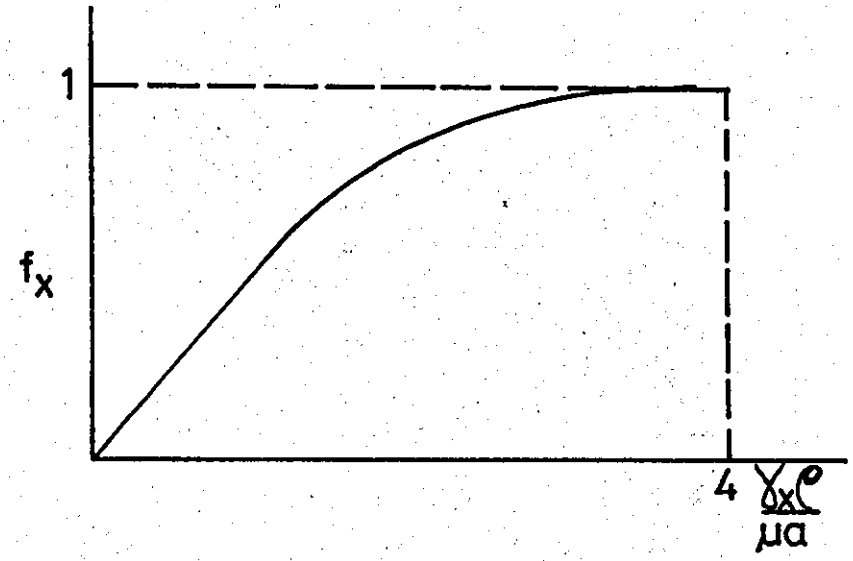

friction, which says that the slip must oppose the tangential force acting between the surfaces. This suggests that the assumed shape of the area of adhesion was not correct.

Johnson compared his theory with experimental results obtained by rolling a ball on an inclined plane, and showed that the theoretical creep was less than the measured creep for a particular force, the maximum difference being about 25%.

This work was extended by Johnson and Vermeulen, Ref. 9, for elliptical contact areas, i.e. for the contact of non-spherical bodies, but again for creep in one direction only. Similar assumptions to Ref. 6 were made in that the area of adhesion was assumed to be an ellipse just touching the leading edge of the contact ellipse, and the total traction was given by the difference of two traction distributions, one over the whole contact area and the other over the area of adhesion. Experimental results were given for lateral creep due to lateral tangential force on contact ellipses with (a/b) ratios from 0.276 to 2.47. Again the theoretical creep was less than the experimental creep for a particular force, the maximum difference being about 25%.

Haines and Ollerton, Ref. 11, put forward an approximate theory for the case of elliptical contact with creep in the direction of rolling only. The contact area was divided into a number of strips parallel to the rolling direction, interaction between the strips was ignored and each strip studied using the Carter/Poritsky two dimensional theory. It follows from this assumption that the leading edge of the area of adhesion touches the leading edge of the contact area, while the trailing edge of the area of adhesion is the trailing edge of the contact area shifted parallel to itself, in the rolling direction. This approximation was best for a contact ellipse narrow in the direction of rolling. The theory was supported by an experimental investigation using a photoelastic frozen stress technique to give the surface traction stresses.

This showed that the assumption of the tangential traction in the slip region being a constant proportion of the normal pressure at any point, was correct. The experimental work also showed that the shape of the area of adhesion was that assumed in the approximate theory of the authors.

In Haines, Ref. 31, a similar investigation was carried out for elliptical contact areas with a shearing traction applied at right angles to the rolling direction.

A report given by Halling, Ref. 14, describes another approximate solution for the case of a circular contact area with creep in one direction only. Although the area of adhesion in this investigation was assumed to be elliptical, almost the shape found by Haines and Ollerton, an error was introduced because the ellipse slightly overlapped the leading edge of the contact area. Halling also carried out some experiments on a steel ball rolling along a flat steel plate under various loads, and found that the results agreed more with his theory than with Johnson's.

The first solution to the creep problem with spin present was given by Johnson, Ref. 7. The motion of an elastic sphere rolling on an elastic plane was studied with the sphere having an angular velocity of spin about an axis normal to the plane. Johnson gave an expression for the lateral creep which was observed to accompany rolling with spin, assuming small spins, circular contact area and small amounts of slip. It was not possible to make a supposition for the area of adhesion once slip had developed, and this result assumes that the area of adhesion covers the whole contact area. Measurements of the creep on a simple thrust bearing agreed with the theory.

This work was continued in a later report, Johnson Ref. 8, where theoretical relationships were derived for the lateral creep due to both applied tangential force and spin. The assumptions of small

spin, small tangential force and circular contact area were again made.

An extension to this work is given by Johnson, Ref. 10, where the shape of the adhesion area was observed for the case of rolling with spin (no applied tangential force), by rolling a rubber ball on a transparent plate onto which a screen of ink spots had been previously printed. With increasing spin the slip regions spread leaving a pear shaped area of adhesion touching the leading edge, with its longitudinal axis in the direction of rolling. The widest part of the pear shape was towards the leading edge.

Johnson, Ref. 10, also reports investigations into the rolling contact of cylinders having different elastic constants, together with a study of a ball rolling in a closely conforming groove where the contact area is a narrow ellipse. This problem is solved by using the Haines/Ollerton strip theory approach.

Similar work was carried out independently by Halling, Ref. 15, for the creep due to a rolling element in a closely conforming track with an applied tangential force. The general case of elliptical contact was developed assuming an ellipse narrow in the rolling direction, the contact area being divided into strips and the two dimensional Carter/Poritsky theory applied. Halling concludes that wear can be minimised when the combined effect of conformity and tangential force reduces the creep ratio to zero. The special case of a ball rolling along a flat plate was considered and theoretical results were compared with the experimental results of Johnson, Ref. 6 and Halling, Ref. 14 with very good agreement.

A more refined solution for the three dimensional case of circular contact with infinitesimal creepage and spin is given by De Pater, Ref. 12. The area of adhesion is assumed to cover the entire contact area, and Poissons ratio is assumed to be zero. This restriction is lifted by Kalker, Ref. 13, where a complete analytical solution is

given for the more complicated problem in which $\sigma \neq 0$. A comparison between Kalker's theory and the experimental results of Johnson, Ref. 6, is made in Ref. 12 and shows very good agreement.

All the theories mentioned so far have had some restriction on their use, e.g. some apply for circular contact areas only, some for creep in one direction only, some for zero Poissons ratio, etc. One of the main difficulties encountered by investigators has been defining the area of adhesion. Solutions have been obtained for the limiting case of infinitesimal creepage and spin, where it is assumed there is no slip anywhere in the contact area and μ tends to infinity. These have been discussed in the previous paragraphs. The opposite case has also been investigated, i.e. the case of very large creepage and spin where complete slip is assumed throughout the contact area. This was the basic assumption made by Lutz, Refs. 17, 18 and 19 and Wernitz, Refs. 20 and 21. They also assumed that the influence of the elastic deformation of the bodies could be neglected in calculating the local slip, i.e. the slip was regarded as pure rigid body rotation, and was specified by the creepage and spin alone. Knowing the direction of the local slip, and therefore the direction of the traction, the total tangential force and moment could be calculated, since the magnitude of the local tractions was also known. Lutz, Ref. 18, considered a circular contact area which is a special case of the results given by Wernitz, Ref. 20, for elliptic contact areas, both assuming creep in one direction only.

Apart from these limiting cases for infinitesimal creepage and spin and for very large creepage and spin, the only case for which there existed a theoretical relationship was that for pure creepage. Unfortunately most cases of practial interest, especially in the railway wheelset application, lie between the two limiting theories and generally involve both creep and spin.

A big step forward was made by Kalker, Ref. 22, where a numerical method was given for the three dimensional case of arbitrary creep and spin. This theory is mainly of academic interest for the case of pure creepage, but for creep and spin occurring together it was the first available method for predicting the forces. The theory was developed in more detail by Kalker, Ref. 23, where results were compared with the experimental results of Johnson, Refs. 6, 7, 8, 9 and Haines and Ollerton, Ref. 11.

In general, theory and experiment agreed very well for the cases tested, and graphs showing these comparisons are given later in Section 2.3. The numerical method failed to converge for(a/b) ratios greater than 2, and can be used only for near circular contact areas. In view of its possible application to the railway wheelset problem it is discussed in more detail, together with its limitations, in Section 3.

Also in Ref. 23, the Lutz-Wernitz theory for large creepage and spin was extended by lifting the restriction of having the creepage along one of the principal axes of the contact ellipse only. Integral expressions are given for the forces which can be solved numerically. This method is also discussed in Section 3.

The case of infinitesimal creepage and spin has been treated by Johnson, Ref. 7, De Pater, Ref. 12 and Kalker, Ref. 13, for circular contact areas. This theory was generalised in Ref. 23 for elliptical contact areas, details of the method being given in Section 3.

In Ref. 24, Kalker generalises the strip theory of Haines and Ollerton, Ref. 11, and Johnson, Ref. 10, to take account of lateral creep and also spin, to a limited extent. Thus in a sense it is a general theory for arbitrary creep and spin, but due to other limitations it is not used in the present analysis. In this theory the complicated relationships between the elastic displacements and the tractions in the contact area are simplified by ignoring some of the cross dependence terms. It is argued that this approximation is less severe than the

following strip theory assumptions which are also made:

(a) the traction distribution is assumed to change slowly in the lateral direction, so that the slip is assumed constant in this direction. (From this assumption it follows that best results are achieved for contact ellipses which are narrow in the direction of rolling)

(b) the traction distribution for a fixed lateral ordinate is the difference of two half elliptical traction distributions, one acting over the whole contact width and the other over the area of adhesion.

Two types of solution are considered:

(a) when there is no area of adhesion; and

(b) when there is an area of adhesion

In the latter case the Carter traction distribution is assumed, and it follows from the boundary conditions that in order for the area of slip to touch the trailing edge and for the law of friction to hold in the area of adhesion, then a restriction must be placed on the spin parameter. This condition says that $|\psi| < 1$

where $$\psi = \frac{\omega_3 a}{2\mu A} \qquad (10)$$

a = semiaxes of contact ellipse in rolling direction

b = semiaxes of contact ellipse in lateral direction

and $$A = \frac{3N}{2\pi ab\,G}$$

In Ref. 24, the theory is tested for the case of pure creepage and the case of pure spin. In the case of pure creepage the results are good for the total tangential force when the contact ellipse is narrow in the direction of rolling, but in the case of circular contact area, the results are poor, with errors of up to 25%. For the pure spin case, errors of the order of 20% are possible when

(a/b) = 0.2 and as high as 40% for circular contact areas. In both cases Poissons ratio is not accurately accounted for. In the limiting case of $|\psi| = 1$, the area of adhesion vanishes, while for $|\psi| > 1$ no area of adhesion forms at all, and this leads to a vanishing total force. This contradicts the numerical theory and Johnson's experiments, which show that the tangential force only vanishes in the limit when $|\psi|$ tends to ∞

In the rolling wheelset problem, contact is either on the tread of the wheel or on the flange. In the former case, contact areas are near circular in shape and since the creeps and spins are generally small, the numerical theory or the infinitesimal creep theory can be used without difficulty. For flange contact conditions the contact ellipse is very elongated in the rolling direction, and because of the large cone angle the spin is great. These conditions make the strip theory totally inadequate and therefore it has not been used in the present analysis.

For cases of rolling contact involving creep without spin on elliptical contact areas, the theories of Johnson and Vermeulen, Ref. 9, Haines and Ollerton, Ref. 11, and Kalker, Ref. 24, have already been mentioned. Johnson and Vermeulen's theory has been shown to give rise to errors of up to 20% while Haines and Ollerton and Kalker are good for slender contact ellipses (slender in the rolling direction), but for other shapes, even circular they are less accurate. In Ref. 25, Kalker proposes an empirical formula which is tested against the theories just mentioned and also against the numerical method of Ref. 23. Agreement between these results and the proposed formula are generally within 10%.

A limited amount of work has been done on the rolling contact of bodies with different elastic constants. In this case the normal pressure and the tangential tractions are not independent of each other as is normally assumed. Johnson, Ref. 10, gives some qualitative

conclusions about the effect of slip for the case of two cylinders in rolling contact, while Bentall and Johnson, Ref. 26, solve the problem approximately using a numerical method, showing that the effect of slip on the rolling friction is generally small. Kalker, Ref. 30, gives the creep/force relationships for elastically dissimilar cylinders for a complete range of values of μ. These results are derived from a minimum principle for the law of dry friction which leads to a linear programming problem. This method does not assume the shape of the adhesion area before starting to solve the problem, as this is taken care of in the mathematical analysis.

Kalker has also investigated transient phenomena for the two dimensional case of cylinders rolling over each other in Ref. 27, 28, 29 and 30. He has devised a step-by-step numerical method and found that the tangential force distribution given by Carter, Ref. 3, for this case, could be achieved after two contact widths had been traversed. A similar result was achieved for dissimilar cylinders in contact, and he concluded that most cases of practical interest, in which the tangential force changes during rolling, can be regarded as a succession of steady states. The same problem is considered in Ref. 30 using linear programming.

Brief mention should be made to a completely different approach to the problem of rolling contact taken by Nayak, Ref. 32, who presents a theory which does not assume either smooth surfaces or that Coulombs law of friction is valid in the contact region. Nayak argues that experimental investigations in rolling contact do not always produce results which agree with the smooth surface theories, and although there are many possible reasons for these disagreements (and these are discussed later) his main criticism is the assumption of Coulombs law in the contact region. In his theory the law of friction is based on experimental observations of junction deformations.

This theory, which postulates surface roughness effects to be

important, is given in a refined form in Ref. 33. The theory only applies for two dimensional contact of similar bodies, and to be able to use the theory a profilometric examination of the body surfaces has to be made to calculate a surface roughness parameter. Results given compare qualitatively with experimental results and Nayak concludes that surface roughness effects are not important for smooth rolling bodies or when the contact pressure is high.

The rolling contact phenomenon is still being investigated by Kalker and recently he has proposed a theory in which the displacement differences (u, v) and the tractions (X, Y) are connected by simple expressions

$$\left.\begin{aligned} u &= S_x X \\ v &= S_y Y \end{aligned}\right\} \qquad (11)$$

where Sx, Sy are called the inverse stiffnesses. This is an obvious simplification on the exact theory where the relationships between these parameters are very complicated. This so called Simplified Theory adapts the governing parameters in a special way so that there is agreement between the results it predicts and the numerical theory.

Although this theory is still being developed at Delft, a brief report has been written on it, Ref. 36, and with the author's permission, the essence of this is given in Appendix 2. This theory, although it has not been proven experimentally, has obvious advantages for use in the present work since it can treat the case of creep with spin on any shape contact ellipse and because of this it is discussed in more detail in Section 3.

The numerical method of Kalker, Ref. 23, has also been recently modified and it can now treat the case of elongated ellipses, although the actual program is still rather cumbersome to use.

This modified version, which is still being developed, has not been used in the present work, although Dr. Kalker has run his program for selected cases to compare with experimental results produced later. These are given in Section 8.

Summing up, this review of theoretical work in the field of rolling contact shows that much progress has been made since Carter published his two dimensional analysis in 1926, to reach the sophisticated numerical techniques which Kalker is developing for the completely general case of arbitrary creep and spin. It seems that a solution will soon be available which predicts the forces for this general case. Even then it will be rather cumbersome, taking a lot of computer time if used, say in the complete dynamic calculations of a railway vehicle. In view of this, some of the approximate theories have obvious attractions for use in particular cases, such as, for example normal tread contact of a wheelset where the creeps and spin are small. Theories which can be used for different types of contact in the railway wheelset situation are given in more detail in Section 3, and a computer program has been written for each method. A comparison of results using these different theories is given in Section 5.

2.3 Experimental Review

Many experiments have been carried out in the field of rolling contact. Some have been directly applicable to railway wheelsets and the tests have been carried out using scale wheels on a rail/wheel machine, generally called a roller rig, while in other experiments real wheels on real tracks have been used. Probably the most accurate creep measurements have been made using apparatus designed specifically for this purpose, and usually comprise a sphere rolling on a flat surface giving a circular contact area.

Experimental evidence falls into three categories: (a) longitudinal creep, (b) lateral creep and (c) lateral forces due to spin. In the early days the main interest in creep phenomena was due to the adhesion of railway wheels or more specifically to the lack of it. This meant an interest in longitudinal creep, and Carters theory, Ref. 3, published in 1928, applied to this case. In a survey report by Hobbs, Ref. 34, there is mention of a British Rail report by Loach published in 1935, in which experiments were carried out on a roller rig using two cylindrical rollers. The longitudinal force due to varying amounts of longitudinal creep was measured. The results have been manipulated by Hobbs into non-dimensional form and are reproduced in Fig. 2.5, along with other longitudinal creep experiments, to show the comparison between them and Kalkers numerical theory. The varying contact conditions are taken care of in the non-dimensional parameter plotted, which was proposed by Johnson and Vermeulen, Ref. 9, for their elliptical contact work.

This experiment was probably one of the first creep/force measurements to be carried out. There had been earlier attempts to measure the coefficient of friction (or coefficient of adhesion, which is more appropriate in railway terminology) and this, of course, is the limiting case for large creeps.

The first experiments on forces due to lateral creep were carried out by Davies, Ref. 41. In this report, in which the author is concerned with the lateral oscillations of railway vehicles, experiments were described using a 1/5 scale model of a four wheeled vehicle with cylindrical steel wheels rolling on flat topped steel rails. A brake force could be applied to one of the wheels to give longitudinal creep and lateral creep was achieved by banking the track. As the experiments were conducted with either "line contact" or point contact, it is not possible to compare Davies's results with any of the theories. In this report the author compares his longitudinal creep experimental

results with Carters theory showing good agreement over the linear region, but for larger tangential forces the creep is greater than Carter's theory predicts. The creep/force curves of Davies are asymptotic to a line, indicating a coefficient of friction of 0.125 which is also the value obtained from the experiment by locking the wheels, i.e. the coefficient of sliding friction. Changing the speed did not affect the results for either longitudinal or lateral creep.

The most extensive experimental work in the field of rolling contact has been carried out by K. L. Johnson, using various pieces of apparatus. He has measured forces due to longitudinal creep, lateral creep and spin, generally on spheres rolling on a flat or inclined plane, and thus the results apply for circular contact areas only. The spheres have always had a very good surface finish of probably 0.025 to 0.05 μm C.L.A., and in order to get repeatable results lubricated surfaces, and therefore low coefficients of friction, have nearly always been used. To avoid any hydrodynamic lubrication effects, the experiments have been carried out at very low speeds. The contact pressures have been high with average pressures greater than 483 MN/m^2. Although most of the experiments have been mentioned briefly in Section 2.2 they are discussed in more detail here.

Johnson, Ref. 6, describes an experiment which measures creep due to both longitudinal and lateral tangential forces separately. For longitudinal creep measurements, the experiment consisted of two hardened steel balls of 25 mm diameter mounted on a spindle. These balls rolled on a hardened steel strip in a direction normal to the axis of the spindle, and could be loaded by means of two hangers mounted on ball races at the ends of the spindle. Longitudinal creep was investigated by tilting the plane and measuring the creep with a micrometer after traversing the ball up and down the plane, the system being restrained from free rolling by strings parallel to the plane passing over pulleys at the top of the plane. Both the balls and the plane had very good

surface finishes and the balls were cleaned, washed in benzene and wiped dry before each experiment. The coefficient of rolling friction was measured as being 0.09 compared with a value of 0.12 - 0.14 for the sliding coefficient.

Lateral creep experiments were carried out on the same piece of apparatus by tilting the plane through an angle perpendicular to the angle of rolling, but maintaining it horizontal. The balls were rolled by hand at very small velocities, less than 3 m/min. and the creep was measured with a micrometer. The coefficient of rolling friction for lateral creep was measured as 0.11.

These experiments were performed 'dry' and also with surfaces flooded with lubricating oil. In view of the very low velocities involved, the hydrodynamic effect of the oil was negligible, but even so the coefficient of friction only fell from 0.11 to 0.09 with the lubricated surfaces. Johnson concludes from this that a thin grease film must have been present for his 'dry' runs.

The longitudinal results are shown in Fig. 2.5 and the lateral results in Fig. 2.6, where it can be seen that agreement between Johnson's experimental results and Kalker's numerical theory is very good for this case where (a/b) = 1. These results are also shown in Fig. 2.7 where they are plotted using Kalkers non-dimensional creep parameters referred to in Section 3.

In Johnson and Vermeulen, Ref. 9, experimental results are given for lateral tangential force due to lateral creep on elongated contact ellipses with the following ratio of semiaxes: (a/b) = 0.276, 0.683, 1.57 and 2.47. The experimental procedure is not described in detail but the measured coefficients of friction are tabulated as 0.11, 0.16, 0.17 and 0.11 respectively. The authors use the following expressions to correlate their results for the various (a/b) ratios:

FIG.2·5 Comparison of Longitudinal Creep Measurements with Kalker's Theory

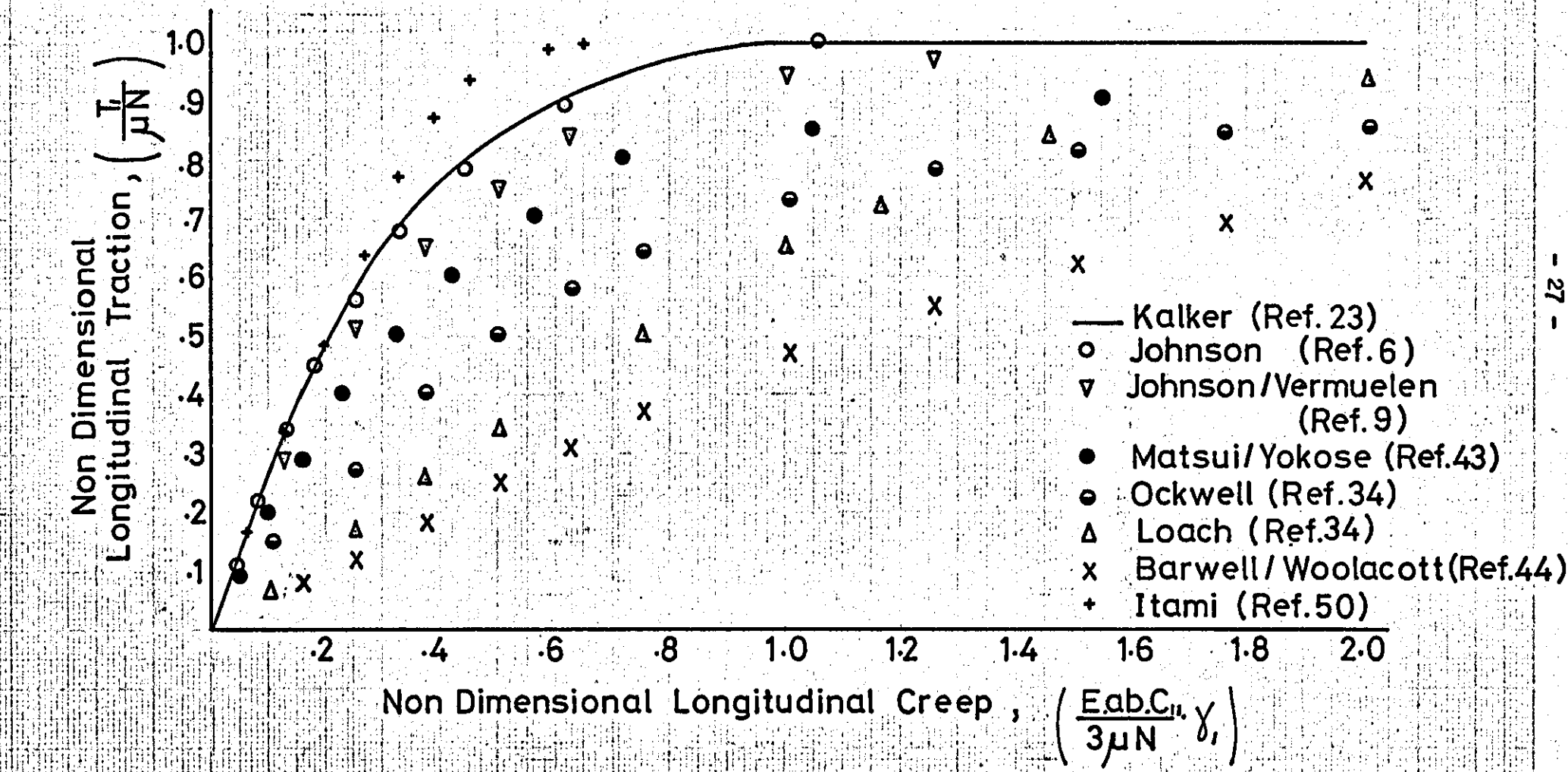

FIG.2·6 Comparison of Lateral Creep Measurements with Kalker's Theory

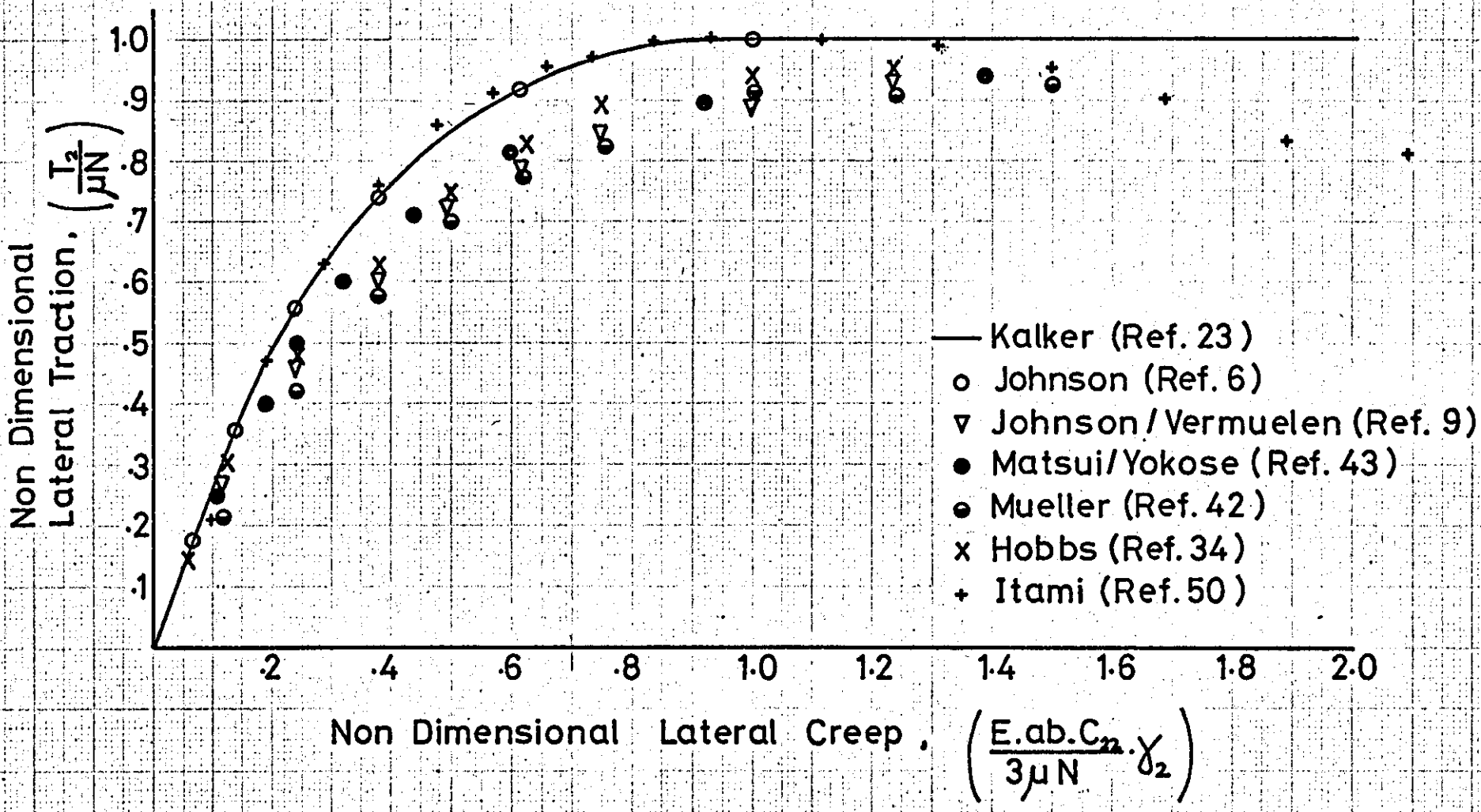

FIG.2.7 The Total Force Due to Longitudinal and Lateral Creepage ($a/b=1, \sigma=0.28, \chi=0$)

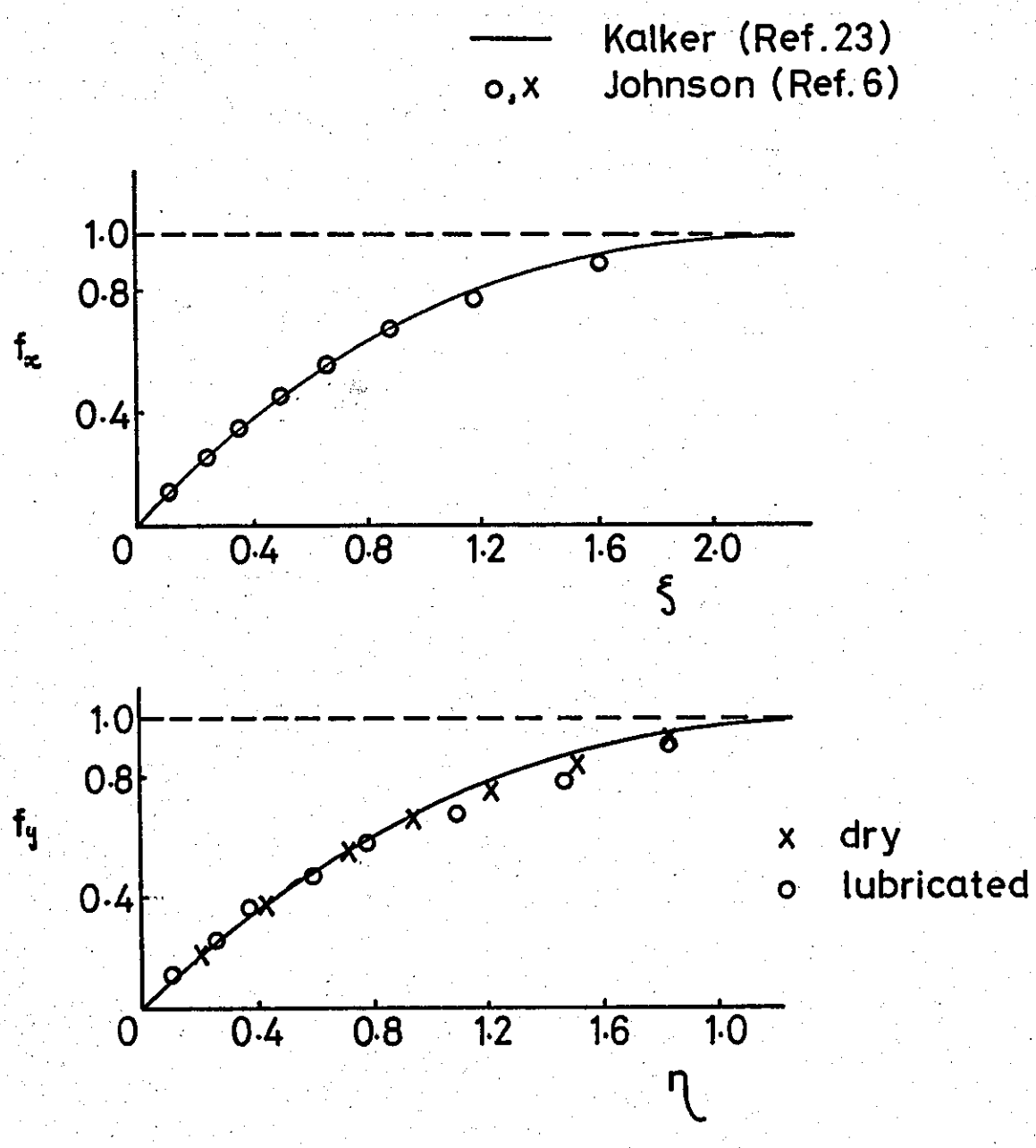

$$\frac{E a b C_{11}' \gamma_1}{3 \mu N} \quad \text{and} \quad \frac{E a b C_{22}' \gamma_2}{3 \mu N}$$

These expressions have been used in Figs. 2.5 and 2.6, where it can be seen that agreement between experiment and theory is not as good as for the circular contact experiments mentioned previously. This may be due to unwanted creep being present in the experiment, or more likely that the coefficient of friction assumed was not correct. By a different choice of μ all points can be brought closer to the theoretical curve; this means, however, that points corresponding to complete sliding lie above the curve. This could be explained by assuming the coefficient of friction increases with increasing slip.

The problem of finding a correlation function for pure creepage in either longitudinal or lateral directions is discussed further by Kalker, Ref. 25. A very complicated function is derived which correlates the experimental evidence of Johnson, Ref. 6, Johnson and Vermeulen, Ref. 9, and the numerical theory of Kalker, better than the correlation function mentioned above. This empirical formula compares well with the exact theory when (a/b) = 0.2, but the agreement becomes worse with increasing (a/b) ratio. Kalker suggests that the formula used by Johnson and Vermeulen is best when (a/b) is large.

Johnson's first spin experiments are described in Ref. 7 where measurements were made of the lateral creep which accompanies rolling with spin. The apparatus consisted of a simple thrust bearing with flat horizontal races, the load being transmitted through three symmetrically spaced balls. Spin is generated by rotating the top race relative to the bottom, and the lateral creep is given by the outward displacement of the balls, measured with a micrometer. Various normal loads and ball diameters were used, the experiments being performed at low velocities to ensure centrifugal forces were negligible.

The effect of different coefficients of friction was obtained by having different surface conditions on the races which were either 'hard' or 'soft', in an "as ground" or polished condition, the balls at all times being hard and polished. Some measurements were made dry but most had a lubricant present. The coefficient of sliding friction was measured in each case and varied between 0.12 to 0.25, depending little on surface finish and hardness. The creep measurements, however, did show a marked change when the races were polished. From his observations of this and other experiments Johnson concludes that the rolling coefficient of friction cannot be compared with the steady sliding value.

Agreement between these experiments and Kalker's numerical theory is good over the linear region. An attempt was made to measure the spin moment by measuring the twisting moment on the bearings and subtracting the elastic hysterisis moment. For small spins the hysterisis effect was much larger than the spin moment and so no comparison was possible, but for larger spins the total twisting moment departs from its linear dependence and approaches a limiting value.

Further spin experiments are described by Johnson, Ref. 8, where separate apparatus were designed to measure creep under the action of small tangential forces for small spins, and for large spins, so that each of the parameters could be varied independently. The apparatus for small spins consisted of a hardened steel ball rolling between two hard flat surfaces. The upper flat was fixed and could be loaded with weights, while the lower flat was constrained to slide in a circular arc about a pivot point, causing the ball to roll and introduce a small angular velocity of spin. A force could be applied to the ball by means of a thread attached on its axis of rotation. The lower flat was reciprocated by hand and for a large enough number of traversals, the radial displacement due to the tangential force and spin could be measured with a micrometer. This is the lateral creep, since the

direction of creep resulting from spin and lateral force is independent of the rolling direction. The spin parameter was varied by changing ball size and track radius, while the creep was measured for a range of forces.

The apparatus for large spins was similar to that used by Johnson, Ref. 7, in that it consisted of two identiaal hardened steel discs, the lower one being fixed while the upper disc was free to rotate about its axis. Load was transmitted through three equally spaced hardened steel balls separating the discs. These balls ran in shallow grooves of large radius ground in the disc face, ensuring that the contact area was almost circular. As the disc rotated the balls moved radially outwards until they reached a steady state position where the force due to spin was reacted by the component of the normal forces at the contact points. The angle of inclination to the contact plane could then be measured and the tangential force found, the creep being given by the radial displacement of the balls. A range of ball diameters and discs were investigated giving a wide range of spins.

Johnson found that for the large spin parameters, where there is considerable slip taking place in the contact area, there was a lot of scatter in the results due to slight differences in the surface conditions, such as roughness and the presence of lubricant, affecting the creep. There was noticeably more scatter in the second set of experiments than the first. A comparison between Johnson's experimental results and Kalker's numerical theory is shown in Fig. 2.8 and Fig. 2.9. As the coefficient of friction was not known it was adjusted to obtain the best correlation. Fig. 2.8 shows the lateral force parameter f_y plotted against spin parameter for zero creep; the value of μ used is 0.094 and using this the correlation is very good. Fig. 2.9 shows the correlation between theory and experiment for combined lateral creep and spin over the linear region for a range of spins. As μ was not

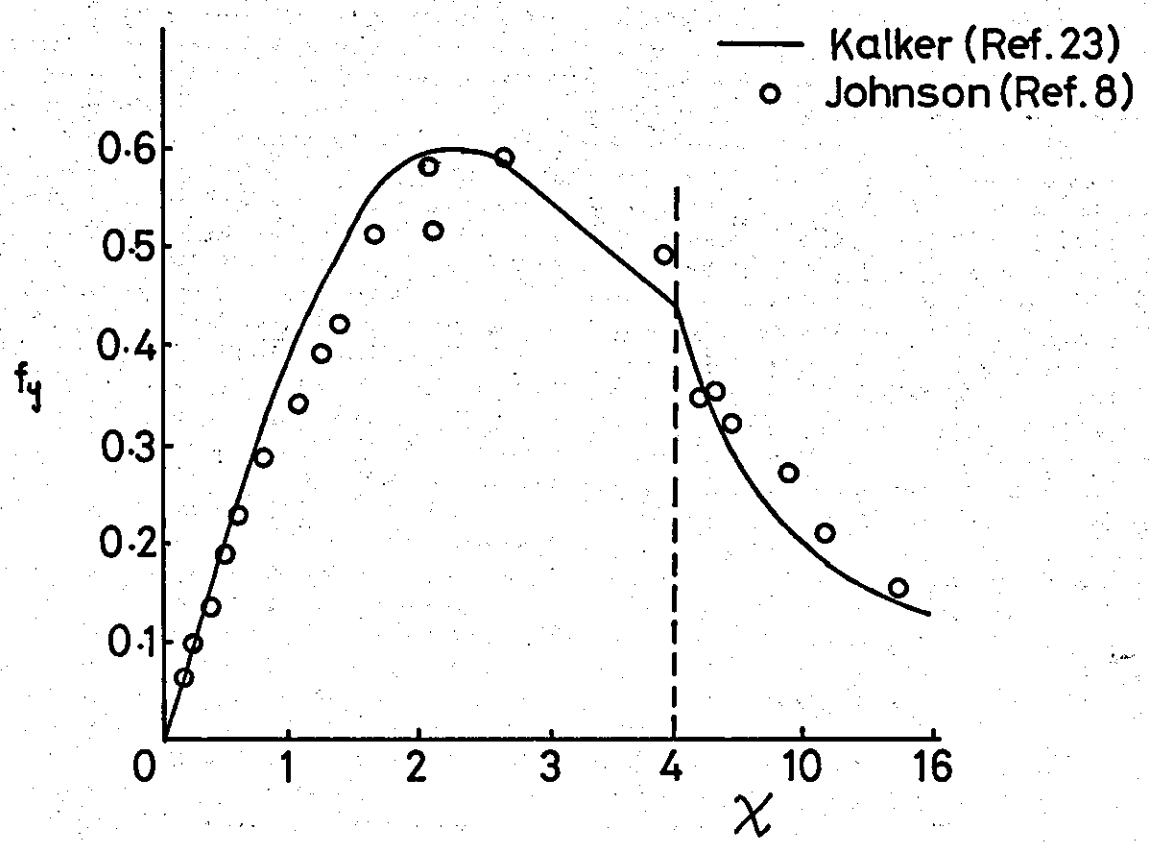

FIG.2·8 The Total Force Due to Spin (a/b=1, σ =0·28)

FIG.2·9 The Total Force Due to Combined Lateral Creepage and Spin (a/b=1, σ=·28)

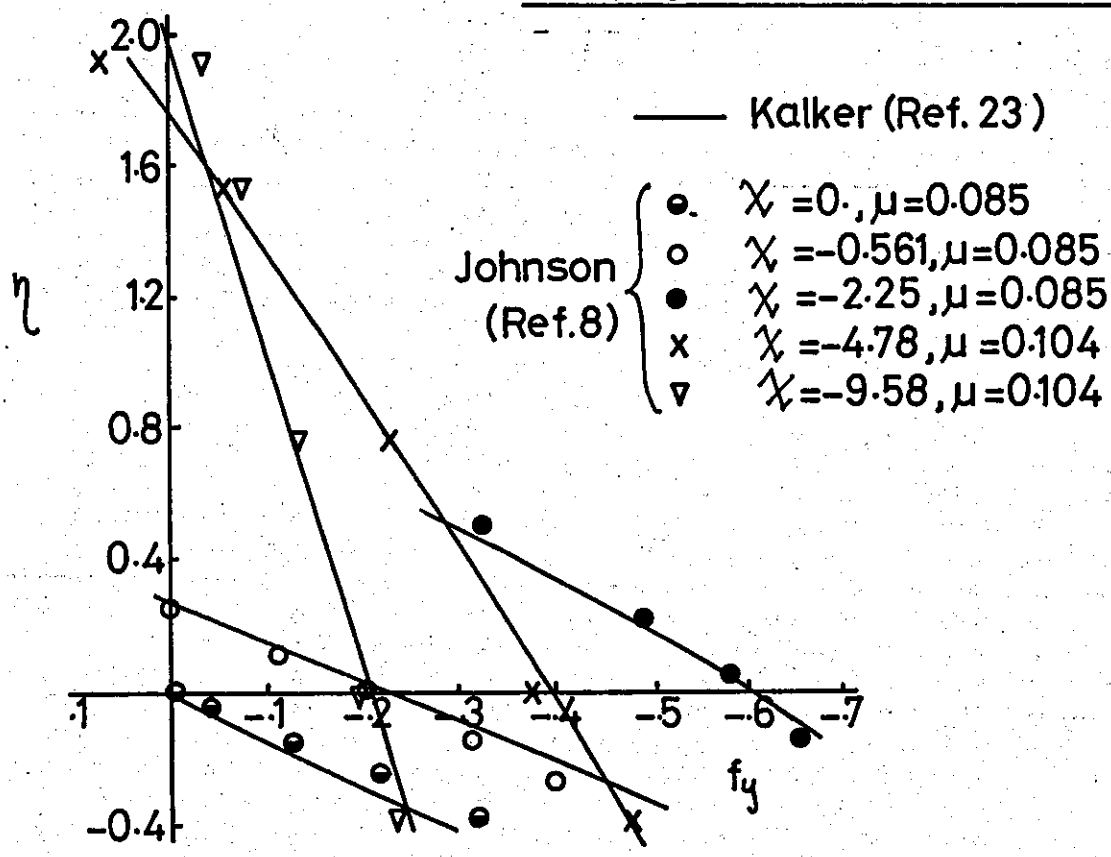

known it was assumed that $\mu = 0.085$ for curves obtained using the small spin experiment and $\mu = .104$ for results using the large spin experiment. It can be seen that as the spin increases the slope also increases with good correlation over the linear region for this case of circular contact area and very low coefficient of friction.

Johnson's experiments were carried out using very smooth balls with high contact pressures resulting in very low coefficients of friction. Much larger values of μ were found by Mueller, Ref. 42, who carried out full scale experiments on a railway wheelset with cylindrical wheels. Some experiments, to measure lateral creep, were performed on very clean dry rails and values of μ between 0.43 and 0.54 were found to exist, while others were carried out on wet rails with μ varying between 0.23 and 0.58. These results are plotted in Fig. 2.6 showing reasonable agreement between them and the numerical theory.

Recently published work in Japan by Matsui and Yokose, Ref. 43, give lateral and longitudinal creep results on 1/5th and 1/10th scale models. The tests were carried out on a rig which consisted of a coned wheelset placed upon a roller, with freedom to yaw and to be displaced laterally. Lateral forces and yawing moments could be applied to the wheelset and the resulting yaw and lateral displacement measured, the former giving a measure of the lateral creep and the latter the longitudinal creep. Some of the results are plotted in Fig. 2.5 and Fig. 2.6 showing good agreement between theory and experiment. All experiments were carried out at low speeds of less than 3 m/s and with estimated coefficients of friction between 0.25 and 0.35. Further tests using a model bogie with a wheelset strain gauged to measure lateral and longitudinal tread forces yielded less satisfactory creep results.

British Rail at Derby have carried out some lateral creep tests on a 1/5th scale unrestrained wheelset mounted on a roller rig, Hobbs, Ref. 34. The wheelset had cylindrical treads to reduce longitudinal creep and was made from aluminium alloy so that wheel loads could be reduced and creepages scaled. The wheelset was suspended from a yoke which was in turn pivotted about a point approximately 1 m ahead of the wheelset. This arrangement coupled yaw with lateral displacement so that the system was stable in the lateral plane under the action of lateral forces. Lateral creep was directly proportional to yaw angle and the experiment was carried out by applying varying lateral forces to the wheelset and measuring the resulting yaw angle optically. The wheel was run at speeds of between 2 m/s and 22m/s showing no correlation between speed and creep over this range. The wheels were slightly abraded to achieve repeatable results and coefficients of friction between 0.125 and 0.39 were recorded. Reductions of 50% in the creep coefficients were observed when lubricant was applied to the wheels. The averaged results which are within 10% of the theoretical values are plotted in Fig. 2.6. Attempts made to measure lateral creep due to spin by using a radiused wheelset were unsuccessful.

Although Barwell and Woolacott, Ref. 44, were mainly interested in the coefficient of adhesion between rail and wheel, they do publish some longitudinal creep results obtained using the same apparatus used by Loach mentioned earlier. The rig, which was basically a roller rig, was enclosed in an air conditioning unit so that humidity and temperature of the surroundings could be controlled as well as surface treatments of the rail and wheel. In order to obtain repeatable results for 'dry' conditions, it was found necessary to abrade the surfaces with 'wet and dry' carborundum paper. These dry results are plotted in Fig. 2.5 and when compared with Kalker's theory they show about twice the theoretical value of creepage for the same force. This discrepancy

could be due to one of several reasons such as: (a) surface vibration in the roller rig due to out of balance; (b) lateral creep being present, or (c) since the experiments were carried out at fairly high speed it could be due to hydrodynamic lubrication being present. It is interesting to note that the coefficient of friction was affected by atmospheric conditions and/or surface contamination, with μ varying from 1.0 for well sanded surfaces to 0.1 for surfaces with considerable organic material on them. Changes in humidity had drastic effects, reducing the coefficient of friction by almost 50% for a relative humidity greater than 75%. The effect of humidity on μ is shown in Fig. 2.10.

Halling, Ref. 14, carried out similar experiments to Johnson using a steel ball on a flat surface, and measured the longitudinal creep due to a longitudinal force. A series of balls with various diameters were investigated for a range of loads with high contact pressures (average pressure > 800 MN/m^2) and low velocities. Good agreement between Halling's theory and experiment was obtained by assuming $\mu = 0.075$. The coefficient of sliding friction measured was 0.090, giving the ratio of rolling to sliding coefficients of friction as $(0.075/0.090) = 0.85$. This is the same ratio found by Johnson.

Halling and Brothers, Ref. 45, investigated the longitudinal creep on a smooth ball subjected to various normal and tangential surface tractions when rolling on planes of various surface finishes. The surfaces investigated had roughnesses between 0.1 and 0.84 μm C.L.A. They found surface roughness had no apparent effect on creeps, or on the coefficient of sliding friction, providing a large normal load was maintained. In all their tests the average contact pressure was greater than 760 MN/m^2.

FIG.2·10 Variation of Adhesion with Relative Humidity

(Ref. 44)

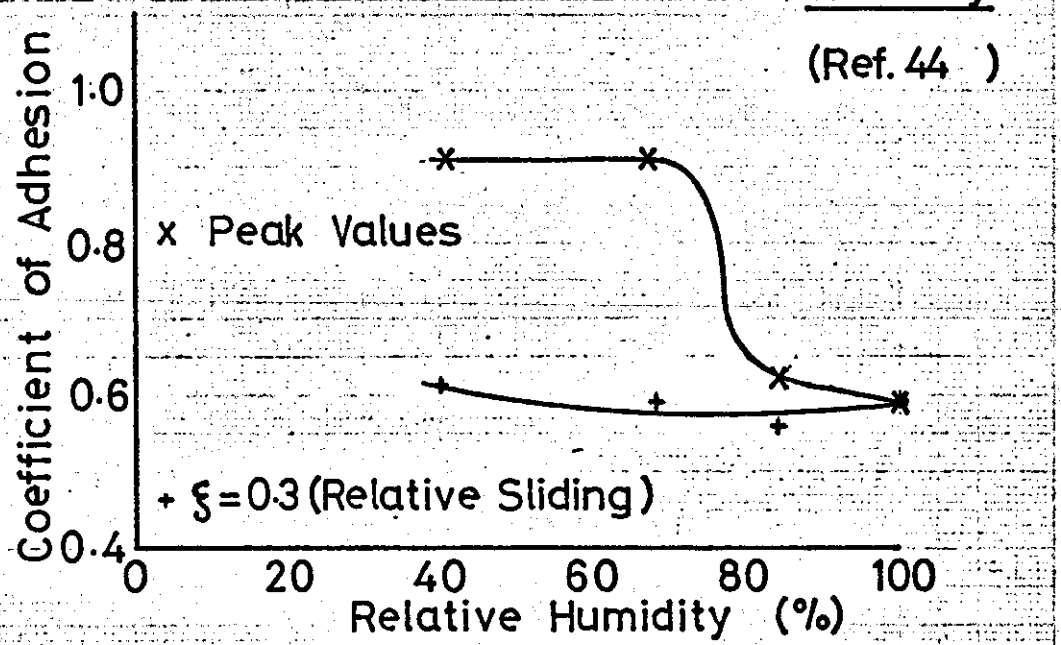

FIG.2·11 Variation of Friction Coefficient with Wheel Load

(Ref. 50)

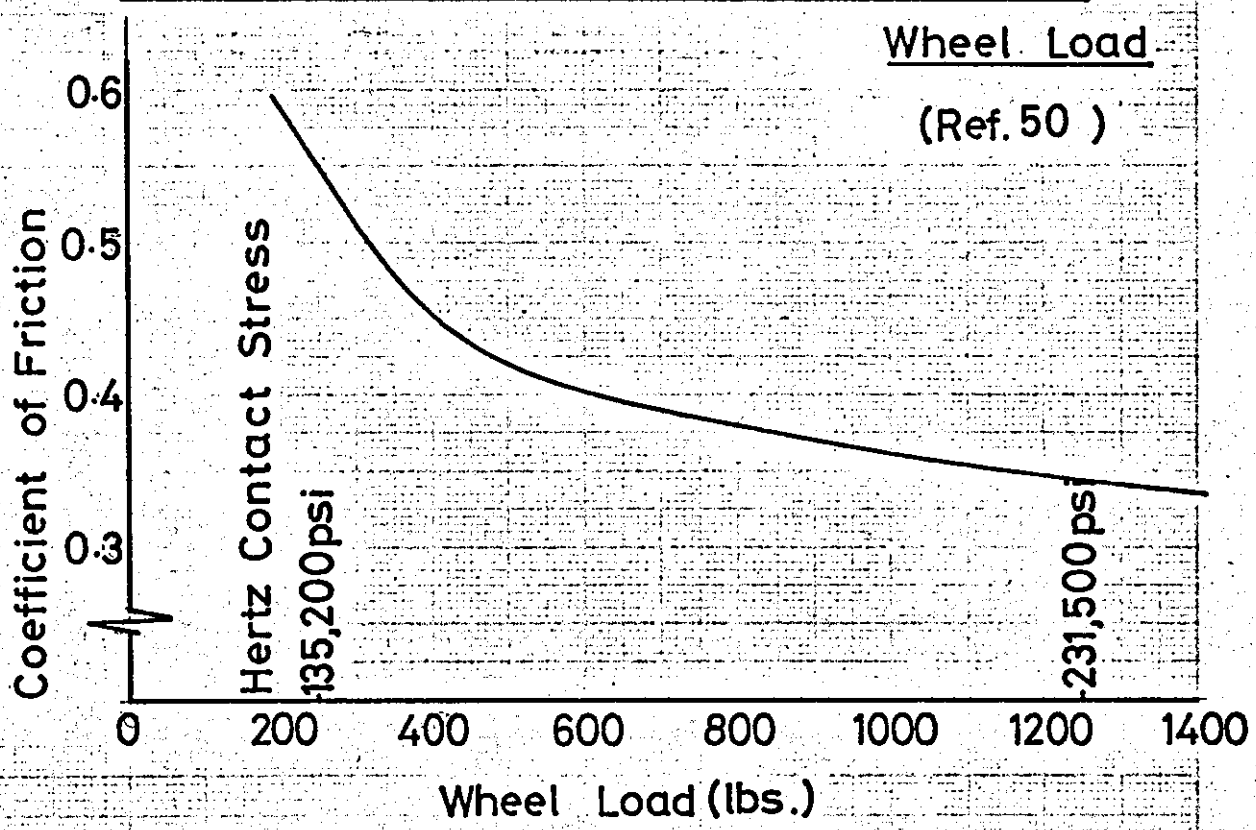

In a paper by Halling and Al-Qishtaini, Ref. 46, other factors affecting the contact conditions between a ball and track were investigated. They measured the longitudinal creep for a circular contact area with dry surfaces and found difficulty in obtaining consistent results at large normal loads, N, or when the tangential force approached its limiting value of μN. They suggested this was due to wear debris on the rolling contact surfaces, and to overcome this they continuously removed the debris with a clean dry pad, thereby achieving consistent results. They found that μ was greater at the higher normal loads, causing great difficulty in the choice of μ to correlate theory and experiment.

Vibration effects were investigated by varying the frequency and amplitude of the normal load, but results showed no significant deviation from those obtained using a constant load. This is an interesting result as variations in normal load must often occur in practice and the present results show that such conditions do not necessarily invalidate the steady state creep/force theories. This result was also predicted by Kalker.

Experimental work on rolling contact and in particular when spin is present, has been carried out by Poon and Haines, Ref. 47 and Poon, Refs. 48 and 49. The aims of the experiments described in Ref. 47 was to measure forces due to varying amounts of spin, using different types of lubricant. The results of this investigation are outside the scope of the present work but the rig used was very interesting and has possibilities regarding further spin experiments. The arrangement consisted of a ball in contact with a flat top roller. The roller was supported on a circular inner ring which in turn was supported on a fixed outer ring. The inner ring could be moved relative to the outer ring and had a vernier scale marked on to measure the relative rotation. The ball resting on top of the roller was mounted on a

shaft which could slide in a semi-circular vertical ring, constrained by an extended strain gauge ring, allowing movement in the plane of the ring only. This strain gauge ring was in turn mounted through flexible cross springs to a moveable platform. The strain gauge ring had eight strain gauges attached and by selecting different combinations of them, the longitudinal force, F_x, lateral force, F_y and moment M_z could be found in the plane of the contact area between ball and roller. Poon and Haines found, in fact, that the moment associated with rolling plus spin was too small to be measured.

The normal load could be varied through cords attached to the spindle of the ball, the lateral creep could be varied by rotating one support ring relative to the other and the spin could be varied by rotating the spindle of the ball around the vertical ring. Although Poon and Haines only investigated a ball on a flat top roller, giving a circular contact area, it would be possible using a similar rig to look at elliptical contact areas by having rollers with different radii. The authors carried out their experiments using hardened steel balls with very fine surface finishes of 0.05 to 0.06 μm C.L.A. and they remark that below speeds of 3 m/min the load was entirely supported by direct asperity contact, even though the surfaces were lubricated.

In Ref. 48, Poon studies the surface shear traction arising from two bodies in rolling contact with spin present, using the frozen stress photoelastic technique. The experiment consisted of two spheres, made from Araldite casting resin, in rolling contact enclosed in a heated oven. When removed, the contact area was sliced into strips and by observing the slices using the normal photoelastic technique, the shear traction boundary could be found. When compared with Kalker's strip theory there was very good agreement.

Poon, Ref. 49, investigates rolling with spin for a circular

contact area but with elasto hydrodynamic lubrication present.

An extensive series of creep experiments were carried out by Itami, Ref. 50, to measure longitudinal creep, lateral creep and a combination of both, without spin, on a roller rig using 1/5 scale wheels. The tests were designed to give further insight into friction, creep and effect of certain parameters on contact conditions of railway locomotive wheels. Wheels with diameters of 150 mm, 200 mm and 250 mm were used with profile radii adjusted so that (a/b) = 1.57 in each case, this being the ratio of contact ellipse semiaxes found in practice. Wheel normal loads were varied giving a range of contact pressures between 930 MN/m^2 and 1810 MN/m^2 (maximum contact pressure). This is the sort of value found on locomotives. Wheels of different hardness were used, while surface roughness was always between 0.51 and 0.76 μm C.L.A. In each case the effect of speed on creep and friction was investigated through the limited range 8 to 24 km/hour.

The experiments were carried out dry after the wheels were thoroughly cleaned with vythene. When running the surfaces were continuously wiped with cheesecloth. Some difficulty was experienced in obtaining force readings when the longitudinal creep was large enough to cause complete sliding in the contact area; flat spots quickly appeared on the wheel which then had to be removed by regrinding.

Longitudinal creep results showed good agreement over the linear region with Kalker's and Johnson/Vermeulen's results, but not so good over the remainder of the curve. A sample of these results is plotted in Fig. 2.5. The coefficients of friction were found to be fairly high, in the range 0.55 to 0.67.

A sample of the lateral creep results is plotted in Fig. 2.6 and shows that as the lateral creep is increased, the lateral force reaches a maximum and then drops to level off at a value which is about

80% of the maximum. Although this effect is common in automobile tyres it has not been observed in other lateral creep experiments.

The experiments showed no apparent speed effect, while the effect of increasing contact pressure caused a drop in the coefficient of friction; this result is reproduced in Fig. 2.11. Changes in surface hardness did not affect the results, but it must be noted that the contact pressure was always high. Itami also observed the effects of humidity, noticing that on days of high humidity the coefficient of friction was low, and in fact he discontinued his tests on days when the relative humidity was greater than 50%.

To compliment the creep experiments just discussed, the Electro Motive Division of General Motors carried out a series of full scale experiments to measure longitudinal creep on a railway locomotive. Their results are published in a report by Marta, Mels & Itami, Ref. 51, which discusses the field tests in conjunction with the laboratory tests and compares the results. The locomotive used had 1 m diameter wheels giving a maximum contact pressure of around 1400 MN/m^2. It was fully instrumented and creep measurements were made at speeds between 8 and 16 km/hr for wet, dry and sanded conditions, but always with a typically contaminated rail. Insufficient information is given in the report in order to plot the results on Fig. 2.5, but a comparison is made in Fig. 2.12 between Johnson and Vermeulen's formula and the field results. Agreement is reasonable considering the difficulties encountered in making full scale measurements such as these.

In a U.S. Department of Transportation report by Nayak et al, Ref. 33, a theory of creep is presented which is based on surface roughness. The aim of this work is to try and account for the differences which exist between the smooth surface theory of Kalker and many of the experimental results evident in Fig. 2.5. To support

FIG 2·12 Variation of Friction Coefficient with Longitudinal Creep

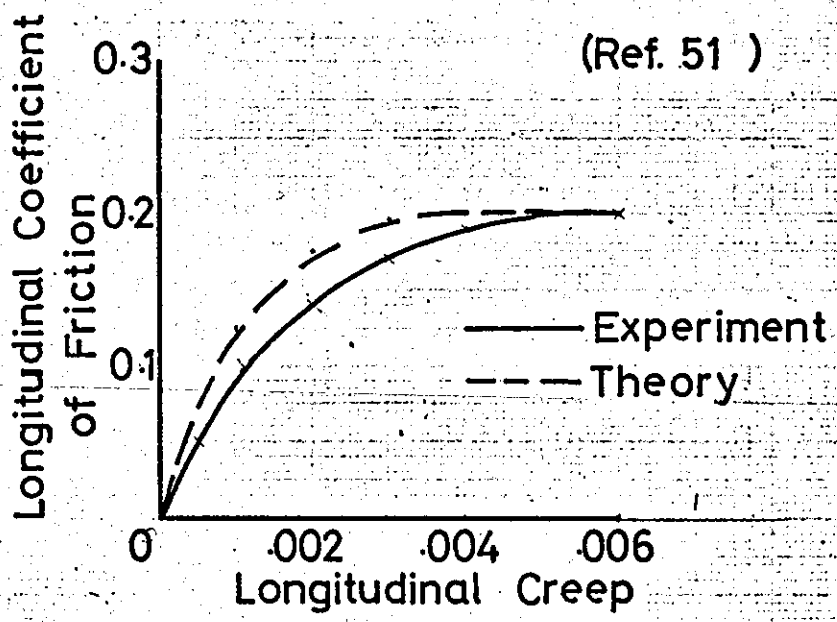

FIG. 2·13 Experimental Variation of Creep with Normal Load

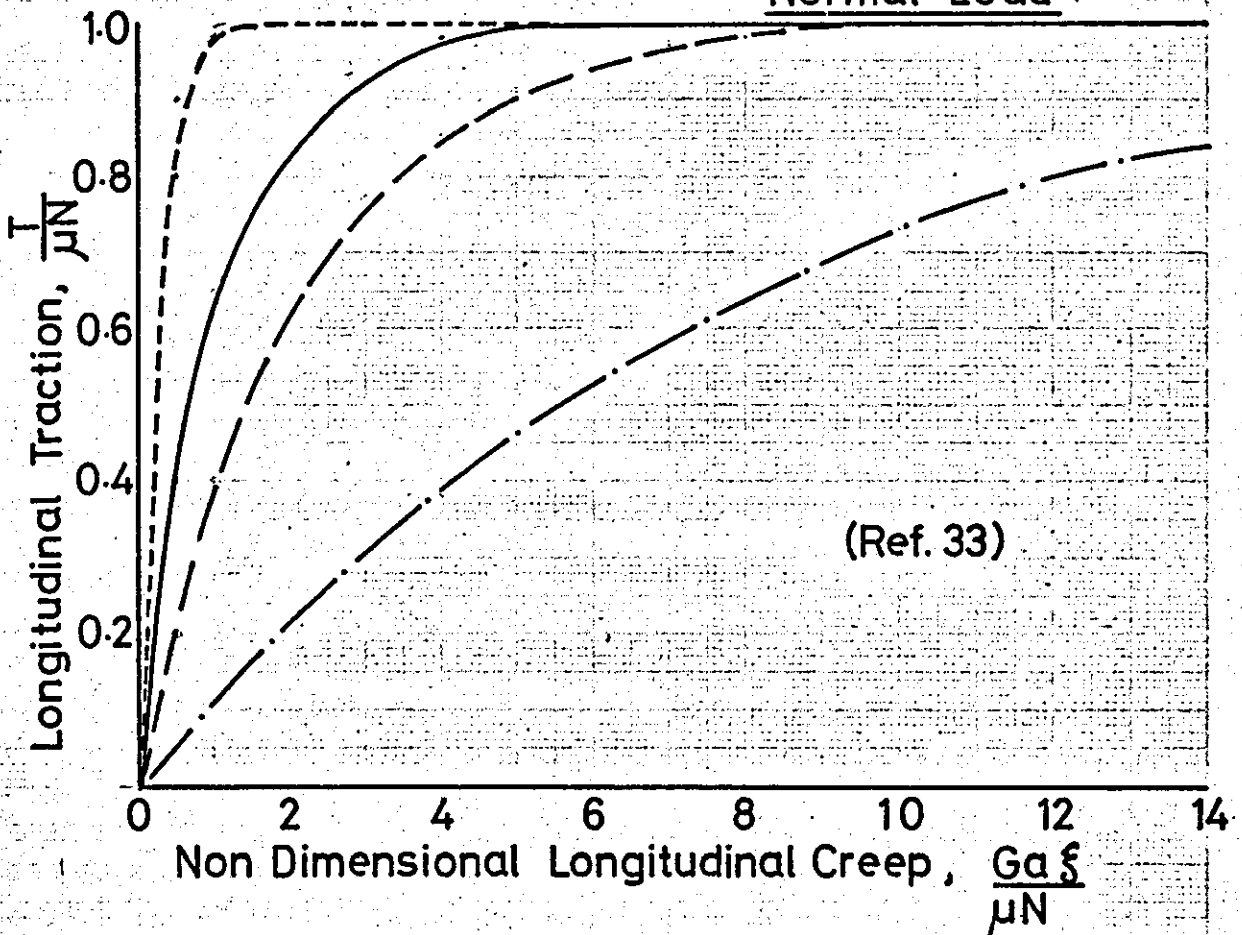

Curve	N (lb/in)	μ	2a(ins) x 10^3	Max.pres.(psi)
—·——·—	3·7	0·172	3·04	1,500
— — —	76	0·189	13·8	7,000
———	400	0·179	31·6	16,200
- - - - - - -	Smooth	Surface	Theory	

their new theory the authors carried out some longitudinal creep tests with an aluminium cylinder on a flat surface, giving a rectangular contact area. The surface of the cylinder was roughened with 100 emery cloth and the surfaces run in before creep measurements were made, in order that the surface roughness was held fairly constant. The normal load was also kept constant and the creep measured for varying tangential loads. A summary of the results obtained is reproduced in Fig. 2.13, where they are compared with smooth surface theory. A considerable amount of scatter was experienced at high loads. The results support qualitatively the rough surface theory of Nayak in that increasing normal loads bring closer correlation between smooth surface theory and experiment.

Some experiments were also carried out by vibrating one of the contact surfaces and measuring the creep for a constant normal and tangential load, but varying amplitude and frequency. These results seem to indicate a decrease in effective coefficient of friction due to surface vibration, a result which has also been observed by Tolstoi, Ref. 52 and Rabinowicz, Ref. 53. Tolstoi showed that the coefficient of friction during sliding depended on the stiffness and damping of the contacting bodies.

Brief mention should be made of other creep tests which have been carried out, generally with cylindrical wheels, such as those of Cabble, Refs. 54 and 55. In these, where the contact area was not elliptical, but rectangular, the author measured the longitudinal creep on a 1/10th scale wheel with maximum contact pressures between 650 MN/m^2 and 1180 MN/m^2. Coefficients of friction varied between 0.6 and 0.66 for dry conditions, but dropped drastically to between 0.1 and 0.11 in the presence of oil or water. The contact pressure was found to have no effect on μ, probably because it was very high anyway, while μ decreased slightly with increasing speed. The latter result is unusual.

Similar tests were carired out by Cress and Talbert, Ref. 56, to measure the lateral force due to lateral creep on a misaligned steel roller, again the contact area being rectangular in shape. The roller used was 25 mm wide by 100 mm diameter. The experiment was carried out at speeds of about 1.5 m/min. with yaw angles up to 3° being investigated. The surfaces were ground, giving a coefficient of friction of 0.16. Some tests were carried out on rusted surfaces, this being achieved by repeated applications of a warm aqueous solution of salt and hydrochloric acid, and the coefficient of friction was then found to be 0.22.

Some full scale lateral creep tests are described by Koci and Marta, Ref. 57, in which a fully instrumented wheelset was used to study creep and transverse load reactions resulting between a wheel and rail during curve negotiation. Measurements were made on ordinary contaminated track and showed a coefficient of friction of 0.29, while complete sliding occurred for about 1° of wheel yaw.

Finally, since the theme of the present work is the forces on railway wheelsets due to the creep phenomenon, it is useful to bear in mind the range of values of μ found in practice on railway tracks. A very comprehensive report on recent research into rail/wheel adhesion is given by Collins and Pritchard, Ref. 58. This report does not measure creep as such, but looks at conditions on running rails, and tries to correlate them with laboratory experiments giving detailed examination to surface contamination and its effect on μ.

A histogram showing the values of μ obtained in good weather is reproduced in Fig. 2.14. Fig. 2.15 shows the effect of oil and humidity on the coefficient of friction, measured in the laboratory, but using oil wiped from actual track. This was found to be very

FIG. 2.14 Frequency of Adhesion Values Obtained on a Main Line in Good Weather

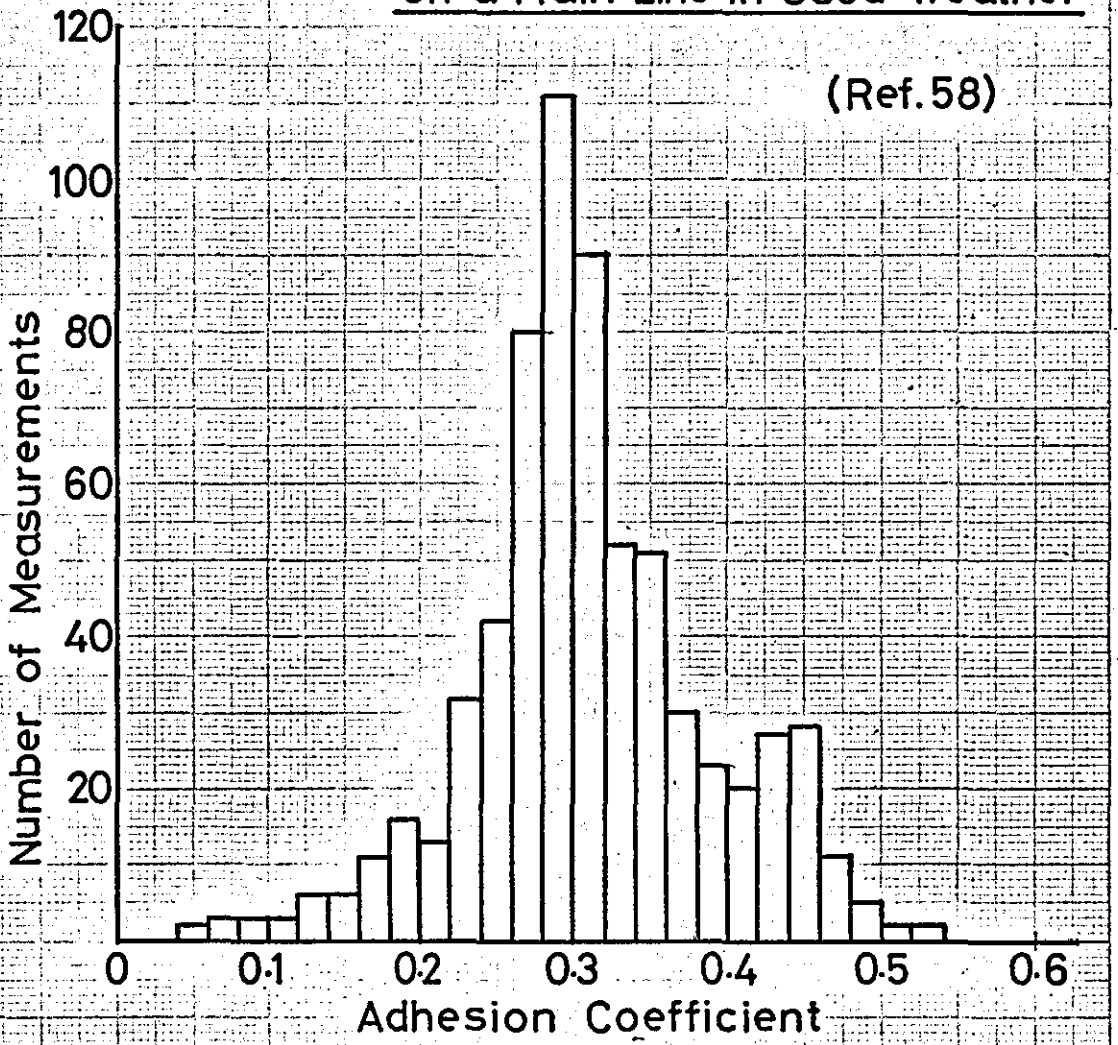

FIG. 2.15 Effect of Oil and Humidity on the Coefficient of Friction

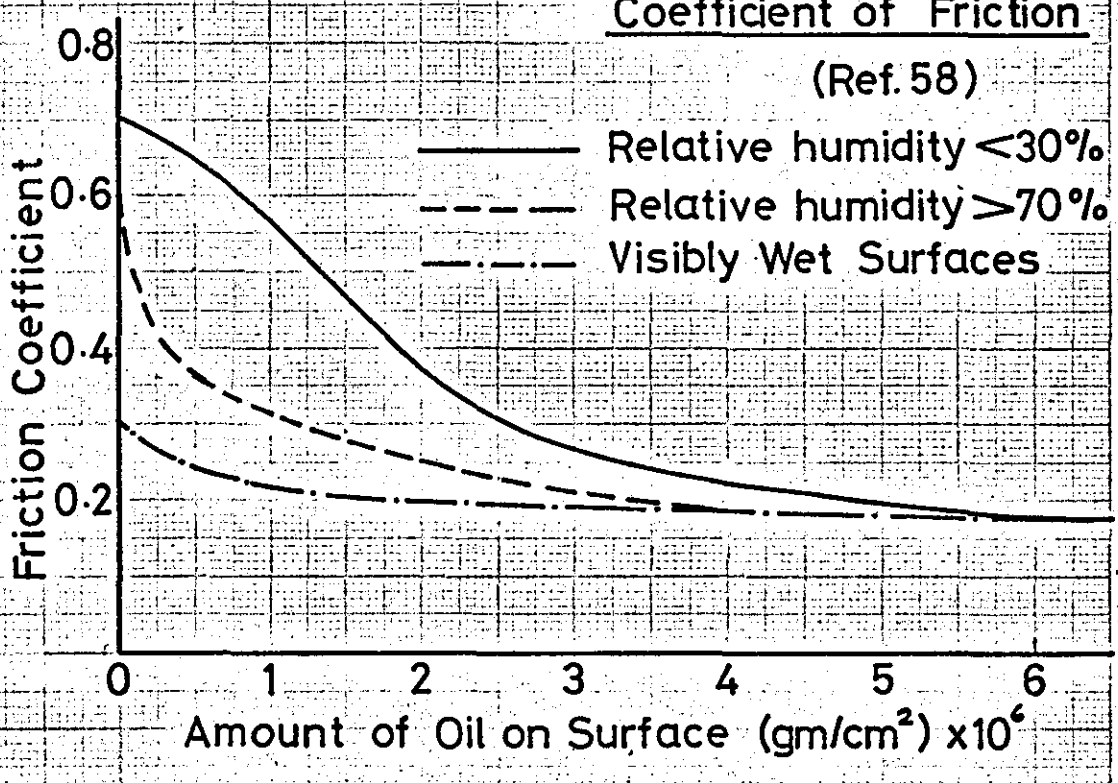

surface active and more viscous than ordinary gearbox oil. It can be seen that μ can drop from 0.7 to 0.2 with only small amounts of oil present when accompanied by humidity changes.

3. Theories used in Present Analysis

This section describes in more detail, those theories which have been used later in the report to calculate the forces on a wheelset. Section 3.1 presents the theory of infinitesimal creep and spin, Section 3.2 the limiting case of large creepage and spin, and Section 3.3 two theories for arbitrary creepage and spin. In each case the theories are discussed with a view to applying them to the railway wheelset problem. Each of the theoretical methods has been programmed in Fortran IV and all the programs and subroutines mentioned in this Section are listed in Appendix 5, together with brief descriptions of their methods.

A comparison between the results obtained for the forces on a wheelset using the different theories is made later, in Section 5.

3.1 The Limiting Case of Infinitesimal Creepage and Spin

The theory of De Pater, Ref. 12, and Kalker, Ref. 13, is generalised in Kalker, Ref. 23, for arbitrary Poissons ratio and elliptical contact areas. The basic approximation in this theory is that the creepage and spin are assumed to be so small that an area of adhesion covers the entire contact area and there is no slip. Thus the relative slip equations, from Appendix 1, become:

$$s_x = \gamma_x - \omega_z y + \frac{\partial u}{\partial x} = 0 \qquad (1)$$

$$s_y = \gamma_y + \omega_z x + \frac{\partial v}{\partial x} = 0 \qquad (2)$$

As it is impossible to have no area of slip when there is creepage and spin present, this assumption leads to a solution with an infinite traction force at the edge of the contact area, which implies that this

point is in an area of slip. However Kalker shows, in Ref. 23, that even with these assumptions, no slip takes place at the leading edge.

In Ref. 23 a set of linear equations are derived, called the load-displacement equations, which give the relationships between the normal and traction forces and the surface displacements. These are solved for a set of boundary conditions, after first removing the singularity from the leading edge, giving the total forces and moment in the plane of the contact area in terms of a set of creepage and spin coefficients, which are tabulated.

The forces in the contact area are given by

$$F_1 = -f_{11}\,\gamma_1 \tag{3}$$

$$F_2 = -f_{22}\,\gamma_2 - f_{23}\,\omega_3 \tag{4}$$

and the couple about axis (3) is

$$M_3 = f_{23}\,\gamma_2 - f_{33}\,\omega_3 \tag{5}$$

The creepage and spin, $\gamma_1, \gamma_2 \& \omega_3$ were given in the previous section, while f_{ij} are defined as

$$\left.\begin{aligned} f_{11} &= G\,(ab)\,C_{11} \\ f_{22} &= G\,(ab)\,C_{22} \\ f_{23} &= G\,(ab)^{\frac{3}{2}}\,C_{23} \\ f_{33} &= G\,(ab)^{2}\,C_{23} \end{aligned}\right\} \tag{6}$$

The creepage and spin coefficients, C_{ij} are tabulated in Ref. 23 for various (a/b) ratios and Poisson's ratio based on the modulus of rigidity, G. They are also plotted and tabulated in Hobbs, Ref. 34, for a Poisson's ratio of 0.3, based on Youngs modulus. The definitions for f_{ij} then become:

$$\left.\begin{aligned} f_{11} &= E\,(ab)\,C_{11}' \\ f_{22} &= E\,(ab)\,C_{22}' \\ f_{23} &= E\,(ab)^{\frac{3}{2}} C_{23}' \\ f_{33} &= E\,(ab)^{2} C_{33}' \end{aligned}\right\} \qquad (7)$$

These coefficients are reproduced in Table 3.1

For values of $(a/b) > 10$ the following approximate formulae should be used to calculate C_{11}, C_{22}, C_{23} and C_{33}:

$$C_{11} = \frac{2\pi}{(\Lambda - 2\sigma)q}\left\{1 + \frac{3 - \ln 4}{\Lambda - 2\sigma}\right\} \qquad (8)$$

$$C_{22} = \frac{2\pi}{[(1-\sigma)\Lambda + 2\sigma]q} \cdot \left\{1 + \frac{(3-\ln 4)(1-\sigma)}{(1-\sigma)\Lambda + 2\sigma}\right\} \qquad (9)$$

$$C_{23} = -C_{32} = \frac{2\pi}{3q\sqrt{q}} \cdot \left\{\frac{1}{(1-\sigma)\Lambda - 2 + 4\sigma}\right\} \qquad (10)$$

$$C_{33} = \frac{\pi}{4} \cdot \frac{(1-2\sigma)\Lambda - 2 + 6\sigma}{(1-\sigma)\Lambda - 2 + 4\sigma} \qquad (11)$$

where $\Lambda = \ln(16/q^2)$

(These asymptotic formulae were given to the author by Dr. Kalker in a private communication).

A subroutine called COEFF has been written which interpolates values of C_{ij} for any (a/b) ratio and this includes the asymptotic formulae given above.

The values of the coefficients C_{11}, C_{22}, C_{23} have been compared in Ref. 23 with Johnson's experimental results, Refs. 6 and 8, for the case of circular contact area, showing good agreement. C_{11}, C_{22} for elliptical contact areas have been compared with the experimental results of Johnson and Vermeulen, Ref. 9, showing differences of up to 7%.

Table 3.1 Creepage and Spin Coefficients for $\sigma = 0.3$

		C_{11}'	C_{22}'	C_{23}'	C_{33}'
	1	1.35	0.98	0.195	3.34
	2	1.37	1.01	0.242	1.74
	3	1.40	1.06	0.288	1.18
	4	1.44	1.11	0.328	0.925
a/b	.5	1.47	1.18	0.368	0.766
	.6	1.50	1.22	0.410	0.661
	.7	1.54	1.28	0.451	0.588
	.8	1.57	1.32	0.493	0.533
	.9	1.60	1.39	0.535	0.492
	1.	1.65	1.43	0.579	0.458
	.9	1.70	1.49	0.628	0.425
	.8	1.75	1.56	0.689	0.396
	.7	1.81	1.65	0.768	0.366
	.6	1.90	1.76	0.875	0.336
b/a	.5	2.03	1.93	1.04	0.304
	.4	2.21	2.15	1.27	0.275
	.3	2.51	2.54	1.71	0.246
	.2	3.08	3.26	2.64	0.215
	.1	4.60	5.15	5.81	0.183

The forces can also be expressed in terms of non-dimensional force and moment parameters given by

$$f_1 = \frac{F_1}{\mu N} = -\frac{3(1-\sigma)E\,C_{11}\,\xi}{4\pi\sqrt{g}} \qquad (12)$$

$$f_2 = \frac{F_2}{\mu N} = -\frac{3(1-\sigma)E}{4\pi\sqrt{g}}\left(C_{22}\eta + C_{23}\chi\right) \qquad (13)$$

and

$$m_3 = \frac{M_3}{\mu N c} = \frac{3(1-\sigma)E}{4\pi\sqrt{g}}\left(C_{23}\eta - C_{33}\chi\right) \qquad (14)$$

where E is the complete elliptic integral of the second kind (Plotted in Fig. A9.2)

ξ, η, χ are non-dimensional creepage and spin parameters defined as

$$\xi = \frac{\gamma_1 a}{\mu c}\,, \qquad \eta = \frac{\gamma_2 a}{\mu c}\,, \qquad \chi = \frac{\omega_3 a}{\mu} \qquad (15)$$

and g = min (a/b, b/a)

One of the problems in using this "small creep theory" is deciding whether in fact the creepages and spin in a particular problem are small enough for the method to give reasonable values for f_1, f_2 and m_3. As a general guide it is suggested that the following tests are carried out:

The maximum and minimum values for f_1 (from equation 12) are ∓ 1

$$\therefore\ \xi_{max.} = \frac{-4\pi\sqrt{g}}{3(1-\sigma)E\,C_{11}}\,, \qquad \xi_{min.} = \frac{4\pi\sqrt{g}}{3(1-\sigma)E\,C_{11}} \qquad (16)$$

$\therefore\ \xi$ should lie between these values

Similarly for f_2 from equation 13, the maximum and minimum values are ± 1

$$\therefore\ \text{when } \chi = 0,\ \eta_{max.} = \frac{-4\pi\sqrt{g}}{3(1-\sigma)E\,C_{22}},\ \eta_{min.} = \frac{4\pi\sqrt{g}}{3(1-\sigma)E\,C_{22}} \qquad (17)$$

$\therefore\ \eta$ should lie between these values.

and when $\eta = 0$,

$$\chi_{max.} = \frac{-4\pi\sqrt{g}}{3(1-\sigma)E\,C_{23}}\,, \quad \chi_{min} = \frac{4\pi\sqrt{g}}{3(1-\sigma)E\,C_{23}} \qquad (18)$$

$\therefore$ χ should lie between these values.

It should be noted that these conditions are necessary but not sufficient.

To ensure that the creepages and spin are sufficiently small for the theory to apply, the following should also hold:

$$(\xi^2+\eta^2) < \tfrac{1}{4}(\xi_{max.}^2 + \eta_{max.}^2)$$

and $|\chi| < \frac{1}{2}|\chi_{max.}|$

(this is generally true for $a/b > 1$ and less accurate for $a/b < 1$)

In order to use the method, a subroutine called SMALL has been written which calculates the force parameters from the creeps, spin and contact ellipse semi axes. To increase its generality, certain extensions to the theory have been built in to the method from a knowledge of results obtained using the numerical theory described in Section 3.3.1. These are as follows:

(a) the values of $\xi + \eta$ are transferred to polar coordinates where $\xi = V\cos\alpha$ + $\eta = V\sin\alpha$
f_1 is then assumed to lie between zero and $\cos\alpha$

(b) f_2 is assumed to lie between $\sin\alpha$ and $f_{2(\xi=\eta=0)}$ for the particular value of χ is question.

$f_{2(\xi=\eta=0)}$ is obtained from results given for the numerical theory, Ref. 23 where curves of (f_2 v χ) are plotted, with for (a/b) ratios of 0.2, 0.5, 1. and 2. These results are shown in Fig. 3.1 where it can be seen that for small values of χ the curves are linear with slope increasing for increasing (a/b). From these results, Fig. 3.2 has been produced, which only applies for small spins. An interpolation subroutine, called MAXFY, has been written

FIG.3.1 f_2 v χ for various values of $(\frac{a}{b})$ ratio

σ=0.28, $\xi = \eta = 0$.

(Kalker, ref. 23)

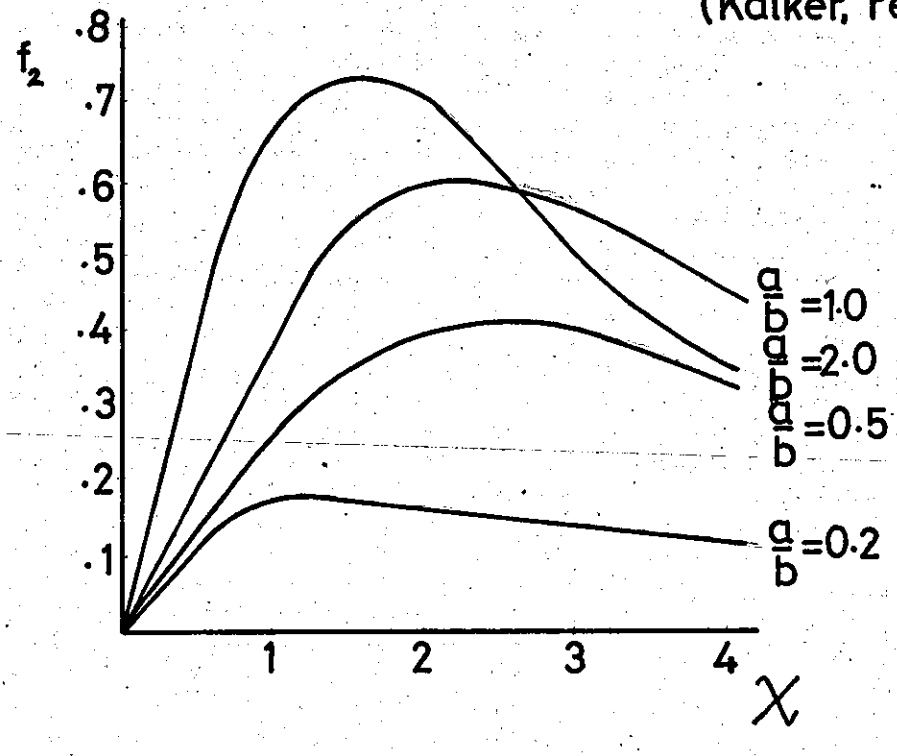

FIG.3.2 $(\frac{\chi}{f_2})$ v $(\frac{b}{a})$, $\xi = \eta = 0$. (for small spins only)

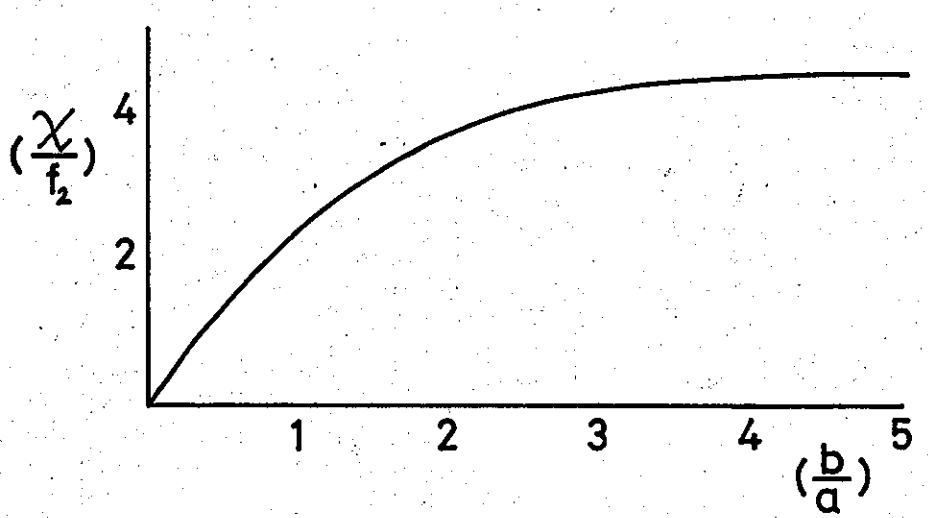

based on this graph, to calculate the value of $f_{2(\xi=\eta=0)}$

Forces have been calculated on a railway wheelset using this "small creep theory" and results are given in Section 5. It may be noted that there is no restriction on (a/b) ratio using this method and so it can be applied, in principle, to both tread and flange contact points providing the creeps and spin are "small".

3.2 The Limiting Case of Large Creepage and Spin

The case of very large creepage and spin has been treated by Lutz, Refs. 17, 18 and 19 and Wernitz, Refs. 20, 21. Lutz considered only circular contact areas, and Wernitz elliptical areas, but with the restriction of creep in one direction only, which is the situation in friction drives - the application considered by both Lutz and Wernitz. This restriction is lifted in Kalker, Ref. 23, where a solution is given for elliptical contact areas and creep in any direction.

The basic assumption in this method is that the creep and spin are so large that the influence of elastic deformation on local slip can be neglected, and the contact area has no area of adhesion. Thus the expressions for the relative slip in steady rolling, from Appendix 1, become

$$s_x = \gamma_x - \omega_z y + \frac{\partial u}{\partial x} \quad \underline{\underline{\sim}} \quad \gamma_x - \omega_z y \qquad (19)$$

$$s_y = \gamma_y + \omega_z x + \frac{\partial v}{\partial x} \quad \underline{\underline{\sim}} \quad \gamma_y + \omega_z x \qquad (20)$$

The slip is then regarded as pure rigid body rotation about a "spin pole" whose coordinates are given by $x' = \frac{-\gamma_y}{\omega_z}$, $y' = \frac{\gamma_x}{\omega_z}$ (21)

The surface traction at a point in the contact area is perpendicular to a line from the point to (x', y') and its magnitude is given by

$$\left|(X, Y)\right| = \mu Z = \frac{3\mu N}{2\pi ab}\sqrt{1-\left(\frac{x}{a}\right)^2-\left(\frac{y}{b}\right)^2} \qquad (22)$$

The total force and moment can then be found by integrating over the surface. Lutz and Wernitz integrate first with respect to x and obtain a result involving complete elliptic integrals of the first and second kind, which are then integrated numerically to give the result. In the general case of an elliptical contact area and creep in any direction, the result also contains elliptic integrals of the third kind. Kalker, Ref. 23, introduces new variables, $x = a\sin\theta\cos\psi$ and $y = b\sin\theta\sin\psi$ giving repeated integrals which can be solved numerically. These are:

$$f_1 = \frac{-3\sqrt{\gamma}\,\mathrm{sign}(\chi)}{2}\int_0^{\frac{\pi}{2}}\sin^2\theta\,d\theta\int_0^{2\pi}\sqrt{\left(\sqrt{\gamma}\sin\theta\cos\psi+\frac{\eta}{\chi}\right)^2+\left(\frac{\sin\theta\sin\psi}{\sqrt{\gamma}}-\frac{\xi}{\chi}\right)^2}\sin\psi\,d\psi \qquad (23)$$

$$f_2 = \frac{3\,\mathrm{sign}(\chi)}{2\pi\sqrt{\gamma}}\int_0^{\frac{\pi}{2}}\sin^2\theta\,d\theta\int_0^{2\pi}\sqrt{\left(\sqrt{\gamma}\sin\theta\cos\psi+\frac{\eta}{\chi}\right)^2+\left(\frac{\sin\theta\sin\psi}{\sqrt{\gamma}}-\frac{\xi}{\chi}\right)^2}\cos\psi\,d\psi \qquad (24)$$

$$m_3 = \frac{3\,\mathrm{sign}(\chi)}{2\pi}\int_0^{\frac{\pi}{2}}\sin\theta\cos^2\theta\,d\theta\int_0^{2\pi}\sqrt{\left(\sqrt{\gamma}\sin\theta\cos\psi+\frac{\eta}{\chi}\right)^2+\left(\frac{\sin\theta\sin\psi}{\sqrt{\gamma}}-\frac{\xi}{\chi}\right)^2}\,d\psi - \left(\frac{\eta}{\chi}\right)f_2 - \left(\frac{\xi}{\chi}\right)f_1 \qquad (25)$$

These formulae apply for $\chi \neq 0$, $a < b$, $\frac{c\eta}{\chi} \geqslant 0$, $\frac{c\xi}{\chi} \geqslant 0$

If $\chi = 0$, $f_1 = \frac{\xi}{\nu}$, $f_2 = \frac{\eta}{\nu}$ where $\nu = \sqrt{\xi^2+\eta^2}$

For values outside this range, the following symmetry relationships hold:

Assuming $\frac{\xi}{\chi} = \alpha$, $\frac{\eta}{\chi} = \beta$ then

$$\left.\begin{aligned} f_1(\alpha,-\beta) &= f_1(\alpha,\beta) \\ f_2(\alpha,-\beta) &= -f_2(\alpha,\beta) \\ m_3(\alpha,-\beta) &= m_3(\alpha,\beta) \end{aligned}\right\} \qquad (26)$$

$$\left.\begin{aligned} f_1(-\alpha,\beta) &= -f_1(\alpha,\beta) \\ f_2(-\alpha,\beta) &= f_2(\alpha,\beta) \\ m_3(-\alpha,\beta) &= m_3(\alpha,\beta) \end{aligned}\right\} \qquad (27)$$

$$\left.\begin{aligned} f_1(a,b,\alpha,\beta) &= -f_2(b,a,-\beta,-\alpha) \\ m_3(a,b,\alpha,\beta) &= m_3(b,a,\beta,\alpha) \end{aligned}\right\} \qquad (28)$$

A subroutine called LARGE, which calculates f_1, f_2 and m_3 using equations 23, 24 and 25, has been written incorporating the above symmetry relationship. The integrations are carried out numerically using Simpson's rule, and a subroutine, called SIMPSON, has been written for this purpose.

As before, the difficulty in applying this method is to judge when the creepages and spin are, this time, large enough to give reasonable values for f_1, f_2 and m_3 . As a general guide the following should hold:

$$|\chi| > \delta \chi_{max.} \qquad (\chi_{max.} \text{ is given in Section 3.1})$$

where $\delta \gg 1$ i.e. the spin parameter should be very much greater than $\chi_{max.}$ The reason for this is as follows: the theory assumes that f_1 is solely dependent on ξ , f_2 on η and m_3 on χ , but the numerical method of Section 3.3.1 shows that f_2 is dependent on η and χ (see Fig. 3.1). This has also been shown in Johnson's experiments, Ref. 8, where the lateral force due to spin has been measured. Results of both theory and experiment show that as χ is increased, f_2 rises to a maximum, then falls off as $\chi \to \infty$. Therefore for the method to give a good approximation for f_2 , χ should be so large that the lateral force due to spin is negligible. This is not so critical for f_1 , thus δ can be an order of magnitude less if only f_1 is required.

The above condition is not the only criteria for using this method. It can be observed from the numerical results of Kalker,

Ref. 23, that in the space (f_1 , f_2 , χ) the parameter $\nu/(\chi)$ is of interest. This is discussed further in Section 3.3.1 but a further condition for using "large creep theory" can be stated as

$$\frac{\nu}{\max.\left(1, \frac{|\chi|}{\chi_{max}}\right)} > \delta' \nu_{max.}$$

where $\nu = \sqrt{\xi^2 + \eta^2}$ and $\nu_{max.} = \sqrt{\xi_{max.}^2 + \eta_{max.}^2}$

Forces have been calculated on a railway wheelset using this "large creep theory" and results are given in Section 5. As for the previous method, there is no restriction on (a/b) ratio.

3.3 Arbitrary Creepage and Spin

3.3.1 Numerical Theory

In Kalker, Ref. 22, a numerical method is described which gives a solution to the case of arbitrary creepage and spin, with or without bodily sliding. This theory is given in more detail in Ref. 23. The load displacement equations mentioned in Section 3.1 are further developed for the case where the tangential tractions vanish at the edge of the contact area. The boundary conditions are written down in the form of an integral over the surface which is divided into 3 factors and can only be satisfied if at every point of the contact area one of the factors vanish. The first factor vanishes on the edge of the contact area, the second in an area of slip and the third in an area of adhesion. The tractions given by the load displacement equations are introduced into the integral, which is then minimised to give a solution.

A computer program was written in ALGOL-60 by Kalker and was used to produce a set of results which are tabulated in Ref. 35 for the following parameters:

$\sigma = 0.28$,	$a/b = 2$,	$\chi = 0,\ .5,\ 1.,\ 2.,\ 3.5$ & 7	variable $\xi + \eta$
"	$a/b = 1$	$\chi = 0,\ .5,\ 1,\ 2,\ 5, 10$	"
"	$a/b = 0.5$	$\chi = 0,\ 1,\ 2,\ 3,\ 5,\ 10$	"
"	$a/b = 0.2$	$\chi = 0,\ .5,\ 1.,\ 2,\ 5,\ 10$	"

where ξ , η and χ are the non-dimensional creepage and spin parameters.

In the tables, ξ and η are given is polar coordinates defined by

$$\xi = \nu\cos\alpha \qquad \eta = \nu\sin\alpha$$

The results are only tabulated for the following ranges:

$$\chi = 0\ ,\ \xi \geqslant 0\ ,\ \eta \geqslant 0$$
$$\chi \neq 0\ ,\ \chi > 0,\ \xi \geqslant 0$$

For values outside these ranges the following symmetry relationships must be applied:

$$f_1(\xi,\eta,\chi) = -f_1(-\xi,\eta,\chi) = f_1(\xi,-\eta,-\chi) = -f_1(-\xi,-\eta,-\chi) \quad (29)$$

$$f_2(\xi,\eta,\chi) = f_2(-\xi,\eta,\chi) = -f_2(\xi,-\eta,-\chi) = -f_2(-\xi,-\eta,-\chi) \quad (30)$$

$$m_3(\xi,\eta,\chi) = m_3(-\xi,\eta,\chi) = -m_3(\xi,-\eta,-\chi) = -m_3(-\xi,-\eta,-\chi) \quad (31)$$

An example of these results is given in Fig. 3.1, where the lateral force due to spin is shown for zero creep and various (a/b) ratios. The complete results of f_1 and f_2 for the case $(a/b) = 1$, $\chi = 0$ are given in Fig. 3.3, for $\chi = 2$ in Fig. 3.4 and for $\chi = 5$ in Fig. 3.5. On inspection of these 3 graphs one can imagine the three combined into the three dimensional space (f_1, f_2, χ). The surfaces of constant creepage $\nu = \sqrt{\xi^2 + \eta^2}$

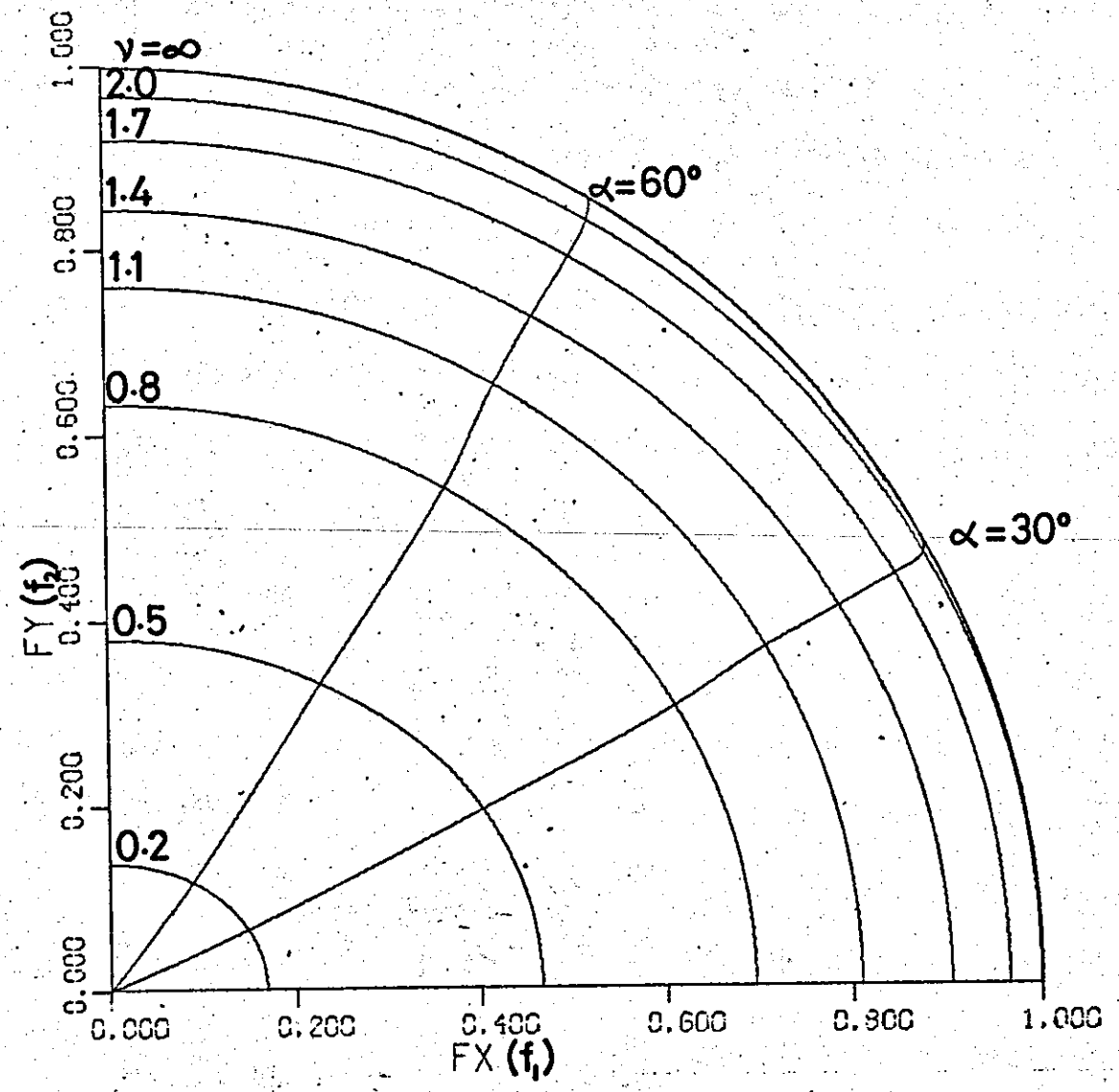

FIG. 33 Numerical Theory Results, ($a/b=1$, $\chi=0$)

FIG.3·4 Numerical Theory Results, ($a/b=1, \chi=2$)

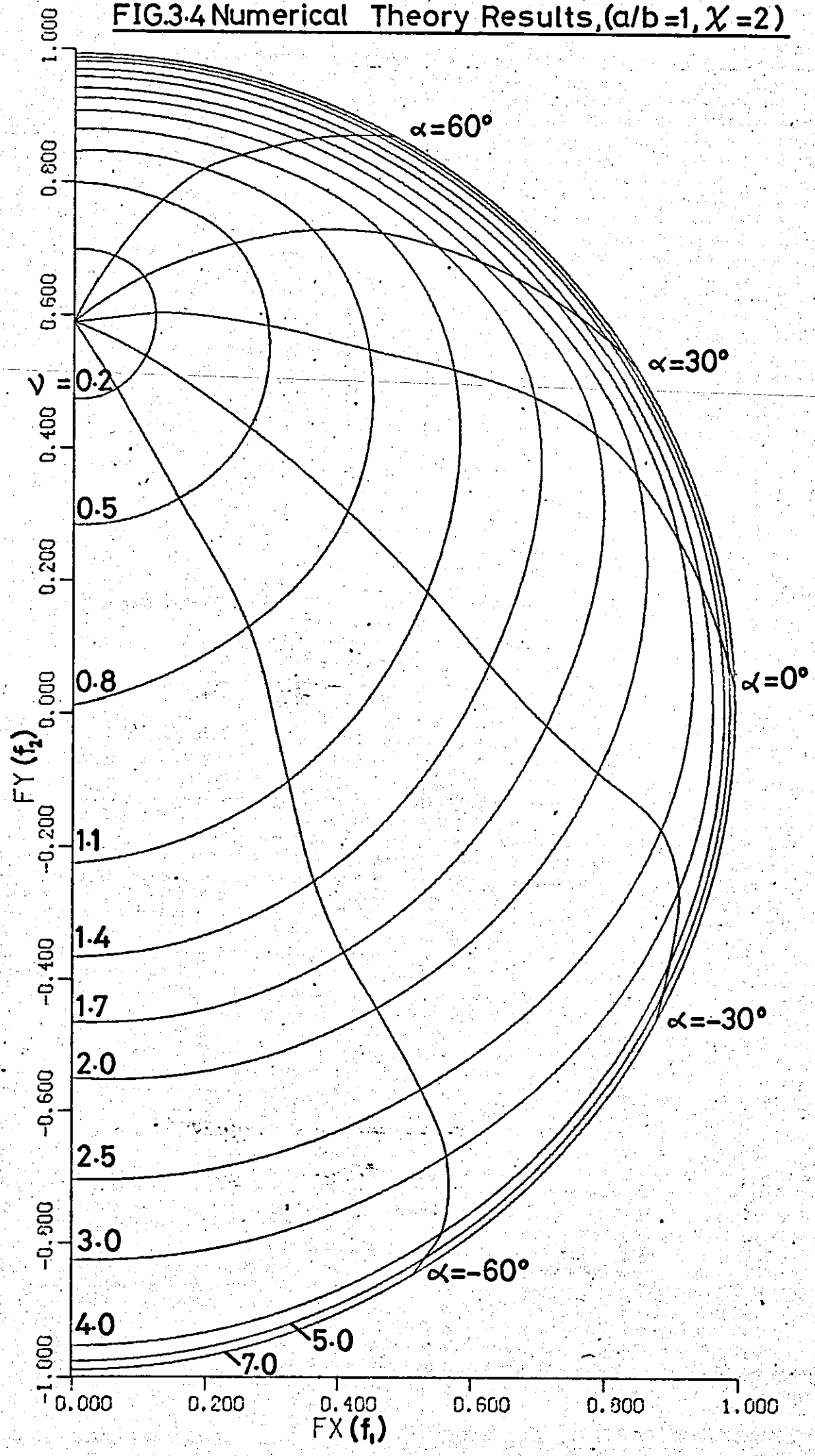

FIG.3.5 Numerical Theory Results

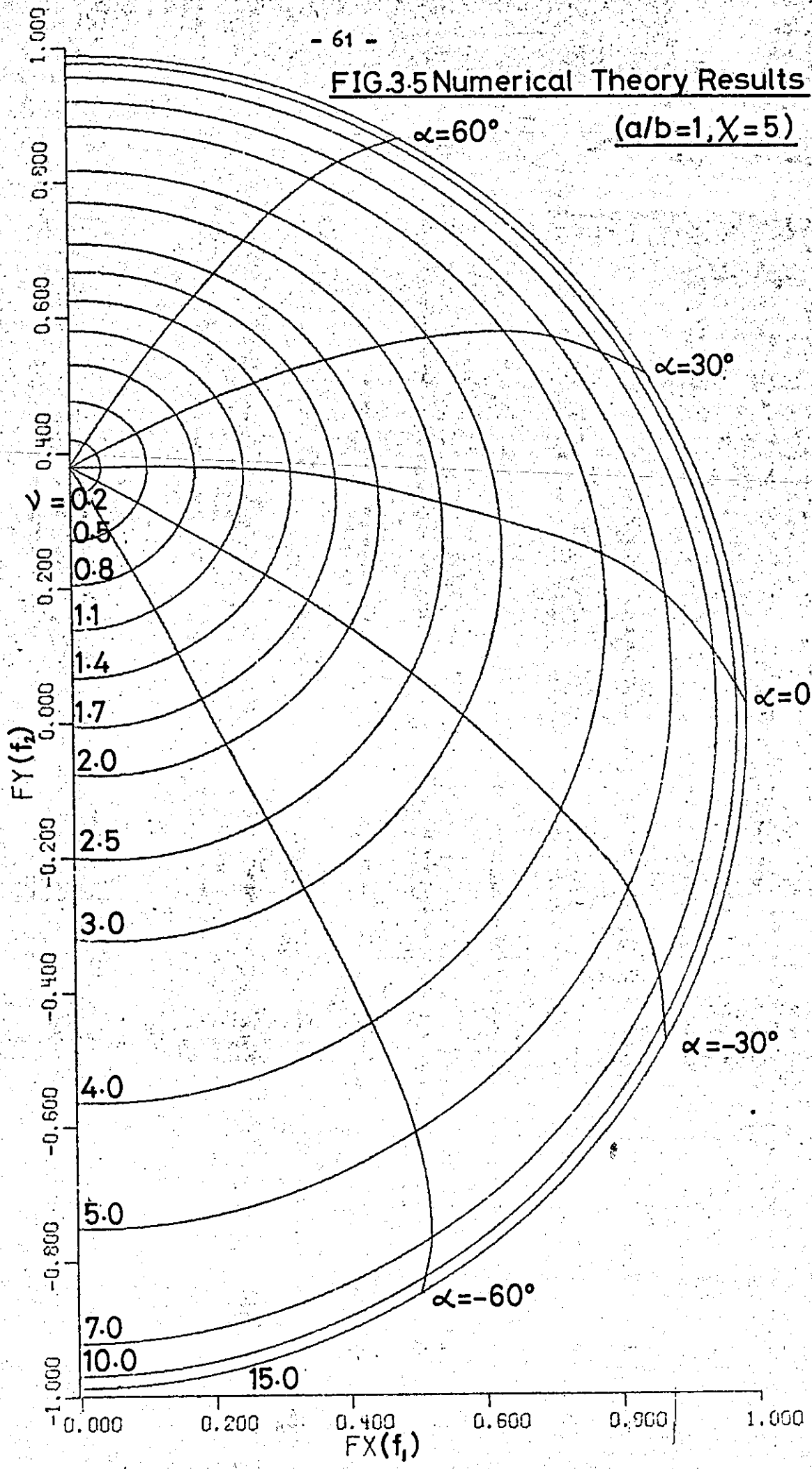

form "tubes" which lie inside the cylinder $(f_1^2 + f_2^2) = 1$ and have roughly circular intersection with the planes χ = constant. The radius of the "tube" increases as ν increases, and as the spin χ is increased, the radius decreases with the "eye" moving to the origin. Thus the radius of the "tube" is roughly determined by the quantity $\nu/|\chi|$.

Kalker has compared his results with the various experiments of Johnson, Refs. 6 and 8, and Haines and Ollerton, Ref. 11, showing good agreement between the force parameters for the cases of pure creepage, pure spin and lateral creep with spin, the total force being within 10% in all cases. The experiments mentioned have been discussed in Section 2.3, and the actual comparisons plotted in Figs. 2.5, 2.6, 2.7, 2.8 and 2.9. The correlation between moments did not agree, but this was probably due to the fact that the moment due to elastic hysterisis, which was present in the experiments, was of the same order as the moment due to surface friction. (The moment is unimportant in the present work so this disagreement is irrelevant). It is worthwhile noting that all the experimental results were for circular contact areas. The theory has not been tested for elliptical contact areas apart from the coefficients Cij, which were compared with the results of Johnson and Vermeulen, Ref. 9.

The program developed by Kalker, using much computer time to produce each result, failed to converge on a solution for contact areas with (a/b) ratios greater than 2, and even for (a/b) = 2 aberrations were found in the results near the peak of the f_2 v χ curve ($\xi = \eta = 0$). In view of this it was decided not to use the program in the present application, but instead to interpolate the results given in Ref. 35, where appropriate.

Since these were only given for (a/b) ratios of 0.2, 0.5, 1 and 2 they could obviously not be used for elongated contact ellipses such as those found on the flange.

A subroutine, called NUMERIC, put the inputs a/b, ξ, η, χ in suitable form and applied the symmetry relationships given by equation 29, 30 and 31. This then called on another subroutine, TAPE, which interpolated the results, previously stored on magnetic tape, to give the appropriate values of f_1, f_2 and m_3. Apart from interpolating the given values, the subroutine will also extrapolate for (a/b) ratios of up to 3.0. For values greater than this it was felt errors could be excessive.

In this way the results of the numerical theory could be used without having to run the program for each case. The processing time on the computer was very short but errors due to the interpolation were incurred.

In recent months Kalker has produced a new numerical theory which has not yet been published. This new method, which is still being developed, can also handle cases with slender contact ellipases, but is as slow as the old method to run on the computer. Preliminary results show agreement between the old and new numerical methods. Although this new numerical method has not been used in the presentwork, Dr. Kalker has run his computer program for several cases to compare with experimental results obtained later in the report.

3.3.2 Simplified Theory

This theory has recently been developed by Kalker, Ref. 36, and in it the complicated relationships of the half space theory, mentioned in the previous section, are replaced by much simpler ones. Using this method it is possible to give an analytical solution for the non linear cases of pure longitudinal and pure lateral creepage, and also the linearised case where the contact area is assumed to be all adhesion. For arbitrary creepage and spin a numerical method is proposed, which by adapting the governing parameters in a special way, achieves reasonable agreement between this method and the numerical theory discussed in the previous section. According to Kalker, although discrepancies do occur they generally happen where the numerical theory is of doubtful quality, and so it is not necessarily the simplified theory which is at fault. A more refined numerical method for the solution of the simplified theory is still under development at Delft and the results are awaited with interest.

It is assumed, and this is the basic simplification, that the displacement differences (u, v) and the tractions (X, Y) are connected by:

$$\left.\begin{aligned} u &= S_x X \\ v &= S_y Y \end{aligned}\right\} \qquad (32)$$

where S_x and S_y are called the inverse stiffnesses.

These simple relationships replace the complicated load-displacement equations of the exact theory which are approximated in the previous numerical method.

Since the theory has not yet been published it is reproduced in Appendix 2 with Dr. Kalker's permission. A subroutine,

called ROL, has been written in Fortran based on the method, and results obtained using it are compared with Kalker's results in Appendix 4.

Basically the contact ellipse is divided into a grid of points, the program starts at the leading edge of each y ordinate and tests whether there is adhesion or slip. If there is adhesion, then the tractions can be calculated directly. If there is slip, the equations are singular and special precautions have to be taken to calculate the starting value of θ, where in the slip area

$$\left.\begin{aligned} X &= \mu Z \cos\theta \\ Y &= \mu Z \sin\theta \end{aligned}\right\} \qquad (33)$$

These are incorporated in the program.

Having solved the leading edge condition, the program is stepped along the y ordinate and tested to find whether there is adhesion or slip in the new point and the corresponding equations used to give the traction forces.

Having covered the whole contact area in this way, the program prints out values of the slip/stick boundaries together with pressure, traction forces and relative slips at the grid points. These are integrated over the area to find the total forces. A correction is made if the pressure integrated over this area does not equal the normal force.

A suggested method for adapting the governing parameters for use in the simplified theory together with the calculations for the inverse stiffnesses are given in Appendix 3. A subroutine, called SIMP, has been written which carries out these operations and the simplified theory can then be used by calling subroutine ROL. The grid size can be varied according to the shape of the

contact ellipse. A (13 x 13) grid has been used for tread contact points while a (41 x 3) grid has generally been used for the very elongated contact ellipses of the flange. The ~~slip~~ step length can also be varied and 0.02 was found to be the optimum as regards accuracy and computer time.

A comparison between simplified theory and numerical theory is shown in Fig. 3.7 where f_2 is plotted against χ for the case of pure spin when (a/b) = 1. For $\chi < 2$ the agreement is very good, but for χ greater than this, there are differences of up to 20%. Results using simplified theory for the case $\chi = 5$, a/b = 1 are given in Fig. 3.6 and these may be compared with Fig. 3.5 which are the equivalent results using numerical theory.

The simplified theory can be used for elongated contact ellipses but cannot be compared with the numerical theory under these conditions. A comparison between the author's experimental results for elongated contact ellipses and the simplified theory is made later.

In the wheelset application, the simplified theory has been used to calculate forces for both tread and flange contacts and these are given in Section 5.

FIG. 3.6 Simplified Theory Results

(a/b=1, χ = 5)

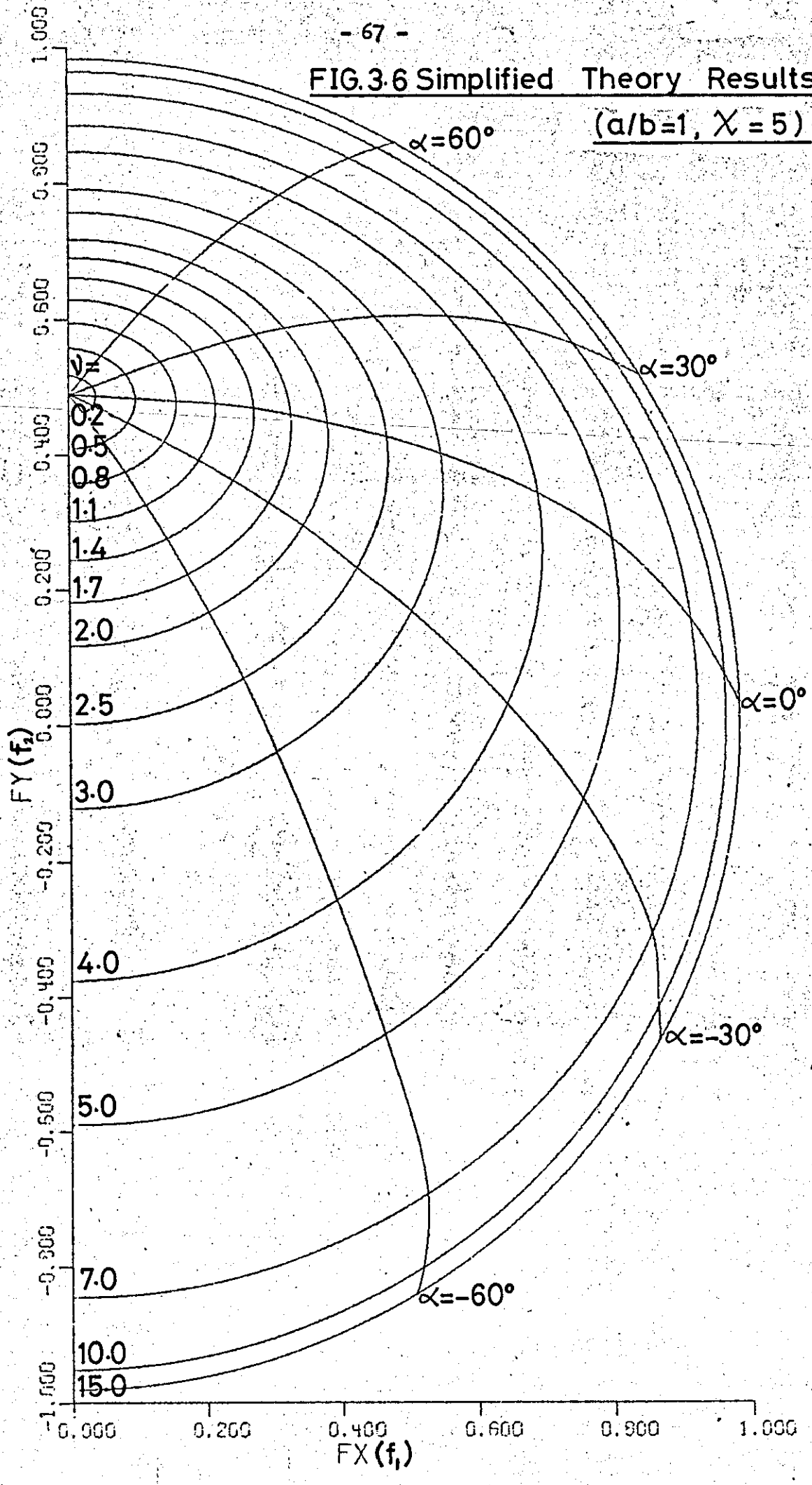

FIG. 3.7 Comparison of Numerical Theory & Simplified Theory

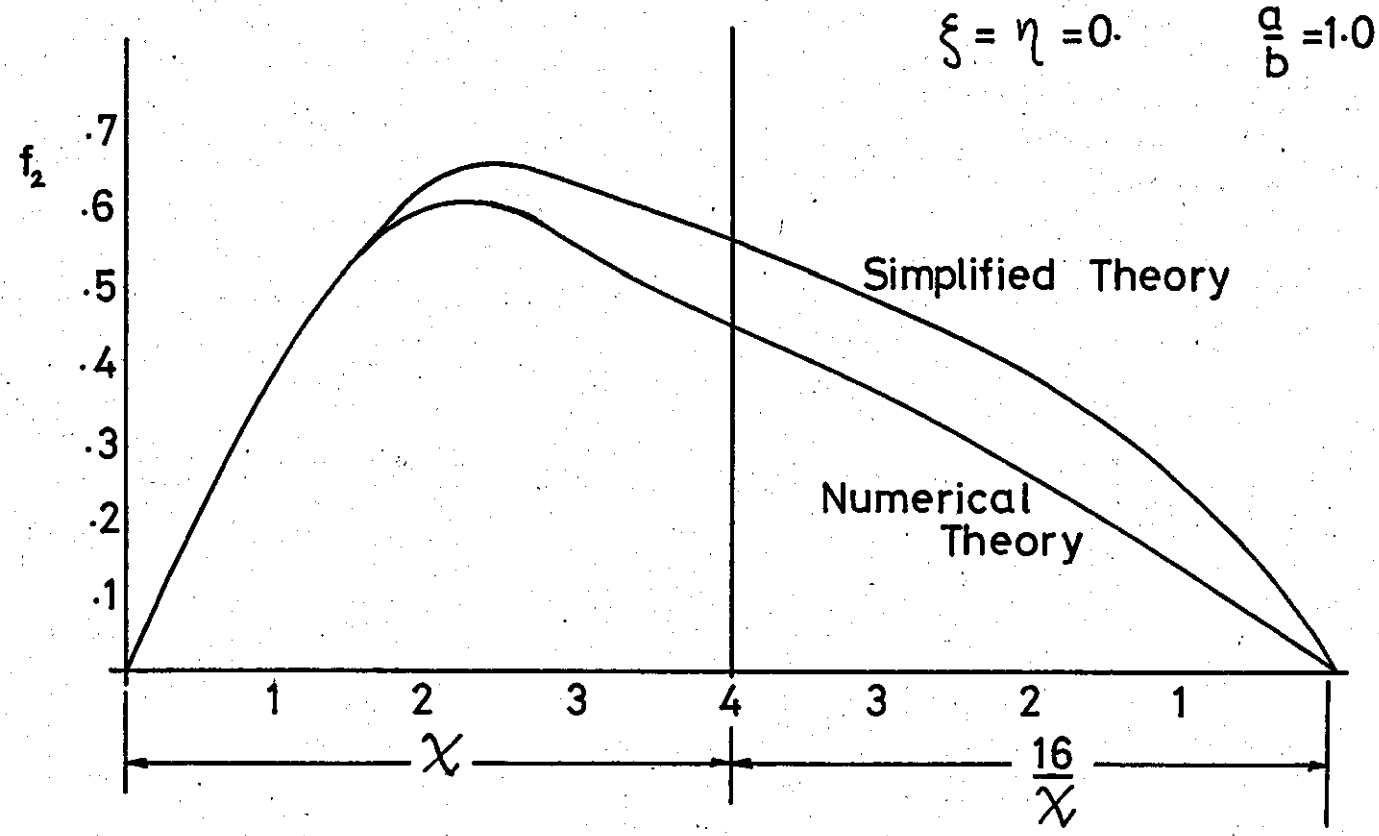

4. Mathematical Model of Wheelset and Track

4.1 Introduction

In this section a theoretical model of a wheelset rolling along track in a steady state displaced position is given. The model is based on a real wheelset rolling on real track. The forces and moments between wheel and rail due to creepage can be calculated using the theories described in Section 3. These forces can then be resolved and summed to give the total forces on the wheelset. The analysis allows the wheelset to be yawed and/or moved laterally with either tread or flange contact.

The geometry of the system is defined in Sections 4.2 and 4.3. The rail is based on a BS110A profile and the coordinates of which are calculated in Track Axes in 4.2. Wear of the rail can be taken into account in these calculations. The wheelset is defined in Wheelset Axes in 4.3 and is assumed to have a British Rail RD4 "worn" tyre profile. Coordinates are calculated for the complete tyre profile including tread and flange portions.

Having defined the wheelset and track, the three dimensional equations of each are calculated in their own axes systems. By allowing translation and rotation of one axes system relative to the other, movement of the wheelset relative to the track can be achieved and the contact points found for various lateral displacements and yaw angles. Computer programs have been written which calculate the contact points numerically and these are described in Section 4.4. In these programs two or three contact points can exist between the wheelset and the track.

Knowing the position of the contact points, the semiaxes of the contact ellipses are calculated in Section 4.5.

The wheelset is assumed to roll along perfectly straight track at a constant velocity in a displaced position. Having found the coordinates of the contact points, the creepages and spin at these points are then calculated in Section 4.6. From these the contact area forces can be calculated using the various theories of Section 3. These forces are resolved and summed to give the total forces and moments on the wheelset in Section 4.7. A computer program is described which calculates the total forces and moments for any displaced position of the wheelset using any of the theories of Section 3. This program iterates to find the angular velocity corresponding to a zero rolling moment of the wheelset about its axes, and calculates the creepages and forces for this condition.

Results obtained using this program are given in Section 5.

All the programs and subroutines referred to in this Section are described in Appendix 5 together with computer listings.

4.2 Rail Geometry

The rail head profile is based on a British Standard 110A. This is a flat bottom rail section weighing 100 lb/yd., the basic dimensions of which are shown in Fig. 4.1.

The track, which is assumed to be straight, is made up of two rails canted inwards at a slope of 1 in 20, a distance apart equal to the gauge, G. Track Axes are defined with origin midway between the rails and at a distance of 0.75" (19 mm) below the top of the rails, this being the point where the gauge is measured. The Track Axes are shown in Fig. 4.2 and denoted by a suffix t.

FIG. 4·1 B.S.110A Rail Section & Railhead Axes

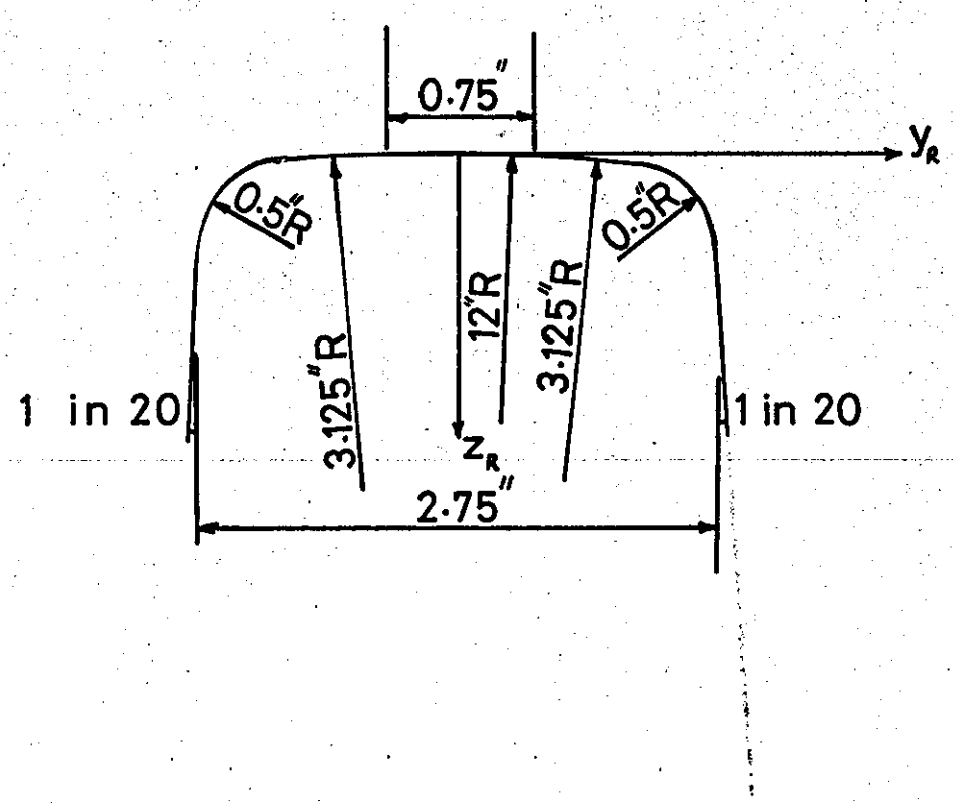

FIG. 4·2 Track Axes

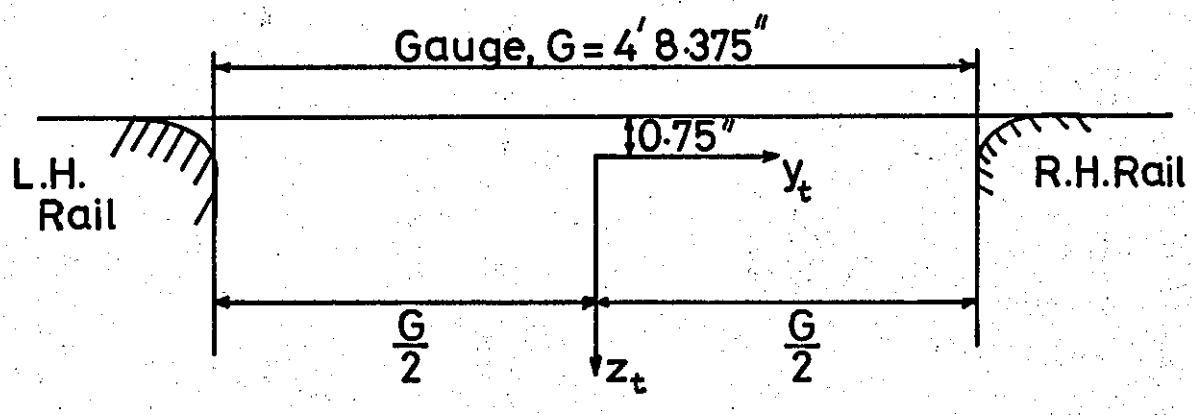

It can be seen in Fig. 4.1 that the rail-head profile is made up of five circular arcs which blend in to each other. The coordinates of the crossover points between these arcs can be calculated in Rail head Axes shown, together with the equation of each circular arc. The end points, where the 1 in 20 lines run in to the 0.5" radii, can also be calculated. These points are called ① for the $-ve$ y_R point, and ⑥ for the $+ve$ y_R point. Crossover points ② to ⑤ lie between these.

A point can also be found where a line with a 1 in 20 slope is tangent to the rail-head, this being the top most point when the rail is canted over, ($y_{T_{TOP}}$, $z_{T_{TOP}}$).

The transformation from Rail-head Axes to Track Axes may be considered as a transformation and rotation, shown in Fig. 4.3(a), where

$$y_t = y_o + y_R \cos\theta + z_R \sin\theta \qquad (1)$$

$$z_t = z_o + z_R \cos\theta - y_R \sin\theta \qquad (2)$$

The value of y_o can be found from equation 1 where

$$y_o = \frac{G}{2} - y_{R_1} \cos\theta - z_{R_1} \sin\theta \qquad (3)$$

and z_o can be found from equation 2 where

$$z_o = -.75 - z_{R_{TOP}} \cos\theta + y_{R_{TOP}} \sin\theta \qquad (4)$$

Knowing (y_o, z_o), the coordinates of all the crossover points and equations of the profile arcs, can be calculated in Track Axes using equations 1 and 2.

A computer subroutine, called RAILAT, has been written based on the above equations to calculate the crossover points and coefficients of the circular arc equations for the rail in Track Axes. Since one of the objectives of the present investigation is to look at wear effects

FIG.4.3 Transformation of Axes

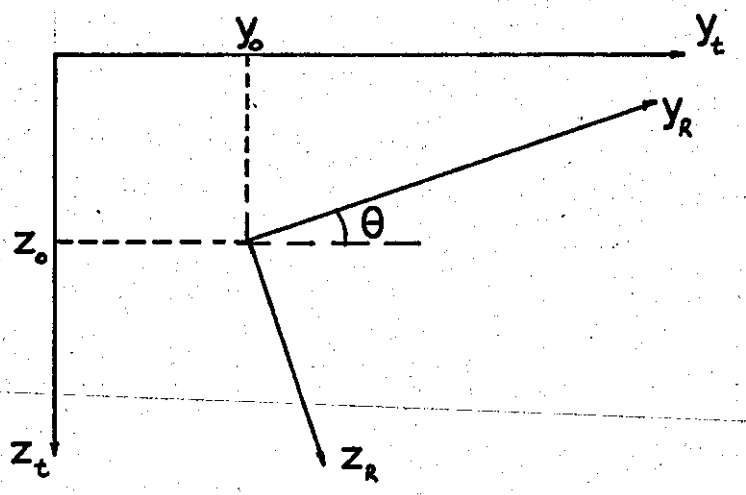

(a) Railhead axes to Track axes

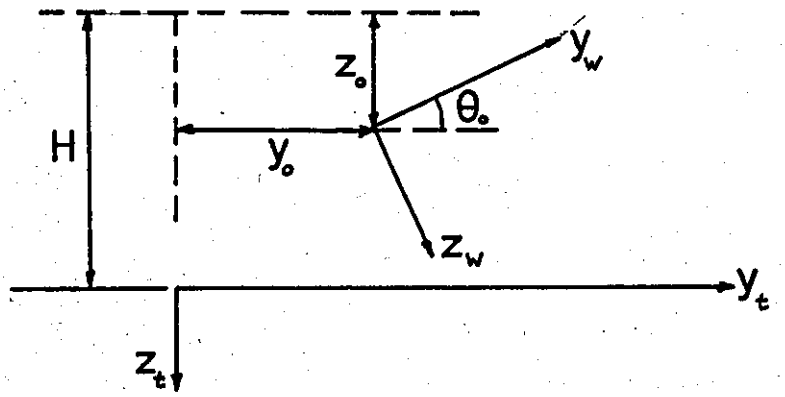

(b) Wheelset moved laterally

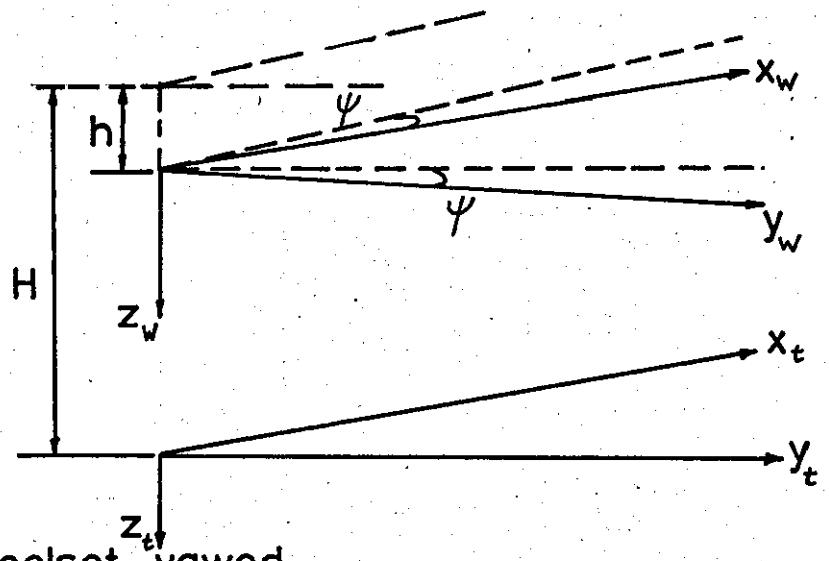

(c) Wheelset yawed

on wheelset forces, the program allows the corner radius, nominally 0.5", to be varied.

Results obtained using this program are given in Table 4.1 where the crossover points and coefficients are listed for a "standard" 0.5" corner radius rail, and for a "worn" 0.7" corner radius rail. A comparison of these two rail profiles is shown in Fig. 4.4.

The equations of the circular arcs are given by

$$(y_t - A)^2 + (z_t - B)^2 = R^2 \qquad (5)$$

where the coefficients A and B are the coordinates of the centre of the arc of radius R.

4.3 Wheel Geometry

The standard tyre used on British Rail wheels is basically made up of two cones, the tread portion with a very small cone angle of 1 in 20, or about 2 degrees, and the flange with a cone angle of about 68°. The wheel contacts the rail either on the tread, which is the point of load support, or the flange which is the point of guidance. Between these points there is a gap on the tyre where contact rarely occurs until the tyre becomes worn. This means that wear is concentrated in a very narrow band, approximately 14 mm wide, and as a result the tyre wears very rapidly to a different, more hollow profile. As this occurs the wear band gets wider and the process slows down until a terminal profile is reached where wear is distributed over the whole width of the tread.

Because of this, it was felt by British Rail to be more sensible to design vehicles to operate on "worn" profiles, as it is only with this type of profile that any degree of long term stability of

Table 4.1 Rail Profile Coordinates and Equations (Track Axes)

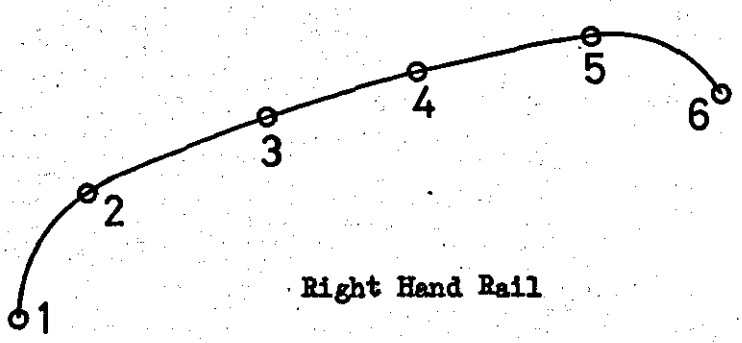

Right Hand Rail

Point	Standard Rail r_c = 12.70 (0.5")		Worn Rail r_c = 17.78 (0.7")	
	y_t	z_t	y_t	z_t
1	715.96	-3.054	716.16	+ 0.849
2	725.16	-15.261	730.15	-16.522
3	740.63	-18.084	740.63	-18.084
4	759.65	-19.036	759.65	-19.036
5	775.33	-17.772	775.33	-17.772
6	785.69	- 6.545	785.69	- 6.545

	y_t max.	z_t max.
Standard Rail	761.14	-19.05
Worn Rail	761.14	-19.05

Equation of Circular Arc $(y_t - A)^2 + (z_t - B)^2 = R^2$

Arc	Standard Rail			Worn Rail		
	R	A	B	R	A	B
1-2	12.70	728.66	- 3.054	17.78	733.94	0.849
2-3	79.375	747.07	61.029	79.375	747.06	61.029
3-4	304.8	765.37	285.71	304.8	765.37	285.71
4-5	79.375	761.14	60.33	79.375	761.14	60.325
5-6	12.70	773.06	- 5.277	17.78	773.05	- 5.277

All dimensions in mm.

FIG.4.4 Comparison of New and Worn Rail Profiles

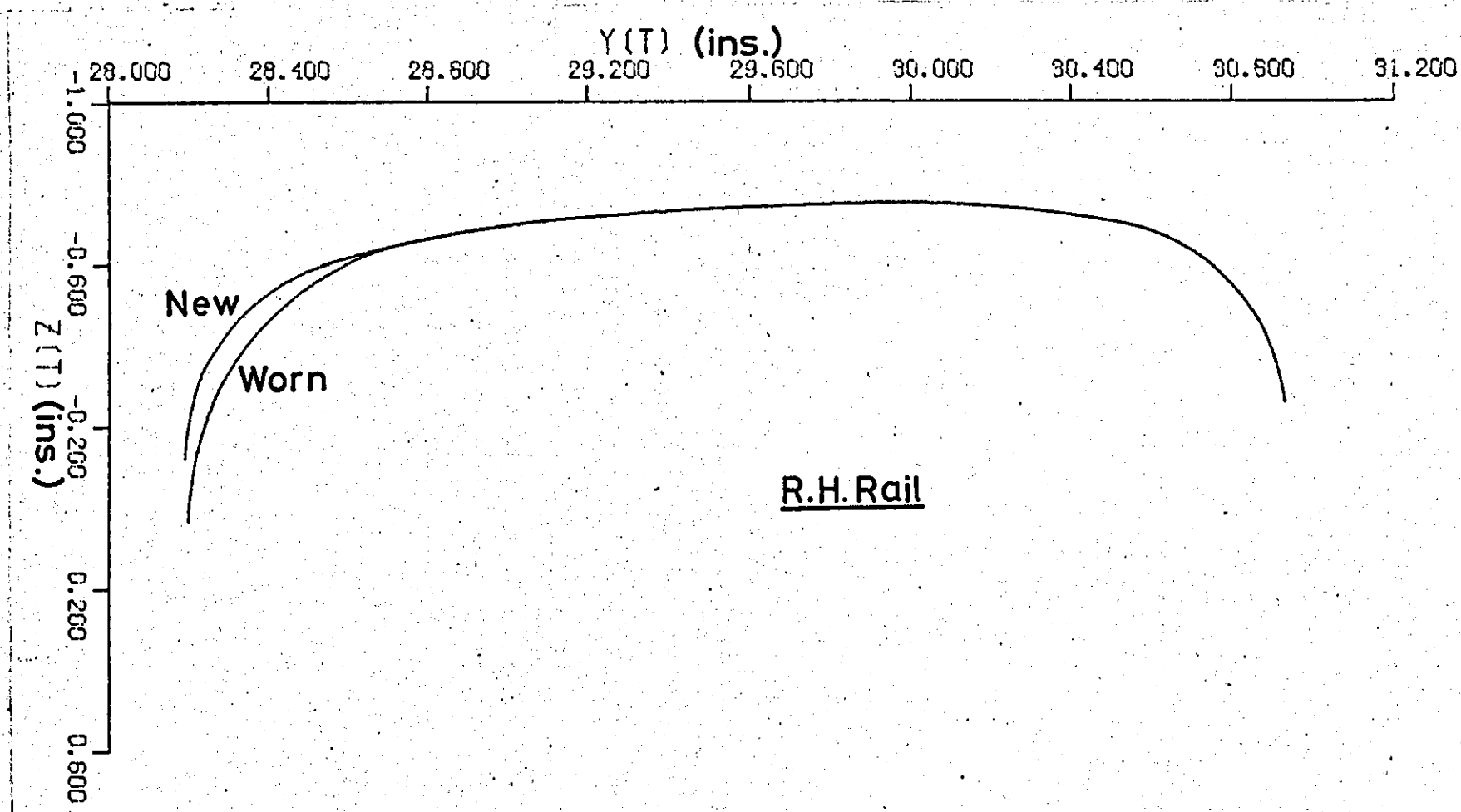

wheel/rail contact conditions occur. This fact was realised 38 years ago by Professor Heumann who pointed out in Ref. 37, the desirability of starting with a "worn" profile.

British Rail commissioned Heumann to design a tyre profile based on his researches. The design of this profile, and the practical aspects of its use, are discussed by Koffman, Ref. 38. British Rail themselves have continued this work, mainly as a by-product of their research on vehicle stability, and have produced four standard "worn" profiles that they claim "will improve tyre life between turning, reduce Hertzian contact stresses by increasing contact area, and improve guidance on curves". The four profiles are designated RD4, RD5, RD6 and RD5A. The RD5 and RD5A are basically improvements on the Heumann profile. It is proposed that eventually coned wheels will not be required on any vehicles, and RD4 and RD6 will remain as the only profiles in common use. A brief description of the design of these new profiles is given by King, Ref. 39.

Because of the likelihood of its widespread future use on trains such as the Advanced Passenger Train, the wheels in the present analysis are assumed to have RD4 Tyre Profiles, the dimensions of which are given in Fig. 4.5. The diameter of the wheel measured at point A is taken to be 750 mm and the distance across flange backs as 1360 mm.

Each wheel can be considered as a three dimensional body of revolution about an axis sytem passing through the centre of the wheelset as shown in Fig. 4.6. This axis system is referred to as Wheelset Axes and denoted by a suffix w. The shape of the body is defined by the tyre profile which is made up of four circular arcs and two straight sections. The parts of the wheel with a circular profile can be represented by the equations

FIG.4.5 R.D.4 Tyre Profile

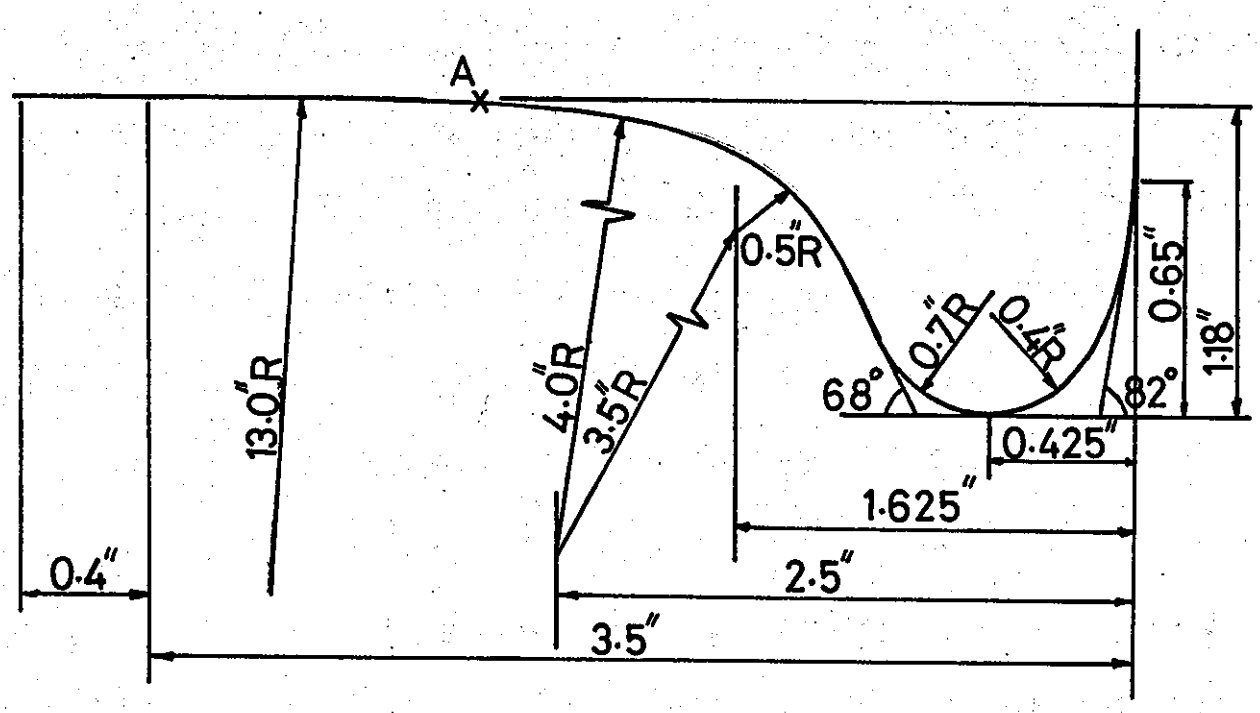

FIG.4.6 Wheelset Axes

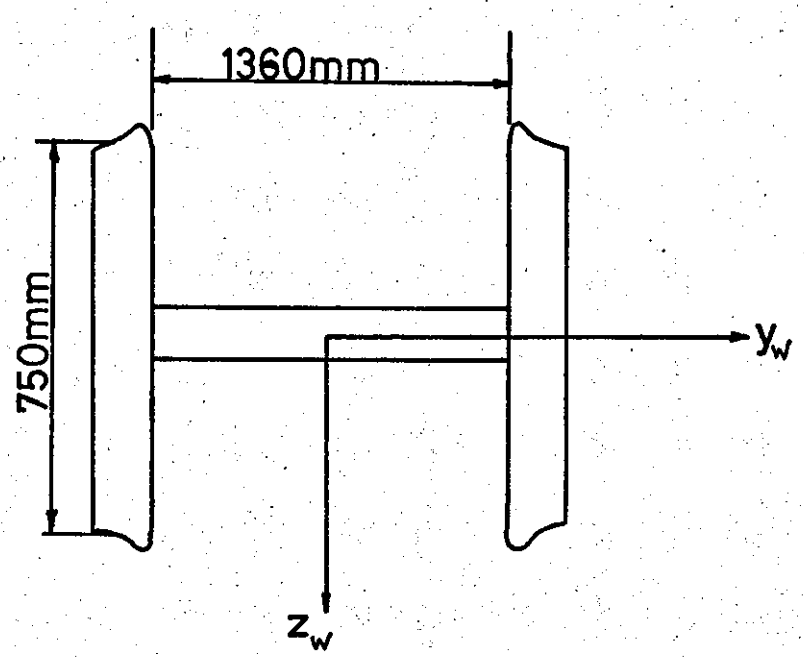

$$(y_w - a)^2 + (R - b)^2 = r^2 \quad (6)$$

$$R^2 = x_w^2 + z_w^2 \quad (7)$$

where a, b are the coordinates of the centre of the circular arc of radius r in the $x_w = 0$ plane.

Sections with straight profiles can be represented by the equations

$$R = m\, y_w + c \quad (8)$$

and equation 7 above.

where m = slope and c = intercept on the plane $x_w = 0$

Using the dimensions given in Fig. 4.5 and the equations 6, 7 and 8, the coordinates of the intersection points between each part of the tyre profile can be calculated together with the constants a, b, m and C. Knowing these values the wheelset is completely defined as a three dimensional body in wheelset axes.

A subroutine called WHEEL has been written to perform these calculations based on the above equations and results obtained using this program are given in Table 4.2.

4.4 Contact Points

Having defined the wheelset and track, this section describes how one may be moved relative to the other and the resulting contact points found. Before this can be done the datum or zero position has to be found where the wheelset is in the central position. This is described in 4.4.1 and the vertical distance between wheelset axes origin and track axes origin found, together with the contact point coordinates.

Table 4.2 Wheel Profile Coordinates and Equations (Wheelset Axes)

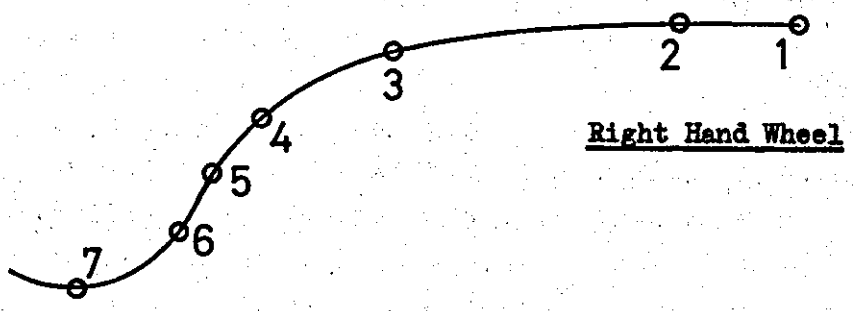

Point	y_w	Z_w
1	780.10	375.37
2	769.94	375.37
3	733.25	377.41
4	719.14	380.01
5	710.54	387.55
6	707.61	394.79
7	691.83	405.89

Equation of Circular Arc $(y_w - a)^2 + (Z_w - b)^2 = r^2$

Equation of Straight Section $Z_w = y_w + C$

Arc	a	b	r
2 - 3	769.94	705.57	330.2
3 - 4	744.54	478.39	101.6
4 - 5	722.31	392.31	12.70
6 - 7	691.13	388.13	17.78

Straight Section	m	C
1-2	0	375.37
5-6	-62.867	2146.19

All dimensions in mm.

There are, of course, two contact points between the wheelset and track when it is in the central position, a left hand contact point and a right hand contact point, both on the treads.

For displacement of the wheelset from this central position, three separate programs have been written to calculate the contact points. In Section 4.4.2 a program is described which allows the wheelset to be moved laterally, without yaw, to any position including flange contact, while Section 4.4.3 contains a program which allows the wheelset to be yawed without lateral displacement. In Section 4.4.4 a numerical iteration method is described which calculates the contact points when a wheelset is moved laterally until the flange contacts the rail and then yawed with the flange remaining in contact with the rail.

4.4.1 Wheelset in Central Position

With the wheelset in the central position, the contact points between the rail and wheel have to be found together with the vertical distance between the Wheelset Axes origin and the Track Axes origin. If this vertical distance is called H, then the transformation between the two axes systems is

$$\left.\begin{aligned} x_t &= x_w \\ y_t &= y_w \\ z_t &= z_w - H \end{aligned}\right\} \qquad (9)$$

The slope at any point on the rail is given by differentiating equation 5 to give:

$$\left(\frac{\partial z}{\partial y}\right)_R = \frac{A - y_t}{z_t - B} \qquad (10)$$

and the slope on a circular arc of the wheel is given by differentiating equation 6 to give:

$$\left(\frac{\partial z}{\partial y}\right)_W = \frac{a - y_T}{z_t + H - b} \qquad (11)$$

An iterative technique can be employed to calculate the contact points by finding where the rail and wheel slopes match. The corresponding value of H follows from the equations.

This iteration is carried out in a subroutine called FINDH, giving the following values for the right hand side contact point:

Standard rail: y_t = 739.83 mm, z_t =-18.015 mm, H = 394.76 mm

Worn rail: y_t = 739.83 mm, z_t =-18.015 mm, H = 394.74 mm

(The left hand side contact point is a mirror image of the right hand side).

The contact point lies on a rail profile radius of 79.375 mm and a wheel radius of 330.2 mm. Fig. 4.7 shows the right hand side contact point with the wheelset in the central position on a "standard" rail.

4.4.2 Wheelset moved laterally only

When the centre of the wheelset is moved laterally a distance y_o, the contact points remain in the plane x_t = 0, while the centre undergoes a vertical displacement z_o and an angle of roll θ_o. Qualitatively, as the wheelset is displaced laterally towards the right hand rail, the contact point moves along the tread until a point is reached when the flange also contacts the rail. For this particular value of y_o there are three contact points between wheelset and track, two on the right hand wheel and one on the left hand wheel. For further lateral displacement the flange of the right hand wheel climbs up the rail with the tread now lifted off while the left hand wheel remains in tread contact. This displacement can be achieved by the transformation of axes shown in

FIG.4.7 Wheelset in Central Position. Standard Rail. R.H.Side.

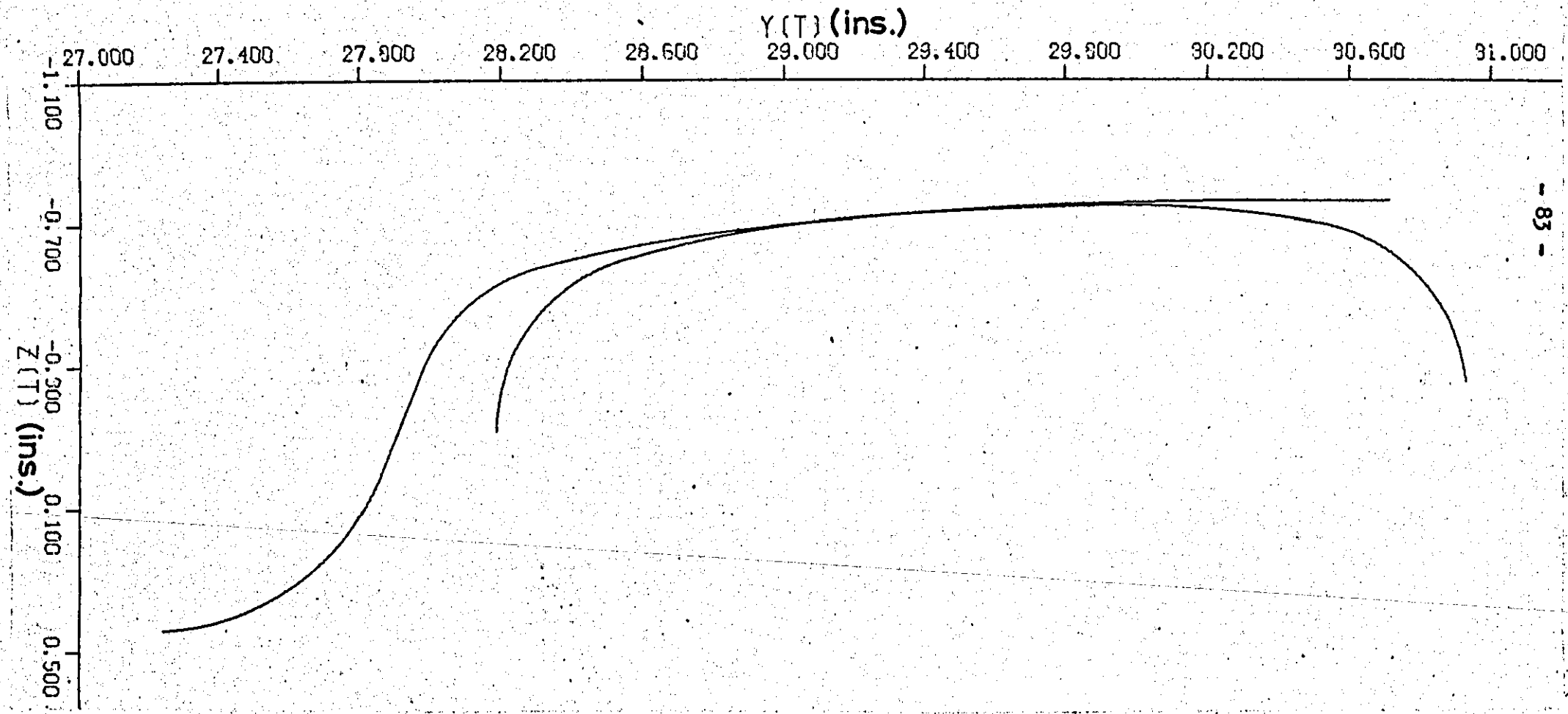

Fig. 4.3(b) which is given by the following equations:

$$\left.\begin{aligned} y_w &= (z_o - z_t - H)\sin\theta_o + (y_t - y_o)\cos\theta_o \\ z_w &= -(z_o - z_t - H)\cos\theta_o + (y_t - y_o)\sin\theta_o \end{aligned}\right\} \qquad (12)$$

Using these equations, any point on the wheelset can be expressed in Track Axes for given values of y_o, z_o and θ_o.

According to equations 6 and 7, for circular arcs of the tyre profile

$$(y_w - a)^2 + (z_w - b)^2 = r^2 \quad \text{(When } x_w = 0) \qquad (13)$$

Differentiating this equation gives:

$$\left(\frac{\partial z}{\partial y}\right)_w = \frac{a - y_w}{z_w - b} \qquad (14)$$

Substituting for y_w and z_w from equation 12 into equation 13 gives:

$$\begin{aligned} &y_t^2 + z_t^2 - 2y_t(y_o + a\cos\theta_o + b\sin\theta_o) - 2z_t(z_o - H - a\sin\theta_o + b\cos\theta_o) \\ &+\left[(z_o - H)^2 + y_o^2 + 2(z_o - H)(b\cos\theta_o - a\sin\theta_o) + 2y_o(a\cos\theta_o + b\sin\theta_o)\right. \\ &\qquad \left. + a^2 + b^2 - r^2\right] = 0 \end{aligned} \qquad (15)$$

(This could be written in the form $(y_t - a')^2 + (z_t - b')^2 = r'^2$ if required).

Substituting for y_w and z_w from equation 12 into equation 14 gives:

$$\frac{\partial z_t}{\partial y_t} = \frac{y_o + a\cos\theta_o + b\sin\theta_o - y_t}{z_t - (z_o - H) + a\sin\theta_o - b\cos\theta_o} \qquad (16)$$

According to equations 7 and 8 for straight profiles:

$$z_w = m y_w + o \qquad (17)$$

Differentiating this equation gives:

$$\frac{\partial z_w}{\partial y_w} = m \qquad (18)$$

Substituting for y_w and z_w from equation 12 into equation 17 gives:

$$\begin{aligned} &y_t(\sin\theta_o - m\cos\theta_o) + z_t(\cos\theta_o + m\sin\theta_o) - (z_o - H)(\cos\theta_o + m\sin\theta_o) \\ &\qquad - y_o(\sin\theta_o - m\cos\theta_o) - c = 0 \end{aligned} \qquad (19)$$

Substituting for y_w and z_w from equation 12 into equation 18 gives:

$$\frac{\partial z_t}{\partial y_t} = \frac{m\cos\theta_o - \sin\theta_o}{\cos\theta_o + m\sin\theta_o} \tag{20}$$

Thus equations 15, 16, 19 and 20 define points and slopes on the wheel profile in the displaced position.

Points on the rail profile are given by equation 5 which is

$$(y_t - A)^2 + (z_t - B)^2 = R^2 \tag{21}$$

Differentiating equation 5 gives:

$$\frac{\partial z_t}{\partial y_t} = \frac{A - y_t}{z_t - B} \tag{22}$$

For a given lateral displacement of the wheelset, y_o, there are six unknowns to be found: $(y_t , z_t)_{R.H.S.}$, $(y_t, z_t)_{L.H.S.}$, z_o and θ_o.

The six equations available for the solution of these parameters are listed below:

1. The rail equation for the right hand side (from equation 21)

$$(y_{t_R} - A_R)^2 + (z_{t_R} - B_R)^2 = R_R^2 \tag{23}$$

2. The rail equation for the left hand side (from equation 21)

$$(y_{t_L} - A_L)^2 + (z_{t_L} - B_L)^2 = R_L^2 \tag{24}$$

3. The wheel equation for the right hand side (either equation 15 or equation 19)

Either

$$y_{t_R}^2 + z_{t_R}^2 - 2y_{t_R}(y_o + a_R\cos\theta_o + b_R\sin\theta_o) - 2z_{t_R}(z_o - H - a_R\sin\theta_o + b_R\cos\theta_o)$$
$$+ [(z_o - H)^2 + y_o^2 + 2(z_o - H)(b_R\cos\theta_o - a_R\sin\theta_o) + 2y_o(a_R\cos\theta_o + b_R\sin\theta_o)$$
$$+ a_R^2 + b_R^2 - r_R^2] = 0 \tag{25}$$

Or

$$y_{t_R}(\sin\theta_o - m_R\cos\theta_o) + z_{t_R}(\cos\theta_o + m_R\sin\theta_o)$$
$$- (z_o - H)(\cos\theta_o + m_R\sin\theta_o) - y_o(\sin\theta_o - m_R\cos\theta_o) - c_R = 0$$

4. The wheel equation for the left hand side (either equation 15 or equation 19)

Either

$$y_{t_L}^2 + z_{t_L}^2 - 2y_{t_L}(y_o + a_L\cos\theta_o + b_L\sin\theta_o) - 2z_{t_L}(z_o - H - a_L\sin\theta_o + b_L\cos\theta_o)$$
$$+\left[(z_o-H)^2 + y_o^2 + 2(z_o-H)(b_L\cos\theta_o - a_L\sin\theta_o) + 2y_o(a_L\cos\theta_o + b_L\sin\theta_o)\right.$$
$$\left. + a_L^2 + b_L^2 - r_L^2\right] = 0$$

Or

$$y_{t_L}(\sin\theta_o - m_L\cos\theta_o) + z_{t_L}(\cos\theta_o + m_L\sin\theta_o)$$
$$-(z_o-H)(\cos\theta_o + m_L\sin\theta_o) - y_o(\sin\theta_o - m_L\cos\theta_o) - c_L = 0 \qquad (26)$$

5. Equating rail and wheel slope on right hand side (equation 22 and either equation 16 or equation 20)

$$\frac{A - y_{t_R}}{z_{t_R} - B} = \frac{y_o + a_R\cos\theta_o + b_R\sin\theta_o - y_{t_R}}{z_{t_R} - (z_o - H) + a_R\sin\theta_o - b_R\cos\theta_o} \qquad (27)$$

6. Equating rail and wheel slope on left hand side (equation 22 and either equation 16 or equation 20)

$$\frac{A - y_{t_L}}{z_{t_L} - B} = \frac{y_o + a_L\cos\theta_o + b_L\sin\theta_o - y_{t_L}}{z_{t_L} - (z_o - H) + a_L\sin\theta_o - b_L\cos\theta_o} \qquad (28)$$

Since these equations are non-linear the problem of reducing the variables is very cumbersome, even if some of the variables are assumed to be small. This problem is complicated further since it is not known which arc on the rail profile touches which arc or straight line on the wheel profile and because of this, a numerical iterative technique was used for the solution of the equations. A computer program called LATERAL WHEELSET was written for this purpose, based on the following approach: Considering one side only, say the right hand side of the wheelset, three equations can be applied, 23, 25 and 27. In these equations there are four unknowns, y_{t_R}, z_{t_R}, θ_o and z_o. If one of these unknowns is assumed, say θ_o, then the other three can be calculated.

Similarly for the left hand side there are three equations, 24, 26 and 28 and assuming a value for θ_0; y_{t_L}, z_{t_L} and z_0 can be found, but z_0 should be the same on either side since the two sides are connected. Thus the correct solution is when z_0 for the right hand side is equal to z_0 for the left hand side.

This is the basis of the program called LATERAL WHEELSET, but since the rail profile is made up of several circular arcs and the tyre profile both circular arcs and straight lines, solutions have to be sought for each combination of these. A subroutine called STRWH, was written to solve the equations for straight profiles and a subroutine, called CIRWH, to solve the equations for circular profiles. The value of θ_0 is varied until values of z_0 are equal on both sides and when this occurs the coordinates of the contact points on either side can be calculated.

In practice, since it is known approximately where the contact points will be, some of the combinations can obviously be discarded and it was found using the program that there was generally only one sensible solution left. As a check, the rail and wheel profiles were then drawn in their displaced position on the computer graph plotter, 5 x full size, to make sure that they just touched and did not cross anywhere.

The program worked well and results showed (for the "standard" rail) that as the wheelset is moved laterally towards the right hand rail, the contact points move along the tread until when y_0 = 6.11 mm there are three contact points between wheelset and track. One contact point is on the tread of the left hand wheel, one on the tread of the right hand wheel and one on the flange of the right hand wheel. For larger values of y_0 there is a contact point on the left hand wheel tread and one on the right hand wheel flange.

Results are given in Table 4.3 for the "standard" rail and in Table 4.4 for the "worn" rail. The contact point coordinates for both cases are given for lateral displacements of 0 to 7.62 mm.

Figs. 4.8 to 4.14 show pictorially the wheel and rail in the displaced position for various amounts of lateral displacement. Figs. 4.8 to 4.11 are using the "standard" rail profile while Figs. 4.12 to 4.14 are using the "worn" rail profile.

4.4.3 Wheelset Yawed Only

When the wheelset is rotated through an angle of yaw, the contact point moves along the rail in the x_t direction, and also moves vertically by a small amount. However, since there is no lateral displacement, there is no accompanying roll. Therefore the three dimensional equations for the wheelset and track have to be used to find the contact points, but due to symmetry, there is only need to consider one side of the wheelset.

The transformation from Wheelset Axes to Track Axes as the wheelset is yawed through an angle ψ and allowed to move vertically by an amount h is shown in Fig. 4.3(c). The equations which give this transformation are:

$$\left.\begin{aligned} x_w &= x_t \cos\psi + y_t \sin\psi \\ y_w &= -x_t \sin\psi + y_t \cos\psi \\ z_w &= z_t + H - h \end{aligned}\right\} \qquad (29)$$

Using these equations any point on the wheelset can be expressed in Track Axes for given values of ψ and h

According to equations 6 and 7, for circular arcs of the tyre profile

$$(y_w - a)^2 + (R' - b)^2 = r^2 \qquad (30)$$

where

$$R'^2 = x_w^2 + z_w^2 \qquad (31)$$

Table 4.3 Coordinates of Contact Points. Wheelset Moved Laterally Only. Standard Rail

All dimensions in mm

y_o	θ_o (rad)	z_o	L.H. WHEEL (A)			R.H. WHEEL (B)			R.H. WHEEL (C)		
			y_t	z_t	y_w	y_t	z_t	y_w	y_t	z_t	y_w
0	0	0	-739.83	-18.015	-739.83	739.83	-18.015	739.83	-	-	-
2.54	0.00033	- .01067	-743.85	-18.329	-746.51	738.96	-17.930	736.29	-	-	-
3.81	0.00046	- .05232	-759.67	-19.037	-763.65	738.53	-17.884	734.54	-	-	-
5.08	0.00057	- .11857	-760.09	-19.042	-765.39	736.99	-17.704	731.69	-	-	-
6.10	0.00069	- .19710	-760.43	-19.047	-766.78	733.17	-17.117	726.82	-	-	-
6.12	0.00070	- .20193	-760.45	-19.047	-766.83	733.06	-17.099	726.67	716.88	-7.803	710.49
6.22	0.00119	- .58039	-760.59	-19.047	-767.27	-	-	-	716.88	-7.798	710.20
6.35	0.00181	-1.0528	-760.77	-19.05	-767.80	-	-	-	716.88	-7.790	709.82
6.60	0.00284	-1.9558	-761.08	-19.05	-768.76	-	-	-	716.87	-7.777	709.16
7.11	0.00559	-3.9573	-761.59	-19.05	-770.81	-	-	-	716.89	-7.808	707.58
7.62	0.00735	-5.3137	-761.73	-19.05	-772.12	-	-	-	717.38	-8.882	706.86

Table 4.4 Coordinates of Contact Points. Wheelset Moved Laterally Only. Worn Rail

y_o	θ_o (rad)	z_o	L.H. WHEEL (A)			R.H. WHEEL (B)			R.H. WHEEL (C)		
			y_t	z_t	y_w	y_t	z_t	y_w	y_t	z_t	y_w
0	0	0	-739.83	-18.015	-739.83	739.83	-18.015	739.83	-	-	-
5.08	0.000574	-.1430	-760.08	-19.043	-765.38	736.96	-17.700	731.67	-	-	-
7.53	0.00091	-.3801	-760.93	-19.050	-769.00	729.95	-16.477	724.00	717.39	-5.6439	710.00
7.62	0.0014	-.7239	-761.07	-19.050	-769.22	-	-	-	717.44	-5.7887	709.28

All dimensions in mm

FIG.4·8 Wheelset Displaced Laterally. Standard Rail. R.H.Side.

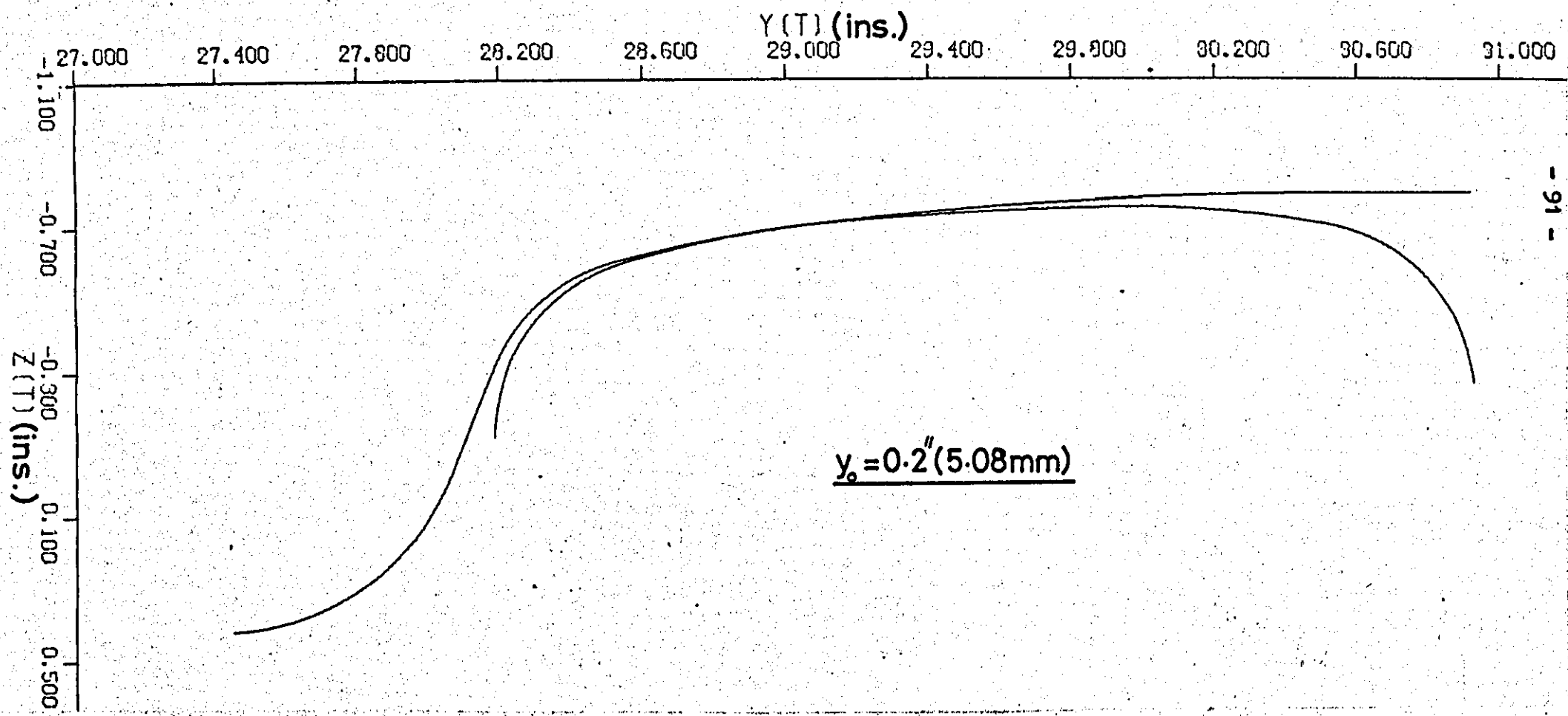

FIG.4.9 Wheelset Displaced Laterally. Standard Rail.

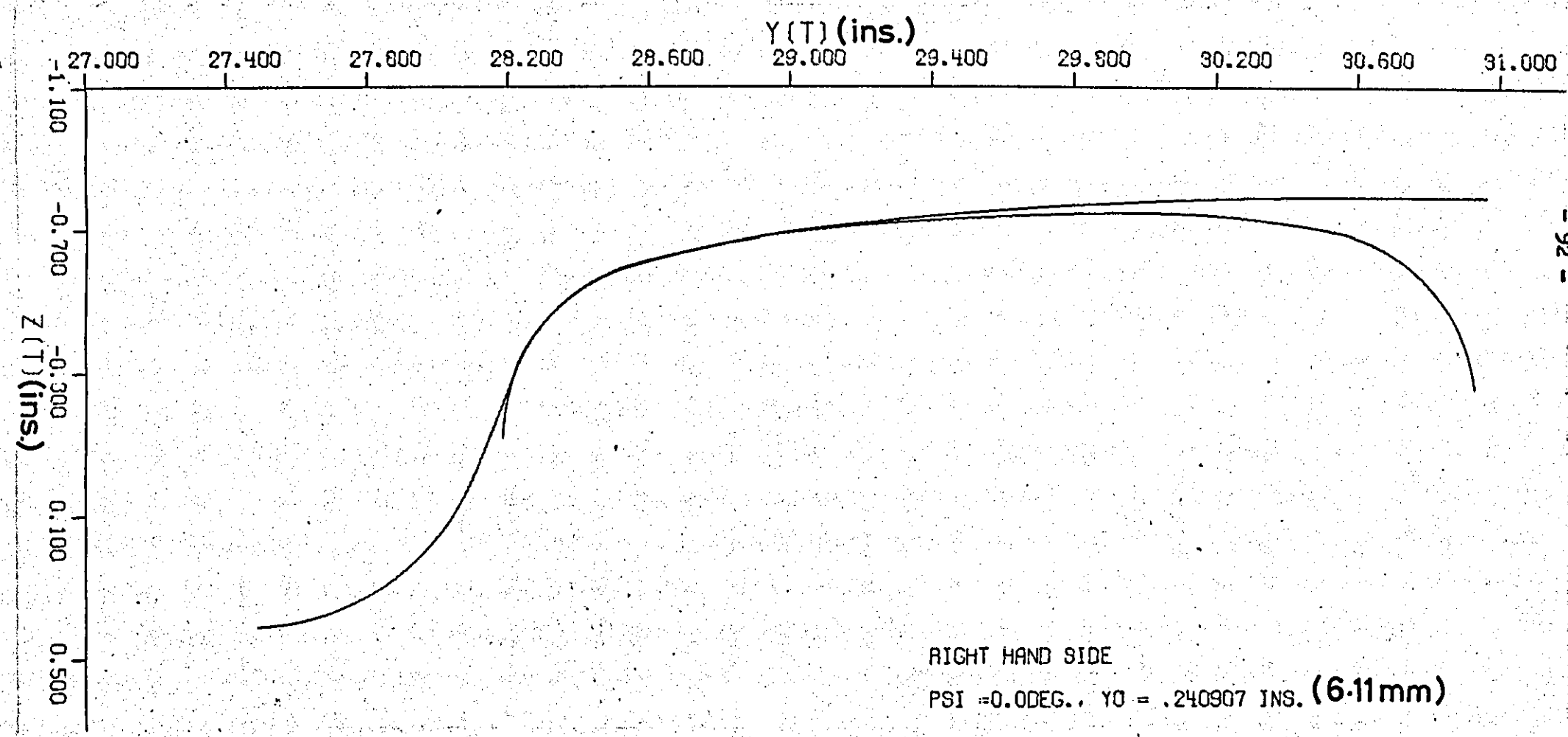

FIG.4.10Wheelset Displaced Laterally. Standard Rail.

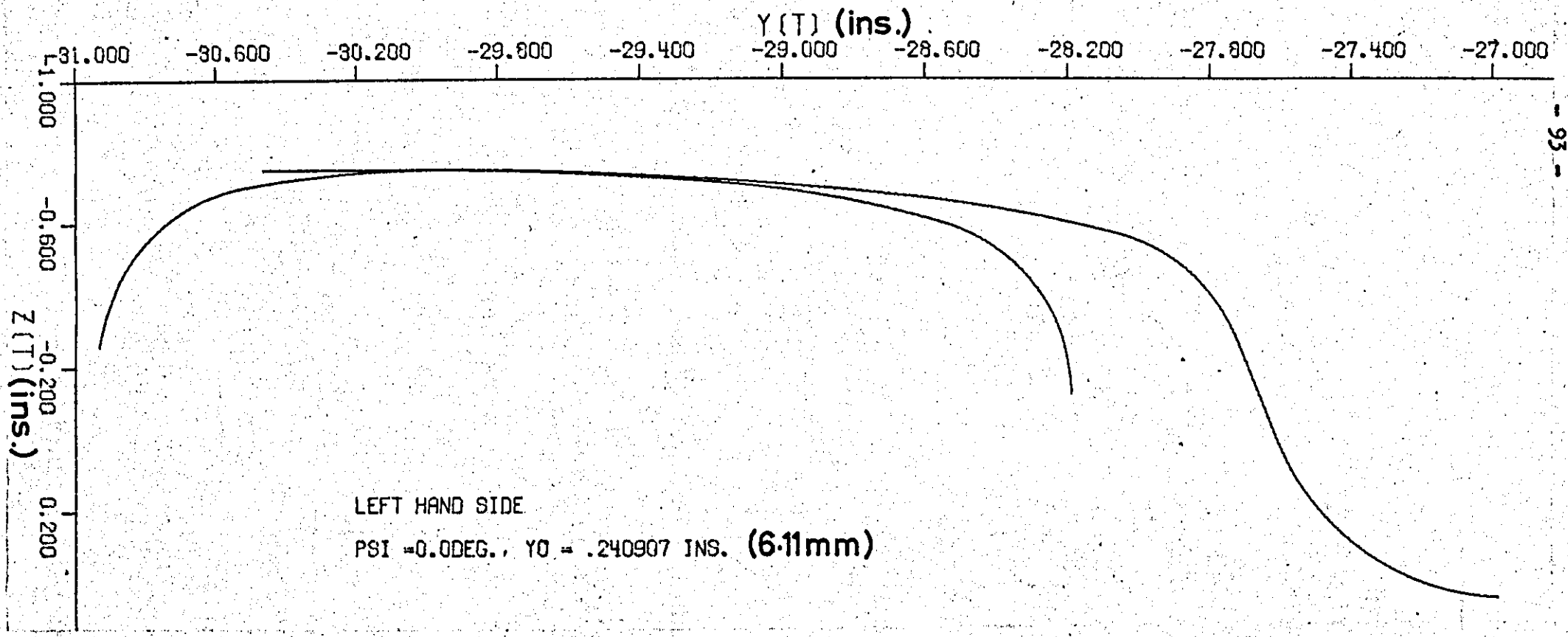

FIG 4.11 Wheelset Displaced Laterally. Standard Rail. R.H. Side.

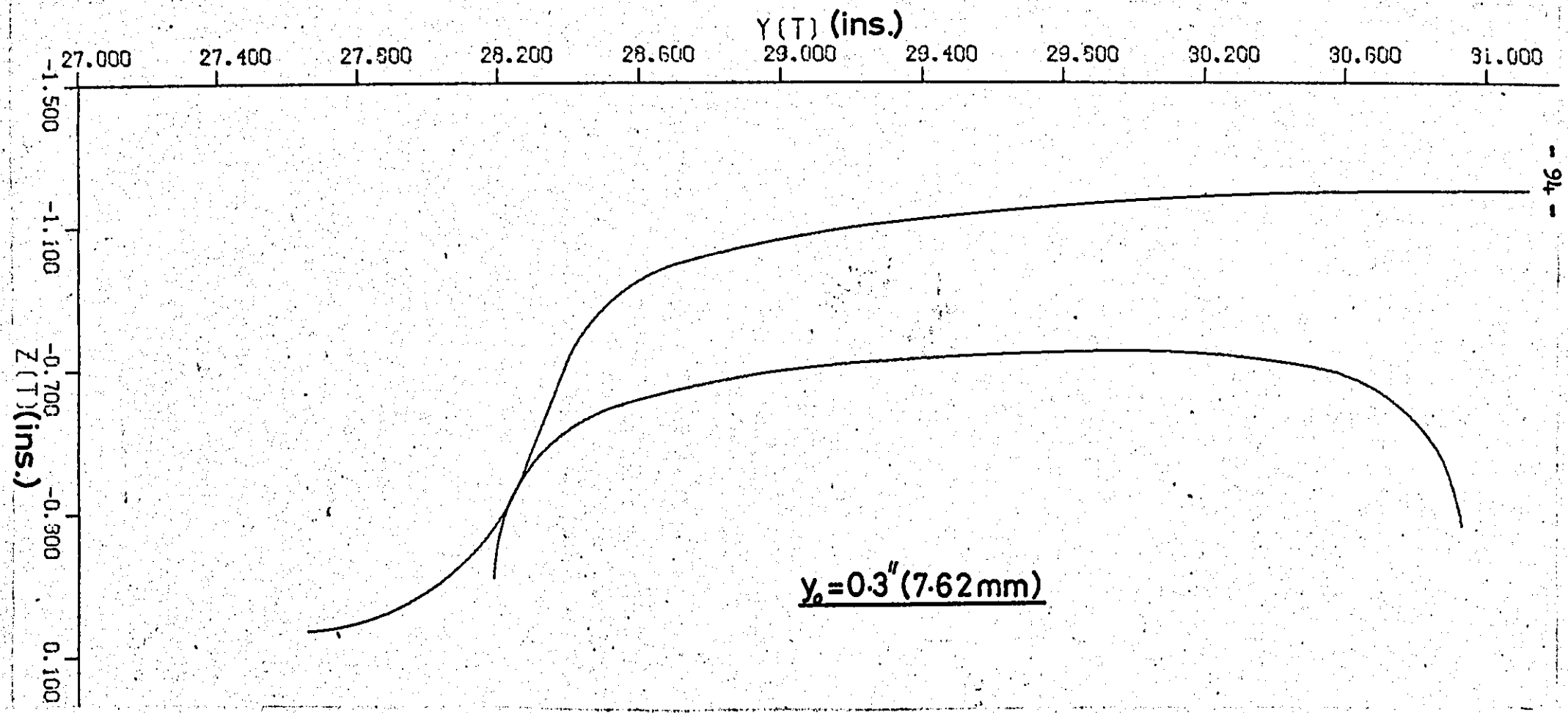

FIG. 4.12 Wheelset Displaced Laterally. Worn Rail. R H Side.

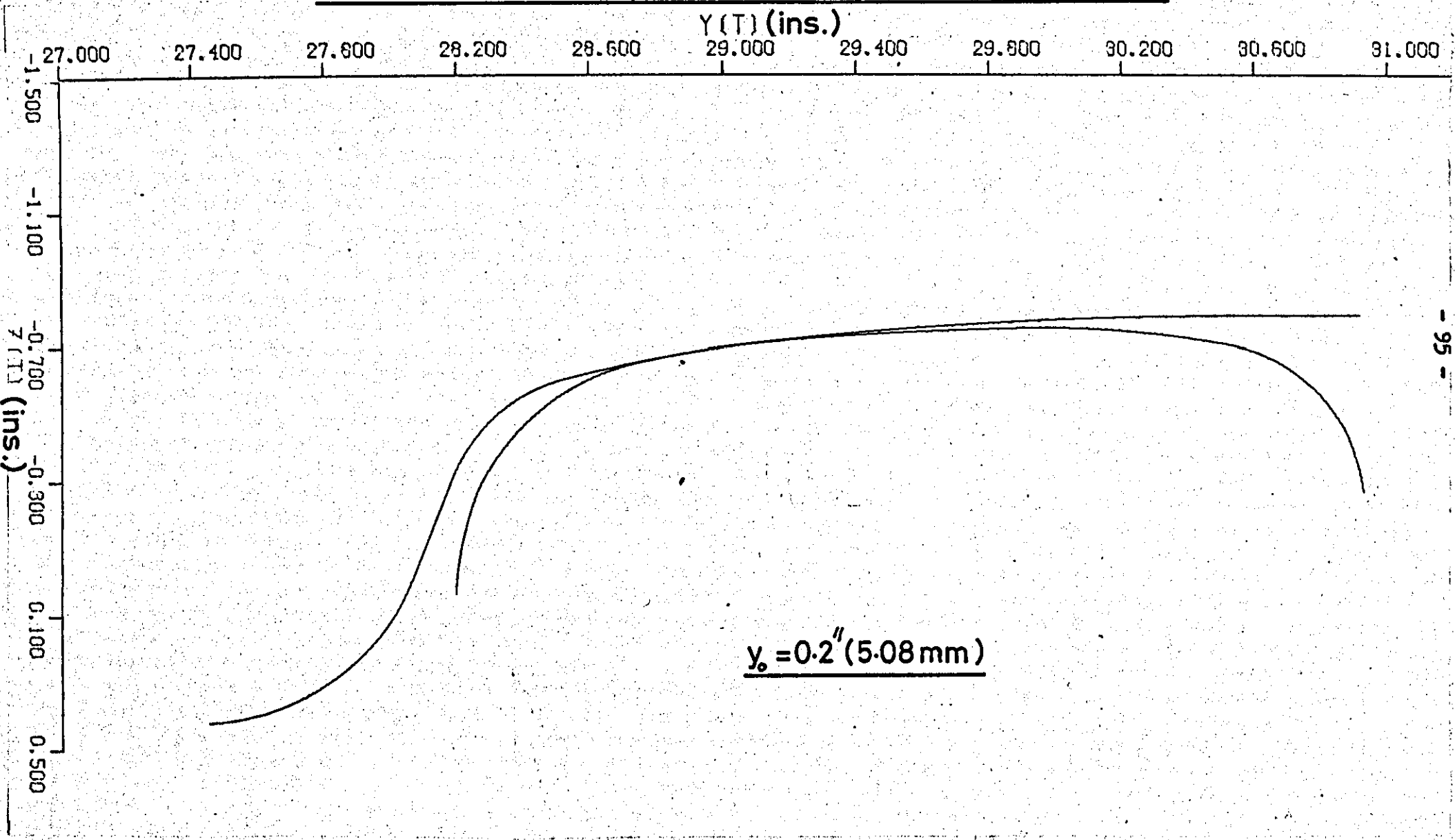

FIG.4.13 Wheelset Displaced Laterally. Worn Rail. R.H.Side.

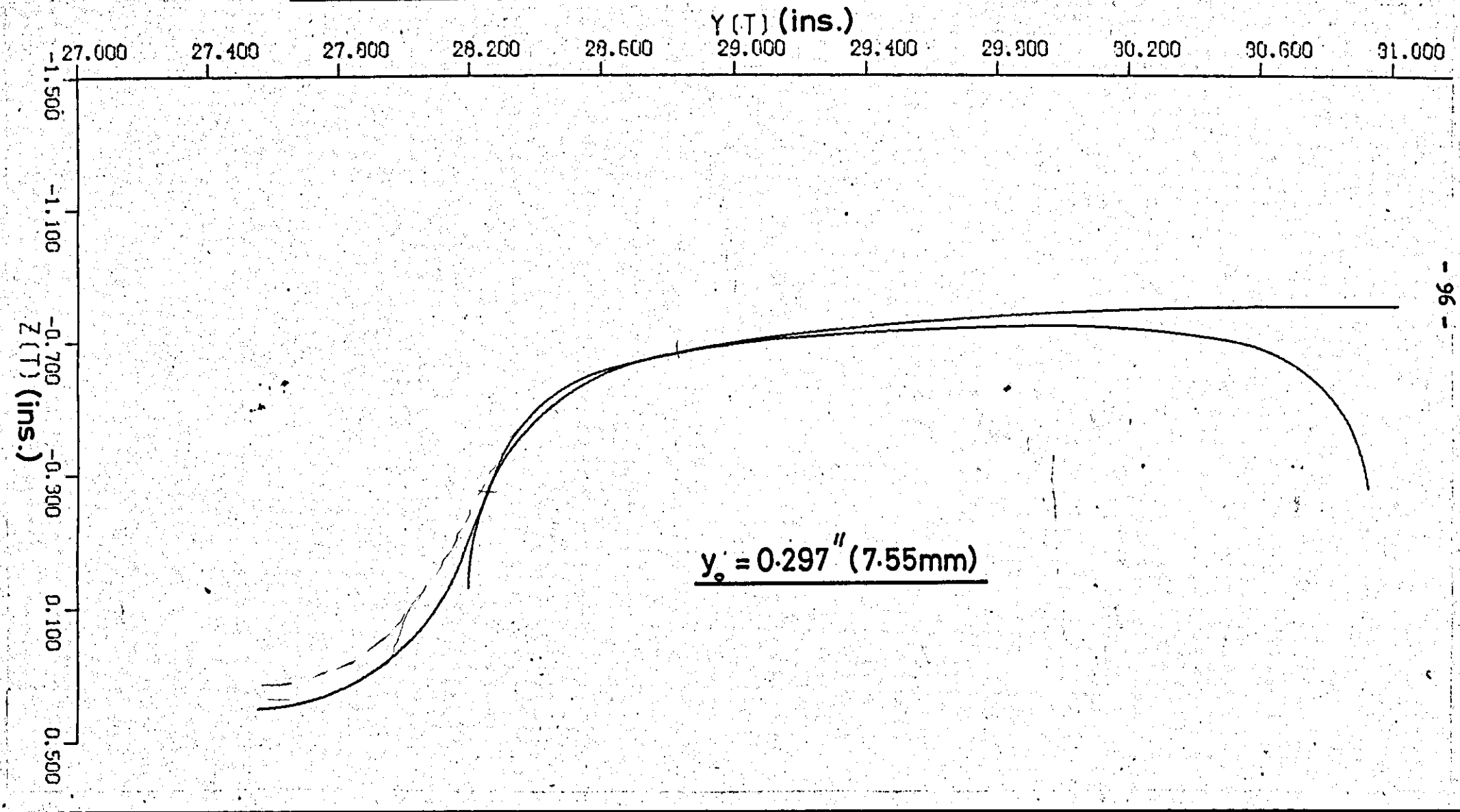

FIG.4.14Wheelset Displaced Laterally. Worn Rail. R.H. Side.

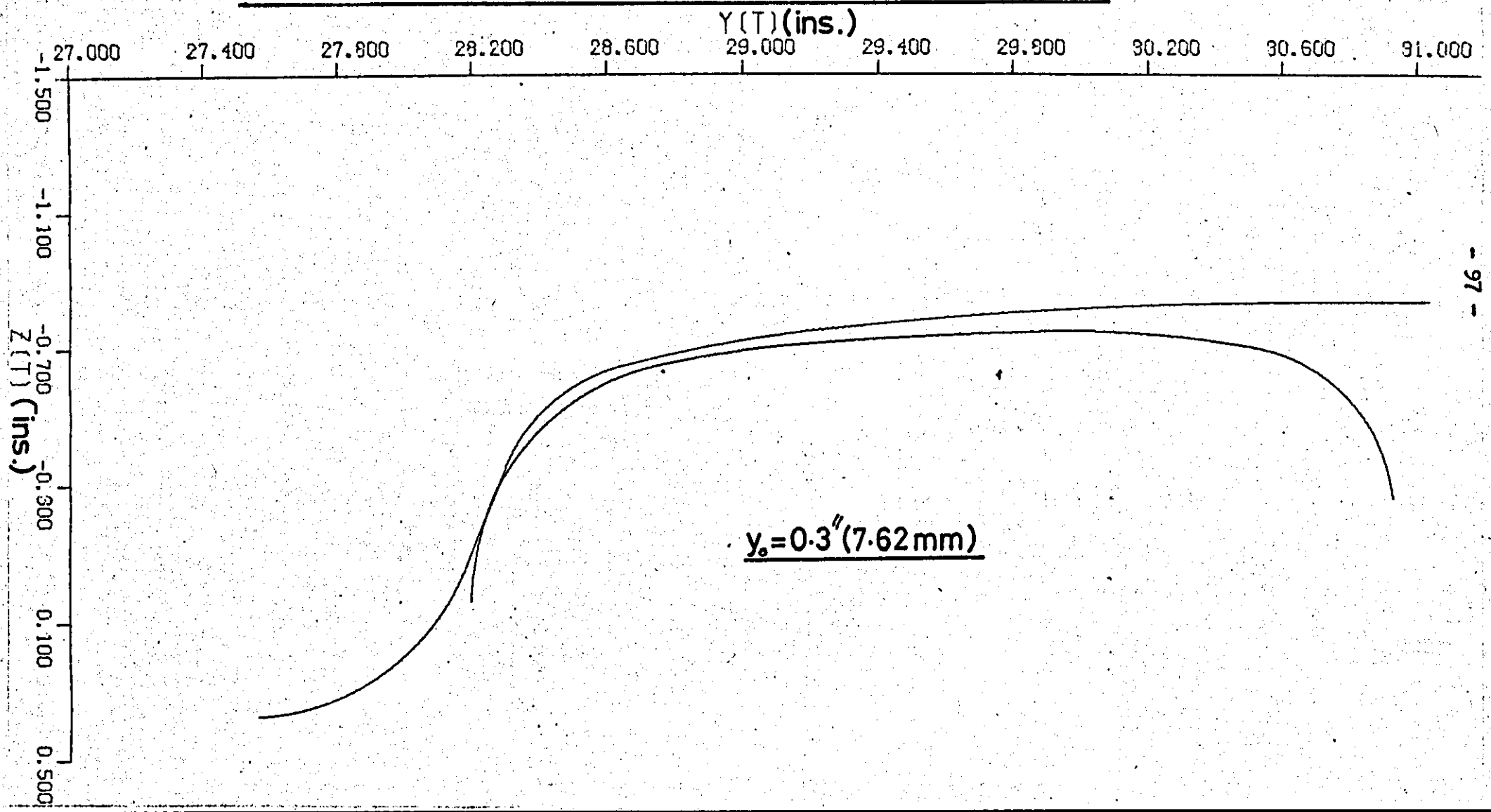

Substituting for x_w, y_w, z_w from equation 29 into equations 30 and 31 gives:

$$y_t^2 + x_t^2 + z_t^2 + 2a x_t \sin\psi - 2a y_t \cos\psi + 2z_t(H-h) + a^2 + b^2 + (H-h)^2 \pm 2b\sqrt{X} = r^2 \quad (32)$$

where $X = x_t^2 \cos^2\psi + 2x_t y_t \cos\psi \sin\psi + y_t^2 \sin^2\psi + z_t^2 + 2z_t(H-h) + (H-h)^2$

The slopes can be found by differentiating equation 32 giving:

$$\frac{\partial z_t}{\partial y_t} = \frac{-y_t + a\cos\psi \mp b(X)^{-\frac{1}{2}}(x_t \cos\psi \sin\psi + y_t \sin^2\psi)}{z_t + (H-h) \pm b(X)^{-\frac{1}{2}}(z_t + H - h)} \quad (33)$$

and

$$\frac{\partial y_t}{\partial x_t} = \frac{-x_t - a\sin\psi \mp b(X)^{-\frac{1}{2}}(x_t \cos^2\psi + y_t \cos\psi \sin\psi)}{y_t - a\cos\psi \pm b(X)^{-\frac{1}{2}}(x_t \cos\psi \sin\psi + y_t \sin^2\psi)} \quad (34)$$

(The third slope may be found from these two if required)

For straight sections of the tyre profile, according to equations 7 and 8

$$R^1 = m\, y_w + o \quad (35)$$

$$R^{1/2} = x_w^2 + z_w^2 \quad (36)$$

Substituting for x_w, y_w, z_w from equation 29 into equations 35 and 36

$$x_t^2(\cos^2\psi - m^2\sin^2\psi) + y_t^2(\sin^2\psi - m^2\cos^2\psi) + z_t^2 + 2x_t y_t \cos\psi\sin\psi(1+m^2) + 2mc\,x_t\sin\psi - 2mc\,y_t\cos\psi + 2z_t(H-h) + (H-h)^2 - c^2 = 0 \quad (37)$$

The slopes can be found by differentiating equation 37 giving:

$$\frac{\partial z_t}{\partial y_t} = \frac{-y_t(\sin^2\psi - m^2\cos^2\psi) - y_t\cos\psi\sin\psi(1+m^2) + mc\cos\psi}{z_t + H - h} \quad (38)$$

and

$$\frac{\partial y_t}{\partial x_t} = \frac{-x_t(\cos^2\psi - m^2\sin^2\psi) - y_t\cos\psi\sin\psi(1+m^2) - mc\sin\psi}{y_t(\sin^2\psi - m^2\cos^2\psi) + x_t\cos\psi\sin\psi(1+m^2) - mc\cos\psi} \quad (39)$$

The problem is to find (x_t, y_t, z_t) at the point of contact between rail and wheel using the above equations. A variable, h, has been introduced which is dependent on (x_t, y_t, z_t) making four unknowns to be found for a particular value of yaw angle, ψ. The four equations available for the solution of these parameters are listed below:

1. The rail equation (from equation 21)

$$(y_t - A)^2 + (z_t - B)^2 = R^2 \qquad (40)$$

2. The wheel equation (either equation 32 or equation 37)

Either $$y_t^2 + x_t^2 + z_t^2 + 2a x_t \sin\psi - 2a y_t \cos\psi + 2z_t(H-h) + a^2 + b^2 + (H-h)^2 \pm 2b\sqrt{X} = r^2$$

where $$X = x_t^2\cos^2\psi + 2x_t y_t \cos\psi\sin\psi + y_t^2\sin^2\psi + z_t^2 + 2z_t(H-h) + (H-h)^2 \qquad (41)$$

Or

$$x_t^2(\cos^2\psi - m^2\sin^2\psi) + y_t^2(\sin^2\psi - m^2\cos^2\psi) + z_t^2 + 2x_t y_t \cos\psi\sin\psi(1+m^2) + 2mc x_t \sin\psi - 2mc y_t \cos\psi + 2z_t(H-h) + (H-h)^2 - c^2 = 0$$

3. Equating rail and wheel slope, $\left(\frac{\partial z_t}{\partial y_t}\right)$ (from equation 22 and equation 33 or 38)

$$\frac{A - y_t}{z_t - B} = \frac{-y_t + a\cos\psi \mp b(X)^{-\frac{1}{2}}(x_t\cos\psi\sin\psi + y_t\sin^2\psi)}{z_t + (H-h) \pm b(X)^{-\frac{1}{2}}(z_t + H - h)}$$

or

$$\frac{-y_t(\sin^2\psi - m^2\cos^2\psi) - x_t\cos\psi\sin\psi(1+m^2) + mc\cos\psi}{z_t + H - h} \qquad (42)$$

4. Equating rail and wheel slope, $\left(\frac{\partial y_t}{\partial x_t}\right)$ (from equation 34 or 39)

$$0 = -x_t - a\sin\psi \mp b(X)^{-\frac{1}{2}}(x_t\cos^2\psi + y_t\cos\psi\sin\psi)$$

(43)

or $$-x_t(\cos^2\psi - m^2\sin^2\psi) - y_t\cos\psi\sin\psi(1+m^2) - mc\sin\psi$$

A computer program has been written, called YAWING WHEELSET, which solves these equations and calculates the values of (x_t, y_t, z_t) and h for a given angle of yaw. Since the wheel equations are different depending on whether the contact point lies on a circular arc, or a straight section of the profile, separate subroutines have been written to solve the equations for these cases. For circular arcs the subroutine is called CIRCLE2 and for straight sections it is called STRGHT2. The main program is based on the following method: A value of z_t is assumed, (z_{t_0} = -19 mm), which is increased in steps. The corresponding value of y_t is calculated from the rail equation 40 and knowing these two values, the slope of the rail ($\partial z_t / \partial y_t$) can be calculated. The same values are

used in the wheel equations and the slope ($\partial z_t / \partial y_t$) of the wheel found using the appropriate equations for one of the wheel sections. If the two values for ($\partial z_t / \partial y_t$) are within a certain pre-set limit, then the program iterates over this value of z_t in very small steps, until a point is found where the slopes are equal. If the slopes do not match for any value of z_t then the next tyre section is investigated. The point where the slopes are equal is assumed to be the contact point and the values of x_t, y_t and h are printed out.

Although this program was only used in the present investigation to calculate contact points with a British Rail RD4 tyre profile, it could be adapted, without too much difficulty, to give contact points for any "worn" measured profile, providing it could be divided into a series of circular arcs and straight lines.

The program was used to find contact points between rail and wheel for a range of yaw angles from 0° to 3°. Results are given in Table 4.5 for "standard" and "worn" rail profiles with an RD4 tyre profile.

4.4.4 Wheelset Moved Laterally and Yawed

In the previous two sections methods were described for finding the contact point when the wheelset is displaced by an amount y_o, or yawed through an angle ψ. The completely general case of arbitrary yawing plus arbitrary lateral displacement would be very complicated to solve and does not have much practical significance in the present context. To railway engineers derailment of a wheelset is considered to begin when it is shifted laterally

Table 4.5 Coordinates of Contact Points. Wheelset Yawed. Right Hand Side

All dimensions in mm

ψ°	STANDARD RAIL				WORN RAIL			
	x_t	y_t	z_t	h	x_t	y_t	z_t	h
0	0	739.83	-18.015	0	0	739.83	-18.015	0
.1	- 1.2319	739.83	-18.015	0.004674	-1.2309	739.83	-18.015	-0.019431
.3	- 3.6932	739.83	-18.015	0.006604	-3.6932	739.83	-18.015	-0.019380
.5	- 6.1544	739.83	-18.015	0.007874	-6.1544	739.83	-18.015	-0.01763
1.0	-12.3114	739.85	-18.016	0.015316	-12.3139	739.84	-18.015	-0.01026
2.0	-24.651	739.93	-18.024	0.06614	-24.6532	739.92	-18.024	-0.03665
3.0	-37.041	740.10	-18.039	0.09370	-37.046	740.10	-18.039	-0.06825

so that the flange of the wheel just touches the rail, and in this position three contact points exist between the wheelset and the track. This Section describes a method which enables the coordinates of these three contact points to be found for a wheelset yawed through an angle ψ, and then moved laterally by an amount y_o until the flange just touches the rail.

It is possible to set up equations at each of the contact points, but the idea of reducing the variables to solve these equations analytically was abandoned when it was realised there were eleven unknowns in the system. These are $(x, y, z)_t$ for each of the three contact points, together with the roll angle and the vertical movement of the wheelset in being displaced. Instead of this, a numerical method is employed which is divided into two distinct parts, the first finding the contact points approximately and the second iterating on these approximate values to converge on a solution.

The approximate contact points are found by yawing the wheelset by the required amount and using the method described in Section 4.4.3 to find the contact points on the tread. The flange contact is assumed to be at the point where the distance between the wheelset in the yawed position and the rail is a minimum. These contact points are only approximate since the wheelset rolls and moves vertically as it is displaced laterally from the yawed position, and both the tread and flange contact points will change.

A basically similar method was used by Johansen, Ref.40, who found the flange contact point graphically, by yawing the wheelset and then drawing wheel sections in vertical planes at different values of x_t. This involved drawing projections of the

basic tyre and rail profiles. The minimum lateral distance between each section and the rail profile was then measured, and the minimum of all these was assumed to be the lateral displacement needed for the flange to touch the rail. The position of the flange contact point was assumed to coincide with this minimum point. In order to achieve any accuracy using this method the drawings had to be very large, and Johansen claims to have worked some of them 16 x full size, and even then only guarantees 5% accuracy. This does not include the errors involved when the wheelset is then displaced laterally by the calculated amount, since the accompanying roll and vertical movement are not accounted for.

In the present investigation the approximate contact points are calculated on a digital computer using the method described earlier. The program given in Section 4.4.3, called YAWING WHEELSET, calculates the tread contact points and also sets up the three dimensional equations for the yawed wheelset in Track Axes. Having found these it is a small step to calculate, firstly, the wheel profile for any value of x_t, and secondly, the minimum distance between wheel and rail for each profile. The flange contact point is assumed to lie at the value of x_t where this distance is a minimum.

A subroutine, called JOHANSEN, has been written based on this method and when used in conjunction with YAWING WHEELSET gives the coordinates of the approximate contact points.

Another program has been written, called ACCURATE, which then uses these points and iterates to find more accurate values for the coordinates of the contact points. This program requires as input data the approximate (x_t, y_t, z_t)coordinates of each of the three contact points together with estimated values of y_o, z_o and θ_o. The wheelset is assumed to be displaced towards the right

hand rail with contact point A on the left hand tread, contact point B on the right hand tread and contact point C on the right hand flange. A grid of values (x_{t_o}, y_{t_o}) is set up at each of the approximate contact points. Since the wheelset is yawed through an angle ψ the transformation given by equation 29 can be used to find the equivalent values of (x_w, y_w) for the grid points

This is

$$\left.\begin{aligned} x_w &= x_{t_o}\cos\psi + y_{t_o}\sin\psi \\ y_w &= -x_{t_o}\sin\psi + y_{t_o}\cos\psi \end{aligned}\right\} \qquad (44)$$

Knowing the values of (x_w, y_w) on the wheel, the corresponding value of z_w can be found using the appropriate wheel equations:

$$\left.\begin{aligned} &(y_w-a)^2 + (R'-b)^2 = r^2 \\ \text{or}\quad &R' = m y_w + c \\ \text{where}\quad &R'^2 = x_w^2 + z_w^2 \end{aligned}\right\} \qquad (45)$$

The corresponding value of x_{t_o} can then be calculated at each grid point since $z_w = z_{t_o} + H - h$ (from equation 29) (46)

If the wheelset is then displaced laterally by an amount y_o, vertically by z_o and rolled through an angle θ_o, the coordinates of the grid points become

$$\left.\begin{aligned} x_t &= x_{t_o} \\ y_t &= y_{t_o}\cos\theta_o + z_{t_o}\sin\theta_o + y_o \\ z_t &= z_{t_o}\cos\theta_o - y_{t_o}\sin\theta_o + z_o - H + h \end{aligned}\right\} \qquad (47)$$

The next part of the program considers each contact point in turn. Firstly the wheelset is shifted laterally until the flange just touches the rail, i.e. y_o is varied until contact point C just touches the rail. Secondly, the wheelset is raised vertically until contact point B just touches the rail, i.e. z_o is varied and finally the wheelset is rolled about contact B until the left hand tread just touches the rail at A. In rolling the wheelset about this point, the centre of the wheelset goes through vertical and

horizontal displacements, and therefore new values are obtained for (y_o, z_o, θ_o).

This process is repeated until the vertical distance between wheel and rail at points A, B and C is less then 25×10^{-7} mm. The program then stops and prints out the solution for the contact points together with values of y_o, z_o and θ_o.

This program worked well and values of y_o, z_o, θ_o, x_t y_t, z_t are plotted against ψ in Figs. 4.15 to 4.20 using a 'standard' rail. The actual tyre and rail profiles are shown in Fig. 4.21 and Fig. 22 for $\psi = 1^\circ$ and in Figs. 4.23 and 4.24 for $\psi = 3^\circ$.

4.5 Contact Ellipses

According to the theory of Hertz when two bodies of revolution are pressed together the area of contact formed between them is elliptical in shape. The wheel and rail may be considered as bodies of revolution, and before the forces can be calculated at the contact points, the creepages and the size of the contact ellipse have to be found. The complete analysis for the contact ellipse is given in Love, Ref. 1, and Timoshenko and Goodier, Ref. 2. The theory used for calculating the contact ellipse is given in Appendix 9 where it can be seen that the actual size of the contact ellipse depends on the radii of the bodies and the normal force, but the shape of the ellipse i.e. the ratio of the semiaxes (a/b), depends only on the radii.

A program has been written, called CONTACT, based on the theory of Appendix 9, which calculates the principal radii of curvature at the contact points, the angle between them, the constants A and B and the angle θ. This program requires as input data: ψ, y_o, z_o, θ_o plus the

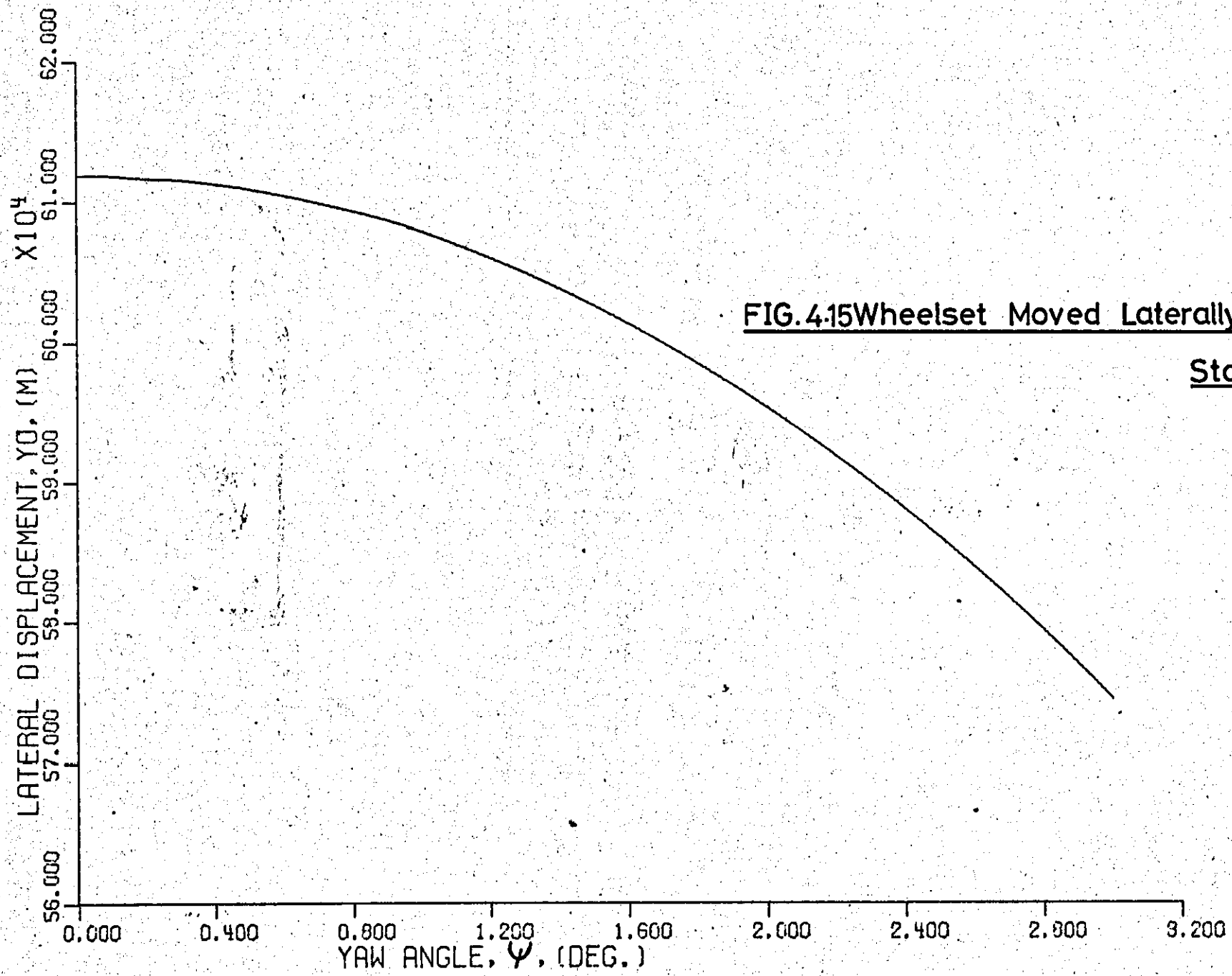

FIG. 4.15 Wheelset Moved Laterally and Yawed.

Standard Rail

y_o v ψ

FIG.4.16 Wheelset Moved Laterally and Yawed. Standard Rail.

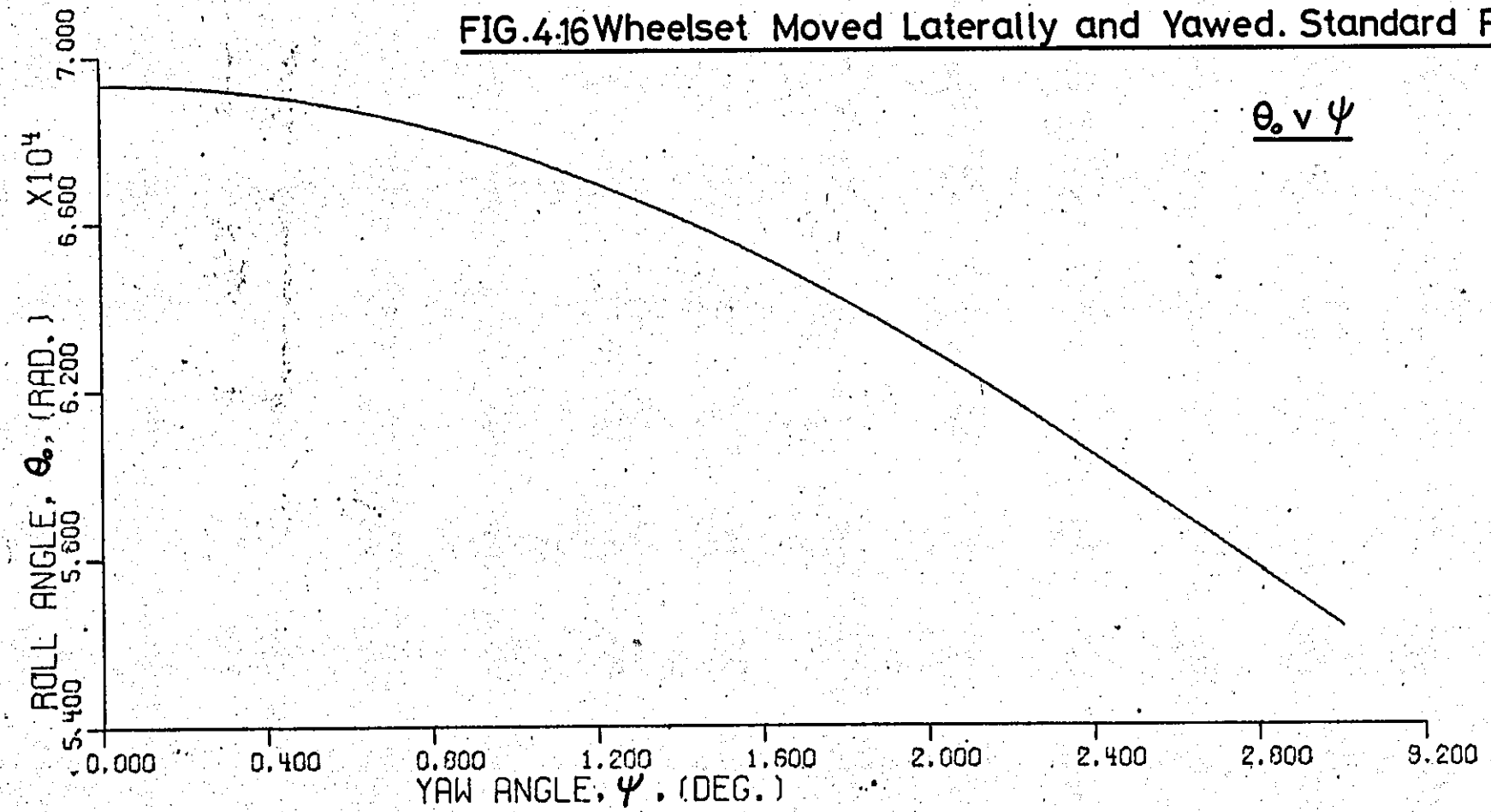

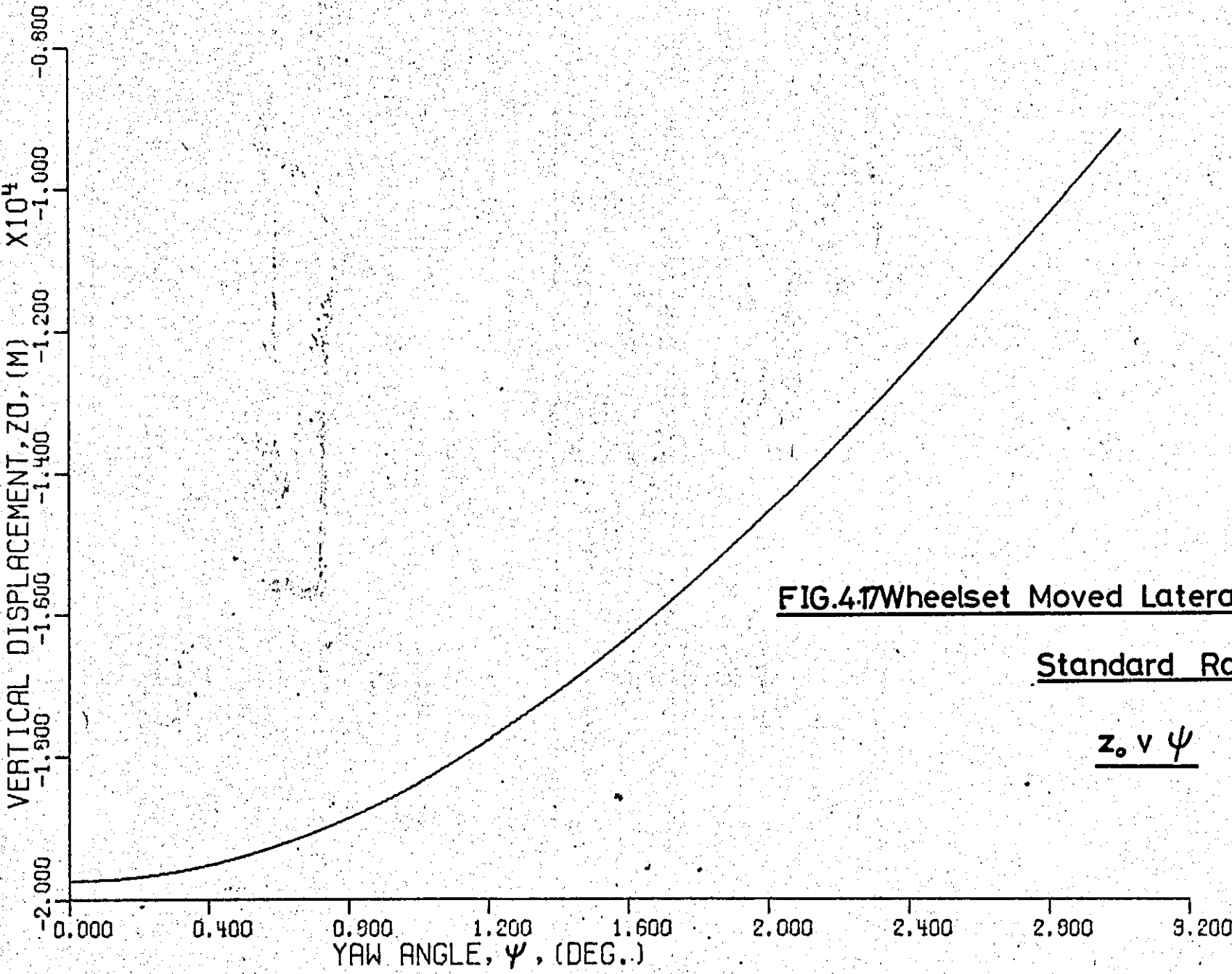

FIG.4.17 Wheelset Moved Laterally and Yawed

Standard Rail

z_o v ψ

FIG.4.18 Wheelset Moved Laterally and Yawed. Standard Rail

x_t v ψ, for contact points A, B & C

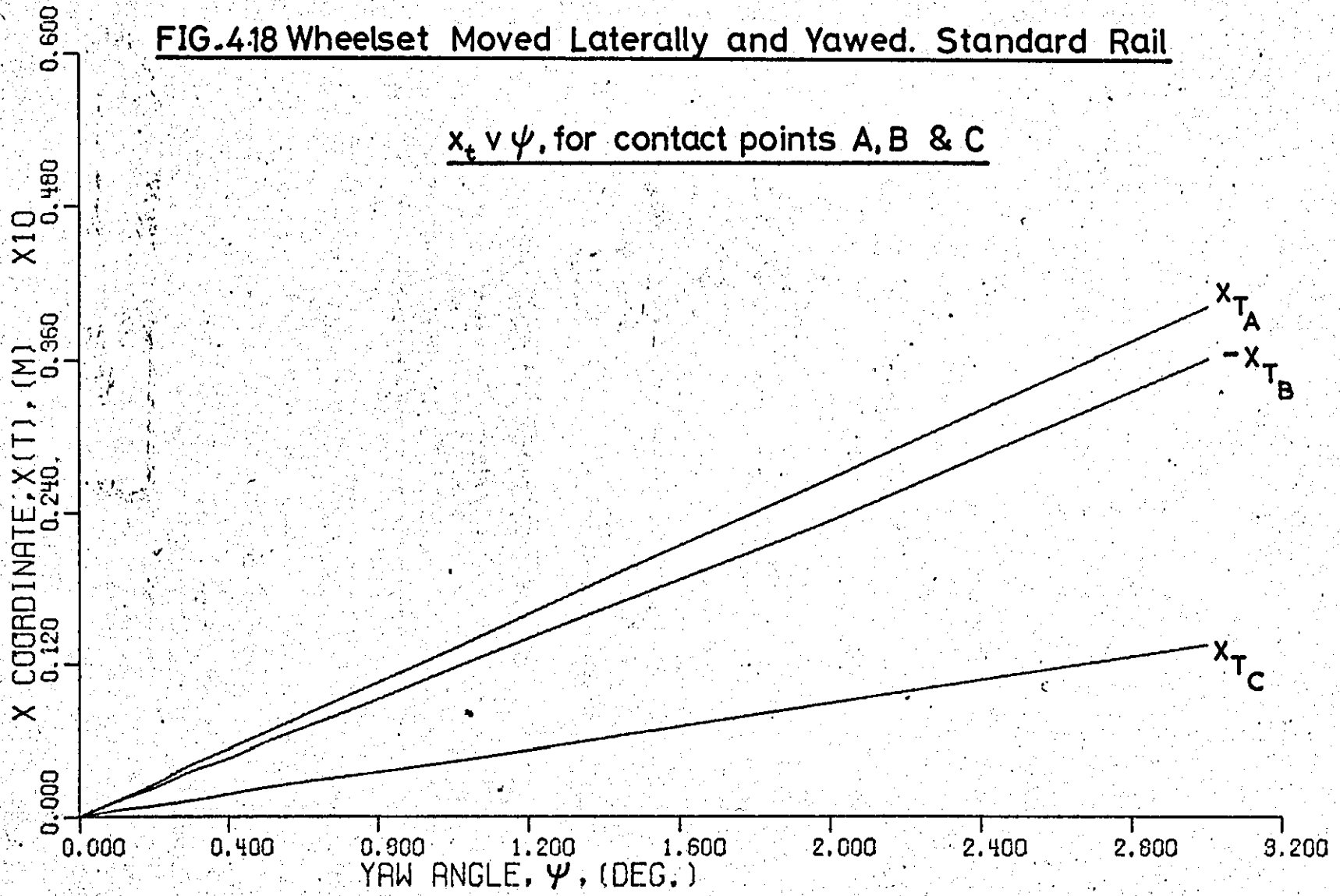

FIG.419 Wheelset Moved Laterally and Yawed. Standard Rail.

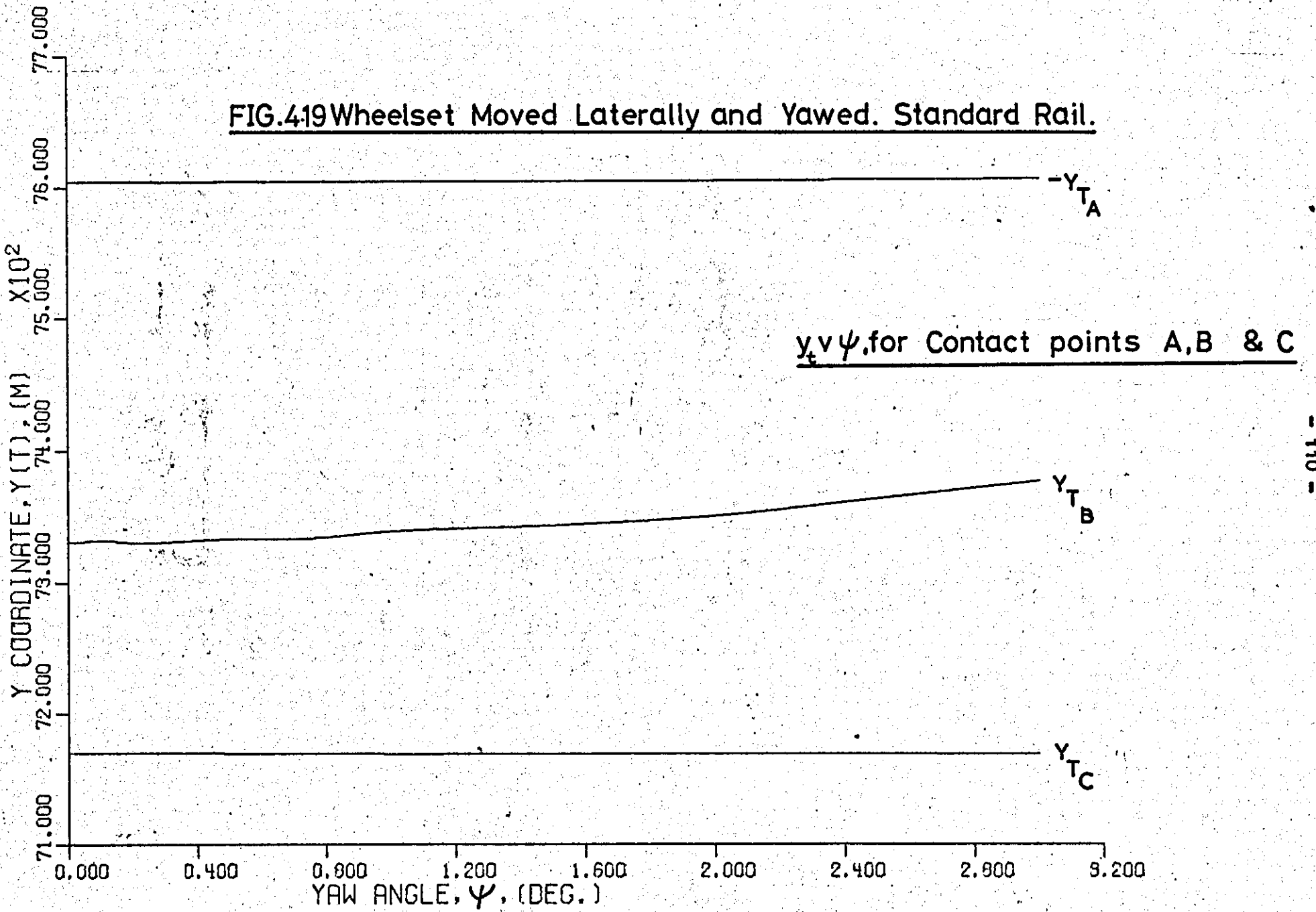

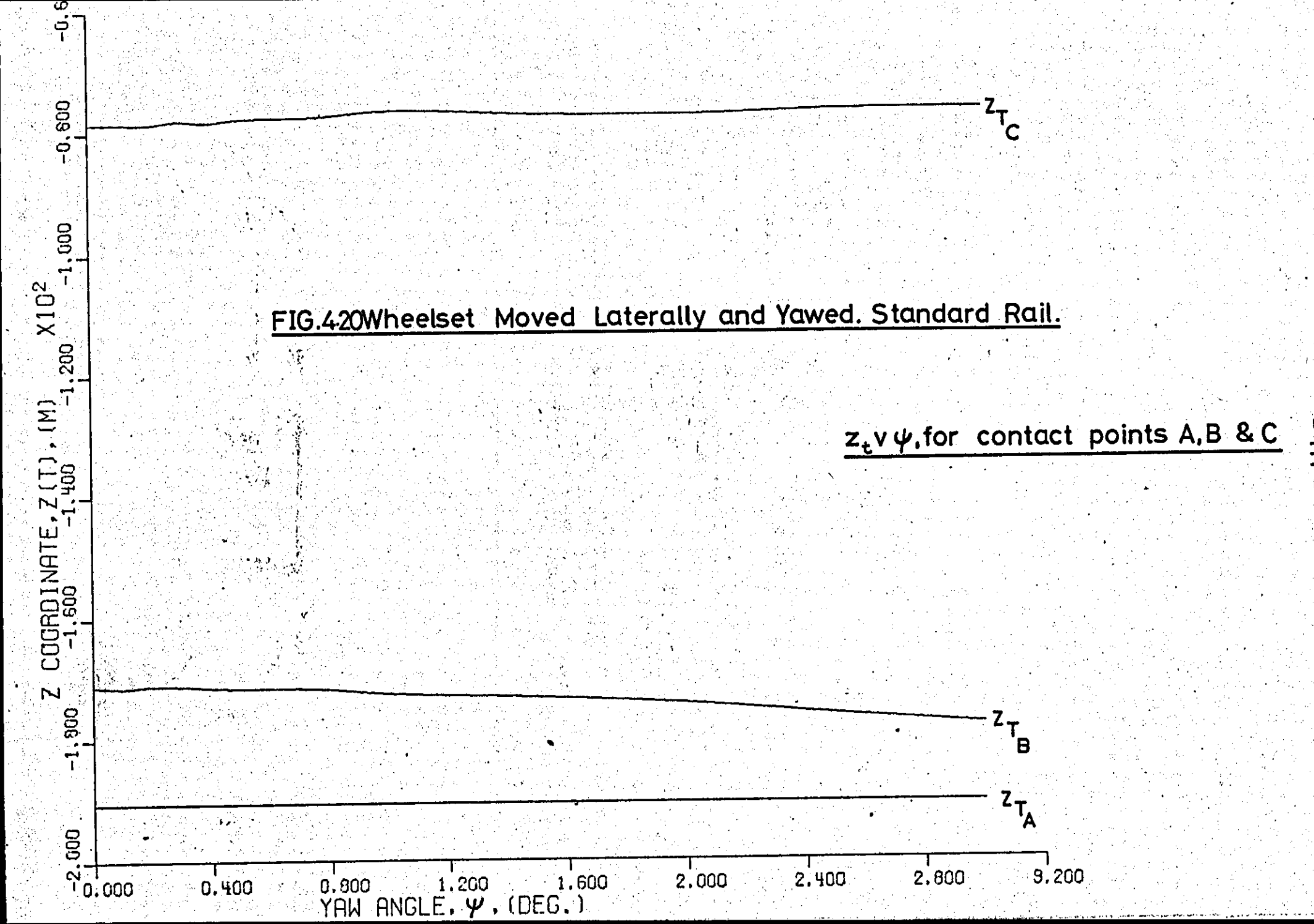

FIG.4.20Wheelset Moved Laterally and Yawed. Standard Rail.

z_t v ψ, for contact points A, B & C

FIG.4.21 Wheelset Displaced Laterally and Yawed. Standard Rail.

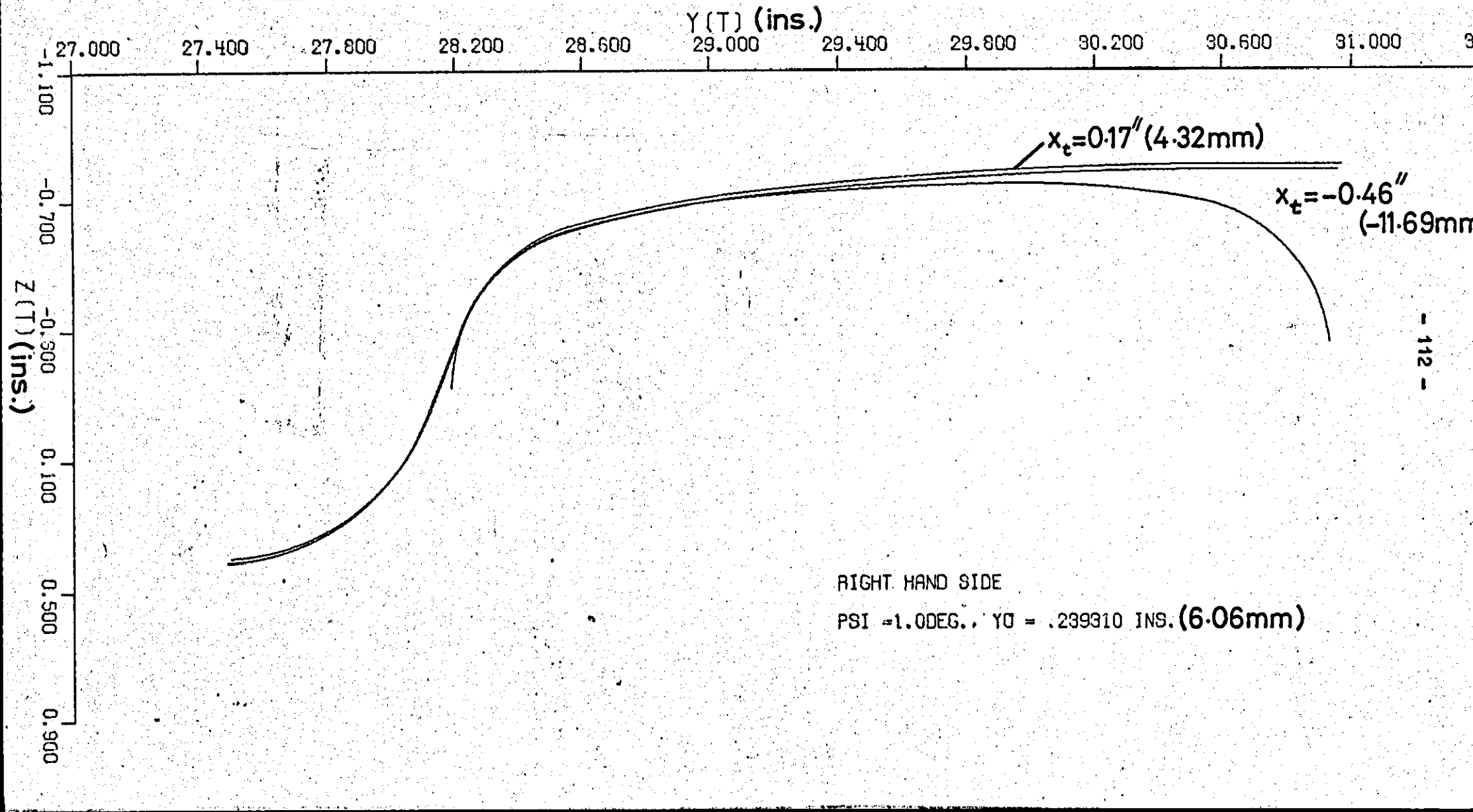

FIG.4.22 Wheelset Displaced Laterally and Yawed. Standard Rail.

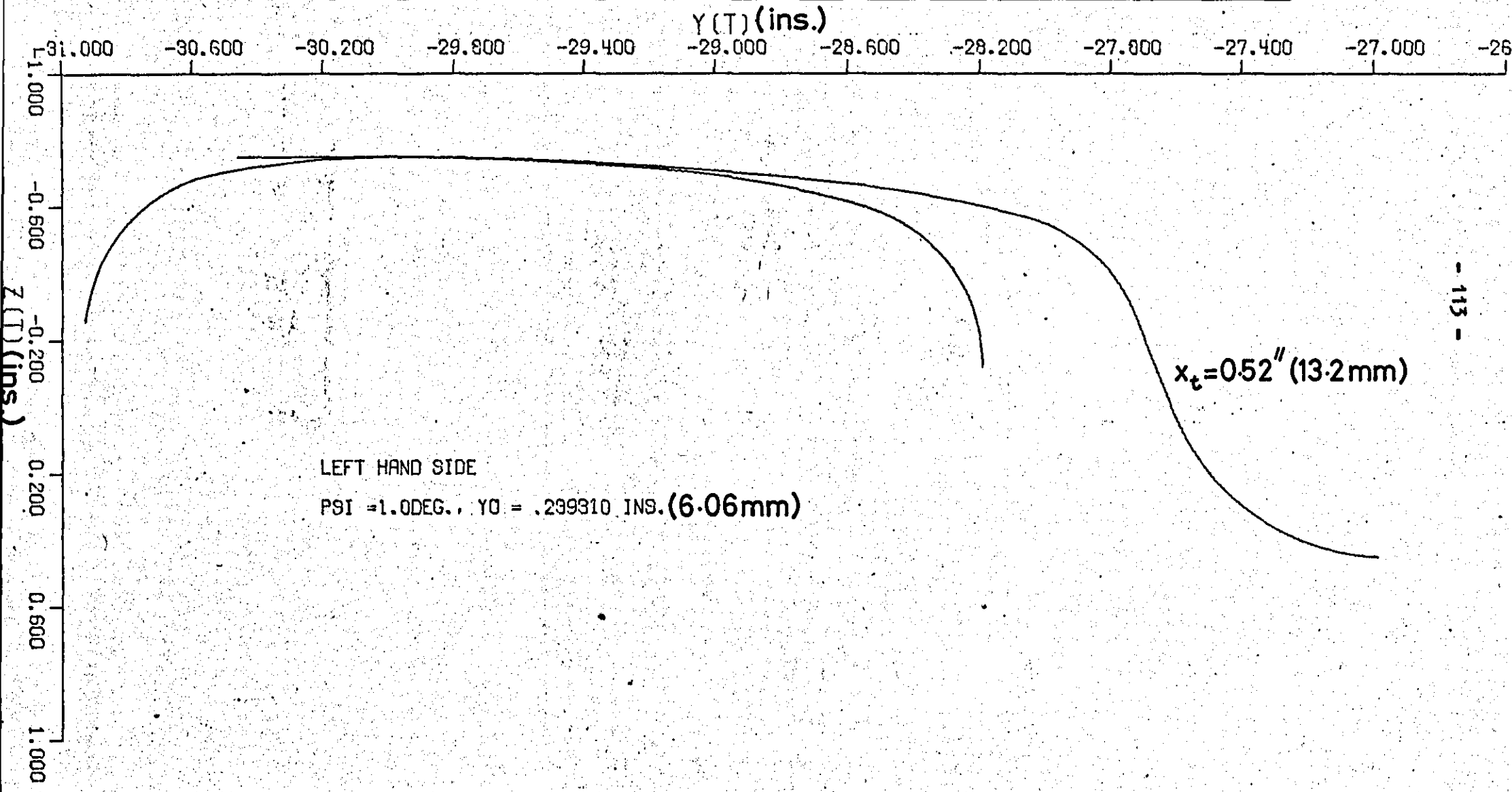

FIG.423 Wheelset Displaced Laterally and Yawed. Standard Rail.

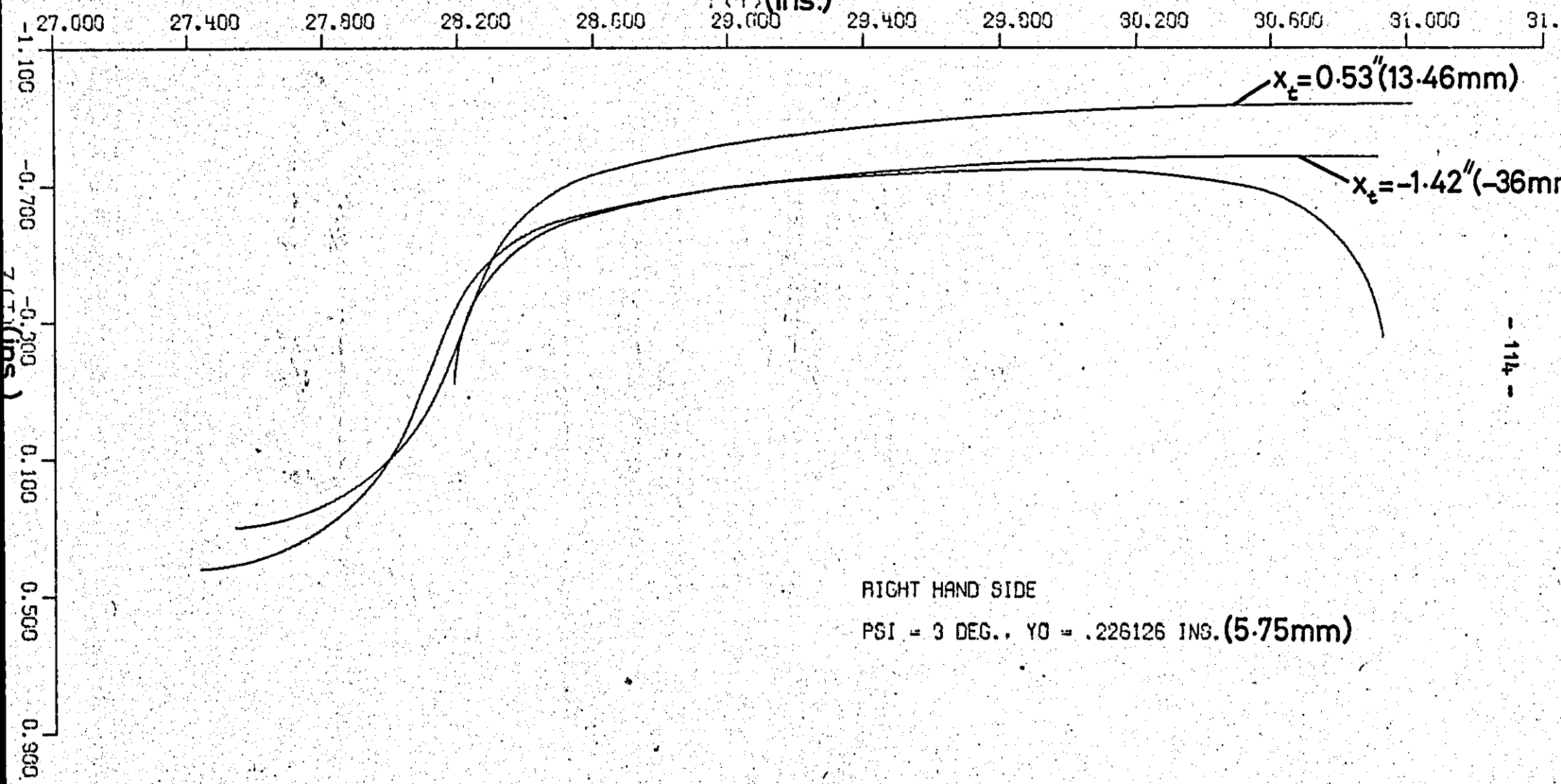

FIG.4.24 Wheelset Displaced Laterally and Yawed. Standard Rail.

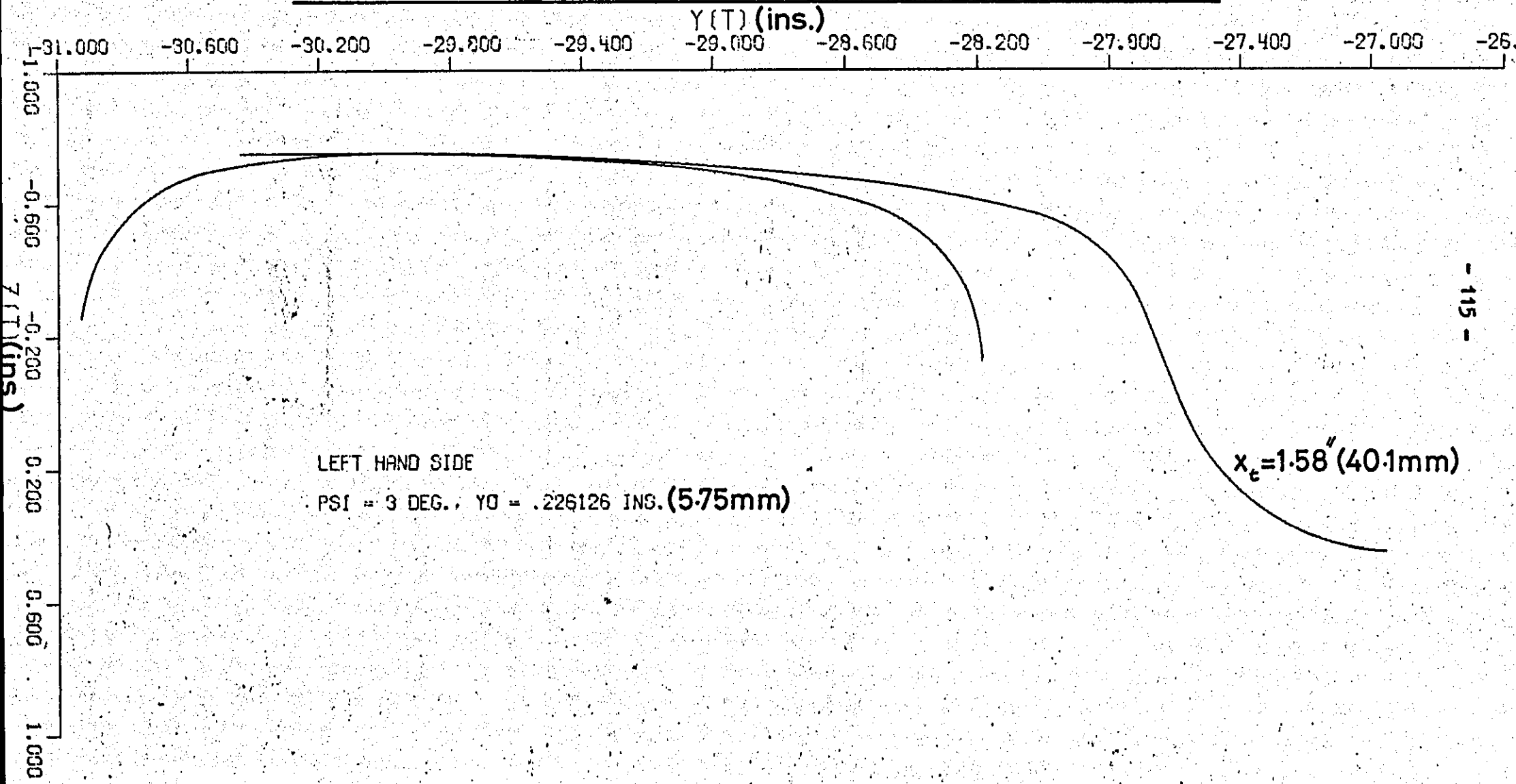

coordinates of the contact points in Track Axes.

In calculating the angle between principal radii, the equations of the planes containing these radii are found from the coordinates of 3 points in the plane. The theory for this and for subsequently finding the angle is given in Appendix 6.

Since the tyre and rail profiles are made up of various circular arcs, the ratio of contact ellipse semiaxes, (a/b), varies depending on the position of the contact point. Although the arcs blend in to each other and therefore the slopes at the crossover points match, there are discrete radii changes and therefore discrete changes in (a/b) ratio. Generally it may be said that for tread contact points the contact ellipses are near circular while for flange contact points they are very elongated in the rolling direction. Fig. 4.25 shows how the (a/b) ratio changes as the wheelset is displaced laterally.

4.6 Creepages and Spin

The wheelset is assumed to be rolling freely along perfectly straight track in a displaced position, at a constant velocity, V, and with an angular velocity, $\dot{\Phi}$. It is yawed through an angle, ψ , and displaced laterally by an amount, y_o, from its central position. There can be two or three points of contact between wheelset and track, as shown in Fig. 4.26, where axes 1 and 2 are defined in the plane of the contact area and axis 3 normal to it. In deriving expressions for the creepages, both the yaw angle and lateral displacement are assumed constant i.e. there are no $\dot{\psi}$ and $\dot{y}_o$ terms included.

A simplified plan view of the wheelset is shown in Fig. 4.27. At contact point A, the velocity of the contact ellipse around the wheel

FIG.4.25 Variation of $\frac{a}{b}$ Ratio as Wheelset is Displaced Laterally

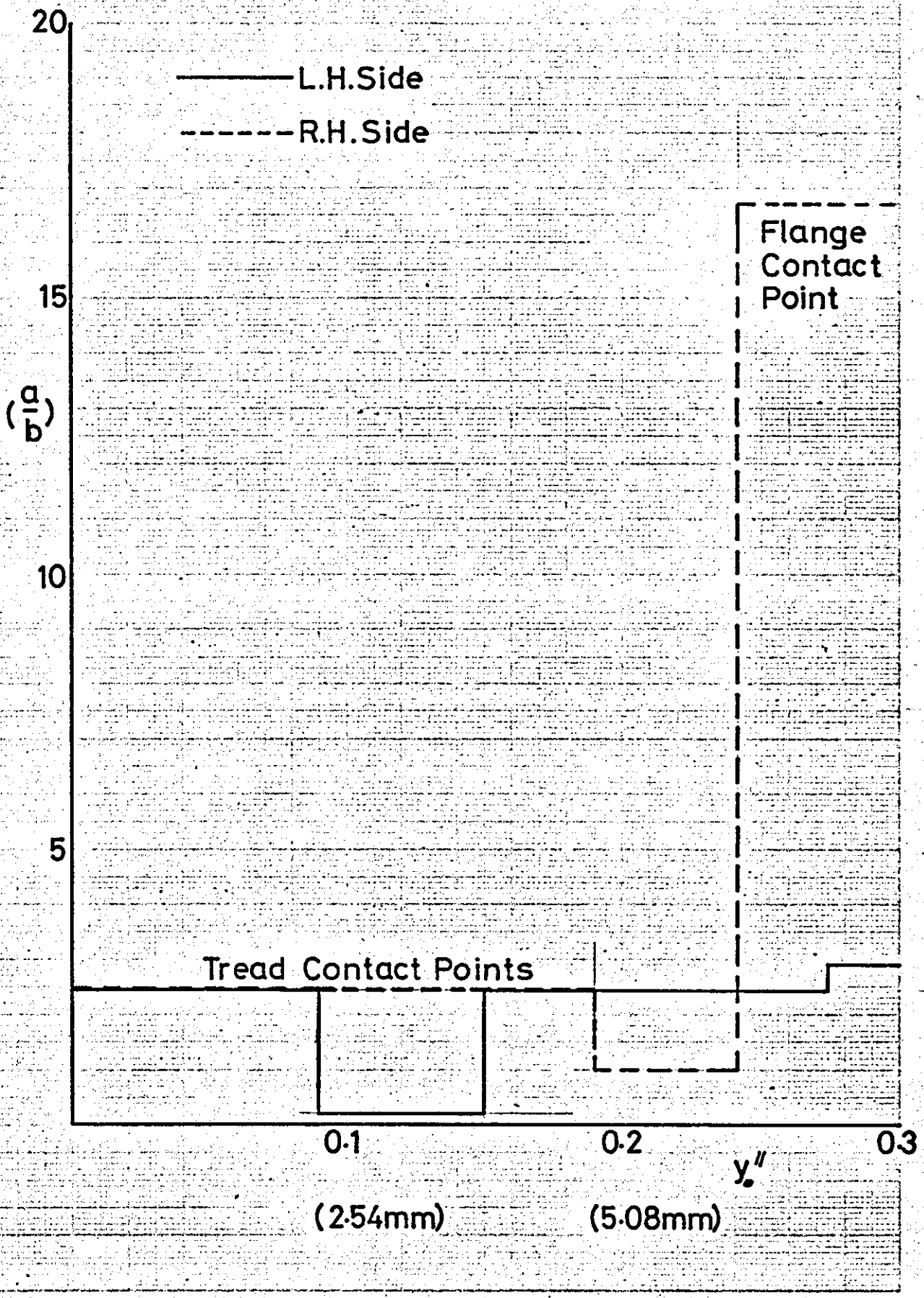

FIG.4.26 Contact Area Axes

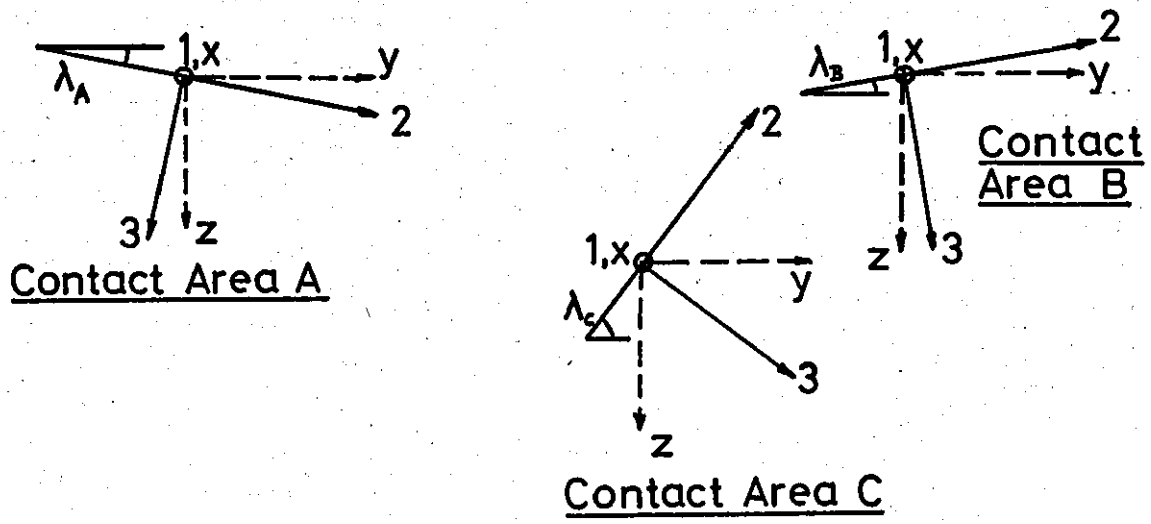

FIG.4.27 Plan View of Wheelset

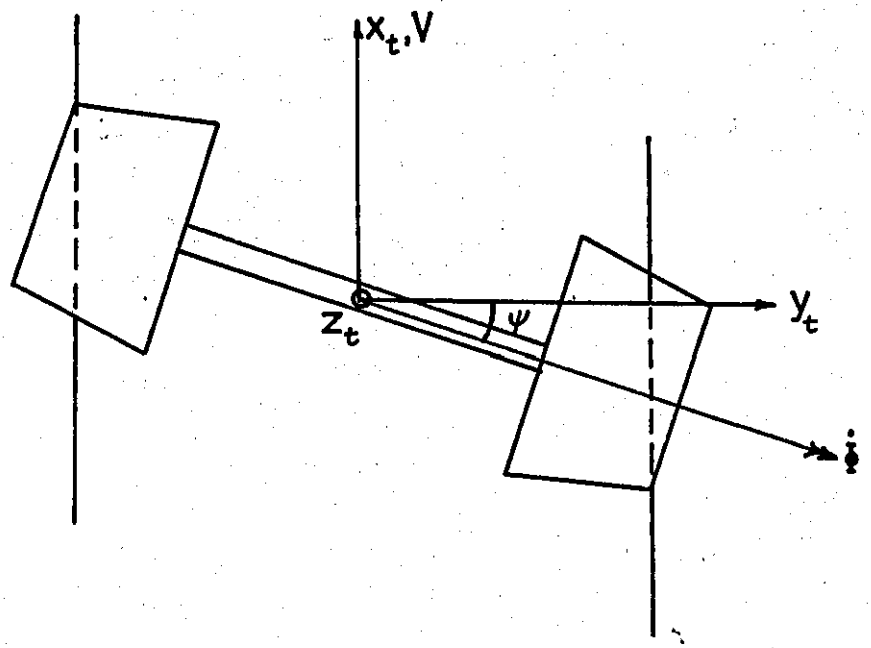

in direction 1 $= -\dot{\Phi} r_A \cos\psi = V_{1_A}'$

and similarly at contact points B and C

$$\left.\begin{aligned} V_{1_B}' &= -\dot{\Phi} r_B \cos\psi \\ V_{1_C}' &= -\dot{\Phi} r_C \cos\psi \end{aligned}\right\} \quad (48)$$

The velocity of the contact ellipses around the wheel in direction 2 are:

$$\left.\begin{aligned} V_{2_A}' &= -\dot{\Phi} r_A \sin\psi \cos\lambda_A \\ V_{2_B}' &= -\dot{\Phi} r_B \sin\psi \cos\lambda_B \\ V_{2_C}' &= -\dot{\Phi} r_C \sin\psi \cos\lambda_C \end{aligned}\right\} \quad (49)$$

where r_A, r_B, r_C are the wheel radii at the points of contact.

The velocity of the contact ellipses along the rail in directions 1 are:

$$V_{1_A} = V_{1_B} = V_{1_C} = V \quad (50)$$

The velocity of the contact ellipses along the rail in direction 2 are:

$$V_{2_A} = V_{2_B} = V_{2_C} = 0 \quad (51)$$

The <u>longitudinal creepage</u> is defined as,

$$\gamma_1 = \frac{V_1 - V_1'}{\frac{1}{2}(V_1 + V_1')} \quad (52)$$

The <u>lateral creepage</u> is defined as,

$$\gamma_2 = \frac{V_2 - V_2'}{\frac{1}{2}(V_1 + V_1')} \quad (53)$$

and substituting from equations 48, 49, 50 and 51 into equations 52 and 53 the creepages for each contact point become:

$$\gamma_{1_A} = \frac{V + \dot{\Phi} r_A \cos\psi}{\frac{1}{2}(V - \dot{\Phi} r_A \cos\psi)} \qquad \gamma_{2_A} = \frac{\dot{\Phi} r_A \sin\psi \cos\lambda_A}{\frac{1}{2}(V - \dot{\Phi} r_A \cos\psi)}$$

$$\gamma_{1_B} = \frac{V + \dot{\Phi} r_B \cos\psi}{\frac{1}{2}(V - \dot{\Phi} r_B \cos\psi)} \quad (54) \qquad \gamma_{2_B} = \frac{\dot{\Phi} r_B \sin\psi \cos\lambda_B}{\frac{1}{2}(V - \dot{\Phi} r_B \cos\psi)} \quad (55)$$

$$\gamma_{1_C} = \frac{V + \dot{\Phi} r_C \cos\psi}{\frac{1}{2}(V - \dot{\Phi} r_C \cos\psi)} \qquad \gamma_{2_C} = \frac{\dot{\Phi} r_C \sin\psi \cos\lambda_C}{\frac{1}{2}(V - \dot{\Phi} r_C \cos\psi)}$$

(it can be seen from equations 55 that when $\psi = 0$, the lateral creepages are also zero).

If Ω_3 and Ω'_3 are the angular velocities of spin of the rail and wheel respectively, about axis (3) then:

$$\Omega_{3_A} = \Omega_{3_B} = \Omega_{3_C} = 0 \tag{56}$$

$$\left.\begin{aligned} \Omega'_{3_A} &= -\dot{\Phi}\cos\psi\sin\lambda_A \\ \Omega'_{3_B} &= \dot{\Phi}\cos\psi\sin\lambda_B \\ \Omega'_{3_C} &= \dot{\Phi}\cos\psi\sin\lambda_C \end{aligned}\right\} \tag{57}$$

The <u>spin</u> is defined as, $\omega_3 = \dfrac{\Omega'_3 - \Omega_3}{\frac{1}{2}(V_1 + V_1')}$ (58)

and substituting from equations 56 and 57 into 58, the spin at each contact point becomes

$$\left.\begin{aligned} \omega_{3_A} &= \frac{-\dot{\Phi}\cos\psi\sin\lambda_A}{\frac{1}{2}(V - \dot{\Phi} r_A\cos\psi)} \\ \omega_{3_B} &= \frac{\dot{\Phi}\cos\psi\sin\lambda_B}{\frac{1}{2}(V - \dot{\Phi} r_B\cos\psi)} \\ \omega_{3_C} &= \frac{\dot{\Phi}\cos\psi\sin\lambda_C}{\frac{1}{2}(V - \dot{\Phi} r_C\cos\psi)} \end{aligned}\right\} \tag{59}$$

According to these definitions, the longitudinal and lateral creepage are non-dimensional while the spin has dimensions $(\text{length})^{-1}$.

In the present investigation non-dimensional creepage and spin parameters are used. These are defined as

$$\xi = \frac{\gamma_1 \ell}{\mu c}, \qquad \eta = \frac{\gamma_2 \ell}{\mu c}, \qquad \chi = \frac{\omega_3 \ell}{\mu} \tag{60}$$

where ℓ = characteristic length = $1 / \frac{1}{2}(A + B)$ (from Section 4.5)

μ = coefficient of friction

$c = \sqrt{ab}$ = geometric mean of contact ellipse semiaxes.

It can be seen that, according to the above equations, the creepage and spin at the contact points are calculated from the velocities V and $\dot{\Phi}$, the cone angle λ and wheel radius r. The contact area

forces can be calculated from the creepages using the theories described in Section 3. A program to calculate the total forces on the wheelset is described in the next Section, and in this program the creepages are calculated as an intermediate step using equations 54, 55, 59 and 60.

4.7 Forces

The contact area forces T_1 and T_2 are defined in the plane of the contact area; T_1 in the longitudinal direction and T_2 in the lateral direction. A moment M_3 is defined about an axis normal to the plane of the contact area. The moment and forces can be calculated from the creepages using any of the creep force theories described in Section 3.

The total forces and moments on the wheelset can be calculated by resolving and summing the appropriate contact area forces as follows:

$$\left.\begin{aligned} T_{x_A} &= T_{1_A} \\ T_{y_A} &= T_{2_A}\cos\lambda_A - T_{3_A}\sin\lambda_A \\ T_{z_A} &= T_{3_A}\cos\lambda_A + T_{2_A}\sin\lambda_A \\ M_{y_A} &= -M_{3_A}\sin\lambda_A \\ M_{z_A} &= M_{3_A}\cos\lambda_A \end{aligned}\right\} \qquad (61)$$

$$\left.\begin{aligned} T_{x_B} &= T_{1_B} \\ T_{y_B} &= T_{2_B}\cos\lambda_B + T_{3_B}\sin\lambda_B \\ T_{z_B} &= T_{3_B}\cos\lambda_B - T_{2_B}\sin\lambda_B \\ M_{y_B} &= M_{3_B}\sin\lambda_B \\ M_{z_B} &= M_{3_B}\cos\lambda_B \end{aligned}\right\} \qquad (62)$$

$$\left.\begin{aligned} T_{x_C} &= T_{1_C} \\ T_{y_C} &= T_{2_C}\cos\lambda_C + T_{3_C}\sin\lambda_C \\ T_{z_C} &= T_{3_C}\cos\lambda_C - T_{2_C}\sin\lambda_C \\ M_{y_C} &= M_{3_C}\sin\lambda_C \\ M_{z_C} &= M_{3_C}\cos\lambda_C \end{aligned}\right\} \qquad (63)$$

If the following non-dimensional force and moment parameters are defined as:

$$f_1 = \frac{T_1}{\mu T_3} \quad , \quad f_2 = \frac{T_2}{\mu T_3} \quad , \quad M_3 = \frac{M_3}{\mu T_3 c} \tag{64}$$

Then, by substitution into equations 61, 62 and 63, forces normal to the plane of the contact area may be written as

$$\left.\begin{aligned} T_{3_A} &= \frac{T_{z_A}}{\cos\lambda_A + \mu f_{2_A} \sin\lambda_A} \\ T_{3_B} &= \frac{T_{z_B}}{\cos\lambda_B + \mu f_{2_B} \sin\lambda_B} \\ T_{3_C} &= \frac{T_{z_C}}{\cos\lambda_C + \mu f_{2_C} \sin\lambda_C} \end{aligned}\right\} \tag{65}$$

It may be noted that in order to calculate T_3, the lateral force parameter, f_2, has first to be calculated. This is done by the appropriate creep/force theory, using the non-dimensional creep and spin parameters. However, in order to calculate these parameters, T_3 has first to be known.

An iterative procedure is used to calculate the normal force, T_3, which assumes as a first approximation that

$$T_3 = \frac{T_z}{\cos\lambda} \tag{66}$$

The total forces and moments on the wheelset, in Track Axes, are found by summing equations 61, 62 and 63 giving:

$$\begin{aligned} T_x &= T_{x_A} + T_{x_B} + T_{x_C} \\ T_y &= T_{y_A} + T_{y_B} + T_{y_C} \\ T_z &= T_{z_A} + T_{z_B} + T_{z_C} = -W \\ M_x &= -T_{y_A} r_A - T_{z_A} l_A - T_{y_B} r_B + T_{z_B} l_B - T_{y_C} r_C + T_{z_C} l_C \\ M_y &= M_{y_A} + M_{y_B} + M_{y_C} + T_{x_A} r_A + T_{x_B} r_B + T_{x_C} r_C - T_{z_A} x_A - T_{z_B} x_B - T_{z_C} x_C \\ M_z &= M_{z_A} + M_{z_B} + M_{z_C} + T_{x_A} l_A - T_{x_B} l_B - T_{x_C} l_C + T_{y_A} x_A + T_{y_B} x_B + T_{y_C} x_C \end{aligned} \tag{67}$$

where $r_A = z_A - z_o + H$, $r_B = z_B - z_o + H$, $r_C = z_C - z_o + H$

and $l_A = y_o - y_A$, $l_B = y_B - y_o$, $l_C = y_C - y_o$

(x, y, z) are the coordinates of the contact points in Track Axes.

A program, called FORCES, has been written which calculates the forces on a displaced wheelset for any weight distribution and speed. The required inputs are the coordinates of the contact points $(x_t, y_t, z_t)_A$, $(x_t, y_t, z_t)_B$, $(x_t, y_t, z_t)_C$, the vertical forces T_{z_A}, T_{z_B}, T_{z_C} and the forward velocity V. If one of the vertical forces is zero then it is assumed that the respective contact point just touches and does not contribute to the force system. In the program, an angular velocity, $\dot{\Phi}$, is assumed, the creep and spin parameters calculated, and from these, the non-dimensional force parameters found by using the required theory. Subroutines have been written for each of the creep/force theories mentioned in Section 3 and any one of these may be called in the main program since they all have the same format, and calculate the same force parameters. It is possible in the program to use one theory for one contact point and a different theory for another contact point. The total forces and moments are then found using equations 67. $\dot{\Phi}$ is varied until the total rolling moment of the wheelset is zero, i.e. the moment about the wheel bearings, M_{y_w}, is zero. This may involve several iterations of the complete program but when this condition is reached, the velocity, creepages and forces are printed out.

This program was used to calculate all the results given in Sections 5, 6 and 7.

5. Comparison of Theories

5.1 Introduction

From the literature survey on rolling contact theories, Section 2, it was obvious that very few of them were adaptable enough to calculate the forces on a railway wheelset, most were very limited in application. The theories that were suitable have been described in more detail in Section 3. Two of these were limiting theories, the first given in 3.1 assumes infinitesimal creepage and spin, while the theory described in 3.2 applies for very large creepage and spin. The first of these is particularly attractive as it is a linear theory and as such can conveniently be incorporated into the dynamic analysis of a wheelset or a complete vehicle. The large creep theory is not very convenient to use as it involves time consuming numerical integrations and some gross approximations.

Only two suitable theories exist for arbitrary creep and spin. The first of these, the numerical theory of Section 3.3.1, has been proven experimentally over most of its range of application, but suffers from the disadvantage of not converging for elongated contact ellipses. The second theory, the simplified theory, has not been proven experimentally, apart from comparisons with the numerical theory over some of the range of values.

In this section the theories are compared by calculating the total forces and moments on a wheelset using the program FORCES, described in the previous section in conjunction with the various subroutines which have been written for each of the theories.

5.2 Results

The theories are compared for 3 different cases which have different load distributions and angles of yaw, the results being given in Tables 5.1, 5.2 and 5.3. In these tables contact point A is on the left hand tread, B on the right hand tread and C on the right hand flange. The wheelset is assumed to have an RD4 tyre profile and run along track with a BS110A railhead profile.

In the program which calculates the forces, the forward velocity, V, is assumed constant and is fixed at 30.5 m/s for each case, while the angular velocity $\dot{\Phi}$ is varied until a condition exists where $M_{y_w} = 0$, i.e. a zero moment about the axle of the wheelset. (This would only be achieved in real life if the wheelset ran in frictionless bearings).

The total weight of the wheelset is assumed fixed at 164.58 kN.

Table 5.1: The wheelset is displaced laterally (no yaw) until the flange almost touches the rail (y_o = 6.11 mm). There are two contact points, one on the tread of each wheel and it is assumed that T_{z_A} =-82.29 kN, T_{z_B} = -82.29 kN, T_{z_C} = 0.

Table 5.2: The wheelset is displaced laterally (no yaw) with the flange just touching the rail, while the tread of the same wheel is just lifting off. (y_o = 6.11 mm). There are therefore two contact points, one on the tread of the left hand wheel and one on the flange of the right hand wheel and it is assumed that T_{z_A} =-82.29 kN, T_{z_B} = 0, T_{z_C} =-82.29 kN.

Table 5.1 FORCES AND CREEPAGES

Wheelset Moved Laterally

$M_{y_w} = 0$, $y_o = 6.11$ mm, $T_{z_A} = T_{z_B} = -82.29$ kN, $T_{z_C} = 0$, $\psi = 0°$

$(a/b)_A = 2.38$, $(a/b)_B = 1.04$ $\gamma_{2A} = \gamma_{2B} = \eta_A = \eta_B = 0$, $V = 30.5$ m/s

A = Tread Contact Point on L.H.Wheel
B = Tread Contact Point on R.H. Wheel

Case	A Numerical B Theory	A Small Creep B Theory	A Simplified B Theory	A Large Creep B Theory
$\dot{\Phi}$ (rad/s)	- 80.8855	- 80.8007	- 80.8125	- 81.0475
γ_{1A}	0.0024	0.0035	0.0033	0.0004
ω_{3A} (m^{-1})	0.0233	0.023	0.023	0.0233
ξ_A	0.6857	0.9753	0.9342	0.1165
χ_A	0.0306	0.0302	0.0302	0.0303
f_{x_A}	0.7900	1.0	0.5252	0.9845
f_{y_A}	0.0220	0.	0.0114	0.
m_{z_A}	0.0066	0.0066	0.0021	0.1206
γ_{1B}	- 0.0027	- 0.0017	- 0.0019	- 0.0048
ω_{3B} (m^{-1})	- 0.468	- 0.469	- 0.469	- 0.470
ξ_B	- 1.3919	- 0.8644	- 0.9421	- 2.4051
χ_B	- 1.2958	- 1.4006	- 1.4007	- 1.4027
f_{x_B}	- 0.7837	- 0.9855	- 0.5244	- 0.9637
f_{y_B}	- 0.3515	- 0.1699	- 0.4382	0.
m_{z_B}	- 0.1680	- 0.4275	- 0.2026	- 0.1233
M_{x_T} (kNm)	5.95	6.20	4.21	7.56
M_{z_T} (kNm)	-24.2	-30.55	-16.08	-30.2
T_{y_T} (kN)	- 7.13	-10.50	- 5.19	-14.1

Table 5.2 FORCES AND CREEPAGES

Wheelset Moved Laterally

$M_{y_W} = 0$, $y_o = 6.11$ mm, $T_{z_A} = T_{z_C} = -82.29$ kN, $T_{z_B} = 0$, $\psi = 0^\circ$

$(a/b)_A = 2.38$, $(a/b)_C = 16.68$, $\gamma_{2_A} = \gamma_{2_C} = \eta_A = \eta_C = 0$, $V = 30.5$ m/s

A = Tread Contact Point on L.H. Wheel

C = Flange Contact Point on R.H.Wheel

Case	1	2	3	4	5	6
	A. Numerical Theory			A Simplified Theory	A Small Creep Theory	A Large Creep Theory
	C Small Creep Theory	C Simplified Theory	C Large Creep Theory	C. Simplified Theory		
$\dot{\Phi}$ (rad/s)	-78.8023	-80.4054	-79.0476	-80.2802	-80.3786	-80.3785
γ_{1_A}	0.0285	0.0084	0.0254	0.0099	0.0087	0.0087
$\omega_{3A}(m^{-1})$	0.023	0.023	0.023	0.023	0.023	0.023
ξ_A	8.0253	2.3682	7.1504	2.7948	2.4497	2.4500
χ_A	0.0298	0.0305	0.0299	0.0301	0.0301	0.0301
f_{x_A}	1.0	0.9996	1.0	0.9524	1.0	1.0
f_{y_A}	0.0	0.0052	0.0	0.0073	0.0	0.0
m_{z_A}	0.0	0.0057	0.0	0.0031	0.0066	0.0067
γ_{1_C}	-0.0010	- 0.0210	- 0.0041	- 0.0195	- 0.0208	- 0.0208
ω_{3C} (m^{-1})	-2.40	- 2.42	- 2.40	- 2.42	- 2.42	- 2.42
ξ_C	-0.0490	- 1.0174	- 0.1797	- 0.9483	- 1.0072	- 1.0072
χ_C	-0.4816	- 0.4854	- 0.4823	- 0.4860	- 0.4863	- 0.4863
f_{x_C}	-0.5479	- 0.4823	- 0.3472	- 0.4566	- 0.4785	- 0.4785
f_{y_C}	-0.8366	- 0.5257	- 0.	- 0.5310	- 0.5273	- 0.5273
m_{z_C}	-0.1624	- 0.1239	- 1.4844	- 0.1108	- 0.1223	- 0.1223
M_{x_T}(kNm)	51.1	60.5	82.9	60.0	60.0	60.0
M_{z_T}(kNm)	-29.9	-29.9	-29.2	-28.4	-29.9	-29.9
T_{y_T}(kN)	-123.	-146.	-205.6	-145.8	-145.9	-145.9

Table 5.3 FORCES AND CREEPAGES

Wheelset Yawed and Moved Laterally

$My_W = 0$, $\psi = 3^\circ$, yo = 5.75 mm, $Tz_A = Tz_C = -82{,}29$ kN, $T_{zB} = 0$,

$(a/b)_A = 2.4$, $(a/b)_C = 16.68$ V = 30.5 m/s

A = Tread Contact Point on L.H. Wheel

C = Flange Contact Point on R.H.Wheel

	A. Numerical Theory		
	C. Small Creep Theory	C. Simplified Theory	C. Large Creep Theory
$\dot{\Phi}$ (rad/s)	- 79.5515	- 79.5547	- 79.0936
γ_{1A}	0.0205	0.0207	0.0262
γ_{2A}	- 0.0519	- 0.0519	- 0.0517
ω_{3A} (m^{-1})	0.0292	0.0200	0.0289
ξ_A	5.7435	5.8057	7.3646
η_A	- 14.5653	- 14.5677	- 14.5231
χ_A	0.0381	0.0262	0.0379
f_{xA}	0.3586	0.3621	0.4481
f_{yA}	- 0.9039	- 0.9030	- 0.8799
m_{zA}	- 0.9152	- 0.9173	- 0.3509
γ_{1C}	- 0.0085	- 0.0092	- 0.0028
γ_{2C}	- 0.0204	- 0.0191	- 0.0203
ω_{3C} (m^{-1})	- 2.39	- 2.42	- 2.39
ξ_C	- 0.4429	- 0.4711	- 0.1396
η_C	- 1.0566	- 0.9754	- 1.0236
χ_C	- 0.4801	- 0.4855	- 0.4788
f_{xC}	- 0.3866	- 0.2032	- 0.2332
f_{yC}	- 0.9222	- 0.9295	- 0.7109
m_{zC}	19.1891	0.0549	0.7752
M_{xT} (kNm)	41.6	44.0	47.0
M_{zT} (kNm)	- 16.0	- 11.61	- 13.18
T_{yT} (kN)	- 94.6	-101.1	-108.2

Table 5.3: The wheelset is yawed through 3^{o} and then moved laterally until the flange touches the rail, while the tread of the same wheel is just lifting off. Therefore there are two contact points as before and it is again assumed that

$T_{z_A} = -82.29$ kN, $T_{z_B} = 0$, $T_{z_C} = -82.29$ kN.

In each case the creepages and forces are tabulated.

5.3 Discussion

5.3.1 Wheelset Displaced Laterally, No Yaw, $T_{z_A} = -82.29$ kN = T_{z_B}, $T_{z_C} = 0$ (Results in Table 5.1)

In this case the contact points are on the tread of each wheel, the wheelset being displaced towards the right hand side giving a contact ellipse on the left hand wheel of (a/b) = 2.38 and on the right hand wheel of (a/b) = 1.04. The difference in these ratios is due to the left hand wheel contact being on a railhead radius of 79.375 mm while the right hand wheel contact is on a railhead radius of 304.8 mm. As (a/b) = 2.38 is only just outside the tabulated range of values given for the numerical theory, the results were extrapolated to give the forces at this contact point. Table 5.1 gives results obtained using each theory for both contact points where $\dot{\Phi}$ was varied to give the condition $M_{y_w} = 0$ in each case.

The numerical theory gives the total lateral force needed to keep the wheelset in this position, $T_y = -7.13$ kN while the simplified theory gives $T_y = -5.19$ kN. It must be remembered looking at the results that since $\dot{\Phi}$ is different in each case, the creepages are different and therefore the forces will be different anyway. The $\dot{\Phi}$'s are only different because the force

coefficients predicted by each theory are different. Thus differences in the theories are accumulative in the final answer. For example if $\dot{\Phi}$ = - 80.8125 rad/s (given by simplified theory) and numerical theory is used then f_{x_A} = .8882 (.5252), f_{y_A} = .0187 (.0114), f_{x_B} = - .6021 (- .5244), f_{y_B} = - .4001 (- .4382). (The simplified theory results given in brackets). This is comparing like with like and offers a better comparison between the two theories. M_y and therefore $\dot{\Phi}$ are affected because of these differences in f_x. Kalker experienced some difficulty in obtaining results for the case (a/b) = 2 and since these results are used to obtain results when (a/b) = 2.38 it is possible that the simplified theory gives a better answer than the numerical theory for this case.

The small creep theory predicts a total lateral force of - 10.50 kN, which is greater than that given by the numerical and simplified theories. Applying the tests outlined in Section 3.1 to check whether the creepages and spins are small

$$\xi_{max.A} = .586 \qquad \xi_{max.B} = 3.91$$

$$\chi_{max.A} = 1.025 \qquad \chi_{max.B} = 2.5$$

Comparing these values with the values for ξ and χ given in Table 5.1 it can be seen that on side A, $\xi > \xi_{max}$ and therefore the small creep theory predicts too large a value for f_x. On side B, $\xi < \xi_{max}$, therefore small creep theory should predict a reasonable answer, although probably still on the high side. These values affect $\dot{\Phi}$ and thus the overall results are different.

In general small creep theory is a good approximation for tread contact and in view of it being a linear theory is used by some European Railway Administrations to calculate the forces on

a wheelset for such conditions. The large creep theory should not be used for tread contact since $\nu < \nu_{max}$ and $|\chi| < \chi_{max}$. Since the lateral loads for tread contact are small anyway, the differences shown are not physically significant.

5.3.2 Wheelset Displaced Laterally, No Yaw, $T_{z_A} = -82.29$ kN $T_{z_B} = 0$, $T_{z_C} = -82.29$ kN (Results in Table 5.2)

In this case the contact area on the left hand wheel has an (a/b) ratio of 2.38 and on the right hand wheel of (a/b) = 16.68, the latter ratio being well outside the range of numerical theory results and thus cannot be used. In cases 1, 2 and 3 numerical theory is used for the left hand contact point, while small creep theory, simplified theory and large creep theory are used for the flange contact point respectively. The remaining three cases analysed use simplified theory for the flange contact point with simplified theory, case 4; small creep theory, case 5; and large creep theory, case 6; for the tread contact point respectively.

In all cases the left hand wheel, with the tread contact, is shown to be sliding along the track with $f_{x_A} = 1$, $f_{y_A} = 0$. The real problem is deciding which theory should be used on the flange, in each case widely different results are obtained, e.g.

using small creep theory on the flange $T_{y_T} = -123$ kN

using simplified " " " " $T_{y_T} = -146$ kN

using large creep " " " " $T_{y_T} = -206$ kN

The main contribution to the total lateral force is the lateral force at C, i.e. the right hand flange contact. Using the large creep theory f_{y_C} is always zero (since the lateral creep is zero) and so the only lateral force is due to resolved component of the normal force. Therefore this theory produces a very high value for the total lateral force on the wheelset.

$\chi_{max_C} = .0613$ and therefore $\chi \gg \chi_{max}$. This means small creep theory should not be used at this point. If it is used, will over estimate the lateral force due to spin, and the total lateral force on the wheelset will be very small.

It may be noted that the large creep theory produces a reasonable value for f_{x_C}, and therefore $\dot{\Phi}$, but to produce a closer value for f_y, χ needs to be an order of magnitude larger.

When the simplified theory is used on the flange it produces a result in between the small creep theory and the large theory and this one would expect.

Since the left hand tread is shown to be sliding, cases 4, 5 and 6 all show the same results since simplified theory is used for the flange contact point in each case.

5.3.3 Wheelset Displaced Laterally and Yawed, $\psi = 3^\circ$

$T_{z_A} = -82.29$ kN, $T_{z_B} = 0$, $T_{z_C} = -82.29$ kN

(Results in Table 5.3)

The three cases analysed all use numerical theory for the tread contact with small creep theory, simplified theory and large creep theory for the flange contact point. In each case

the tread on the left hand side is found to be sliding. Numerical theory cannot be used on the flange because the (a/b) ratio is well out of range of the tabulated results as in the previous set of results.

When the wheelset is yawed the lateral creepage increases. On the flange, the lateral force due to spin and the lateral force due to lateral creepage act in the same direction, both tending to lift the wheel off the rail.

Using large creep theory the lateral force due to spin is assumed to be zero while the lateral force due to lateral creep gives $f_{y_c} = -0.7109$; this compares with $f_{y_c} = 0$ when $\psi = 0$. Therefore using this theory, there is a large change in the total lateral force as the wheelset is yawed; T_{yT} drops from - 206 kN when $\psi = 0^\circ$ to - 108 kN when $\psi = 3^\circ$. Since the effect of spin is not accounted for, this theory still produces a slightly higher value for the lateral force on the wheelset, than the other theories.

The simplified theory and the small creep theory give similar values for T_{y_T}. This is because the wheelset has been yawed through such a large angle that the lateral creepage is very large and the force due to it, combined with the lateral force due to the spin, shows the wheelset to be almost sliding on the flange.

As before the simplified theory gives a value for T_{y_T} in between the other two theories:

Small creep theory	$T_{yT} = -94.6$ kN
Simplified theory	$T_{y_T} = -101.1$ kN
Large Creep theory	$T_{y_T} = -108.2$ kN

5.4 Conclusions

One of the objectives of the present investigation is to compare the available creep/force theories and give their limitations when applied to the problem of a wheelset rolling along a railway track in a displaced position. It has been shown that the problem can be separated into two distinct regions, tread contact and flange contact conditions.

The numerical method of Kalker, Ref. 23, is based on exact theory and should give the best available results within the range in which it can be used. It has been compared with experimental results and found to give good correlation. The numerical method failed to converge for (a/b) greater than 2 and for this reason cannot be used for flange contact. It is impractical to run Kalker's program for each case required but the method can be utilised by interpolating his given tabulated results. This can be done numerically on the computer if the tabulated results are stored on disc or magnetic tape. In this way it is convenient to use the method for tread contact, the creepages and spins tabulated easily cover the range of values found in the wheelset problem.

The linearised or small creep theory is easy to use and gives good answers if the creepages and spin are small enough to be in the linear region of the creep/force curves. In order to check this, certain tests are outlined in Section 3.1. These tests have been carried out on the present results. Basically values of ξ_{max}, η_{max}, χ_{max} are calculated for the contact ellipse in question and depending on whether ξ, η, χ are greater or less than these values, the creepages and spin can be called "large" or "small".

The small creep theory used in this report has been modified by giving limiting values for f_x and f_y for a particular creepage and spin. (These modifications have been described in Section 3.1). The results given in Tables 5.1, 5.2 and 5.3 show that even this modified version gives unacceptable results for flange contact except near the sliding condition when the yaw angle, and therefore the lateral creepage, is very large. The theory can be used on the tread giving acceptable results, and has the obvious advantage of being a linearised theory.

The large creep theory, discussed in Section 3.2 has very limited use. Its main disadvantage is that the lateral force given by the theory is independent of the spin. Thus the theory can only be used when the spin is sufficiently large so that the lateral force due to it is negligible. This is not the only restriction on its use, another was given in Section 3.2, but it excludes its use for tread contact where the spin is relatively small. The theory predicts high lateral forces necessary to keep the wheelset in flange contact since the contribution from the spin is zero.

The simplified theory, is not yet fully developed but it seems to be a good "engineering" approach to the subject. The displacements and the tractions are assumed to be connected by the simple relationships $u = S_x X$, $v = S_y Y$. The stiffnesses S_x and S_y are then calculated from the initial slopes of the creep/force curves, i.e. from the coefficients C_{11} , C_{22} . This theory can be used for any value of (a/b) as long as C_{11} , etc. are known. These can be calculated outside the tabulated range of Ref. 23 using the asymptotic formulae given in Section 3.1. This theory was found to be easy to use and has an advantage over the numerical theory in that better accuracy can be obtained by taking smaller step lengths at the expense of extra computer time. The results

lay between the two limiting theories, as would be expected, but apart from this it is not possible at this stage to say quantitatively whether the answers are right or wrong since there is nothing to compare the results with.

The main problem lays in calculating the forces at the flange where the spin is large and the contact ellipse very elongated. The numerical method cannot be used for such conditions and the simplified theory has not been checked experimentally for these kind of values. In view of this an experimental program was initiated to provide data for the creep/force relationship on elongated contact ellipses with a large amount of spin present, e.g. flange ~~tyre~~ type conditions. Measurements were made of the lateral force due to varying amounts of lateral creep and spin between wheels with an elongated contact ellipse. These results, together with a full description of the rig, are given in Section 8, where they are compared with simplified theory.

Brief mention should be made of the fact that Kalker is presently working on a numerical method which can also treat the elongated contact ellipse case. Although this method is not yet available, Dr. Kalker has very kindly run his program as it stands to compare with some of the author's experimental results given later, and these have been superimposed on the graphs.

6. Comparison of wheelset forces using new and worn rails

6.1 Introduction

There is very little information available neither theoretical nor experimental, for the forces and moments on a wheelset when in flange contact with the rail. The cases analysed in the previous section were very limited as they applied only for one yaw angle and for one side-to-side load distribution. Since the computer programs discussed in Section 4 were available, a whole range of cases have been calculated for different side-to-side load distributions, different flange-to-tread load distributions and different angles of yaw. Results have been calculated using both the standard BS110A rail head profile with the 0.5" (12.7 mm) corner radius and the 'worn' profile with the 0.7" (17.8 mm) corner radius. In all cases, numerical theory has been used for the tread contact point(s) and simplified theory for the flange contact point.

6.2 Results

The program FORCES has again been used to calculate the results. In all cases the forward velocity V is assumed constant and is fixed at 30.5 m/s while the angular velocity $\dot{\Phi}$ is varied until the condition exists when the rolling moment about the axle, M_{y_w}, is zero. The total weight of the wheelset is assumed fixed at 164.58 kN, and it is assumed to have an RD4 tyre profile. As before contact point A is on the left-hand tread, B on the right-hand tread and C on the right-hand flange.

Results using the 'standard' rail profile are given in Figs. 6.1 to 6.12 and using the 'worn' rail profile in Figs. 6.13 to 6.18. For each profile three side-to-side load distributions have been

considered; (a) $T_{z_A} = -41.15$ kN, $(T_{z_B} + T_{z_C}) = -123.44$ kN, (b) $T_{z_A} = -82.29$ kN, $(T_{z_B} + T_{z_C}) = -82.29$ kN, (c) $T_{z_A} = -123.44$ kN $(T_{z_B} + T_{z_C}) = -41.15$ kN, and for these, three flange-to-tread distributions. In all cases yaw angles were varied from -1° to 3°. The coefficient of friction was taken as 0.25 for all cases.

In Figs. 6.1 to 6.6 the creeps and spins are plotted against yaw angle for the 'standard' rail cases.

In Figs. 6.7 to 6.12 the total forces and moments on the wheelset are plotted versus yaw angle for the 'standard' rail.

In Figs. 6.13 to 6.18 the total forces and moments on the wheelset are plotted versus yaw angle for the 'worn' rail.

6.3 Discussion and Conclusions

Considering the 'standard' rail results it can be seen in Figs. 6.7, 6.9 and 6.11, where T_{y_T} is plotted for each of the three side-to-side wheel load distributions, that the lateral force increases as the load carried on the flange increases. The lateral force drops off as the yaw angle increases since the lateral creep also increases, and the effect of this is to lift the wheel up. The shape of the three curves on each of these graphs is interesting and can be explained as follows. When all the load is carried on the tread, where the cone angle is very small, the effect of spin is negligible and the shape of the curve is dependent on the lateral creep/lateral force relationship. Thus the curve goes from sliding in one direction to sliding in the other direction between $\psi = \pm 0.5^\circ$. When all the load is on the flange, where the spin is large, the lateral force due to this is also large, and the effect of

changing lateral creep is not so significant. On the graphs this can be seen where the curves become more 'S' shaped as the load is transferred from flange to tread.

The total lateral force on the wheelset is, of course, dominated by the lateral force on the flange and this is evident in the curves of T_{y_C} v ψ , Figs. 6.7, 6.9 and 6.11. This effect is reduced as the vertical load carried on the flange is reduced.

The rolling moment, M_{x_T}, plotted in Figs. 6.8, 6.10 and 6.12 for the three distributions, is largely dependent on the vertical and lateral forces at the contact points, thus the shapes of these curves are similar to the T_{y_C} curves. A +ve rolling moment indicates a restoring moment, i.e. one tending to pull the wheelset down onto the right-hand rail. The only time it is -ve is in Fig. 6.8 when there is a vertical load of - 41.15 kN on the tread at point A and - 123.44 kN on the tread at point B, which is probably an unreal situation. Generally the rolling moment increases as the vertical load is transferred from the right-hand side to the left-hand side. It may be noted that in real life the load distribution would sort itself out to the state where the rolling moment about the vehicle centre of gravity was zero. Knowing the height of a vehicle c.g. above the wheelset centre this condition can be evaluated from the results presented.

All the results were calculated by varying the angular velocity of the wheelset until the rolling moment was zero. This condition generally occurs when the speeds on the right-hand side are nearly matched. This is the side towards which the wheelset is displaced and has the larger rolling radii. As a result, the longitudinal creep is small on this side but large on the left-hand side. The yawing moment is largely dependent on the longitudinal forces which in turn depend on the longitudinal creeps. Thus the yawing moment is largely

dependent on what happens at contact point A where the spin is negligible. M_{z_T} is a maximum when f_{x_A} is a maximum, i.e. when $f_y = 0$ or the yaw angle is zero. When the flange is taking all the load, the longitudinal creep on the left-hand side is very large and is hardly affected by changes of yaw angle. Alternatively when the tread is taking all the load the longitudinal creep is small, and therefore greatly affected by yaw angle changes. This explains the shape of the M_{z_T} curves as the load is transferred from flange to tread in Figs. 6.8, 6.10 and 6.12.

Comparing results using the 'standard' rail with the 'worn' rail results given in Figs. 6.13 to 6.18, there is practically no difference between the two. If anything, the lateral force required to keep the wheelset in flange contact for the 'worn' rail is slightly less and this would be expected. The 'worn' profile used was based on measured profiles on the Glasgow Suburban Railway and results indicate that the wheelset forces are little changed by this amount of wear. The rails obviously have to be sideout by a much greater amount before performance is affected. (This is discussed further in Section 7.)

It may be noticed that the results plotted in this section are slightly different from the equivalent results tabulated in the previous section. This is because an improved version of the subroutine SIMP was used to obtain the present results.

In conclusion, the results given for the forces and moments on a wheelset are calculated using the latest creep/force theories and cover a wide range of yaw angles and load distributions. Although they are given for a specific rail and wheel, it is the first time that flange forces have been calculated using rolling contact theories, and the results should prove valuable in future derailment studies.

FIG. 6.1 Creepage & Spin Parameters v Yaw Angle

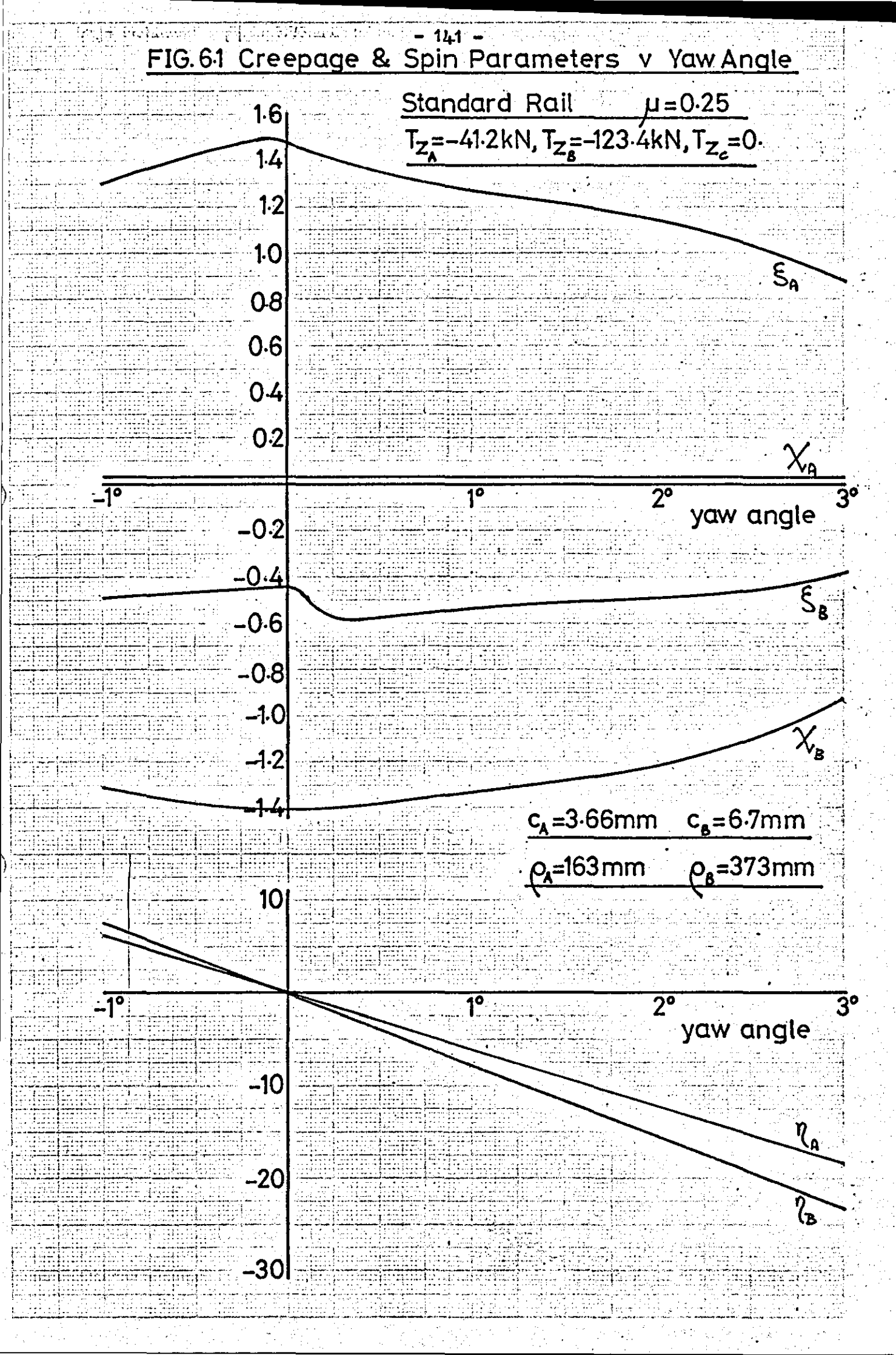

FIG. 6.2 Creepage & Spin Parameters v Yaw Angle

Standard Rail. $\mu = 0.25$. $T_{Z_A} = -41.2$kN, $T_{Z_B} = 0.$, $T_{Z_C} = -123.4$kN

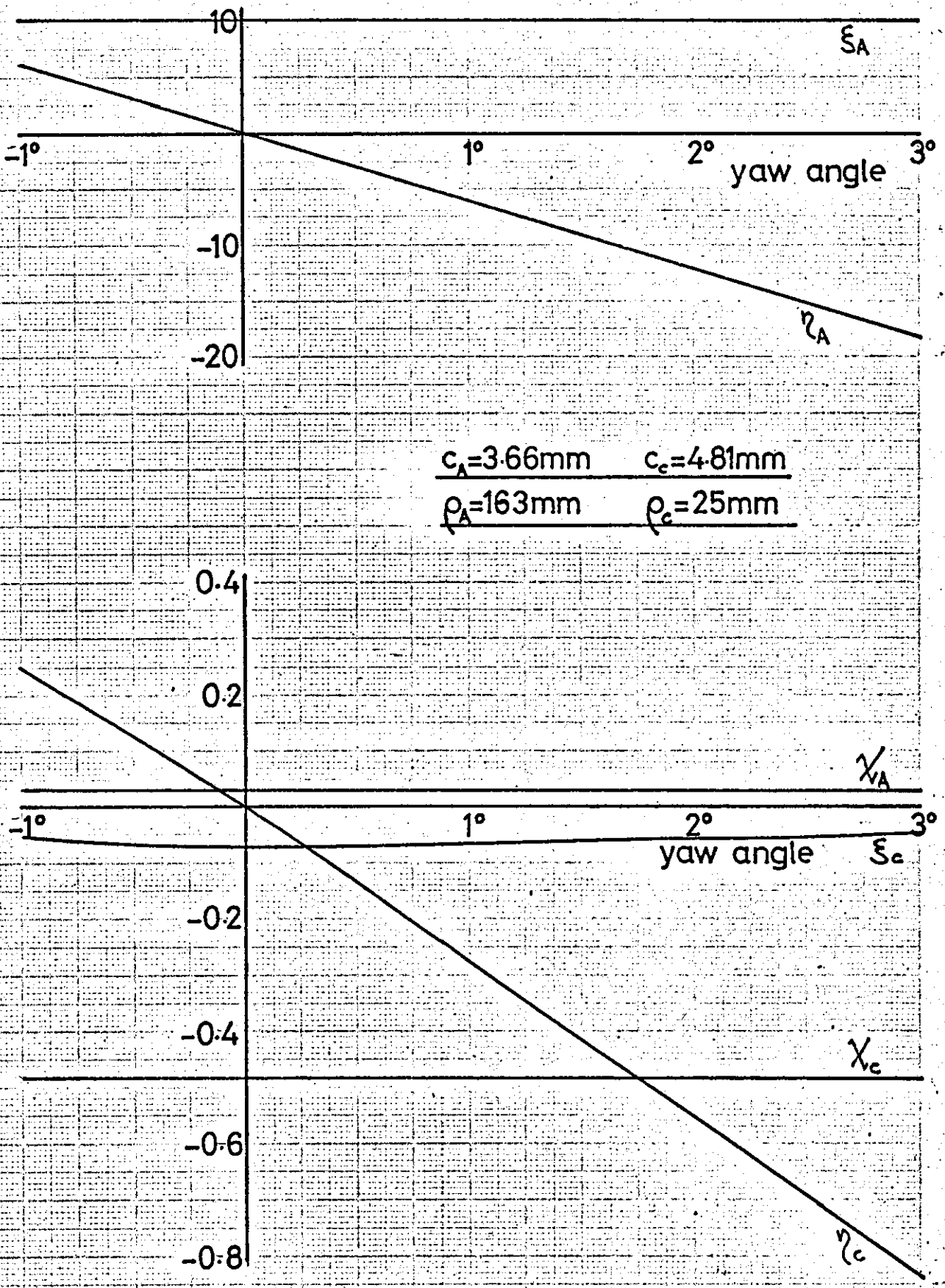

FIG.6.3 Creepage & Spin Parameters v Yaw Angle

Standard Rail. μ=0.25. T_{z_A}=-82.3kN, T_{z_B}=-82.3kN, T_{z_C}=0.

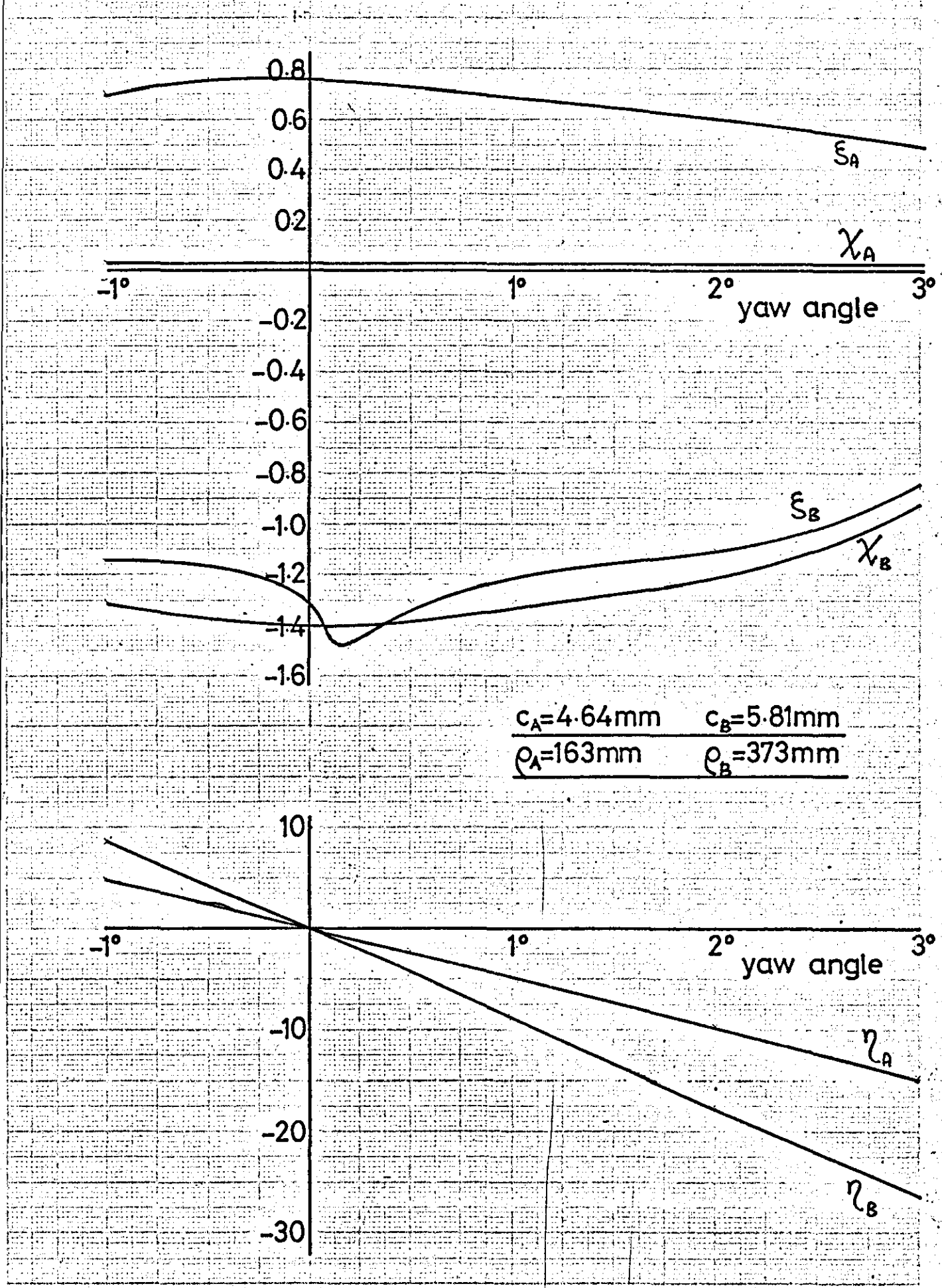

FIG. 6·4 Creepage & Spin Parameters v Yaw Angle

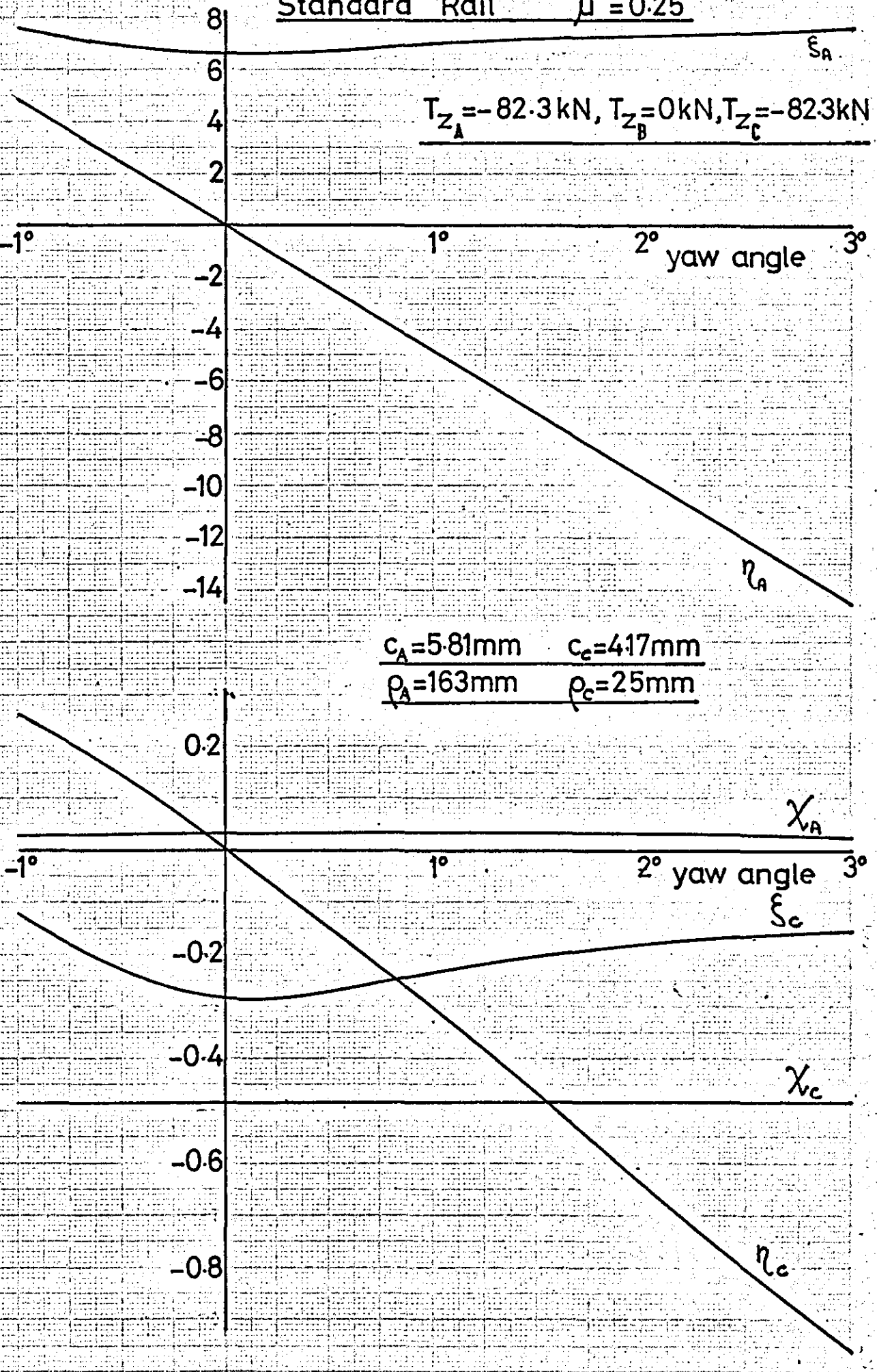

FIG. 6.5 Creepage & Spin Parameters v Yaw Angle

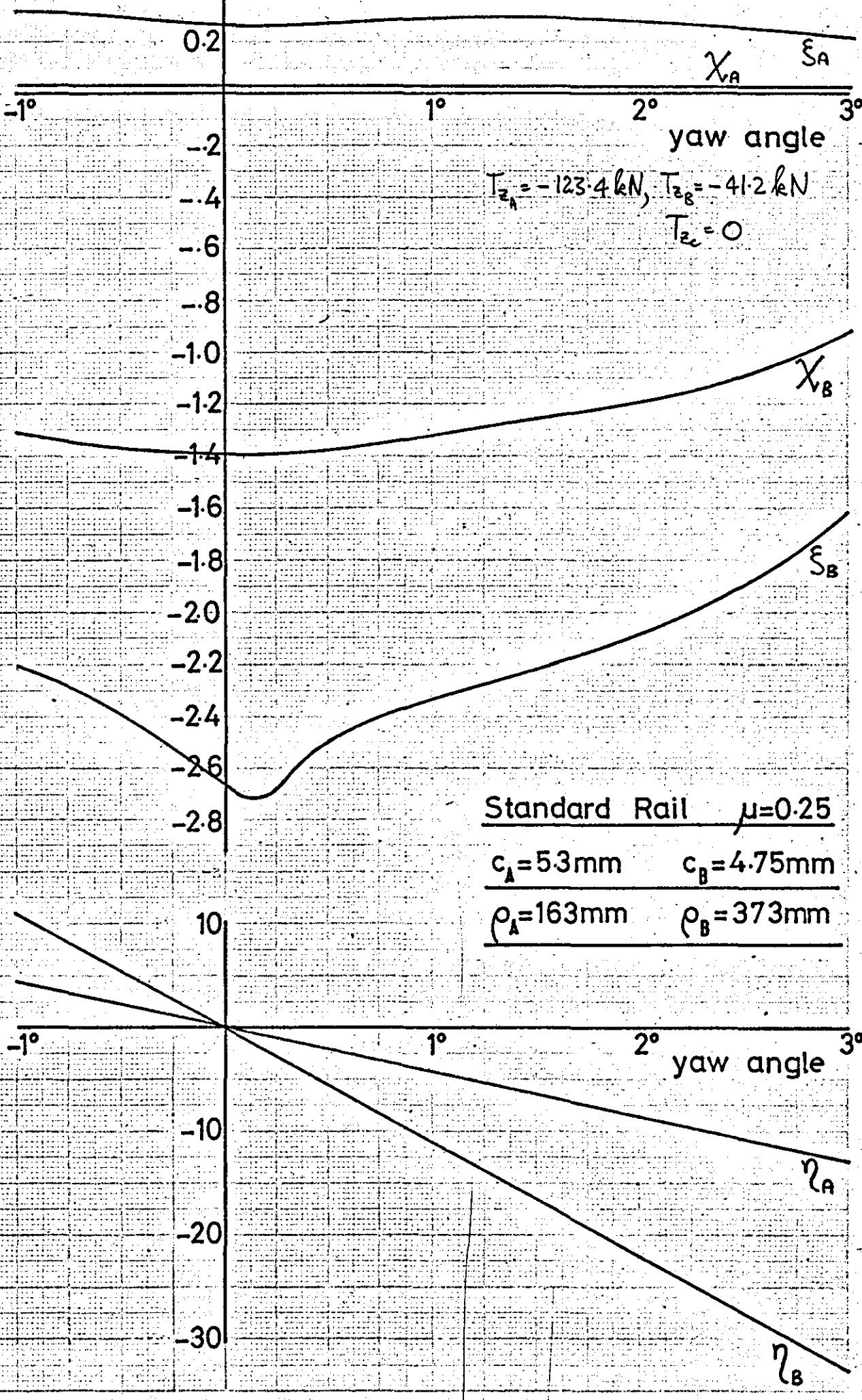

FIG. 6·6 Creepage & Spin Parameters v Yaw Angle

Standard Rail $\mu = 0.25$

$T_{z_A} = -123.4\,kN$, $T_{z_B} = 0\,kN$, $T_{z_C} = -41.2\,kN$

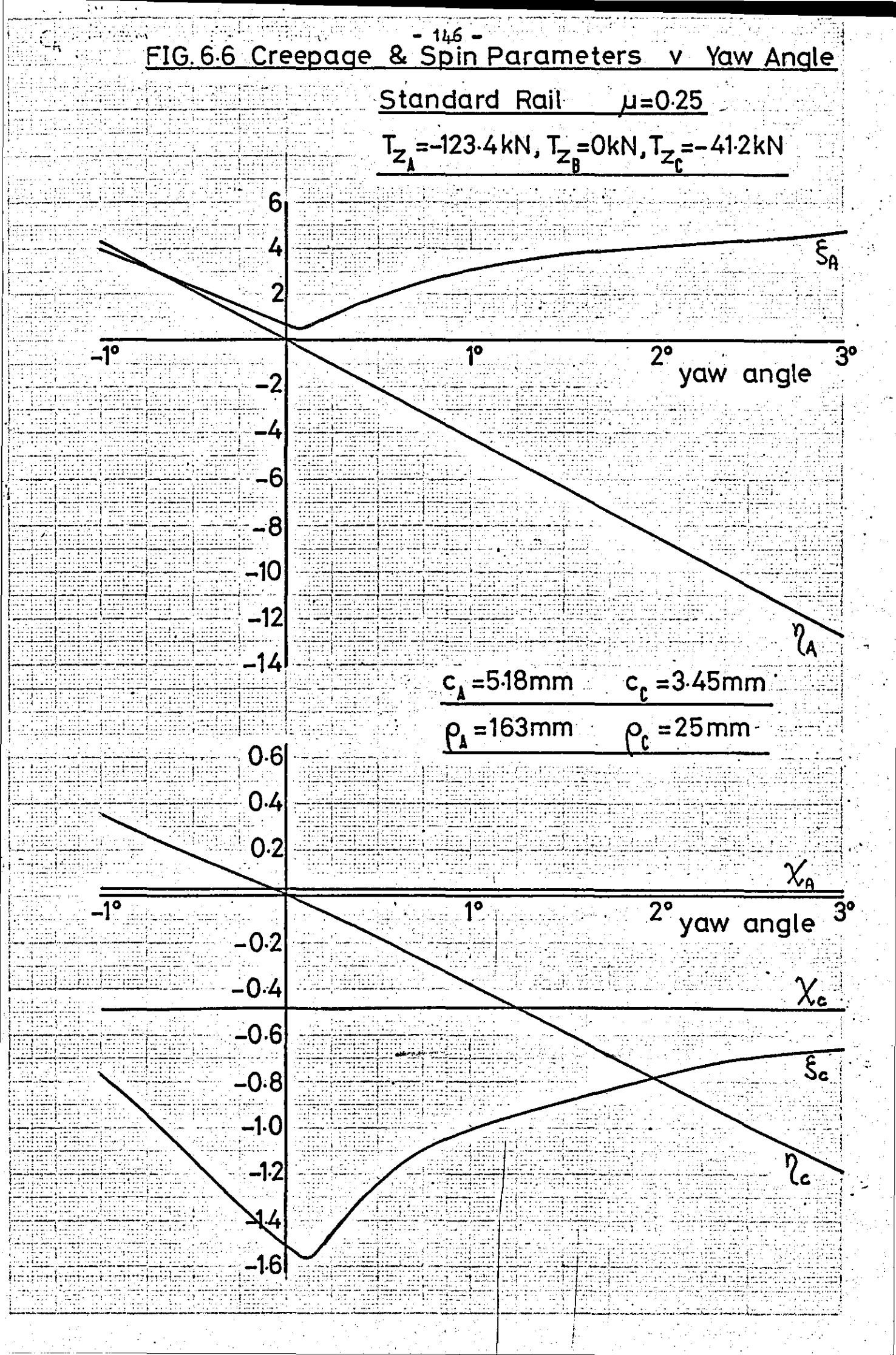

FIG.6·7 Wheelset Forces T_{y_T}, T_{y_C} v Yaw Angle

Standard Rail $\mu=0.25$

$T_{z_A}=-41.2kN, (T_{z_B}+T_{z_C})=-123.4kN$

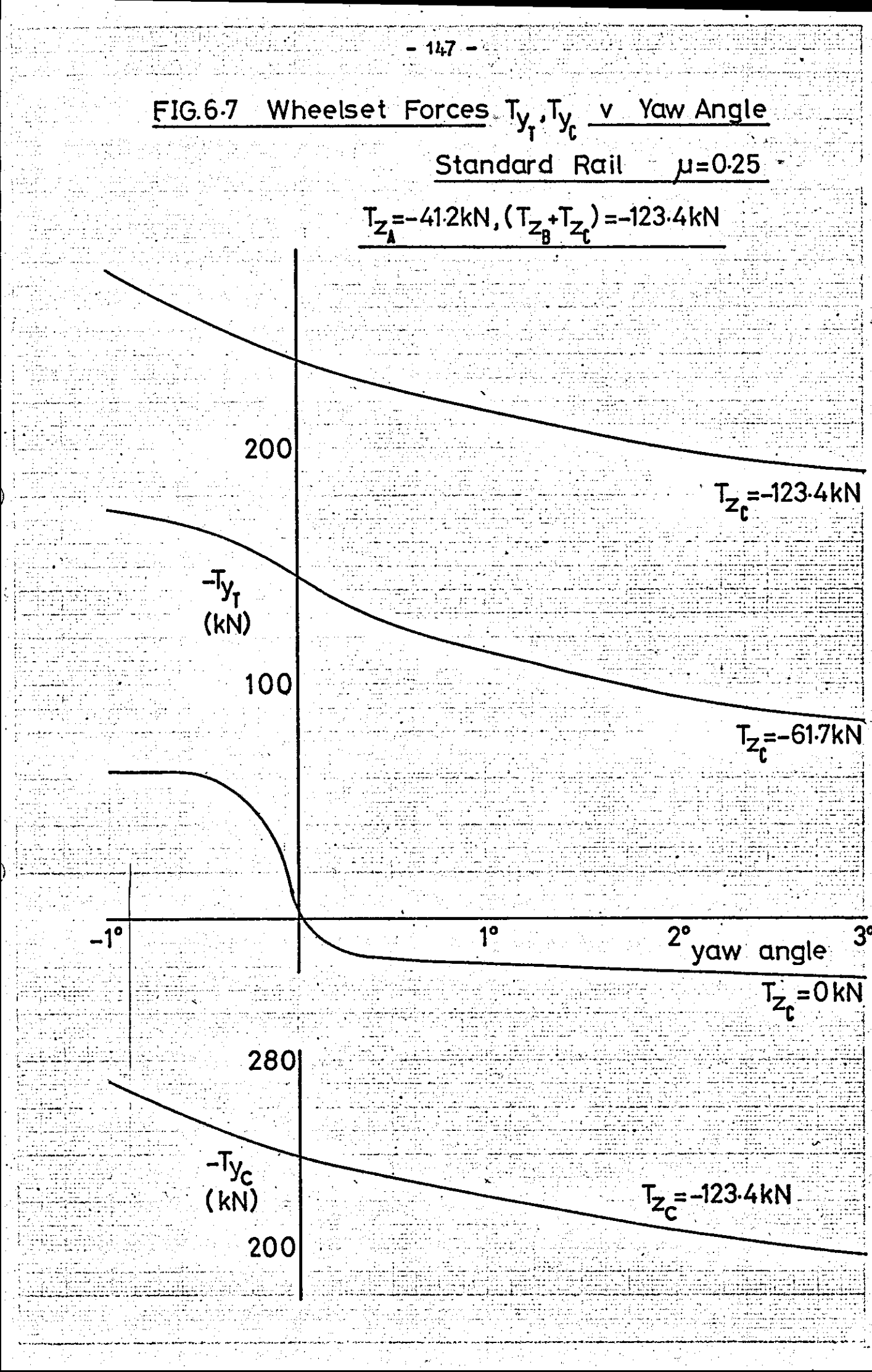

FIG. 6·8 Wheelset Moments M_{X_T}, M_{Z_T} v Yaw Angle

Standard Rail. $\mu = 0.25$

$T_{Z_A} = -41.2kN$, $(T_{Z_B} + T_{Z_C}) = -123.4kN$

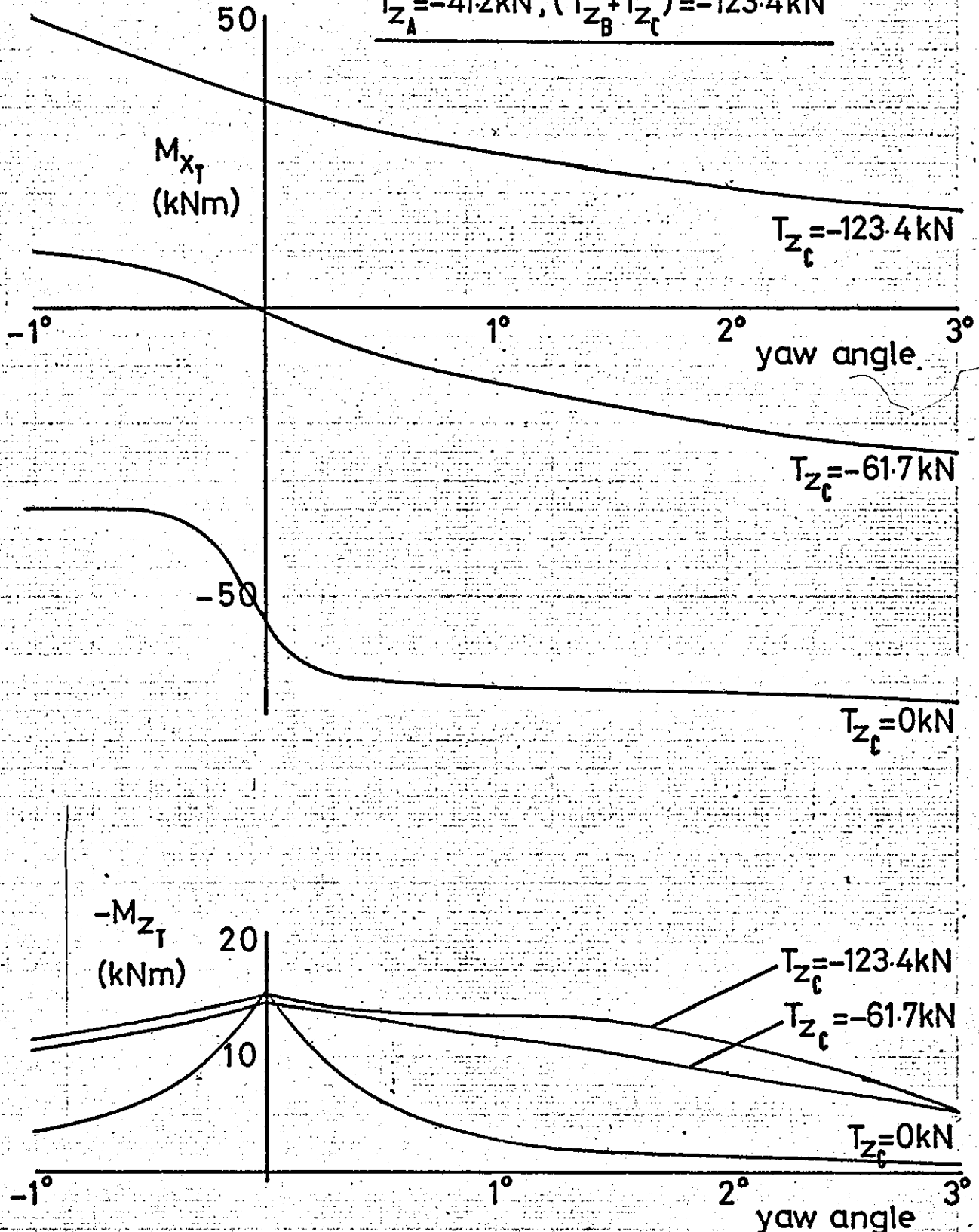

FIG. 6.9 Wheelset Forces T_{y_T}, T_{y_C} v Yaw Angle

Standard Rail. $\mu = 0.25$

$T_{z_A} = -82.3\text{kN}, (T_{z_B} + T_{z_C}) = -82.3\text{kN}$

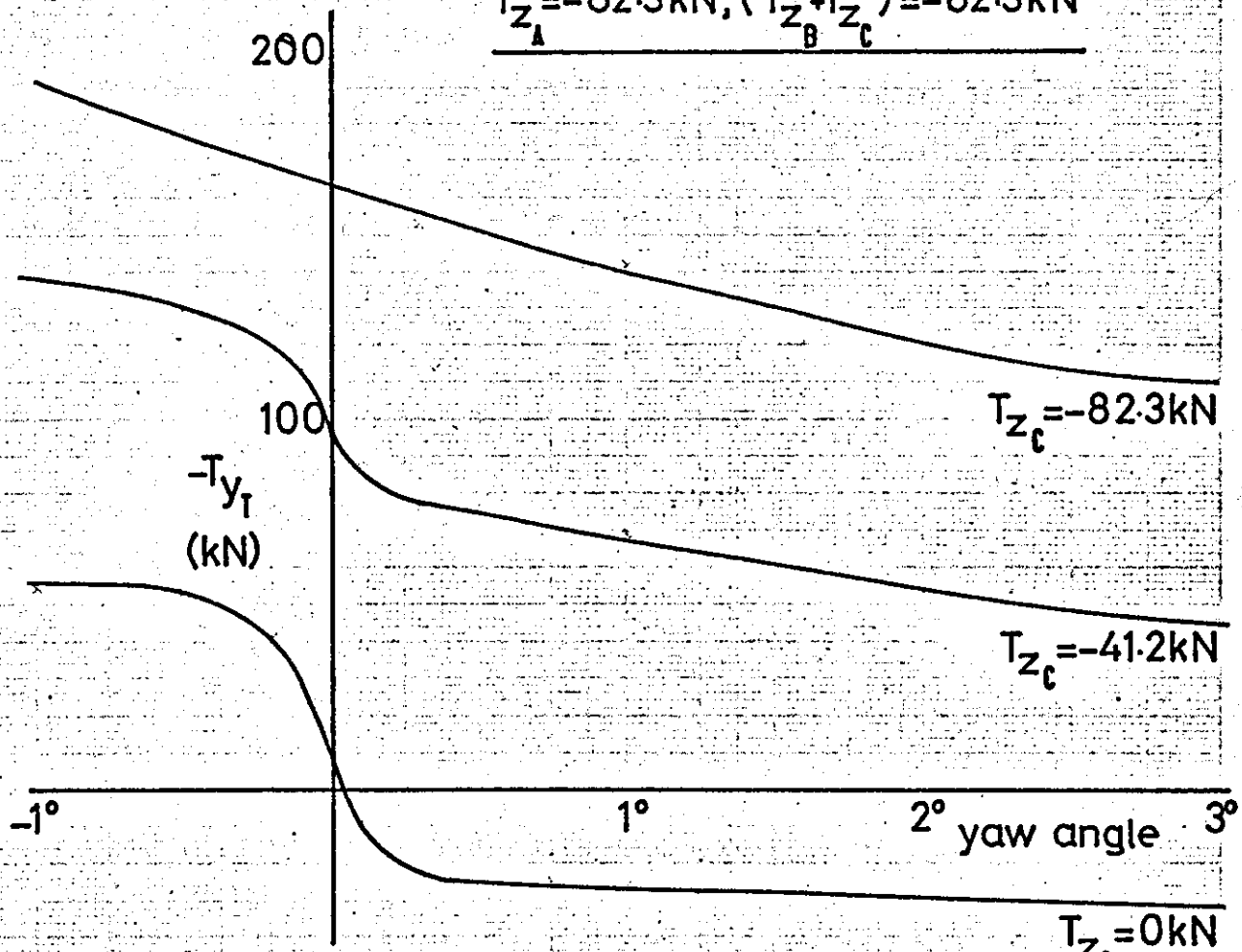

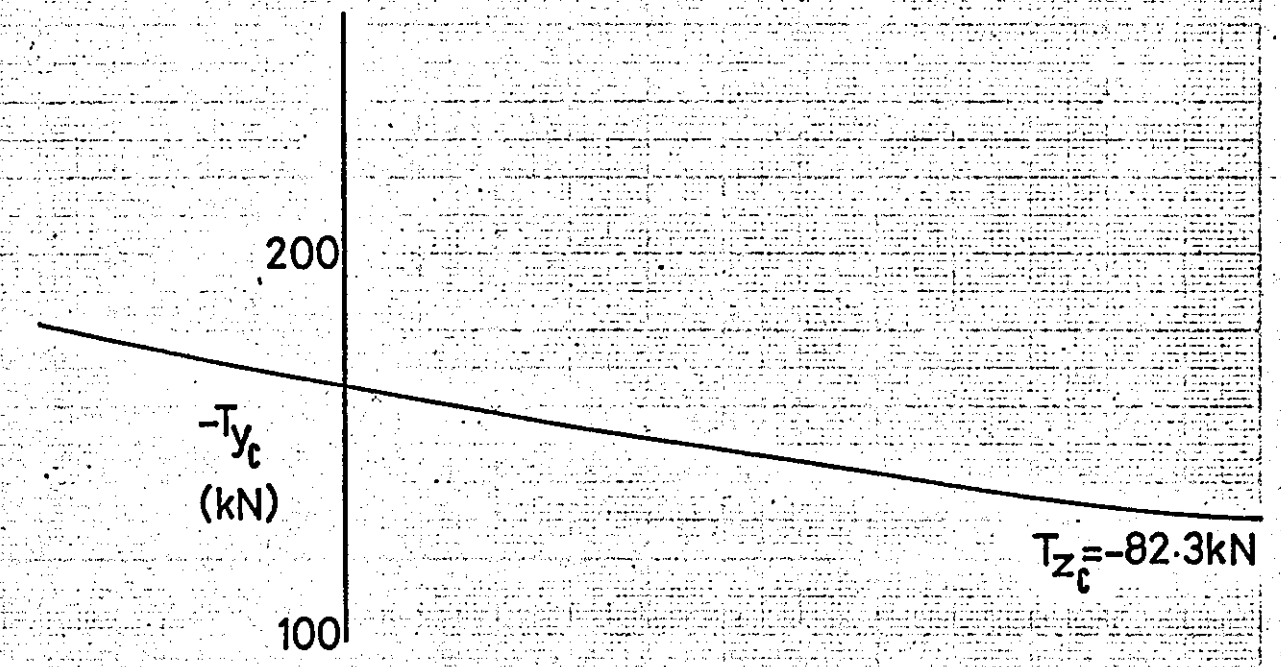

FIG. 6·10 Wheelset Moments M_{x_T}, M_{z_T} v Yaw Angle

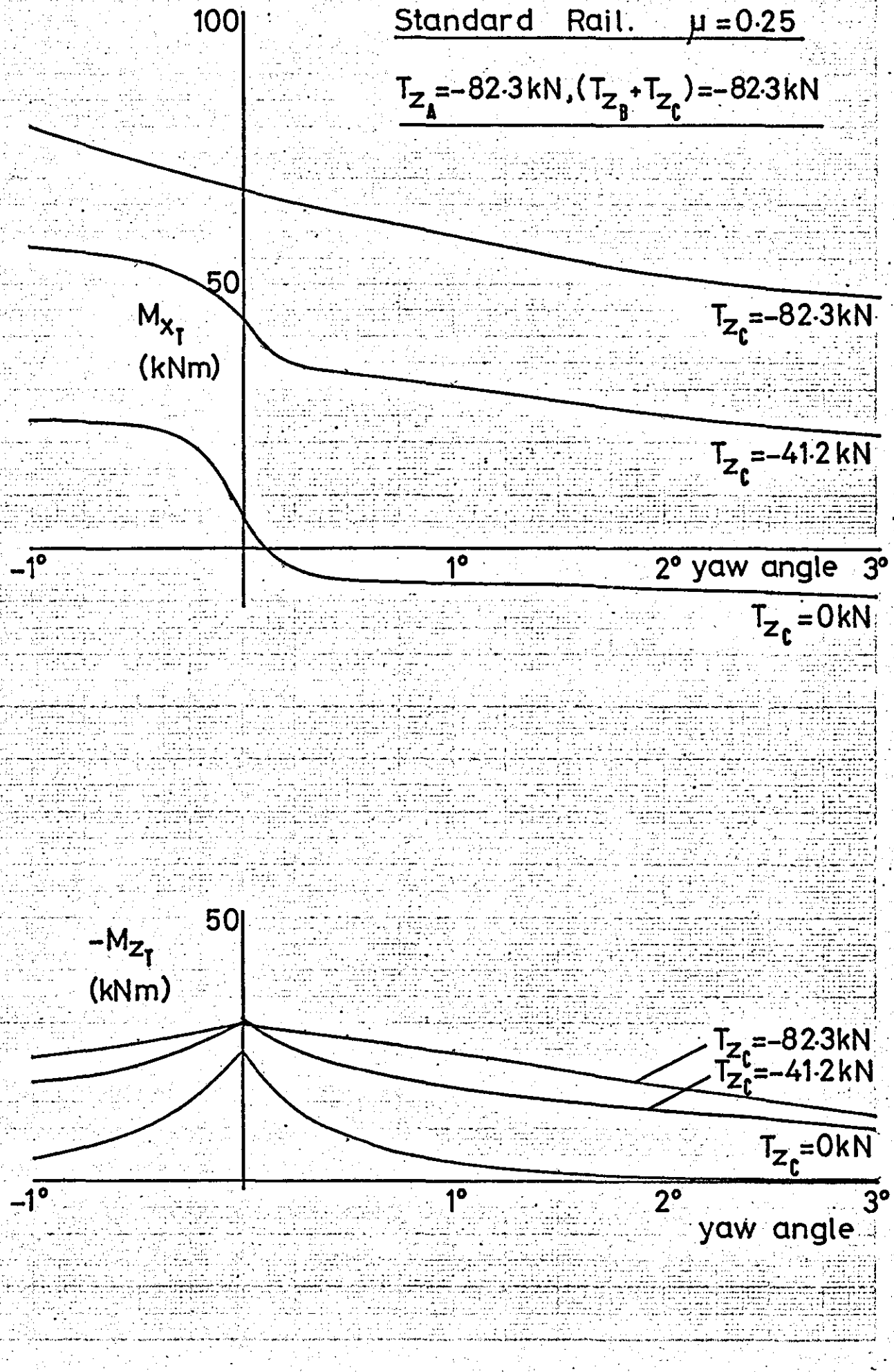

FIG. 6.11 Wheelset Forces T_{y_T}; T_{y_C} v Yaw Angle

Standard Rail $\mu=0.25$

$T_{Z_A}=-123.4kN$, $(T_{Z_B}+T_{Z_C})=-41.2kN$

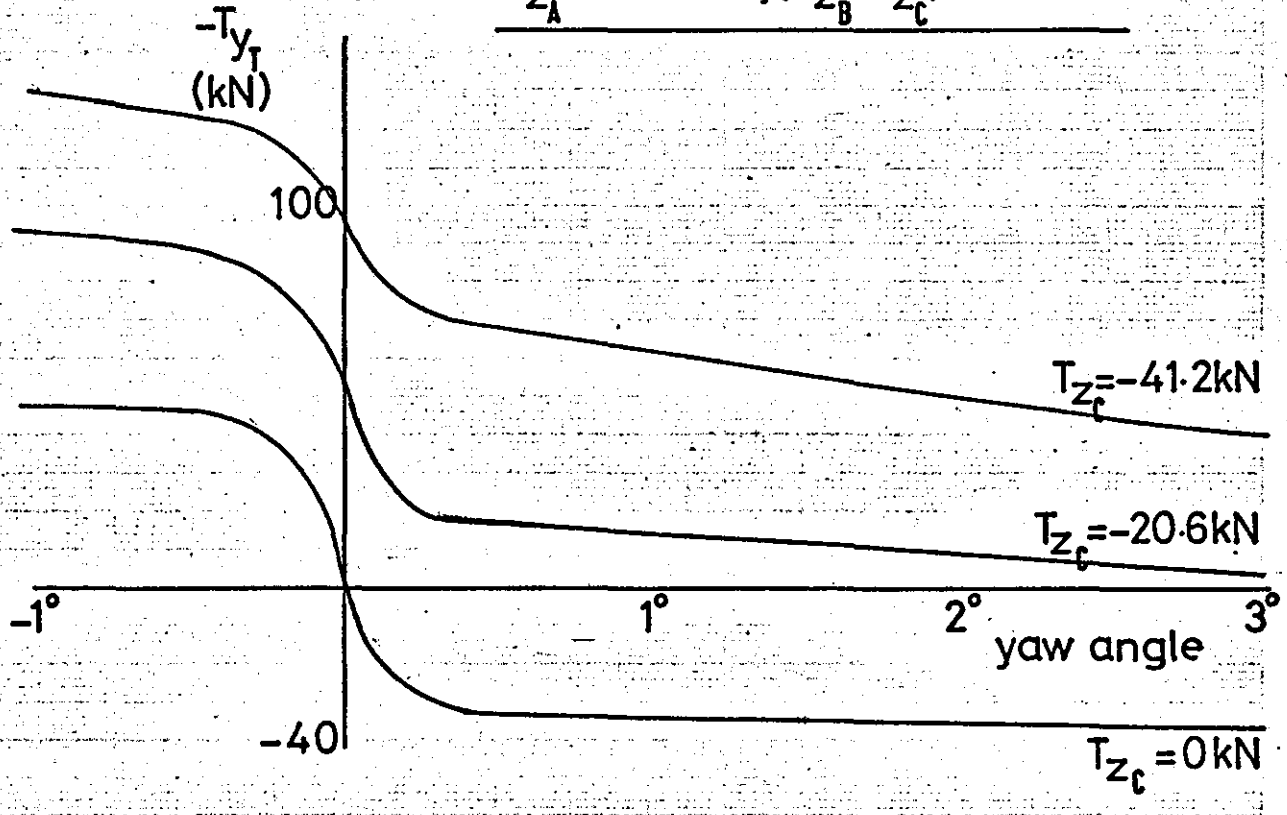

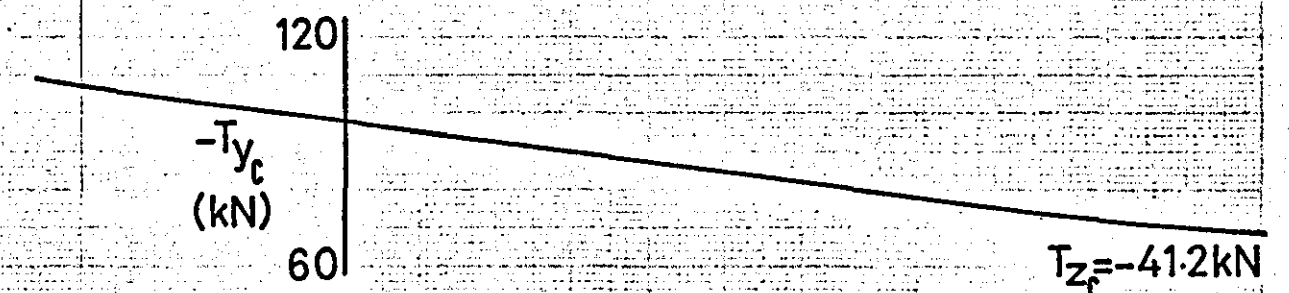

FIG. 6.12 Wheelset Moments M_{x_T}, M_{z_T} v Yaw Angle

Standard Rail $\mu = 0.25$

$T_{z_A} = -123.4\,kN, (T_{z_B} + T_{z_C}) = -41.2\,kN$

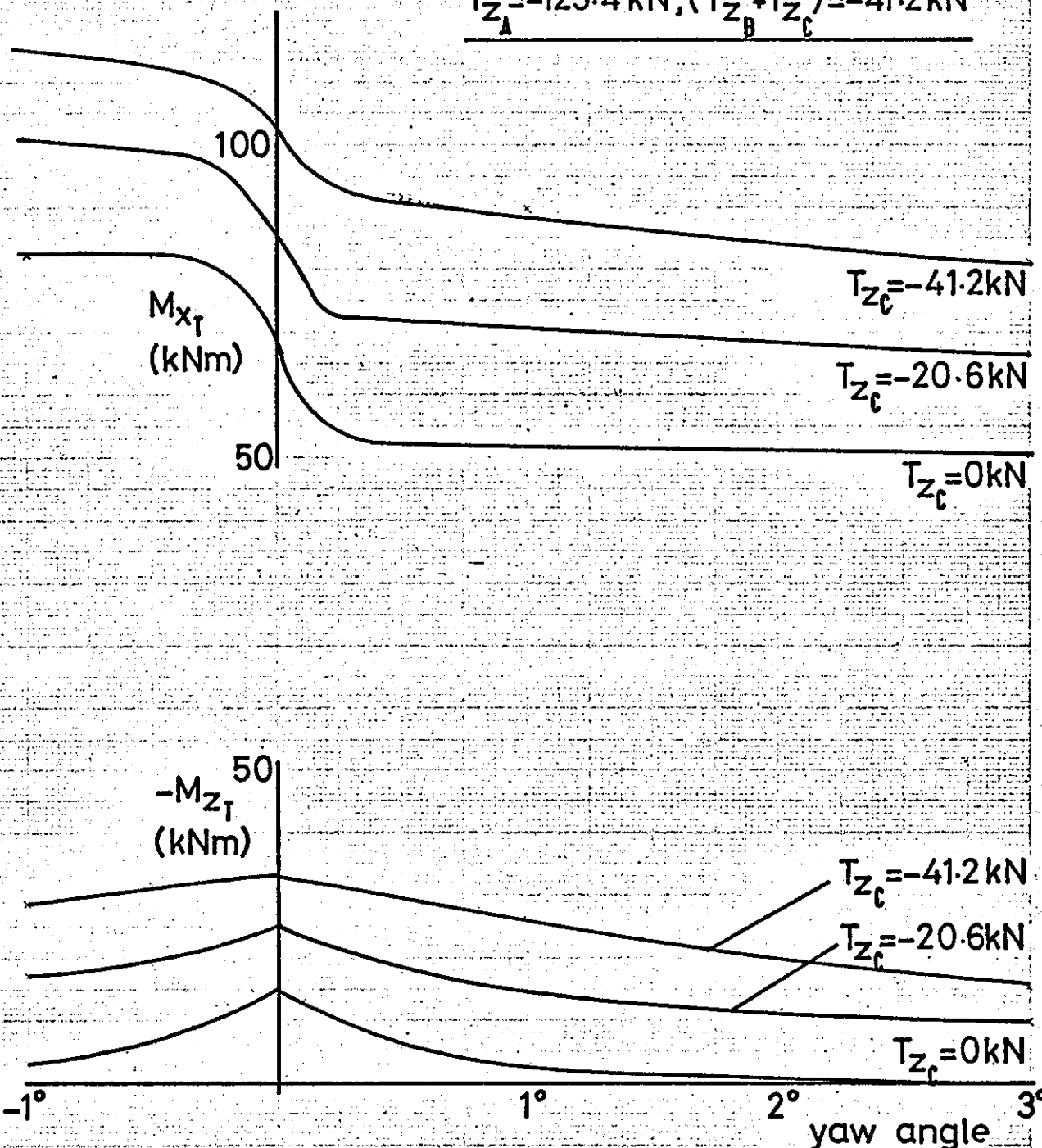

FIG. 6.13 Wheelset Forces T_{y_f}, T_{y_c} v Yaw Angle

Worn Rail $\mu = 0.25$

$T_{z_A} = -41.2\,kN$, $(T_{z_B} + T_{z_c}) = -123.4\,kN$

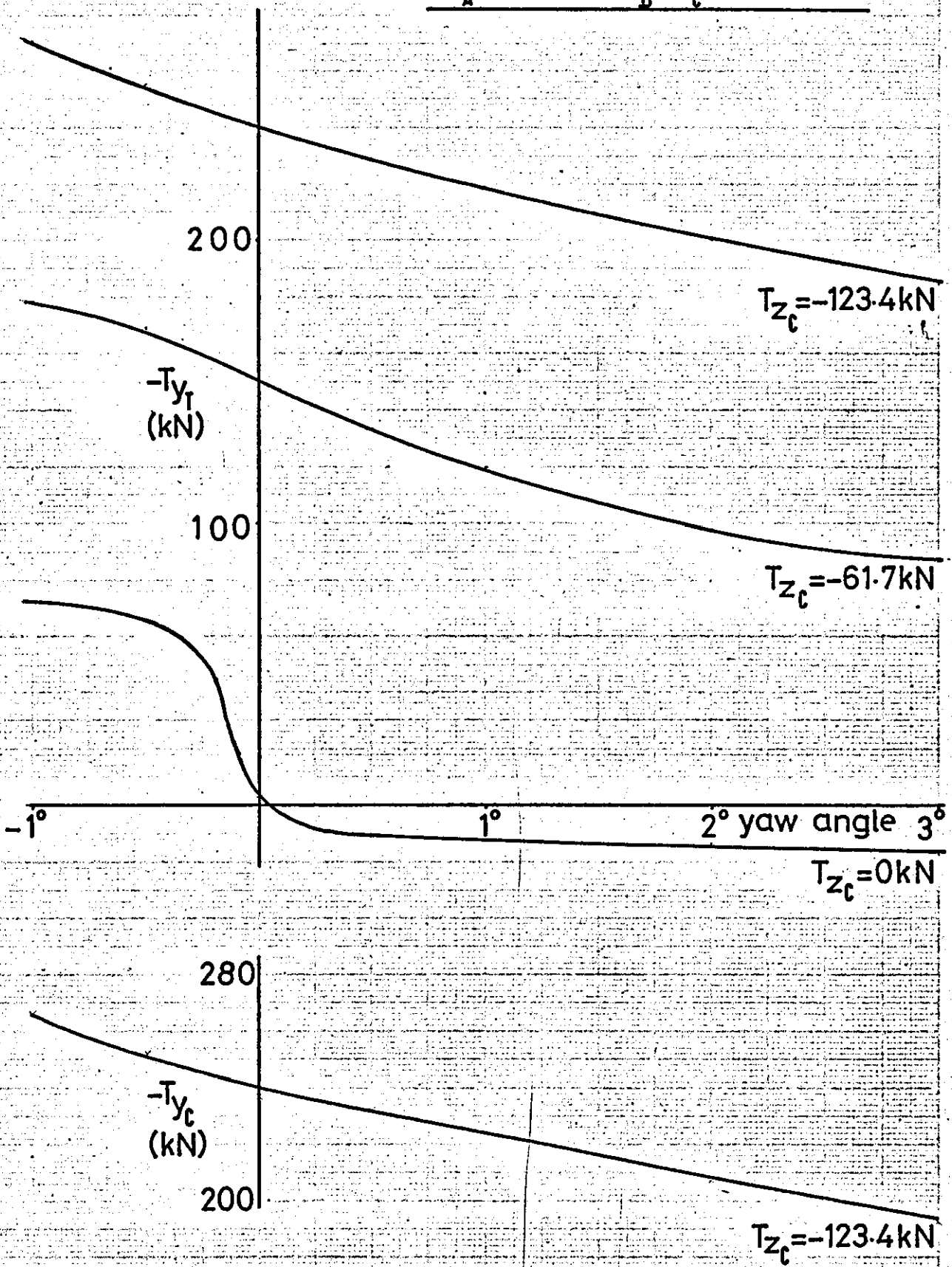

FIG. 6.14 Wheelset Moments M_{x_T}, M_{z_T} v Yaw Angle

Worn Rail $\mu = 0.25$

$T_{z_A} = -41.2\,kN$, $(T_{z_B} + T_{z_C}) = -123.4\,kN$

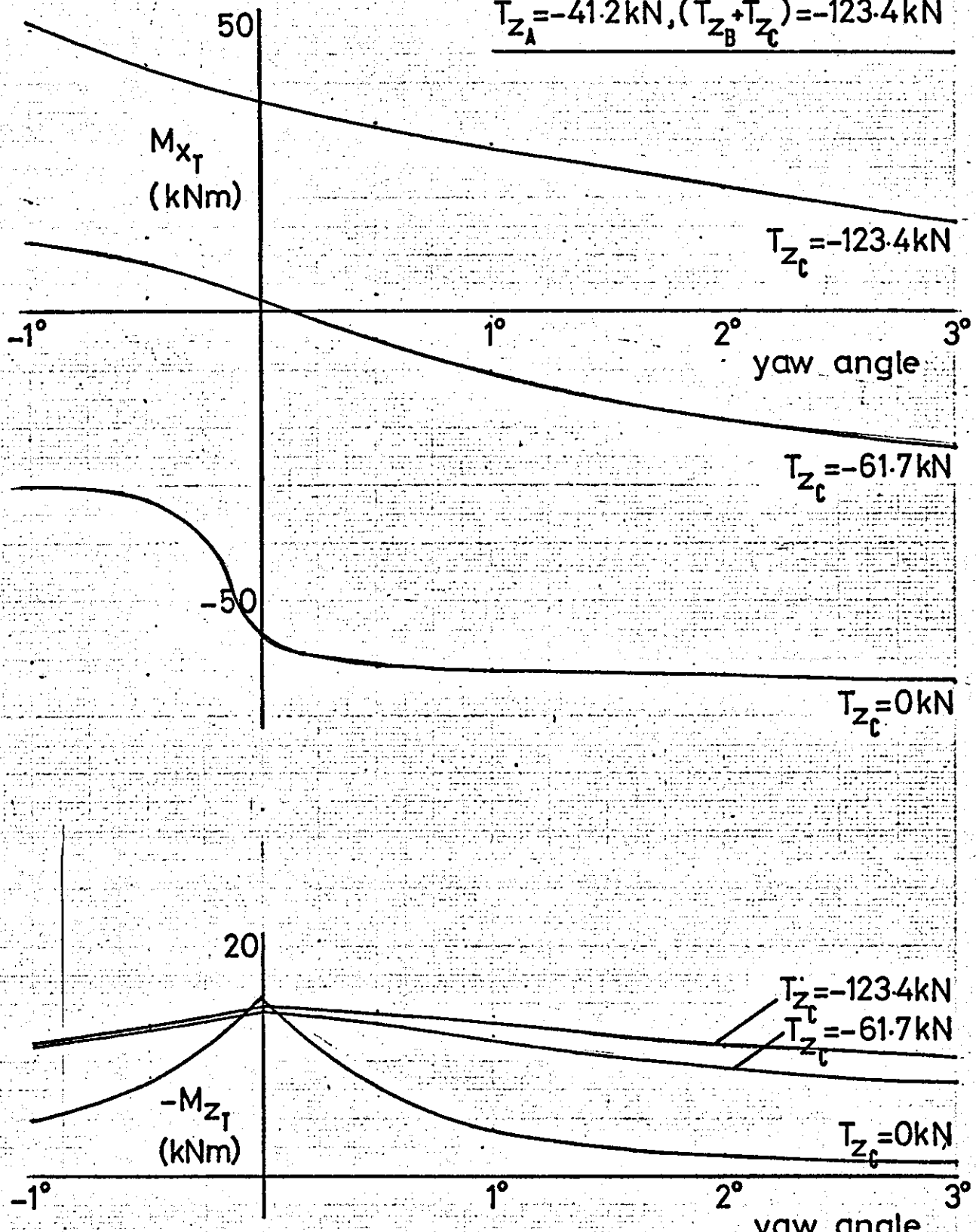

FIG. 6·15 Wheelset Forces T_{y_f}, T_{y_c} v Yaw Angle

Worn Rail $\mu = 0.25$

$T_{z_A} = -82.3kN, (T_{z_B} + T_{z_C}) = -82.3kN$

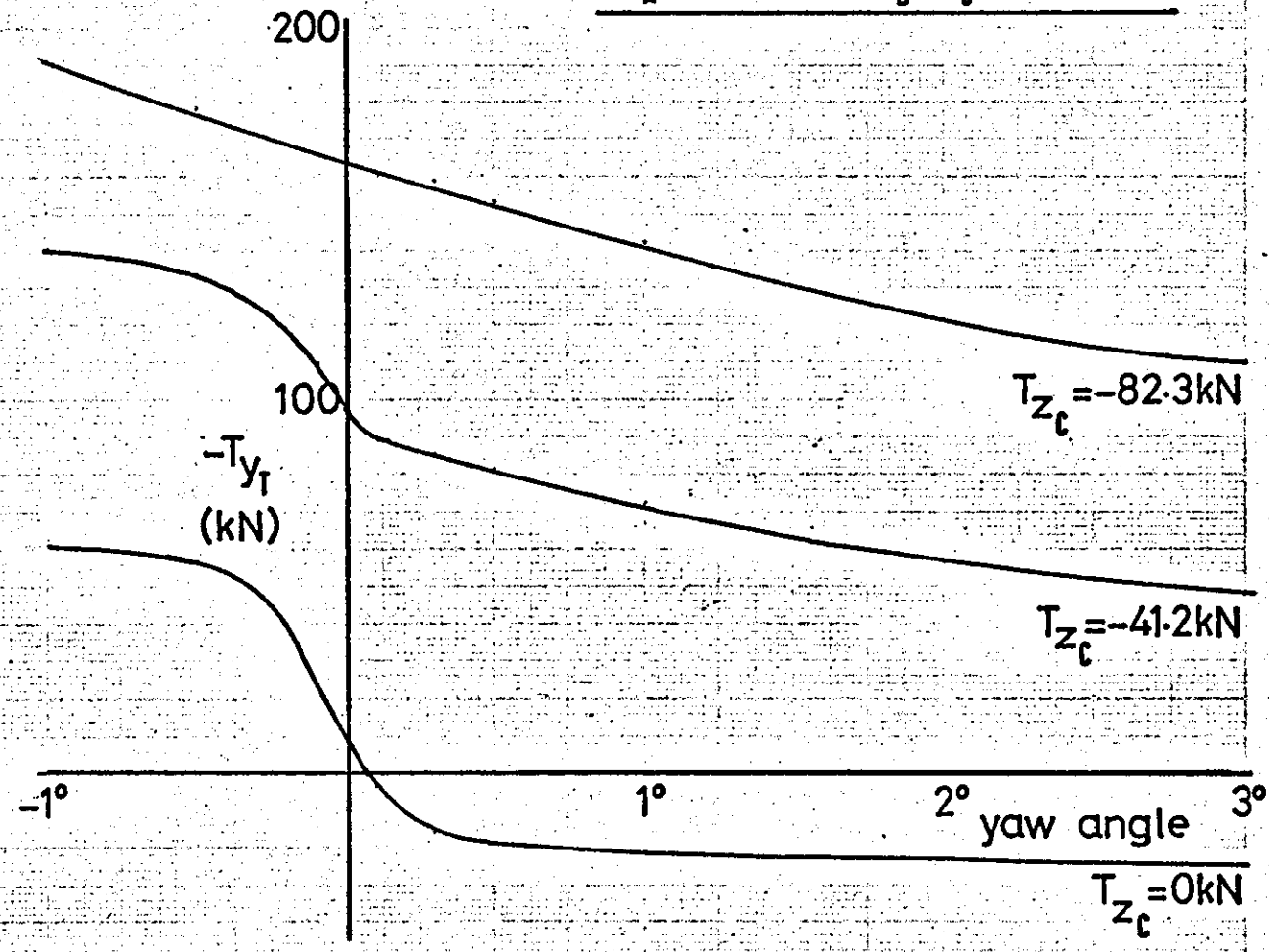

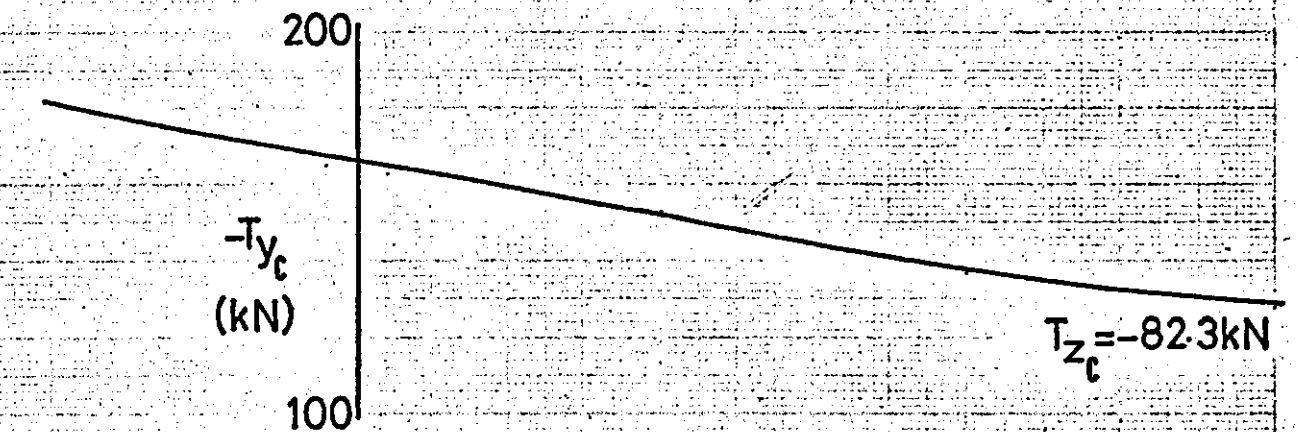

FIG. 6.16 Wheelset Moments M_{x_T}, M_{z_T} v Yaw Angle

Worn Rail $\mu = 0.25$

$T_{z_A} = -82.3\,kN$, $(T_{z_B} + T_{z_C}) = -82.3\,kN$

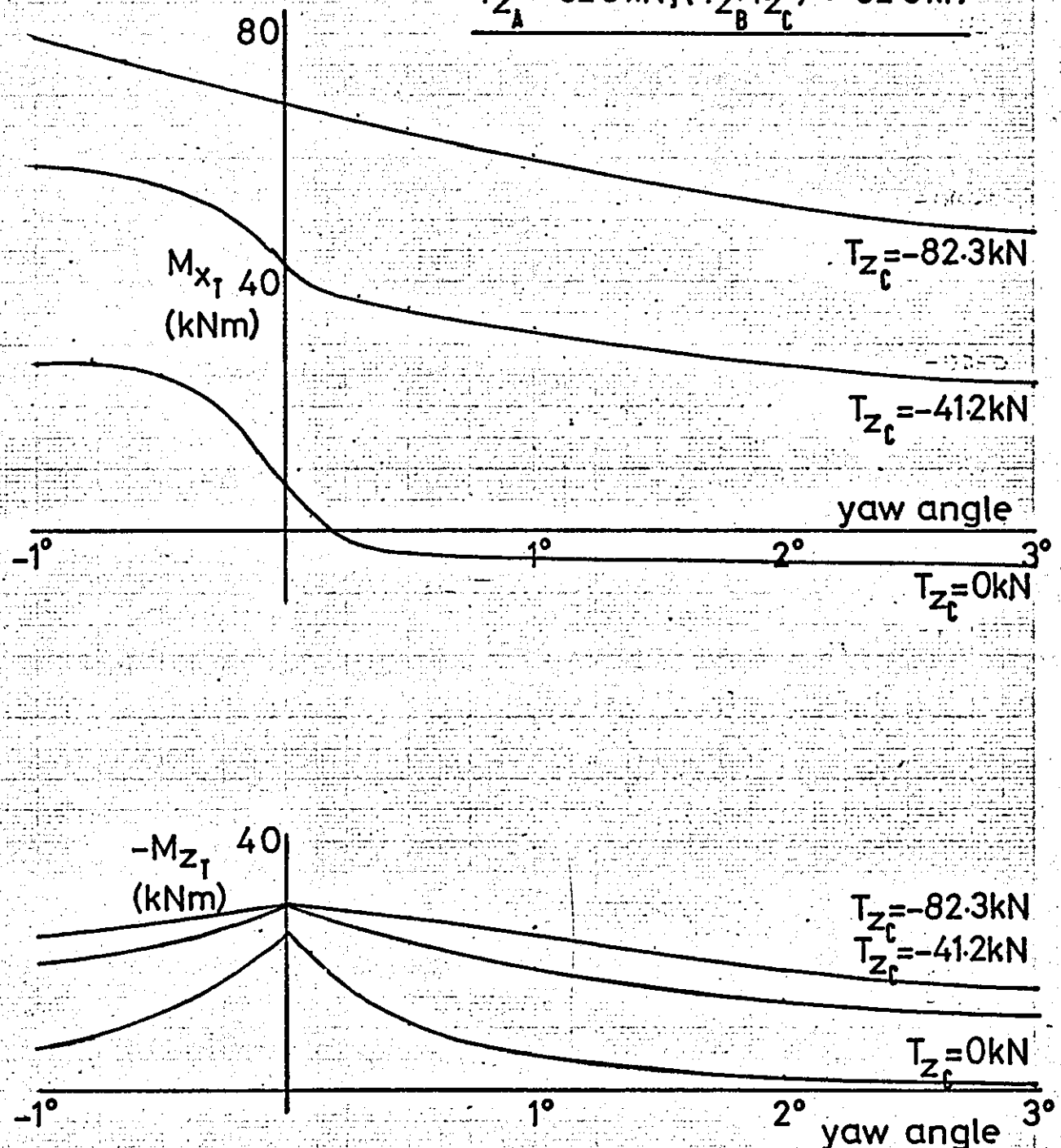

FIG. 6·17 Wheelset Forces T_{y_T}, T_{y_C} v Yaw Angle

Worn Rail $\mu = 0.25$

$T_{z_A} = -123.4\,kN$, $(T_{z_B} + T_{z_C}) = -41.2\,kN$

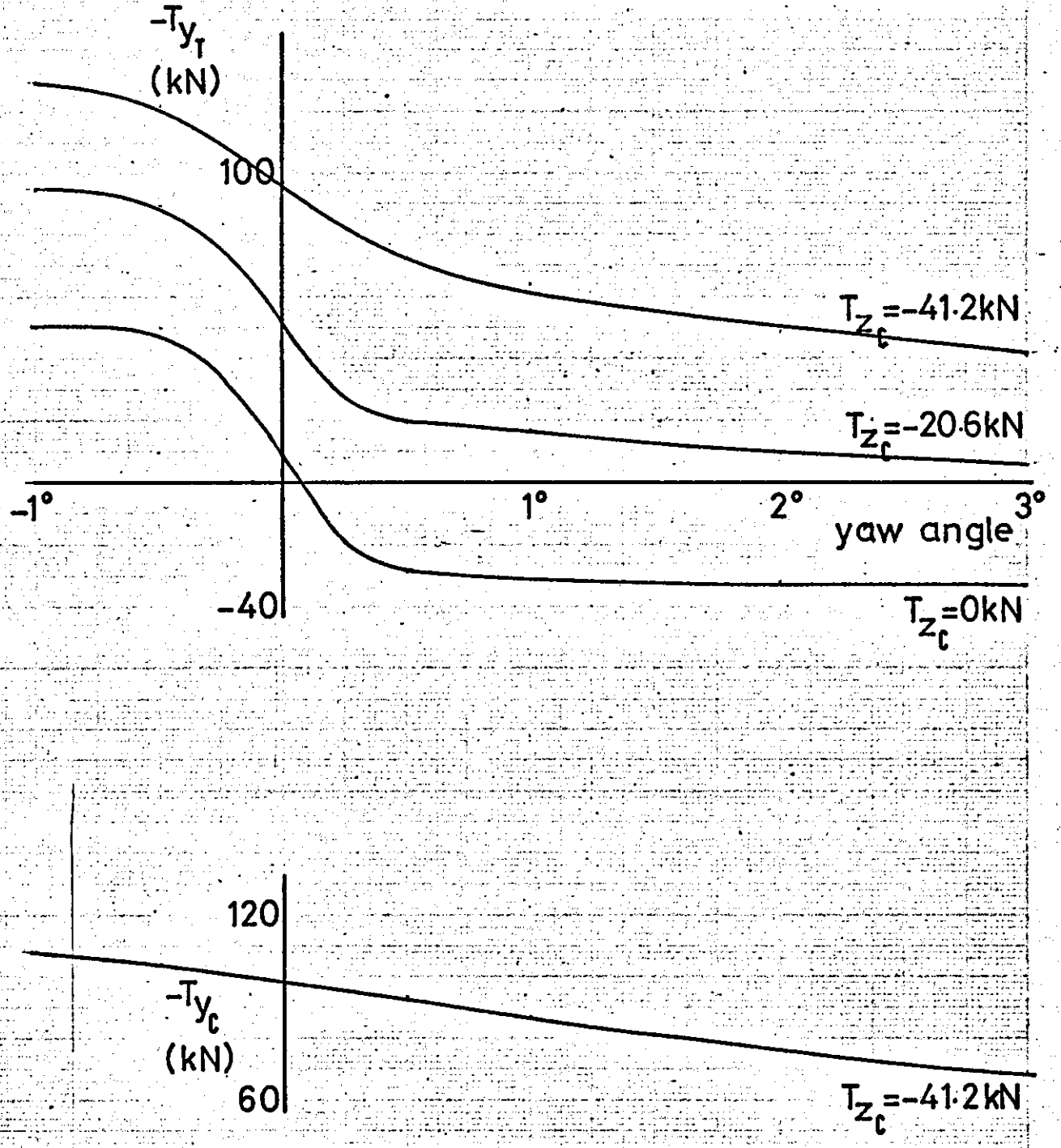

FIG. 6·18 Wheelset Moments M_{x_T}, M_{z_T} v Yaw Angle

Worn Rail $\mu=0{\cdot}25$

$T_{z_A}=-123{\cdot}4\,kN, (T_{z_B}+T_{z_C})=-41{\cdot}2\,kN$

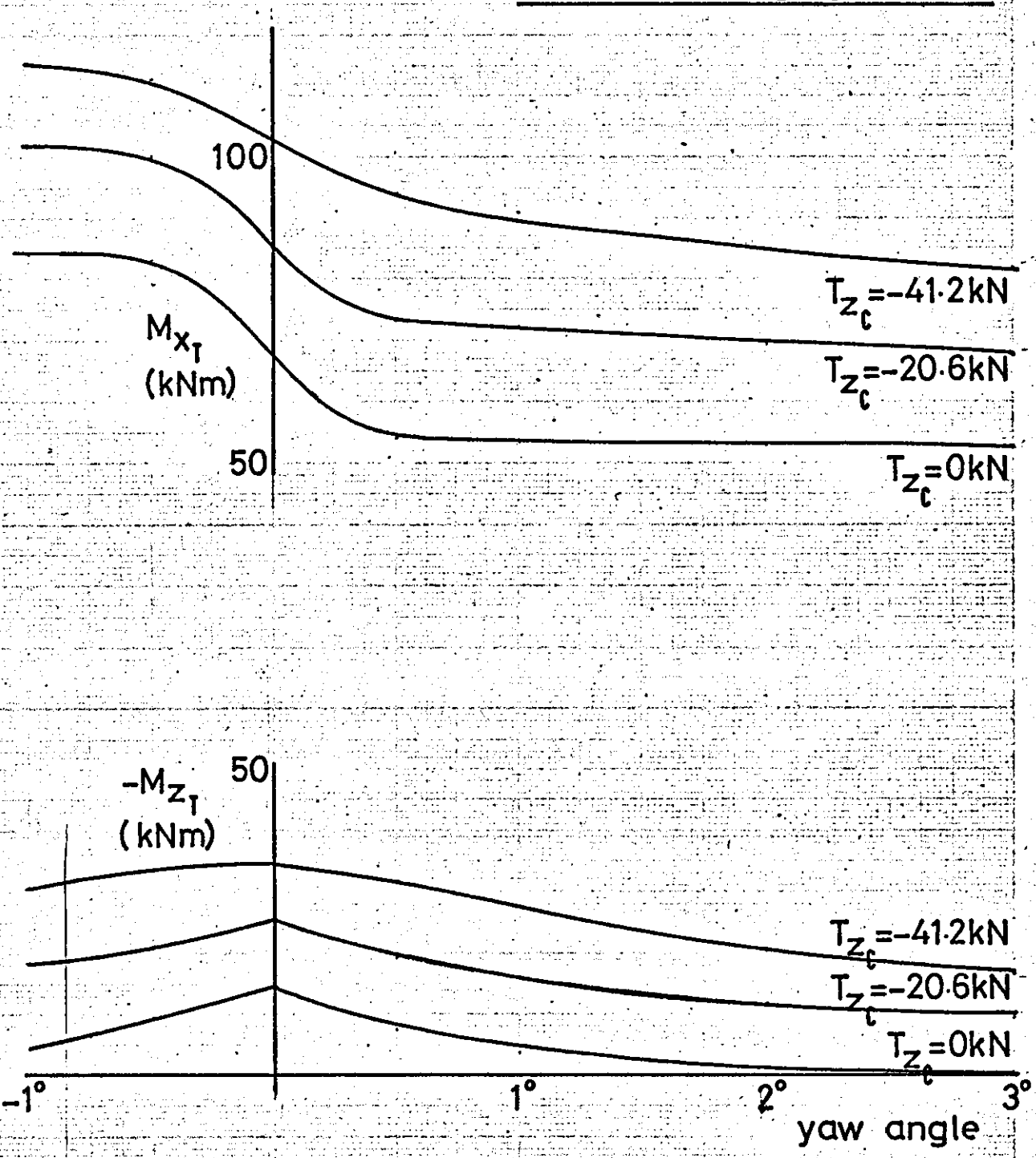

7. Derailment Ratio

7.1 Introduction

With railway trains operating at ever increasing speeds the question of safety arises, and this requires a better understanding of the derailment phenomena. Since the forces between wheel and rail are so complex, especially when the flange contacts the rail, little work has been done in this area. The problem is complicated further since it depends on many other factors, one of these being the condition of wheel and track, which varies from one vehicle to another. This problem is also of interest to the railway civil engineer who needs to know how much wear can be tolerated on the track before it is taken out of service and renewed.

As a guide to derailment proneness various formulae have been proposed which give a (lateral force/vertical force) ratio for a particular rail/wheel combination. This ratio is usually called the 'derailment ratio' or 'derailment quotient' and is denoted by (F/W).

The wheelset normally runs along the track near its neutral position with a point of contact on the tread of each wheel. If a side force acts on the wheelset it moves laterally until the flange of one wheel also contacts the rail. If this side force is increased further a load transfer takes place until there is only contact on the flange of one wheel and the tread of the opposite wheel. This condition is considered to be the start of derailment and if F and W are the lateral and vertical forces at the flange, respectively, then the derailment ratio (F/W) is used as a measure of the running safety of vehicles.

Since the forces have been calculated on a wheelset, during the present investigation, for both new and worn rails for a range of yaw angles, Section 6, it is a small step to compare the (F/W) ratios for these results with existing formula for the same theoretical wheelset. The

present analysis is the first time any rolling contact theory has been used to predict flange forces, and since it includes spin effects, should give a more accurate estimate of the (F/W) ratio.

The existing formulae are described in Section 7.2, followed in 7.3 by a comparison between these formulae and the present results. A discussion of the correlation between the two follows in Section 7.4.

7.2 Existing formulae for Derailment Ratio

7.2.1 Nadal's Formula

This formula is very simple and very approximate since it does not allow for yawing of the wheel relative to the rail and does not take account of spin effects due to the flange cone angle. It assumes the flange is sliding on the rail and as such is the limiting value for very large lateral creeps, i.e. very large yaw angles.

If, in Fig. 7.1, F and W are the lateral and vertical forces at the flange respectively, and T_2 and T_3 are the forces in the plane, and normal to the contact area respectively.

Then $$F = T_2 \cos\lambda - T_3 \sin\lambda \qquad (1)$$

and $$-W = T_3 \cos\lambda + T_2 \sin\lambda \qquad (2)$$

Assuming $$T_2 = \mu T_3$$

Then $$\frac{F}{W} = \frac{\tan\lambda - \mu}{1 + \mu\tan\lambda} \qquad (3)$$

Equation 3 is Nadal's formula for the derailment ratio.

FIG. 7.1 Forces at Flange Contact Point

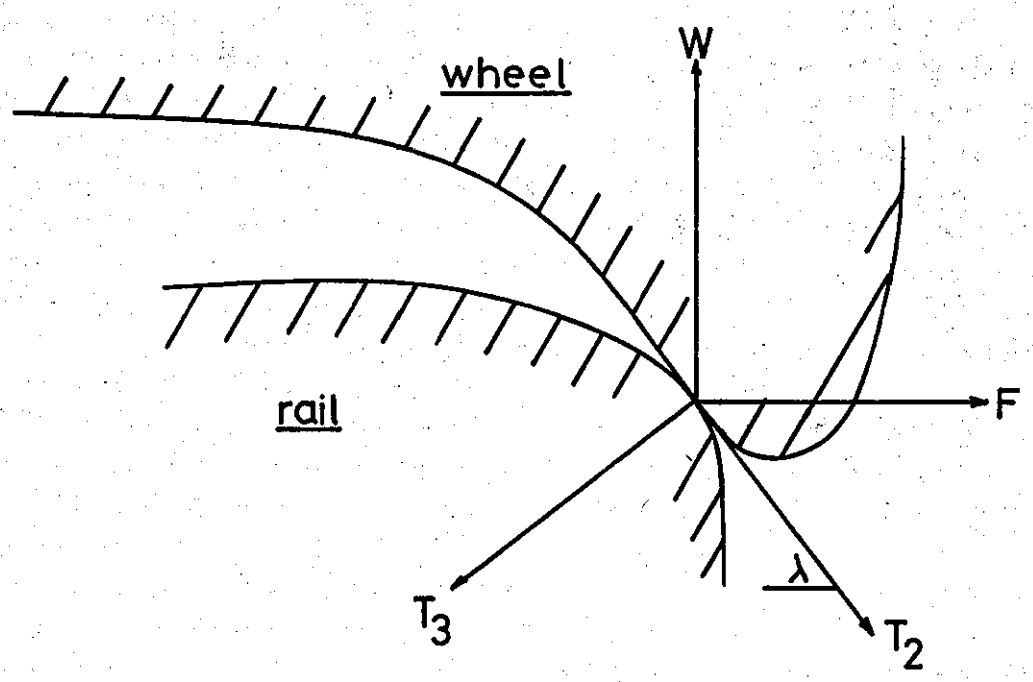

FIG. 7.2 Flange Contact Point, showing forward shift due to yaw

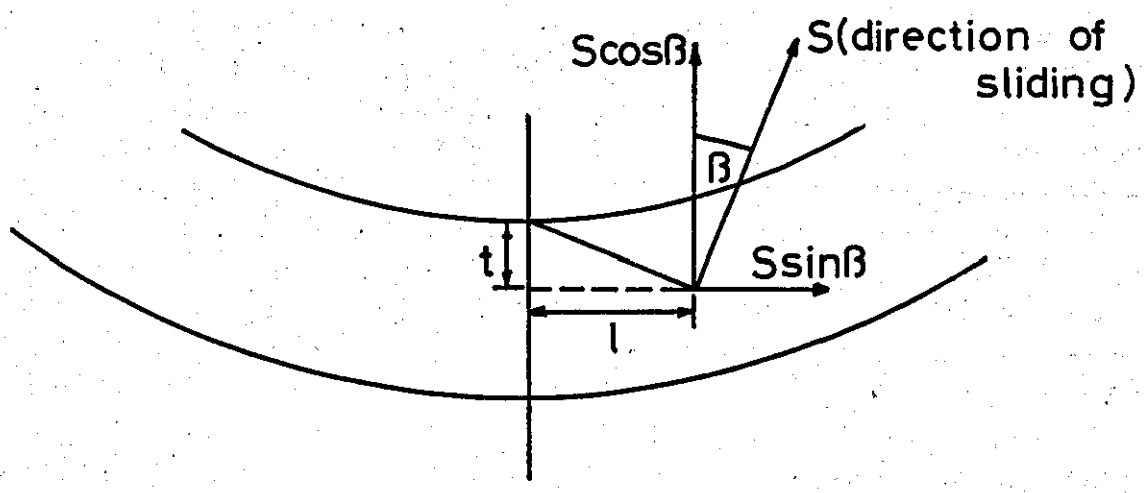

7.2.2 Wagner's Formula

This is more refined than the previous formula since it takes account of the yaw angle between wheel and rail, and allows the flange contact point to move forward as the yaw angle is changed. It still does not take care of spin effects and again assumes the flange is sliding on the rail, i.e. very large yaw angles.

The flange shown in Fig. 7.2 is assumed to be yawed relative to the rail, and the contact point has moved horizontally and vertically by amounts l and t, respectively, from the tread contact point. As a result the lateral force S no longer acts in a vertical plane but at an angle β to the vertical as shown.

Wagner's formula can be derived from equations 1 and 2, assuming $T_2 = \mu T_3$

Thus $F = T_3 (\mu \cos\lambda - \sin\lambda)$

and $-W = T_3 (\cos\lambda + \mu \sin\lambda)$

i.e. $$T_3 = \frac{F}{\mu\cos\lambda - \sin\lambda} = \frac{-W}{\cos\lambda + \mu\sin\lambda} \qquad (4)$$

i.e. $$W\sin\lambda = \mu W\cos\lambda + F\cos\lambda + \mu F\sin\lambda \qquad (5)$$
$$= S$$

When the wheel is yawed relative to the rail the component of the vertical force in the plane of the contact area, $W\sin\lambda = S\cos\beta$

Thus $W\sin\lambda = (\mu W\cos\lambda + F\cos\lambda + \mu F\sin\lambda)\cos\beta$

and $$\frac{F}{W} = \frac{\sin\lambda - \mu\cos\lambda\cos\beta}{(\cos\lambda + \mu\sin\lambda)\cos\beta}$$

i.e. $$\frac{F}{W} = \frac{\tan\lambda - \mu\cos\beta}{(1 + \mu\tan\lambda)\cos\beta} \qquad (6)$$

(To be correct this is a modified version of Wagner's formula due to Heumann. The original equation by Wagner did not contain the term $\mu\cos\beta$ in the numerator and as such does not tend to

Nadal's formula, equation 3, as it should).

$$\frac{1}{\cos\beta} = \sqrt{1 + \left(\frac{t}{l}\right)^2} \qquad \text{where } l = r \sin\psi \tan\lambda \quad (7)$$

and r = distance between tread contact point and axle.

(This equation for the forward movement of the contact point as the wheel is yawed, is proved in Appendix 7).

Equation 6 contains an obvious irrationality in that as $l \longrightarrow 0$, $\cos\beta \longrightarrow 0$ and $(F/W) \longrightarrow \infty$. This irrationality arises because the formula inherently assumes that the angle of yaw is large by saying $T_2 = \mu T_3$.

7.2.3 Johansen's Formula

In this formula as in Wagner's formula, the forward movement of the flange contact point as the wheel is yawed is catered for, although the flange is assumed to be sliding on the rail, i.e. $S = \mu T_3$, and again the lateral force due to spin is not allowed for.

The formula may be derived from equations 1 and 2 where it is assumed that $T_2 = S \cos\beta \;\&\; S = \mu T_3$

Thus $F = \mu T_3 \cos\beta \cos\lambda - T_3 \sin\lambda$

and $-W = T_3 \cos\lambda + \mu T_3 \cos\beta \sin\lambda$

Thus $$\frac{F}{W} = \frac{\sin\lambda - \mu\cos\lambda \cos\beta}{\cos\lambda + \mu\cos\beta \sin\lambda}$$

i.e. $$\frac{F}{W} = \frac{\tan\lambda - \mu\cos\beta}{1 + \mu\tan\lambda \cos\beta} \qquad (8)$$

This formula does not contain the irrationality of Wagner's formula since as $\cos\beta \longrightarrow 0$, $(F/W) \longrightarrow \tan\lambda$, which is the expected result if the spin effect is ignored.

Johansen calculates β in a slightly different way to Wagner but the end result is practically the same for large cone angles.

$$\tan\beta = \frac{t}{l}\sin\lambda$$

Thus $$\frac{1}{\cos\beta} = \sqrt{1 + \left(\frac{t}{l}\sin\lambda\right)^2} \qquad (9)$$

As $\cos\beta \longrightarrow 1$ $\quad \frac{F}{W} \longrightarrow \frac{\tan\lambda - \mu}{1 + \mu\tan\lambda}$ (Nadal's formula)

This was also true of Wagner's formula, equation 6.

7.3 Results

In Section 6 forces were calculated on a wheelset using simplified theory for the flange contact point, and numerical theory for the tread contact points. Results were calculated for various load distributions for a standard rail with a 0.5" corner radius and for a 'worn' rail with a 0.7" corner radius. These results were plotted in Figs. 6.1 to 6.18.

In these results the derailment ratio, (F/W) is given by (T_{y_C}/T_{z_C}) when $T_{z_B} = 0$. Since three side-to-side load distributions were analysed, three curves can be drawn for (T_{y_C}/T_{z_C}) v ψ for the standard rail and three for the worn rail. The results for the worn rail are plotted in Fig. 7.3. The results for the standard rail are indistinguishable from these results.

FIG. 7.3 Derailment Ratio v Yaw Angle

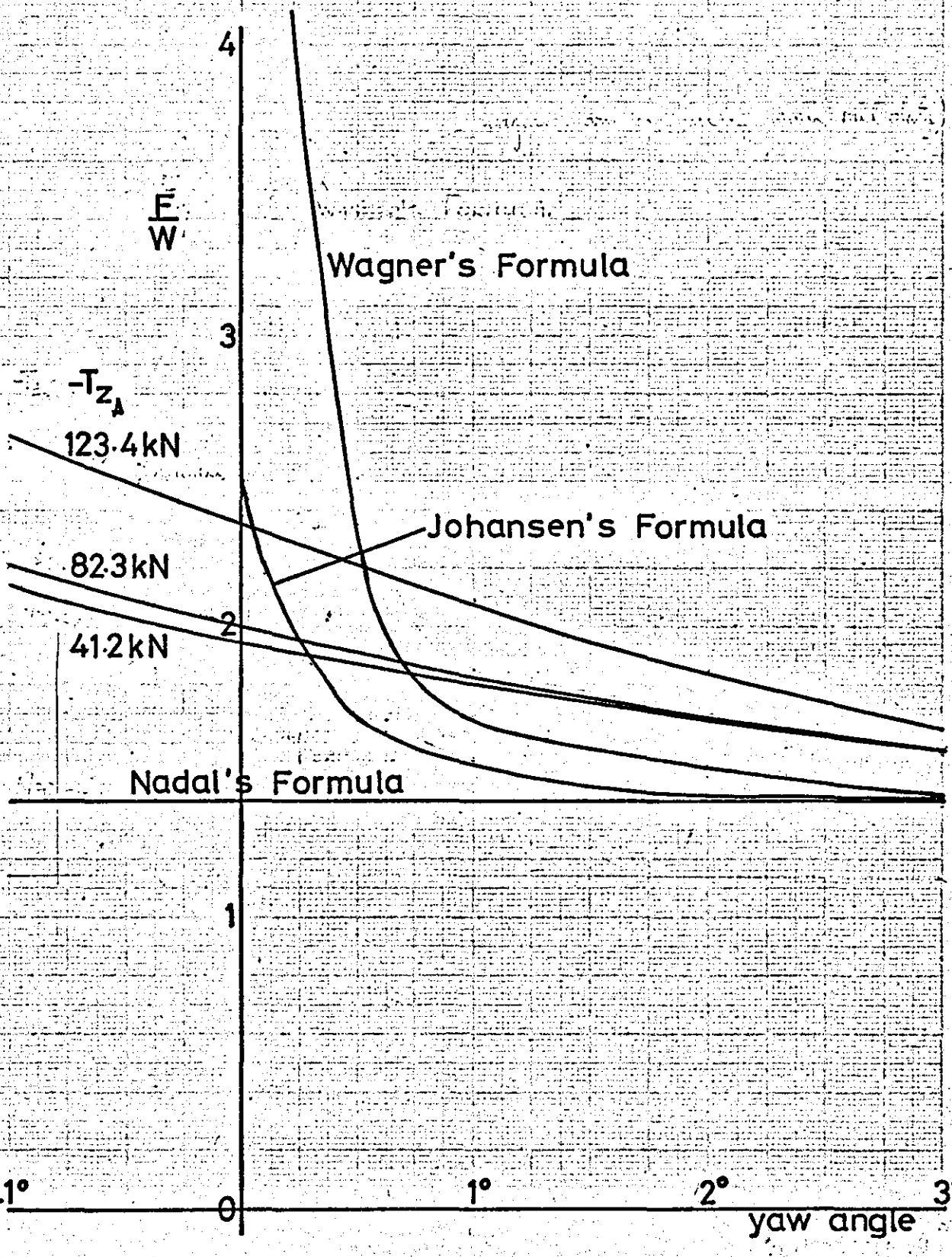

The results for (F/W) using the three formulae just described in Sections 7.2.1, 7.2.2 and 7.2.3 are also plotted in Fig. 7.3 from results given in Table 7.1. The values in Table 7.1 are obtained from the coordinates of the contact points using the 'worn' rail.

Table 7.1 Derailment Ratio's for 'Worn' Rail

ψ°	(t/l)	$1/\cos\beta$ (7.7)	$1/\cos\beta$ (7.9)	F/W (Wagner)	F/W (Johansen)
0	∞	∞	∞	∞	2.5
0.1	6.56	6.64	6.19	9.85	2.22
0.3	2.18	2.4	2.25	3.51	1.87
0.5	1.3	1.64	1.57	2.35	1.68
1.0	0.64	1.19	1.26	1.68	1.54
2.0	0.35	1.06	1.05	1.52	1.42
3.0	0.23	1.03	1.04	1.42	1.41

7.4 Discussion and Conclusions

The derailment ratio is a qualitative measure of how easy a particular rail/wheel combination is to derail. The greater this ratio is the better, since the lateral force needed to maintain flange contact is greater and thus less likely to occur in practice.

The various formulae that have been proposed are very crude and none of them account for spin effects. Nadal's formula assumes the flange is sliding on the rail and takes no account of the yaw angle between wheel and rail. As a result it gives the worst case and results will tend to this value at large angles of yaw. For the present rail/wheel combination it is 1.4.

Wagner's formula is an attempt to take account of the forward movement of the contact point as the wheelset is yawed, but again assumes the flange to be sliding on the rail, and does not allow for spin. The resulting formula tends to 1.4 for large angles of yaw but has an irrationality at $\psi = 0^{\circ}$ where (F/W) tends to infinity.

Johansen's formula is better since at $\psi = 0^{\circ}$, $(F/W) = \tan \lambda$, but again spin is not accounted for. The flange is assumed to be sliding on the rail and the results tend to 1.4 for large yaw angles, the value given by Nadal's formula.

It can be seen that as $\cos \beta$ tends to 1 both Wagner's formula and Johansen's formula tend to Nadal's formula.

The basic difference between Wagner's formula and Johansen's formula can be seen by referring to Figs. 7.1 and 7.2. Wagner assumes that the inclined force S is given by

$$S = \frac{W \sin \lambda}{\cos \beta}$$

while Johansen assumes

$$S = \frac{T_2}{\cos \beta}$$

Since the latter result is the correct one, Johansen's formula should give more sensible results for the derailment ratio.

The effect of lateral force due to lateral creep for positive yaw angles is to tend to lift the wheel off the rail. The effect of spin is the same. Thus Johansen's formula, which does not cater for spin, gives too large a value for the derailment ratio at $\psi = 0^{\circ}$ and too low a value at large +ve yaw angles.

The (F/W) ratio variation with yaw angle plotted in Fig. 7.3, using the present theoretical results, is the first time a rolling contact theory has been used to predict this ratio and the simplified theory used on the flange takes account of spin and lateral creep. Curves for three different side-to-side load distributions are shown in Fig. 7.3. The curves tend to Nadal's values for large yaw angles but lie between Nadal's value and Johansen's value at $\psi = 0^{\circ}$. The curves show that the (F/W) ratio falls as the yaw angle is increased and the minimum values from these curves are (F/W) = 1.94 at $\psi = 0^{\circ}$ and (F/W) = 1.57 at 3°.

In Johansen's report, Ref. 40, he predicts very low values for the (F/W) ratio, e.g. for a new tyre and new rail (not the profiles used in the present analysis) at $\psi = 5^{\circ}$ and $\mu = 0.25$, (F/W) is as low as 1.0. In Ref. 40 the contact points are found by drawing sections through the rail and wheel about 16x full size. By drawing different projections of the wheel he is able to measure the distances between flange and rail and assumes that if the wheel were displaced laterally by the calculated amount, that is where the flange contact point would be. Errors are involved in this procedure since roll and vertical displacement of the wheelset as it is moved laterally are not allowed for, and apart from this there are inaccuracies involved in the drawing process.

According to Baguley, Ref. 61, the value of (F/W) ratio used by British Rail as a standard is 1.04 and this was probably based on Johansen's work or on Nadal's formula. It has been shown in the present analysis that for values of yaw less than 3° (which is probably a very large value in practice) these formulae predict rather low values for (F/W). It must be remembered when quoting these results that they are calculated assuming steady loads and do not apply to impulsive loads.

Matsui, Ref. 60, describes some experiments which were carried out by the Japanese National Railways to measure the derailment ratio on 1/10 and 1/5 scale model wheels. They found (F/W) tended to Nadal's value for angles of yaw greater than 1° and tended to $\tan \lambda$ at $\psi = 0^{\circ}$. These tests were carried out with a standard J.N.R. wheel which has a 60° cone angle.

The (F/W) ratio used by J.N.R. on their high speed Tokaido line is 0.8, which is a very low value in view of the fact that the cone angle used is 70°.

It seems that values of (F/W) ratios used by railway authorities are minimum values and therefore safe values. However, the present results give the variation of (F/W) with yaw angle, taking account of spin, and show that in fact the (F/W) ratio is larger than the approximate formulae predicted over most of the range. This would mean that more wear can be tolerated between rail and wheel than using present standards, thus improving the economics of the railways.

8. Experimental Investigation

8.1 Introduction

For normal running of a wheelset on track, contact exists between the tread of the wheel and the rail. Under such conditions the contact area is almost circular in shape and the creepage and spin are both small. Various theories exist, which have been proven experimentally, to calculate the contact area forces for these conditions.

It has been shown in the previous sections, that when the flange contacts the rail conditions are very different; the contact ellipse becomes elongated and the spin is large due to the large cone angle. Although theories exist which can predict contact area forces for such conditions, there is no experimental evidence available to support them.

Because of this, an experimental program of work was commenced to provide data on elongated contact ellipses with varying amounts of creep and spin present. It was argued that if experimental and theoretical results correlated for a scale wheel of known geometry then the theories could be used with some safety to predict wheelset forces under flange contact conditions. In this situation it is the lateral force which is of prime importance and this arises due to both lateral creep and spin. Because of this longitudinal forces due to longitudinal creep were eliminated as far as possible in the design of the rig.

The rig simulates flange contact of a railway wheel and enables lateral force due to varying amounts of lateral creep and spin to be measured on wheels with elongated contact ellipses.

The rig is described in Section 8.2 and the theory given in 8.3. The procedure adopted in carrying out the tests is given in 8.4. Various combinations of wheels were tested giving different contact ellipses and different amounts of spin. For each case the lateral creep, contact pressure and speed were varied. The results of these tests are given in Section 8.5 and a discussion of the correlation between them and theory follows in 8.6. Conclusions and recommendations are given in Section 8.7.

8.2 Rig Description

The rig which was designed to meet the following objectives, is shown in Figs. 8.1, 8.2, 8.3 and diagramatically in Fig. 8.4:

1. To simulate flange contact conditions as closely as possible with longitudinal creep eliminated.

2. To vary the lateral creep at the contact point throughout the range from pure rolling to gross sliding.

3. To vary the spin.

4. To vary the shape of the contact ellipse and particularly to investigate elongated contact ellipses (long in the direction of rolling).

5. To measure changes in lateral force due to variations of lateral creep and spin.

6. To investigate speed effects.

7. To vary the pressure between contact surfaces.

FIG. 8.1 Overall View of Roller Rig

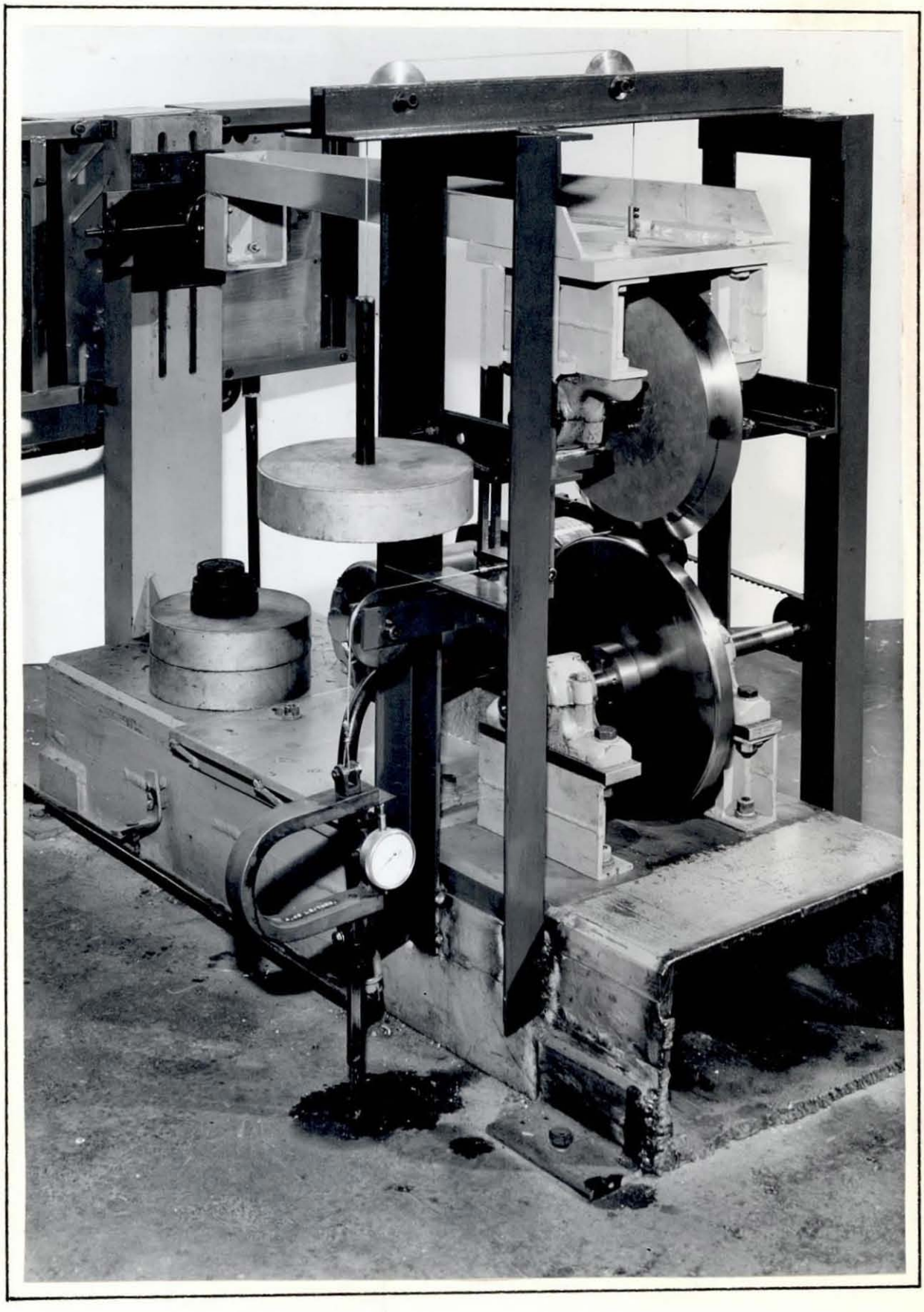

FIG. 8.2 Rear End View of Roller Rig

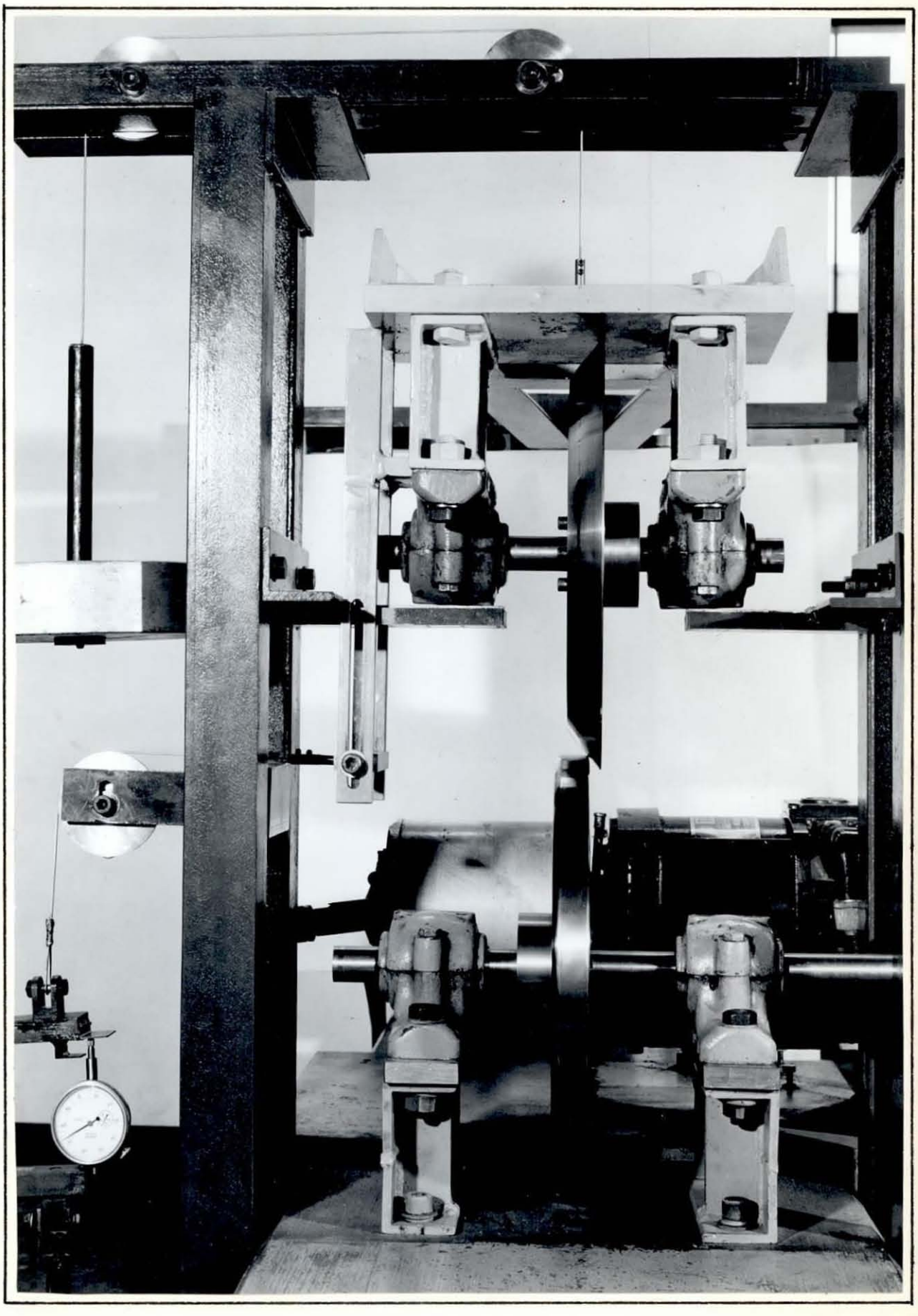

FIG. 8.3 Front End View of Roller Rig

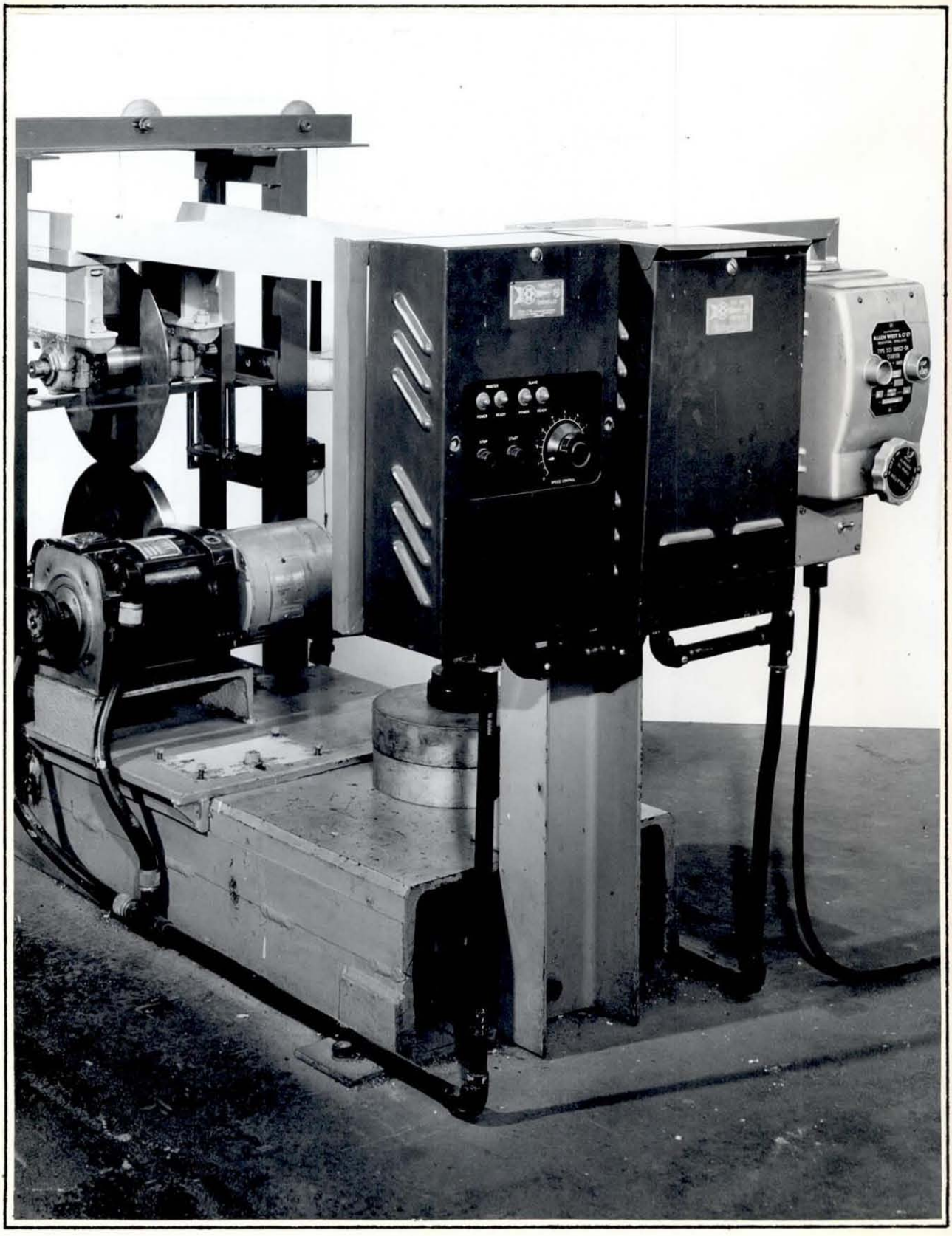

FIG. 8.4 Roller Rig

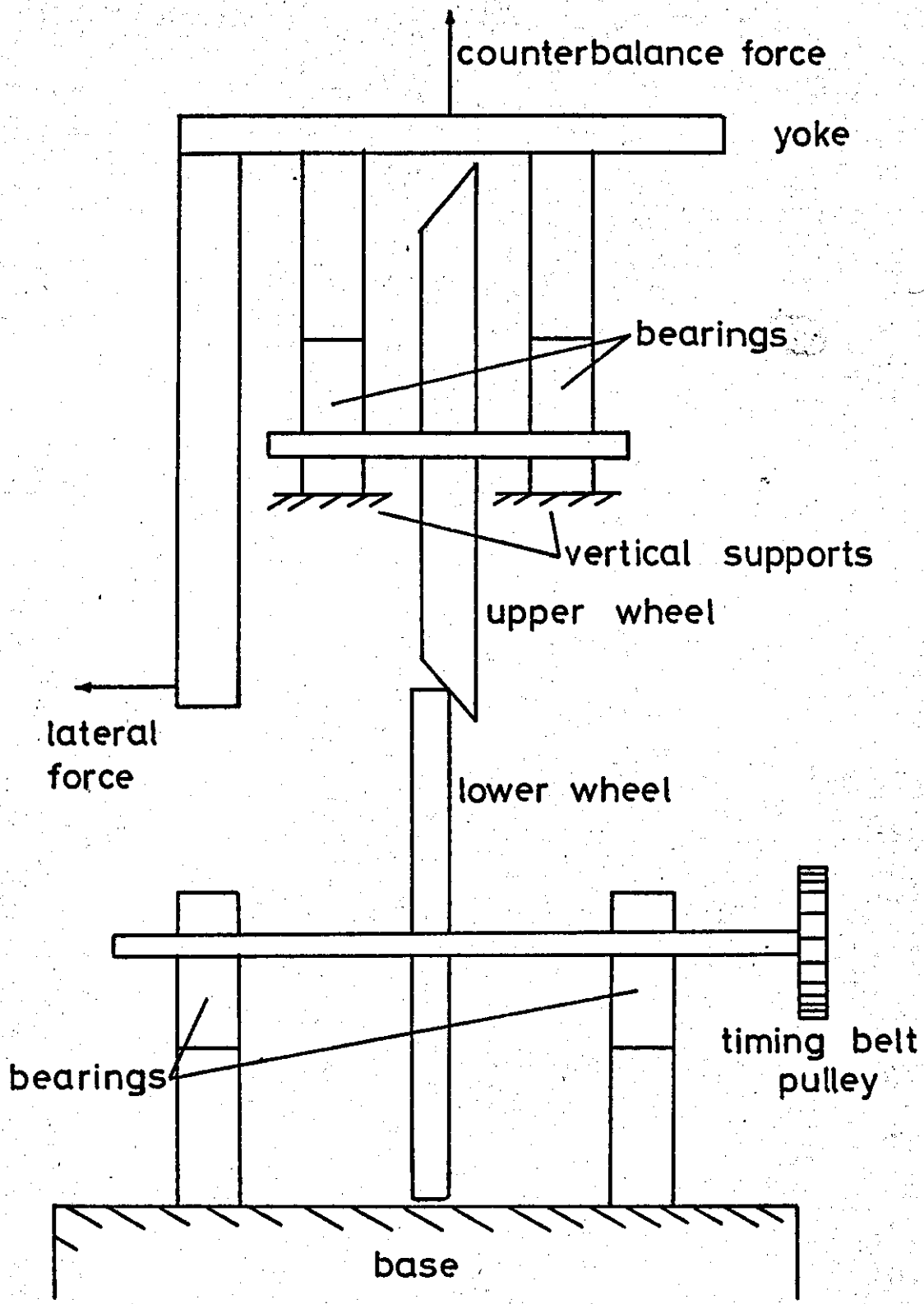

8. To conform as closely as possible to assumptions made in the theories, namely that the bodies in contact have smooth surfaces and that Coulomb or dry friction exists between them.

The rig consists of a hardened steel wheel of approximately 0.305 m dia. which is driven at constant speed in contact with a similar wheel which is free to rotate in its bearings. The lower, or driven wheel, (or 'rail') has a profile radius machined around its periphery, while the upper, or free wheel, has a straight conical profile. The upper wheel is mounted on a short stub shaft and is supported in self-aligning bearings; these in turn are attached to a yoke which is pivotted about a point approximately 1 m ahead of the wheel axis to a rigid frame. The pivot is a Hookes Joint which allows the upper wheel to pitch and yaw relative to the lower wheel, but prevents roll. The Hookes Joint can be moved along a horizontal slider and clamped in any position so that an angle of yaw can be set between the two wheels. The horizontal displacement of this pivot is measured with a dial test indicator calibrated to 0.0025 mm. The yaw angle is given by the DTI measurement divided by the distance from the pivot to the wheel axis. It will be shown later that the lateral creep is directly related to the yaw angle.

The spin is varied by using upper wheels with different cone angles, while the contact ellipse shape is varied by using lower wheels with different profile radii. Longitudinal creep was eliminated by allowing one wheel to freely rotate on the other with as little friction as possible in the bearings.

Initially the weight of the upper wheel and yoke is supported on its bearing caps by two vertical supports attached to the frame of the rig. These are adjustable in height so that the rolling radius on

the upper wheel can be selected. The yoke can be loaded, or the weight counter balanced through a system of pulleys, to investigate variation of contact pressure between the rolling surfaces. A lateral force can be applied to the upper wheel through an arm welded to the yoke, the point of application of this force being adjustable to ensure that it passes through the centre of the contact area. The actual force is applied by a wire passing over a pulley attached to a load ring and turn buckle.

Having set the required angle of yaw and started the motor, the lateral force is then increased until the upper wheel begins to climb up the lower wheel. This is observed by the upper wheel bearing caps lifting off the supports. At this point the forces are in balance, and the contact area forces can be calculated from the measured lateral and vertical forces. Thus the lateral force corresponding to known amounts of lateral creep and spin can be found, while the shape of the contact area can be calculated from the wheel geometry.

The equations for the creep, spin and forces on the rig are derived in Section 8.3 while the experimental procedure adopted is given in more detail in 8.4. A detailed explanation of the various parts of the rig follows.

The wheels used are shown in Figs. 8.5 and 8.6. Their main dimensions and physical properties are given in Table 8.1. Each was machined, case hardened and then ground to its final profile. The hardness and roughness of each wheel was measured before running and is also given in Table 8.1.

Shafts on which the wheels are mounted, Fig. 8.7, are made from mild steel with a collar welded on to react thrust loads. The lower shaft, which is mounted in self aligning bearings attached rigidly to the base, has a 'Fenner' timing belt pulley which transmits

Table 8.1 Physical Properties of Wheels

	Lower Wheels			Upper Wheels	
Wheel	a	b	c	d	e
Corner radius(mm)	101.5	6.35	3.18	-	-
Cone angle	-	-	-	49°	67°
Outside dia.(mm)	304.8	304.8	304.8	304.8	188.0
Width(mm)	34.9	25.4	25.4	25.4	25.4
Material	EN36	EN36	EN36	EN36	EN36
Hardness Rockwell No.	58	60	60	60	54
Roughness (μm)	.508	.610	.457	.178	.457

Table 8.2 Parameters of Cases Tested

Case	1	2	3	4	5	6
Lower wheel	a	a	b	b	c	c
Upper wheel	d	e	d	e	d	e
r_c (mm)	101.5	101.5	6.35	6.35	3.18	3.18
λ^o	49	67	49	67	49	67
r_r (mm)	141.3	117.5	149.2	148.0	151.3	150.5
r_w (mm)	141.3	76.2	135.0	67.9	142.4	71.4
ρ (mm)	209.6	218.4	24.0	24.1	12.4	12.4
(a/b)	1.038	1.111	6.45	6.75	10.0	10.3
K($N^{\frac{1}{3}}$)	3616.	6222.	717.	1200.	431.	721.
$\chi_{max.}$	2.46	2.34	0.262	0.256	0.122	0.122

($\chi_{max.}$ = value of χ when $f_2 = 1$ for the case $\xi = \eta = 0$ according to linearised theory)

Table 8.3 Spin Parameter for the Cases Tested

Case	1	2	3	4	5	6
$\mu = .6$	3.72	7.26	0.426	0.795	0.212	0.392
$\mu = .7$	3.19	6.22	0.365	0.681	0.182	0.336

FIG. 8.5 Lower Wheels

Scale = $\frac{1}{2}$ x full size

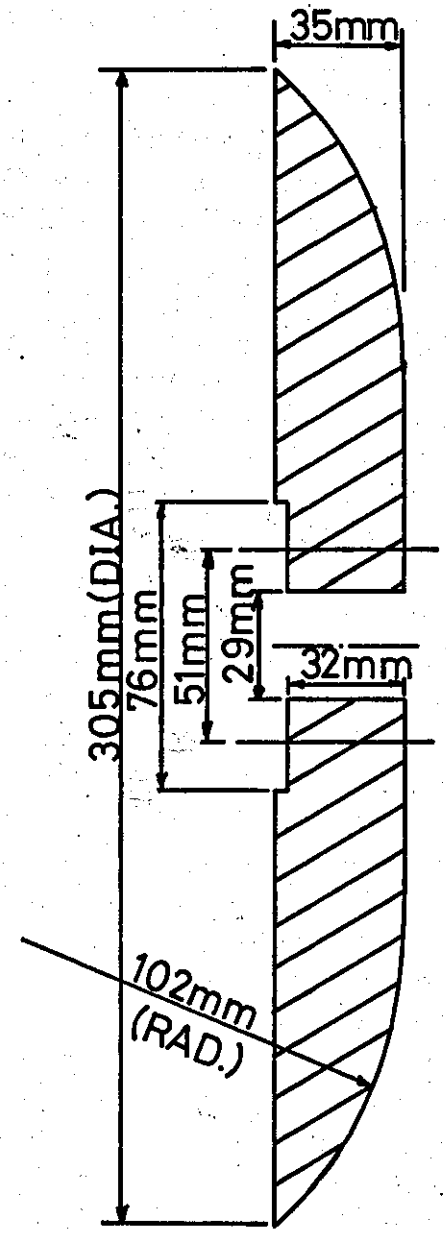

wheel a

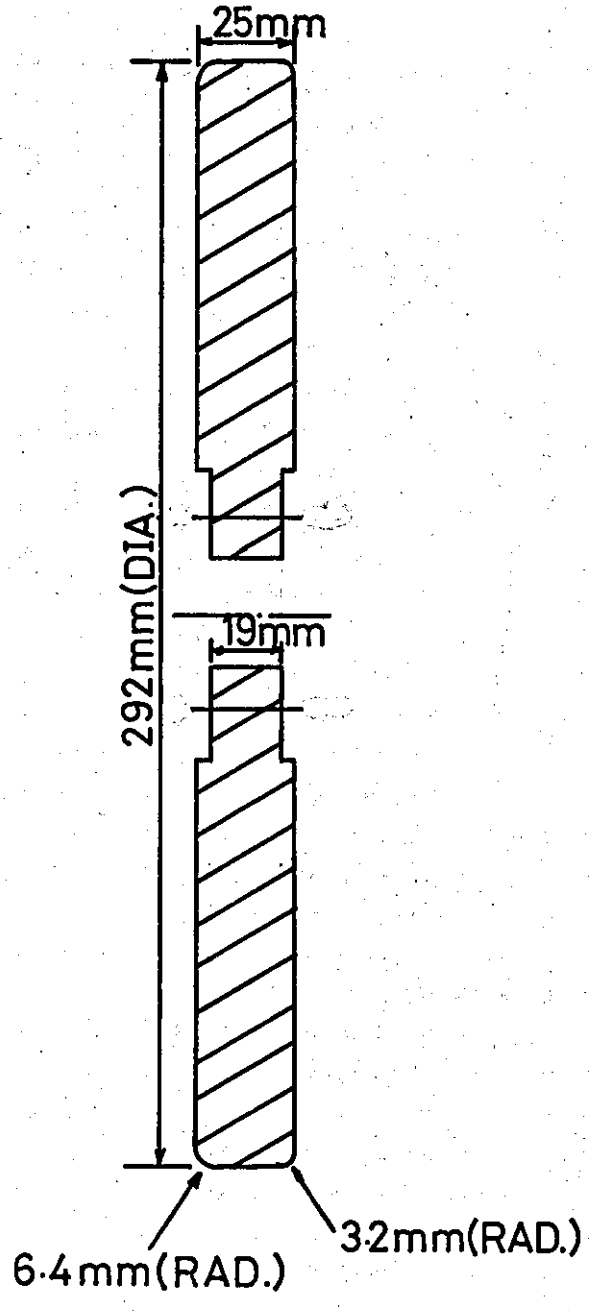

wheel b & c

FIG. 8·6 Upper Wheels

Scale = $\frac{1}{2}$ x full size

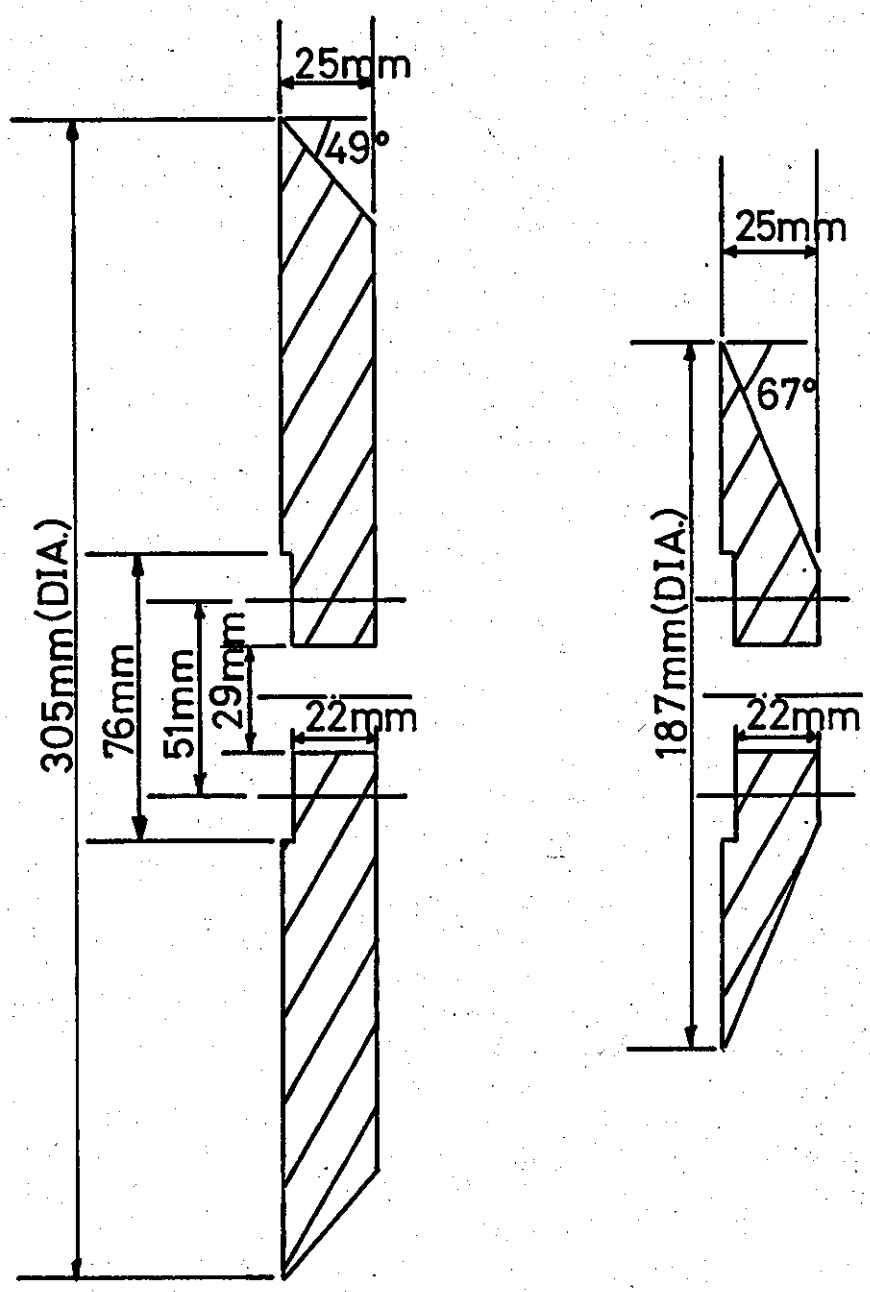

wheel d wheel e

FIG. 8.7 Wheel Shafts

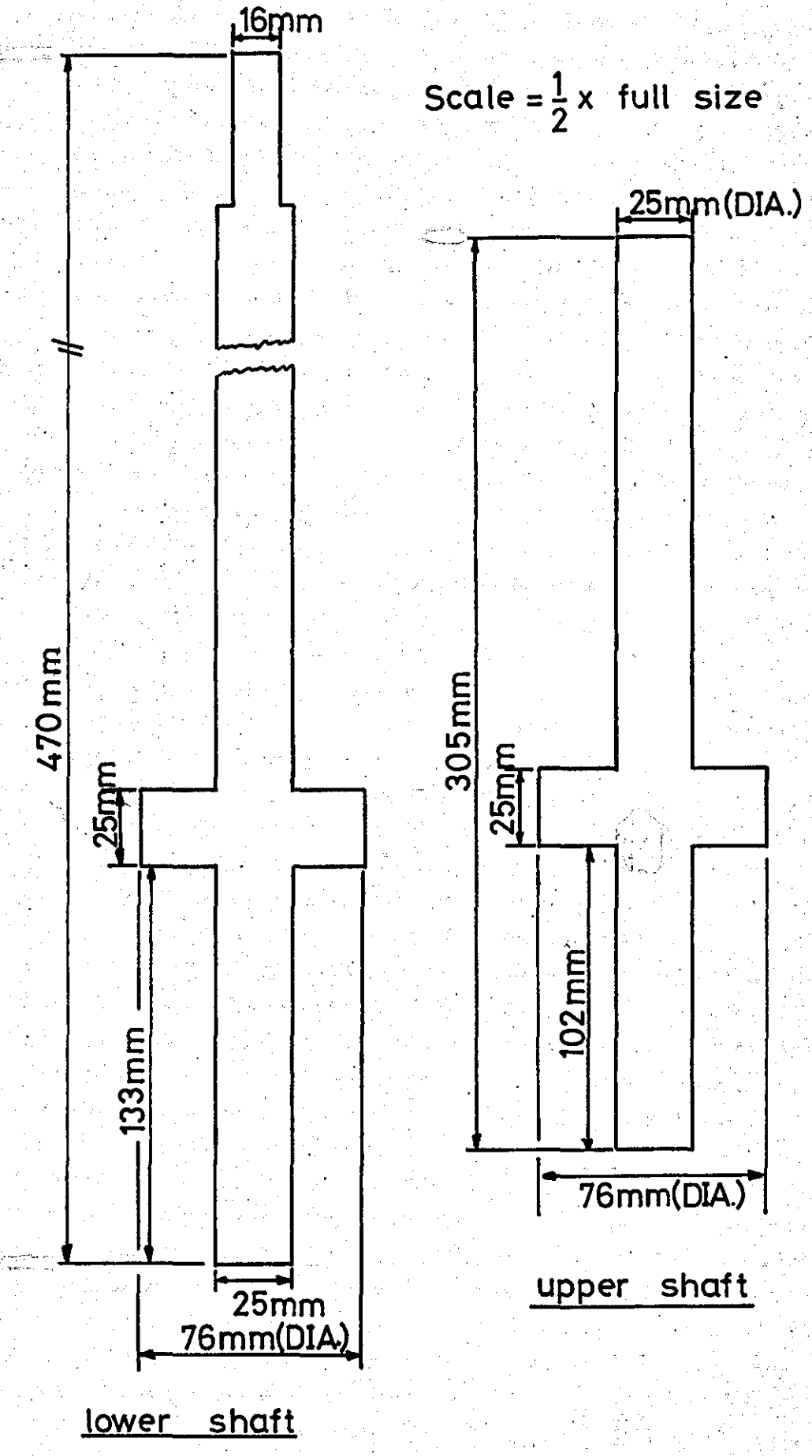

the drive from the electric motor to the lower wheel, via a flexible timing belt.

The lower wheel is driven by a $\frac{3}{4}$ h.p. constant speed motor through an eddy current coupling in which the speed of the wheel is kept constant by a feedback system using the voltage produced by a magslip. The required speed could be set on the Speed Control Unit shown in Fig. 8.3.

The upper wheel is attached through its bearings to a rigid yoke, Fig. 8.8, roughly triangular in shape. During manufacture the yoke was placed on the bed of a milling machine and the distance from pivot point to bearing centre accurately measured.

A close up of the Hookes Joint arrangement is shown in Fig. 8.9. In order to accommodate different size wheels on the rig, the whole pivot point can be moved vertically in two slots, ensuring that the yoke is horizontal for each wheel tested.

The lateral load is applied either by means of weights, for light loads, or using a load ring and turn buckle for larger loads. In each case the force is applied via a pulley to an arm welded on to the yoke. The force is applied in a line horizontal with the contact point and normal to the lower wheel.

Summarising the main features of the roller rig it fulfills its main objectives as follows:

1. It eliminates longitudinal creep by ensuring the upper wheel is free to rotate in its bearings.

2. Lateral creep can be varied by changing the angle of yaw of one wheel relative to the other.

FIG. 8.8 Yoke

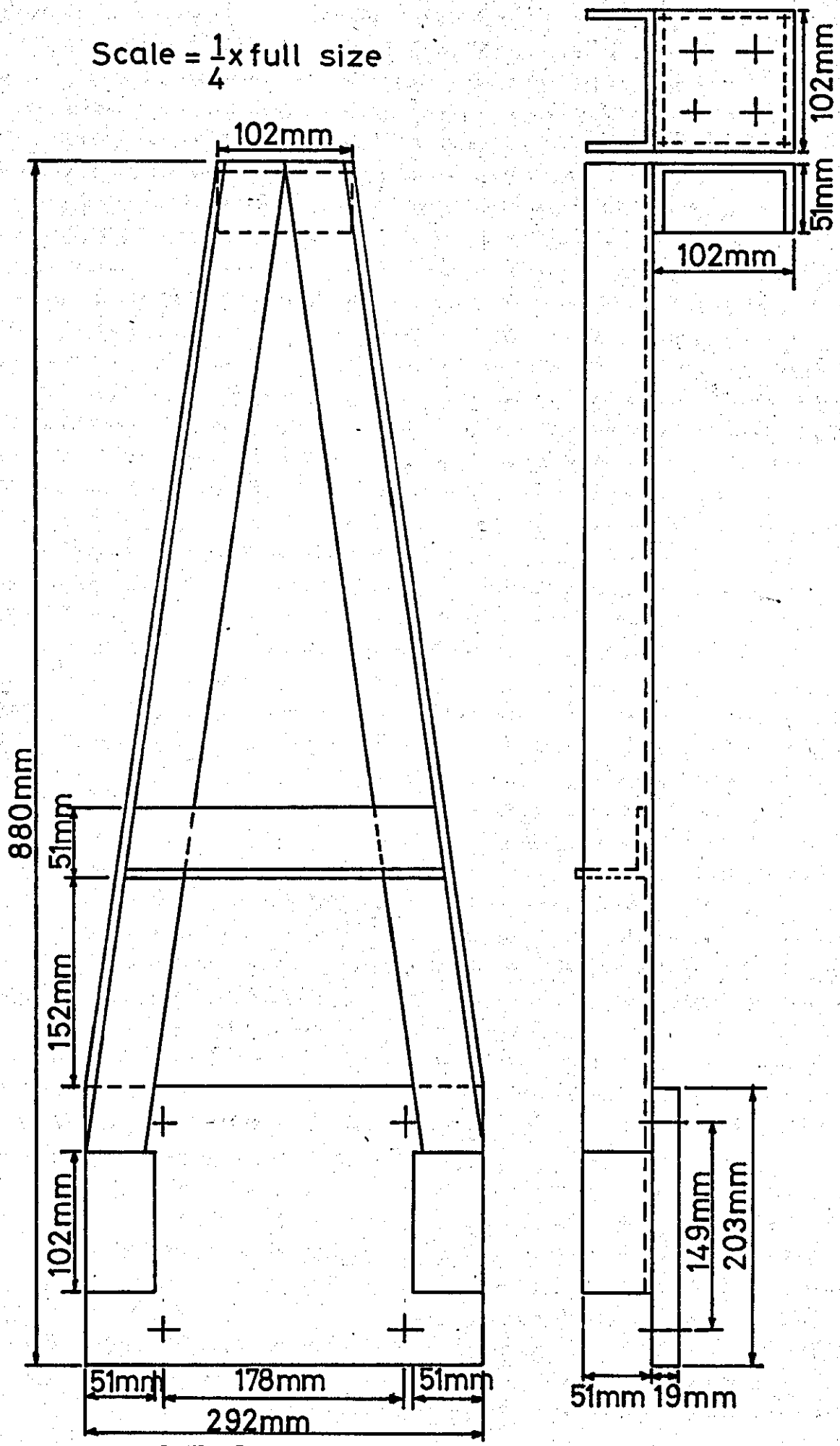
Scale = 1/4 x full size
102mm
880mm
51mm
152mm
102mm
51mm
178mm
51mm
292mm
102mm
51mm
102mm
149mm
203mm
51mm
19mm

FIG. 8.9 Hookes Joint

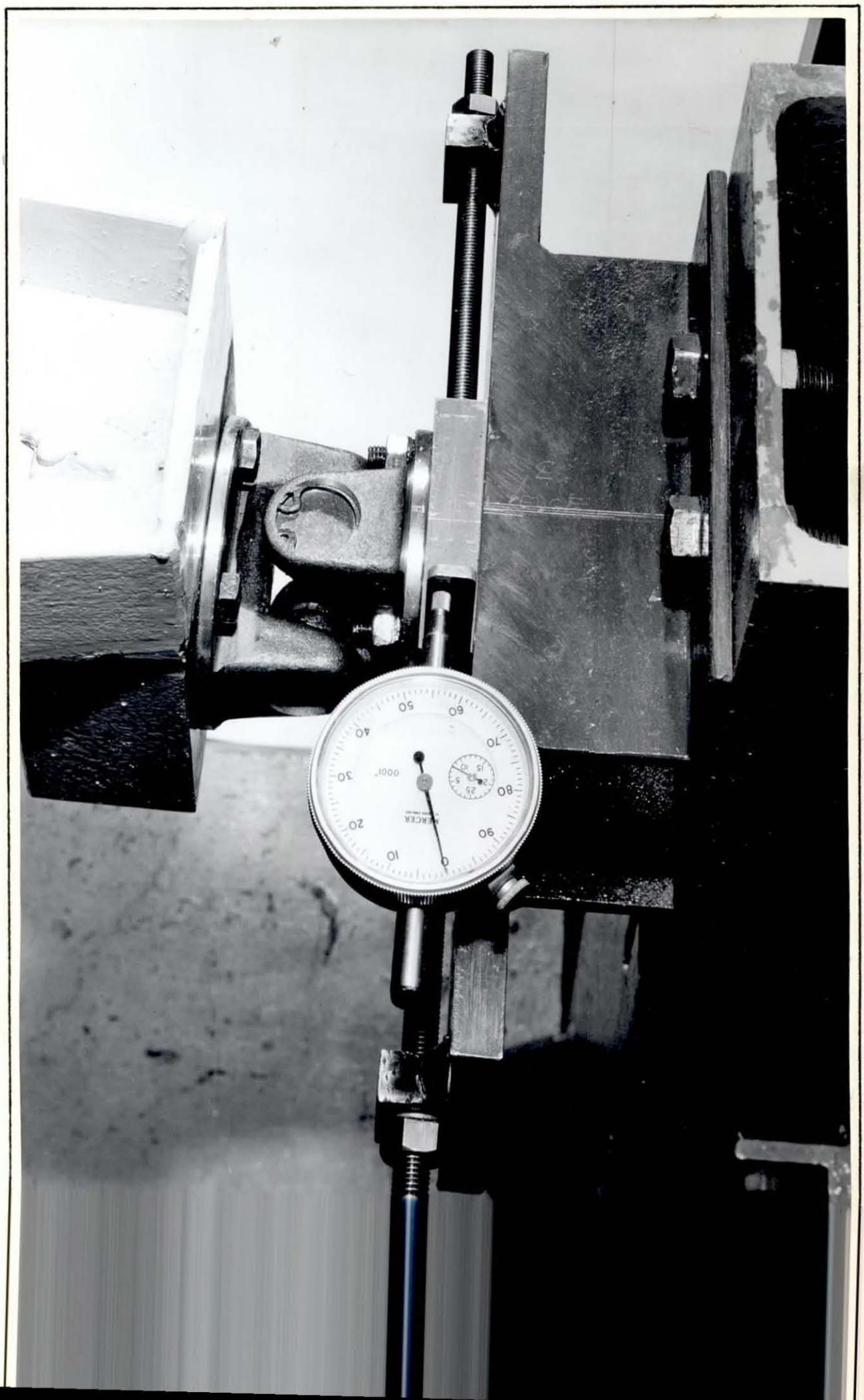

3. Spin can be varied by using upper wheels with different cone angles.

4. The ratio of contact ellipse semi axes can be varied by using wheels with different diameters and different profile radii.

5. Lateral force due to lateral creep and spin can be measured.

6. The speed can be varied using the Speed Controller.

7. The contact pressure can be varied by changing the vertical load through the contact point.

8. The assumptions made in the rolling contact theories are adhered to, i.e. the rolling contact surfaces were ground, high contact pressures were maintained and the experiments were run dry.

The next section derives the expressions for creep, spin and forces on the rig.

8.3 Creepages and Forces

Creepages

Expressions for the longitudinal creepage, γ_1, lateral creepage γ_2, and spin, ω_3 are derived in Appendix 7 for the roller rig using vector analysis.

Since the upper wheel is free to rotate when in contact with the lower driven wheel, it is assumed that the longitudinal creep is zero, i.e. $\gamma_1 = 0$.

From equation 8 of Appendix 7

$$\dot{\Phi}_w r_w = - \dot{\Phi}_R r_R \qquad (1)$$

where $\dot{\Phi}_w$, $\dot{\Phi}_R$ are the angular velocities of the upper and lower wheels respectively and r_w, r_R are the respective rolling radii.

The <u>lateral creep</u> is given by equation 9 which is

$$\gamma_2 = \frac{-\dot{\Phi}_R r_R \psi}{\cos\lambda |V|} \qquad (2)$$

where ψ = yaw angle, λ = cone angle and V = mean velocity. (It can be seen from this equation that the sign of γ_2 depends on the direction of rotation of the wheel).

The <u>spin</u> is given by equation 10 which is

$$\omega_3 = \sin\lambda \left(\frac{1}{r_w} + \frac{1}{r_R} \right) \qquad (3)$$

(The spin is independent of the rolling direction).

Non-dimensional creep and spin parameters are defined as:

$$\xi = \frac{\gamma_1 e}{\mu c} \qquad \eta = \frac{\gamma_2 e}{\mu c} \qquad \chi = \frac{\omega_3 e}{\mu}$$

where e is the characteristic length of the bodies, given by

$$\frac{1}{e} = \frac{(A+B)}{2} = \frac{1}{4}\left(\frac{1}{R_x^+} + \frac{1}{R_x^-} + \frac{1}{R_y^+} + \frac{1}{R_y^-} \right)$$

$R_{x,y}^{\pm}$ are the principal radii of curvature of the lower (+) and upper (-) wheels, taken +ve when the corresponding centre of curvature lies inside the half space under consideration.

Thus $R_x^+ = \frac{r_R}{\cos\lambda}$ $\qquad R_x^- = \frac{r_w}{\cos\lambda}$

$R_y^+ = r_c$ $\qquad R_y^- = \infty$

r_c = profile radius of lower wheel

μ = coefficient of friction

$c = \sqrt{ab}$, where a, b are the semiaxes of the contact ellipse which can be calculated using the method given in Appendix 9. (eqn. 10)

Forces

On the roller rig, a lateral force is applied to the upper wheel in a horizontal line with the contact point. This force is increased until the upper wheel just begins to lift off its vertical supports. At this point it is assumed that the forces are in balance and can be resolved to give a force in the plane of the contact area and a force normal to it.

If axes are defined at the contact point, as in Fig. 8.10 then

$$T_y = T_2 \cos\lambda - T_3 \sin\lambda \qquad (4)$$

and $$T_z = T_3 \cos\lambda + T_2 \sin\lambda \qquad (5)$$

If W and F are the measured vertical and horizontal reactions

then $T_z = -W$ and $T_y = F$

If f_2 is a non-dimensional force parameter, defined as $T_2 = \mu T_3 f_2$

Then $$T_3 = N = \frac{-W}{(\cos\lambda + \mu f_2 \sin\lambda)} \qquad (6)$$

and $$\mu f_2 = \frac{W\sin\lambda - F\cos\lambda}{F\sin\lambda + W\cos\lambda} \qquad (7)$$

By varing the angle of yaw, and therefore the lateral creep, the relationship between the lateral force parameter, f_2 , and the lateral creep can be found for a constant value of spin.

For large values of lateral creep, the value of f_2 tends to 1 and therefore at large +ve and - ve angles of yaw, μf_2 tends to the value of μ . This is useful as it enables a value of μ to be estimated from the results.

FIG. 8.10 Forces at Contact Point

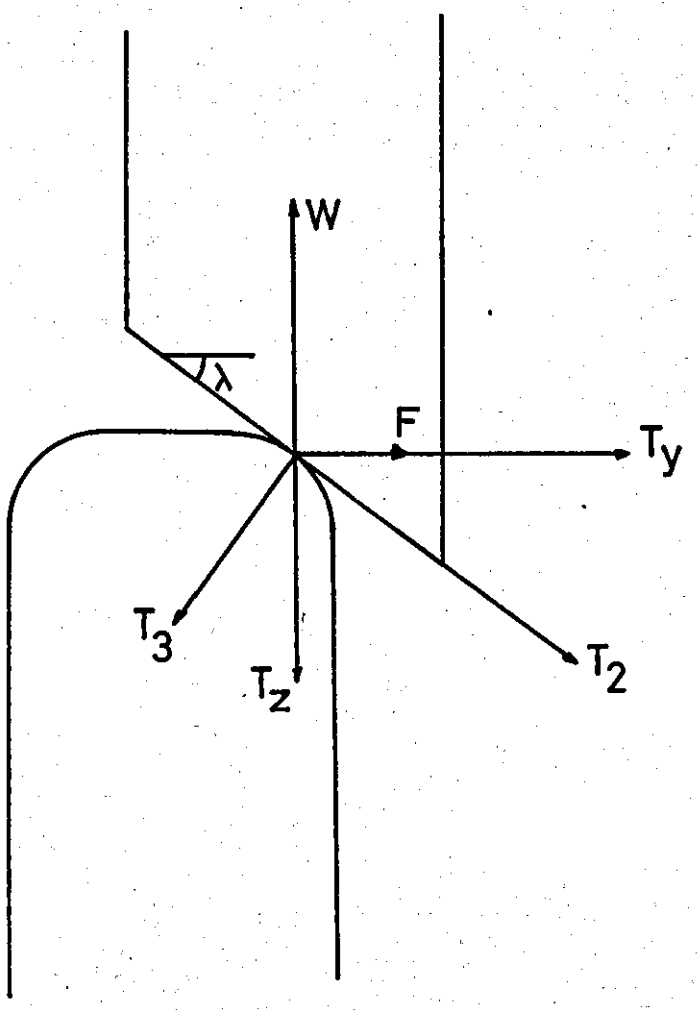

Having found μf_2, the normal force N is given by equation 6. It may be noticed that since f_2 varies with the angle of yaw, ψ, then the normal force N also varies with ψ. (This feature also occurs in the case of a real railway wheel). To overcome this disadvantage results are plotted in the form μf_2 v ($\psi / N^{\frac{1}{3}}$). The reason for this is that since $f_2 = f(\eta)$, it is logical to plot results in the form (f_2 v η). In order to calculate η, μ has to be known, but in this case μ is unknown and has to be estimated from the results. To do this it is best to plot the results in the form (μf_2 v $\mu\eta$)

$$\text{But} \quad \mu\eta = \frac{\gamma_2 e}{c} = \frac{-\dot{\Phi}_R r_e \psi e}{|V| \cos\lambda \left(\frac{3N(1-\sigma)E e}{4\pi G\sqrt{q}} \right)^{\frac{1}{3}}} \tag{8}$$

$$= \frac{\psi}{N^{\frac{1}{3}}} \left[\frac{-\dot{\Phi}_R r_e}{|V|} \cdot \frac{e}{\cos\lambda} \sqrt[3]{\frac{4\pi G\sqrt{q}}{3(1-\sigma)eE}} \right]$$

The terms inside the square brackets are either constant or solely dependent on the geometry of the system. (Note that $|\dot{\Phi}_R r_R| = |V|$ therefore the term $\frac{-\dot{\Phi}_R r_R}{|V|}$ dictates the sign).

When the yaw angle is large, the lateral force needed to lift the wheelset off its supports is also large. Because of this the terms containing F in equation 7 are very much larger than those containing W and in the limit $\mu f_2 \longrightarrow \frac{-\cos\lambda}{\sin\lambda} = -\cot\lambda$. Thus when $\lambda = 67^\circ$, $\mu f_2 \longrightarrow -.364$ and when $\lambda = 49^\circ$ $\mu f_2 \longrightarrow -.869$. If the value of μ existing between the surfaces is greater than this limiting value, then at large +ve yaw angles the results will be asymptotic to this value rather than μ.

8.4 Procedure

This section is roughly divided into three parts. The method of setting up the rig is given, followed by the cleaning routine for the rolling contact surfaces and finally the actual experimental procedure is discussed.

Before mounting the wheels on the rig they were first measured, weighed and the cone angles checked. The wheels were mounted on their shafts and put between centres on a lathe to measure flatness. The roughness of the conical surfaces was measured on a Talysurf 3 and the roughness of the radii measured with a datum attachment using the same machine.

The pair of wheels to be tested was selected and each was mounted in its bearings. The vertical position of the Hookes Joint pivot was chosen to give the required rolling radius on the upper wheel with the yoke horizontal. The rolling radius on the lower wheel was fixed by the cone angle. The bearing supports for the upper wheel were raised so that the bearing caps rested on them with the yoke horizontal. The vertical positions of the supports and pivot were fixed in these positions throughout the test. These positions were only altered when another rolling radius of the upper wheel was required, or the wheels were to be changed.

Having set the yoke horizontal, the counterbalance wire pulley was adjusted so that the wire was vertical. Sideways adjustment could be achieved by moving the pulley in a slot while fore and aft adjustment was possible by packing with washers. In some tests a counterbalance weight was used and in others the weight of the yoke plus wheel assembly gave the required contact pressure. This wire also provided a convenient way of finding the weight of the yoke and upper wheel assembly acting through the contact point by adding counterbalance weights until the wheel

just lifted off its supports. This weight included a clinometer mounted on the yoke to measure roll angles.

The lateral force was applied in the same horizontal plane as the contact point by a wire attached to an arm welded to the yoke. This wire passed over a pulley and the actual load was applied vertically, either by hanging weights on the wire or via a turn buckle and load ring. The turn buckle was used for forces greater than 67 N while the weights were used for forces less than this value. The calibration curve for the load ring is given in Fig. 8.11. The vertical distance between the contact point and the base was measured with a height gauge and the horizontal wire set at the same distance from the base.

Having set the wheels up and adjusted the wires, the angle of yaw of one wheel relative to the other was varied by sliding the pivot point sideways in slots. By measuring this sideways displacement with a DTI and dividing by the distance from the pivot to the contact point the yaw angle could be calculated.

It was important to define the zero yaw or datum position accurately because spin was always present in the tests, due to the large cone angle of the upper wheel and this meant a lateral force at zero yaw angle. Thus the DTI had to be set to zero with the two wheels perfectly in line. Two methods were used to locate this zero position. The first was an optical method where the principle was to shine a slit of light on to the back faces of the wheels, thus getting two reflected slits on a screen. The angle of yaw between the wheels was then changed until these slits were in line, this being the zero yaw position. Either the back faces of the wheels, or mirrors attached to them could be used to reflect the light slit. With mirrors there was a possibility of errors being introduced if the mirror was not perfectly flat against the wheel, while the disadvantage of using the actual wheel face was a poorer quality

FIG. 8.11 Calibration Curve for Load Ring

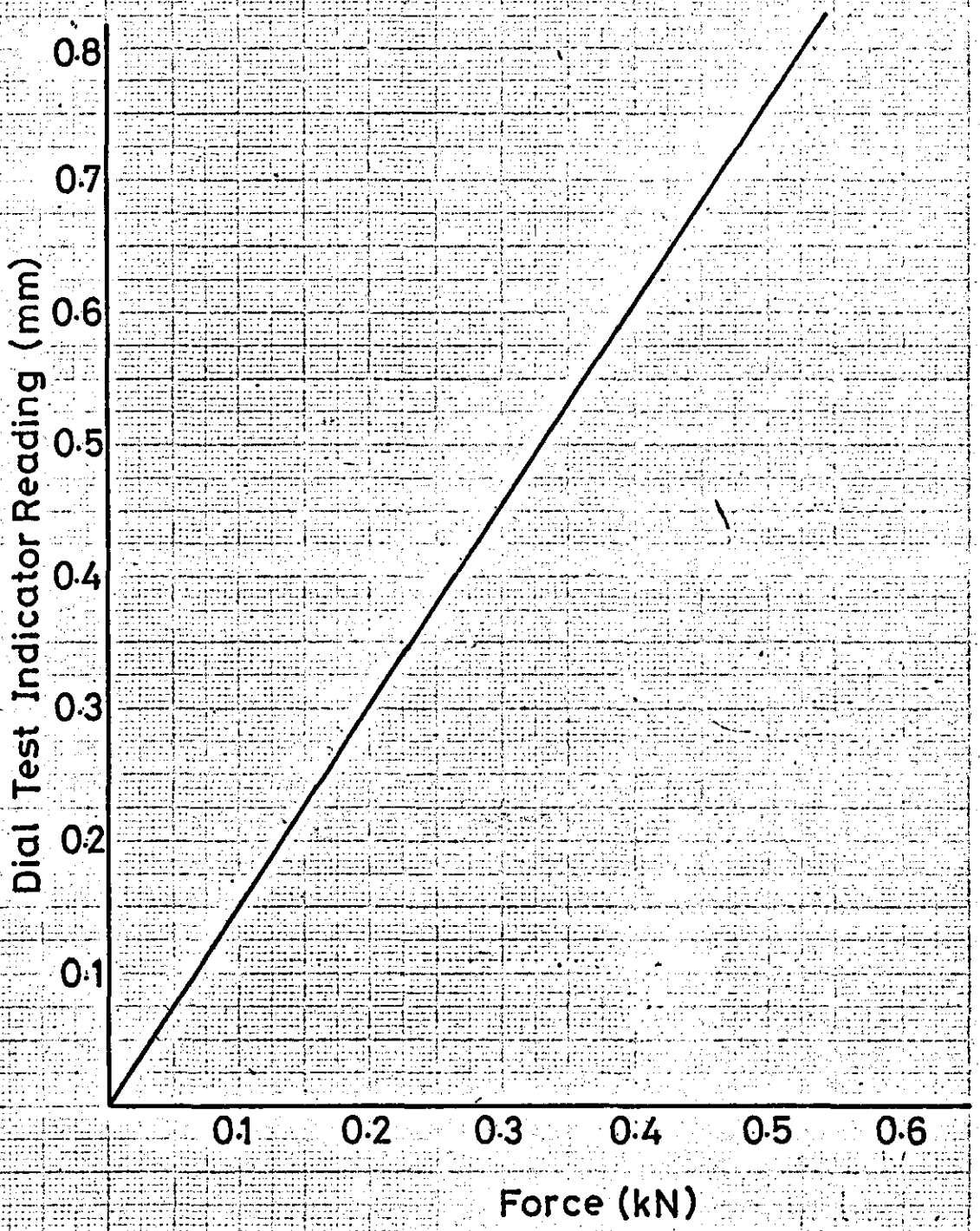

reflected image.

The light source used was a mercury vapour bulb which was set up on an optical bench with a telescope lens and an adjustable slit as shown in Fig. 8.12. An optical mirror was used to reflect the slit on to the junction of the two wheels and a screen was placed about 4 m away to view the images.

The zero yaw position was found by sliding the pivot from left to right and taking the DTI reading when the slits lined up, then moving the pivot from right to left and again taking the reading. This was repeated several times for different wheel positions and the average reading taken as the zero position. Having set the zero yaw position in this way it was then checked with the wheels rotating. However, the definition of the reflected slit on the screen was of poor quality due to the 'grain' effect of the wheel surface, and made accurate dynamic measurements difficult.

The second method for setting the zero was based on the fact that when the direction of rotation of the wheels is changed, the lateral force due to lateral creep changes direction, while the lateral force due to spin acts in the same direction. Thus, if lateral force is plotted against lateral creep for the wheels rotating in different directions a crossover point can be found on the curves where the lateral force due to creep is zero, this being the zero yaw position. In most cases this method served as a check on the previous one, although with the 101.5 mm radius wheel it was the only method that could be applied, since the whole face of the wheel was curved and therefore it was not possible to reflect the light slit.

The shape of the contact ellipse was calculated from the rolling radii. These were easily measured since the point where the wheels touched was clearly visible as a ring of wear debris on each wheel.

FIG. 8-12 Optical System for Locating Zero Yaw Position

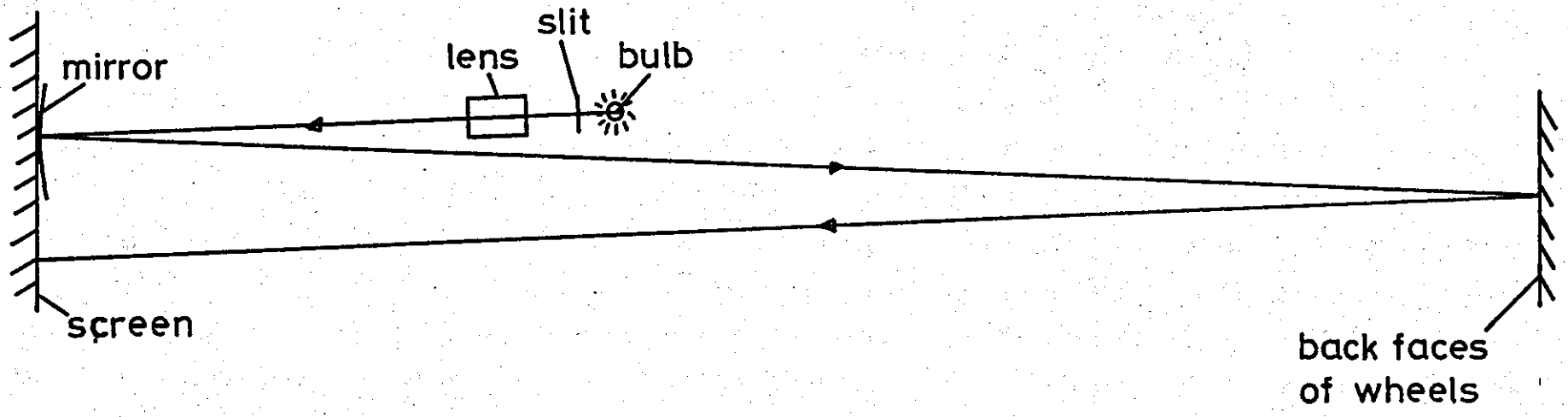

A check on the shape of the contact ellipse was also made by inserting carbon paper between the wheels (when they were stationary) to obtain an imprint of the contact area. This was not very accurate because of the poor definition around the contact area edges, but it was possible to say whether the (a/b) ratio was 1 : 1, 3 : 1, or 10 : 1 and did give some reassurance to the calculations.

Various methods of cleaning the rolling contact surfaces were tried in order to obtain repeatable results. It was important to obtain consistent rolling contact surfaces throughout the test and this was difficult when operating with dry surfaces because of wear taking place.

At the start of testing the wheels were degreased with carbon tetrachloride, then abraded with 600 wet and dry paper and wiped dry with a tissue. They were then allowed a short running-in period, under load, before measurements were actually taken. A 'run' consisted of setting the wheels to various angles of yaw and measuring the lateral force needed for the upper wheel to just lift off its supports. The wheels were wiped with a dry tissue after setting each yaw angle. The load was then increased as rapidly as possible so that the reading could be taken before wear debris built up on the surface. Other investigators have continuously wiped this off, but in view of the possibility of introducing longitudinal creep this method was not adopted here.

The debris on the surface was an iron oxide powder similar in colour to rust and was observed to build up quickly at the large yaw angles and large loads. By wiping the wheels between each reading, the amount of debris on the surface was kept relatively constant. This gave repeatable results, but with large coefficients of friction. A certain lack of repeatability was noted on days when the relative humidity was high. Each wheel combination was tested on several different days and

with different loads so that repeatability could be checked.

The forces were assumed to be in balance when the lateral force was such that the upper wheel had just lifted off its supports and a 0.050 mm feeler gauge could be slid between the bottom of the bearing cap and the support. Various methods were tried in order to indicate when the wheel had lifted off, such as DTI's, micro switches etc. but all were discarded in favour of the feeler gauge.

In general the system was stable since as the wheel starts to lift off its supports it also tends to move sideways, thus increasing the angle of yaw, which means it needs a larger force to maintain its new position. The opposite situation was true when the direction of rotation was reversed. In this case the wheel was leading the pivot point rather than trailing it which was a very unstable situation. Having increased the lateral force to make the upper wheel just lift off its supports, the tendency was to increase the angle of yaw so that the lateral force required to keep it in the new position was now less and the wheel just kept climbing.

For normal rotation the tests were conducted from large -ve angles of yaw to large +ve angles, thus the lateral force needed to lift the wheel was greater for each successive yaw angle setting. At large -ve angles of yaw the rig was very unstable and oscillated violently, probably due to the large amount of surface sliding present exciting the natural frequencies of the rig. At large +ve angles of yaw the wheel frequencies were excited, probably for the same reasons, resulting in a high pitch squeeling noise. This also indicates the very dry conditions present in the contact area. This effect has also been observed by Barwell, Ref. 59, during some recent traction tests on a locomotive. Quoting from Ref. 59, "When the locomotive driving wheels were just on the point of slipping, a ringing noise was to be heard".

At each yaw setting the speed of the lower wheel was checked with a hand tachometer when the wheel was just lifting off. If necessary the speed control was finely adjusted to maintain the same speed for all the results.

The readings taken at each yaw angle were as follows:-

(1) the lateral displacement of the pivot point;

(2) the lateral force needed to just lift the upper wheel off its supports;

(3) the angle of roll on the clinometer;

(4) the speed of the lower wheel.

A sample experimental data sheet is given in Appendix 10.

Having gone through the range of yaw angles, the direction of rotation of the motor was changed, and readings were taken around the zero yaw position. The two sets of results should cross at the point $\psi = 0$. Because of the unstable nature of the wheel when run in this direction, only sufficient readings were taken to define the curve and thus establish the crossover point.

Each wheel combination was tested on different days at two different speeds and generally with three different vertical weights. By plotting results in the form (μf_2) v $(\psi / N^{\frac{1}{3}})$, they could all be shown on the same graph. The actual results from the tests are given in the next section.

8.5 Results

Each of the three lower wheels a, b and c (Table 8.1) were tested with each of the two upper wheels d and e giving a total of 6 cases. Each case was run with different vertical weights and at different

speeds. The 6 cases have different (a/b) ratios and spins, this can be seen in Table 8.2 where the main parameters are listed for each case.

The results are plotted in the form (μf_2) v $(\psi / N^{\frac{1}{3}})$ for reasons described in Section 8.3. Using this parameter, results obtained for different vertical weights can be plotted on the same graph.

If required, the value of the lateral creep parameter, η, corresponding to a value of $(\psi / N^{\frac{1}{3}})$ can be found using equation 8, which is

$$\mu\eta = \frac{\psi}{N^{\frac{1}{3}}}\left[\left(\frac{-\dot{\Phi}_R r_R}{|V|}\right)\cdot\frac{\rho}{\cos\lambda}\sqrt[3]{\frac{4\pi G\sqrt{g}}{3(1-\sigma)\rho E}}\right]$$

$$\text{or}\quad \mu\eta = \frac{\psi}{N^{\frac{1}{3}}}\cdot\left(\frac{-\dot{\Phi}_R r_R}{|V|}\right)\cdot K$$

where K for each case is tabulated in Table 8.2 (p.178) assuming $G = 79.6\ GN/m^2$ and $\sigma = 0.3$.

The spin parameter, χ, can be found from equation 3 using the values given in Table 8.2. The values of χ corresponding to $\mu = 0.6$ and $\mu = 0.7$ for each case are tabulated in Table 8.3 (p.178).

The effect of varying rolling speed is shown in Fig. 8.13 for case 1 where μf_2 is plotted against V.

The main results are plotted in Figs. 8.14 to 8.19 for cases 1 to 6 respectively. In all cases the speed of the lower wheel was constant at 160 rev/min which is approximately equivalent to a linear velocity of 2.4 m/s. Average contact pressures for these cases are given in Table 8.4.

Table 8.4 Average Contact Pressure

Case	W (N)	$\frac{\psi}{N^{\frac{1}{3}}}$ ($N^{-\frac{1}{3}}$) x 10^3	Average Contact Pressure (MN/m^2)
1	129	-.170	200.6
		-.046	206.8
		.530	338.8
	262	-.462	247.1
		0	266.1
		.347	324.5
2	133	-.336	271.3
		-.255	229.6
		.360	315.7
	311	-.596	260.3
		0	311.4
		.108	334.5
3	129	-.340	316.8
		0	320.6
		.587	462.9
	262	-.167	404.7
		-.015	412.8
		.533	565.5
	396	-.066	689.5
		0	472.3
		.431	595.0
4	44	.010	265.4
		.617	518.5
	178	.010	399.8
		.435	560.4
5	89	-.141	744.6
		.608	1110.1
6	36	.444	772.2
		.596	1158.3

FIG. 8.13 Effect of Varying Rolling Speed

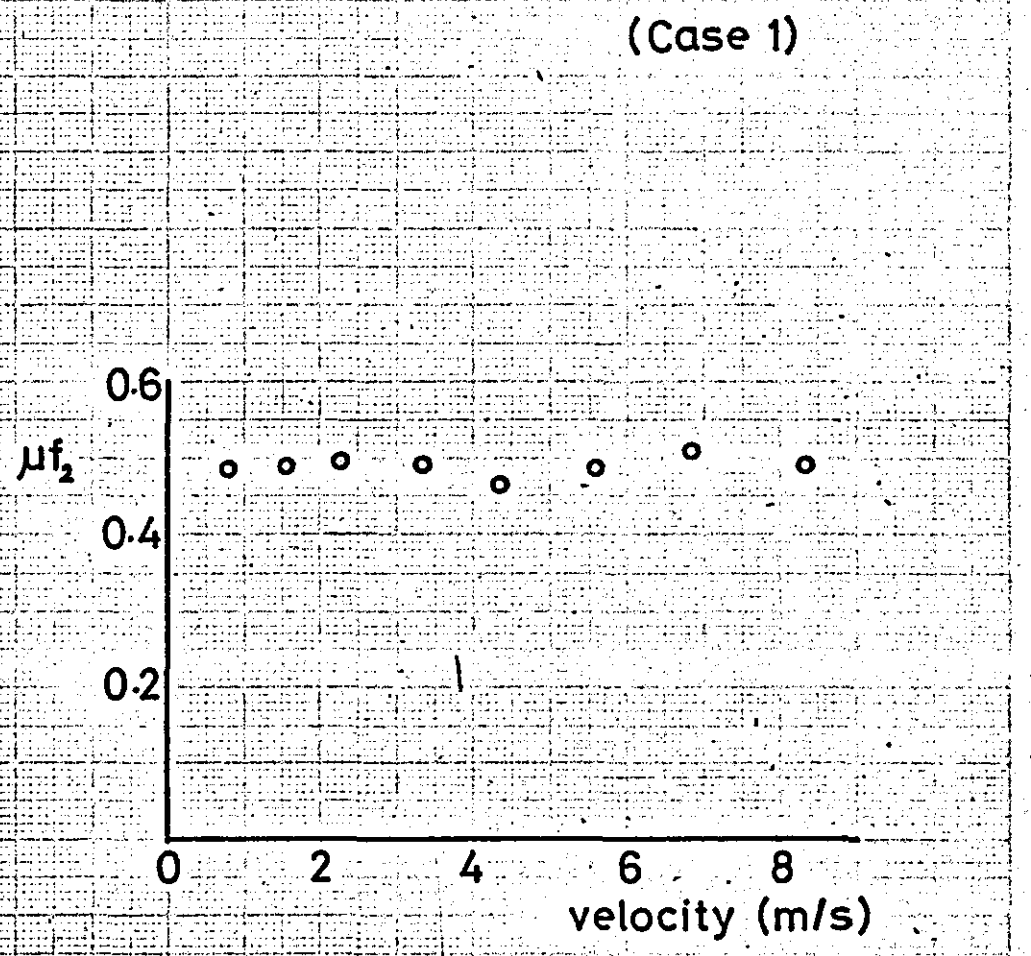

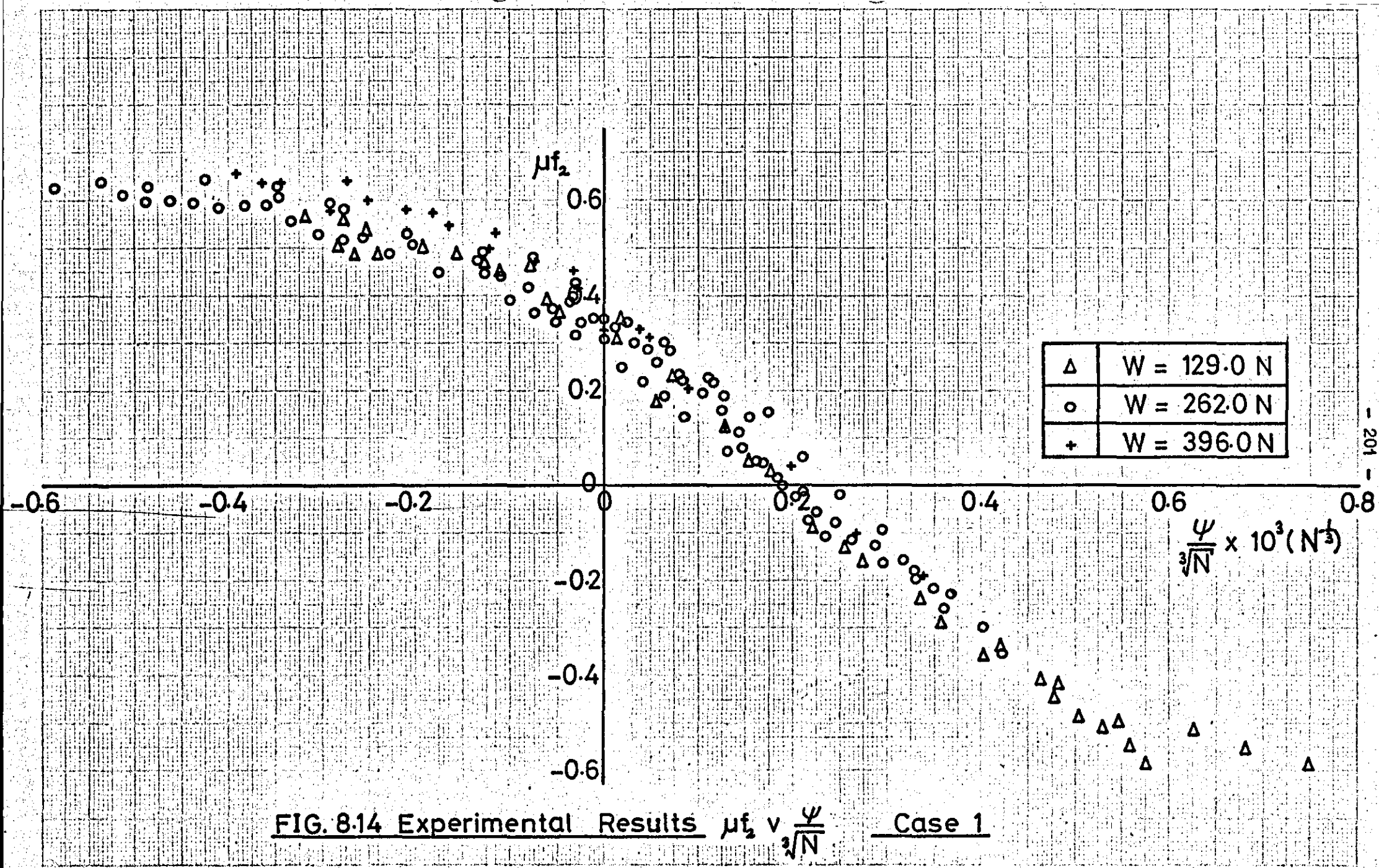

FIG. 8.14 Experimental Results μf_2 v $\frac{\Psi}{\sqrt[3]{N}}$ Case 1

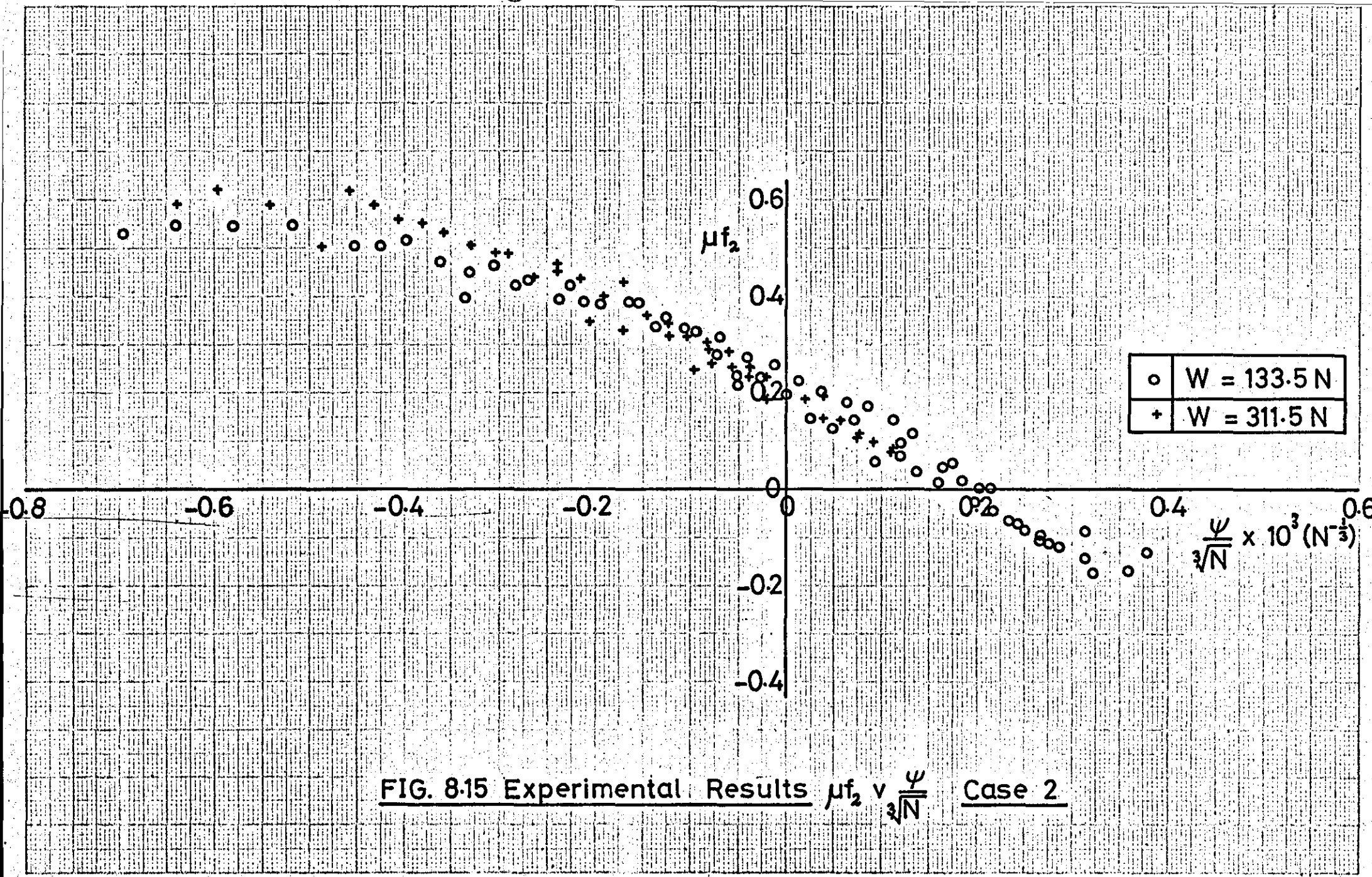

FIG. 8.15 Experimental Results μf_2 v $\frac{\Psi}{\sqrt[3]{N}}$ Case 2

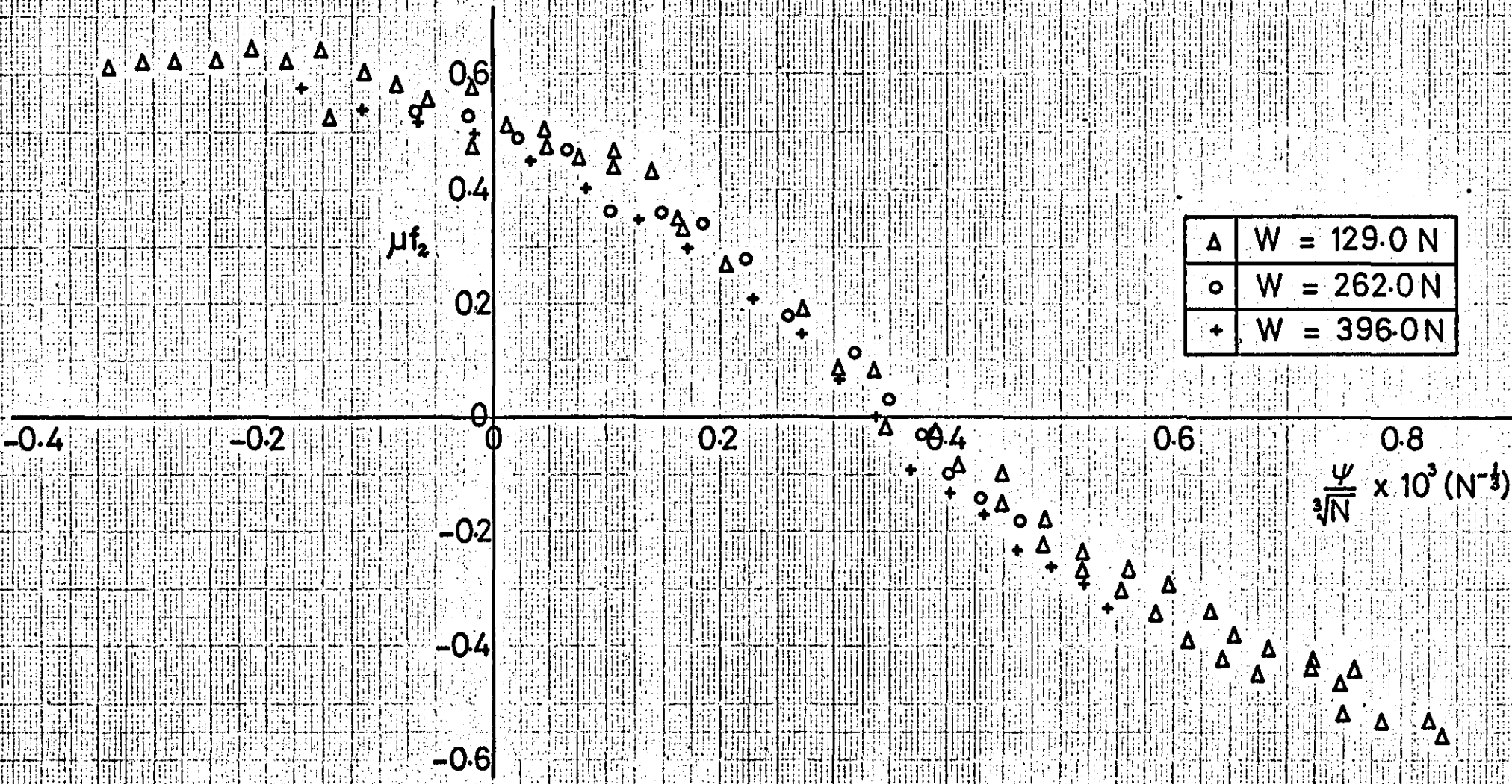

FIG. 8.16 Experimental Results μf_2 v $\frac{\Psi}{\sqrt[3]{N}}$ Case 3

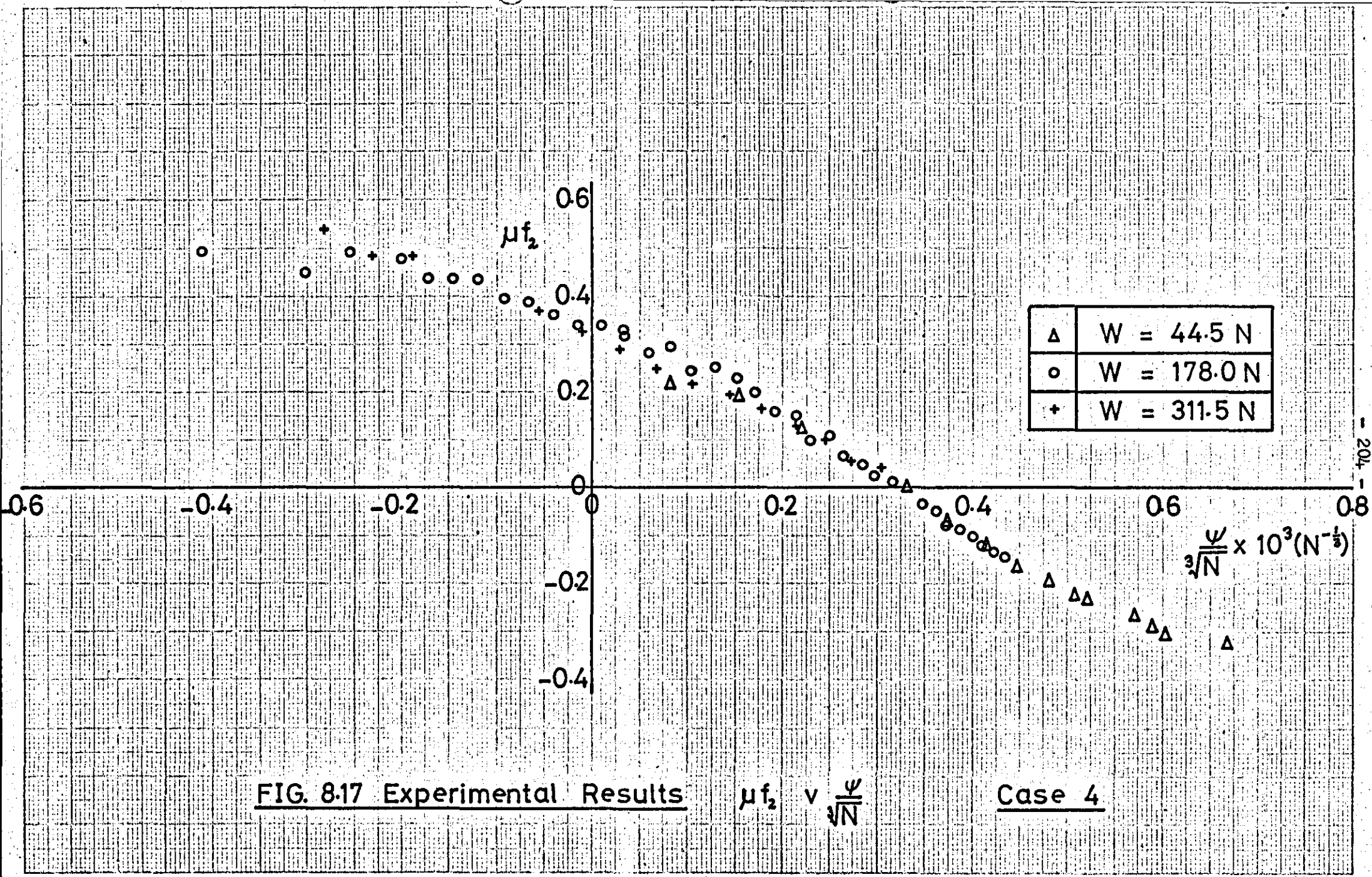

FIG. 8.17 Experimental Results μf_2 v $\frac{\Psi}{\sqrt[3]{N}}$ Case 4

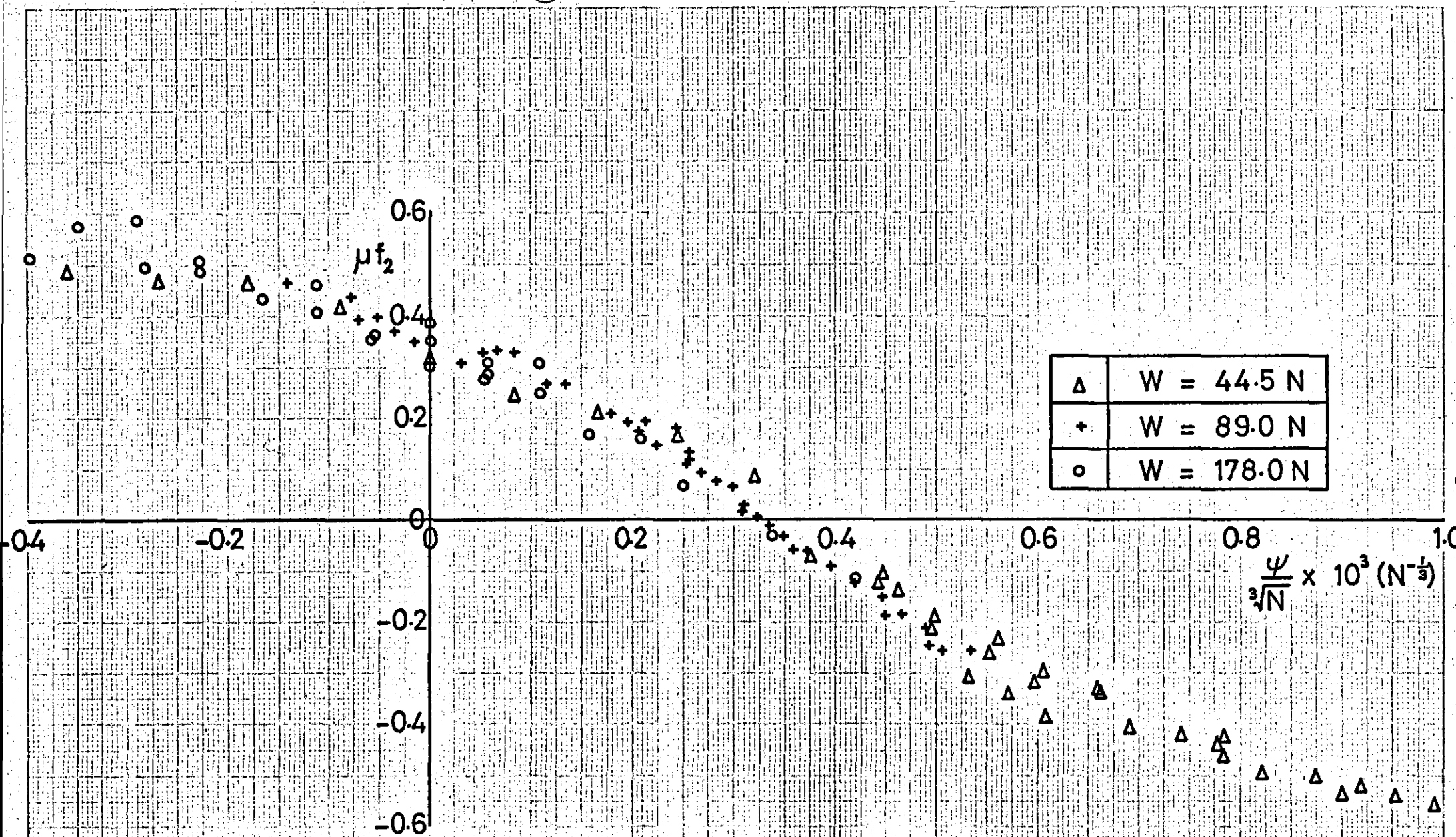

FIG. 8.18 Experimental Results μf_2 v $\frac{\Psi}{\sqrt[3]{N}}$ Case 5

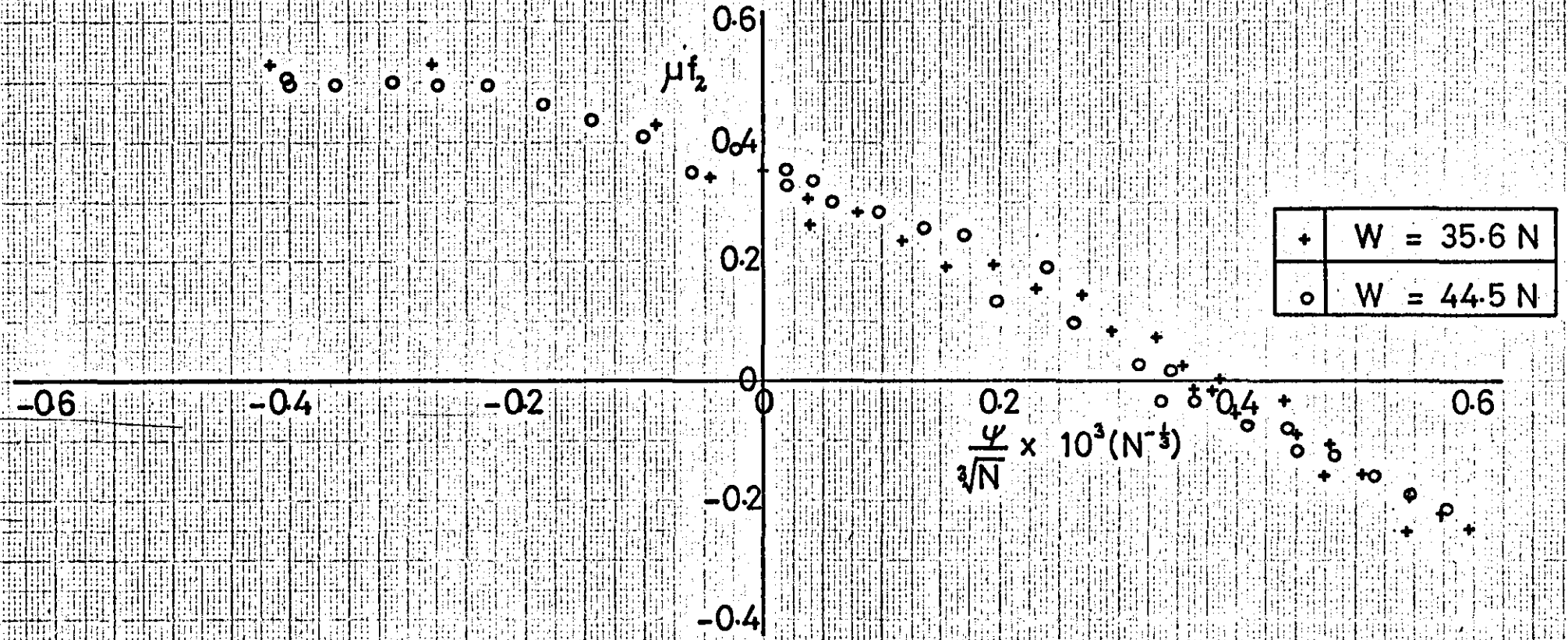

FIG. 8·19 Experimental Results μf_2 v $\frac{\Psi}{\sqrt[3]{N}}$ Case 6

8.6 Discussion

8.6.1 Validity, Accuracy and Repeatability of Results

The prime objective of the experimental investigation was to provide test data on the lateral force due to varying amounts of lateral creep and spin on bodies in rolling contact forming elongated contact ellipses. During the tests various other effects were investigated, such as different ratios of contact ellipse semiaxes, speed effects and different contact pressures. Conditions existing on the rig were similar in several respects to the contact between a railway wheel and the track when in flange contact. Firstly, the vertical load was constant as the angle of yaw was varied, thereby giving different loads normal to the plane of the contact area for different yaw angles, while the amount of spin remained constant. Secondly, as the angle of yaw was changed the contact point moved either forward or backward by a small amount.

The roller rig model did not represent actual wheel to rail interaction in the following ways: (a) longitudinal creep was excluded from the roller rig by having one surface freely rotating on the other, and (b) there were the obvious differences in scale, materials, surface finishes, contamination of the track, amounts of vibration, etc. The rig was not designed to simulate such conditions, but to conform as closely as possible to assumptions made in the rolling contact theories. These are that the bodies in contact have smooth surfaces and that Coulomb friction exists between them.

The latter assumption was valid since all the results presented in Figs. 8.14 to 8.19 were obtained with "dry" conditions. The rig was in fact designed on this basis and could provide lateral

forces corresponding to the large coefficients of friction measured between the surfaces under such conditions. Some tests were carried out with lubricated surfaces, but because of the low coefficient of friction (of the order of 0.1), the changes in lateral force due to yaw angle were so small as to be undistinguishable. Another disadvantage in running with lubricated surfaces was that the speed needed to be very low in order to avoid hydrodynamic lubrication effects, and this was not possible on the rig. The minimum speed that could be obtained was 0.8 m/s. As a comparison Johnson, Ref. 6, ran his lubricated tests with speeds as low as 3.1 m/min. The main advantage of running at such low speeds and with lubricated surfaces is that the amount of wear is reduced.

In order to keep wear to a minimum on the present rig, since the surfaces were to be run dry, the material used for the wheels was a case hardened steel. Each wheel was machined, case hardened and then ground to its final surface finish, which varied from wheel to wheel between 0.18 μm CLA and 0.61 μm CLA. This was not as good as the surface finishes achieved by Johnson, but it was hoped that by maintaining fairly high contact pressures and relatively low speeds, roughness effects would be minimised and that a comparison with smooth surface theory was valid. This had been the conclusion reached by Halling, Ref. 15, and Nayak, Ref. 33.

Since the bodies were accurately ground and the rig was carefully assembled, the amount of surface vibration on the wheels when running was minimal. According to Tolstoi, Ref. 52, the effect of vibration is to reduce the effective coefficient of friction and there is no evidence of this in the results.

The ratio of contact ellipse semi-axes was calculated from the principal radii of curvature of the rolling bodies, Appendix 9, which in turn depended on the rolling and profile radii of the wheels. The profile radius of each wheel was checked on a Talysurf machine with a datum attachment, by setting the nominal radius on the machine and then following the profile around. When the radius was correct, the resulting trace was a straight line with the roughness superimposed. The rolling radius of each wheel could be measured easily since a wear band around the wheel was clearly visible after each test.

A check was also made on the calculations for (a/b) ratio, by sliding carbon paper between the wheels when stationary and obtaining an imprint of the contact area. This served only as a rough guide, and no quantitative measurements could be made, since the edges of the ellipse were poorly defined.

It was assumed in the experiments that longitudinal creep was zero because the upper wheel was allowed to roll freely on the lower wheel. No attempt was made to measure differences in speed of the two wheels since the rolling radii which occur on a highly curved body of revolution, could not be measured with sufficient accuracy to justify measuring velocity differences. The results themselves do not show longitudinal creep being present, as this would be indicated by curves with a slope somewhat less than the theory. There is no evidence of this and in fact the opposite is true in some cases.

The amount of lateral creep present was calculated from the yaw angle according to equation 2. This formula takes into account the forward or backward movement of the contact point as the wheel is yawed, which incidentally, makes considerable

difference to the results. Initially it was excluded from the calculations and obvious differences in slope occurred between the experimental and theoretical values. The yaw angle was calculated by measuring the lateral displacement of the pivot point on a dial test indicator reading to 0.0025 mm, and dividing this by the distance from the pivot to the contact point. The latter distance was measured accurately before testing with the yoke placed on the bed of a milling machine. Ideally the pivot point should move in a circular arc with centre at the contact point. The error introduced by moving the pivot laterally was very small, since the maximum lateral displacement of the pivot was $\pm$ 5 mm, compared with the radius of 806 mm. The fore and aft movement of the contact point due to yaw, mentioned above, was several orders of magnitude greater than this shift.

Both upper wheels tested had large cone angles, 49° and 67°, which meant large amounts of spin present in all cases. As a result, at zero yaw angle or zero lateral creep, there was a considerable lateral force due to spin. Since this was one of the parameters being investigated some method had to be found of accurately determining the zero yaw position, as it was not possible to deduce this from the results alone.

Two methods were used for finding this. The principle of the first was to shine a slit of light at the junction of the two wheels in their static position and then to examine the reflected image on a screen some distance away from the rig. The wheels were assumed to be in the zero yaw position when the images of the two slits were in line. This was done for various positions of the wheels and the average taken as the zero position.

The vertical weight was also varied and the zero found corresponding to each weight used. It was noticeable that the zero position varied slightly as the vertical load was increased, for example in Case 4 the zero was found to be at 6.06 mm when W = 44.5 N, at 5.66 mm when W = 178 N and at 5.49 mm when W = 311.5 N. A similar trend was observed for all the wheel combinations tested.

Possible explanations for this behaviour are that it may be due to deflection of the vertical supports or due to roll of the upper wheel. Considering deflection of the vertical supports, since the zero is being set with the wheels static, the weight of the wheel assembly is supported, thus causing deflection of the supports and therefore lateral displacement of the upper wheel. This deflection would be different for different vertical weights. The deflection of the supports was actually measured in Test 1 of Appendix 11 and found to be approximately 0.25 mm when W = 396 N. This is not a significant amount, and in any case, causes a displacement in the opposite direction to the observed effect.

The second possible effect is due to the counterbalance wire not being vertically above the contact point. This would cause a rolling moment which would be dependent on the amount of counterbalance force. On inspection of the rig it was possible for the effset between the line of action of the counterbalance wire and the contact point to be as much as 13 mm, and although the Hookes Joint theoretically restrained the wheel assembly in roll, a certain flexibility was possible at the contact point in this direction.

A rolling moment causes the upper wheel to roll about an axis passing through the centre of the Hookes Joint. Since this is at some distance above the contact point, very small roll angles can result in significant lateral displacements at the contact point, e.g. with the 49° upper wheel, a roll angle of $2'$ results in a lateral displacement at the contact point of 0.25 mm. Lateral displacement also occurs when the upper wheel rolls relative to the lower wheel, since apart from effectively changing the cone angle (and therefore the amount of spin), the point of contact is also shifted.

It seems likely that the observed lateral shift of the zero yaw position for different vertical weights is a combination of these effects. It was not possible to make an accurate check of the zero yaw position with the wheels rotating using the optical method, due to the poor quality of the reflected images.

The second method used for finding the zero yaw position was to obtain two sets of results of lateral force versus yaw angle with the wheels rotating in opposite directions and to plot these on the same graph. The zero should then lie at the cross-over point of the two curves. This is possible since the lateral force due to spin is independent of the direction of rotation of the wheels, while the lateral force due to lateral creep depends on the direction of rotation.

These results also indicated a shift in the zero yaw position for different vertical weights, in the same direction as noted previously. The same argument can be applied as before, i.e. as the counterbalance load increases, the rolling moment increases resulting in a roll angle and thus a lateral shift of the

zero. Differences in zero positions indicated by the 'crossover' method and the 'optical' method were within 4% of each other and can be explained as the difference between the 'static' zero position and the 'dynamic' zero position.

In the 'crossover' method the lateral load was increased until the wheel just lifted off its supports. At this point all the loads passed through the contact point and the wheel was in its natural position, free of any restraints. Changes in roll angle between 'static' and 'dynamic' settings result in displacement of the zero yaw position. For a -ve change of roll angle the displacement is to the left, and for a +ve change of roll angle displacement of the zero is to the right.

Other effects have also been investigated to explain possible differences between 'static' and 'dynamic' zero positions. As the lateral load is increased, the vertical load on the supports is reduced until it is zero when the measurements are actually taken. Thus the upper wheel moves vertically upwards by some small amount as the lateral load is increased, and in so doing must also move sideways, effectively shifting the zero yaw position.

The wire which applies the lateral load is set horizontal with the wheels in the static position. As the lateral load is increased the upper wheel moves upwards resulting in an anti-clockwise rolling moment applied to the yoke. This tends to shift the zero position towards the left relative to the 'static' zero position.

Since the displacement of the vertical support is small, less than 0.25 mm for the range of weights tested, both these effects are considered to be second order compared with the change of roll angle from 'static' to 'dynamic' position of the wheel. The

experimental evidence agrees with this hypothesis since the zero found by the 'crossover' method is sometimes to the left and sometimes to the right of the zero found optically.

It was not possible in all cases, to use both methods for locating the zero, for example, the 101.5 mm radius wheel (a) was radiused almost to its centre and so the 'optical' method could not be used. In all the other cases tested the zero yaw position was fixed by considering both the zero's from the 'optical' method and the 'crossover' method. It was not automatically assumed that the 'dynamic' zero given by the 'crossover' method was the most accurate, since the wheel had to be run in a very unstable condition to obtain this value. This shift of the zero yaw position for different amounts of counterbalance has been incorporated in the results present in Figs. 8.14 to 8.19 and the results for each weight are based on the zero indicated by the above methods.

The shift of the zero yaw position for different vertical weights raises a further question as to whether it also shifts as the lateral force increases. The effect of this would be to change the slope of the results since, as the yaw angle increases, the lateral load required to lift the wheel off its supports also increases.

A possible way in which this situation could arise, is if the lateral force were not applied in a horizontal line with the contact point. The effective rolling moment would then increase as the lateral load increased.

The main reasons for assuming this did not occur are that, firstly, the load wire was accurately set at the same height as the contact point prior to each test and secondly, the roll

angle was continuously monitored for each run and did not vary by more than 3′ throughout the lateral load range.

Apart from this, a further series of roll tests were carried out by deliberately offsetting the lateral load by known amounts and observing the effects. When the wire was offset by 6 mm, the roll angle varied by as much as 10′ throughout the range of lateral loads. These tests are reported in Appendix 11 where the results are shown graphically. They show that when the wire is offset, it is apparent from the results since the roll angle progressively increases as the lateral load increases. The tests also show that even when the wire is offset by these relatively large amounts, the change to the overall results is not very great.

In a second series of tests, which are also reported in Appendix 11, a dial test indicator was used to measure the lateral displacement of the upper wheel just above the contact point. This showed that the wheel was displaced by about 0.64 mm from the 'static' to 'dynamic' positions, but for changes of yaw angle the variation was less than 0.25 mm throughout the range.

The roll angle was measured throughout the main series of tests and where this was different from the angle of roll at the zero yaw position, the corresponding lateral displacement in the plane of the contact point has been calculated and the results corrected. Since the angles of roll throughout the range of loads were within 3′, this correction makes very little difference to the measured values.

The variation of lateral force due to lateral creep is represented in Figs. 8.14 to 8.19, by the slope of the graphs, while

the amount of lateral force due to spin can be estimated from the zero yaw value of f_2. The amount of spin is given by equation 3 which is

$$\omega_3 = \sin\lambda \left(\frac{1}{r_w} + \frac{1}{r_e} \right)$$

This shows that spin is a function of cone angle and rolling radii and the validity of each of these parameters has been checked. The cone angle was accurately ground on the wheel and the rolling radii could be measured easily, since the contact of the two wheels left a clearly marked track on the surface. The effect of roll angle on spin has already been mentioned and is negligible, since measured angles of roll were less than $3'$, and this makes very little difference to the $\sin\lambda$ term in the above equation.

The non-dimensional spin parameter used in the analysis is defined as $\chi = \frac{\omega_3 a}{\mu}$

This shows that χ is dependent on the coefficient of friction but independent of the normal load, which means in the present investigation, that it is constant for variation of yaw angle. Values of χ are tabulated in Table 8.3 for each case corresponding to $\mu = 0.6$ and $\mu = 0.7$.

When the various theories were discussed earlier, the curve (f_2 v χ) for $\xi = \eta = 0$ was mentioned. This curve increases linearly for small values of χ and then non-linearly until it reaches a maximum value. As χ is further increased the value of f_2 falls. The value of χ when the initial slope reaches $f_2 = 1$ has been called $\chi_{max.}$ and occurs approximately at the maximum f_2 position. This function, χ_{max}, has been calculated using equation 3.18 and is tabulated for each case in Table 8.2. It can be seen that by comparing Table 8.2 with Table 8.3, $\chi > \chi_{max.}$ in each case. The graph (f_2 v χ) for $\xi = \eta = 0$

has not been plotted for the experimental results since there are only two values, corresponding to the two cone angles, for each (a/b) ratio. Instead, these values are tabulated in Table 8.5, assuming $\mu = 0.7$.

The results plotted in Figs. 8.14 to Figs. 8.19 are presented in the form (μf_2), v $(\psi / N^{\frac{1}{3}})$. This parameter takes care of the variation in normal load as the yaw angle is changed and thus allows results with different vertical loads to be plotted on the same graph. At large angles of yaw (both +ve and -ve) f_2 theoretically tends to 1 and the curves therefore level off at the value of μ existing between the wheels.

The value of μ was unknown in the tests since it could not be measured directly and it is not necessarily the same as the steady sliding value of μ. The only indication of its value was from the method mentioned above, i.e. the asymptotes of the results, but there were difficulties in running the rig at large angles of yaw to obtain these, since the contact area was then nearly all sliding resulting in a lot of wear taking place. (Brothers and Halling, Ref. 45, have done experimental work on this subject and shown that wear increases as the creep increases). Because the surfaces were sliding over each other, vibrations were excited in the rig. At the large -ve angles where the contact pressure is low, the whole rig oscillated and it was very difficult to take readings. At the large +ve angles, with high contact pressures, wheel frequencies were excited and a high pitch squeeling noise was emitted with a lot of surface debris being collected. This noise indicated the dry conditions present. (Itami, Ref. 50, also encountered difficulty in obtaining readings in this region).

TABLE 8.5 MEASURED VALUES OF f_2 WHEN $\xi = \eta = 0$

Case	μf_2	f_2	X	$X_{max.}$
1	0·34	0·49	3·19	2·46
2	0·22	0·31	6·22	2·34
3	0·51	0·73	0·37	0·26
4	0·34	0·49	0·68	0·26
5	0·36	0·52	0·18	0·12
6	0·35	0·50	0·34	0·12

(ASSUMING $\mu = 0.7$)

At the very large +ve yaw angles, where the lateral force required to lift the wheel off its supports was large, increasing the lateral load had little effect. This can be seen by referring to equation 7 which is

$$\mu f_2 = \frac{W\sin\lambda - F\cos\lambda}{F\sin\lambda + W\cos\lambda}$$

For very large values of F, μf_2 tends to $-\cot\lambda$, thus results are asymptotic to the line - 0.424 for the 67° wheel and - 0.869 for the 49° wheel. Since the latter value is greater than the value of μ, the results are asymptotic to μ for this case.

Apart from this, limitations of the rig itself prevented lateral loads great than 750 N being applied. This meant, for some cases, stopping the run well before reaching the asymptotic value of μf_2.

Because of the various reasons mentioned it was difficult to obtain results at large +ve or large -ve angles of yaw. However, from the results that were obtained, a value of $\mu = 0.7$ in most cases, $\mu = 0.6$ in others, was indicated. This is very large, but considering that the tests were carried out dry and that the wheels were abraded and wiped before each run, it is not unreasonable. Johnson's experiments, where μ was found to be approximately 0.1, were carried out with very smooth surfaces which were generally lubricated.

The lateral creep tests of Itami, Ref. 50, indicated a coefficient of friction between 0.55 and 0.67 with clean, dry, rolling contact surfaces. Itami plotted a graph, reproduced in Fig. 2.11 showing how the coefficient of friction changed with wheel load. This graph indicates a value of $\mu > 0.6$ with the contact pressures used in the present investigation.

Initially various methods were tried to obtain repeatable results. The difficulty was in obtaining consistent rolling contact surfaces throughout the test when operating with dry surfaces. This was finally overcome by abrading the wheels with a fine carborundum paper between each run and then wiping with a tissue, so that the amount of wear debris on the surface was kept to a minimum. Hobbs, Ref. 34, and Barwell and Woolacott, Ref. 44, also found that they had to abrade the rolling contact surfaces to obtain repeatable results.

It was observed that if the wheels were allowed to run for a long period under pressure then the contaminant layer built up and the lateral load required to make the wheel lift off its supports changed. Because of this readings were taken as quickly as possible after the surfaces had been wiped, but it was inevitable at the higher loads that readings took slightly longer. Evidence shows, Ref. 33, that the oxide layer formed by wear has a smaller tendency to form a strong adhesive bond with itself than does the metal, consequently the presence of an oxide layer usually reduces the coefficient of friction.

On days when the relative humidity was high, more scatter than usual was noticed in the results and testing was in fact curtailed on very humid days.

8.6.2 Correlation with theory

In order to be able to compare the experimental results with existing theories, a program was written, called LAB, which simulated the conditions on the roller rig by incorporating the equations for the creepages and forces given in Section 8.3. The

contact area forces are calculated from the creepages by calling on one of the subroutines for the individual theories described in Section 3. Results were calculated for a range of yaw angles and for a range of friction coefficients. Each case was considered in turn by inputting to the program the appropriate rolling radii, cone angle and vertical weight. Results were output from the program in the form (μf_2) v $(\psi / N^{\frac{1}{3}})$ so that they could be compared with experimental results directly.

The only theories available which predict the contact area forces for arbitrary creep and spin are the numerical theory (Section 3.3.1) and the simplified theory (Section 3.3.2). Since the numerical theory can only be used for contact areas with (a/b) ratios up to 2, it is only possible to compare the results of cases 1 and 2, where $(a/b) \simeq 1$, with this theory. Simplified theory can be used on elongated contact ellipses and the results of all the cases are compared with this. It has been mentioned previously that Kalker is still developing a numerical theory which can also treat elongated contact ellipses and he has run his program as it stands for several points on each of the cases with elongated contact ellipses.

The main objective of the experimental work was to provide data on the lateral force due to lateral creep and spin on elongated contact ellipses. This is done in cases 3 and 4 where $(a/b) \simeq 6.6$ and cases 5 and 6 where $(a/b) \simeq 10$. However, it was decided that a check on the rig should first be made by investigating a case with a near circular contact area, since the numerical theory had been proven for this case for a wide range of spins by Johnson's experimental results, Ref. 8. This is done in cases 1 and 2.

In Fig. 8.20 the experimental results for case 1 are reproduced from Fig. 8.14 and compared with numerical theory results. The comparison with simplified theory is made in Fig. 8.21. In each case theoretical results are plotted corresponding to $\mu = 0.6$ and $\mu = 0.7$.

The correlation between numerical theory and experimental results for this case is good, especially over the linear region where the value of f_2 for $\psi = 0$ is in good agreement as is the case when $f_2 = 0$. The major area of disagreement is at large yaw angles where some difficulty was experienced in obtaining results. It is also worth mentioning that the numerical theory has not been proven in this region, since Johnson's experimental results were for the linear region only.

The comparison of case 1 results with simplified theory, Fig. 8.21, shows a disagreement in slope for the same value of μ.

Case 2 has a larger amount of spin than case 1 since the cone angle is 67° as compared with 49°, but the contact area remains circular in shape. The comparison between experimental results and numerical theory is shown in Fig. 8.22 and simplified theory in Fig. 8.23. The slopes of the experimental results and numerical theory results agree well and correlation between the two is good. Using simplified theory, the predicted curves have less slope than the experimental results, as in the previous case. The inverse stiffnesses, S_x and S_y, of the simplified theory have been calculated according to the method outlined in Section 3.3.2 and Appendix 3. If the bodies were covered in a thin layer of material which was stiffer than the bulk of the body then the values of S_x and S_y would be reduced, resulting in a steeper f_2 v ψ curve and better correlation with experiment.

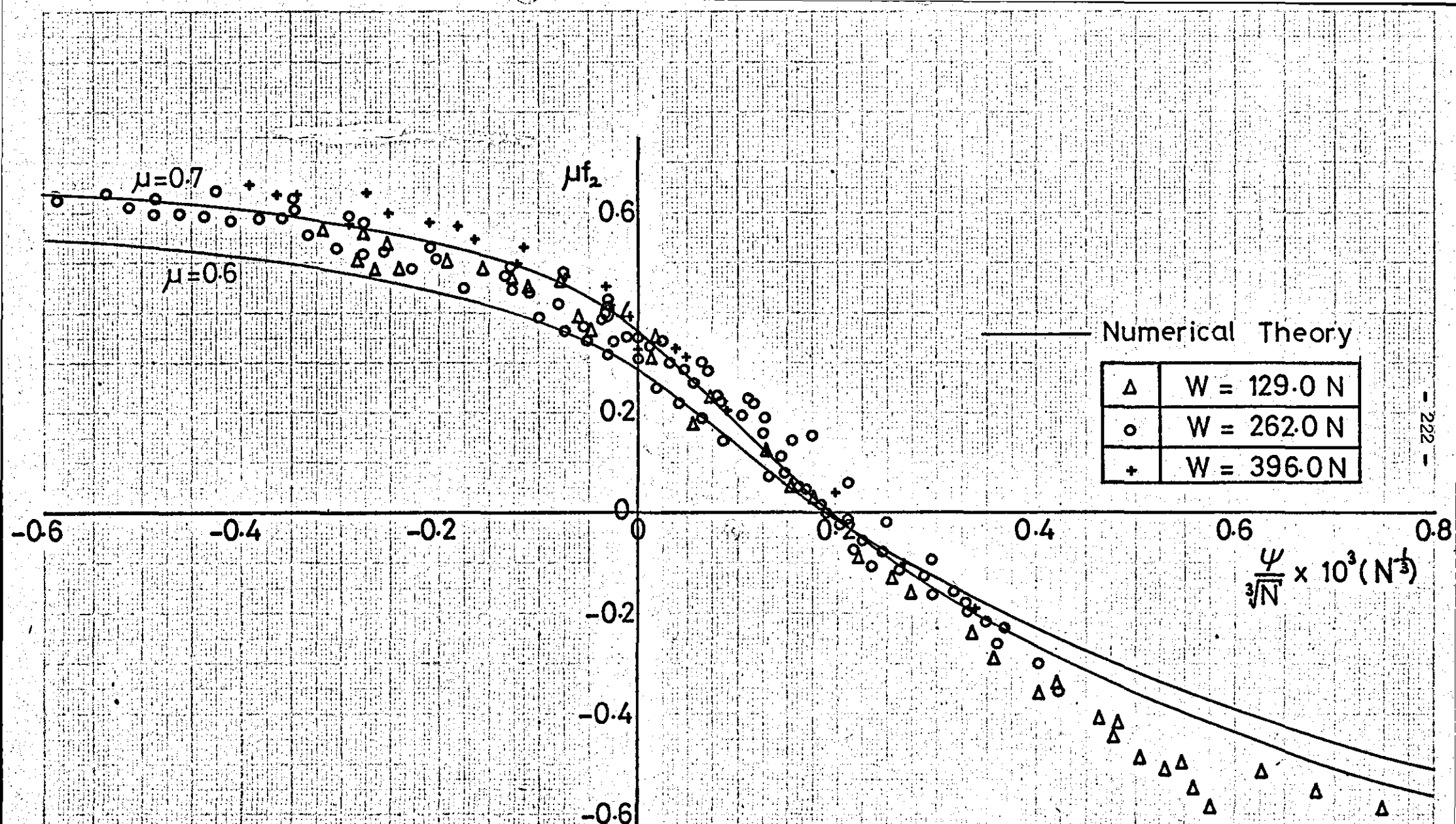

FIG. 8·20 Comparison of Experimental Results with Numerical Theory Case 1

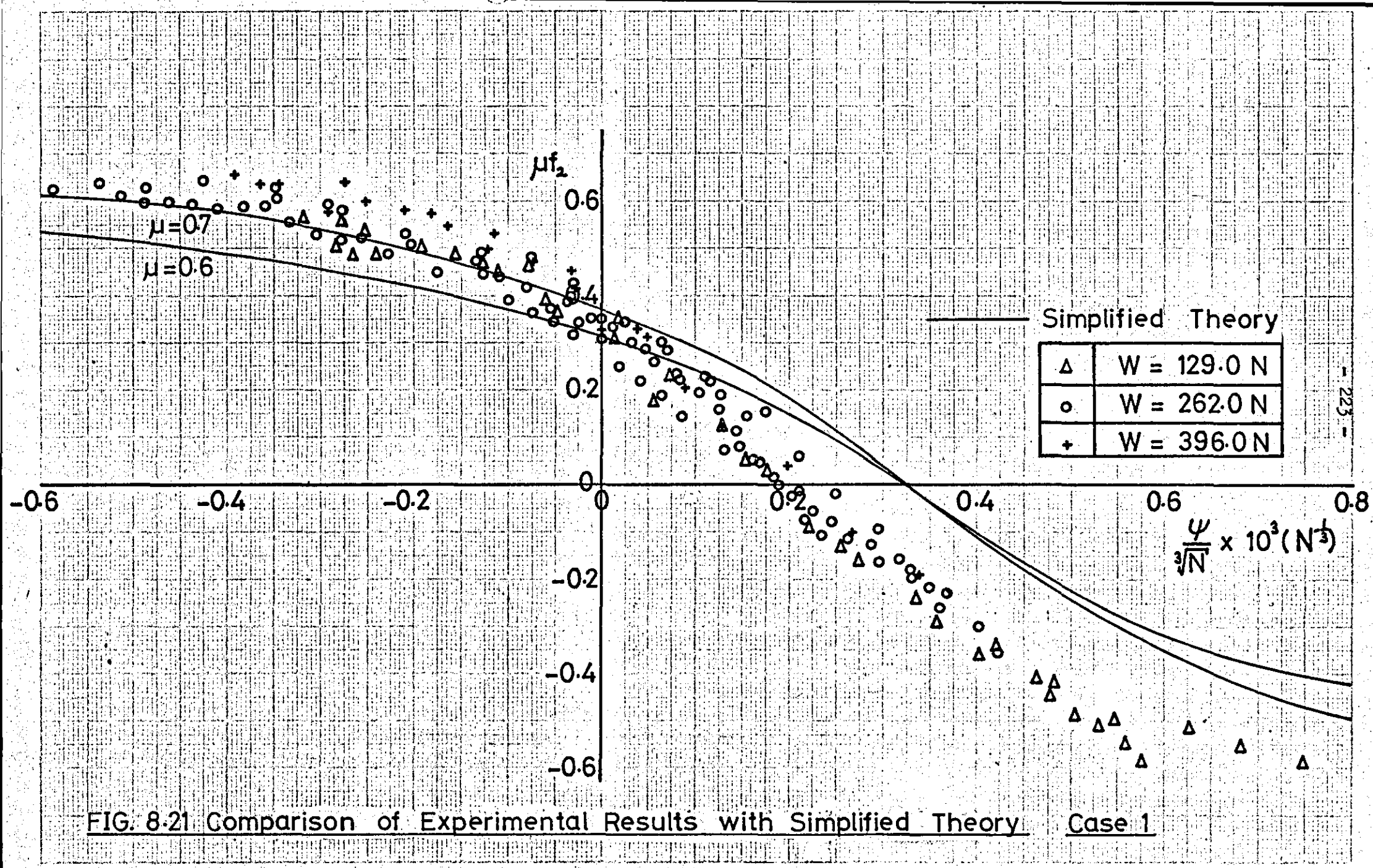

FIG. 8.21 Comparison of Experimental Results with Simplified Theory Case 1

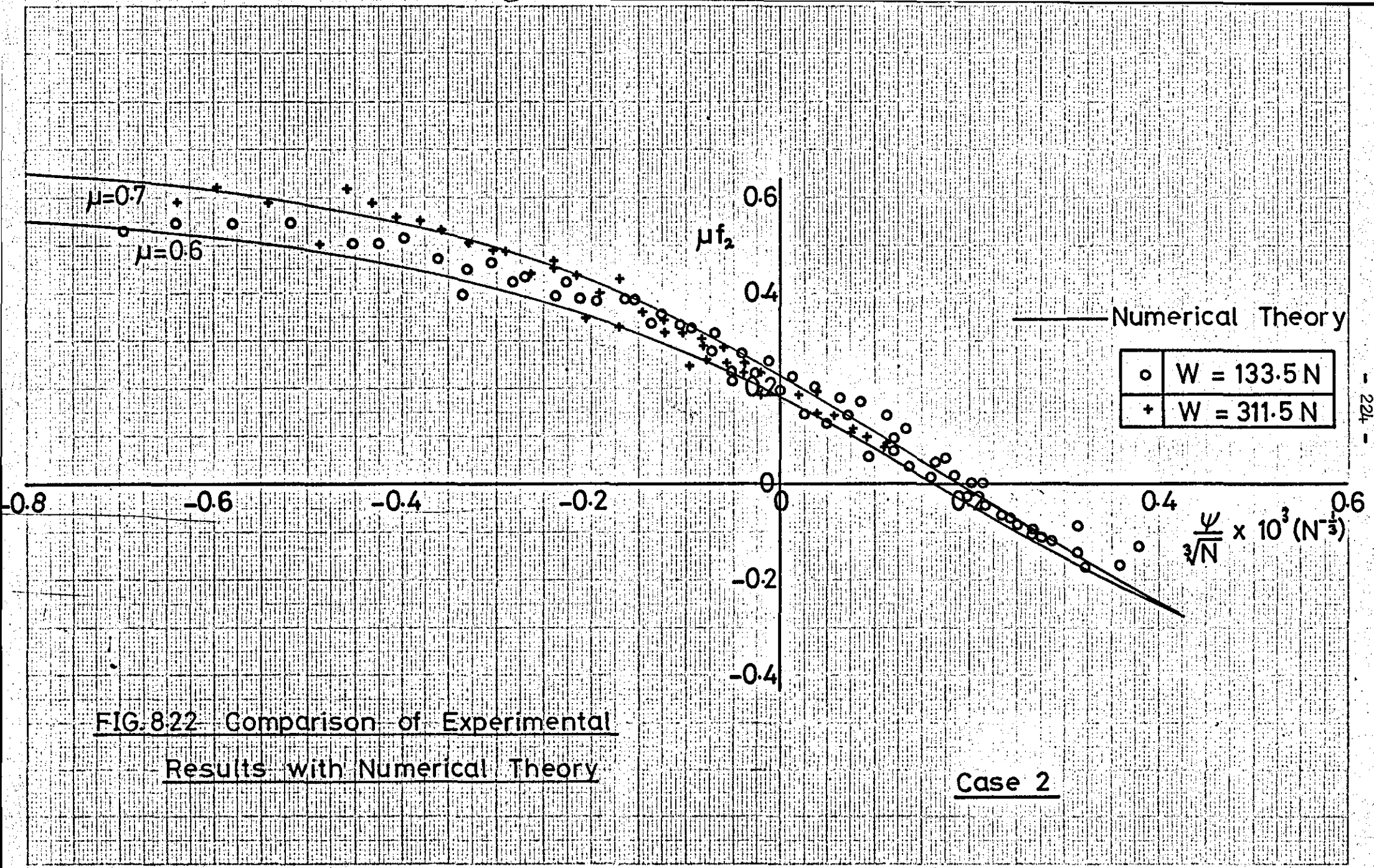

FIG. 8.22 Comparison of Experimental Results with Numerical Theory

Case 2

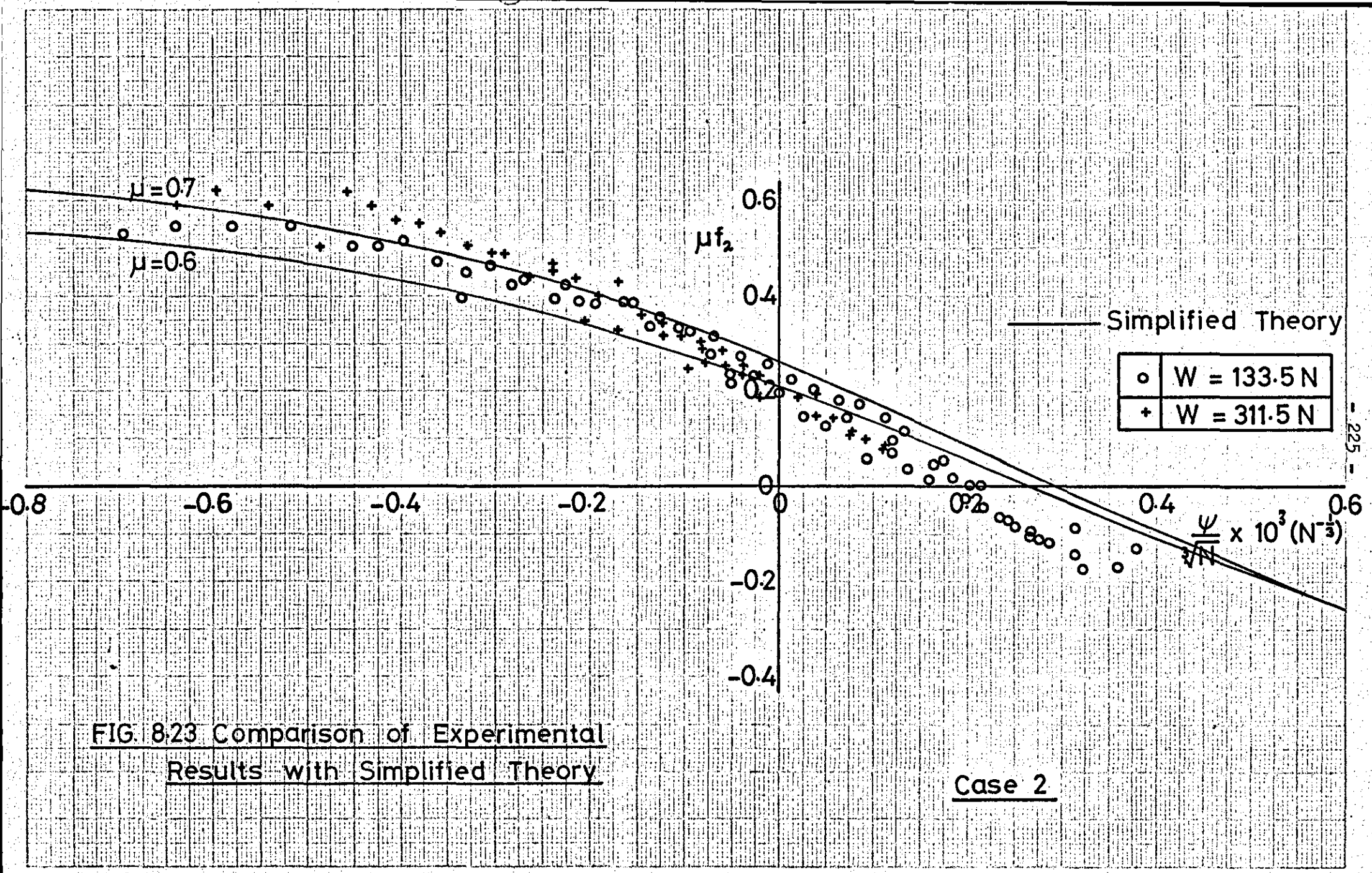

FIG. 8.23 Comparison of Experimental Results with Simplified Theory

Experimental results with the circular contact area just discussed, were encouraging, since there was good agreement between them and the numerical theory. Previously the numerical theory had been compared with the experiments of Johnson which were carried out using a ball rolling between inclined surfaces to give a circular contact area and the required amount of spin. The present results were achieved between two wheels which, by design, had radii giving a circular contact area, and cone angle which gave the required amount of spin. This is more like the physical problem of a railway wheel contacting the rail.

For cases 3, 4, 5 and 6 with the elongated contact ellipses, the experiments are only correlated with simplified theory and with a few points using Kalker's new numerical theory. The latter are all calculated assuming $\mu = 0.7$ while the simplified theory results are calculated for $\mu = 0.6$ and $\mu = 0.7$. Agreement between the new numerical method and the simplified theory is generally good, but Kalker admits that in fact both theories could over estimate the lateral force due to spin by as much as 10%.

For $(a/b) \simeq 6.6$ case 3 results are plotted in Fig. 8.24 and case 4 results for the larger cone angle in Fig. 8.25. Fig. 8.24 shows good agreement between the shape of the experimental and theoretical curves, but one curve appears to be shifted relative to the other. Since there is no justification for shifting the experimental results across to match the theory, it must be concluded that the effect of spin in the simplified theory is over emphasised. There is good correlation between the experimental results using different vertical weights, but it is difficult to estimate the value of μ from them. From the simplified theory slopes it appears that μ for the experimental

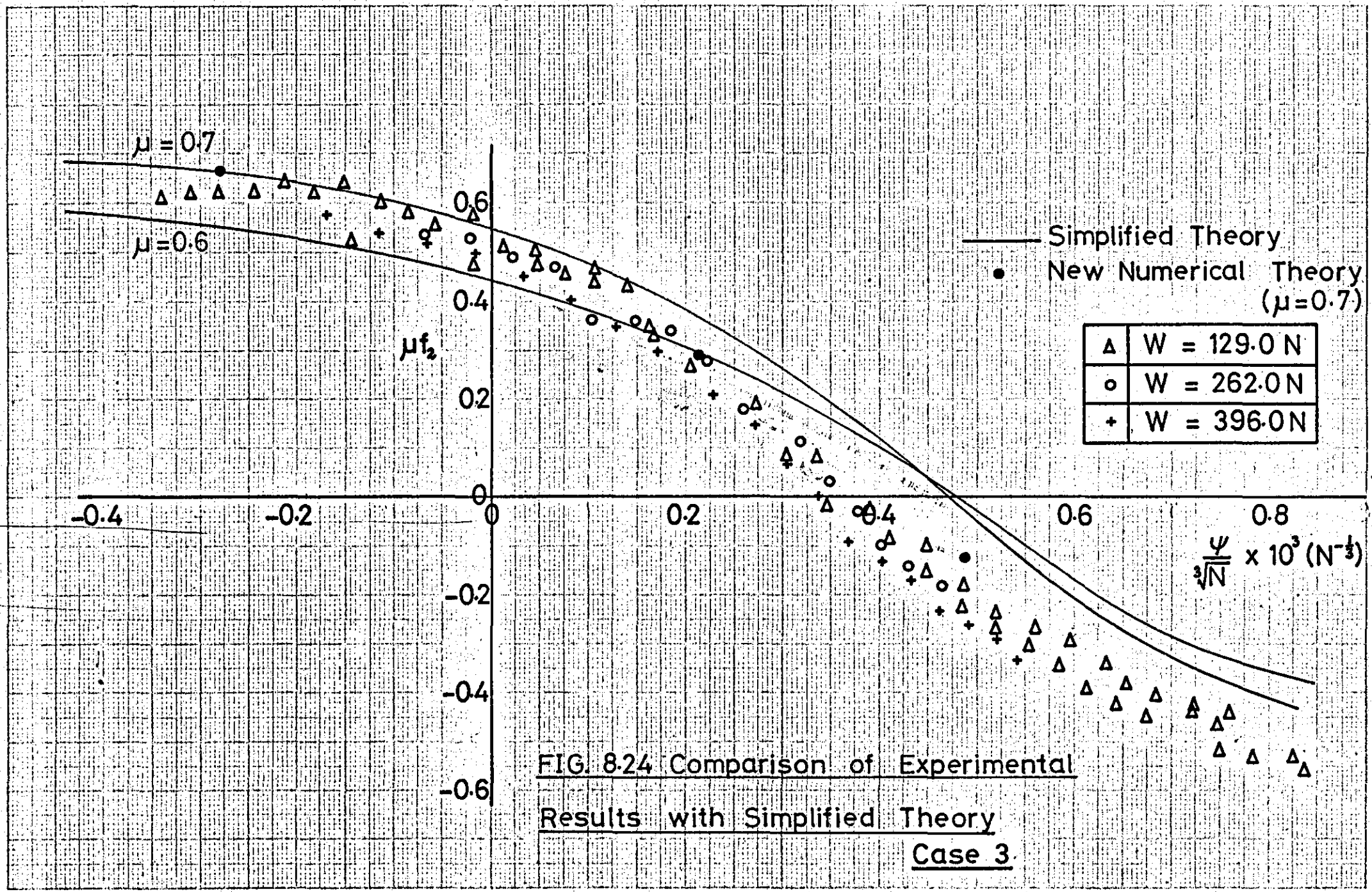

FIG. 8.24 Comparison of Experimental Results with Simplified Theory Case 3

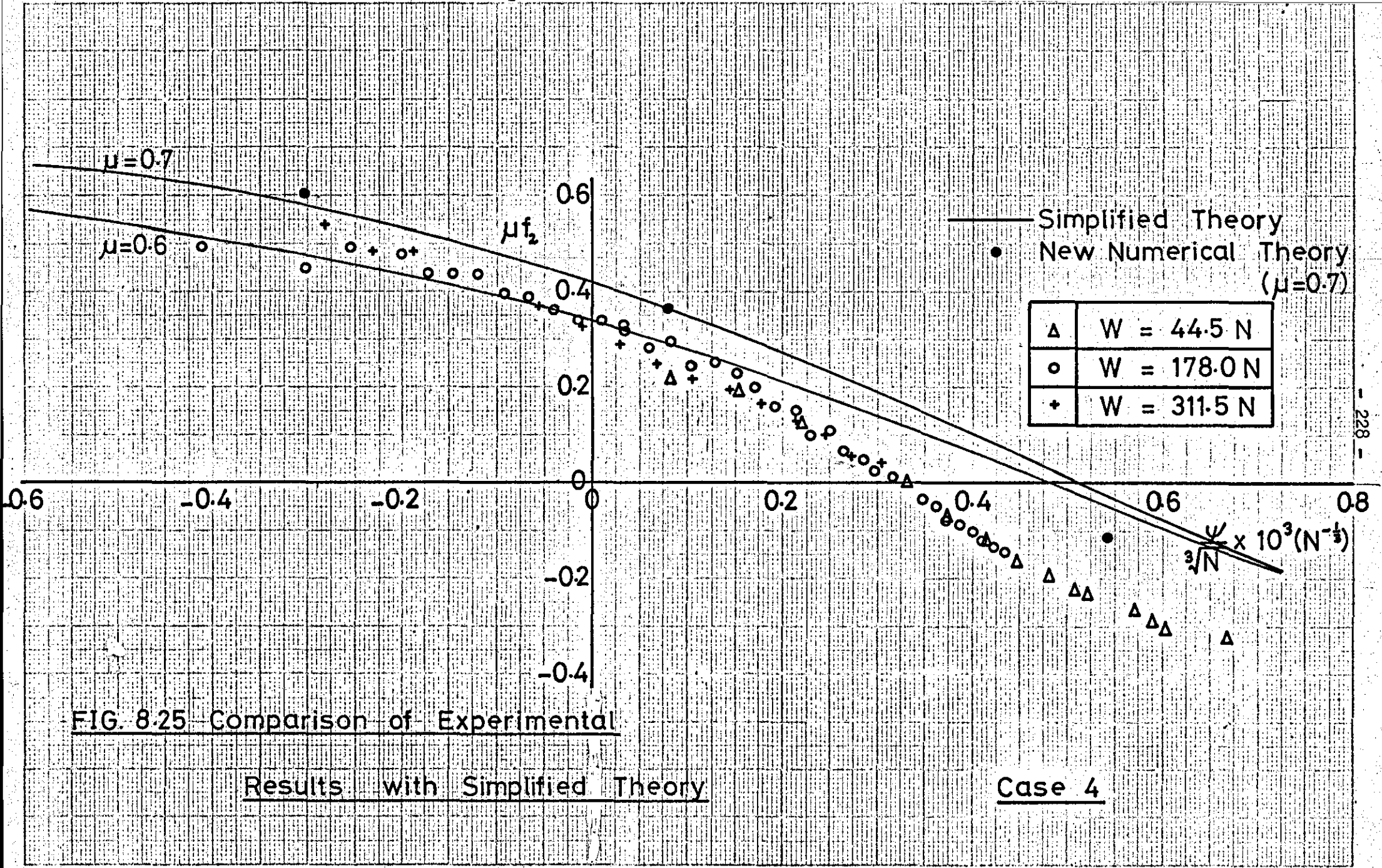

FIG. 8.25 Comparison of Experimental Results with Simplified Theory

Case 4

results is between 0.7 and 0.8, but this probably over estimates the value [illegible] and it is in fact between 0.6 and 0.7. The new numerical theory points lie closer to the experimental values than the simplified theory, but both theories probably over-estimate the effect of spin.

Case 4 in Fig. 8.25 again shows a difference in slope between experiment and simplified theory, while the new numerical theory points indicate a slope somewhere between the two. Correlation between the experimental results for the different weights is very good and since the roll effects have been fully explored in Section 8.6.1, there is no justification for further changing the slope of the experimental points.

When (a/b) = 10, cases 5 and 6, Figs. 8.26 and 8.27 respectively, the same trends are shown as in the previous two cases. The simplified theory and new numerical theory agree very well for these cases. In Fig. 8.26 the simplified theory curve corresponding to $\mu = 0.5$ is also plotted since there is some indication from the experimental results that perhaps μ is between 0.5 and 0.6. This is possible since the surface finishes of the wheels used in these tests (3.18 mm radius and 49°) were better than the other wheels used.

8.7 Conclusions and Recommendations

In general the experimental results were repeatable and consistent, and show the variation of lateral force with lateral creep on two surfaces in rolling contact with an elongated contact ellipse between them. Results were obtained for two ratios of contact ellipse

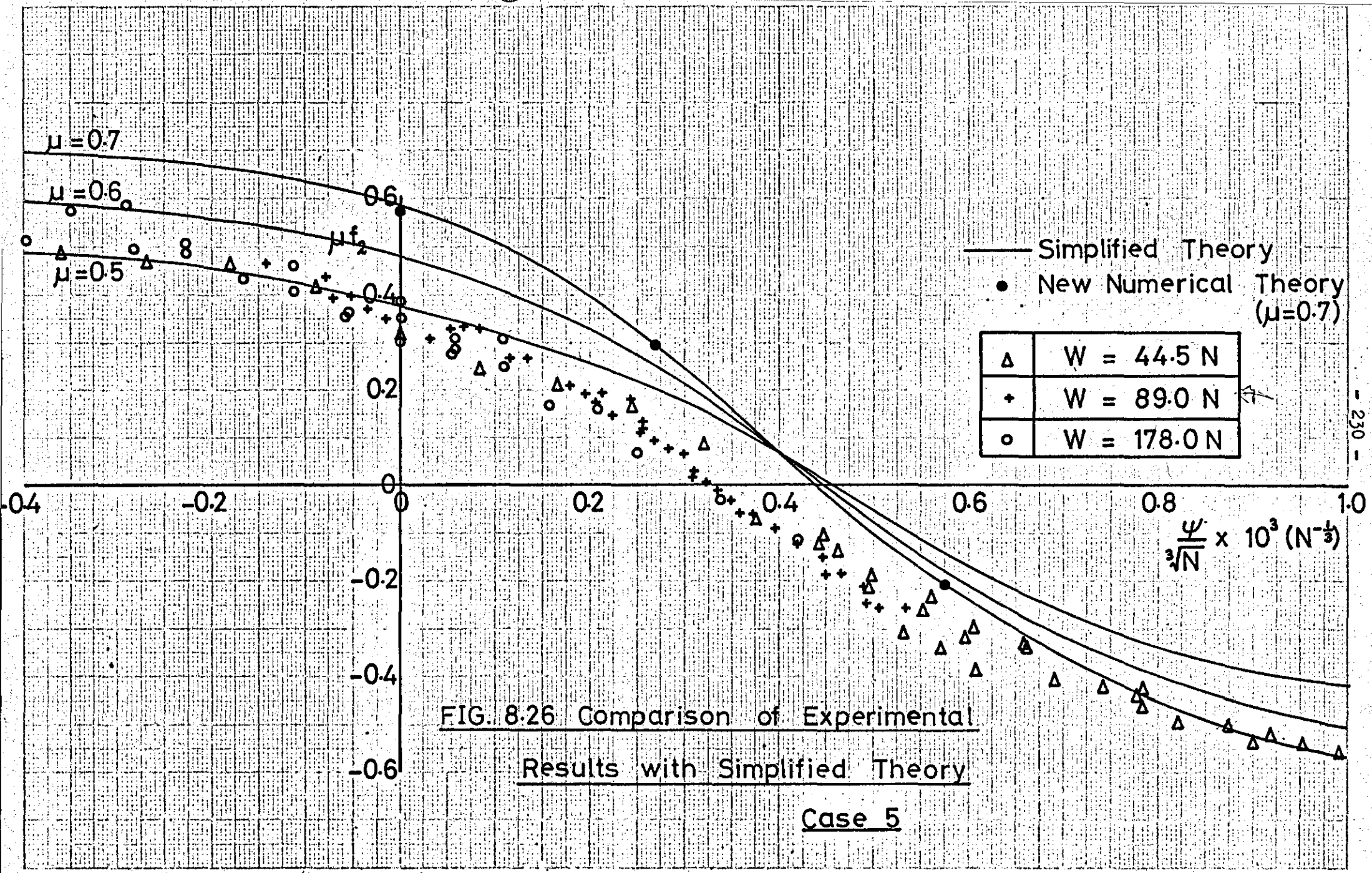

FIG. 8.26 Comparison of Experimental Results with Simplified Theory

Case 5

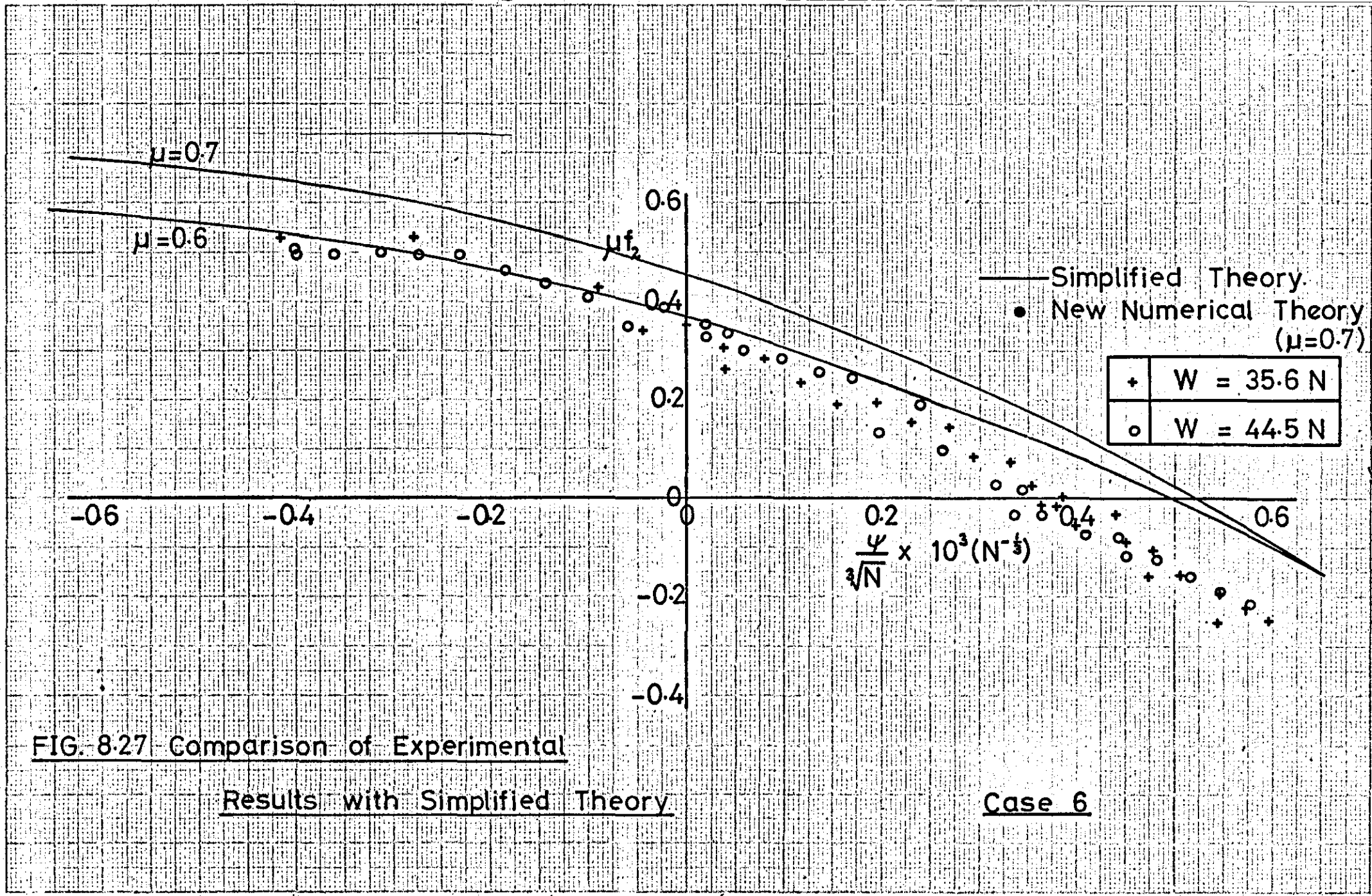

FIG. 8.27 Comparison of Experimental Results with Simplified Theory Case 6

semi-axes, (a/b) = 6.6 and (a/b) = 10 and for two values of spin. In each case the lateral creep was varied by varying the angle of yaw between the rolling contact surfaces. The contact pressure was also varied. Apart from this, a set of results was also produced for a circular contact area, since the numerical theory had been proven for this case by Johnson's experiments, Ref. 8, and this served as a check on the rig.

The rig was designed to conform as closely as possible to assumptions made in the rolling contact theories, i.e. smooth surfaces and Coulomb friction. This was achieved by using wheels made out of case hardened steel which were then ground to a good surface finish. The experiments were carried out "dry" at relatively low speeds and high contact pressures. The wheels were abraded before each test and wiped before each reading. This achieved consistent surfaces and therefore repeatable results.

The value of μ estimated from the results, approximately 0.7 was high but not altogether unexpected in view of the dry conditions present. There is no evidence to show that μ varied with contact pressure within the range tested. Speed effects were negligible, again within the range tested, and although longitudinal creep was not measured, there seems little doubt that it was so small as to not affect the results.

Possible errors in the results have been discussed in some detail in the previous section. These include the calculation of the yaw angle between the wheels, fixing the zero yaw position and roll effects. The yaw angle was calculated by measuring the lateral displacement of a pivot point on a dial test indicator and dividing this by the distance from the pivot to the contact point. This was not a very direct way of measuring the yaw angle at the actual contact point and

could have led to some inaccuracy. The expression for the lateral creep on the rig included a term which took account of the fore and aft movement of the contact point as the wheel was yawed.

As there was a large amount of spin present in each test it was important to be able to fix the zero yaw position so that the amount of lateral force due to spin could be estimated. Two methods were used to do this and each one suffered from some disadvantage, but even so the difference in results was small. Both methods showed that the zero position changed for different vertical weights. This effect has been allowed for in the results and has been discussed at some length in Section 8.6 where the main conclusion is that it is due to roll effects of the counterbalance wire.

The Hookes Joint arrangement for yawing one wheel relative to the other was theoretically restrained in roll, but because of play in the bearings and flexibility in the rig has been shown to allow a certain degree of roll. These effects were investigated by a further series of tests and all the results have been "roll" corrected, although this made very little difference to the measured values.

Correlation between theory and experiment was good, especially when the results were compared with numerical theory for the case (a/b) = 1. Johnson's experiments for this case were carried out with a ball on a flat surface, thereby giving a circular contact area, while the present results were achieved under conditions more like those found on a railway wheel, with both rolling surfaces being bodies of revolution.

All the results, including those with elongated contact ellipses, have been compared with simplified theory, which is the only available theory for arbitrary creep and spin that can be used for such conditions. It seems apparent from the results that either the spin or the inverse stiffness is not well accounted for in the simplified and new numerical

theories and in fact Kalker admits that both might over-estimate the effect of spin by as much as 10%.

In general the results were encouraging and show reasonable agreement between simplified theory and experiment for flange type contact conditions. In view of the uncertainty in knowing the coefficient of friction in the real case, it would seem that simplified theory can be used to give a good estimate of forces between a wheelset and the track when in flange contact.

Several recommendations can be made with respect to the rig. It could be improved by having a more direct method of measuring the yaw angle such as the one attempted in the experiment, e.g. by shining a slit of light onto the back faces of the wheels and measuring the angle from the reflected images when in motion. In the present investigation the reflected image was not consistent enough to allow accurate measurements with the wheels rotating, and so the method was only adopted as a setting-up procedure. In future tests it would be advisable to have the back faces of the wheels polished and perhaps even silvered, thus enabling angles to be measured directly at the rolling contact surfaces and eliminating errors inherent in the present system due to flexibilities.

Another improvement would be either to stiffen the yoke, or better still to have a different arrangement for supporting the upper wheel, perhaps more along the lines of the rig used by Poon, Ref. 49. This is not only a stiffer arrangement but also allows the spin to be infinitely variable. It would also mean that the wheels could be run in the reverse direction and without the inherent instability of the present rig.

9. General Discussion and Conclusions

With the present trend of higher speeds showing better economics for rail travel, railway designers of late have shown renewed interest in the field of railway vehicle dynamics. In the past an empirical approach was sufficient, but at high speeds a number of phenomena need to be investigated more thoroughly. The basic force inputs to the dynamic calculations of a railway vehicle are those which arise between the wheel and rail and are due to the phenomenon known as creepage. This phenomenon was first analysed by Carter, Ref. 3, who considered the rolling of a cylinder on a flat surface.

A railway wheelset comprises two wheels on a fixed axle. The wheels are coned to provide a measure of stability; the cone angle of the tread is approximately 3° while the cone angle of the flange is approximately 70°. During normal running, the wheelset rolls on its treads with the creepage forces providing the necessary guidance. Lateral displacement of the wheelset produces longitudinal creepage, while a yaw angle displacement produces lateral creepage. A spin component is also present due to the cone angles of the tread and flange.

The creepage forces are non-conservative and can lead to a dynamic instability at high speeds, known as hunting, which is caused by a combination of these forces and the suspension parameters. This is characterised by a violent swaying of the wheelset from side-to-side with the flanges of the wheels in contact with the rails. Although actual running speeds, which are governed by the lateral dynamics of the wheelset, are based on comfort criteria, it is important from the safety viewpoint to know the order of magnitude of the forces involved when the flange contacts the rail. This is generally considered the start of derailment. For a wheelset to derail, it has to move sideways (with or without an angle of yaw) until the flange contacts the rail and then, if the lateral force is increased further, it climbs up the rail until it eventually jumps off.

Various theories exist which predict the forces in the plane of the contact area, due to creepage and spin, of two bodies of revolution in rolling contact. This report set out to investigate these theories and to select, compare and recommend those most appropriate to the railway wheelset problem. This included calculations of the creepages and forces for various lateral and angular displacements of a wheelset from its central position, including flange contact conditions.

A historical review of the work done in the field of rolling contact is given in Section 2 which is divided in two parts, a theoretical review in 2.2 and an experimental review in 2.3.

Most of the theories which have been developed have some restrictions placed upon them, e.g. some apply to circular contact areas only, some apply for small creeps, others for large creeps and so on. For application to the railway wheelset problem it is desirable to use a theory which can take account of varying amounts of longitudinal creep, lateral creep and spin, and also apply to various shapes of contact ellipse. For tread contact this area is near circular in shape, while on the flange the contact ellipse is very elongated in the rolling direction. The spin, which is a function of cone angle, also varies considerably from the small cone angle of the tread to the large flange cone angle.

All but one of the existing theories have as basic assumptions that both bodies in rolling contact have smooth surfaces and that Coulomb friction exists between them. In postulating such theories, the difficulty has been to define which part of the contact area is an area of slip and which part is adhesion. One type of theory assumes that the creepage and spin are infinitesimal and there is no slip anywhere in the contact area. This type is discussed in Section 3.1 and is useful for railway wheelset problems when displacements from the central position are small, i.e. tread contact points only. Since the relationship between creepage and force is linear, it can be incorporated easily in a dynamic

analysis of a wheelset rolling on its treads, and is in fact used by some railway authorities for this purpose. For more general use, a check should always be made on the relative magnitude of the creeps and spin before use. The way in which this can be done is outlined in Section 3.1 where certain modifications are also suggested in order to extend its use, for approximate analysis, to very large creeps and spins.

A second type of theory assumes that the creepage and spin are very large and there is complete slip throughout the contact area. This type is discussed in Section 3.2, and again one of the problems in using it is deciding whether the creepage and spin are large enough for the approximations to be valid. This theory, in fact, assumes that the spin is so large that the lateral force due to it is negligible. It is felt that this is a gross approximation, and because of it the large creep theory has limited use for railway wheelset application.

Another approach to the problem has been to divide the contact area into a number of strips parallel to the rolling direction and each strip is then considered as two-dimensional. These theories generally predict good results when the contact ellipse is narrow in the rolling direction, but results are poor even for circular contact areas. Because of this, strip theory is not seen to have any application in the railway wheelset problem and as such has not been used in the present analysis.

The final type of smooth surface theories are those which apply for arbitrary creep and spin. Kalker, Ref. 23, presents a numerical theory which can be applied for the three-dimensional case of arbitrary creep and spin and this is described in Section 3.3.1. The disadvantage of using this method is that it is very cumbersome as regards computer time, and the numerical iterations fail to converge for (a/b) ratios greater than two. For (a/b) ratios less than two Kalker has published tables of results of non-dimensional force parameters for various creeps, spins and contact ellipses.

In the railway wheelset application this theory is useful for accurate values of forces due to creeps and spin for tread contact, but cannot be used on the flange due to the very elongated contact ellipses present. It is probably most convenient to use the method, as has been done in the present analysis, by interpolating the tabulated results to obtain the required values.

Kalker is at present working on a new numerical theory which can also treat elongated contact ellipses. This work is as yet unfinished but, if successful, should prove useful for flange contact problems.

Another theory for arbitrary creep and spin is the simplified theory described in Section 3.3.2, where the complicated relationships between displacement and traction of the numerical theory are replaced by very simple relationships. By adapting the governing parameters in a special way, solutions can be found for the forces due to arbitrary creeps and spin on any shape contact ellipse including elongated ellipses. The simplified theory is in fact the only theory available at present for arbitrary creep and spin, which can be used to predict the forces for flange contact of a railway wheelset.

Unlike the smooth surface theories just mentioned, a theory due to Nayak, Ref. 32, does not make the same basic assumptions of smooth surfaces and Coulomb friction. The theory only applies for two-dimensional contact of similar bodies, and to be able to use the theory a profilometric examination of the body surfaces has to be made. Therefore it is impractical for use in railway contact problems.

Experimental work in the field of rolling contact, reviewed in Section 2.3, can generally be divided into two groups:

(a) experiments carried out on real wheelsets or with scale wheels on roller rigs; and

(b) experiments using apparatus specifically designed for the purpose.

Up until the last decade adhesion studies were the main concern of railway engineers and as a result most experiments in group (a) were designed to measure longitudinal creep. Recently some experiments have been carried out where lateral creep was also measured, but in all cases only tread contact has been considered. Generally, experimental results obtained from real wheel tests have not agreed well with the theories, probably because of the difficulty in controlling all the parameters accurately in such tests, especially the coefficient of friction between the surfaces.

The most accurate creep measurements have been made on apparatus designed specifically for the purpose, group (b), and have usually comprised a sphere rolling on a flat or inclined surface, giving a circular contact area. Experiments of this type have been carried out by Johnson, Refs. 6, 7, 8 and 10, for longitudinal creep, lateral creep and creep with spin, all for circular contact areas. Johnson and Vermeulen, Ref. 9, carried out tests on elliptical contact areas with (a/b) ratios up to 2.5 and measured the lateral force due to lateral creep. All these tests were carried out with extremely smooth surfaces and at very low speeds, generally with the surfaces lubricated. As a result, estimated coefficients of friction were very low, of the order of 0.1.

The numerical theory of Ref. 23 has been compared with Johnson's experimental results for a wide range of creeps and spins, and the total forces have been within 10% of each other in all cases. The creepage and spin coefficients of the small creep theory have been compared with these experimental results together with Johnson and Vermeulen's results, again with very good agreement. For cases where both creep and spin were present, the numerical theory has only been compared with experimental results for circular contact areas, while for cases without spin, contact ellipses with (a/b) ratios up to 2.5 have been compared.

The simplified theory has only been compared with numerical theory results, and since the latter can only be found for (a/b) ratios up to 2, it has not been proven for elongated contact ellipses.

In view of the lack of experimental results available for more elongated contact ellipses, especially with spin present, as is the case with flange contact of a railway wheel, a series of tests were carried out during the present investigation. The experimental rig is described in Section 8 and was designed to provide data on elongated contact ellipses with varying amounts of lateral creep and spin present. Longitudinal creep was excluded from the rig by allowing one surface to roll freely on the other.

The rig basically consists of two wheels in rolling contact, one driven and one free. The lateral creep is varied by yawing one wheel relative to the other, and spin and contact ellipse shape are varied by using wheels with various cone angles and radii, while contact pressure and speed can also be varied on the rig. In order to achieve repeatable results the experiments were run 'dry' at low speeds and with relatively high contact pressures. The principle of the rig was to increase the lateral force until one wheel tended to ride up on the other. At this point the forces were in balance and the lateral force corresponding to known amounts of lateral creep and spin could be calculated.

A set of results were produced first for a circular contact area by using wheels of suitable radii. This allowed a comparison with proven theories to be made and served as a check on the rig. Good correlation was achieved between the experimental results and numerical theory for the two values of spin tested.

The coefficient of friction present had to be estimated from the results and they were presented in such a way that this was possible, values of $\mu \simeq 0.7$ were found to exist between the rolling surfaces. This is

not altogether surprising in view of the dry conditions present and similar values have been found by other investigators for similar conditions.

Results were produced for contact ellipses with semi-axes ratios of (a/b) = 6.6 and (a/b) = 10. These results, together with the circular contact area results, were compared with simplified theory, which is the only theory existing that can be used for arbitrary creep and spin on elongated contact ellipses. In all cases the slopes of the theoretical and experimental results were different. This also applied for the circular contact area results which had previously agreed well with numerical theory. This seems to indicate that perhaps the lateral force due to spin is overestimated by the simplified theory.

Possible errors in the experimental results have been discussed in Section 8. These include the measurements of yaw angle between the wheels, locating the zero yaw position, possible roll effects and difficulties in estimating the coefficient of friction present.

Possible errors in the simplified theory could be due to either the inverse stiffness or the spin not being well accounted for. Kalker, in fact, admits that the effect of spin could be overestimated by as much as 10%, and his own checks with numerical theory show this. Since the spin parameter is dependent on the value of μ, this would affect the slope of the results and the lateral force due to spin.

However, since the simplified theory and experimental results show reasonable agreement, within 15% of each other, and in view of the uncertainty in knowing the coefficient of friction and the other parameters for the real case, it would seem that simplified theory can be used to give an estimate of forces between a wheelset and track when in flange contact.

It has been pointed out earlier in this discussion that one of the objectives of the investigation was to calculate the creepages and forces on a

wheelset for various amounts of lateral and angular displacement from its central position, including flange contact conditions. A comparison between forces calculated using the various rolling contact theories could then be made as well as an estimate of the forces on the wheelset with the flange in contact with the rail. Previous calculations of flange forces had not taken into account the force due to spin and assumed the flange to be sliding on the rail. Using the present theories this information could be updated. A third objective was to investigate wear effects and assess how the forces changed with rail wear.

Before the forces on a wheelset could be calculated using the rolling contact theories it was necessary to define a mathematical model of a real wheelset and real track so that representative values of creep, spin and contact ellipse were used in the analysis. This model is described in Section 4, and is based on a BS 110A rail section and a British Rail RD4 tyre profile on a 750 mm diameter wheel. Three-dimensional equations were calculated for both track (assuming it to be straight) and wheelset, these being written in the form of computer subroutines. The program which defined the rail allowed the corner radius to be varied so that rail wear could be simulated. The RD4 tyre profile was chosen as it is one of British Rail's 'worn' profiles - they found standard profiles wore very rapidly to a profile which then remained relatively constant for the life of the wheel and the RD4 worn profile was based on this shape. Programs were written to enable the wheelset to be displaced laterally, and also yawed, relative to the track and the resulting contact points found. This included large displacements so that the flange contacted the rail. Vertical displacements and angles of roll were accounted for in the programs, together with fore and aft movement of the contact point, as the wheelset was displaced.

The creepages were calculated assuming the wheelset to be rolling along the track at a constant velocity in a displaced position. From

these the contact area forces were calculated using the subroutine appropriate to the required theory. A computer program was written, for each of the theories in the same input and output format ao that any one of them could be used to obtain the forces. The total forces on the wheelset were then calculated by summing and resolving the contact area forces.

A program was written which carried out these calculations and varied the angular velocity of the wheelset, and therefore the creepages, until the total rolling moment was zero. The program then printed out the creepages, contact area forces and total forces on the wheelset for the appropriate lateral displacement and angle of yaw.

In Section 5 this model and its accompanying programs were used to calculate the total forces and moments on the wheelset using different combinations of theories for the tread and flange contact points. Three cases were analysed (a) tread contact only, (b) flange contact with zero angle of yaw, and (c) flange contact with 3° angle of yaw. For case (a) there was reasonable agreement between numerical theory, simplified theory and small creep theory. Although contact remained on the treads, the displacement was in fact large. Small creep theory being a linearised theory has obvious attractions for tread contact points but would not normally be used for such large displacements. When the flange was in contact with the rail, cases (b) and (c), the numerical theory could not be used because of the very elongated contact ellipse. The large creep theory produced a large lateral force necessary to keep the wheelset in flange contact because the effect of lateral force due to spin, which tends to lift the wheel up, is not accounted for in this theory. The modified small creep theory produced a small lateral force necessary to maintain flange contact since the lateral force due to spin is over-estimated. The simplified theory produced results between the latter theories, as would be expected. It is interesting to note that for large angles of yaw all three theories produce very similar results since the lateral force due to both the lateral creep and the spin components are large. The differences between the theories

are much more noticeable at zero yaw angle, i.e. zero lateral creep.

The cases mentioned above were only a sample of all the results obtained. The complete results using both a new and worn rail profile are presentedin Section 6 for a range of yaw angles, lateral displacements and load distributions. In all cases numerical theory was used for tread contact points and simplified theory for flange contact points. The 'new' rail had a 12.7 mm corner radius while the 'worn' rail considered in the analysis had a 17.8 mm corner radius. Since there was practically no difference between the wheelset forces calculated for the two cases it must be concluded that rails have to be sidecut by much greater amounts before performance is affected. Although the results presented apply for a particular rail/wheel combination, it is the first time that flange forces have been calculated using rolling contact theories and the results should prove useful in future derailment studies.

In this connection, the results have been used in Section 7 to calculate the 'derailment ratio' or 'derailment quotient'. This is a parameter used by railway engineers as a measure of how easy a particular rail/wheel combination is to derail. It is simply the ratio of lateral force/vertical force at the flange contact point. Previously this ratio has been calculated using various approximate formulae which have not taken account of spin effects and usually assume the flange to be sliding on the rail. These formulae are reviewed in Section 7 and compared with the present results. The formula used by British Rail is the limiting case for very large angles of yaw. At small or zero yaw angles the present work shows that the derailment ratio is considerably greater than the limiting value which means the lateral force is less likely to occur in practice. The value used by British Rail is therefore a safe limit.

In conclusion, the present investigation has shown that for tread contact of a railway wheel linearised theory can be used to predict the contact area forces and results compare favourably with numerical theory. The latter

theory is very cumbersome to use directly but existing results can be effectively and easily interpolated, and in this form, is a possibility to use for tread contact points where greater accuracy is required. The linearised theory has been modified in the present analysis and as such can be used to give acceptable results for a wider range of displacements.

For flange contact points the only available theory at present which can be used to calculate the contact area forces is simplified theory. This has been compared with experiments in the present investigation and shown to give reasonable results for flange type contact conditions. The lateral force due to spin seems to be over-estimated by the simplified theory, but even so results were always within 15% of each other. Results have been calculated on a theoretical wheelset using numerical theory for the tread contact points and simplified theory for the flange contact point. These results show the magnitude of forces and moments on a wheelset when the flange contacts the rail and should prove useful in future derailment studies. The derailment ratio has been calculated from these results and is the first time spin effects have been included in the calculations of this ratio.

It is possible that in the not too distant future other theories will appear which can be used for elongated contact ellipses and as such could be used to calculate the forces at the flange. The experimental results presented could be used as a check on these theories as and when they appear.

10. References

1. LOVE, A. E. H. — A treatise on the mathematicl theory of elasticity. 4th Edition. Cambridge University Press. 1952.

2. TIMOSHENKO, S. and GOODIER, J. N. — Theory of elasticity. McGraw-Hill Book Co., Inc., New York. 1951.

3. CARTER, F. W. — On the action of a locomotive driving wheel Proc. Roy. Soc. A112 (1926) p.151-157.

4. PORITSKY, H. — Stresses and Deflections of Cylindrical Bodies in Contact with applications to contact of gears and of locomotive driving wheels. J. Appl. Mech., 17 (1950), 191-201.

5. CAIN, B. S. — Discussion of Ref. 4 by PORITSKY. J. Appl. Mech., 17 (1950) 465.

6. JOHNSON, K. L. — The effect of a tangential contact force upon the rolling motion of an elastic sphere on a plane. J. Appl. Mech., 25 (1958), 339-346.

7. JOHNSON, K. L. — The effect of spin upon the rolling motion of an elastic sphere upon a plane. J. Appl. Mech. 25 (1958), 332-338.

8. JOHNSON, K. L. — The influence of elastic deformation upon the motion of a ball rolling between two surfaces. Proc. Inst. Mech. Engs. 173 (1959) 34 p.795-810.

9. JOHNSON, K. L. and VERMEULEN, P. J. — Contact of non-spherical bodies transmitting tangential forces. J. Appl. Mech. (1964) p.338-340.

10. JOHNSON, K. L. — Tangential tractions and microslip in rolling contact. Proc. Symp. Rolling Contact Phenomena. Ed. J. B. Bidwell, Elsevier 1962, p.6-28.

11. HAINES, D. J. and OLLERTON, E. — Contact stress distributions on elliptical contact surfaces subjected to radial and tangential forces. Proc. Inst. Mech. Engrs. Vol. 177 (1963) p.95-114.

12. DE PATER, A. D. — On the reciprocal pressure between two bodies. Proc. Symp. Rolling Contact Phenomena. Ed. J. B. Bidwell, Elsevier 1962 p.29-75.

13. KALKER, J. J. — The transmission of force and couple between two elastically similar rolling spheres. Proc. Kon. Ned. Akad. Wet. Amsterdam, B67 (1964) p.135-177.

14. HALLING, J. — The rolling of a ball subjected to normal and tangential loads. Wear 7 (1964) 516-534.

15. HALLING, J. — The microslip between a rolling element and its track arising from geometric conformity and applied surface tractions. J. Mech. Eng. Sci. 6 (1964) 64.

16. JOHNSON, K. L. — A review of the theory of rolling contact stresses. Wear 9 (1966) p.4-19.

17. LUTZ, O. Grundsatzliches uber stufenlos verstellbare Walzgetriebe.Konstruktion 7 (1955) 9, p.330-335.

18. LUTZ, O. Grundsatzliches uber stufenlos verstellbare Walzgetriebe.Konstruktion 9 (1957) 5, p.169-171.

19. LUTZ, O. Grundsatzliches uber stufenlos verstellbare Walzgetriebe. Konstruktion 10 (1958) 11, p.424-427.

20. WERNITZ, W. Walz-Bohreibung. F. Vieweg and Sohn. Braunschweig 1958, p.68-81.

21. WERNITZ, W. Friction at Hertzian contact with combined roll and twist. Proc. Symp. Rolling Contact Phenomena. Ed. J. B. Bidwell, Elsevier 1962, p.132-156.

22. KALKER, J. J. Rolling with slip and spin in the presence of dry friction. Wear 9 (1966), p.20-38.

23. KALKER, J. J. On the rolling contact of two elastic bodies in the presence of dry friction. Doctoral thesis. Delft (1967).

24. KALKER, J. J. A strip theory for rolling with slip and spin. Proc. Kon. Ned. Akad. Wet. Amsterdam, B70 (1967) p.10-62.

25. KALKER, J. J. The tangential force transmitted by two elastic bodies rolling over each other with pure creepage. Wear 11 (1968) p 421-430.

26. BENTALL, R. H. and JOHNSON, K. L. — Slip in the rolling contact of two dissimilar elastic rollers. Int. J. Mech. Sci 9 (1967) p.389-404.

27. KALKER, J. J. — Transient phenomena in two elastic cylinders rolling over each other with dry friction. J. of Appl. Mech. 37, Trans ASME, Vol. 92 Series E 1970 p.677-688.

28. KALKER, J. J. — Transient rolling contact phenomena (to be published in ASLE Transactions)

29. KALKER, J. J. — Transient phenomena in two elastically similar rolling cylinders in the presence of dry friction. Delft University of Technology. WTHD Report M, 1969.

30. KALKER, J. J. — A minimum principle for the law of dry friction, with application to elastic cylinders in rolling contact. J. Appl. Mechanics, Vol. 38 Series E No. 4 December 1971.

31. HAINES, D. J. — Contact stresses in flat elliptical contact surfaces which support radial and shearing forces during rolling. Proc. Inst. Mech. Engrs. Vol 179 (1964-65) Part 3J.

32. NAYAK, P. R. — A new theory of rolling contact. Ph.D. Thesis, Dept. of Mechanical Engineering, MIT (1968).

33. NAYAK, P. R. et al — Friction and Creep in Rolling Contact. U.S. Dept. of Transportation, Ref. FRA-RT-71-64. PB-196-707. November 1970.

34. HOBBS, A. E. W. — A survey of creep. B.R. Ref. DYN 52 (1967)

35. KALKER, J. J. — On the rolling contact of two elastic bodies in the presence of dry friction. Numerical results. Delft (1967).

36. KALKER, J. J. — A simplified theory of rolling contact. Delft (1971).

37. HEUMANN, H. — Zur Frage des Radreifen - Umrisses. Organ, 15th September 1934.

38. KOFFMAN, J. L. — Heumann tyre profile tests on British Railways. Railway Gazette, 2nd April 1965.

39. KING, B. L. — New tyre profiles for British Railways. Railway Gazette, 19th January 1968.

40. JOHANSEN, F. C. — Graphical study of derailing tendency of flanged wheels. B.R. Report No. W.1, Ref. ER/2/13.

41. DAVIES, R. D. — Some experiments on the lateral oscillation of railway vehicles. J. Inst. Civil Eng. 11 (1939) p 224-261.

42. MUELLER, C. Th. — Memo to O.R.E. Sub-Committee C.9.

43. MATSUI, N. and YOKOSE, K. — On the creep phenomenon between wheel and rail. Railway Technical Research Institute, J.N.R. (1966), 3.

44. BARWELL, F. T. and WOOLACOTT, R. G. — The N.E.L. contribution to adhesion studies. Proc. Con. Adhesion. I.Mech.E. (1963) p.145-160.

45. HALLING, J. and BROTHERS, B. G. — The effect of surface finish on the creep and wear of a rolling ball subjected to normal and tangential surface tractions. Wear, 9 (1966) p.199-208.

46. HALLING, J. and AL-QISHTAINI, M. A. — An experimental study of some of the factors affecting the contact conditions and the slip between a rolling ball and its track. Proc. Inst. Mech. Engrs. (1967/68), Vol. 182 Pt. 1, No. 37.

47. POON, S.Y. and HAINES, D. J. — Frictional behaviour of lubricated rolling contact elements. Proc. Inst. Mech. Engrs. (1966/67) Vol. 181 Pt.1, No. 16.

48. POON, S. Y. — An experimental study of the shear traction distribution in rolling with spin. Wear 10 (1967) No. 1. p.61-69.

49. POON, S. Y. — Some calculations to assess the effect of spin on the tractive capacity of rolling contact drives. Proc. Inst. of Mech. Engrs. (1970-71) Vol. 185 76/71.

50. ITAMI, G. S. — The study of friction-creep phenomenon of adhesion between steel wheels and rail. Thesis submitted to General Motors Institute, July 1968.

51. MARTA , H. A.
MELS, K. D.
ITAMI, G. S. — Friction creep phenomenon of adhesion between steel wheels and rails. IEEE/ASME Rail Transportation Conference, April 1971.

52. TOLSTOI, D. M. — Significance of the normal degree of freedom and natural normal vibrations in contact friction. Wear 10, (1967) p.199-213.

53. RABINOWICZ, E. — Friction and wear of materials. John Wiley & Sons, Inc., New York (1965).

54. CABBLE, G. M. — Adhesion between rails and wheels of railway motive power. Doctoral Thesis. University of Illinois (1958).

55. CABBLE, G. M. — Understanding wheel rail adhesion. ASME Publication. No. 60-RR-3. (1960).

56. CRESS, H. A. and
TALBERT, S. G. — Experimental determination of lateral forces developed by a misaligned steel roller on a steel rail. ASME Publication No. 63-WA-298. (1963).

57. KOCI, L. F. and
MARTA, H. A. — Lateral loading between locomotive truck wheels and rail due to curve negotiation. ASME Publication No. 65-WA/RR-4. (1965).

58. COLLINS, A. H. and PRITCHARD, C. — Recent research into wheel/rail adhesion. Paper given to I.Mech.E. Railway Division, Derby. April 1972.

59. BARWELL, F. T. — The contribution of tribology to the development and operation of railways. Proc. Inst. Mech. Engrs. Vol. 187. (1973).

60. MATSUI, N. — On the derailment quotient Q/P J.N.R. (1966).

61. BAGULEY, R. W. — Vehicle testing for higher speeds. REJ, Inst. Mech. Engrs. March 1973.

11. Acknowledgements

My thanks go to Professor F.D.Hales for his help and supervision, and to British Rail who sponsored the work, particularly to Dr. A.O.Gilchrist and Mr. A.E.W.Hobbs for their assistance and encouragement.

I should like to thank also Dr. J.J.Kalker, of Technische Hogeschool Delft, for his advice and for making available to me his latest theories.

I thank Mrs. J.Lynn who typed the thesis, and I express my gratitude to my wife and children for their support and forbearance during the last three years.

12. APPENDICES

APPENDIX 1

Derivation of the Relative Slip Equations for Steady Rolling

Assuming two bodies touch each other along an elliptical contact area which lies in the plane z = 0. The centre of the ellipse is taken as the origin and the axes of the ellipse are the coordinate axes x and y, the positive x axis is assumed to coincide with the rolling direction.

A particle that lies in (x, y, z) in the undeformed state lies in (x + u, y + v, z + w) in the deformed state, where $\underline{u}$ (u, v, w) is the elastic displacement of the particle.

In the undeformed state the velocity is $\underline{V}_r$ where

$$\underline{V}_r = \left(\frac{dx}{dt}, \frac{dy}{dt}, \frac{dz}{dt}\right)$$

In the deformed state the velocity is V where

$$\underline{V} = \underline{V}_r + \frac{\partial u}{\partial t} + \underline{V}_r \cdot \text{grad}\, \underline{u} \qquad (1)$$

The slip is defined as the velocity of the upper body with respect to the lower body in the deformed state (+ refers to lower body; - refers to upper body). Then $(\underline{V}^- - \underline{V}^+) = (\underline{V}_r^- - \underline{V}_r^+) + \frac{\partial(\underline{u}^- - \underline{u}^+)}{\partial t} + \frac{1}{2} \times$

$(\underline{V}_r^- - \underline{V}_r^+) \cdot \text{grad}\, (\underline{u}^+ + \underline{u}^-) + \frac{1}{2} (\underline{V}_r^- + \underline{V}_r^+) \cdot \text{grad}\, (\underline{u}^- - \underline{u}^+)$ (2)

The third term in the above equation may be ignored compared with the first term since the displacement gradients are small compared with unity. The material of the bodies flows through the coordinate system in the direction of the -ve x axis, therefore $\frac{1}{2} (\underline{V}_r^- + \underline{V}_r^+)$ (-V, 0, 0) i.e. the opposite of the rolling velocity.

The last term in equation 2 then becomes $- V \frac{\partial(u^- - u^+)}{\partial x}$

and $(\underline{V}^- - \underline{V}^+) = (\underline{V}_r^- - \underline{V}_r^+) - V \frac{\partial(u^- - u^+)}{\partial x}$ for steady rolling. (3)

Now the velocity of the undeformed bodies can be regarded as a velocity at the origin and a rotation about the z axis i.e.

$$\frac{dx^+}{dt} = \left(\frac{dx^+}{dt}\right)_0 - \Omega_z^+ y, \quad \frac{dy^+}{dt} = \left(\frac{dy^+}{dt}\right)_0 + \Omega_z^+ x \qquad (4)$$

and similarly for the upper body

where $\Omega_z^+ + \Omega_z^-$ are the angular velocities of lower and upper body respectively.

The creeps are then defined as

$$\gamma_x = \frac{1}{V}\left(\frac{dx^-}{dt} - \frac{dx^+}{dt}\right)_0, \quad \gamma_y = \frac{1}{V}\left(\frac{dy^-}{dt} - \frac{dy^+}{dt}\right)_0$$

and the spin as $\omega_z = \frac{1}{V}\left(\Omega_z^- - \Omega_z^+\right)$ (5)

Now $\underline{V}_r^- - \underline{V}_r^+ = \left(\frac{dx^-}{dt} - \frac{dx^+}{dt}, \frac{dy^-}{dt} - \frac{dy^+}{dt}\right)$

where from equations 4 and 5

$$\frac{dx^-}{dt} = -V + \frac{1}{2}V\gamma_x - y\Omega_z^-, \quad \frac{dx^+}{dt} = -V - \frac{1}{2}V\gamma_x - y\left(\Omega_z^- - V\omega_z\right)$$

$$\frac{dy^-}{dt} = \frac{1}{2}V\gamma_y + x\Omega_z^-, \quad \frac{dy^+}{dt} = -\frac{1}{2}V\gamma_y + x\left(\Omega_z^- - V\omega_z\right) \qquad (6)$$

$$\therefore \quad \underline{V}_r^- - \underline{V}_r^+ = \left(V\gamma_x - V_y\omega_z, V\gamma_y + Vx\omega_z\right)$$

The relative slip $\underline{s}\ (s_x, s_y)$ is defined as

$$\underline{s}\ (s_x, s_y) = \frac{1}{V}\left(\underline{V}^- - \underline{V}^+\right)$$

$$= \left(\gamma_x - y\omega_z + \frac{\partial(u^+ - u^-)}{\partial x}, \gamma_y + x\omega_z + \frac{\partial(V^+ - V^-)}{\partial x}\right)$$

if the elastic displacement differences are written as $u = u^+ - u^-$, $v = v^+ - v^-$

Then

$$\left.\begin{aligned} s_x &= \gamma_x - \omega_z y + \frac{\partial u}{\partial x} \\ s_y &= \gamma_y + \omega_z x + \frac{\partial v}{\partial x} \end{aligned}\right\} \quad \text{for steady rolling} \qquad (7)$$

APPENDIX 2

Simplified Theory (Kalker, Ref. 36)

(Values such as $\bar{a}$, $\bar{b}$, $\bar{Z}$ refer to simplified theory values)

The relative slip is given by: (Appendix 1)

$$s_x = \gamma_x - \omega_z y + \frac{\partial u}{\partial x} \tag{1}$$

$$s_y = \gamma_y + \omega_z x + \frac{\partial v}{\partial x} \tag{2}$$

The basic approximation of the method assumes the displacement differences (u, v) and the tractions (X, Y) are connected by

$$u = S_x X \tag{3}$$

$$v = S_y Y \tag{4}$$

where S_x, S_y are called the inverse stiffnesses

Then

$$\frac{\partial u}{\partial x} = S_x X' \tag{5}$$

$$\frac{\partial v}{\partial x} = S_y Y' \tag{6}$$

If N is the normal force then call parameter $foo = \frac{3N}{2\pi ab}$

In the half space theory of Ref. 23, the normal pressure Z was of the form

$$Z = foo\sqrt{1-\left(\frac{x}{a}\right)^2-\left(\frac{y}{b}\right)^2} \tag{7}$$

This pressure has a vertical tangent at the edge of the contact area which means that the tractions X and Y will have also. In the simplified theory these would give rise to infinite relative slips. Because of this, a different pressure distribution is used here which is closely akin to that given by equation 7.

$$\bar{Z} = \overline{foo}\left(1-\left(\frac{x}{a}\right)^2-\left(\frac{y}{b}\right)^2\right) \tag{8}$$

Assuming Z and $\bar{Z}$ are equal over the contact area then

$$N = \int Z\,dx\,dy = \int \bar{Z}\,dx\,dy = \frac{2}{3}\pi a b f_{oo} = \frac{\pi \bar{a}\bar{b} f_{\bar{o}\bar{o}}}{2} \tag{9}$$

$$\therefore \quad f_{\bar{o}\bar{o}} = \frac{4}{3}\cdot\frac{ab}{\bar{a}\bar{b}}\cdot f_{oo}$$

Comparison of linearised theory creepage and spin coefficients

This theory assumes that the contact area is all adhesion and the relative slip is zero. i.e. equations 1 and 2 become

$$\left.\begin{aligned} \gamma_x - \omega_z y + S_x X' &= 0 \quad (10) \\ \text{and} \qquad \gamma_y + \omega_z x + S_y Y' &= 0 \quad (11) \end{aligned}\right\}$$

If the leading edge is given by

$$x = L(y) = a\sqrt{1 - \left(\frac{y}{b}\right)^2} \tag{12}$$

then equations 10 and 11 have the solution

$$X(x, y) = \frac{(\gamma_x - \omega_z y)(L(y) - x)}{S_x} \tag{13}$$

$$\text{and } Y(x, y) = \frac{\gamma_y (L(y) - x) + \frac{1}{2}\omega_z (L^2(y) - x^2)}{S_y} \tag{14}$$

since the traction force is zero on the leading edge.

The total forces and moment are then given by:

$$F_x = \iint_E X(x,y)\,dx\,dy = \frac{8\bar{a}^2\bar{b}}{3 S_x}\gamma_x \tag{15}$$

$$F_y = \iint_E Y(x,y)\,dx\,dy = \frac{8\bar{a}^2\bar{b}}{3 S_y}\gamma_y + \frac{\pi \bar{a}^3 \bar{b}}{4 S_y}\omega_z \tag{16}$$

$$M_z = \iint_E (Y_x - X_y)\,dx\,dy = \frac{8\bar{a}^2\bar{b}^3}{15 S_x}\omega_z - \frac{\pi \bar{a}^3 \bar{b}}{4 S_y}\gamma_y \tag{17}$$

The equivalent forces given by the linearised theory are

$$F_x = G a b C_{11} \gamma_x \tag{18}$$

$$F_y = G a b C_{22} \gamma_y + G(ab)^{\frac{3}{2}} C_{23} \omega_z \tag{19}$$

$$M_z = -G(ab)^{\frac{3}{2}} C_{23} \gamma_y + G(ab)^2 C_{33} \omega_z \tag{20}$$

Hence the equivalent simplified theory coefficients are

$$\overline{C_{11}} = \frac{8a}{3G S_x} \quad ; \quad \overline{C_{22}} = \frac{8a}{3G S_y} \quad ; \quad \overline{C_{23}} = \frac{\pi a}{4G S_y \sqrt{\frac{a}{b}}} \quad ;$$

$$\overline{C_{33}} = \frac{8b}{15 G S_x} \tag{21}$$

Arbitrary Creepage and Spin

(a) Area of Adhesion

In the area of adhesion, the relative slip is zero, therefore equations 1 and 2 become

$$\delta_x = 0 = \gamma_x - \omega_z y + S_x X' \tag{22}$$

$$\delta_y = 0 = \gamma_y + \omega_z x + S_y Y' \tag{23}$$

If the value of x where the particle enters this area of adhesion is x_a and the traction forces at this point X_a, Y_a then solving equations 22 and 23 for X and Y they become

$$X = -\frac{(\gamma_x - \omega_z y)(x - x_a)}{S_x} + X_a \tag{24}$$

$$Y = -\frac{\gamma_y (x - x_a) + \frac{1}{2}\omega_z (x^2 - x_a^2)}{S_y} + Y_a \tag{25}$$

This area of adhesion extends from x_a until $X^2 + Y^2 > \mu^2 Z^2$

(b) Area of Slip

In the area of slip

$$X = \mu Z \cos\theta \tag{26}$$

$$Y = \mu Z \sin\theta \tag{27}$$

$$\left.\begin{aligned} s_x &= \gamma_x - \omega_z y + S_x X' = \lambda X \quad (28)\\ s_y &= \gamma_y + \omega_z x + S_y Y' = \lambda Y \quad (29) \end{aligned}\right\} \lambda > 0$$

Differentiating equations 26 and 27

$$X' = \mu Z' \cos\theta - \mu Z \theta' \sin\theta \tag{30}$$

$$Y' = \mu Z' \sin\theta + \mu Z \theta' \cos\theta \tag{31}$$

Substituting in equations 28 and 29

$$\gamma_x - \omega_z y + S_x(\mu Z' \cos\theta - \mu Z \theta' \sin\theta) = \lambda \mu Z \cos\theta \tag{32}$$

$$\gamma_y + \omega_z x + S_y(\mu Z' \sin\theta + \mu Z \theta' \cos\theta) = \lambda \mu Z \sin\theta \tag{33}$$

Eliminating λ from equations 32 and 33 gives

$$\begin{aligned} \mu Z \theta'(S_x \sin^2\theta + S_y \cos^2\theta) &= (\gamma_x - \omega_z y)\sin\theta \\ &\quad - (\gamma_y + \omega_z x)\cos\theta + \mu Z'(S_x - S_y)\cos\theta \sin\theta \end{aligned} \tag{34}$$

This equation can be solved numerically for θ, except at the edges of the contact area where the pressure Z is zero and the equation singular. X and Y then follow from equations 26 and 27.

When λ becomes -ve adhesion sets in. This may be formulated by multiplying equation 28 by $S_y X$ and equation 29 by $S_x Y$ and adding

$$\begin{aligned} \lambda(S_y X^2 + S_x Y^2) &= S_y X(\gamma_x - \omega_z y + S_x X') \\ &\quad + S_x Y(\gamma_y + \omega_z x + S_y Y') \end{aligned}$$

Substituting for X and Y from equations 26 and 27, X' and Y' from equations 30 and 31

$$\lambda = \frac{S_y \mu Z \cos\theta (\gamma_x - \omega_z y + S_x \mu Z' \cos\theta - \mu Z \theta' \sin\theta S_x)}{S_y \mu^2 Z^2 \cos^2\theta + S_x \mu^2 Z^2 \sin^2\theta}$$

$$+ \frac{S_x \mu Z \sin\theta (\gamma_y + \omega_z x + S_y \mu Z' \sin\theta + S_y \mu Z \theta' \cos\theta)}{S_y \mu^2 Z^2 \cos^2\theta + S_x \mu^2 Z^2 \sin^2\theta}$$

$$= \frac{S_y \cos\theta (\gamma_x - \omega_z y) + S_x \sin\theta (\gamma_y + \omega_z x) + S_x S_y \mu Z'}{\mu Z (S_x \sin^2\theta + S_y \cos^2\theta)}$$

the condition for slip is when

$$S_y \cos\theta (\gamma_x - \omega_z y) + S_x \sin\theta (\gamma_y + \omega_z x) + S_x S_y \mu Z' > 0 \qquad (35)$$

Adhesion to slip transition : $X^2 + Y^2 - \mu^2 Z^2$ becomes +ve

Slip to adhesion transition : $S_y \cos\theta (\gamma_x - \omega_z y) + S_x \sin\theta (\gamma_y + \omega_z x) + S_x S_y \mu Z'$ becomes -ve.

As this is a step by step solution, the leading edge conditions have first to be established. As Z = 0 on the leading edge, the condition for adhesion is

$$(X')^2 + (Y')^2 \leqslant \mu^2 (Z')^2 \qquad (36)$$

substituting for X' and Y' from equations 22 and 23

if $$\left\{ -\frac{(\gamma_x - \omega_z y)}{S_x} \right\}^2 + \left\{ -\frac{(\gamma_y + \omega_z x)}{S_y} \right\}^2 \leqslant \mu^2 (Z')^2$$

there is adhesion.

If there is not adhesion at the leading edge then equation 34 is singular and it becomes

$$(\gamma_x - \omega_z y) \sin\theta_o - (\gamma_y + \omega_z x) \cos\theta_o + \mu Z' (S_x - S_y) \sin\theta_o \cos\theta_o = 0 \qquad (37)$$

θ_o can be found numerically using Newton's method.

To be able to move away from the leading edge, the starting value θ_o' must also be found by differentiating equation 37.

Having solved the leading edge condition move along the y ordinate in small steps and test at each point if there is slip or adhesion. Use the appropriate equations to find the tractions.

APPENDIX 3

Adaption of governing parameters for use in simplified theory

(a, b refer to the semi-axes of the contact ellipse and ξ, η, χ are the longitudinal, lateral and spin parameters. $c = \sqrt{a\,b}$

Barred terms, such as $\bar{a}$, refer to the adapted parameters).

The first requirement is that the maximum possible total force will be the same in the simplified theory as in the exact theory.

Thus $\bar{F}_{max.} = \int_E \mu \bar{z}\, dx\, dy = \frac{\pi}{2} \bar{a}\bar{b}\, f_{\bar{o}\bar{o}}\, \mu$

and $F_{max.} = \int_E \mu z\, dx\, dy = \frac{2}{3} \pi a b\, f_{oo}\, \mu$

} from equation 9 in Appendix 2

and since $\bar{F}_{max.} = F_{max.}$

$$f_{\bar{o}\bar{o}} = \frac{4}{3} \cdot \frac{ab}{\bar{a}\bar{b}} \cdot f_{oo} \qquad (1)$$

Also the maximum possible moments should be equal in the two theories.

Thus $\bar{M}_{max.} = \frac{8}{15} s \bar{l}^2 \mu f_{\bar{o}\bar{o}} \underline{\bar{E}} = \frac{\pi}{4} s l^2 \mu f_{oo} \underline{E} = M_{max}$

where l, s are the major and minor semi-axes of the contact ellipse respectively, and $\underline{E}$ is a complete elliptic integral of the 2nd kind.

For reasons which become apparent later, all moments calculated by the simplified theory are multiplied by a factor γ

Thus $\bar{\bar{M}}_Z = \gamma \bar{M}_Z$

i.e. $\gamma \cdot \frac{8}{15} \cdot s \bar{l}^2 \mu f_{\bar{o}\bar{o}} \underline{\bar{E}} = \frac{\pi}{4} \cdot s l^2 \cdot \mu f_{oo} \underline{E}$

On substituting for $\left(\frac{f_{oo}}{f_{\bar{o}\bar{o}}}\right)$ from equation 1

$$\gamma = \frac{45\pi}{128} \cdot \frac{l \underline{E}}{\bar{l} \underline{\bar{E}}} \qquad (2)$$

Another requirement is that the initial slopes of the force and moment must be equal in the simplified and linearised theories. Thus from equations 15 and 18

$$\frac{8\bar{a}^2\bar{b}}{3S_x} = G\,ab\,C_{11}$$

Therefore $$GS_x = \frac{8\bar{a}^2\bar{b}}{3ab\,C_{11}} \qquad (3)$$

From equations 16 and 19 in Appendix 2

$$\bar{F}_{y_{\omega_z=0}} = \frac{8\bar{a}^2\bar{b}\,\gamma_y}{3S_y} = Gab\,C_{22}\gamma_y = F_{y_{\omega_z=0}}$$

Therefore $$GS_y = \frac{8\bar{a}^2\bar{b}}{3ab\,C_{22}} \qquad (4)$$

Also from the same equations

$$\bar{F}_{y_{\gamma_y=0}} = \frac{\pi\bar{a}^3\bar{b}\,\omega_z}{4S_y} = G(ab)^{\frac{3}{2}}C_{23}\,\omega_z = F_{y_{\gamma_y=0}}$$

Therefore $$GS_y = \frac{\pi\bar{a}^3\bar{b}}{4(ab)^{\frac{3}{2}}C_{23}} \qquad (5)$$

From equations 17 and 20 in Appendix 2

$$\bar{\bar{M}}_{z_{\omega_z=0}} = \frac{-\gamma\pi\bar{a}^3\bar{b}\,\gamma_y}{4S_y} = -G(ab)^{\frac{3}{2}}C_{23} = M_{z_{\omega_z=0}}$$

Thus $$GS_y = \frac{\gamma\pi\bar{a}^3\bar{b}}{4(ab)^{\frac{3}{2}}C_{23}} \qquad (6)$$

Also from the same equations

$$\bar{\bar{M}}_{z_{\gamma_y=0}} = \frac{\gamma 8\bar{a}^2\bar{b}^3\omega_z}{15S_x} = G(ab)^2C_{33}$$

Thus $$GS_x = \frac{\gamma 8\bar{a}^2\bar{b}^3}{15(ab)^2C_{33}} \qquad (7)$$

It can be seen that equations 1 to 7 constitute seven equations to find 6 unknowns, namely $\bar{a}$, $\bar{b}$, S_x, S_y, $f_{\bar{o}\bar{o}}$ and γ . Because of this one equation has to be dropped and this is a matter of choice. Obviously equations 3, 4 and 5 should be retained since they ensure the correct slope of the forces results. Kalker has suggested that equation 6 be dropped since there is not much significance to this equation and there is some evidence to show that C_{23} changes as the spin increases. Anyway, if $\gamma \triangleq 1$ equation 5 guarantees the dependence of M_z on γ_y.

Thus the equations that are retained are 1, 2, 3, 4, 5 and 7, and the parameters calculated in the following way:

1) Find C_{11}, C_{22}, C_{23} and C_{33} either from Ref. 23 or the asymptotic formulae given in Section 3.1 (or from C_{11} etc. given in Table 3.1)

2) Assume $c = 1$ and $N = 1$

Then
$$f_{oo} = \frac{3N}{2\pi ab} = \frac{3}{2\pi} = 0.4775$$

3) Equating equations 4 and 5 gives
$$\bar{a} = \frac{32}{3\pi} \cdot \frac{C_{23}}{C_{22}} \cdot c \qquad (8)$$

Thus $\bar{a}$ can be calculated.

4) Equating equations 3 and 7 gives
$$\gamma b^2 = \frac{5ab\,C_{33}}{C_{11}}$$

Thus from equation 2, substituting for γ gives
$$b^2 = \frac{128}{9\pi} \cdot \frac{C_{33}}{C_{11}} \cdot \frac{\bar{E}}{E} \cdot \bar{\ell}\bar{s} \qquad (9)$$

By considering equations 8 and 9 expressions can be obtained for

$$\bar{g} = \min.(\bar{a}/\bar{b},\ \bar{b}/\bar{a})$$

If $\bar{s} = \bar{b} \leqslant \bar{a} = \bar{l}$

Then $$\bar{g}^2 = \left(\frac{\bar{b}}{\bar{a}}\right)^2 = \frac{4}{3} \cdot \frac{\bar{E}}{\underline{E}} \cdot \frac{C_{33} C_{22} \sqrt{\gamma}}{C_{23} C_{11}} \qquad (10)$$

If $\bar{l} = \bar{b} \geqslant \bar{a} = \bar{s}$

Then $$\bar{g} = \frac{\bar{a}}{\bar{b}} = \frac{3 \underline{E} C_{23} C_{11}}{4 \bar{E} C_{22} C_{33} \sqrt{\gamma}} \qquad (11)$$

Thus $\bar{g}$ can be calculated from either equation 10 or equation 11. Note, however, that $\bar{\underline{E}}$ depends on $\bar{g}$ and thus an iteration is necessary to find the value of $\bar{g}$. Since $\bar{\underline{E}}$ only varies between 1 and $\pi/2$ this is not very difficult.

5) $\bar{b}$ follows from $\bar{a}$ and $\bar{g}$.

6) $G = \dfrac{3(1-\sigma)\underline{E}}{4\pi\sqrt{\gamma}}$ where $\underline{E}$ depends on g.

7) S_x can be calculated from equation 3 where

$$S_x = \frac{8\bar{a}^2 \bar{b}}{3ab\, C_{11} G}$$

and S_y can be calculated from equation 4 where

$$S_y = \frac{8\bar{a}^2 \bar{b}}{3ab\, C_{22} G}$$

The traction bound used in the simplified theory described in Appendix 2 is of the form

$$\mu \bar{t} = \mu f_{\infty} \left[1 - \left(\frac{x}{a}\right)^2 - \left(\frac{y}{b}\right)^2\right] \qquad (12)$$

This differed from the exact theory where the traction bound was

$$\mu \bar{t} = \mu f_{\infty} \sqrt{1 - \left(\frac{x}{a}\right)^2 - \left(\frac{y}{b}\right)^2} \qquad (13)$$

The reason this was not used in the simplified theory was because it would give rise to infinite slips.

Using the traction bound of equation 12 leads to

$$f_{\bar{o}\bar{o}} = \frac{4ab}{3\bar{a}\bar{b}} f_{oo}$$

However Kalker has recently modified the implementation of the simplified theory and has tried the traction bound of equation 13. This met with little success and consequently the latest form of the simplified theory uses a combination of both. $\mu \bar{Z}$ being of the form given by equation 12 near the edge of the contact area and given by equation 13 inside the contact area.

Using the traction bound of equation 13 gives

$$f_{\bar{o}\bar{o}} = \frac{ab}{\bar{a}\bar{b}} . f_{oo} \qquad (14)$$

This is the value for $f_{\bar{o}\bar{o}}$ used in the latest form of the simplified theory while all the other parameters stay the same.

APPENDIX 4

Comparison of results obtained using subroutine RØL with Kalker's simplified theory program

The following cases were compared:

Case	σ	a/b	ξ	η	χ
1	.3	10.	0	- .355	.181
2	.3	10.	0	0	.181
3	.3	1.04	0	- 1.288	3.174
4	.3	6.54	0	- .219	.355
5	.3	2.695	0	- .565	1.221
6	.3	2.38	.686	0	.031

Results:

	Case	1	2	3	4	5	6
KALKER	Grid Size	(13,13)	(13, 13)	(13, 13)	(13, 13)	(13, 13)	(13,13)
	Step	.03	.03	.02	.03	.02	.02
	f_x	0	0	0	0	0	.7800
	f_y	-.3027	.8258	.1683	.5116	.4428	.0244
	m_z	.748	.345	.511	.610	.484	.007
RØL	Grid Size	(13,13)	(13,13)	(13, 13)	(13, 13)	(13, 13)	(13, 13)
	Step	.02	.02	.02	.02	.02	.02
	f_x	0	0	0	0	0	0
	f_y	-.3158	.8282	.1719	.5136	.4420	.0244
	m_z	.725	.331	.515	.605	.486	.007
RØL	Grid Size	(13, 13)	(13,13)	(13, 13)	(13, 13)	(13, 13)	(13, 13)
	Step	.01	.01	.01	.01	.01	.01
	f_x	0	0	0	0	0	0
	f_y	-.3158	.8282	.1719	.5136	.4420	.0244
	m_z	.725	.331	.515	.605	.486	.007

APPENDIX 5

Program Descriptions

The following programs and subroutines were developed and used in the present investigation. A brief description of each is given in Section A followed by a complete listing in Section B.

Program Number	Name	Reference Section	Description Page Number	Listing Page Number
1	SMALL	3.1	270	296
2	COEFF	3.1	271	296
3	ELLIP	3.1	271	301
4	MAXFY	3.1	272	301
5	LARGE	3.2	272	302
6	SIMPSN	3.2	274	303
7	NUMERIC	3.3.1	274	303
8	TAPE	3.3.1	275	305
9	SIMP	3.3.2	277	308
10	ROL	3.3.2	278	311
11	RAILAT	4.2	279	315
12	FR1	4.2	280	317
13	WHEEL	4.3	281	318
14	FINDH	4.4.1	282	319
15	LATERAL WHEELSET	4.4.2	283	321
16	STRWH	4.4.2	284	324
17	CIRWH	4.4.2	285	324
18	YAWING WHEELSET	4.4.3	286	326
19	CIRCLE2	4.4.3	286	326
20	STRGHT2	4.4.3	287	330
21	Z200B	4.4.3	288	332
22	JOHANSEN	4.4.4	289	334
23	CIRY	4.4.4	290	337
24	LINY	4.4.4	291	338
25	ACCURATE	4.4.4	291	338
26	CONTACT	4.5	292	348
27	FORCES	4.7	293	354
28	LAB	8.6.2	294	359

Section A

1. SUBROUTINE SMALL (G, K, T, U, E, FX, FY, ZM)

PURPOSE

To calculate the non-dimensional force parameters f_1, f_2, m_3 from the creepage and spin parameters ξ, η, χ and the ratio (a/b), using the small creep theory of Section 3.1.

DESCRIPTION OF PARAMETERS

G	Minimum (a/b, b/a) = g	Input
K	= 1 if g = (a/b); = 2 if g = (b/a)	
T	Spin parameter, χ	
U	Lateral creep parameter, η	
E	Longitudinal creep parameter, ξ	
FX	Longitudinal force parameter, f_1	Output
FY	Lateral force parameter, f_2	
ZM	Moment parameter, m_3	

SUBROUTINES USED

COEFF, ELLIP, MAXFY

METHOD

The creep and spin coefficients C_{ij} are calculated in COEFF for a Poissons ratio of 0.3 and required (a/b) ratio.

The value of E is found in ELLIP for the required (a/b) ratio.

The values of f_1, f_2, m_3 are found from equations 12, 13 and 14 of Section 3.1. The remainder of the program checks that the values obtained are within the bounds mentioned in Section 3.1, using MAXFY to give the value of $f_{2(\xi=\eta=0)}$

2. SUBROUTINE COEFF (G, K, C11, C22, C23, C33)

PURPOSE

To calculate the creepage and spin coefficients, C_{ij}, for any (a/b) ratio.

DESCRIPTION OF PARAMETERS

G	Minimum (a/b, b/a) = g	Input
K	= 1 if g = (a/b); = 2 if g = (b/a)	Input
C11	C_{11}	Output
C22	C_{22}	Output
C23	C_{23}	Output
C33	C_{33}	Output

SUBROUTINES USED

None

METHOD

The coefficients are linearly interpolated from the values given in Table 3.1 for Poissons ratio of 0.3. For values of a/b $>$ 10 the asymptotic formulae given in Section 3.1 are used. Before using this subroutine the values given in Table 3.1 must be read into the array COF(19, 4).

3. SUBROUTINE ELLIP (G, E)

PURPOSE

To calculate E, the complete elliptic integral of the 2nd kind for the required value of g.

DESCRIPTION OF PARAMETERS

G	Minimum (a/b, b/a) = g	Input
E	E, complete elliptic integral of 2nd kind	Output

SUBROUTINES USED

None

METHOD

The value of $\underline{E}$ is linearly interpolated from values of $\underline{E}$ given on page 58 of Ref.23.

4. SUBROUTINE MAXFY (BA, S, FYM)

PURPOSE

To give an estimated value of f_2 due to spin when the longitudinal and lateral creeps are zero.

DESCRIPTION OF PARAMETERS

BA	ratio (b/a) of contact ellipse semi axes	Input
S	spin parameter, χ	Input
FYM	estimated value of f_2	Output

SUBROUTINES USED

None

METHOD

For a given (b/a) ratio, the value of (χ /f_2) is linearly interpolated from Fig. 3.2. Knowing the spin, f_2 is calculated. Should only be applied for small spins.

5. SUBROUTINE LARGE (G, K, T, EW, ET, FX, FY, ZM)

PURPOSE

To calculate the non-dimensional force parameters f_1, f_2, and m_3 from the creepage and spin parameters ξ, η, χ and the ratio (a/b), using the large creep theory of Section 3.2.

DESCRIPTION OF PARAMETERS

G	Minimum (a/b, b/a) = g	Input
K	= 1 if g = (a/b), = 2 if g = (b/a)	
T	spin parameter, χ	
EW	lateral creep parameter, η	
ET	longitudinal creep parameter, ξ	
FX	longitudinal force parameter, f_1	Output
FY	lateral force parameter, f_2	
ZM	moment parameter, m_3	

SUBROUTINES USED

SIMPSN, FUNC1, FUNC2, FUNC3, FUNC4, FUNC5

METHOD

Since the integrals given in Section 3.2 only apply for $\chi \neq 0$, $a < b$, $\frac{c\eta}{\chi} \geqslant 0$, $\frac{c\xi}{\chi} \geqslant 0$ this is checked at the beginning of the subroutine. If any of the parameters are outside this range, the symmetry relations given in 3.2 are applied.

The double integration, using the formulae given in 3.2, is carried out using the Simpsons rule subroutine, SIMPSN, to calculate f_1, f_2 and m_3.

The actual terms to be integrated are calculated in the following function sub programs:

FUNC1 $= \sqrt{\left(\sqrt{g}\sin\theta\cos\psi + \frac{\eta}{\chi}\right)^2 + \left(\frac{\sin\theta\sin\psi}{\sqrt{g}} - \frac{\xi}{\chi}\right)^2}\,\sin\psi$

FUNC2 $= \sqrt{\left(\sqrt{g}\sin\theta\cos\psi + \frac{\eta}{\chi}\right)^2 + \left(\frac{\sin\theta\sin\psi}{\sqrt{g}} - \frac{\xi}{\chi}\right)^2}\,\cos\psi$

FUNC3 $= \sqrt{\left(\sqrt{g}\sin\theta\cos\psi + \frac{\eta}{\chi}\right)^2 + \left(\frac{\sin\theta\sin\psi}{\sqrt{g}} - \frac{\xi}{\chi}\right)^2}$

FUNC4 $= K\sin^2\theta$

FUNC5 $= K\cos^2\theta\sin\theta$

6. SUBROUTINE SIMPSN (X, Y, N, R)

PURPOSE

To give $y = \int f(x)$ using Simpsons rule for numerical integration.

DESCRIPTION OF PARAMETERS

X	array X(N), value of x_i	Input
Y	array Y(N), value of $y_i = f(x_i)$	Input
N	number of points, must be an odd number	Input
R	value of integral	Output

SUBROUTINES USED

None

METHOD

Numerical integration using standard Simpsons rule formula.

7. SUBROUTINE NUMERIC (G, K, T, U, E, FA, FB, CM, IF, IT)

PURPOSE

To calculate the non-dimensional force parameters, f_1, f_2, m_3 from the creepage and spin parameters ξ, η, χ and the ratio (a/b), using the numerical theory of Section 3.3.1.

DESCRIPTION OF PARAMETERS

G	Minimum (a/b, b/a) = g	Input
K	= 1 if g = a/b, = 2 if g = b/a	Input
T	spin parameter, χ	Input
U	lateral creep parameter, η	Input
E	Longitudinal creep parameter, ξ	Input
FA	longitudinal force parameter, f_1	Output
FB	lateral force parameter, f_2	Output
CM	moment parameter, m_3	Output

IF this counter is normally set at 1 but if the value of (a/b) is outside the range (.2 - 3.) then the method cannot be applied and this counter is set to 2.

IT if this subroutine is used several times in a program there is only need to read the tabulated results off magnetic tape once.

To ensure this is done, this counter is initially set to 1 and after the results have been read it is automatically set to 2 so they will not be read again.

SUBROUTINES USED

TAPE

METHOD

The input values of ξ, η and χ are checked to ensure they lie within the tabulated results of Ref. 35. If not the symmetry relations given in Section 3.3.1 are applied. ξ, η are changed to polar coordinates. The values of f_1, f_2, m_3, given in Ref. 35, are stored on magnetic tape for various creeps and spins and for (a/b) ratios of 0.2, 0.5, 1. and 2. . This subroutine calls on TAPE which interpolates these values to give f_1, f_2 and m_3 for the input values of ξ, η and χ for the four (a/b) ratios. These results are then interpolated again in this subroutine for the required (a/b) ratio. For $2 < (a/b) < 3$ the results are extrapolated. The subroutine sets IF = 2 if $3 < a/b < .2$ and no results are given.

8. SUBROUTINE TAPE (SPP, ALP, VP, IT)

PURPOSE

To interpolate the tabulated results of Ref. 35 to find the non-dimensional force parameters f_1, f_2 and m_3 from the creepage and spin parameters in polar coordinates χ, ν and λ for (a/b) ratios of 0.2,

0.5, 1.0, 2.0 .

DESCRIPTION OF PARAMETERS (Input)

SPP	spin parameter, χ
ALP, VP	polar coordinates for the longitudinal and lateral creep parameters where ξ = VP cos (ALP) and η = VP sin (ALP)
IT	= 1 if tabulated results have to be read off magnetic tape = 2 if tabulated results have been read off magnetic tape. (This is explained more fully in the write up on subroutine NUMERIC)

SUBROUTINES USED

None

METHOD

The complete set of results given in Ref. 35 are read off magnetic tape into the subroutine. The results are firstly interpolated for the required value of ν giving 156 values of f_1, f_2 and m_3 . These are then interpolated for the required value of α giving 24 values of f_1, f_2, m_3 . Finally these are again interpolated for the required value of χ giving 4 values of f_1, f_2 and m_3 corresponding to (a/b) ratios of 0.2, 0.5, 1.0 and 2.0 . These values are held in arrays T1/F1(4), F2(4), F3(4).

9. SUBROUTINE SIMP (AAAAA, BBBBB, CCCCC, F, K, NA, NB, FXM, FYM, AMZM, JIF)

PURPOSE

To calculate the non-dimensional force parameters, f_1, f_2, m_3 from the creepage and spin parameters ξ, η, χ and the ratio (a/b) using the simplified theory of Section 3.3.2.

DESCRIPTION OF PARAMETERS

AAAAA	longitudinal creep parameter, ξ	Input
BBBBB	lateral creep parameter, η	
CCCCC	spin parameter, χ	
F	minimum (a/b, b/a) = g	
K	= 1 if g = (a/b), = 2 if g = (b/a)	
NA	number of +ve x ordinates not including x = 0	
NB	number of +ve y ordinates not including y = 0	
FXM	longitudinal force parameter, f_1	Output
FYM	lateral force parameter, f_2	
AMZM	moment parameter, m_3	
JIF	if this counter set to 3 on entry to the subroutine some intermediate steps in the subroutine are printed out. For normal use JIF $\neq$ 3.	

SUBROUTINE USED

COEFF, ELLIP, ROL, SIMPSN

METHOD

The governing parameters are adapted for use in the simplified theory in the manner outlined in Appendix 3. The values of C_{11}, C_{22} and C_{33} are found in subroutine COEFF while E is found in subroutine ELLIP. The stiffnesses are calculated as per Section 3.3.2. These parameters are then put into arrays which are carried into subroutine ROL in the COMMON/GRP. These arrays are described in the write up on ROL. The

actual simplified theory outlined in Appendix 2 is the basis of subroutine ROL. On return from ROL the values of f_1 and f_2 calculated are modified by a factor found by comparing the normal force on the contact area with the pressure integrated over the area. This numerical integration is carried out over the grid of points using Simpsons rule in the form of subroutine SIMPSN.

The traction forces and the relative slips calculated at each of the grid points are found in ROL and carried into this subroutine. The condition of the leading edge at each y ordinate is also given together with the values of x along each y ordinate where a slip/stick boundary occurs.

In the present work the simplified theory was used mainly to calculate the total forces in the contact area and a counter JIF was put in the subroutine to suppress this latter information if not required as a print out.

10. SUBROUTINE ROL

PURPOSE

To calculate the force parameters f_1, f_2, m_3 using the simplified theory of Section 3.3.2 from the governing parameters calculated in subroutine SIMP.

DESCRIPTION OF PARAMETERS

The following parameters are transferred between this subroutine and subroutine SIMP in the COMMON/GRP.

CS(1) longitudinal creep parameter, ξ

CS(2) lateral creep parameter, η

CS(3) adapted spin parameter, $\bar{\chi}$

GEL(1) S_x, longitudinal inverse stiffness

GEL(2) S_y, lateral inverse stiffness

GEL(3)	$\bar{a}$, semi-axis of adapted contact ellipse
GEL(4)	$\bar{b}$, semi-axes of adapted contact ellipse
GEL(5)	step length
X, Y	traction arrays
VX, VY	slip arrays
G	array of slip/stick boundaries
AMUZ	$f_{\bar{o}\bar{o}}$

SUBROUTINES USED

None

METHOD

This method is based on the theory given in Appendix 2.

Having divided the contact area into a grid of points the program starts at the leading edge of each y ordinate and tests if there is adhesion or slip. If there is adhesion there is no problem, but if there is slip the equations are singular and special precautions have to be taken to calculate the starting value of θ, where in the slip area, $X = \mu Z \cos\theta$ and $Y = \mu Z \sin\theta$.

Having solved the leading edge condition, the program is stepped along the y ordinate and tested to find whether there is adhesion or slip in the new point and corresponding to which it is, the respective equations used to give the traction forces. The traction forces are then integrated to give the total force.

11. SUBROUTINE RAILAT

PURPOSE

To calculate rail profile coordinates and centres of rail profile radii in track axes.

DESCRIPTION OF PARAMETERS

R1	Crown radius (12")	Input
R2	Radius either side of crown (3.125")	
RCI	Inside corner radius of right-hand rail (nominally 0.5")	
RCØ	Outside corner radius of right-hand rail (nominally 0.5")	
YDR	Width of profile with radius R1 (0.75")	
W	Width of railhead (2.75")	
YT(I)	y coordinate of point i in track axes	Output
ZT(I)	z coordinate of point i in track axes	
AL(I)	y coordinate of centre of radius i in track axes	
BL(I)	z coordinate of centre of radius i in track axes	
RL(I)	radius i	

SUBROUTINES USED

None

METHOD

The coordinates of the points are firstly calculated in Railhead axes and then transformed to Track axes using the method described in Section 4.2.

The values R1 to W listed above have to be read into the subroutine. The values of these variables for a BS110A rail are given in brackets.

The arrays YT, ZT, AL, BL, RL are filled and can be transferred to any other subroutine using COMMON/RAIL

12. SUBROUTINE FR1 (Y, Z, K)

PURPOSE

To calculate z_t coordinate of rail if y_t is known or to calculate y_t if z_t is known.

DESCRIPTION OF PARAMETERS

Y — y_t coordinate of rail

Z — z_t coordinate of ril

K — = 1 if z_t is known and y_t to be calculated

= 2 if y_t is known and z_t to be calculated

SUBROUTINES USED

RAILAT

METHOD

The profile radius in which the desired point lies is first located and the (y/z) coordinate found using the corresponding equation, (already calculated in RAILAT).

If $y_t(1) > y > y_t(6)$ — $z_t = 10.0$

If $z_t < -0.75''$ — $y_t = 100.0$

If $z_t > z_t(1)$ — $y_t = y_t(1)$

} limits

13. SUBROUTINE WHEEL

PURPOSE

To calculate wheel profile coordinates and centres of wheel profile radii in Wheelset axes.

DESCRIPTION OF PARAMETERS

R — wheel radius at point A (29.6")

YW(1) — y_w of point 1 (30.7125")

YW(2) — y_w of point 2 (30.3125")

YW(7) — y_w of point 7 (27.2375")

YA — y_w of point A (29.5625")

Z7 — vertical distance between A and 7 (1.18")

AN(1) — y_w of centre of radius RD(1) (30.3125")

AN(2)	y_w of centre of radius RD(2)	(29.3125")
AN(3)	y_w of centre of radius RD(3)	(28.4375")
RD(1)	radius between 2 and 3	(13.")
RD(2)	radius between 3 and 4	(4.")
RD(3)	radius between 4 and 5	(0.5")
RD(4)	radius between 6 and 7	(0.7")

SUBROUTINES USED

None

METHOD

The tyre profile is based on a British Rail RD4 'worn' profile and the coordinates of the points are calculated in Wheelset axes. (The actual values of the inputs are in brackets).

The points referred to above are shown in Table 4.2.

The arrays QM, C, BN, AN, YW, ZW, RD are calculated in the subroutine and stored in COMMON/WHEEL/.

(QM, C are the slope and intercept of the straight line portions of profile).

14. SUBROUTINE FINDH (H, Y)

PURPOSE

To calculate the vertical distance between Track axes origin and Wheelset axes origin with wheelset in central position, also, to give coordinates (in Track axes) of contact point on right-hand wheel with wheelset in central position.

DESCRIPTION OF PARAMETERS

H	vertical distance between wheelset axes origin and track axes origin.	Output
Y	y_t, y coordinate (Track axes) of contact point on right hand wheel	Output

SUBROUTINES USED

None

METHOD

An initial approximation is made for the value of y_t. The corresponding values of z_t and slope on the rail are found. The value of y_t is then stepped until the slopes on both rail and wheel are equal. This is then the contact point and values of y_t, z_t, $(\partial z/\partial y)_t$ and H are printed out.

15. LATERAL WHEELSET

PURPOSE

To give points of contact between rail and wheel when wheelset is displaced laterally by an amount y_o.

INPUT PARAMETERS

YO lateral displacement of wheelset (y_o)

TH angle of roll due to lateral displacement (θ) (assumed).

SUBROUTINES USED

RAILAT, WHEEL, FINDH, STRWH, CIRWH

METHOD

The initial value of θ is read into the program. The right-hand side and left-hand side are considered separately, and the values of y_t, z_t and z_o calculated for each rail/wheel profile segment combination using the equations given inSection 4.4.2. The actual equations are solved in subroutine STRWH for straight tyre profiles and in subroutine CIRWH for circular tyre profiles.

The program prints out possible solutions for the left-hand and right-hand wheels corresponding to the input value of θ. θ is then stepped and

another set of solutions found. These results can then be interpolated to give a solution where the calculated values of Z_o on either side are identical. The coordinates of the contact points then follow.

16. SUBROUTINE STRWH (YO, TH, A, B, R, Q, C, YT, ZT, DZT, ZØ, H)

PURPOSE

To solve equations between straight tyre profiles and circular rail profiles when wheelset is displaced laterally.

DESCRIPTION OF PARAMETERS

YO	lateral displacement of wheelset, y_o	Input
TH	angle of roll, θ	
A	Y_t of centre of rail profile arc	
B	Z_t of centre of rail profile arc	
R	radius of rail profile arc	
Q	slope of straight tyre profile	
C	intercept of straight tyre profile	
YT	solution for y_t	Output
ZT	solution for z_t	
DZT	solution for $(\partial z/\partial y)_t$	
ZØ	solution for z_o	
H	vertical distance between origin of wheelset axes and track axes (wheelset central)	

SUBROUTINES USED

None

METHOD

The values of y_t, z_t, z_o, $(\partial z/\partial y)_t$ are calculated using equations 23 to 28 for input values of y_o and θ.

17. SUBROUTINE CIRWH (YO, TH, A, B, R, AN, BN, RD, H, YTX, ZTX, DZX, ZØX)

PURPOSE

To solve equations between circular tyre profiles and circular rail profiles when wheelset is displaced laterally.

DESCRIPTION OF PARAMETERS

YO	lateral displacement of wheelset, y_o	Input
TH	angle of roll, θ	
A	y_t of centre of rail profile arc	
B	z_t of centre of rail profile arc	
R	radius of rail profile arc	
AN	y_w of centre of tyre profile arc	
BN	z_w of centre of tyre profile arc	
RD	radius of tyre profile arc	
H	vertical distance between origin of wheelset axes and track axes (wheelset central)	
YTX	solution for y_t	Output
ZTX	solution for z_t	
DZX	solution for $(\partial z/\partial y)_t$	
ZØX	solution for z_o	

SUBROUTINES USED

None

METHOD

The values of y_t, z_t, z_o and $(\partial z/\partial y)_t$ are calculated using equations 23 to 28 of Section 4.4.2 for input values of y_o and θ.

18. YAWING WHEELSET

PURPOSE

To find contact points when wheelset is yawed through an angle ψ

INPUT PARAMETERS

PSI angle of yaw of wheelset, ψ

SUBROUTINES USED

RAILAT, WHEEL, FINDH, CIRCLE2, STRGHT2

METHOD

The contact points are found using the method outlined in Section 4.4.3. Each tyre profile segment is investigated in turn by either calling CIRCLE2, which solves the equations for circular tyre profile segments, or STRGHT2, which solves the equations for straight tyre profile segments. If no solution is found in a particular segment then the program goes on to the next segment, and so on until a solution is found.

The coordinates of the contact point are output in track axes and wheelset axes.

19. SUBROUTINE CIRCLE2 (P, A, B, R, G, IP1, IP2, NSTØP)

PURPOSE

To solve equations between a circular tyre profile segment and the rail when the wheelset is yawed.

DESCRIPTION OF PARAMETERS (Input)

P	angle of yaw of wheelset, ψ
A	y_w of centre of tyre profile arc
B	z_w of centre of tyre profile arc
R	radius of tyre profile arc

H — vertical distance between origin of wheelset axes and track axes (wheelset central).

IP1, IP2 — point IP1 to point IP2 on tyre profile

NSTOP — = 1 normally, but set to 2 if a solution is found

SUBROUTINES USED

RAILAT, WHEEL, Z200B

METHOD

The value of z_t is initially set to - .75" and this is increased in steps of .01". The corresponding values of y_t and $(\partial z_t/\partial y_t)_R$ are found from the rail equation. These values of y_t and z_t are then put in the wheel equations given in Section 4.3, which are solved for x_t and h. A fourth order equation has to be solved to give x_t and this is done numerically by calling subroutine Z200B. Only real roots are retained and tests are carried out on all the roots to ensure the correct one is used. The value of $(\partial z_t/\partial y_t)_W$ is calculated and compared with the equivalent value for the rail, if the two values are within a preset limit the program iterates over this value of z_t in very small steps until the slopes are equal.

If no solution is found then the subroutine says so and returns to the master program.

20. SUBROUTINE STRGHT2 (P, Q, C, H, IP1, IP2, NSTØP)

PURPOSE

To solve equations between a straight tyre profile segment and the rail when wheelset is yawed.

DESCRIPTION OF PARAMETERS (Input)

P	angle of yaw of wheelset, ψ
Q	slope of straight tyre profile
C	intercept of straight tyre profile
H	vertical distance between origin of wheelset axes and track axes (wheelset central)
IP1, IP2	point IP1 to point IP2 on tyre profile
NSTØP	= 1 normally but set to 2 if a solution is found

SUBROUTINES USED

RAILAT, WHEEL

METHOD

The method is basically the same as outlined for the previous subroutine except that this time equations 7 and 8 of Section 4.3 are solved. These second order equations are solved within the subroutine.

21. SUBROUTINE Z200B (A, R, GI, KAD, N)

PURPOSE

To find the root of a n'th order polynomial equation

DESCRIPTION OF PARAMETERS

A	array of coefficients starting with $a_n x^{n-1}$	Input
R	array of real parts or roots	Output
GI	array of imaginary parts of roots	Output
KAD	= 2 if method fails (normally = 1)	Output
N	order of polynomial, n	Input

SUBROUTINE USED

None

METHOD

This subroutine is based on a standard procedure for finding the roots of a polynomial equation in one variable of the form $x^n + a_1x^{n-1}$ $+ \_ \_ \_ \_ \_ \_ + a_r x^{n-r} + a_n$ where all the a's are real numbers. The maximum degree of the equation which the program can solve is 40. The method used is an iterative procedure derived by Bairstow.

The program can fail if a large number of iterations are required to reach a solution, if there are a large number of zero coefficients in the equation or if the equation is ill conditioned, e.g. coincident roots.

22. SUBROUTINE JOHANSON

PURPOSE

To find the minimum lateral distance and its position, between flange and rail when wheelset is yawed.

DESCRIPTION OF PARAMETERS (transferred in COMMON/JOH)

PSI angle of yaw of wheelset, ψ

H vertical distance between origin of wheelset axes and track axes (wheelset central)

SUBROUTINES USED

LINY, CIRY, RAILAT, WHEEL, FINDH, Z200B

METHOD

The shape of the tyre profile is found for different values of x_t at intervals of 0.5" using equation 29 of Section 4.4.3. These equations represent vertical planes through the wheel. The shortest lateral distance between the tyre profile and the rail profile is then found in each of these planes. The value of x_t where the minimum distance occurs follows. The program then goes back to the beginning

of the interval and increases x_t in smaller steps of 0.05" and the same procedure carried out.

The minimum distance between flange and rail is printed out along with the values of x_t, z_t, yt_{rail} and yt_{wheel} where this occurs.

23. SUBROUTINE CIRY (X, Z, K1, K2, YS)

PURPOSE

To calculate the value of y_t on a circular tyre profile arc knowing x_t and z_t when the wheelset is yawed.

DESCRIPTION OF PARAMETERS

X	x_t	Input
Z	z_t	Input
K1, K2	point lies in section K1 to K2	Input
YS	calculated value of y_t	Output

SUBROUTINES USED

Z200B

METHOD

The yaw angle and vertical distance between Track Axis origin and Wheelset Axis origin, are transferred in COMMON/JOH. Equation 32 of Section 4.4.3 is solved to find y_t. This is a 4th order polynomial equation which expresses points on circular tyre profile arcs in track coordinates when the wheelset is yawed.

24. SUBROUTINE LINY (X, Z, K1, K2, YS)

PURPOSE

To calculate the value of y_t on a straight tyre profile section knowing x_t and z_t when the wheelset is yawed.

DESCRIPTION OF PARAMETERS

X	x_t	Input
Z	z_t	Input
K1, K2	point lies in section K1 to K2	Input
YS	calculated value of y_t	Output

METHOD

Similar to above except that equation 37 of Section 4.4.3 is solved to find y_t.

25. ACCURATE

PURPOSE

To calculate the contact points for a wheelset yawed and then moved laterally until the flange contacts the rail.

INPUT PARAMETERS

PSI	ψ , yaw angle (radius)
HL	h_1, amount wheelset moves vertically in being yawed through ψ
H	vertical distance between origin of track axes and wheelset axes, wheelset in central position.
YO	approximate lateral distance to touch flange
TH	approximate roll angle
ZO	approximate vertical movement
XA5, XB5, XC5	approximate values of x_t for contact point A (left-hand tread), B (right-hand tread), C (right-hand flange)

YA5, YB5, Similarly for y_t.

YC5

SUBROUTINES USED

RAILAT, WHEEL, FINDH, FR1

METHOD

The method outlined in Section 4.4.4 is used to find the three contact points by a process of iteration from the approximate values input. The iteration continues until the vertical distance between rail and wheel at points A, B and C is less than .0000001".

The solution should be checked to make sure x_{A_t}, x_{B_t}, x_{C_t}, y_{A_t}, y_{B_t} are within ± .04" of the approximate input values and y_{C_t} is within ± .02". (This is the range of values in which a solution is sought).

26. CONTACT

PURPOSE

To calculate the principal radii of curvature at contact points between a wheelset and track. The program also calculates the angle between the principal radii and the constants A and B.

INPUT PARAMETERS

YO	lateral displacement of wheelset
ZO	vertical displacement of wheelset
PSI	angle of yaw
TH	angle of roll
XA,YA,ZA	coordinates of contact point A, in track axes
XB,YB,ZB	coordinates of contact point B, in track axes
XC,YC,ZC	coordinates of contact point C, in track axes

SUBROUTINES USED

RAILAT, WHEEL, FINDH

METHOD

Each contact point is considered in turn and the principal radii of curvature calculated. The equations of the planes containing the principal radii are also calculated, using the method given in Appendix 6, together with the angle between the planes. The constants A and B are calculated from the principal radii using the formulae given in Appendix 9. All these parameters are output on the line printer.

27. FORCES

PURPOSE

To calculate the creepages and forces on a displaced wheelset which has up to three contact points between itself and the track. Various load distributions, speeds and coefficients of friction can be input to the program.

INPUT PARAMETERS

UM	coefficient of friction
V	velocity
PD	initial guess at value of angular velocity to give zero rolling moment.
TZA,TZB, TZC	vertical loads carried at contact points A, B and C respectively.
XTA,YTA, ZTA	coordinates of contact point A, in track axes
XTB,YTB, ZTB	coordinates of contact point B, in track axes
XTC,YTC, ZTC	coordinates of contact point C, in track axes

YO	lateral displacement of wheelset
PSI	yaw angle
APBA, APBB, APBC	(A + B) for contact points A, B, C respectively
GA,GB,GC	minimum (a/b, b/a) for contact point A, B, C respectively
AL,BL,CL	cone angle at contact point A, B, C respectively

SUBROUTINES USED

NUMERIC, TAPE, SMALL, COEFF, LARGE, ELLIP, SIMP, ROL.

METHOD

If one of the input vertical loads is zero then the program assumes there is no contact at this point. The creepages and spin at each contact point are calculated using the assumed value of angular velocity $\dot{\Phi}$. The forces in the planes of the contact areas are calculated using the required theory by calling on the appropriate subroutine. The total forces and moments on the wheelset are then calculated. $\dot{\Phi}$ is varied and the whole process repeated until the total rolling moment on the wheelset is zero. When this is achieved after several iterations, the program stops and the creepages and forces are output on the line printer.

28. LAB

PURPOSE

To calculate forces on experimental roller rig for various wheel combinations and for various amounts of yaw angle, using any of the rolling contact theories.

INPUT PARAMETERS

RR	rolling radius of lower wheel
RW	rolling radius of upper wheel

AL	cone angle of upper wheel
APBA	(A + B) for contact area
GA	minimum (a/b, b/a)
W	vertical weight

SUBROUTINES USED

NUMERIC, TAPE, SMALL, COEFF, LARGE, ELLIP, SIMP, ROL.

METHOD

The program simulates conditions on the roller rig by incorporating the equations for the creepages and forces given in Section 8.3. The contact area forces are calculated from the creepages using any one of the rolling contact theories. Results are calculated for a range of yaw angles and coefficients of friction and output in the form μf_2 and $\psi / N^{\frac{1}{3}}$.

Section B GENERAL LISTING (XRLP) 28/06/73

```
      SUBROUTINE SMALL(G,K,T,U,E,FX,FY,ZM)
      COMMON/CFF/COF(19,4)
      CALL COEFF(G,K,C11,C22,C23,C33)
      PI=3.141592654
      TMAX=T
      UMAX=U
      EMAX=E
      CALL ELLIP(G,E)
      FX1=3.*.7*E*C11*EMAX/(4.*PI*SQRT(G))
      FY1=3.*.7*E*(C22*UMAX+C23*TMAX)/(4.*PI*SQRT(G))
      ZM=3.*.7*E*(C33*TMAX-C23*UMAX)/(4.*PI*SQRT(G))
      FX=FX1
      FY=FY1
      AT=ABS(TMAX)
      CALL MAXFY(G,AT,FYM)
      IF(FYM.GT.1.) FYM=1.
      ALPHA=ATAN(UMAX/EMAX)
      SALP=SIN(ALPHA)
      CALP=COS(ALPHA)
      AFX=ABS(FX1)
      IF(AFX.LT.CALP) GO TO 10
      AFX=CALP
      FX=SIGN(AFX,FX1)
   10 CONTINUE
      IF(TMAX)20,30,30
   30 IF(SALP.LT.FYM) GO TO 40
      IF(FY1.GT.SALP) FY=SALP
      IF(FY1.LT.FYM) FY=FYM
      GO TO 60
   40 IF(FY1.GT.FYM) FY=FYM
      IF(FY1.LT.SALP) FY=SALP
      GO TO 60
   20 FY2=-FY1
      IF(SALP.LT.FYM) GO TO 70
      IF(FY2.GT.SALP) FY=-SALP
      IF(FY2.LT.FYM) FY=-FYM
      GO TO 60
   70 IF(FY2.GT.FYM) FY=-FYM
      IF(FY2.LT.SALP) FY=-SALP
   60 CONTINUE
      FXM=SQRT(FX*FX+FY*FY)
      IF(FXM.LT.1.) GO TO 80
      FMM=SQRT(1.-FX*FX)
      FY=SIGN(FMM,FY1)
   80 CONTINUE
      RETURN
      END
      SUBROUTINE COEFF(G,K,C11,C22,C23,C33)
      COMMON/CFF/COF(19,4)
      PI=3.141592654
      IF(K.EQ.2) GO TO 10
      IF(G-.1)11,12,13
   11 WRITE(2,100)
  100 FORMAT(10X,17HA/B LESS THAN 0.1)
   12 C11=COF(1,1)
      C22=COF(1,2)
      C23=COF(1,3)
```

```
      C33=COF(1,4)
      GO TO 102
   13 IF(G-.2)14,15,16
   14 C11=(COF(2,1)-COF(1,1))*(G-.1)/.1+COF(1,1)
      C22=(COF(2,2)-COF(1,2))*(G-.1)/.1+COF(1,2)
      C23=(COF(2,3)-COF(1,3))*(G-.1)/.1+COF(1,3)
      C33=(COF(2,4)-COF(1,4))*(G-.1)/.1+COF(1,4)
      GO TO 102
   15 C11=COF(2,1)
      C22=COF(2,2)
      C23=COF(2,3)
      C33=COF(2,4)
      GO TO 102
   16 IF(G-.3)17,18,19
   17 C11=(COF(3,1)-COF(2,1))*(G-.2)/.1+COF(2,1)
      C22=(COF(3,2)-COF(2,2))*(G-.2)/.1+COF(2,2)
      C23=(COF(3,3)-COF(2,3))*(G-.2)/.1+COF(2,3)
      C33=(COF(3,4)-COF(2,4))*(G-.2)/.1+COF(2,4)
      GO TO 102
   18 C11=COF(3,1)
      C22=COF(3,2)
      C23=COF(3,3)
      C33=COF(3,4)
      GO TO 102
   19 IF(G-.4)20,21,22
   20 C11=(COF(4,1)-COF(3,1))*(G-.3)/.1+COF(3,1)
      C22=(COF(4,2)-COF(3,2))*(G-.3)/.1+COF(3,2)
      C23=(COF(4,3)-COF(3,3))*(G-.3)/.1+COF(3,3)
      C33=(COF(4,4)-COF(3,4))*(G-.3)/.1+COF(3,4)
      GO TO 102
   21 C11=COF(4,1)
      C22=COF(4,2)
      C23=COF(4,3)
      C33=COF(4,4)
      GO TO 102
   22 IF(G-.5)23,24,25
   23 D=(G-.4)/.1
      C11=(COF(5,1)-COF(4,1))*D+COF(4,1)
      C22=(COF(5,2)-COF(4,2))*D+COF(4,2)
      C23=(COF(5,3)-COF(4,3))*D+COF(4,3)
      C33=(COF(5,4)-COF(4,4))*D+COF(4,4)
      GO TO 102
   24 C11=COF(5,1)
      C22=COF(5,2)
      C23=COF(5,3)
      C33=COF(5,4)
      GO TO 102
   25 IF(G-.6)26,27,28
   26 D=(G-.5)/.1
      C11=(COF(6,1)-COF(5,1))*D+COF(5,1)
      C22=(COF(6,2)-COF(5,2))*D+COF(5,2)
      C23=(COF(6,3)-COF(5,3))*D+COF(5,3)
      C33=(COF(6,4)-COF(5,4))*D+COF(5,4)
      GO TO 102
   27 C11=COF(6,1)
      C22=COF(6,2)
      C23=COF(6,3)
      C22YC/FR6V2[
      C33=COF(6,4)
```

```
      GO TO 102
   28 IF(G-.7)29,30,31
   29 D=(G-.6)/.1
      C11=(COF(7,1)-COF(6,1))*D+COF(6,1)
      C22=(COF(7,2)-COF(6,2))*D+COF(6,2)
      C23=(COF(7,3)-COF(6,3))*D+COF(6,3)
      C33=(COF(7,4)-COF(6,4))*D+COF(6,4)
      GO TO 102
   30 C11=COF(7,1)
      C22=COF(7,2)
      C23=COF(7,3)
      C33=COF(7,4)
      GO TO 102
   31 IF(G-.8)32,33,34
   32 D=(G-.7)/.1
      C11=(COF(8,1)-COF(7,1))*D+COF(7,1)
      C22=(COF(8,2)-COF(7,2))*D+COF(7,2)
      C23=(COF(8,3)-COF(7,3))*D+COF(7,3)
      C33=(COF(8,4)-COF(7,4))*D+COF(7,4)
      GO TO 102
   33 C11=COF(8,1)
      C22=COF(8,2)
      C23=COF(8,3)
      C33=COF(8,4)
      GO TO 102
   34 IF(G-.9)35,36,37
   35 D=(G-.8)/.1
      C11=(COF(9,1)-COF(8,1))*D+COF(8,1)
      C22=(COF(9,2)-COF(8,2))*D+COF(8,2)
      C23=(COF(9,3)-COF(8,3))*D+COF(8,3)
      C33=(COF(9,4)-COF(8,4))*D+COF(8,4)
      GO TO 102
   36 C11=COF(9,1)
      C22=COF(9,2)
      C23=COF(9,3)
      C33=COF(9,4)
      GO TO 102
   37 IF(G-1.)38,39,40
   38 D=(G-.9)/.1
      C11=(COF(10,1)-COF(9,1))*D+COF(9,1)
      C22=(COF(10,2)-COF(9,2))*D+COF(9,2)
      C23=(COF(10,3)-COF(9,3))*D+COF(9,3)
      C33=(COF(10,4)-COF(9,4))*D+COF(9,4)
      GO TO 102
   39 C11=COF(10,1)
      C22=COF(10,2)
      C23=COF(10,3)
      C33=COF(10,4)
      GO TO 102
   40 WRITE(2,103)
  103 FORMAT(10X,20HA/B GREATER THAN 1.0)
      GO TO 101
   10 IF(G-.1)41,42,43
   41 VINV=ALOG(16./(G*G))
      C11=2.*PI*(1.+1.6137/(VINV-.6))/(VINV-.6)/G
      C22=2.*PI*(1.+1.6137*.7/(.7*VINV+.6))/(.7*VINV+.6)/G
      C23=2.*PI/(3.*G*SQRT(G)*(.7*VINV-.8))
      C33=PI*(.4*VINV-.2)/4./(.7*VINV-.8)
      C11=C11*.384
```

```
176           C22=C22*.384
177           C23=C23*.384
178           C33=C33*.384
179           GO TO 102
180        42 C11=COF(19,1)
181           C22=COF(19,2)
182           C23=COF(19,3)
183           C33=COF(19,4)
184           GO TO 102
185        43 IF(G-.2)44,45,46
186        44 C11=(COF(19,1)-COF(18,1))*(.2-G)/.1+COF(18,1)
187           C22=(COF(19,2)-COF(18,2))*(.2-G)/.1+COF(18,2)
188           C23=(COF(19,3)-COF(18,3))*(.2-G)/.1+COF(18,3)
189           C33=(COF(19,4)-COF(18,4))*(.2-G)/.1+COF(18,4)
190           GO TO 102
191        45 C11=COF(18,1)
192           C22=COF(18,2)
193           C23=COF(18,3)
194           C33=COF(18,4)
195           GO TO 102
196        46 IF(G-.3)47,48,49
197        47 C11=(COF(18,1)-COF(17,1))*(.3-G)/.1+COF(17,1)
198           C22=(COF(18,2)-COF(17,2))*(.3-G)/.1+COF(17,2)
199           C23=(COF(18,3)-COF(17,3))*(.3-G)/.1+COF(17,3)
200           C33=(COF(18,4)-COF(17,4))*(.3-G)/.1+COF(17,4)
201           GO TO 102
202        48 C11=COF(17,1)
203           C22=COF(17,2)
204           C23=COF(17,3)
205           C33=COF(17,4)
206           GO TO 102
207        49 IF(G-.4)50,51,52
208        50 C11=(COF(17,1)-COF(16,1))*(.4-G)/.1+COF(16,1)
209           C22=(COF(17,2)-COF(16,2))*(.4-G)/.1+COF(16,2)
210           C23=(COF(17,3)-COF(16,3))*(.4-G)/.1+COF(16,3)
211           C33=(COF(17,4)-COF(16,4))*(.4-G)/.1+COF(16,4)
212           GO TO 102
213        51 C11=COF(16,1)
214           C22=COF(16,2)
215           C23=COF(16,3)
216           C33=COF(16,4)
217           GO TO 102
218        52 IF(G-.5)53,54,55
219        53 C11=(COF(16,1)-COF(15,1))*(.5-G)/.1+COF(15,1)
220           C22=(COF(16,2)-COF(15,2))*(.5-G)/.1+COF(15,2)
221           C23=(COF(16,3)-COF(15,3))*(.5-G)/.1+COF(15,3)
222           C33=(COF(16,4)-COF(15,4))*(.5-G)/.1+COF(15,4)
223           GO TO 102
224        54 C11=COF(15,1)
225           C22=COF(15,2)
226           C23=COF(15,3)
227           C33=COF(15,4)
228           GO TO 102
229        55 IF(G-.6)56,57,58
230        56 C11=(COF(15,1)-COF(14,1))*(.6-G)/.1+COF(14,1)
231           C22=(COF(15,2)-COF(14,2))*(.6-G)/.1+COF(14,2)
232           C23=(COF(15,3)-COF(14,3))*(.6-G)/.1+COF(14,3)
233           C33=(COF(15,4)-COF(14,4))*(.6-G)/.1+COF(14,4)
234           GO TO 102
```

```
235        57 C11=COF(14,1)
236           C22=COF(14,2)
237           C23=COF(14,3)
238           C33=COF(14,4)
239           GO TO 102
240        58 IF(G-.7)59,60,61
241        59 C11=(COF(14,1)-COF(13,1))*(.7-G)/.1+COF(13,1)
242           C22=(COF(14,2)-COF(13,2))*(.7-G)/.1+COF(13,2)
243           C23=(COF(14,3)-COF(13,3))*(.7-G)/.1+COF(13,3)
244           C33=(COF(14,4)-COF(13,4))*(.7-G)/.1+COF(13,4)
245           GO TO 102
246        60 C11=COF(13,1)
247           C22=COF(13,2)
248           C23=COF(13,3)
249           C33=COF(13,4)
250           GO TO 102
251        61 IF(G-.8)62,63,64
252        62 C11=(COF(13,1)-COF(12,1))*(.8-G)/.1+COF(12,1)
253           C22=(COF(13,2)-COF(12,2))*(.8-G)/.1+COF(12,2)
254           C23=(COF(13,3)-COF(12,3))*(.8-G)/.1+COF(12,3)
255           C33=(COF(13,4)-COF(12,4))*(.8-G)/.1+COF(12,4)
256           GO TO 102
257        63 C11=COF(12,1)
258           C22=COF(12,2)
259           C23=COF(12,3)
260           C33=COF(12,4)
261           GO TO 102
262        64 IF(G-.9)65,66,67
263        65 C11=(COF(12,1)-COF(11,1))*(.9-G)/.1+COF(11,1)
264           C22=(COF(12,2)-COF(11,2))*(.9-G)/.1+COF(11,2)
265           C23=(COF(12,3)-COF(11,3))*(.9-G)/.1+COF(11,3)
266           C33=(COF(12,4)-COF(11,4))*(.9-G)/.1+COF(11,4)
267           GO TO 102
268        66 C11=COF(11,1)
269           C22=COF(11,2)
270           C23=COF(11,3)
271           C33=COF(11,4)
272           GO TO 102
273        67 IF(G-1.)68,69,70
274        68 C11=(COF(11,1)-COF(10,1))*(1.-G)/.1+COF(10,1)
275           C22=(COF(11,2)-COF(10,2))*(1.-G)/.1+COF(10,2)
276           C23=(COF(11,3)-COF(10,3))*(1.-G)/.1+COF(10,3)
277           C33=(COF(11,4)-COF(10,4))*(1.-G)/.1+COF(10,4)
278           GO TO 102
279        69 C11=COF(10,1)
280           C22=COF(10,2)
281           C23=COF(10,3)
282           C33=COF(10,4)
283           GO TO 102
284        70 WRITE(2,105)
285       105 FORMAT(10X,20HB/A GREATER THAN 1.0)
286       101 CONTINUE
287       102 CONTINUE
288           C11=C11/.384
289           C22=C22/.384
290           C23=C23/.384
291           C22*C22*(384
292           C33=C33/.384
293           RETURN
```

```
      END
      SUBROUTINE ELLIP(G,E)
      IF(G-.05)10,20,30
   10 E=1.+.2*G
      GO TO 1000
   20 E=1.01
      GO TO 1000
   30 IF(G-.1)40,50,60
   40 E=1.01+.2*(G-.05)
      GO TO 1000
   50 E=1.02
      GO TO 1000
   60 IF(G-.18)70,80,90
   70 E=1.02+(1.04-1.02)*(G-.1)/(.18-.1)
      GO TO 1000
   80 E=1.04
      GO TO 1000
   90 IF(G-.26)100,110,120
  100 E=1.04+(1.08-1.04)*(G-.18)/(.26-.18)
      GO TO 1000
  110 E=1.08
      GO TO 1000
  120 IF(G-.36)130,140,150
  130 E=1.08+(1.13-1.08)*(G-.26)/(.36-.26)
      GO TO 1000
  140 E=1.13
      GO TO 1000
  150 IF(G-.47)160,170,180
  160 E=1.13+(1.19-1.13)*(G-.36)/(.47-.36)
      GO TO 1000
  170 E=1.19
      GO TO 1000
  180 IF(G-.62)190,200,210
  190 E=1.19+(1.29-1.19)*(G-.47)/(.62-.47)
      GO TO 1000
  200 E=1.29
      GO TO 1000
  210 IF(G-.79)220,230,240
  220 E=1.29+(1.41-1.29)*(G-.62)/(.79-.62)
      GO TO 1000
  230 E=1.41
      GO TO 1000
  240 E=1.41+(1.57-1.41)*(G-.79)/(1.-.79)
 1000 CONTINUE
      RETURN
      END
      SUBROUTINE MAXFY(BA,S,FYM)
      IF(BA.GT.0..AND.BA.LE..5) DXF=1.25*BA/.5
      IF(BA.GT..5.AND.BA.LE.1.) DXF=1.25+1.*(BA-.5)/.5
      IF(BA.GT.1..AND.BA.LE.1.5) DXF=2.25+.84*(BA-1.)/.5
      IF(BA.GT.1.5.AND.BA.LE.2.) DXF=3.09+.63*(BA-1.5)/.5
      IF(BA.GT.2..AND.BA.LE.2.5) DXF=3.72+.27*(BA-2.)/.5
      IF(BA.GT.2.5.AND.BA.LE.3.) DXF=3.99+.13*(BA-2.5)/.5
      IF(BA.GT.3..AND.BA.LE.3.5) DXF=4.12+.10*(BA-3.)/.5
      IF(BA.GT.3.5.AND.BA.LE.4.)DXF=4.22+.08*(BA-3.5)/.5
      IF(BA.GT.4..AND.BA.LE.4.5) DXF=4.3+.04*(BA-4.)/.5
      IF(BA.GT.4.5.AND.BA.LE.5.) DXF=4.34+.03*(BA-4.5)/.5
      IF(BA.GT.5.) DXF=4.38
      DFX=1./DXF
```

```
      FYM=DFX*S
      RETURN
      END
      SUBROUTINE LARGE(G,K,T,EW,ET,FX,FY,ZM)
      DIMENSION PS(73),FC1(73),FC2(73),FC3(73),TH(19),R1(19),R2(19),R3(
     19),FP1(19),FP2(19),FP3(19)
      IF(K.EQ.2) GO TO 5
      GO TO 6
    5 EWM=-ET
      ETM=-EW
      EW=EWM
      ET=ETM
    6 CONTINUE
      PI=3.141592654
      PR=(PI*5.)/180.
      NT=19
      NP=73
      TH(1)=0.
      DO 10 ITH=1,18
      KTH=ITH+1
   10 TH(KTH)=TH(ITH)+PR
      DO 40 ITH=1,19
      PS(1)=0.
      DO 20 IPS=1,72
      KPS=IPS+1
   20 PS(KPS)=PS(IPS)+PR
      DO 30 IFN=1,73
      FC1(IFN)=FUNC1(PS(IFN),G,EW,ET,T,TH(ITH))
      FC2(IFN)=FUNC2(PS(IFN),G,EW,ET,T,TH(ITH))
   30 FC3(IFN)=FUNC3(PS(IFN),G,EW,ET,T,TH(ITH))
      CALL SIMPSN(PS,FC1,NP,R1(ITH))
      CALL SIMPSN(PS,FC2,NP,R2(ITH))
      CALL SIMPSN(PS,FC3,NP,R3(ITH))
   40 CONTINUE
      DO 50 IFN=1,19
      FP1(IFN)=FUNC4(TH(IFN),R1(IFN))
      FP2(IFN)=FUNC4(TH(IFN),R2(IFN))
   50 FP3(IFN)=FUNC5(TH(IFN),R3(IFN))
      CALL SIMPSN(TH,FP1,NT,RA)
      CALL SIMPSN(TH,FP2,NT,RB)
      CALL SIMPSN(TH,FP3,NT,RC)
      ST=SIGN(1.,T)
      FX=-3.*SQRT(G)*ST*RA/(2.*PI)
      FY=3.*ST*RB/(2.*PI*SQRT(G))
      ZM=3.*ST*RC/(2.*PI)
      ZM=ZM-FY*(EW/T)-FX*(ET/T)
      IF(K.EQ.1) GO TO 51
      FXM=-FY
      FYM=-FX
      FX=FXM
      FY=FYM
      EW=-ETM
      ET=-EWM
   51 CONTINUE
      RETURN
      END
      FUNCTION FUNC1(PS,G,EW,ET,T,TH)
      A=SQRT(G)
      F1=A*SIN(TH)*COS(PS)+EW/T
```

```
      F1=F1*F1
      F2=(SIN(TH)*SIN(PS)/A)-ET/T
      F2=F2*F2
      FUNC1=SQRT(F1+F2)*SIN(PS)
      RETURN
      END
      FUNCTION FUNC2(PS,G,EW,ET,T,TH)
      A=SQRT(G)
      F1=A*SIN(TH)*COS(PS)+EW/T
      F1=F1*F1
      F2=(SIN(TH)*SIN(PS)/A)-ET/T
      F2=F2*F2
      FUNC2=SQRT(F1+F2)*COS(PS)
      RETURN
      END
      FUNCTION FUNC3(PS,G,EW,ET,T,TH)
      A=SQRT(G)
      F1=A*SIN(TH)*COS(PS)+EW/T
      F1=F1*F1
      F2=(SIN(TH)*SIN(PS)/A)-ET/T
      F2=F2*F2
      FUNC3=SQRT(F1+F2)
      RETURN
      END
      FUNCTION FUNC4(A,B)
      FUNC4=SIN(A)*SIN(A)*B
      RETURN
      END
      FUNCTION FUNC5(A,B)
      FUNC5=SIN(A)*COS(A)*COS(A)*B
      RETURN
      END
      SUBROUTINE SIMPSN(X,Y,N,R)
      DIMENSION X(N),Y(N)
      H=(X(N)-X(1))/(N-1)
      J=N-2
      K=N-1
      SH=0.
      DO 10 I=3,J,2
   10 SH=SH+Y(I)
      TH=0.
      DO 20 I=2,K,2
   20 TH=TH+Y(I)
      R=H*(Y(1)+Y(N)+2.*SH+4.*TH)/3.
      RETURN
      END
      SUBROUTINE NUMERIC(G,K,T,U,E,FA,FB,CM,IF,IT)
      DIMENSION F1S(4),F2S(4),F3S(4)
      COMMON/T1/F1(4),F2(4),F3(4)/T2/ABF(4),SPS(24),ALS(156),VS(1785),F
     1S(1785),FYS(1785),ZMS(1785),NVS(156),NKS(24),NAS(4)
      IF(K.EQ.2) GO TO 10
      AT=G
      IF(AT.GT.3..OR.AT.LT..2) GO TO 20
      GO TO 30
   20 IF=2
      GO TO 102
   10 AT=1./G
      IF(AT.GT.3..OR.AT.LT..2) GO TO 20
   30 CONTINUE
```

```
      IF(U.EQ.0.) GO TO 9
      W=SQRT(E*E+U*U)
      GO TO 8
    9 W=ABS(E)
    8 CONTINUE
C
   19 FORMAT(5X,4E20.6)
C  SYMMETRY RELATIONS
      IF(E.LT.0..AND.T.GE.0.) GO TO 32
      IF(E.GE.0..AND.T.LE.0.) GO TO 40
      IF(E.LT.0..AND.T.LE.0.) GO TO 50
      IF(E.EQ.0..AND.U.EQ.0.) GO TO 150
      IF(E.EQ.0..AND.U.GT.0.) GO TO 132
      IF(E.EQ.0..AND.U.LT.0.) GO TO 140
      ALP=ATAN(U/E)
      ALP=ALP*57.3
      GO TO 134
  150 ALP=0.
      GO TO 134
  132 ALP=90.
      GO TO 134
  140 ALP=-90.
  134 CALL TAPE(T,ALP,W,IT)
      GO TO 60
   32 CONTINUE
      ALP=ATAN(U/(-E))
      ALP=ALP*57.3
  133 CALL TAPE(T,ALP,W,IT)
      DO 31 I=1,4
   31 F1(I)=-F1(I)
      GO TO 60
   40 IF(E.EQ.0.) GO TO 135
      ALP=ATAN(-U/E)
      ALP=ALP*57.3
      GO TO 141
  135 IF(U.GT.0.) ALP=-90.
      IF(U.LT.0.) ALP=90.
      IF(U.EQ.0.) ALP=0.
  141 CALL TAPE(-T,ALP,W,IT)
      DO 41 I=1,4
      F2(I)=-F2(I)
   41 F3(I)=-F3(I)
      GO TO 60
   50 ALP=ATAN((-U)/(-E))
      ALP=ALP*57.3
      CALL TAPE(-T,ALP,W,IT)
      DO 51 I=1,4
      F1(I)=-F1(I)
      F2(I)=-F2(I)
   51 F3(I)=-F3(I)
   60 CONTINUE
      F1S(1)=F1(4)
      F1S(2)=F1(2)
      F1S(3)=F1(1)
      F1S(4)=F1(3)
      F2S(1)=F2(4)
      F2S(2)=F2(2)
      F2S(3)=F2(1)
      F2S(4)=F2(3)
```

```
      F3S(1)=F3(4)
      F3S(2)=F3(2)
      F3S(3)=F3(1)
      F3S(4)=F3(3)
      DO 61 I=1,4
      F1(I)=F1S(I)
      F2(I)=F2S(I)
   61 F3(I)=F3S(I)
      IF(.2-AT)70,80,80
   80 FA=F1(1)
      FB=F2(1)
      CM=F3(1)
      GO TO 99
   70 IF(.5-AT)71,72,73
   73 FA=(F1(2)-F1(1))*(AT-.2)/.3+F1(1)
      FB=(F2(2)-F2(1))*(AT-.2)/.3+F2(1)
      CM=(F3(2)-F3(1))*(AT-.2)/.3+F3(1)
      GO TO 99
   72 FA=F1(2)
      FB=F2(2)
      CM=F3(2)
      GO TO 99
   71 IF(1.-AT)74,75,76
   76 FA=(F1(3)-F1(2))*(AT-.5)/.5+F1(2)
      FB=(F2(3)-F2(2))*(AT-.5)/.5+F2(2)
      CM=(F3(3)-F3(2))*(AT-.5)/.5+F3(2)
      GO TO 99
   75 FA=F1(3)
      FB=F2(3)
      CM=F3(3)
      GO TO 99
   74 IF(2.-AT)79,78,79
   79 FA=(F1(4)-F1(3))*(AT-1.)/1.+F1(3)
      FB=(F2(4)-F2(3))*(AT-1.)/1.+F2(3)
      CM=(F3(4)-F3(3))*(AT-1.)/1.+F3(3)
      GO TO 99
   78 FA=F1(4)
      FB=F2(4)
      CM=F3(4)
   99 CONTINUE
      IF(FA.LT.1..AND.FA.GT.-1.) GO TO 101
      FA=SIGN(1.,FA)
  101 AFA=ABS(FA)
      IF(AFA.EQ.1..AND.U.EQ.0.) GO TO 200
      FAB=SQRT(FA*FA+FB*FB)
      IF(FAB.LT.1.) GO TO 102
  202 FORMAT(20X,32HSQRT(FX*FX+FY*FY) GREATER THAN 1)
      BFB=SQRT(1.-FA*FA)
      FB=SIGN(BFB,FB)
       GO TO 102
  200 FB=0.
  102 CONTINUE
      RETURN
      END
      SUBROUTINE TAPE(SPP,ALP,VP,IT)
      DIMENSION AB(4),SP(24),AL(156),V(1785),FX(1785),FY(1785),ZM(1785)
     1NV(156),NK(24),NA(4)
      COMMON/T1/F1(4),F2(4),F3(4)/T2/ABF(4),SPS(24),ALS(156),VS(1785),F
     1S(1785),FYS(1785),ZMS(1785),NVS(156),NKS(24),NAS(4)
```

```
      IF(IT.EQ.2) GO TO 1000
C
      REWIND 6
      DO 199 I=1,156
  199 READ(6)NVS(I)
      DO 201 I=1,24
  201 READ(6)NKS(I)
      DO 202 I=1,4
  202 READ(6)NAS(I)
      DO 50 I=1,4
   50 READ(6)ABF(I)
      DO 51 I=1,24
   51 READ(6)SPS(I)
      DO 52 I=1,156
   52 READ(6)ALS(I)
      DO 53 I=1,1785
      READ(6)VS(I)
      READ(6)FXS(I)
      READ(6)FYS(I)
   53 READ(6)ZMS(I)
      IT=2
      REWIND 6
 1000 CONTINUE
      DO 700 I=1,156
      NV(I)=NVS(I)
  700 AL(I)=ALS(I)
      DO 701 I=1,24
      NK(I)=NKS(I)
  701 SP(I)=SPS(I)
      DO 702 I=1,4
      NA(I)=NAS(I)
  702 AB(I)=ABF(I)
      DO 703 I=1,1785
      V(I)=VS(I)
      FX(I)=FXS(I)
      FY(I)=FYS(I)
  703 ZM(I)=ZMS(I)
C          TO SOLVE FOR VP(NU)
C
      K=0
      DO 2 J=1,156
      DO 3 I=1,NV(J)
      K=K+1
      SOL=VP-V(K)
      IF(SOL)30,31,32
   32 CONTINUE
    3 CONTINUE
      I=I-1
      FX(J)=COS(AL(J)*3.141592653589/180.)
      FY(J)=SIN(AL(J)*3.141592653589/180.)
      K2=K-1
      ZM(J)=ZM(K)+(ZM(K)-ZM(K2))*(VP-V(K))/(V(K)-V(K2))
      IF(ZM(K).GT.0..AND.ZM(K2).GT.0..AND.ZM(J).LT.0.) GO TO 50
      IF(ZM(K).LT.0..AND.ZM(K2).LT.0..AND.ZM(J).GT.Q.) GO TO 50
      GO TO 28
  502 ZM(J)=0.
      GO TO 28
   31 FX(J)=FX(K)
      FY(J)=FY(K)
```

```
      ZM(J)=ZM(K)
      GO TO 28
   30 IF(I.EQ.1) GO TO 147
      K2=K-1
      FX(J)=((FX(K)-FX(K2))*(VP-V(K2))/(V(K)-V(K2)))+FX(K2)
      FY(J)=((FY(K)-FY(K2))*(VP-V(K2))/(V(K)-V(K2)))+FY(K2)
      ZM(J)=((ZM(K)-ZM(K2))*(VP-V(K2))/(V(K)-V(K2)))+ZM(K2)
      GO TO 28
  147 K3=K+1
      FX(J)=FX(K3)-(FX(K3)-FX(K))*(V(K3)-VP)/(V(K3)-V(K))
      FY(J)=FY(K3)-(FY(K3)-FY(K))*(V(K3)-VP)/(V(K3)-V(K))
      ZM(J)=ZM(K3)-(ZM(K3)-ZM(K))*(V(K3)-VP)/(V(K3)-V(K))
   28 K=K-I+NV(J)
    2 CONTINUE
C
C          TO SOLVE FOR ALP(ALPHA)
C
      K=0
      DO 101 J=1,24
      DO 102 I=1,NK(J)
      K=K+1
      SOL=ALP-AL(K)
      IF(SOL)130,131,132
  132 CONTINUE
  102 CONTINUE
  131 FX(J)=FX(K)
      FY(J)=FY(K)
      ZM(J)=ZM(K)
      GO TO 128
  130 IF(I.EQ.1) GO TO 1301
      K2=K-1
      FX(J)=((FX(K)-FX(K2))*(ALP-AL(K2))/(AL(K)-AL(K2)))+FX(K2)
      FY(J)=((FY(K)-FY(K2))*(ALP-AL(K2))/(AL(K)-AL(K2)))+FY(K2)
      GO TO 128
      ZM(J)=((ZM(K)-ZM(K2))*(ALP-AL(K2))/(AL(K)-AL(K2)))+ZM(K2)
 1301 ALP2=-ALP
      K=K-1
      DO 1302 I=1,NK(J)
      K=K+1
      SOL=ALP2-AL(K)
      IF(SOL)1303,1304,1305
 1305 CONTINUE
 1302 CONTINUE
 1304 FX(J)=FX(K)
      FY(J)=FY(K)
      ZM(J)=ZM(K)
      GO TO 1281
 1303 K2=K-1
      FX(J)=((FX(K)-FX(K2))*(ALP2-AL(K2))/(AL(K)-AL(K2)))+FX(K2
      FY(J)=((FY(K)-FY(K2))*(ALP2-AL(K2))/(AL(K)-AL(K2)))+FY(K2
      ZM(J)=((ZM(K)-ZM(K2))*(ALP2-AL(K2))/(AL(K)-AL(K2)))+ZM(K2
 1281 FY(J)=-FY(J)
      ZM(J)=-ZM(J)
      GO TO 128
  128 K=K-I+NK(J)
  101 CONTINUE
C
C          TO SOLVE FOR SPP(KI)
C
```

```
      K=0
      DO 401 J=1,4
      DO 402 I=1,NA(J)
      K=K+1
      SOL=SPP-SP(K)
      IF(SOL)430,431,432
  432 CONTINUE
  402 CONTINUE
      K2=K-1
      FX(J)=FX(K)+(FX(K)-FX(K2))*(SPP-SP(K))/(SP(K)-SP(K2))
      FY(J)=FY(K)+(FY(K)-FY(K2))*(SPP-SP(K))/(SP(K)-SP(K2))
      ZM(J)=ZM(K)+(ZM(K)-ZM(K2))*(SPP-SP(K))/(SP(K)-SP(K2))
      GO TO 428
  431 FX(J)=FX(K)
      FY(J)=FY(K)
      ZM(J)=ZM(K)
      GO TO 428
  430 K2=K-1
      FX(J)=((FX(K)-FX(K2))*(SPP-SP(K2))/(SP(K)-SP(K2)))+FX(K2)
      FY(J)=((FY(K)-FY(K2))*(SPP-SP(K2))/(SP(K)-SP(K2)))+FY(K2)
      ZM(J)=((ZM(K)-ZM(K2))*(SPP-SP(K2))/(SP(K)-SP(K2)))+ZM(K2)
  428 K=K-I+NA(J)
      F1(J)=FX(J)
      F2(J)=FY(J)
      F3(J)=ZM(J)
  401 CONTINUE
   19 FORMAT(5X,4E20.6)
      RETURN
      END
      SUBROUTINE SIMP(AAAAA,BBBBB,CCCCC,F,K,NA,NB,FXM,FYM,AMZM,JIF)
      DIMENSION XDIM(41),YDIM(21),Z(41,21)
      DIMENSION XINT(41),YINT(41),YY(21),R(21)
      COMMON/CFF/COF(19,4)
      COMMON/GRP/CS(3),GEL(5),X(41,21),Y(41,21),VX(41,21),VY(41,21),G(2
     1,10),IE(21),ALE(21),AMUZ,NX,NY,FX,FY,AMZ,NDI,NDJ
      CS(1)=AAAAA
      CS(2)=BBBBB
      NX=NA
      NY=NB
      PI=3.1415926536
      POI=.3
      AMUZ=2./PI
C         NX = NO. OF +VE X ORDINATES NOT INCLUDING X = 0
C         NY = NO. OF +VE Y ORDINATES NOT INCLUDING Y = 0
      NADI=2*NX+1
      NADJ=2*NY+1
      CALL COEFF(F,K,C11,C22,C23,C33)
    4 FORMAT(5X,4HC11=,F7.4,2X,4HC22=,F7.4,2X,4HC23=,F7.4,2X,4HC33=,F7.
     1)
   14 CONTINUE
      IMARK=1
      IF(CCCCC.GE.0.) GO TO 5
      IMARK=2
      CS(2)=-CS(2)
      CCCCC=-CCCCC
    5 CONTINUE
      GEL(3)=3.395*C23/C22
      IF(K.EQ.1) GO TO 6
      BDD=5.*C33*GEL(3)*SQRT(F)/C11
```

```
      BDD=SQRT(BDD)
      GBAR=BDD/GEL(3)
      GBAR3=GBAR
      CALL ELLIP(F,E)
    7 CONTINUE
      CALL ELLIP(GBAR,EBAR)
      GBAR2=GBAR3*SQRT(EBAR/E)
      GDIF=GBAR2-GBAR
      GA=ABS(GDIF)
      IF(GA.LE..0001) GO TO 8
      GBAR=GBAR2
      GO TO 7
    8 CONTINUE
      GEL(4)=GBAR*GEL(3)
   12 GEL(1)=(8.*GEL(3)*GEL(3)*GEL(4)*4.*3.1415926536*SQRT(F))/(3.*C11*
     1.*(1.-POI)*E)
      GEL(2)=(8.*GEL(3)*GEL(3)*GEL(4)*4.*3.1415926536*SQRT(F))/(3.*C22*
     1.*(1.-POI)*E)
      AMUZ=.4775/(GEL(3)*GEL(4))
      CS(3)=CCCCC
      GO TO 9
    6 BDD=5.*C33*SQRT(F)/C11
      GBAR=GEL(3)/BDD
      CALL ELLIP(F,E)
   10 CONTINUE
      CALL ELLIP(GBAR,EBAR)
      GBAR2=GBAR*E/EBAR
      GDIF=GBAR2-GBAR
      GA=ABS(GDIF)
      IF(GA.LE..0002) GO TO 11
      GBAR=GBAR2
      GO TO 10
   11 CONTINUE
      GEL(4)=GEL(3)/GBAR
      GO TO 12
    9 CONTINUE
      GEL(5)=.04
      IF(JIF.NE.3) GO TO 130
      WRITE(2,30)(CS(I),I=1,3)
   30 FORMAT(5X,5HUX = ,F7.4,2X,5HUY = ,F7.4,2X,5HPH = ,F7.4)
      WRITE(2,40)(GEL(I),I=1,5)
   40 FORMAT(5X,5HSX = ,F7.4,2X,5HSY = ,F7.4,2X,4HA = ,F7.4,2X,4HB = ,F
     1.4,2X,5HDM = ,F7.4)
      WRITE(2,21)NX,NY
   21 FORMAT(5X,5HNX = ,I2,5X,5HNY = ,I2)
  130 CONTINUE
      NDI=2*NX-1
      NDJ=2*NY-1
      NTIM=2*NX
      CALL ROL
      IF(JIF.NE.3) GO TO 131
      WRITE(2,45)FX,FY,AMZ
   45 FORMAT(5X,5HFX = ,F7.4,2X,5HFY = ,F7.4,2X,5HMZ = ,F7.4)
      WRITE(2,50)
   50 FORMAT(5X,12HCONTACT AREA)
  131 CONTINUE
      H=GEL(3)/NX
      XDIM(1)=-GEL(3)
      YDIM(1)=-GEL(4)
```

```
      DO 60 I=2,NADI
      J=I-1
   60 XDIM(I)=XDIM(J)+H
      AK=GEL(4)/NY
      DO 70 I=2,NADJ
      J=I-1
   70 YDIM(I)=YDIM(J)+AK
      NK=NDJ+1
      NKK=NADJ
      IF(JIF.NE.3) GO TO 174
      DO 80 I=1,NDJ
      NK=NK-1
      NKK=NKK-1
      IF(G(NK,1).LT.0.) GO TO 72
      WRITE(2,71)YDIM(NKK),(G(NK,J),J=2,10)
   71 FORMAT(5X,4HY = ,F7.4,2X,11HL.E. STICKS,9F7.4)
      GO TO 74
   72 WRITE(2,73)YDIM(NKK),(G(NK,J),J=2,10)
   73 FORMAT(5X,4HY = ,F7.4,2X,11HL.E. SLIPS ,9F7.4)
   74 CONTINUE
   80 CONTINUE
  174 CONTINUE
      DO 85 J=1,NADJ
      DO 85 I=1,NADI
      P=1.-XDIM(I)*XDIM(I)/GEL(3)/GEL(3)-YDIM(J)*YDIM(J)/GEL(4)/GEL(4)
      Z(I,J)=0.
      IF(P.GT.0.) Z(I,J)=AMUZ*SQRT(P)
   85 CONTINUE
      NTY=2*NY
      NK=NDJ+1
      NKK=NADJ
      IF(JIF.NE.3) GO TO 175
      DO 90 J=2,NTY
      NK=NK-1
      NKK=NKK-1
      WRITE(2,81)YDIM(NKK)
   81 FORMAT(5X,4HY = ,F7.4)
      WRITE(2,82)
   82 FORMAT(11X,1HX,10X,1HZ,9X,2HTX,9X,2HTY,9X,2HVX,9X,2HVY,9X,2HXY,9X
     11HV)
      XLE=GEL(3)*SQRT(1.-YDIM(NKK)*YDIM(NKK)/GEL(4)/GEL(4))
      XTE=-XLE
      DO 90 I=2,NTIM
      IF(XDIM(I).GE.XLE.OR.XDIM(I).LE.XTE) GO TO 90
      XARG=SQRT(X(I,NK)*X(I,NK)+Y(I,NK)*Y(I,NK))
      VARG=SQRT(VX(I,NK)*VX(I,NK)+VY(I,NK)*VY(I,NK))
      WRITE(2,83)XDIM(I),Z(I,NKK),X(I,NK),Y(I,NK),VX(I,NK),VY(I,NK),XAR
     1,VARG
   83 FORMAT(7X,F7.4,4X,F7.4,4X,F7.4,4X,F7.4,4X,F7.4,4X,F7.4,4X,F7.4,4X
     1F7.4)
   90 CONTINUE
  175 CONTINUE
      FXM=FX
      FYM=FY
      AMZM=AMZ
      IF(IMARK.EQ.1) GO TO 161
      FYM=-FYM
      AMZM=-AMZM
  161 CONTINUE
```

```
      RETURN
      END
      SUBROUTINE ROL
      COMMON/GRP/CS(3),GEL(5),X(41,21),Y(41,21),VX(41,21),VY(41,21),G(2
     1,10),IE(21),ALE(21),AMUZ,NX,NY,FX,FY,AMZ,NDI,NDJ
      UX=CS(1)
      UY=CS(2)
      PH=CS(3)
      DM=GEL(5)
      SX=GEL(1)
      SY=GEL(2)
      A=GEL(3)
      B=GEL(4)
      H=A/NX
      AK=B/NY
      PI=3.1415926536
      CZP=AMUZ*2./A/A
      KSET=2*NY-1
      J=-(KSET-1)/2-1
      DO 100 JCOUNT=1,KSET
      J=J+1
      ALE(JCOUNT)=A*SQRT(1.-AK*AK*J*J/B/B)
      IE(JCOUNT)=.99*ALE(JCOUNT)/H
      ICOUNT=2*NX+1
      I=-NX-1
      DO 110 NCASE=1,ICOUNT
      I=I+1
      IF(I.LT.-IE(JCOUNT).OR.I.GT.IE(JCOUNT)) GO TO 111
      GO TO 112
  111 X(NCASE,JCOUNT)=0.
      Y(NCASE,JCOUNT)=0.
      VX(NCASE,JCOUNT)=0.
      VY(NCASE,JCOUNT)=0.
  112 CONTINUE
  110 CONTINUE
      DO 120 I=1,10
  120 G(JCOUNT,I)=-3.*A
  100 CONTINUE
      IF(UX-PH*B.GT.0.) GO TO 121
      THV=-1.
      GO TO 122
  121 THV=1.
  122 CONTINUE
      THV=THV*ATAN(UY/(ABS(UX-PH*B)+.00000001))+PI*(1.-THV)/2.
      MIE=IE(1)
      IF(KSET.EQ.1) GO TO 124
      DO 123 JC=2,KSET
      MIE=MAXO(MIE,IE(JC))
  123 CONTINUE
  124 CONTINUE
      KSET=2*NY-1
      J=-(KSET-1)/2-1
      DO 150 JC=1,KSET
      J=J+1
      Q=J*AK
      P=ALE(JC)
      PG=P
      CUX=UX-PH*Q
```

```
      NPIJL=2
      CUY=UY+PH*P
      CALL AMAAKZ(P,Q,ZN,CZ,CZP,A,B,AMUZ)
      XG=0.
      YG=0.
      XV=0.
      YV=0.
      VV=0.
      I=IE(JC)
      IC=MIE+I+2
      G(JC,1)=1.
      IF(CZ*CZ-CUX*CUX/SX/SX-CUY*CUY/SY/SY.GT.0.) GO TO 50
C         SLIP AT THE LEADING EDGE. DETERMINE T(HETA)
      G(JC,1)=-1.
      IF(CUX.GT.0.) GO TO 1
      T=-1.
      GO TO 2
    1 T=1.
    2 CONTINUE
      T=T*ATAN(CUY/(ABS(CUX)+.00000001))+PI*(1.-T)/2.
   10 S=SIN(T)
      C=COS(T)
      ANU=(CUX*S-CUY*C-CZ*(SX-SY)*C*S)/(CUX*C+CUY*S-CZ*(SX-SY)*(C*C-S*S
     1)
      T=T-ANU
      IF(ABS(ANU).GT..001) GO TO 10
      THV=T
      C=COS(T)
      S=SIN(T)
C         THE STARTING VALUE OF T HAS BEEN FOUND.
C         THE DERIVATIVE IS DETERMINED IN A SPECIAL WAY.
      TP=(PH*C+CZP*(SX-SY)*C*S)/(CUX*C+CUY*S-CZ*((3.*C*C-1.)*(SX-SY)-SX
     1)
   20 IF((P-DM).LT.(I*H+.000001)) GO TO 21
      D=-DM
      GO TO 22
   21 D=I*H-P
   22 CONTINUE
      PN=P+D
      CALL AMAAKZ(PN,Q,ZN,CZ,CZP,A,B,AMUZ)
      TN=T+D*TP
      S=SIN(TN)
      C=COS(TN)
      CUY=UY+PH*PN
      TPN=(CUX*S-CUY*C-CZ*C*S*(SX-SY))/ZN/(SY*C*C+SX*S*S)
      T=T+.5*D*(TP+TPN)
      S=SIN(T)
      C=COS(T)
      XN=ZN*C
      YN=ZN*S
      V=CUX*SY*C+CUY*SX*S-CZ*SX*SY
      IF(V.LT.-.00004) GO TO 25
      GO TO 26
   25 IF(ABS(VV).LT..0000000001) GO TO 23
      AN=VV/(VV-V)
      GO TO 24
   23 AN=.9
   24 CONTINUE
      VV=0.
```

```
      AV=1.-AN
      PG=AV*P+AN*PN
      G(JC,NPIJL)=PG
      NPIJL=NPIJL+1
      P=PG
      IF(NPIJL.GT.10) NPIJL=10
      XV=AV*XV+AN*XN
      XG=XV
      YG=AV*YV+AN*YN
      YV=YG
      GO TO 30
   26 CONTINUE
C          SLIP IN THE NEW POINT
      XV=XN
      YV=YN
      P=PN
   40 TP=(CUX*S-CUY*C-CZ*C*S*(SX-SY))/ZN/(SY*C*C+SX*S*S)
      IF(P.GT.(I*H+.000001)) GO TO 20
      X(IC,JC)=XN
      Y(IC,JC)=YN
      XP=-ZN*S*TP-CZ*C
      YP=ZN*C*TP-CZ*S
      VX(IC,JC)=CUX+SX*SP
      VY(IC,JC)=CUY+SY*YP
      VV=V
      I=I-1
      IC=IC-1
      IF(I.LT.-IE(JC)) GO TO 150
      GO TO 20
   50 CONTINUE
C          ADHESION AT L.E.
      IF(CUX.GT.0.) GO TO 41
      T=-1.
      GO TO 42
   41 T=1.
   42 CONTINUE
      THV=T*ATAN((UY+PH*P)/(ABS(CUX)+.00000001))+PI*(1.-T)/2.
   30 PN=I*H
      XN=CUX*(PG-PN)/SX+XG
      YN=(UY+.5*PH*(PG+PN))*(PG-PN)/SY+YG
      CALL AMAAKZ(PN,Q,ZN,CZ,CZP,A,B,AMUZ)
      V=ZN-SQRT(XN*XN+YN*YN)
      IF(V.LT.-.00004*AMUZ) GO TO 31
C          TRUE/SLIP                FALSE/STICK
      GO TO 36
   31 CONTINUE
C          SLIP
      IF(ABS(VV).LT..0000000001) GO TO 32
      AN=VV/(VV-V)
      GO TO 33
   32 AN=.9
   33 CONTINUE
      AV=1.-AN
      P=AV*P+AN*PN
      G(JC,NPIJL)=P
      VV=0.
      NPIJL=NPIJL+1
      XV=AV*XV+AN*XN
      YV=AV*YV+AN*YN
```

```
      IF(NPIJL.GT.10) NPIJL=10
      IF(XV.GT.0.) GO TO 34
      T=-1.
      GO TO 35
   34 T=1.
   35 CONTINUE
      CUY=UY+PH*P
      T=T*ATAN(YV/(ABS(XV)+.00000001))+PI*(1.-T)/2.
      C=COS(T)
      S=SIN(T)
      CALL AMAAKZ(P,Q,ZN,CZ,CZP,A,B,AMUZ)
      GO TO 40
   36 VV=V
C          STICK
      X(IC,JC)=XN
      XV=XN
      Y(IC,JC)=YN
      YV=YN
      VX(IC,JC)=0.
      VY(IC,JC)=0.
      I=I-1
      IC=IC-1
      P=PN
      IF(I.GE.-IE(JC)) GO TO 30
  150 CONTINUE
C          THE ARRAYS ARE FILLED. THE INTEGRALS ARE DETERMINED.
      T=4.*AK/3.
      TN=2.*AK
      FX=0.
      FY=0.
      AMZ=0.
      YN=2.*H
      KSET=2*NY-1
      J=-(KSET-1)/2-1
      DO 80 JC=1,KSET
      J=J+1
      I=IE(JC)
      IC=MIE+I+2
      ID=IC-2*I
      NPIJL=I
      P=(ALE(JC)-I*H)/2.-H/3.
      YP=J*AK
      C=P*(X(IC,JC)+X(ID,JC))
      S=P*(Y(IC,JC)+Y(ID,JC))
      D=P*I*H*(Y(IC,JC)-Y(ID,JC))
      P=2.*H/3.
      I=-NPIJL-1
      DO 90 ICC=ID,IC
      I=I+1
      C=C+P*X(ICC,JC)
      D=D+P*I*H*Y(ICC,JC)
      S=S+P*Y(ICC,JC)
      P=YN-P
   90 CONTINUE
      FX=FX+T*C
      FY=FY+T*S
      AMZ=AMZ+T*(D-YP*C)
      T=TN-T
   80 CONTINUE
```

```
      RETURN
      END
      SUBROUTINE AMAAKZ(P,Q,WZ,DZ,D2Z,A,B,AMUZ)
      AL=.9
      S=SQRT(1.-AL*AL)
      AW=A*SQRT(1.-Q*Q/B/B)
      PI=3.1415926536
      F=AMUZ*PI/2./A/(ATAN(AL/S)+(2./3.-AL+AL*AL*AL/3.)/S)
      IF(P.GT.(AL*AW)) GO TO 10
      WZ=F*SQRT(AW*AW-P*P)-F/2.*AW*S
      DZ=F*P/SQRT(AW*AW-P*P)
      GO TO 20
   10 WZ=F*(AW*AW-P*P)/2./AW/S
      DZ=F*P/AW/S
      D2Z=F/AW/S
   20 CONTINUE
      RETURN
      END
      SUBROUTINE RAILAT
      COMMON/RAIL/YT(6),ZT(6),AL(5),BL(5),RL(5)
C          FORMATS
    1 FORMAT(6F0.0)
    2 FORMAT(3X,4HZCR=,F8.6,3X,4HZDR=,F8.6,3X,5HABCR=,F8.6,3X,4HBBC=,F8
     16,3X,4HYBR=,F8.6,3X,4HZBT=,F8.6)
    3 FORMAT(3X,5HAABR=,F8.6,3X,4HBAB=,F8.6,3X,4HYAR=,F8.6,3X,4HZAT=,F8
     16)
    4 FORMAT(3X,5HYTOP=,F8.6,3X,5HZTOP=,F8.6)
    5 FORMAT(3X,4HYTO=,F9.6,3X,4HZTO=,F9.6)
    6 FORMAT(20X,12HRAIL PROFILE)
    7 FORMAT(2X,6HYT(1)=,F9.6,2X,6HYT(2)=,F9.6,2X,6HYT(3)=,F9.6,2X,6HYT
     14)=,F9.6,2X,6HYT(5)=,F9.6,2X,6HYT(6)=,F9.6,2X,6HYTMAX=,F9.6)
    8 FORMAT(2X,6HZT(1)=,F9.6,2X,6HZT(2)=,F9.6,2X,6HZT(3)=,F9.6,2X,6HZT
     14)=,F9.6,2X,6HZT(5)=,F9.6,2X,6HZT(6)=,F9.6,2X,6HZTMAX=,F9.6)
    9 FORMAT(3X,6HAL(1)=,F9.6,3X,6HAL(2)=,F9.6,3X,6HAL(3)=,F9.6,3X,6HAL
     14)=,F9.6,3X,6HAL(5)=,F9.6)
   10 FORMAT(3X,6HBL(1)=,F9.6,3X,6HBL(2)=,F9.6,3X,6HBL(3)=,F9.6,3X,6HBL
     14)=,F9.6,3X,6HBL(5)=,F9.6)
   11 FORMAT(3X,6HRL(1)=,F9.6,3X,6HRL(2)=,F9.6,3X,6HRL(3)=,F9.6,3X,6HRL
     14)=,F9.6,3X,6HRL(5)=,F9.6)
   12 FORMAT(//)
   13 FORMAT(3X,5HABCL=,F10.6,2X,4HYBL=,F10.6,2X,5HZBTL=,F10.6)
   14 FORMAT(3X,5HAABL=,F8.6,3X,5HBABL=,F8.6,3X,4HYAL=,F8.6,3X,5HZATL=,
C
     18.6)
      READ(1,1)R1,R2,RCI,RCO,YDR,W
      YDR=YDR/2.
      YCR=-YDR
      ZCR=R1-SQRT(R1*R1-YCR*YCR)
      ZDR=R1-SQRT(R1*R1-YDR*YDR)
      ACD=0.
      BCD=R1
      ABCR=(R1-R2)*YDR/R1
      ABCL=-ABCR
      B2=(ABCR/YDR)*(R1-ZCR)
      BBC=R1-B2
      DA=W/2.-RCO-ABCR
      FA=W/2.-RCI-ABCR
      BC=R2*DA/(R2-RCO)
      BCL=R2*FA/(R2-RCI)
```

```
      YBR=ABCR+BC
      YBL=ABCL-BCL
      ZBT=BBC-SQRT(R2*R2-(YBR-ABCR)*(YBR-ABCR))
      ZBTL=BBC-SQRT(R2*R2-(YBL-ABCL)*(YBL-ABCL))
      BO=BBC-ZBT
      BOL=BBC-ZBTL
      AO=BO*(R2-RCO)/R2
      AOL=BOL*(R2-RCI)/R2
      BAB=BBC-AO
      BABL=BBC-AOL
      AABR=W/2.-RCO
      AABL=-W/2.+RCI
      HT=RCO/20.
      HTL=RCI/20.
      ZAT=BAB-HT
      ZATL=BABL-HTL
      FL=SQRT(RCO*RCO-HT*HT)
      FLL=SQRT(RCI*RCI-HTL*HTL)
      YAR=AABR+FL
      YAL=AABL-FLL
      WRITE(2,6)
      WRITE(2,12)
      WRITE(2,2)ZCR,ZDR,ABCR,BBC,YBR,ZBT
      WRITE(2,14)AABL,BABL,YAL,ZATL
      WRITE(2,3)AABR,BAB,YAR,ZAT
      WRITE(2,13)ABCL,YBL,ZBTL
C TO CALCULATE POINT AT WHICH A 1/20 LINE IS TANGENT TO THE RAILHEAD.
      AM=SQRT(399.)
      AM=1./AM
      AM1=ABCR+AM*BBC
      AM2=AM
      ZA=1.+AM*AM
      ZB=-2.*(AM1-ABCR)*AM-2.*BBC
      ZC=(AM1-ABCR)*(AM1-ABCR)+BBC*BBC-R2*R2
      ZTOP=-ZB-SQRT(ZB*ZB-4.*ZA*ZC)
      ZTOP=ZTOP/(2.*ZA)
      YTOP=AM1-AM2*ZTOP
      WRITE(2,4)YTOP,ZTOP
C             YTOP  = POSITION OF TOP OF RAIL WHEN CANTED OVER (Y R/H)
C             ZTOP  = POSITION OF TOP OF RAIL WHEN CANTED OVER (Z R/H)
C TO FIND ORIGIN OF RAILHEAD AXES IN TRACK AXES,YTO AND ZTO
      SP=1./20.
      CP=SQRT(399.)/20.
      ZTO=-.75-ZTOP*CP+YTOP*SP
      YTO=28.1875-YAL*CP-ZAT*SP
      WRITE(2,5)YTO,ZTO
C  COORDINATES OF POINTS IN TRACK AXES.
      YT(1)=YTO+YAL*CP+ZATL*SP
      YT(2)=YTO+YBL*CP+ZBTL*SP
      YT(3)=YTO+YCR*CP+ZCR*SP
      YT(4)=YTO+YDR*CP+ZDR*SP
      YTMAX=YTO+YTOP*CP+ZTOP*SP
      YT(5)=YTO+YBR*CP+ZBT*SP
      YT(6)=YTO+YAR*CP+ZAT*SP
      WRITE(2,7)(YT(I),I=1,6),YTMAX
      ZT(1)=ZTO+ZATL*CP-YAL*SP
      ZT(2)=ZTO+ZBTL*CP-YBL*SP
      ZT(3)=ZTO+ZCR*CP-YCR*SP
      ZT(4)=ZTO+ZDR*CP-YDR*SP
```

```
      ZTMAX=ZTO+ZTOP*CP-YTOP*SP
      ZT(5)=ZTO+ZBT*CP-YBR*SP
      ZT(6)=ZTO+ZAT*CP-YAR*SP
      WRITE(2,8)(ZT(I),I=1,6),ZTMAX
      AL(1)=YTO+AABL*CP+BABL*SP
      AL(2)=YTO+ABCL*CP+BBC*SP
      AL(3)=YTO+ACD*CP+BCD*SP
      AL(4)=YTO+ABCR*CP+BBC*SP
      AL(5)=YTO+AABR*CP+BAB*SP
      WRITE(2,9)AL(1),AL(2),AL(3),AL(4),AL(5)
      BL(1)=ZTO+BABL*CP-AABL*SP
      BL(2)=ZTO+BBC*CP-ABCL*SP
      BL(3)=ZTO+BCD*CP-ACD*SP
      BL(4)=ZTO+BBC*CP-ABCR*SP
      BL(5)=ZTO+BAB*CP-AABR*SP
      WRITE(2,10)BL(1),BL(2),BL(3),BL(4),BL(5)
      RL(1)=RCI
      RL(2)=R2
      RL(3)=R1
      RL(4)=R2
      RL(5)=RCO
      WRITE(2,11)RL(1),RL(2),RL(3),RL(4),RL(5)
C
      RETURN
      END
      SUBROUTINE FR1(Y,Z,K)
      COMMON/RAIL/YT(6),ZT(6),AL(5),BL(5),RL(5)
      IF(K.EQ.2) GO TO 100
      IF(Z.GE.ZT(1)) Y=YT(1)
      IF(Z.LT.ZT(1).AND.Z.GT.ZT(2)) Y=AL(1)-SQRT(RL(1)*RL(1)-(Z-BL(1))*
     1Z-BL(1)))
      IF(Z.EQ.ZT(2)) Y=YT(2)
      IF(Z.LT.ZT(2).AND.Z.GT.ZT(3)) Y=AL(2)-SQRT(RL(2)*RL(2)-(Z-BL(2))*
     1Z-BL(2)))
      IF(Z.EQ.ZT(3)) Y=YT(3)
      IF(Z.LT.ZT(3).AND.Z.GT.ZT(4)) Y=AL(3)-SQRT(RL(3)*RL(3)-(Z-BL(3))*
     1Z-BL(3)))
      IF(Z.EQ.ZT(4)) Y=YT(4)
      IF(Z.LT.ZT(4).AND.Z.GE.-.75)  Y=AL(4)-SQRT(RL(4)*RL(4)-(Z-BL(4))*
     1Z-BL(4)))
      IF(Z.LT.-.75) Y=100.
C             IF Z<-.75  PROGRAM PUTS Z=100.
      GO TO 200
  100 CONTINUE
      IF(Y.LT.YT(1)) Z=10.
      IF(Y.EQ.YT(1)) Z=ZT(1)
      IF(Y.GT.YT(1).AND.Y.LT.YT(2)) Z=BL(1)-SQRT(RL(1)*RL(1)-(Y-AL(1))*
     1Y-AL(1)))
      IF(Y.EQ.YT(2)) Z=ZT(2)
      IF(Y.GT.YT(2).AND.Y.LT.YT(3)) Z=BL(2)-SQRT(RL(2)*RL(2)-(Y-AL(2))*
     1Y-AL(2)))
      IF(Y.EQ.YT(3)) Z=ZT(3)
      IF(Y.GT.YT(3).AND.Y.LT.YT(4)) Z=BL(3)-SQRT(RL(3)*RL(3)-(Y-AL(3))*
     1Y-AL(3)))
      IF(Y.EQ.YT(4)) Z=ZT(4)
      IF(Y.GT.YT(4).AND.Y.LT.YT(5)) Z=BL(4)-SQRT(RL(4)*RL(4)-(Y-AL(4))*
     1Y-AL(4)))
      IF(Y.EQ.YT(5)) Z=ZT(5)
      IF(Y.GT.YT(5).AND.Y.LT.YT(6)) Z=BL(5)-SQRT(RL(5)*RL(5)-(Y-AL(5))*
```

```
     1Y-AL(5)))
      IF(Y.EQ.YT(6)) Z=ZT(6)
      IF(Y.GT.YT(6)) Z=10.
C               IF Y<YT(1) OR Y>YT(6) PROGRAM PUTS Z=10.
  200 CONTINUE
      RETURN
      END
      SUBROUTINE WHEEL
      COMMON/WEEEL/QM(2),C(2),BN(4),AN(4),YW(7),ZW(7),RD(4)
C          FORMATS
   10 FORMAT(8F10.0)
  523 FORMAT(8H  ZW(1)=,F9.6,8H  ZW(2)=,F9.6,8H  ZW(3)=,F9.6,8H  ZW(4)=
     1F9.6,8H  ZW(5)=,F9.6,8H  ZW(6)=,F9.6,8H  ZW(7)=,F9.6)
   30 FORMAT(20X,13HWHEEL PROFILE)
   40 FORMAT(//)
  522 FORMAT(8H  YW(1)=,F9.6,8H  YW(2)=,F9.6,8H  YW(3)=,F9.6,8H  YW(4)=
     1F9.6,8H  YW(5)=,F9.6,8H  YW(6)=,F9.6,8H  YW(7)=,F9.6)
  524 FORMAT(8H  AN(1)=,F9.6,8H  AN(2)=,F9.6,8H  AN(3)=,F9.6,8H  AN(4)=
     1F9.6)
  525 FORMAT(8H  BN(1)=,F9.6,8H  BN(2)=,F9.6,8H  BN(3)=,F9.6,8H  BN(4)=
     1F9.6)
  526 FORMAT(8H  RD(1)=,F9.6,8H  RD(2)=,F9.6,8H  RD(3)=,F9.6,8H  RD(4)=
     1F9.6)
  527 FORMAT(8H  QM(1)=,F9.6,8H  QM(2)=,F9.6)
  528 FORMAT(8H   C(1)=,F9.6,8H   C(2)=,F9.6)
      R=14.8
      YW(1)=30.7125
      YW(2)=30.3125
      YW(7)=27.2375
      YA=29.5625
      Z7=1.18
      AN(1)=30.3125
      AN(2)=29.3125
      AN(3)=28.4375
      RD(1)=13.
      RD(2)=4.
      RD(3)=.5
      RD(4)=.7
      BN(1)=R+SQRT(169.-(YA-AN(1))*(YA-AN(1)))
      C(1)=BN(1)-SQRT(169.-(YW(2)-AN(1))*(YW(2)-AN(1)))
      QM(1)=0.
      ZW(1)=C(1)
      ZW(2)=C(1)
      YW(3)=YW(2)-(YW(2)-AN(2))*(RD(1))/(RD(1)-RD(2))
      Z3=BN(1)-SQRT(RD(1)*RD(1)-(YW(3)-AN(1))*(YW(3)-AN(1)))
      ZW(3)=Z3
      BN(2)=Z3+SQRT(RD(2)*RD(2)-(YW(3)-AN(2))*(YW(3)-AN(2)))
      YW(4)=AN(2)-4.*(AN(2)-AN(3))/3.5
      Z4=BN(2)-SQRT(RD(2)*RD(2)-(YW(4)-AN(2))*(YW(4)-AN(2)))
      ZW(4)=Z4
      BN(3)=Z4+SQRT(RD(3)*RD(3)-(YW(4)-AN(3))*(YW(4)-AN(3)))
      QM(2)=-TAN(3.141592653589*68./180.)
      BM=1.+1./(QM(2)*QM(2))
      YW(5)=2.*AN(3)*BM-SQRT(4.*AN(3)*AN(3)*BM*BM-4.*BM*(AN(3)*AN(3)*BM
     1RD(3)*RD(3)))
      YW(5)=YW(5)/(2.*BM)
      Z5=BN(3)-SQRT(RD(3)*RD(3)-(YW(5)-AN(3))*(YW(5)-AN(3)))
      ZW(5)=Z5
      C(2)=Z5-QM(2)*YW(5)
```

```
      ZCB=SQRT((RD(4)*RD(4))/(1.+QM(2)*QM(2)))
      YCA=-QM(2)*ZCB
      YK3=C(2)+QM(2)*YCA-ZCB
      Z7=R+Z7
      YK4=Z7-YK3
      YKA=1.+QM(2)*QM(2)
      ZW(7)=Z7
      YKB=-2.*YW(7)-2.*QM(2)*YK4
      YKC=YW(7)*YW(7)+YK4*YK4-RD(4)*RD(4)
      AN(4)=-YKB+SQRT(YKB*YKB-4.*YKA*YKC)
      AN(4)=AN(4)/(2.*YKA)
      BN(4)=QM(2)*AN(4)+YK3
      YW(6)=AN(4)+YCA
      ZW(6)=YW(6)*QM(2)+C(2)
      WRITE(2,20)
   20 FORMAT(////)
      WRITE(2,30)
      WRITE(2,40)
      WRITE(2,522)(YW(I),I=1,7)
      WRITE(2,523)(ZW(I),I=1,7)
      WRITE(2,524)(AN(I),I=1,4)
      WRITE(2,525)(BN(I),I=1,4)
      WRITE(2,526)(RD(I),I=1,4)
      WRITE(2,527)QM(1),QM(2)
      WRITE(2,528)C(1),C(2)
C
      RETURN
      END
      SUBROUTINE FINDH(H,Y)
      COMMON/RAIL/YT(6),ZT(6),AL(5),BL(5),RL(5)/WEEEL/QM(2),C(2),BN(4),
     1N(4),YW(7),ZW(7),RD(4)
C          Y = APPROX POSITION OF CONTACT POINT
      Y=29.127504
   30 Y=Y-.0001
      IF(YT(5)-Y)40,41,42
   40 WRITE(2,140)
  140 FORMAT(10X,20HY GREATER THAN YT(5))
      GO TO 99
  140 F/."A;R10JV20HK G.EA;E. :HAX K;R5EE
   41 Z=ZT(5)
      DZDY=0.0000000001
      GO TO 100
   42 IF(YT(4)-Y)43,44,45
   43 Z=BL(4)-SQRT(RL(4)*RL(4)-(Y-AL(4))*(Y-AL(4)))
      DZDY=(AL(4)-Y)/(Z-BL(4))
      GO TO 100
   44 Z=ZT(4)
      G/.;/100
   44 SY$;R4E
      DZDY=(AL(4)-Y)/(Z-BL(4))
      GO TO 100
   45 IF(YT(3)-Y)46,47,48
   46 Z=BL(3)-SQRT(RL(3)*RL(3)-(Y-AL(3))*(Y-AL(3)))
      DZDY=(AL(3)-Y)/(Z-BL(3))
      GO TO 100
   47 Z=ZT(3)
      DZDY=(AL(3)-Y)/(Z-BL(3))
      GO TO 100
   48 IF(YT(2)-Y)49,50,51
```

```
      49 Z=BL(2)-SQRT(RL(2)*RL(2)-(Y-AL(2))*(Y-AL(2)))
         DZDY=(AL(2)-Y)/(Z-BL(2))
         GO TO 100
      50 Z=ZT(2)
         DZDY=(AL(2)-Y)/(Z-BL(2))
         GO TO 100
      51 IF(YT(1)-Y)52,52,53
      52 Z=BL(1)-SQRT(RL(1)*RL(1)-(Y-AL(1))*(Y-AL(1)))
         DZDY=(AL(1)-Y)/(Z-BL(1))
         GO TO 100
      53 WRITE(2,54)
      54 FORMAT(10X,17HY LESS THAN YT(1))
         GO TO 99
C     Y,Z AND DZ/DY ARE NOW KNOWN AND CAN BE PUT IN THE WHEEL EQUATIONS
     100 IF(YW(2)-Y)60,62,62
      60 WRITE(2,4)
       4 FORMAT(10X,39HCONTACT POINT ON WHEEL BETWEEN 1 AND 2.)
         GO TO 99
      62 IF(YW(3)-Y)63,63,65
      63 D2=1.+1./(DZDY*DZDY)
         Y2=SQRT((2.*AN(1)*D2)*(2.*AN(1)*D2)-4.*D2*(AN(1)*AN(1)*D2-RD(1)*R
        1(1)))
         Y21=(2.*AN(1)*D2+Y2)/(2.*D2)
         Y22=(2.*AN(1)*D2-Y2)/(2.*D2)
         YA1=ABS(Y-Y21)
         YA2=ABS(Y-Y22)
C        LIMIT OF JUMPING OUT OF LOOP = .0001
         IF(YA1.LT..0001) GO TO 150
         IF(YA2.LT..0001) GO TO 150
         GO TO 30
     150 H=(AN(1)-Y)/DZDY+BN(1)-Z
         GO TO 200
      65 IF(YW(4)-Y)66,66,67
      66 D2=1.+1./(DZDY*DZDY)
         Y2=SQRT((2.*AN(2)*D2)*(2.*AN(2)*D2)-4.*D2*(AN(2)*AN(2)*D2-RD(2)*R
        1(2)))
         Y21=(2.*AN(2)*D2+Y2)/(2.*D2)
         Y22=(2.*AN(2)*D2-Y2)/(2.*D2)
         YA1=ABS(Y-Y21)
         YA2=ABS(Y-Y22)
         IF(YA1.LT..0001) GO TO 151
         IF(YA2.LT..0001) GO TO 151
         GO TO 30
     151 H=(AN(2)-Y)/DZDY+BN(2)-Z
         GO TO 200
      67 IF(YW(5)-Y)68,68,69
      68 D2=1.+1./(DZDY*DZDY)
         Y2=SQRT((2.*AN(3)*D2)*(2.*AN(3)*D2)-4.*D2*(AN(3)*AN(3)*D2-RD(3)*R
        1(3)))
         Y21=(2.*AN(3)*D2+Y2)/(2.*D2)
         Y22=(2.*AN(3)*D2-Y2)/(2.*D2)
         YA1=ABS(Y-Y21)
         YA2=ABS(Y-Y22)
         IF(YA1.LT..0001) GO TO 152
         IF(YA2.LT..0001) GO TO 152
         IFRKA1(#:((0001[ G/ :/ 152
         GO TO 30
     152 H=(AN(3)-Y)/DZDY+BN(3)-Z
         G/ :/ 30
```

```
      GO TO 200
   69 WRITE(2,5)
    5 FORMAT(10X,38HCONTACT POINT ON WHEEL BETWEEN 5 AND 6)
      GO TO 99
  200 WRITE(2,521)
  521 FORMAT(////)
      WRITE(2,7)
    7 FORMAT(8X,16HCENTRAL POSITION)
      WRITE(2,6)Y,Z,DZDY,H
    6 FORMAT(10X,29HCONTACT POINT (TRACK AXES) Y=,F9.6,4H  Z=,F9.6,8H
     1Z/DY=,F9.6,4H  H=,F9.6)
   99 CONTINUE
      1$+DKYVF9(6V4H-HYVF9(6F
C
      RETURN
      END
      MASTER LATERAL WHEELSET
      DIMENSION YTX(2),ZTX(2),DZX(2),ZOX(2),YR(10,5),ZR(10,5),DR(10,5),
     1OR(10,5),YL(10,5),ZL(10,5),ZOL(10,5),DL(10,5),YWR(10,5),ZWR(10,5)
     2YWL(10,5),ZWL(10,5)
      COMMON/RAIL/YT(6),ZT(6),AL(5),BL(5),RL(5)
      COMMON/WEEEL/QM(2),C(2),BN(4),AN(4),YW(7),ZW(7),RD(4)
C
      CALL RAILAT
      CALL WHEEL
      CALL FINDH(H,YTSO)
C
      YO=.3
      WRITE(2,130)
  130 FORMAT(1H1)
      WRITE(2,140)YO
  140 FORMAT(5X,5HYO = ,F10.6)
C
      TH=.001198
      DO 310 ICOUNT=1,200
      TH=TH+.000002
      SP=SIN(TH)
      CP=COS(TH)
C                                  RIGHT HAND WHEEL
      DO 60 KN=1,5
      AKN=AL(KN)
      BKN=BL(KN)
      RKN=RL(KN)
      CALL STRWH(YO,TH,AKN,BKN,RKN,QM(1),C(1),YR(1,KN),ZR(1,KN),DR(1,KN
     1,ZOR(1,KN),H)
      CALL CIRWH(YO,TH,AKN,BKN,RKN,AN(1),BN(1),RD(1),H,YTX,ZTX,DZX,ZOX)
      DO 20 I=1,2
      K=I+1
      YR(K,KN)=YTX(I)
      ZR(K,KN)=ZTX(I)
      DR(K,KN)=DZX(I)
   20 ZOR(K,KN)=ZOX(I)
      CALL CIRWH(YO,TH,AKN,BKN,RKN,AN(2),BN(2),RD(2),H,YTX,ZTX,DZX,ZOX)
      DO 30 I=1,2
      K=I+3
      YR(K,KN)=YTX(I)
      ZR(K,KN)=ZTX(I)
      DR(K,KN)=DZX(I)
   30 ZOR(K,KN)=ZOX(I)
```

```
      CALL CIRWH(YO,TH,AKN,BKN,RKN,AN(3),BN(3),RD(3),H,YTX,ZTX,DZX,ZOX)
      DO 40 I=1,2
      K=I+5
      YR(K,KN)=YTX(I)
      ZR(K,KN)=ZTX(I)
      DR(K,KN)=DZX(I)
   40 ZOR(K,KN)=ZOX(I)
      CALLSTRWH(YO,TH,AKN,BKN,RKN,QM(2),C(2),YR(8,KN),ZR(8,KN),DR(8,KN)
     1ZOR(8,KN),H)
      CALL CIRWH(YO,TH,AKN,BKN,RKN,AN(4),BN(4),RD(4),H,YTX,ZTX,DZX,ZOX)
      DO 50 I=1,2
      K=I+8
      YR(K,KN)=YTX(I)
      ZR(K,KN)=ZTX(I)
      DR(K,KN)=DZX(I)
   50 ZOR(K,KN)=ZOX(I)
   60 CONTINUE
C                                   LEFT HAND WHEEL
      DO 70 KN=1,5
      AKN=-AL(KN)
      BKN=BL(KN)
      RKN=RL(KN)
      CALL STRWH(YO,TH,AKN,BKN,RKN,-QM(1),C(1),YL(1,KN),ZL(1,KN),DL(1,K
     1),ZOL(1,KN),H)
      CALL CIRWH(YO,TH,AKN,BKN,RKN,-AN(1),BN(1),RD(1),H,YTX,ZTX,DZX,ZOX
      DO 80 I=1,2
      K=I+1
      YL(K,KN)=YTX(I)
      ZL(K,KN)=ZTX(I)
      DL(K,KN)=DZX(I)
   80 ZOL(K,KN)=ZOX(I)
      CALL CIRWH(YO,TH,AKN,BKN,RKN,-AN(2),BN(2),RD(2),H,YTX,ZTX,DZX,ZOX
      DO 90 I=1,2
      K=I+3
      YL(K,KN)=YTX(I)
      ZL(K,KN)=ZTX(I)
      DL(K,KN)=DZX(I)
   90 ZOL(K,KN)=ZOX(I)
      CALL CIRWH(YO,TH,AKN,BKN,RKN,-AN(3),BN(3),RD(3),H,YTX,ZTX,DZX,ZOX
      DO 100 I=1,2
      K=I+5
      YL(K,KN)=YTX(I)
      ZL(K,KN)=ZTX(I)
      DL(K,KN)=DZX(I)
  100 ZOL(K,KN)=ZOX(I)
      CALL STRWH(YO,TH,AKN,BKN,RKN,-QM(2),C(2),YL(8,KN),ZL(8,KN),DL(8,K
     1),ZOL(8,KN),H)
      CALL CIRWH(YO,TH,AKN,BKN,RKN,-AN(4),BN(4),RD(4),H,YTX,ZTX,DZX,ZOX
      DO 110 I=1,2
      K=I+8
      YL(K,KN)=YTX(I)
      ZL(K,KN)=ZTX(I)
      DL(K,KN)=DZX(I)
  110 ZOL(K,KN)=ZOX(I)
   70 CONTINUE
C         CHANGING TO WHEELSET AXES
      DO 120 I=1,5
      DO 120 J=1,10
      YWR(J,I)=(ZOR(J,I)-ZR(J,I)-H)*SP+(YR(J,I)-YO)*CP
```

```
      YWL(J,I)=(ZOL(J,I)-ZL(J,I)-H)*SP+(YL(J,I)-YO)*CP
      ZWR(J,I)=(ZR(J,I)+H-ZOR(J,I))*CP+(YR(J,I)-YO)*SP
  120 ZWL(J,I)=(ZL(J,I)+H-ZOL(J,I))*CP+(YL(J,I)-YO)*SP
      WRITE(2,150)
  150 FORMAT(//)
      WRITE(2,160)TH
  160 FORMAT(30X,8HTHETA = ,E13.6)
      WRITE(2,170)
  170 FORMAT(/)
      WRITE(2,430)
  430 FORMAT(10X,35HPOSSIBLE RIGHT HAND WHEEL SOLUTIONS)
      DO 400 IA=1,5
      DO 400 IB=1,10
      IF(IB.EQ.1) GO TO 410
      IF(IB.EQ.2) GO TO 411
      IF(IB.EQ.3) GO TO 411
      IF(IB.EQ.4) GO TO 412
      IF(IB.EQ.5) GO TO 412
      IF(IB.EQ.6) GO TO 413
      IF(IB.EQ.7) GO TO 413
      IF(IB.EQ.8) GO TO 414
      IF(IB.EQ.9) GO TO 415
      GO TO 415
  410 IC=1
      GO TO 420
  411 IC=2
      GO TO 420
  412 IC=3
      GO TO 420
  413 IC=4
      GO TO 420
  414 IC=5
      GO TO 420
  415 IC=6
  420 CONTINUE
      IF(IB.EQ.6.AND.IA.EQ.2) GO TO 400
      IF(IB.EQ.7.AND.IA.EQ.2) GO TO 400
      IF(IB.EQ.4.AND.IA.EQ.3) GO TO 400
      IF(IB.EQ.5.AND.IA.EQ.3) GO TO 400
      IF(IB.EQ.6.AND.IA.EQ.3) GO TO 400
      IF(IB.EQ.7.AND.IA.EQ.3) GO TO 400
      IF(IB.EQ.6.AND.IA.EQ.4) GO TO 400
      IF(IB.EQ.7.AND.IA.EQ.4) GO TO 400
      IF(YR(IB,IA).LT.YT(IA).OR.YR(IB,IA).GT.YT(IA+1)) GO TO 400
      IF(ZR(IB,IA).GT.ZT(IA).OR.ZR(IB,IA).LT.ZT(IA+1)) GO TO 400
      IF(YWR(IB,IA).GT.YW(IC).OR.YWR(IB,IA).LT.YW(IC+1)) GO TO 400
      IF(ZOR(IB,IA).GT.1..OR.ZOR(IB,IA).LT.-1.) GO TO 400
      WRITE(2,440)YR(IB,IA),ZR(IB,IA),YWR(IB,IA),ZOR(IB,IA),IB,IA
  440 FORMAT(10X,5HYT = ,E13.6,5X,5HZT = ,E13.6,5X,5HYW = ,E13.6,5X,5HZ
     1 = ,E13.6,5X,1H(,I2,1H,,I1,1H))
  400 CONTINUE
      WRITE(2,170)
      WRITE(2,450)
  450 FORMAT(10X,34HPOSSIBLE LEFT HAND WHEEL SOLUTIONS)
      DO 500 IA=1,5
      DO 500 IB=1,10
      IF(IB.EQ.1) GO TO 510
      IF(IB.EQ.2) GO TO 511
      IF(IB.EQ.3) GO TO 511
```

```
      IF(IB.EQ.4) GO TO 512
      IF(IB.EQ.5) GO TO 512
      IF(IB.EQ.6) GO TO 513
      IF(IB.EQ.7) GO TO 513
      IF(IB.EQ.8) GO TO 514
      IF(IB.EQ.9) GO TO 515
      GO TO 515
  510 IC=1
      GO TO 520
  511 IC=2
      GO TO 520
  512 IC=3
      GO TO 520
  513 IC=4
      GO TO 520
  514 IC=5
      GO TO 520
  515 IC=6
  520 CONTINUE
      IF(IB.EQ.6.AND.IA.EQ.2) GO TO 500
      IF(IB.EQ.7.AND.IA.EQ.2) GO TO 500
      IF(IB.EQ.4.AND.IA.EQ.3) GO TO 500
      IF(IB.EQ.5.AND.IA.EQ.3) GO TO 500
      IF(IB.EQ.6.AND.IA.EQ.3) GO TO 500
      IF(IB.EQ.7.AND.IA.EQ.3) GO TO 500
      IF(IB.EQ.6.AND.IA.EQ.4) GO TO 500
      IF(IB.EQ.7.AND.IA.EQ.4) GO TO 500
      IF(YL(IB,IA).GT.-YT(IA).OR.YL(IB,IA).LT.-YT(IA+1)) GO TO 500
      IF(YWL(IB,IA).LT.-YW(IC).OR.YWL(IB,IA).GT.-YW(IC+1)) GO TO 500
      IF(ZOL(IB,IA).GT.1..OR.ZOL(IB,IA).LT.-1.) GO TO 500
      WRITE(2,440)YL(IB,IA),ZL(IB,IA),YWL(IB,IA),ZOL(IB,IA),IB,IA
  500 CONTINUE
  310 CONTINUE
 1000 CONTINUE
      STOP
      END
      SUBROUTINE STRWH(YO,TH,A,B,R,Q,C,YT,ZT,DZT,ZO,H)
      SP=SIN(TH)
      CP=COS(TH)
      DZT=(Q*CP-SP)/(CP+Q*SP)
      ZT=B-R/(SQRT(DZT*DZT+1.))
      YT=A-DZT*(ZT-B)
      ZO=YT*(SP-Q*CP)+ZT*(CP+Q*SP)-YO*(SP-Q*CP)-C
      ZO=ZO/(CP+Q*SP)
      ZO=ZO+H
      RETURN
      END
      SUBROUTINE CIRWH(YO,TH,A,B,R,AN,BN,RD,H,YTX,ZTX,DZX,ZOX)
      DIMENSION RI(2),YTX(2),ZTX(2),DZX(2),ZOX(2)
      SP=SIN(TH)
      CP=COS(TH)
      XK1=(AN*SP-BN*CP)*(AN*SP-BN*CP)-AN*AN-BN*BN+RD*RD+(AN*CP+BN*SP)*(
     1N*CP+BN*SP)
      A1=R*R-XK1
      B1=-2.*YO*R*R-2.*AN*CP*R*R-2.*BN*SP*R*R+2.*A*XK1
      C1=R*R*(YO*YO+2.*YO*(AN*CP+BN*SP)+AN*AN*CP*CP+2.*AN*BN*CP*SP+BN*B
     1*SP*SP)-A*A*XK1
      BRA=B1*B1-4.*A1*C1
      IF(A1.EQ.0.) GO TO 31
```

```
      IF(BRA.LT.0.) GO TO 31
      RI(1)=(-B1+SQRT(BRA))/(2.*A1)
      RI(2)=(-B1-SQRT(BRA))/(2.*A1)
      DO 30 I=1,2
      YT=RI(I)
      RR=R*R-(YT-A)*(YT-A)
      IF(RR.LT.0.) GO TO 29
      ZT=B-SQRT(RR)
      DZT=(A-YT)/(ZT-B)
      HDAS=ZT+AN*SP-BN*CP-(ZT-B)*(YO+AN*CP+BN*SP-YT)/(A-YT)
      ZO=HDAS+H
      YTX(I)=YT
      ZTX(I)=ZT
      DZX(I)=DZT
      ZOX(I)=ZO
      GO TO 30
   29 YTX(I)=0.
      ZTX(I)=0.
      DZX(I)=0.
      ZOX(I)=0.
   30 CONTINUE
      GO TO 40
   31 CONTINUE
      DO 32 JJ=1,2
      YTX(JJ)=0.
      ZTX(JJ)=0.
      DZX(JJ)=0.
      ZOX(JJ)=0.
   32 CONTINUE
   40 CONTINUE
      RETURN
      END
#SWITCH
```

GENERAL LISTING (XRLP) 04/07/73

```
      MASTER YAWING WHEELSET
      DIMENSION PS(6)
      COMMON/RAIL/YT(6),ZT(6),AL(5),BL(5),RL(5)
      COMMON/WEEEL/QM(2),C(2),BN(4),AN(4),YW(7),ZW(7),RD(4)
      COMMON/JOH/PSI,H,HL
      COMMON/CON/H11,X,Y,Z,XW3,YW3,ZW31
C          FORMATS
   10 FORMAT(6F10.0)
   12 FORMAT(5X,29HNO SOLUTION IN SECTION 1 TO 2)
   10 F/."A:R6F10(0[
   13 FORMAT(5X,29HNO SOLUTION IN SECTION 2 TO 3)
   14 FORMAT(5X,29HNO SOLUTION IN SECTION 3 TO 4)
   15 FORMAT(5X,29HNO SOLUTION IN SECTION 4 TO 5)
   16 FORMAT(5X,29HNO SOLUTION IN SECTION 5 TO 6)
   17 FORMAT(5X,29HNO SOLUTION IN SECTION 6 TO 7)
   20 FORMAT(1H1)
   21 FORMAT(30X,6HPSI = ,F10.6,7HRADIANS)
   22 FORMAT(/)
      CALL RAILAT
      CALL WHEEL
      CALL FINDH(H,YTSO)
      READ(1,10)(PS(I),I=1,6)
      DO 100 KPS=1,6
      PSI=PS(KPS)/57.3
      WRITE(2,20)
      WRITE(2,21)PSI
      WRITE(2,22)
      NSTOP=1
C          FROM POINT 1 TO POINT 2 ON WHEELSET
      CALL STRGHT2(PSI,QM(1),C(1),H,1,2,NSTOP)
      IF(NSTOP.EQ.2) GO TO 1110
      WRITE(2,12)
C          FROM POINT 2 TO POINT 3 ON WHEELSET
      CALL CIRCLE2(PSI,AN(1),BN(1),RD(1),H,2,3,NSTOP)
      IF(NSTOP.EQ.2) GO TO 1110
      WRITE(2,13)
C          FROM POINT 3 TO POINT 4 ON WHEELSET
      CALL CIRCLE2(PSI,AN(2),BN(2),RD(2),H,3,4,NSTOP)
      IF(NSTOP.EQ.2) GO TO 1110
      WRITE(2,14)
C          FROM POINT 4 TO POINT 5 ON WHEELSET
      CALL CIRCLE2(PSI,AN(3),BN(3),RD(3),H,4,5,NSTOP)
      IF(NSTOP.EQ.2) GO TO 1110
      WRITE(2,15)
C          FROM POINT 5 TO POINT 6 ON WHEELSET
      CALL STRGHT2(PSI,QM(2),C(2),H,5,6,NSTOP)
      IF(NSTOP.EQ.2) GO TO 1110
      WRITE(2,16)
C          FROM POINT 6 TO POINT 7 ON WHEELSET
      CALL CIRCLE2(PSI,AN(4),BN(4),RD(4),H,6,7,NSTOP)
      WRITE(2,17)
 1110 CONTINUE
      CALL JOHANSEN
  100 CONTINUE
      STOP
      END
      SUBROUTINE CIRCLE2(P,A,B,R,H,IP1,IP2,NSTOP)
```

```
      DIMENSION CO(4),RI(4),GI(4),BZ(4),CZ(4)
      COMMON/RAIL/YT(6),ZT(6),AL(5),BL(5),RL(5)
      COMMON/WEEEL/QM(2),C(2),BN(4),AN(4),YW(7),ZW(7),RD(4)
      COMMON/CON/H11,X,Y,Z,XW3,YW3,ZW31
C          FORMATS
   14 FORMAT(//)
   15 FORMAT(6X,45HCOORDINATES OF CONTACT POINT IN TRACK AXES  (,E13.6,
     1H,,E13.6,1H,,E13.6,1H))
   17 FORMAT(/)
   21 FORMAT(6X,22H(DZT/DYT) SHOULD BE = ,E13.6)
   91 FORMAT(10X,6HZTP = ,E13.6)
  212 FORMAT(5X,22HCONTACT POINT BETWEEN ,I1,5H AND ,I1,18H ON WHEELSET
     1  YW(,I1,2H)=,F9.6,5X,3HYW(,I1,2H)=,F9.6)
  213 FORMAT(10X,4HH = ,E13.6)
  214 FORMAT(6X,48HCOORDINATES OF CONTACT POINT IN WHEELSET AXES  (,E13.
     16,1H,,E13.6,1H,,E13.6,1H))
  215 FORMAT(6X,22HCALCULATED(DZT/DYT) = ,E13.6)
    9 FORMAT(10X,22HCONTACT POINT BETWEEN ,I1,5H AND ,I2,40HBUT UNABLE
     10 FIND SOLUTION IN FINE LOOP)
      YW1=YW(IP1)
      YW2=YW(IP2)
      CP=COS(P)
      SP=SIN(P)
      CPP=CP*CP
      SPP=SP*SP
      LOO=1
      ZTP=-.76
      DO 1109 II=1,80
      ZTP=ZTP+.01
      D/ 1109 IIY1V80
C                    ZTP = ASSUMED VALUE OF ZT
      D1 1109 IIK1!80
C                          THIS IS INCREASED IN STEPS OF .01
      D8 1109 II=1<80
C          TO CHECK WHICH PART OF RAIL CURVE ZTP IS IN
      DW 1109 IIY1<80
  103 IF(ZTP-ZT(4))104,105,106
  104 YTP=AL(4)-SQRT(RL(4)*RL(4)-(ZTP-BL(4))*(ZTP-BL(4)))
      DZT=(AL(4)-YTP)/(ZTP-BL(4))
      GO TO 2001
  105 YTP=YT(4)
      DZT=(AL(4)-YTP)/(ZTP-BL(4))
      GO TO 2001
  106 IF(ZTP-ZT(3))107,108,109
  107 YTP=AL(3)-SQRT(RL(3)*RL(3)-(ZTP-BL(3))*(ZTP-BL(3)))
      DZT=(AL(3)-YTP)/(ZTP-BL(3))
      GO TO 2001
  108 YTP=YT(3)
      DZT=(AL(3)-YTP)/(ZTP-BL(3))
      108 K:?YK:R3E
      GO TO 2001
  109 IF(ZTP-ZT(2))110,111,112
  110 YTP=AL(2)-SQRT(RL(2)*RL(2)-(ZTP-BL(2))*(ZTP-BL(2)))
      DZT=(AL(2)-YTP)/(ZTP-BL(2))
      GO TO 2001
  111 YTP=YT(2)
      DZT=(AL(2)-YTP)/(ZTP-BL(2))
      GO TO 2001
  112 IF(ZTP-ZT(1))113,114,114
```

```
      113 YTP=AL(1)-SQRT(RL(1)*RL(1)-(ZTP-BL(1))*(ZTP-BL(1)))
          DZT=(AL(1)-YTP)/(ZTP-BL(1))
          GO TO 2001
      114 YTP=YT(1)
          DZT=99999999999999.
     2001 CONTINUE
          DYT=0.
          GO TO 2003
     2002 IF(LOO-2)1109,31,31
     2003 KAB=1
          Y=YTP
          Z=ZTP
          ALL=1.-CPP
          BLL=2.*A*SP*(2.-CPP)-2.*Y*CP*SP
          CL=Y*Y+A*A*SPP+4.*A*A*SPP-2.*A*Y*CP+A*A+B*B+B*B*CPP*CPP-4.*A*Y*CP*
         1SPP-Y*Y*SPP-2.*B*B*CPP-R*R-A*A*SPP*CPP
          DL=2.*A*Y*Y*SP+2.*A*A*A*SPP*SP-4.*A*A*Y*CP*SP+2.*A*A*A*SP+2.*A*B*B
         1*SP+2.*B*B*Y*CPP*CP*SP-2.*A*A*Y*CP*SPP*SP-2.*A*Y*Y*SPP*SP-2.*B*B*Y
         2*CP*SP-2.*B*B*A*SP*CPP-R*R*2.*A*SP
          EL=Y*Y*A*A*SPP-2.*A*A*A*Y*CP*SPP+A*A*A*A*SPP+A*A*B*B*SPP+B*B*Y*Y*C
         1PP*SPP-A*A*Y*Y*SPP*SPP-2.*B*B*A*Y*CP*SPP-R*R*A*A*SPP
          CO(1)=BLL/ALL
          CO(2)=CL/ALL
          CO(3)=DL/ALL
          CO(4)=EL/ALL
          IF(LOO.EQ.2) GO TO 30
          IJ=4
          CALL Z200B(CO,RI,GI,KAB,IJ,BZ,CZ)
          IF(KAB.EQ.2) GO TO 1109
          DO 81 I=1,4
          IF(GI(I).NE.0.) GO TO 81
          X=RI(I)
       90 B1=(X*CPP+Y*CP*SP)*(X*CPP+Y*CP*SP)*B*B
          B1=B1/((X+A*SP)*(X+A*SP))
          B2=X*X*CPP
          B3=2.*X*Y*CP*SP
          B4=Y*Y*SPP
          B1=B1-B2-B3-B4
          CH=Z*Z-B1
          BH=2.*Z
          BRA=BH*BH-4.*CH
          IF(BRA.LT.0.) GO TO 81
          H11=H+BH/2.-(SQRT(BRA)/2.)
          DZTN=-Y+A*CP+(X+A*SP)*(X*CP*SP+Y*SPP)/(X*CPP+Y*CP*SP)
          DZTD1=Z+H-H11-(X+A*SP)*(Z+H-H11)/(X*CPP+Y*CP*SP)
          DZT1=DZTN/DZTD1
          XW3=CP*X+SP*Y
          YW3=Y*CP-X*SP
          ZW31=Z+H-H11
          RRW31=SQRT(XW3*XW3+ZW31*ZW31)
          IF(YW3.GT.YW1) GO TO 81
```

```
      IF(YW3.LT.YW2) GO TO 81
      IF(RRW31.GT.15.98) GO TO 81
      IF(RRW31.LT.14.778347) GO TO 81
      IF(H11.GT.1..OR.H11.LT.-1.) GO TO 81
      DIF1=DZT-DZT1
      IF(II.EQ.1) GO TO 70
      GO TO 71
   81 CONTINUE
      GO TO 71
      DIF2=0.
      GO TO 1109
   70 DIF2=DIF1
      GO TO 1109
   71 IF(DIF2.EQ.0.) GO TO 72
      IF(DIF1.GT.0..AND.DIF2.LT.0.) GO TO 28
      IF(DIF1.LT.0..AND.DIF2.GT.0.) GO TO 28
   72 DIF2=DIF1
 1109 CONTINUE
      GO TO 982
   28 CONTINUE
      LOO=2
      ZTP=Z-.0101
      DO 31 KK=1,200
      ZTP=ZTP+.0001
      GO TO 103
   30 IJ=4
      CALL Z200B(CO,RI,GI,KAB,IJ,BZ,CZ)
      IF(KAB.EQ.2) GO TO 31
      DO 32 I=1,4
      IF(GI(I).NE.0.) GO TO 32
      X=RI(I)
      B1=+(X*CPP+Y*CP*SP)*(X*CPP+Y*CP*SP)*B*B
      B1=B1/((X+A*SP)*(X+A*SP))
      B2=X*X*CPP
      B3=2.*X*Y*CP*SP
      B4=Y*Y*SPP
      B1=B1-B2-B3-B4
      CH=Z*Z-B1
      BH=2.*Z
      BRA=BH*BH-4.*CH
      IF(BRA.LT.0.) GO TO 32
      H11=H+BH/2.-(SQRT(BRA)/2.)
      DZTN=-Y+A*CP+(X+A*SP)*(X*CP*SP+Y*SPP)/(X*CPP+Y*CP*SP)
      DZTD1=Z+H-H11-(X+A*SP)*(Z+H-H11)/(X*CPP+Y*CP*SP)
      DZT1=DZTN/DZTD1
      XW3=CP*X+SP*Y
      YW3=Y*CP-X*SP
      ZW31=Z+H-H11
      RRW31=SQRT(XW3*XW3+ZW31*ZW31)
      IF(YW3.GT.YW1) GO TO 32
      IF(YW3.LT.YW2) GO TO 32
      IF(H11.GT.1..OR.H11.LT.-1.) GO TO 32
      DIF3=DZT-DZT1
      IF(KK.EQ.1) GO TO 170
      GO TO 171
   32 CONTINUE
      DIF3=0.
```

```
      GO TO 31
  170 DIF4=DIF3
      GO TO 31
  171 CONTINUE
      IF(DIF4.EQ.0.) GO TO 172
      IF(DIF3.GT.0..AND.DIF4.LT.0.) GO TO 128
      IF(DIF3.LT.0..AND.DIF4.GT.0.) GO TO 128
  172 DIF4=DIF3
   31 CONTINUE
      WRITE(2,17)
      WRITE(2,9)IP1,IP2
      WRITE(2,91)Z
      GO TO 981
  128 WRITE(2,17)
      WRITE(2,212)IP1,IP2,IP1,YW1,IP2,YW2
      WRITE(2,14)
      WRITE(2,15)X,Y,Z
      WRITE(2,17)
      WRITE(2,213)H11
      WRITE(2,17)
      WRITE(2,214)XW3,YW3,ZW31
      WRITE(2,17)
      WRITE(2,21)DZT
      WRITE(2,215)DZT1
  981 NSTOP=2
  982 CONTINUE
      RETURN
      END
      SUBROUTINE STRGHT2(P,Q,D,H,IP1,IP2,NSTOP)
      COMMON/RAIL/YT(6),ZT(6),AL(5),BL(5),RL(5)
      COMMON/WEEEL/QM(2),C(2),BN(4),AN(4),YW(7),ZW(7),RD(4)
      COMMON/CON/H11,X,Y,Z,XW3,YW3,ZW31
C          FORMATS
    9 FORMAT(10X,22HCONTACT POINT BETWEEN ,I1,5H AND ,I2,47HBUT METHOD U
     1NABLE TO FIND SOLUTION IN FINE LOOP)
   14 FORMAT(//)
   15 FORMAT(6X,45HCOORDINATES OF CONTACT POINT IN TRACK AXES  (,E13.6,1
     1H,,E13.6,1H,,E13.6,1H))
   17 FORMAT(/)
   21 FORMAT(6X,22H(DZT/DYT) SHOULD BE = ,E13.6)
   91 FORMAT(10X,6HZTP = ,E13.6)
  212 FORMAT(5X,22HCONTACT POINT BETWEEN ,I1,5H AND ,I1,18H ON WHEELSET
     1  YW(,I1,2H)=,F9.6,5X,3HYW(,I1,2H)=,F9.6)
  214 FORMAT(6X,48HCOORDINATES OF CONTACT POINT IN WHEELSET AXES  (,E13.
     16,1H,,E13.6,1H,,E13.6,1H))
  215 FORMAT(6X,22HCALCULATED(DZT/DYT) = ,E13.6)
      PSI=P
      CP=COS(PSI)
      SP=SIN(PSI)
      CPP=CP*CP
      SPP=SP*SP
      L00=1
      Y1=YW(IP1)
      Y2=YW(IP2)
      ZTP=-.76
      DO 1109 I=1,80
      ZTP=ZTP+.01
   29 IF(ZTP-ZT(5))101,102,103
  102 YTP=YT(5)
```

```
      DZT=0.
      GO TO 2001
  103 IF(ZTP-ZT(4))104,105,106
  104 YTP=AL(4)-SQRT(RL(4)*RL(4)-(ZTP-BL(4))*(ZTP-BL(4)))
      DZT=(AL(4)-YTP)/(ZTP-BL(4))
      GO TO 2001
  105 YTP=YT(4)
      DZT=(AL(4)-YTP)/(ZTP-BL(4))
      GO TO 2001
  106 IF(ZTP-ZT(3))107,108,109
  107 YTP=AL(3)-SQRT(RL(3)*RL(3)-(ZTP-BL(3))*(ZTP-BL(3)))
      DZT=(AL(3)-YTP)/(ZTP-BL(3))
      GO TO 2001
  108 YTP=YT(3)
      DZT=(AL(3)-YTP)/(ZTP-BL(3))
      GO TO 2001
  109 IF(ZTP-ZT(2))110,111,112
  110 YTP=AL(2)-SQRT(RL(2)*RL(2)-(ZTP-BL(2))*(ZTP-BL(2)))
      DZT=(AL(2)-YTP)/(ZTP-BL(2))
      GO TO 2001
  111 YTP=YT(2)
      DZT=(AL(2)-YTP)/(ZTP-BL(2))
      GO TO 2001
  112 IF(ZTP-ZT(1))113,114,114
  113 YTP=AL(1)-SQRT(RL(1)*RL(1)-(ZTP-BL(1))*(ZTP-BL(1)))
      DZT=(AL(1)-YTP)/(ZTP-BL(1))
      GO TO 2001
  114 YTP=YT(1)
      DZT=99999999999999.
 2001 CONTINUE
      DYT=0.
  576 XTPN=-YTP*CP*SP-Q*Q*YTP*SP*CP-Q*D*SP
      XTP=XTPN/(CPP-Q*Q*SPP)
      B=2.*ZTP
      BB=B*B
      CB=XTP*XTP*CPP+2.*XTP*YTP*CP*SP+YTP*YTP*SPP+ZTP*ZTP-Q*Q*YTP*YTP*CP
     1P+2.*Q*Q*XTP*YTP*SP*CP-Q*Q*XTP*XTP*SPP-D*D-2.*Q*D*YTP*CP+2.*Q*D*XT
     2P*SP
      BR=SQRT(BB-4.*CB)
      BR=BR/2.
      HP1=H+B/2.-BR
      DZTN=Q*Q*YTP*CPP-Q*Q*XTP*CP*SP+Q*D-XTP*CP*SP-YTP*SPP
      DZT1=DZTN/(ZTP+H-HP1)
      XW3=CP*XTP+SP*YTP
      YW3=YTP*CP-XTP*SP
      ZW31=ZTP+H-HP1
      RRW31=SQRT(XW3*XW3+ZW31*ZW31)
      IF(LOO-2)19,81,81
   19 DIF1=DZT-DZT1
      IF(YW3.GT.Y1) GO TO 23
      IF(YW3.LT.Y2) GO TO 23
      Z1=Y1*Q+D
      Z2=Y2QQ+D
      IF(HP1.GT.1..OR.HP1.LT.-1.) GO TO 23
      IF(I.EQ.1) GO TO 23
      IF(DIF1.GT.0..AND.DIF2.LT.0.) GO TO 25
      IF(DIF1.LT.0..AND.DIF2.GT.0.) GO TO 25
      GO TO 23
   25 LOO=2
```

```
      ZTP=ZTP-.0101
      DO 28 KK=1,200
      ZTP=ZTP+.0001
      GO TO 29
   81 DIF1=DZT-DZT1
      IF(YW3.GT.Y1) GO TO 27
      IF(YW3.LT.Y2) GO TO 27
      IF(HP1.GT.1..OR.HP1.LT.-1.) GO TO 27
      IF(KK.EQ.1) GO TO 27
      IF(DIF1.GT.0..AND.DIF2.LT.0.) GO TO 30
      IF(DIF1.LT.0..AND.DIF2.GT.0.) GO TO 30
   27 DIF2=DIF1
   28 CONTINUE
      GO TO 428
   23 DIF2=DIF1
  101 CONTINUE
 1109 CONTINUE
      GO TO 1999
  428 WRITE(2,17)
      WRITE(2,9)IP1,IP2
      WRITE(2,91)ZTP
      GO TO 2000
   30 WRITE(2,17)
      WRITE(2,212)IP1,IP2,IP1,Y1,IP2,Y2
      WRITE(2,14)
      WRITE(2,15)XTP,YTP,ZTP
      WRITE(2,17)
      WRITE(2,18)HP1
   18 FORMAT(10X,4HH = ,E13.6)
      WRITE(2,17)
      WRITE(2,214)XW3,YW3,ZW31
      WRITE(2,17)
      WRITE(2,21)DZT
      WRITE(2,215)DZT1
 2000 NSTOP=2
 1999 CONTINUE
      H11=HP1
      X=XTP
      Y=YTP
      Z=ZTP
      RETURN
      END
      SUBROUTINE Z200B(A,R,GI,KAD,N,B,C)
      DIMENSION A(N),B(N),C(N),R(N),GI(N)
      ABSF(X)=ABS(X)
      SQRTF(X) = SQRT(X)
      NUMBER=1
      ERROR=.000001
      DO 350 IJKLM=1,NUMBER
      IT=0
      KR=0
   34 IF(N-1)35,4,6
    4 G=-A(1)
      E=0.
      KR=KR+1
      R(KR)=G
      GI(KR)=E
      GO TO 35
    6 IF(N-2)7,7,8
```

```
      7 P=A(1)
        Q=A(2)
        GO TO 28
      8 CONTINUE
     82 P=A(1)
        Q=A(2)
     84 M=1
      9 B(1)=A(1)-P
        B(2)=A(2)-P*B(1)-Q
        DO 10 K=3,N
     10 B(K)=A(K)-P*B(K-1)-Q*B(K-2)
        L=N-1
        C(1)=B(1)-P
        C(2)=B(2)-P*C(1)-Q
        DO 11 J=3,L
     11 C(J)=B(J)-P*C(J-1)-Q*C(J-2)
        DIFF=C(L)-B(L)
        IF(N-3)13,12,13
     12 D=C(N-2)*C(N-2)-DIFF
        GO TO 14
     13 D=C(N-2)*C(N-2)-DIFF*C(N-3)
     14 IF(D)17,15,17
     15 KAD=2
        WRITE(2,16)
     16 FORMAT(29H DIVIDED BY ZERO METHOD FAILS )
        GO TO 35
     17 IF(N-3)19,18,19
     18 DELTP=(B(N-1)*C(N-2)-B(N))/D
        GO TO 20
     19 DELTP=(B(N-1)*C(N-2)-B(N)*C(N-3))/D
     20 DELTQ=(B(N)*C(N-2)-B(N-1)*DIFF)/D
        P=P+DELTP
        Q=Q+DELTQ
    101 SUM=ABSF(DELTP)+ABSF(DELTQ)
        IF(M-1)35,21,22
     21 SUM1=SUM
        GO TO 24
     22 IF(M-25)24,23,240
    240 IF(M-99)24,26,26
     23 IF(SUM-SUM1)24,26,26
     24 M=M+1
     25 IF(SUM-ERROR)28,28,9
   26   IF(IT-N+2)38,39,38
   38   IT=IT+1
        IF(A(IT))381,26,381
  381   P=A(IT+1)/A(IT)
        GO TO 84
        Q=A(IT+2)/A(IT)
     39 KAD=2
        WRITE(2,27)
     27 FORMAT(33H FUNCTIONS DIVERGING METHOD FAILS )
        GO TO 35
     28 G=-P/2.
        F=Q-P*P/4.
        IF(F)29,29,31
     29 E=SQRTF(ABSF(F))
        T=G
        S=E
        E=0.
```

```
      G=T+S
      KR=KR+1
      R(KR)=G
      GI(KR)=E
      N=N-1
      S=-S
      G=T+S
   30 KR=KR+1
      R(KR)=G
      GI(KR)=E
      N=N-1
      IF(N)35,35,32
   31 E=SQRTF(F)
      KR=KR+1
      R(KR)=G
      GI(KR)=E
      E=-E
      N=N-1
      GO TO 30
   32 DO 33 I=1,N
   33 A(I)=B(I)
      IT=0
      GO TO 34
   35 CONTINUE
  350 CONTINUE
      RETURN
      END
      SUBROUTINE JOHANSEN
      DIMENSION YTW(7),CO(4),RI(4),GI(4),ZTW(7),ZW3(7),XW3(7)
      COMMON/RAIL/YT(6),ZT(6),AL(5),BL(5),RL(5)
      COMMON/WEEEL/QM(2),C(2),BN(4),AN(4),YW(7),ZW(7),RD(4)/JOH/PSI,H,HL
C          FORMATS
  702 FORMAT(//)
   61 FORMAT(5X,7HX(T) = ,F5.2)
   62 FORMAT(/)
   60 FORMAT(5X,6E13.6)
   23 FORMAT(3X,7HZ(T) = ,E13.6,3X,13HY(T)(RAIL) = ,E13.6,3X,14HY(T)(WHE
     1EL) = ,E13.6,3X,7HYDIF = ,E13.6,2X,5HPHI= ,F8.4)
  327 FORMAT(20X,48HMINIMUM LATERAL DISTANCE BETWEEN FLANGE AND RAIL)
  328 FORMAT(10X,39HWHEEL COORDINATES AT THIS VALUE OF X(T))
  502 FORMAT(3X,9HYTW(I) = )
  503 FORMAT(3X,9HZTW(I) = )
      SP=SIN(PSI)
      CP=COS(PSI)
      SPP=SP*SP
      CPP=CP*CP
      IL=1
      X=-2.5
   13 CONTINUE
      DO 10 NXS=1,21
      IF(IL.EQ.1) GO TO 703
      X=X+.05
      GO TO 704
  703 X=X+.5
  704 CONTINUE
      DO 50 I=1,7
   50 YTW(I)=(YW(I)+X*SIN(PSI))/COS(PSI)
      DO 500 I=1,7
  500 XW3(I)=X*CP+YTW(I)*SP
```

```
      R1=QM(1)*YW(1)+C(1)
      ZW3S=R1*R1-XW3(1)*XW3(1)
      ZW3(1)=SQRT(ZW3S)
      R1=QM(1)*YW(2)+C(1)
      ZW3S=R1*R1-XW3(2)*XW3(2)
      ZW3(2)=SQRT(ZW3S)
      R3=BN(1)-SQRT(RD(1)*RD(1)-(YW(3)-AN(1))*(YW(3)-AN(1)))
      ZW3(3)=SQRT(R3*R3-XW3(3)*XW3(3))
      R4=BN(2)-SQRT(RD(2)*RD(2)-(YW(4)-AN(2))*(YW(4)-AN(2)))
      ZW3(4)=SQRT(R4*R4-XW3(4)*XW3(4))
      R5=BN(3)-SQRT(RD(3)*RD(3)-(YW(5)-AN(3))*(YW(5)-AN(3)))
      ZW3(5)=SQRT(R5*R5-XW3(5)*XW3(5))
      R1=QM(2)*YW(6)+C(2)
      ZW3(6)=SQRT(R1*R1-XW3(6)*XW3(6))
      R6=BN(4)+SQRT(RD(4)*RD(4)-(YW(7)-AN(4))*(YW(7)-AN(4)))
      ZW3(7)=SQRT(R6*R6-XW3(7)*XW3(7))
      DO 501 I=1,7
  501 ZTW(I)=ZW3(I)+HL-H
      Z=-.33
      DO 20 NZS=1,10
      Z=Z+.01
C         CALCULATE VALUE OF Y ON RAIL
      IF(Z.GT.ZT(4)) GO TO 30
      YR=AL(4)-SQRT(RL(4)*RL(4)-(Z-BL(4))*(Z-BL(4)))
      R1A=RL(4)
      PHI=ATAN((AL(4)-YR)/(Z-BL(4)))
      GO TO 40
   30 IF(Z.GT.ZT(3)) GO TO 31
      YR=AL(3)-SQRT(RL(3)*RL(3)-(Z-BL(3))*(Z-BL(3)))
      R1A=RL(3)
      PHI=ATAN((AL(3)-YR)/(Z-BL(3)))
      GO TO 40
   31 IF(Z.GT.ZT(2)) GO TO 32
      YR=AL(2)-SQRT(RL(2)*RL(2)-(Z-BL(2))*(Z-BL(2)))
      R1A=RL(2)
      PHI=ATAN((AL(2)-YR)/(Z-BL(2)))
      GO TO 40
   32 IF(Z.GT.ZT(1)) GO TO 33
      YR=AL(1)-SQRT(RL(1)*RL(1)-(Z-BL(1))*(Z-BL(1)))
      R1A=RL(1)
      PHI=ATAN((AL(1)-YR)/(Z-BL(1)))
      GO TO 40
   33 Z=ZT(1)
      YR=YT(1)
      R1A=RL(1)
   40 CONTINUE
      PH=PHI*57.3
C         CALCULATE VALUE OF Y ON WHEEL
      IF(Z.GT.ZTW(2)) GO TO 70
      CALL LINY(X,Z,1,2,YS)
      R2A=99999999999999.
      NY=1
      GO TO 71
   70 IF(Z.GT.ZTW(3)) GO TO 72
      CALL CIRY(X,Z,2,3,YS)
      R2A=-RD(1)
      NY=2
      GO TO 71
   72 IF(Z.GT.ZTW(4)) GO TO 73
```

```
      CALL CIRY(X,Z,3,4,YS)
      R2A=-RD(2)
      NY=3
      GO TO 71
   73 IF(Z.GT.ZTW(5)) GO TO 74
      CALL CIRY(X,Z,4,5,YS)
      R2A=-RD(3)
      NY=4
      GO TO 71
   74 IF(Z.GT.ZTW(6)) GO TO 75
      CALL LINY(X,Z,5,6,YS)
      R2A=99999999999999.
      NY=5
      GO TO 71
   75 CALL CIRY(X,Z,6,7,YS)
      R2A=RD(4)
      NY=6
   71 CONTINUE
      YDIF=ABS(YR-YS)
      IF(NZS.EQ.1) GO TO 21
      IF(YDIF.GT.YDIF2) GO TO 22
   21 YDIF2=YDIF
   20 CONTINUE
   22 CONTINUE
      IF(NXS.EQ.1) GO TO 11
      IF(IL.EQ.2) GO TO 80
      IF(YDIF2.GT.YDIFX) GO TO 12
      GO TO 11
   80 IF(YDIF2.GT.YDIFX) GO TO 14
   11 YDIFX=YDIF2
   10 CONTINUE
   12 X=X-1.
      IL=2
      GO TO 13
   14 CONTINUE
      WRITE(2,702)
      WRITE(2,327)
      X=X-.05
      WRITE(2,61)X
      WRITE(2,62)
      WRITE(2,328)
      WRITE(2,502)
      DO 329 I=1,7
  329 YTW(I)=(YW(I)+X*SIN(PSI))/COS(PSI)
      WRITE(2,60)(YTW(I),I=1,7)
      WRITE(2,503)
      DO 300 I=1,7
  300 XW3(I)=X*CP+YTW(I)*SP
      R1=QM(1)*YW(1)+C(1)
      ZW3S=R1*R1-XW3(1)*XW3(1)
      ZW3(1)=SQRT(ZW3S)
      R1=QM(1)*YW(2)+C(1)
      ZW3S=R1*R1-XW3(2)*XW3(2)
      ZW3(2)=SQRT(ZW3S)
      R3=BN(1)-SQRT(RD(1)*RD(1)-(YW(3)-AN(1))*(YW(3)-AN(1)))
      ZW3(3)=SQRT(R3*R3-XW3(3)*XW3(3))
      R4=BN(2)-SQRT(RD(2)*RD(2)-(YW(4)-AN(2))*(YW(4)-AN(2)))
      ZW3(4)=SQRT(R4*R4-XW3(4)*XW3(4))
      R5=BN(3)-SQRT(RD(3)*RD(3)-(YW(5)-AN(3))*(YW(5)-AN(3)))
```

```
      ZW3(5)=SQRT(R5*R5-XW3(5)*XW3(5))
      R1=QM(2)*YW(6)+C(2)
      ZW3(6)=SQRT(R1*R1-XW3(6)*XW3(6))
      R6=BN(4)+SQRT(RD(4)*RD(4)-(YW(7)-AN(4))*(YW(7)-AN(4)))
      ZW3(7)=SQRT(R6*R6-XW3(7)*XW3(7))
      DO 301 I=1,7
  301 ZTW(I)=ZW3(I)+HL-H
      WRITE(2,60)(ZTW(I),I=1,7)
      YDIF=YDIFX
      IF(Z.GT.ZT(4)) GO TO 90
      YR=AL(4)-SQRT(RL(4)*RL(4)-(Z-BL(4))*(Z-BL(4)))
      R1A=RL(4)
      PHI=ATAN((AL(4)-YR)/(Z-BL(4)))
      GO TO 140
   90 IF(Z.GT.ZT(3)) GO TO 91
      YR=AL(3)-SQRT(RL(3)*RL(3)-(Z-BL(3))*(Z-BL(3)))
      R1A=RL(3)
      PHI=ATAN((AL(3)-YR)/(Z-BL(3)))
      GO TO 140
   91 IF(Z.GT.ZT(2)) GO TO 92
      YR=AL(2)-SQRT(RL(2)*RL(2)-(Z-BL(2))*(Z-BL(2)))
      R1A=RL(2)
      PHI=ATAN((AL(2)-YR)/(Z-BL(2)))
      GO TO 140
   92 IF(Z.GT.ZT(1)) GO TO 93
      YR=AL(1)-SQRT(RL(1)*RL(1)-(Z-BL(1))*(Z-BL(1)))
      R1A=RL(1)
      PHI=ATAN((AL(1)-YR)/(Z-BL(1)))
      GO TO 140
   93 Z=ZT(1)
      YR=YT(1)
      R1A=RL(1)
  140 CONTINUE
      PH=PHI*57.3
      YS=YR-YDIF
      WRITE(2,23)Z,YR,YS,YDIF,PH
      RETURN
      END
      SUBROUTINE CIRY(X,Z,K1,K2,YS)
      DIMENSION CO(4),RI(4),GI(4),BZ(4),CZ(4)
      COMMON/WEEEL/QM(2),C(2),BN(4),AN(4),YW(7),ZW(7),RD(4)
      COMMON/JOH/PSI,H,HL
      IF(K1.EQ.2) K3=1
      IF(K1.EQ.3) K3=2
      IF(K1.EQ.4) K3=3
      IF(K1.EQ.6) K3=4
      SP=SIN(PSI)
      CP=COS(PSI)
      SPP=SP*SP
      CPP=CP*CP
      A=AN(K3)
      B=BN(K3)
      R=RD(K3)
      CO(1)=-4.*A*CP
      CO(2)=-2.*R*R-2.*(-X*X-Z*Z-2.*A*X*SP-2.*Z*(H-HL)-A*A-B*B-(H-HL)*(H
     1-HL))+4.*A*A*CPP-4.*B*B*SPP
      CO(3)=4.*R*R*A*CP-4.*X*X*A*CP-4.*Z*Z*A*CP-8.*A*X*SP*A*CP+4.*A*CP*(
     1-2.*Z*(H-HL)-A*A-B*B-(H-HL)*(H-HL))-8.*B*B*X*CP*SP
      E1=(H-HL)*(H-HL)
```

```
      E2=-B*B-E1
      E3=-A*A+E2
      E4=-2.*Z*(H-HL)+E3
      E5=-2.*A*X*SP+E4
      E6=-Z*Z+E5
      E7=-X*X+E6
      CO(4)=R**4+2.*R*R*E7+X**4-2.*X*X*E6+Z**4-2.*Z*Z*E5+4.*A*A*X*X*SPP-
     14.*A*X*SP*E4+4.*Z*Z*E1-4.*Z*(H-HL)*E3+A**4-2.*A*A*E2+B**4+2.*B*B*E
     21+E1*E1-4.*B*B*(X*X*CPP+Z*Z+2.*Z*(H-HL)+E1)
      KAB=1
      IJ=4
      CALL Z200B(CO,RI,GI,KAB,IJ,BZ,CZ)
      DO 20 I=1,4
      IF(GI(I).NE.0.) GO TO 20
      IF(RI(I).GT.Y1) GO TO 20
      IF(RI(I).LT.Y2) GO TO 20
      YS=RI(I)
      GO TO 21
   20 CONTINUE
   21 CONTINUE
      RETURN
      END
      SUBROUTINE LINY(X,Z,K1,K2,YS)
      COMMON/JOH/PSI,H,HL
      COMMON/WEEEL/QM(2),C(2),BN(4),AN(4),YW(7),ZW(7),RD(4)
      IF(K1.EQ.1) K3=1
      IF(K1.EQ.5) K3=2
      SP=SIN(PSI)
      CP=COS(PSI)
      SPP=SP*SP
      CPP=CP*CP
      Q=QM(K3)
      B=C(K3)
      YSA=SPP-Q*Q*CPP
      YSB=2.*X*CP*SP*(1.+Q*Q)-2.*Q*B*CP
      YSC=X*X*(CPP-Q*Q*SPP)+Z*Z+2.*Q*B*X*SP+2.*Z*(H-HL)+(H-HL)*(H-HL)-B*
     1B
      Y=SQRT(YSB*YSB-4.*YSA*YSC)
      YS1=(-YSB+Y)/(2.*YSA)
      YS2=(-YSB-Y)/(2.*YSA)
      IF(YS1.GT.Y1) GO TO 20
      IF(YS1.LT.Y2) GO TO 20
      YS=YS1
      GO TO 30
   20 YS=YS2
   30 CONTINUE
      RETURN
      END
      MASTER ACCURATE
      DIMENSION XA(9),XB(9),XC(9),YA(9),YB(9),YC(9),ZA(9,9),ZB(9,9),ZC(9
     1,9),YCR(9,9),Y(9),YMD(9),ZMD(9),ZCR(9,9),ZDR(9,9),YS1(9,9)
      DIMENSION YBTT(9),ZBTT(9),ZS1(9,9)
      COMMON/RAIL/YT(6),ZT(6),AL(5),BL(5),RL(5)/WEEEL/QM(2),C(2),BN(4),A
     1N(4),YW(7),ZW(7),RD(4)
C
      CALL RAILAT
      CALL WHEEL
      CALL FINDH(H,YTSO)
C
```

```
C          FORMATS
      1 FORMAT(8F10.0)
      2 FORMAT(1H1)
    306 FORMAT(5X,5HYO = ,F9.6,5X,5HZO = ,F9.6,5X,5HTH = ,F9.7,5X,7HZMINC=
     1 ,F9.7)
    310 FORMAT(5X,5HYO = ,F9.6,5X,5HZO = ,F9.6,5X,5HTH = ,F9.7,5X,7HZMINB=
     1 ,F9.7)
    501 FORMAT(5X,5HYO = ,F9.6,5X,5HZO = ,F9.6,5X,5HTH = ,F9.7,5X,7HZMINA=
     1 ,F9.7)
    503 FORMAT(///)
   1000 FORMAT(5X,6HPSI = ,F9.6,2X,5HHL = ,F9.6,2X,4HH = ,F9.6)
   1001 FORMAT(5X,24HAPPROXIMATE INPUT VALUES)
   1002 FORMAT(10X,5HXA =,,F5.3,2X,5HXB = ,F5.3,2X,5HXC = ,F5.3)
   1003 FORMAT(10X,5HYA = ,F8.4,2X,5HYB = ,F7.4,2X,5HYC = ,F7.4)
   1004 FORMAT(10X,5HYO = ,F6.4,2X,5HTH = ,F8.6,2X,5HZO = ,F9.6)
   1005 FORMAT(////)
   1600 FORMAT(5X,4HYBT=,F9.5,5X,4HZBT=,F9.5,5X,4HXBT=,F9.5)
   1601 FORMAT(5X,4HYCT=,F9.5,5X,4HZCT=,F9.5,5X,4HXCT=,F9.5)
   1602 FORMAT(5X,4HYAT=,F9.5,5X,4HZAT=,F9.5,5X,4HXAT=,F9.5)
C
      READ(1,1)PSI,HL,YO,TH,ZO
      READ(1,1)XA5,XB5,XC5,YA5,YB5,YC5
C
      WRITE(2,2)
      WRITE(2,1001)
      WRITE(2,1000)PSI,HL,H
      WRITE(2,1004)YO,TH,ZO
      WRITE(2,1002)XA5,XB5,XC5
      WRITE(2,1003)YA5,YB5,YC5
      WRITE(2,1005)
C
      SP=SIN(PSI)
      CP=COS(PSI)
      SPP=SP*SP
      CPP=CP*CP
      XA(1)=XA5-.04
      XB(1)=XB5-.04
      XC(1)=XC5-.04
      YA(1)=YA5-.04-YO
      YB(1)=YB5-.04-YO
      YC(1)=YC5-.02-YO
C         RANGE OF VALUES OF X(T),Y(T) FOR EACH CONTACT POINT. SOLUTION
C         IS SOUGHT WITHIN THIS RANGE
      DO 5 I=2,9
      J=I-1
      XA(I)=XA(J)+.01
      XB(I)=XB(J)+.01
      XC(I)=XC(J)+.01
      YA(I)=YA(J)+.01
      YB(I)=YB(J)+.01
    5 YC(I)=YC(J)+.005
C
C         VALUES OF (X(T),Y(T)) FOR EACH CONTACT POINT CHANGED TO
C         WHEELSET AXES (X(W),Y(W)) ASSUMING WHEELSET YAWED ONLY.
      DO 10 I=1,9
      DO 10 J=1,9
      XWA=XA(I)*CP+YA(J)*SP
      YWA=YA(J)*CP-XA(I)*SP
      XWB=XB(I)*CP+YB(J)*SP
```

```
      YWB=YB(J)*CP-XB(I)*SP
      XWC=XC(I)*CP+YC(J)*SP
      YWC=YC(J)*CP-XC(I)*SP
C
C          CALCULATING VALUES OF Z(W) FOR CONTACT POINT A
      IF(YWA.GE.-YW(3).AND.YWA.LT.-YW(4)) GO TO 39
      IF(YWA.GE.-YW(2).AND.YWA.LT.-YW(3)) GO TO 40
      IF(YWA.GE.-YW(1).AND.YWA.LT.-YW(2)) GO TO 50
      WRITE(2,60)YWA
   60 FORMAT(10X,6HYWA = ,F8.4)
      GO TO 30
   39 AK=BN(2)-SQRT(RD(2)*RD(2)-(YWA+AN(2))*(YWA+AN(2)))
      GO TO 41
   40 AK=BN(1)-SQRT(RD(1)*RD(1)-(YWA+AN(1))*(YWA+AN(1)))
   41 ZWA=SQRT(AK*AK-XWA*XWA)
      GO TO 30
   50 AK=C(1)
      GO TO 41
   30 ZA(I,J)=ZWA
C          CALCULATING VALUES OF Z(W) FOR CONTACT POINT B
      IF(YWB.GE.YW(5).AND.YWB.LT.YW(4)) GO TO 68
      IF(YWB.GE.YW(4).AND.YWB.LT.YW(3)) GO TO 69
      IF(YWB.GE.YW(3).AND.YWB.LT.YW(2)) GO TO 70
      IF(YWB.GE.YW(2).AND.YWB.LT.YW(1)) GO TO 80
      WRITE(2,90)YWB
   90 FORMAT(10X,6HYWB = ,F8.4)
      GO TO 100
   68 AK=BN(3)-SQRT(RD(3)*RD(3)-(YWB-AN(3))*(YWB-AN(3)))
      GO TO 71
   69 AK=BN(2)-SQRT(RD(2)*RD(2)-(YWB-AN(2))*(YWB-AN(2)))
      GO TO 71
   70 AK=BN(1)-SQRT(RD(1)*RD(1)-(YWB-AN(1))*(YWB-AN(1)))
   71 ZWA=SQRT(AK*AK-XWB*XWB)
      GO TO 100
   80 AK=C(1)
      GO TO 71
  100 ZB(I,J)=ZWA
C
C          CALCULATING VALUES OF Z(W) FOR CONTACT POINT C
      IF(YWC.GE.YW(7).AND.YWC.LT.YW(6)) GO TO 110
      IF(YWC.GE.YW(6).AND.YWC.LT.YW(5)) GO TO 120
      IF(YWC.GE.YW(5).AND.YWC.LT.YW(4)) GO TO 130
      IF(YWC.GE.YW(4).AND.YWC.LT.YW(3)) GO TO 140
      WRITE(2,150)YWC
  150 FORMAT(10X,6HYWC = ,F8.4)
      GO TO 200
  110 AK=BN(4)+SQRT(RD(4)*RD(4)-(YWC-AN(4))*(YWC-AN(4)))
  111 ZWA=SQRT(AK*AK-XWC*XWC)
      GO TO 200
  120 AK=QM(2)*YWC+C(2)
      GO TO 111
  130 AK=BN(3)-SQRT(RD(3)*RD(3)-(YWC-AN(3))*(YWC-AN(3)))
      GO TO 111
  140 AK=BN(2)-SQRT(RD(2)*RD(2)-(YWC-AN(2))*(YWC-AN(2)))
      GO TO 111
  200 ZC(I,J)=ZWA
   10 CONTINUE
C          INITIAL STEP LENGTHS
      BETA=0.
```

```
      DELTA=.0008
      DELTA1=.0005
      DELTA2=.00005
      IJCOUNT=1
      IMARK=1
   11 CONTINUE
C          WHEELSET MOVED LATERALLY UNTIL CONTACT POINT C ALMOST TOUCHES
C          THE RAIL. (YO VARIED)(ZO,TH CONSTANT)
      DO 301 I=1,9
      DO 304 J=1,9
      YS1(I,J)=YC(J)*COS(TH)+ZC(I,J)*SIN(TH)+YO
      ZCR(I,J)=ZC(I,J)*COS(TH)-YC(J)*SIN(TH)+ZO-H+HL
      CALL FR1(YS1(I,J),YCR(I,J),2)
      ZDR(I,J)=YCR(I,J)-ZCR(I,J)
      IF(ZDR(I,J))302,303,303
  302 YO=YO-DELTA
      IMARK=2
      GO TO 11
  303 CONTINUE
  304 CONTINUE
      YMD(I)=AMIN1(ZDR(I,1),ZDR(I,2),ZDR(I,3),ZDR(I,4),ZDR(I,5),ZDR(I,6)
     1,ZDR(I,7),ZDR(I,8),ZDR(I,9))
      IF(YMD(I).EQ.ZDR(I,1)) GO TO 1300
      IF(YMD(I).EQ.ZDR(I,2)) GO TO 1301
      IF(YMD(I).EQ.ZDR(I,3)) GO TO 1302
      IF(YMD(I).EQ.ZDR(I,4)) GO TO 1303
      IF(YMD(I).EQ.ZDR(I,5)) GO TO 1304
      IF(YMD(I).EQ.ZDR(I,6)) GO TO 2305
      IF(YMD(I).EQ.ZDR(I,7)) GO TO 2306
      IF(YMD(I).EQ.ZDR(I,8)) GO TO 2307
      IF(YMD(I).EQ.ZDR(I,9)) GO TO 2308
 1300 CONTINUE
      YBTT(I)=YS1(I,1)
      ZBTT(I)=YCR(I,1)
      GO TO 1305
 1301 YBTT(I)=YS1(I,2)
      ZBTT(I)=YCR(I,2)
      GO TO 1305
 1302 YBTT(I)=YS1(I,3)
      ZBTT(I)=YCR(I,3)
      GO TO 1305
 1303 YBTT(I)=YS1(I,4)
      ZBTT(I)=YCR(I,4)
      GO TO 1305
 1304 YBTT(I)=YS1(I,5)
      ZBTT(I)=YCR(I,5)
      GO TO 1305
 2305 YBTT(I)=YS1(I,6)
      ZBTT(I)=YCR(I,6)
      GO TO 1305
 2306 YBTT(I)=YS1(I,7)
      ZBTT(I)=YCR(I,7)
      GO TO 1305
 2307 YBTT(I)=YS1(I,8)
      ZBTT(I)=YCR(I,8)
      GO TO 1305
 2308 CONTINUE
      YBTT(I)=YS1(I,9)
      ZBTT(I)=YCR(I,9)
```

```
 1305 CONTINUE
  301 CONTINUE
C          DIST. BETWEEN FLANGE AND RAIL = YMIN (VERTICAL)(CONTACT C)
      YMIN=AMIN1(YMD(1),YMD(2),YMD(3),YMD(4),YMD(5),YMD(6),YMD(7),YMD(8)
     1,YMD(9))
       IF(YMIN.EQ.YMD(1)) GO TO 1306
       IF(YMIN.EQ.YMD(2)) GO TO 1307
       IF(YMIN.EQ.YMD(3)) GO TO 1308
       IF(YMIN.EQ.YMD(4)) GO TO 1309
       IF(YMIN.EQ.YMD(5)) GO TO 1310
       IF(YMIN.EQ.YMD(6)) GO TO 2310
       IF(YMIN.EQ.YMD(7)) GO TO 2311
       IF(YMIN.EQ.YMD(8)) GO TO 2312
       IF(YMIN.EQ.YMD(9)) GO TO 2313
 1306 CONTINUE
       YCT=YBTT(1)
       ZCT=ZBTT(1)
       XCT=XC(1)
       GO TO 1311
 1307 YCT=YBTT(2)
       ZCT=ZBTT(2)
       XCT=XC(2)
       GO TO 1311
 1308 YCT=YBTT(3)
       ZCT=ZBTT(3)
       XCT=XC(3)
       GO TO 1311
 1309 YCT=YBTT(4)
       ZCT=ZBTT(4)
       XCT=XC(4)
       GO TO 1311
 1310 YCT=YBTT(5)
       ZCT=ZBTT(5)
       XCT=XC(5)
       GO TO 1311
 2310 YCT=YBTT(6)
       ZCT=ZBTT(6)
       XCT=XC(6)
       GO TO 1311
 2311 YCT=YBTT(7)
       ZCT=ZBTT(7)
       XCT=XC(7)
       GO TO 1311
 2312 YCT=YBTT(8)
       ZCT=ZBTT(8)
       XCT=XC(8)
       GO TO 1311
 2313 CONTINUE
       YCT=YBTT(9)
       ZCT=ZBTT(9)
       XCT=XC(9)
 1311 CONTINUE
C          COORDINATES OF FLANGE CONTACT POINT GIVEN BY XCT,YCT,ZCT
       IF(IMARK.EQ.2) GO TO 305
       YO=YO+DELTA
       GO TO 11
  305 WRITE(2,306)YO,ZO,TH,YMIN
       WRITE(2,1601)YCT,ZCT,XCT
       ZMINC=YMIN
```

```
      IMARK=1
      GO TO 320
  307 ZO=ZO-DELTA1
      IMARK=2
  320 CONTINUE
C          WHEELSET MOVED VERTICALLY UNTIL CONTACT POINT B ALMOST TOUCHES
C          THE RAIL (ZO VARIED) (YO,TH CONSTANT)
      DO 309 I=1,9
      DO 308 J=1,9
      YS1(I,J)=YB(J)*COS(TH)+ZB(I,J)*SIN(TH)+YO
      ZCR(I,J)=ZB(I,J)*COS(TH)-YB(J)*SIN(TH)+ZO-H+HL
      CALL FR1(YS1(I,J),ZDR(I,J),2)
      YCR(I,J)=ZDR(I,J)-ZCR(I,J)
      IF(YCR(I,J))307,308,308
  308 CONTINUE
      YMD(I)=AMIN1(YCR(I,1),YCR(I,2),YCR(I,3),YCR(I,4),YCR(I,5),YCR(I,6)
     1,YCR(I,7),YCR(I,8),YCR(I,9))
      IF(YMD(I).EQ.YCR(I,1)) GO TO 1797
      IF(YMD(I).EQ.YCR(I,2)) GO TO 1800
      IF(YMD(I).EQ.YCR(I,3)) GO TO 1801
      IF(YMD(I).EQ.YCR(I,4)) GO TO 1802
      IF(YMD(I).EQ.YCR(I,5)) GO TO 1796
      IF(YMD(I).EQ.YCR(I,6)) GO TO 2797
      IF(YMD(I).EQ.YCR(I,7)) GO TO 2798
      IF(YMD(I).EQ.YCR(I,8)) GO TO 2799
      IF(YMD(I).EQ.YCR(I,9)) GO TO 2800
 1797 CONTINUE
      YBTT(I)=YS1(I,1)
      ZBTT(I)=ZDR(I,1)
      GO TO 1803
 1800 YBTT(I)=YS1(I,2)
      ZBTT(I)=ZDR(I,2)
      GO TO 1803
 1801 YBTT(I)=YS1(I,3)
      ZBTT(I)=ZDR(I,3)
      GO TO 1803
 1802 YBTT(I)=YS1(I,4)
      ZBTT(I)=ZDR(I,4)
      GO TO 1803
 1796 YBTT(I)=YS1(I,5)
      ZBTT(I)=ZDR(I,5)
      GO TO 1803
 2797 YBTT(I)=YS1(I,6)
      ZBTT(I)=ZDR(I,6)
      GO TO 1803
 2798 YBTT(I)=YS1(I,7)
      ZBTT(I)=ZDR(I,7)
      GO TO 1803
 2799 YBTT(I)=YS1(I,8)
      ZBTT(I)=ZDR(I,8)
      GO TO 1803
 2800 CONTINUE
      YBTT(I)=YS1(I,9)
      ZBTT(I)=ZDR(I,9)
 1803 CONTINUE
  309 CONTINUE
C          DIST. BETWEEN TREAD AND RAIL = ZMIN (VERTICAL)(CONTACT B)
      ZMIN=AMIN1(YMD(1),YMD(2),YMD(3),YMD(4),YMD(5),YMD(6),YMD(7),YMD(8
     1,YMD(9))
```

```
      IF(ZMIN.EQ.YMD(1)) GO TO 1799
      IF(ZMIN.EQ.YMD(2)) GO TO 1804
      IF(ZMIN.EQ.YMD(3)) GO TO 1805
      IF(ZMIN.EQ.YMD(4)) GO TO 1806
      IF(ZMIN.EQ.YMD(5)) GO TO 1798
      IF(ZMIN.EQ.YMD(6)) GO TO 2801
      IF(ZMIN.EQ.YMD(7)) GO TO 2802
      IF(ZMIN.EQ.YMD(8)) GO TO 2803
      IF(ZMIN.EQ.YMD(9)) GO TO 2804
 1799 CONTINUE
      YBT=YBTT(1)
      ZBT=ZBTT(1)
      XBT=XB(1)
      GO TO 1808
 1804 YBT=YBTT(2)
      ZBT=ZBTT(2)
```

```
      XBT=XB(2)
      GO TO 1808
 1805 YBT=YBTT(3)
      ZBT=ZBTT(3)
      XBT=XB(3)
      GO TO 1808
 1806 YBT=YBTT(4)
      ZBT=ZBTT(4)
      XBT=XB(4)
      GO TO 1808
 1798 YBT=YBTT(5)
      ZBT=ZBTT(5)
      XBT=XB(5)
      GO TO 1808
 2801 YBT=YBTT(6)
      ZBT=ZBTT(6)
      XBT=XB(6)
      GO TO 1808.
 2802 YBT=YBTT(7)
      ZBT=ZBTT(7)
      XBT=XB(7)
      GO TO 1808
 2803 YBT=YBTT(8)
      ZBT=ZBTT(8)
      XBT=XB(8)
      GO TO 1808
 2804 CONTINUE
      YBT=YBTT(9)
      ZBT=ZBTT(9)
      XBT=XB(9)
 1808 CONTINUE
C          COORDINATES OF TREAD CONTACT XBT,YBT,ZBT
      IF(IMARK.EQ.2) GO TO 321
      ZO=ZO+DELTA1
      GO TO 320
  321 CONTINUE
      WRITE(2,310)YO,ZO,TH,ZMIN
      WRITE(2,1600)YBT,ZBT,XBT
      ZMINB=ZMIN
      IMARK=1
  903 BETA=BETA+DELTA2
      GO TO 902
  315 BETA=BETA-DELTA2
```

```
      IMARK=2
  902 CONTINUE
C          WHEELSET ROLLED ABOUT CONTACT POINT B UNTIL CONTACT POINT A
C          ALMOST TOUCHES THE RAIL (YO,ZO,TH VARIED)
      DO 317 I=1,9
      DO 317 J=1,9
      YCR(I,J)=YA(J)*COS(TH)+ZA(I,J)*SIN(TH)+YO
      ZCR(I,J)=ZA(I,J)*COS(TH)-YA(J)*SIN(TH)+ZO-H+HL
      YCR(I,J)=YCR(I,J)-YBT
  317 ZCR(I,J)=ZCR(I,J)-ZBT
      DO 900 I=1,9
      DO 901 J=1,9
      CONS=SQRT(YCR(I,J)*YCR(I,J)+ZCR(I,J)*ZCR(I,J))
      ALPHA=ASIN(ZCR(I,J)/CONS)
      ALPHA=3.141593-ALPHA-BETA
      YS1(I,J)=COS(ALPHA)*CONS
      ZS1(I,J)=SIN(ALPHA)*CONS
      YCR(I,J)=YS1(I,J)+YBT
      ZCR(I,J)=ZS1(I,J)+ZBT
      YCR(I,J)=-YCR(I,J)
      CALL FR1(YCR(I,J),ZDR(I,J),2)
      YCR(I,J)=-YCR(I,J)
      YS1(I,J)=ZDR(I,J)-ZCR(I,J)
      IF(YS1(I,J))315,316,316
  316 CONTINUE
  901 CONTINUE
      YMD(I)=AMIN1(YS1(I,1),YS1(I,2),YS1(I,3),YS1(I,4),YS1(I,5),YS1(I,6)
     1,YS1(I,7),YS1(I,8),YS1(I,9))
      IF(YMD(I).EQ.YS1(I,1)) GO TO 1312
      IF(YMD(I).EQ.YS1(I,2)) GO TO 1313
      IF(YMD(I).EQ.YS1(I,3)) GO TO 1314
      IF(YMD(I).EQ.YS1(I,4)) GO TO 1315
      IF(YMD(I).EQ.YS1(I,5)) GO TO 1316
      IF(YMD(I).EQ.YS1(I,6)) GO TO 2317
      IF(YMD(I).EQ.YS1(I,7)) GO TO 2318
      IF(YMD(I).EQ.YS1(I,8)) GO TO 2319
      IF(YMD(I).EQ.YS1(I,9)) GO TO 2320
 1312 CONTINUE
      YBTT(I)=YCR(I,1)
      ZBTT(I)=ZDR(I,1)
      GO TO 1317
 1313 YBTT(I)=YCR(I,2)
      ZBTT(I)=ZDR(I,2)
      GO TO 1317
 1314 YBTT(I)=YCR(I,3)
      ZBTT(I)=ZDR(I,3)
      GO TO 1317
 1315 YBTT(I)=YCR(I,4)
      ZBTT(I)=ZDR(I,4)
      GO TO 1317
 1316 YBTT(I)=YCR(I,5)
      ZBTT(I)=ZDR(I,5)
      GO TO 1317
 2317 YBTT(I)=YCR(I,6)
      ZBTT(I)=ZDR(I,6)
      GO TO 1317
 2318 YBTT(I)=YCR(I,7)
      ZBTT(I)=ZDR(I,7)
      GO TO 1317
```

```
 2319 YBTT(I)=YCR(I,8)
      ZBTT(I)=ZDR(I,8)
      GO TO 1317
 2320 CONTINUE
      YBTT(I)=YCR(I,9)
      ZBTT(I)=ZDR(I,9)
 1317 CONTINUE
  900 CONTINUE
C          DIST. BETWEEN TREAD AND RAIL = ZMIN(VERTICAL)(CONTACT A)
      ZMIN=AMIN1(YMD(1),YMD(2),YMD(3),YMD(4),YMD(5),YMD(6),YMD(7),YMD(8)
     1,YMD(9))
      IF(ZMIN.EQ.YMD(1)) GO TO 1318
      IF(ZMIN.EQ.YMD(2)) GO TO 1319
      IF(ZMIN.EQ.YMD(3)) GO TO 1320
      IF(ZMIN.EQ.YMD(4)) GO TO 1321
      IF(ZMIN.EQ.YMD(5)) GO TO 1323
      IF(ZMIN.EQ.YMD(6)) GO TO 2324
      IF(ZMIN.EQ.YMD(7)) GO TO 2325
      IF(ZMIN.EQ.YMD(8)) GO TO 2326
      IF(ZMIN.EQ.YMD(9)) GO TO 2327
 1318 CONTINUE
      YAT=YBTT(1)
      ZAT=ZBTT(1)
      XAT=XA(1)
      GO TO 1322
 1319 YAT=YBTT(2)
      ZAT=ZBTT(2)
      XAT=XA(2)
      GO TO 1322
 1320 YAT=YBTT(3)
      ZAT=ZBTT(3)
      XAT=XA(3)
      GO TO 1322
 1321 YAT=YBTT(4)
      ZAT=ZBTT(4)
      XAT=XA(4)
      GO TO 1322
 1323 YAT=YBTT(5)
      ZAT=ZBTT(5)
      XAT=XA(5)
      GO TO 1322
 2324 YAT=YBTT(6)
      ZAT=ZBTT(6)
      XAT=XA(6)
      GO TO 1322
 2325 YAT=YBTT(7)
      ZAT=ZBTT(7)
      XAT=XA(7)
      GO TO 1322
 2326 YAT=YBTT(8)
      ZAT=ZBTT(8)
      XAT=XA(8)
      GO TO 1322
 2327 CONTINUE
      YAT=YBTT(9)
      ZAT=ZBTT(9)
      XAT=XA(9)
 1322 CONTINUE
C          COORDINATES OF TREAD CONTACT XAT,YAT,ZAT
```

```
      IF(IMARK.EQ.2) GO TO 500
      GO TO 903
  500 YT10=YO-YBT
      ZT10=ZO-ZBT-H
      CONS=SQRT(YT10*YT10+ZT10*ZT10)
      ALPHA=ASIN(ZT10/CONS)
      ALPHA=3.141593-ALPHA-BETA
      YW20=COS(ALPHA)*CONS
      ZW20=SIN(ALPHA)*CONS
      YTO=YW20+YBT
      ZTO=ZW20+ZBT+H
      YO=YTO
      ZO=ZTO
      TH=BETA+TH
      WRITE(2,501)YO,ZO,TH,ZMIN
      WRITE(2,1602)YAT,ZAT,XAT
      ZMINA=ZMIN
      IMARK=1
      DELTA1=DELTA1/5.
      DELTA2=DELTA2/10.
      IF(IJCOUNT.EQ.2) DELTA=DELTA/10.
      IJCOUNT=2
      WRITE(2,503)
      IF(ZMINA.LT..0000001.AND.ZMINB.LT..0000001.AND.ZMINC.LT..0000001)
     1GO TO 502
      GO TO 11
  502 CONTINUE
      STOP
      END
      MASTER CONTACT
      COMMON/RAIL/YT(6),ZT(6),AL(5),BL(5),RL(5)/WEEEL/QM(2),C(2),BN(4),
     1N(4),YW(7),ZW(7),RD(4)
C
      CALL RAILAT
      CALL WHEEL
      CALL FINDH(H,YTSO)
C
C          FORMATS
    1 FORMAT(9F8.0)
    3 FORMAT(5X,5HXA = ,F10.6,2X,5HYA = ,F10.6,2X,5HZA = ,F10.6)
    4 FORMAT(5X,5HXB = ,F10.6,2X,5HYB = ,F10.6,2X,5HZB = ,F10.6)
    5 FORMAT(5X,5HXC = ,F10.6,2X,5HYC = ,F10.6,2X,5HZC = ,F10.6)
    6 FORMAT(10X,43HCOORDINATES OF CONTACT POINTS IN TRACK AXES)
    7 FORMAT(10X,46HCOORDINATES OF CONTACT POINTS IN WHEELSET AXES)
   10 FORMAT(5X,22HYWC GREATER THAN YW(4))
   18 FORMAT(5X,19HYWC LESS THAN YW(7))
   21 FORMAT(20X,34HFLANGE CONTACT POINT ON R.H. WHEEL)
   22 FORMAT(//)
   23 FORMAT(5X,15HR1A (RAIL)  =  ,E13.6)
   24 FORMAT(5X,23HR1B (RAIL)  =  INFINITY)
   25 FORMAT(5X,15HR2A (WHEEL) =  ,E13.6)
   26 FORMAT(5X,15HR2B (WHEEL) =  ,E13.6)
   27 FORMAT(5X,45HANGLE BETWEEN NORMAL PLANES OF R1A AND R2A = ,E13.6)
   28 FORMAT(/)
   29 FORMAT(5X,6HA+B = ,E13.6,3X,6HB-A = ,E13.6,3X,13HCOS(THETA) = ,E1
     1.6,3X,8HTHETA = ,E13.6,7HDEGREES)
   97 FORMAT(70X,6HPSI = ,F8.6,7HRADIANS)
   98 FORMAT(1H1)
  129 FORMAT(49X,13HCOS(TOR) =   ,E13.6,3X,8HTOR =   ,E13.6,7HDEGREES)
```

```
      140 FORMAT(20X,33HTREAD CONTACT POINT ON R.H. WHEEL)
      141 FORMAT(5X,4HA = ,E13.6,5X,4HB = ,E13.6)
      142 FORMAT(20X,33HTREAD CONTACT POINT ON L.H. WHEEL)
C
      DO 2 NCASES=1,7
      READ(1,1)YO,ZO,TH,PSI
      READ(1,1)XA,YA,ZA,XB,YB,ZB,XC,YC,ZC
      PSI=PSI/57.3
      SP=SIN(PSI)
      CP=COS(PSI)
      SPP=SP*SP
      CPP=CP*CP
      STH=SIN(TH)
      CTH=COS(TH)
C          CHANGING CONTACT POINTS FROM TRACK AXES TO WHEELSET AXES.
      XWA=XA*CP+(YA-YO)*SP*CTH+(ZA-ZO+H)*SP*STH
      XWB=XB*CP+(YB-YO)*SP*CTH+(ZB-ZO+H)*SP*STH
      XWC=XC*CP+(YC-YO)*SP*CTH+(ZC-ZO+H)*SP*STH
      YWA=-XA*SP+(YA-YO)*CP*CTH-(ZA-ZO+H)*STH*CP
      YWB=-XB*SP+(YB-YO)*CP*CTH-(ZB-ZO+H)*STH*CP
      YWC=-XC*SP+(YC-YO)*CP*CTH-(ZC-ZO+H)*STH*CP
      ZWA=(YA-YO)*STH+(ZA-ZO+H)*CTH
      ZWB=(YB-YO)*STH+(ZB-ZO+H)*CTH
      ZWC=(YC-YO)*STH+(ZC-ZO+H)*CTH
      WRITE(2,98)
      WRITE(2,97)PSI
      WRITE(2,6)
      WRITE(2,3)XA,YA,ZA
      WRITE(2,4)XB,YB,ZB
      WRITE(2,5)XC,YC,ZC
      WRITE(2,7)
      WRITE(2,3)XWA,YWA,ZWA
      WRITE(2,4)XWB,YWB,ZWB
      WRITE(2,5)XWC,YWC,ZWC
      YAA=ABS(YA)
      IF(YAA.GT.YT(1).AND.YAA.LT.YT(2)) ACR=-AL(1)
      IF(YAA.GT.YT(1).AND.YAA.LT.YT(2)) BCR=BL(1)
      IF(YAA.GT.YT(2).AND.YAA.LT.YT(3)) ACR=-AL(2)
      IF(YAA.GT.YT(2).AND.YAA.LT.YT(3)) BCR=BL(2)
      IF(YAA.GT.YT(3).AND.YAA.LT.YT(4)) ACR=-AL(3)
      IF(YAA.GT.YT(3).AND.YAA.LT.YT(4)) BCR=BL(3)
      IF(YAA.GT.YT(4).AND.YAA.LT.YT(5)) ACR=-AL(4)
      IF(YAA.GT.YT(4).AND.YAA.LT.YT(5)) BCR=BL(4)
      IF(YAA.GT.YT(5).AND.YAA.LT.YT(6)) ACR=-AL(5)
      IF(YAA.GT.YT(5).AND.YAA.LT.YT(6)) BCR=BL(5)
      DZDYA=(ACR-YA)/(ZA-BCR)
      IF(YB.GT.YT(1).AND.YB.LT.YT(2)) ACR=AL(1)
      IF(YB.GT.YT(1).AND.YB.LT.YT(2)) BCR=BL(1)
      IF(YB.GT.YT(2).AND.YB.LT.YT(3)) ACR=AL(2)
      IF(YB.GT.YT(2).AND.YB.LT.YT(3)) BCR=BL(2)
      IF(YB.GT.YT(3).AND.YB.LT.YT(4)) ACR=AL(3)
      IF(YB.GT.YT(3).AND.YB.LT.YT(4)) BCR=BL(3)
      IF(YB.GT.YT(4).AND.YB.LT.YT(5)) ACR=AL(4)
      IF(YB.GT.YT(4).AND.YB.LT.YT(5)) BCR=BL(4)
      IF(YB.GT.YT(5).AND.YB.LT.YT(6)) ACR=AL(5)
      IF(YB.GT.YT(5).AND.YB.LT.YT(6)) BCR=BL(5)
      DZDYB=(ACR-YB)/(ZB-BCR)
      IF(YC.GT.YT(1).AND.YC.LT.YT(2)) ACR=AL(1)
      IF(YC.GT.YT(1).AND.YC.LT.YT(2)) BCR=BL(1)
```

```
      IF(YC.GT.YT(2).AND.YC.LT.YT(3)) ACR=AL(2)
      IF(YC.GT.YT(2).AND.YC.LT.YT(3)) BCR=BL(2)
      IF(YC.GT.YT(3).AND.YC.LT.YT(4)) ACR=AL(3)
      IF(YC.GT.YT(3).AND.YC.LT.YT(4)) BCR=BL(3)
      IF(YC.GT.YT(4).AND.YC.LT.YT(5)) ACR=AL(4)
      IF(YC.GT.YT(4).AND.YC.LT.YT(5)) BCR=BL(4)
      IF(YC.GT.YT(5).AND.YC.LT.YT(6)) ACR=AL(5)
      IF(YC.GT.YT(5).AND.YC.LT.YT(6)) BCR=BL(5)
      DZDYC=(ACR-YC)/(ZC-BCR)
      WRITE(2,28)
      WRITE(2,143)DZDYA,DZDYB,DZDYC
  143 FORMAT(5X,9H(DZ/DY)A=,F10.6,2X,9H(DZ/DY)B=,F10.6,2X,9H(DZ/DY)C=,F1
     10.6)
C          CONTACT POINT C (FLANGE)(R.H.SIDE)
C          R = RADIUS PC IN BOOK(P.335)
      R=SQRT(XWC*XWC+ZWC*ZWC)
C          TO CALCULATE THETA IN BOOK(P.335)
      IF(YWC-YW(4))8,8,9
    9 WRITE(2,10)
      GO TO 99
    8 IF(YWC-YW(5))11,11,12
   12 DYX=(BN(3)-R)/(YWC-AN(3))
      GO TO 13
   11 IF(YWC-YW(6))14,14,15
   15 DYX=R/(QM(2)*(QM(2)*YWC+C(2)))
      GO TO 13
   14 IF(YWC-YW(7))16,17,17
   16 WRITE(2,18)
      GO TO 99
   17 DYX=(BN(4)-R)/(YWC-AN(4))
   13 CONTINUE
      THB=1./DYX
      THB=ATAN(THB)
      R2B=R/COS(THB)
C          TO CALCULATE ANGLE BETWEEN R1A AND R2A
C          KNOWING 3 POINTS IN A PLANE THE EQUATION OF THE PLANE
C          CONTAINING R2A CAN BE CALCULATED.
C          POINT 1 (XC,YC,ZC)  TRACK AXES
C          POINT 2  XW=0.,YW=YWC,ZW=0.
      X2=-YWC*SP
      Y2=YO+YWC*CP*CTH
      Z2=ZO-H-YWC*CP*STH
C          POINT 3 XW=0.,YW=0.,ZW=0.
      X3=0.
      Y3=YO
      Z3=ZO-H
C          THEREFORE EQUATION OF PLANE CONTAINING R2A (P.35)
      E=(XC*(ZC-Z2)+(X2-XC)*(ZC-Z3))/((Y3-YC)*(ZC-Z2)+(Z3-ZC)*(Y2-YC))
      F=((X2-XC)+E*(Y2-YC))/(ZC-Z2)
      G=-XC-E*YC-F*ZC
C          ANGLE BETWEEN TWO PLANES. (P.34)
      CSPH=1./SQRT(E*E+F*F+1.*1.)
      PH=ACOS(CSPH)
      PHD=PH*57.3
C          TO FIND R1A
      IF(YC.GT.YT(1).AND.YC.LT.YT(2)) R1A=RL(1)
      IF(YC.GT.YT(2).AND.YC.LT.YT(3)) R1A=RL(2)
      IF(YC.GT.YT(3)) GO TO 99
C          TO FIND R2A
```

```
      IF(YWC.GT.YW(7).AND.YWC.LT.YW(6)) R2A=RD(4)
      IF(YWC.GT.YW(6).AND.YWC.LT.YW(5)) R2A=1000000000000.
      IF(YWC.GT.YW(5).AND.YWC.LT.YW(4)) R2A=-RD(3)
      IF(YWC.GT.YW(4)) GO TO 99
      WRITE(2,22)
      WRITE(2,21)
      WRITE(2,23)R1A
      WRITE(2,24)
      WRITE(2,25)R2A
      WRITE(2,26)R2B
      WRITE(2,27)PHD
C CALCULATING HERTZ CONSTANTS
      APB=.5*(1./R1A+1./R2A+1./R2B)
      BMA=(1./R1A)*(1./R1A)+(1./R2A-1./R2B)*(1./R2A-1./R2B)+2.*(1./R1A)
     1(1./R2A-1./R2B)*COS(2.*PH)
      BMA=.5*SQRT(BMA)
      CSTH=BMA/APB
      IF(CSTH.GT.1.) CSTH=1.
      IF(CSTH.LT.-1.) CSTH=-1.
      TH=ACOS(CSTH)
      TH=TH*57.3
      WRITE(2,28)
      WRITE(2,29)APB,BMA,CSTH,TH
      WRITE(2,28)
      TOR=ABS(1./R2B-1./R1A-1./R2A)
      TOR=TOR/(1./R2B+1./R1A+1./R2A)
      ATOR=ACOS(TOR)
      ATOR=ATOR*57.3
      WRITE(2,129)TOR,ATOR
      A=(APB-BMA)/2.
      B=BMA+A
      WRITE(2,141)A,B
C          CONTACT POINT B (TREAD)(R.H.SIDE)
C          TO FIND R1A
      IF(YB.GT.YT(1).AND.YB.LT.YT(2)) R1A=RL(1)
      IF(YB.GT.YT(2).AND.YB.LT.YT(3)) R1A=RL(2)
      IF(YB.GT.YT(3).AND.YB.LT.YT(4)) R1A=RL(3)
      IF(YB.GT.YT(4).AND.YB.LT.YT(5)) R1A=RL(4)
      IF(YB.GT.YT(5).AND.YB.LT.YT(6)) R1A=RL(5)
C          R1B = INFINITY
C          TO FIND R2A
C          TO FIND R2B
      R=SQRT(XWB*XWB+ZWB*ZWB)
      IF(YWB.LT.YW(5)) GO TO 99
      IF(YWB.GT.YW(5).AND.YWB.LT.YW(4)) GO TO 30
      IF(YWB.GT.YW(4).AND.YWB.LT.YW(3)) GO TO 31
      IF(YWB.GT.YW(3).AND.YWB.LT.YW(2)) GO TO 32
      IF(YWB.GT.YW(2).AND.YWB.LT.YW(1)) GO TO 33
      GO TO 99
   30 R2A=-RD(3)
      DYX=(BN(3)-R)/(YWB-AN(3))
      GO TO 34
   31 R2A=-RD(2)
      DYX=(BN(2)-R)/(YWB-AN(2))
      GO TO 34
   32 R2A=-RD(1)
      DYX=(BN(1)-R)/(YWB-AN(1))
      GO TO 34
   33 R2A=1000000000000.
```

```
      DYX=R/(QM(1)*(QM(1)*YWB+C(1)))
   34 CONTINUE
      THB=1./DYX
      THB=ATAN(THB)
      R2B=R/COS(THB)
C          TO CALCULATE ANGLE BETWEEN R1A AND R2A
C          KNOWING 3 POINTS IN A PLANE THE EQUATION OF THE PLANE
C          CONTAINING R2A CAN BE CALCULATED.
C          POINT 1 (XB,YB,ZB) TRACK AXES
C          POINT 2 XW=0.,YW=YWB,ZW=0.
      X2=-YWB*SP
      Y2=YO+YWB*CP*CTH
      Z2=ZO-H-YWB*CP*STH
C          POINT 3 XW=0.,YW=0.,ZW=0.
      X3=0.
      Y3=YO
      Z3=ZO-H
C          THEREFORE EQUATION OF PLANE CONTAINING R2A (P.35)
      E=(XB*(ZB-Z2)+(X2-XB)*(ZB-Z3))/((Y3-YB)*(ZB-Z2)+(Z3-ZB)*(Y2-YB))
      F=((X2-XB)+E*(Y2-YB))/(ZB-Z2)
      G=-XB-E*YC-F*ZC
C          ANGLE BETWEEN TWO PLANES. (P.34)
      CSPH=1./SQRT(E*E+F*F+1.*1.)
      PH=ACOS(CSPH)
      PHD=PH*57.3
      WRITE(2,22)
      WRITE(2,140)
      WRITE(2,23)R1A
      WRITE(2,24)
      WRITE(2,25)R2A
      WRITE(2,26)R2B
      WRITE(2,27)PHD
      APB=.5*(1./R1A+1./R2A+1./R2B)
      BMA=(1./R1A)*(1./R1A)+(1./R2A-1./R2B)*(1./R2A-1./R2B)+2.*(1./R1A)
     1(1./R2A-1./R2B)*COS(2.*PH)
      BMA=.5*SQRT(BMA)
      CSTH=BMA/APB
      IF(CSTH.GT.1.) CSTH=1.
      IF(CSTH.LT.-1.) CSTH=-1.
      TH=ACOS(CSTH)
      TH=TH*57.3
      WRITE(2,28)
      WRITE(2,29)APB,BMA,CSTH,TH
      WRITE(2,28)
      TOR=ABS(1./R2B-1./R1A-1./R2A)
      TOR=TOR/(1./R2B+1./R1A+1./R2A)
      ATOR=ACOS(TOR)
      ATOR=ATOR*57.3
      WRITE(2,129)TOR,ATOR
      A=(APB-BMA)/2.
      B=BMA+A
      WRITE(2,141)A,B
C          CONTACT POINT A (TREAD)(L.H.SIDE)
C          TO FIND R1A
      IF(-YA.GT.YT(1).AND.-YA.LT.YT(2)) R1A=RL(1)
      IF(-YA.GT.YT(2).AND.-YA.LT.YT(3)) R1A=RL(2)
      IF(-YA.GT.YT(3).AND.-YA.LT.YT(4)) R1A=RL(3)
      IF(-YA.GT.YT(4).AND.-YA.LT.YT(5)) R1A=RL(4)
      IF(-YA.GT.YT(5).AND.-YA.LT.YT(6)) R1A=RL(5)
```

```
C           R1B = INFINITY
C           TO FIND R2A
C           TO FIND R2B
          R=SQRT(XWA*XWA+ZWA*ZWA)
          IF(-YWA.LT.YW(5)) GO TO 99
          IF(-YWA.GT.YW(5).AND.-YWA.LT.YW(4)) GO TO 40
          IF(-YWA.GT.YW(4).AND.-YWA.LT.YW(3)) GO TO 41
          IF(-YWA.GT.YW(3).AND.-YWA.LT.YW(2)) GO TO 42
          IF(-YWA.GT.YW(2).AND.-YWA.LT.YW(1)) GO TO 43
          GO TO 99
       40 R2A=-RD(3)
          DYX=(BN(3)-R)/(YWA+AN(3))
          GO TO 44
       41 R2A=-RD(2)
          DYX=(BN(2)-R)/(YWA+AN(2))
          GO TO 44
       42 R2A=-RD(1)
          DYX=(BN(1)-R)/(YWA+AN(1))
          GO TO 44
       43 R2A=1000000000000.
          DYX=R/(-QM(1)*(-QM(1)*YWA+C(1)))
       44 CONTINUE
          THB=1./DYX
          THB=ATAN(THB)
          R2B=R/COS(THB)
C           TO CALCULATE ANGLE BETWEEN R1A AND R2A
C           KNOWING 3 POINTS IN A PLANE THE EQUATION OF THE PLANE
C           CONTAINING R2A CAN BE CALCULATED.
C           POINT 1 (XA,YA,ZA) TRACK AXES
C           POINT 2  XW=0., YW=YWA, ZW=0.
          X2=-YWA*SP
          Y2=YO+YWA*CP*CTH
          Z2=ZO-H-YWA*CP*STH
C           POINT 3 XW=0.,YW=0.,ZW=0.
          X3=0.
          Y3=YO
          Z3=ZO-H
C           THEREFORE EQUATION OF PLANE CONTAINING R2A (P.35)
          E=(XA*(ZA-Z2)+(X2-XA)*(ZA-Z3))/((Y3-YA)*(ZA-Z2)+(Z3-ZA)*(Y2-YA))
          F=((X2-XA)+E*(Y2-YA))/(ZA-Z2)
          G=-XA-E*YA-F*ZA
C           ANGLE BETWEEN TWO PLANES. (P.34)
          CSPH=1./SQRT(E*E+F*F+1.*1.)
          PH=ACOS(CSPH)
          PHD=PH*57.3
          WRITE(2,22)
          WRITE(2,142)
          WRITE(2,23)R1A
          WRITE(2,24)
          WRITE(2,25)R2A
          WRITE(2,26)R2B
          WRITE(2,27)PHD
          APB=.5*(1./R1A+1./R2A+1./R2B)
          BMA=(1./R1A)*(1./R1A)+(1./R2A-1./R2B)*(1./R2A-1./R2B)+2.*(1./R1A)
         1(1./R2A-1./R2B)*COS(2.*PH)
          BMA=.5*SQRT(BMA)
          CSTH=BMA/APB
          IF(CSTH.GT.1.) CSTH=1.
          IF(CSTH.LT.-1.) CSTH=-1.
```

```
      TH=ACOS(CSTH)
      TH=TH*57.3
      WRITE(2,28)
      WRITE(2,29)APB,BMA,CSTH,TH
      WRITE(2,28)
      TOR=ABS(1./R2B-1./R1A-1./R2A)
      TOR=TOR/(1./R2B+1./R1A+1./R2A)
      ATOR=ACOS(TOR)
      ATOR=ATOR*57.3
      WRITE(2,129)TOR,ATOR
      A=(APB-BMA)/2.
      B=BMA+A
      WRITE(2,141)A,B
   99 CONTINUE
    2 CONTINUE
      STOP
      END
      MASTER FORCES
      DIMENSION PPD(10),YYTM(10)
      COMMON/CFF/COF(19,4)
C          FORMATS
    1 FORMAT(19F4.0)
   10 FORMAT(8F10.0)
   11 FORMAT(2E11.4)
   16 FORMAT(3I2)
  166 FORMAT(3E20.6)
  200 FORMAT(1H1)
  201 FORMAT(20X,6HINPUTS,10X,8HCASE NO.,I2)
  202 FORMAT(/)
  203 FORMAT(5X,3HUM=,F3.2,2X,5HAPBA=,F7.6,2X,5HAPBB=,F7.5,2X,5HAPBC=,F
     1.5,2X,3HGA=,F4.3,2X,3HGB=,F4.3,2X,3HGC=,F4.3)
  204 FORMAT(5X,3HAM=,F4.2,2X,3HBM=,F4.2,2X,3HCM=,F4.2,2X,3HAN=,F4.3,2X
     13HBN=,F4.3,2X,3HCN=,F4.3)
  205 FORMAT(5X,4HTZA=,F7.0,2X,4HTZB=,F7.0,2X,4HTZC=,F7.0,2X,4HPSI=,F7.
     1,2X,3HAL=,F5.4,2X,3HBL=,F5.3,2X,3HCL=,F6.4)
  207 FORMAT(5X,4HPOK=,E11.4,2X,4HE  = ,E11.4)
  208 FORMAT(5X,8HPHI DOT=,F8.4)
  209 FORMAT(//)
  210 FORMAT(10X,4HG1A=,E13.6,5X,4HG1B=,E13.6,5X,4HG1C=,E13.6)
  211 FORMAT(10X,4HG2A=,E13.6,5X,4HG2B=,E13.6,5X,4HG2C=,E13.6)
  212 FORMAT(10X,4HG3A=,E13.6,5X,4HG3B=,E13.6,5X,4HG3C=,E13.6)
  213 FORMAT(5X,5HKA  = ,I2,2X,5HKB  = ,I2,2X,5HKC  = ,I2)
  220 FORMAT(10X,3HTA=,E13.6,5X,3HUA=,E13.6,5X,3HEA=,E13.6,5X,3HCA=,E13
     16)
  221 FORMAT(10X,4HFXA=,E13.6,5X,4HFYA=,E13.6,5X,4HMZA=,E13.6,10X,4HTY
     1,E13.6)
  222 FORMAT(10X,3HTB=,E13.6,5X,3HUB=,E13.6,5X,3HEB=,E13.6,5X,3HCB=,E13
     16)
  223 FORMAT(10X,4HFXB=,E13.6,5X,4HFYB=,E13.6,5X,4HMZB=,E13.6,10X,4HTY
     1,E13.6)
  224 FORMAT(10X,3HTC=,E13.6,5X,3HUC=,E13.6,5X,3HEC=,E13.6,5X,3HCC=,E13
     16)
  225 FORMAT(10X,4HFXC=,E13.6,5X,4HFYC=,E13.6,5X,4HMZC=,E13.6,10X,4HTY
     1,E13.6)
  300 FORMAT(5X,4HTZT=,F7.0,2X,4HTXT=,F6.1,2X,4HTYT=,F7.0,2X,4HMZT=,F7
     1,2X,4HMYT=,F10.3,2X,4HMXT=,F7.0,2X,7HMYT(W)=,F10.3)
  400 FORMAT(20X,6HOUTPUT)
  744 FORMAT(5X,5HZO  = ,F9.6,3X,4HH  = ,F9.6,3X,4HV  = ,F4.0,3X,7HPPD(1)
     1F8.4,3X,7HPPD(2)=,F8.4)
```

```
  745 FORMAT(5X,4HXTA=,F10.6,2X,4HXTB=,F10.6,2X,4HXTC=,F10.6)
  746 FORMAT(5X,4HYTA=,F10.6,2X,4HYTB=,F10.6,2X,4HYTC=,F10.6)
  747 FORMAT(5X,4HZTA=,F10.6,2X,4HZTB=,F10.6,2X,4HZTC=,F10.6)
  748 FORMAT(5X,4HXWA=,F10.6,2X,4HXWB=,F10.6,2X,4HXWC=,F10.6)
  749 FORMAT(5X,4HZWA=,F10.6,2X,4HZWB=,F10.6,2X,4HZWC=,F10.6)
  822 FORMAT(5X,100HNUMERIC METHOD CAN NOT BE USED TO CALCULATE THE FORC
     1ES AT POINT A BECAUSE A/B RATIO OUT OF RANGE     )
  826 FORMAT(5X,100HNUMERIC METHOD CAN NOT BE USED TO CALCULATE THE FORC
     1ES AT POINT B BECAUSE A/B RATIO OUT OF RANGE     )
  828 FORMAT(10X,4HT3A=,E13.6)
  829 FORMAT(5X,100HNUMERIC METHOD CAN NOT BE USED TO CALCULATE THE FORC
     1ES AT POINT C BECAUSE A/B RATIO OUT OF RANGE     )
  831 FORMAT(10X,4HT3B=,E13.6)
  832 FORMAT(10X,4HT3C=,E13.6)
 1202 FORMAT(5X,5HYO = ,F5.3,3X,6HPSI = ,F6.3)
      IT=1
      READ(1,1)((COF(I,J),I=1,19)J=1,4)
      READ(1,11)POK,E
      DO 2000 NCASES=1,2
      READ(1,10)PPD(1),PPD(2)
      READ(1,10)UM,APBA,APBB,APBC,GA,GB,GC,YO
      READ(1,16)KA,KB,KC
      READ(1,10)AM,BM,CM,AN,BN,CN
      READ(1,10)TZA,TZB,TZC,PSI,AL,BL,CL
      READ(1,10)YTA,YTB,YTC,XTA,XTB,XTC,ZO,H
      READ(1,10)ZTA,ZTB,ZTC,ZWA,ZWB,ZWC
      READ(1,10)XWA,XWB,XWC,V
      WRITE(2,200)
      WRITE(2,201)NCASES
      WRITE(2,202)
      WRITE(2,1202)YO,PSI
      PSI=PSI/57.3
      WRITE(2,203)UM,APBA,APBB,APBC,GA,GB,GC
      WRITE(2,213)KA,KB,KC
      WRITE(2,204)AM,BM,CM,AN,BN,CN
      WRITE(2,205)TZA,TZB,TZC,PSI,AL,BL,CL
      WRITE(2,207)POK,E
      WRITE(2,744)ZO,H,V,PPD(1),PPD(2)
      WRITE(2,745)XTA,XTB,XTC
      WRITE(2,746)YTA,YTB,YTC
      WRITE(2,747)ZTA,ZTB,ZTC
      WRITE(2,748)XWA,XWB,XWC
      WRITE(2,749)ZWA,ZWB,ZWC
      WRITE(2,209)
      WRITE(2,400)
      WRITE(2,202)
      CP=COS(PSI)
      SP=SIN(PSI)
      CLA=COS(AL)
      CLB=COS(BL)
      CLC=COS(CL)
      SLA=SIN(AL)
      SLB=SIN(BL)
      SLC=SIN(CL)
      PI=3.141593
      XTA=XTA/12.
      XTB=XTB/12.
      XTC=XTC/12.
      ZWA=ZWA/12.
```

```
      ZWB=ZWB/12.
      ZWC=ZWC/12.
      XWA=XWA/12.
      XWB=XWB/12.
      XWC=XWC/12.
      ELA=YO-YTA
      ELB=YTB-YO
      ELC=YTC-YO
      ELA=ELA/12.
      ELB=ELB/12.
      ELC=ELC/12.
      RAR=ZTA-ZO+H
      RBR=ZTB-ZO+H
      RCR=ZTC-ZO+H
      RAR=RAR/12.
      RBR=RBR/12.
      RCR=RCR/12.
      RA=(1./(.5*APBA))/12.
      RB=(1./(.5*APBB))/12.
      IF(APBC.EQ.0.) GO TO 1209
      RC=(1./(.5*APBC))/12.
      GO TO 1210
 1209 RC=0.
 1210 CONTINUE
      APBA=APBA*12.
      APBB=APBB*12.
      APBC=APBC*12.
      DO 21 I=1,10
      IF(I.LE.2) GO TO 12
      IF(I.EQ.3) GO TO 13
      IM1=I-1
      IM2=I-2
      IM3=I-3
      PPD(I)=PPD(IM1)-YYTM(IM1)/((YYTM(IM3)-YYTM(IM2))/(PPD(IM3)-PPD(IM2
     1)))
      GO TO 12
   13 PPD(I)=(YYTM(2)*(PPD(2)-PPD(1)))/(YYTM(1)-YYTM(2))+PPD(2)
   12 PD=PPD(I)
      WRITE(2,208)PD
      VA=0.5*(V-PD*RAR*CP)
      VB=0.5*(V-PD*RBR*CP)
      VC=0.5*(V-PD*RCR*CP)
      G1A=(V+PD*RAR*CP)/VA
      G1B=(V+PD*RBR*CP)/VB
      G1C=(V+PD*RCR*CP)/VC
      G2A=PD*RAR*SP*CLA/VA
      G2B=PD*RBR*SP*CLB/VB
      G2C=PD*RCR*SP*CLC/VC
      G3A=-PD*CP*SLA/VA
      G3B=PD*CP*SLB/VB
      G3C=PD*CP*SLC/VC
      T3A=TZA/CLA
      T3B=TZB/CLB
      T3C=TZC/CLC
      DO 61 J=1,3
      ABA=.75*PI*T3A*POK/APBA
      ABA=ABA*ABA
      ABA=ABA**.3333333
      ABA=AM*AN*ABA
```

```
      CA=SQRT(ABA)
      EA=(G1A*RA)/(UM*CA)
      UA=(G2A*RA)/(UM*CA)
      TA=G3A*RA/UM
      IFA=1
      TV=TA
      GK=GA
      CALL NUMERIC(GA,KA,TA,UA,EA,FXA,FYA,ZMA,IFA,IT)
      IF(IFA.EQ.2) GO TO 261
      T3A2=T3A
      T3A=TZA/(CLA+UM*FYA*SLA)
      DA=T3A-T3A2
   61 CONTINUE
  261 CONTINUE
      IFB=1
      IF(TZB.EQ.0.) GO TO 162
      DO 62 J=1,3
      ABB=.75*PI*T3B*POK/APBB
      ABB=ABB*ABB
      ABB=ABB**.3333333
      ABB=BM*BN*ABB
      CB=SQRT(ABB)
      EB=(G1B*RB)/(UM*CB)
      UB=(G2B*RB)/(UM*CB)
      TB=G3B*RB/UM
      GJ=GB
      TX=TB
      JBJ=1
      IFB=1
      CALL SIMP(EB,UB,TX,GJ,KB,10,3,FXB,FYB,ZMB,JBJ)
      IF(IFB.EQ.2) GO TO 262
      T3B2=T3B
      T3B=TZB/(CLB-UM*FYB*SLB)
      DB=T3B-T3B2
   62 CONTINUE
  262 CONTINUE
      GO TO 163
  162 TZB=0.
      T3B=0.
      FXB=0.
      FYB=0.
      ZMB=0.
  163 CONTINUE
      IFC=1
      IF(TZC.EQ.0.) GO TO 164
      DO 63 J=1,3
      ABC=.75*PI*T3C*POK/APBC
      ABC=ABC*ABC
      ABC=ABC**.3333333
      ABC=CM*CN*ABC
      CC=SQRT(ABC)
      EC=(G1C*RC)/(UM*CC)
      UC=(G2C*RC)/(UM*CC)
      TC=G3C*RC/UM
      GG=GC
      TT=TC
      JJ=1
      CALL SIMP(EC,UC,TT,GG,KC,10,1,FXC,FYC,ZMC,JJ)
      IF(IFC.EQ.2) GO TO 263
```

```
      T3C2=T3C
      T3C=TZC/(CLC-UM*FYC*SLC)
      DC=T3C-T3C2
   63 CONTINUE
  263 CONTINUE
      GO TO 165
  164 TZC=0.
      T3C=0.
      FXC=0.
      FYC=0.
      ZMC=0.
  165 CONTINUE
      IF(IFA.EQ.1) GO TO 821
      WRITE(2,822)
      GO TO 825
  821 CONTINUE
      T1A=UM*T3A*FXA
      A3M=UM*T3A*CA*ZMA
      TYA=UM*T3A*FYA*CLA-T3A*SLA
  825 IF(IFB.EQ.1) GO TO 823
      WRITE(2,826)
      GO TO 827
  823 CONTINUE
      T1B=UM*T3B*FXB
      B3M=UM*T3B*CB*ZMB
      TYB=UM*T3B*FYB*CLB+T3B*SLB
  827 IF(IFC.EQ.1) GO TO 824
      WRITE(2,829)
      GO TO 830
  824 CONTINUE
      T1C=UM*T3C*FXC
      C3M=UM*T3C*CC*ZMC
      TYC=UM*T3C*FYC*CLC+T3C*SLC
  830 CONTINUE
C               TOTAL FORCES
      IF(IFA.EQ.2) GO TO 1000
      IF(IFB.EQ.2) GO TO 1000
      IF(IFC.EQ.2) GO TO 1000
      TXA=T1A
      TXB=T1B
      TXC=T1C
      TXT=TXA+TXB+TXC
      TYT=TYA+TYB+TYC
      TZT=TZA+TZB+TZC
      ZAM=A3M*CLA
      ZBM=B3M*CLB
      ZCM=C3M*CLC
      YAM=-A3M*SLA
      YBM=B3M*SLB
      YCM=C3M*SLC
      ZTM=ZAM+ZBM+ZCM+TXA*ELA+TYA*XTA-TXB*ELB+TYB*XTB-TXC*ELC+TYC*XTC
      YTM=YAM+YBM+YCM+TXA*RAR+TXB*RBR+TXC*RCR-TZA*XTA-TZB*XTB-TZC*XTC
      XTM=-TYA*RAR-TZA*ELA-TYB*RBR+TZB*ELB-TYC*RCR+TZC*ELC
      TXWA=TXA*CP+TYA*SP*CTH+TZA*SP*STH
      TZWA=TYA*STH+TZA*CTH
      TXWB=TXB*CP+TYB*SP*CTH+TZB*SP*STH
      TZWB=TYB*STH+TZB*CTH
      TXWC=TXC*CP+TYC*SP*CTH+TZC*SP*STH
      TZWC=TYC*STH+TZC*CTH
```

```
      WMYA=YAM*CP*CTH-ZAM*STH*CP
      WMYB=YBM*CP*CTH-ZBM*STH*CP
      WMYC=YCM*CP*CTH-ZCM*STH*CP
      YWTM=WMYA+WMYB+WMYC+TXWA*ZWA+TXWB*ZWB+TXWC*ZWC-TZWB*XWB-TZWC*XWC-T
     1ZWA*XWA
      YYTM(I)=YWTM
      WRITE(2,300)TZT,TXT,TYT,ZTM,YTM,XTM,YWTM
      AYTM=ABS(YWTM)
      IF(AYTM.LT..001) GO TO 22
   21 CONTINUE
   22 CONTINUE
      WRITE(2,210)G1A,G1B,G1C
      WRITE(2,211)G2A,G2B,G2C
      WRITE(2,212)G3A,G3B,G3C
      WRITE(2,828)T3A
      WRITE(2,220)TA,UA,EA,CA
      WRITE(2,831)T3B
      WRITE(2,222)TB,UB,EB,CB
      WRITE(2,832)T3C
      WRITE(2,224)TC,UC,EC,CC
      WRITE(2,221)FXA,FYA,ZMA,TYA
      WRITE(2,223)FXB,FYB,ZMB,TYB
      WRITE(2,225)FXC,FYC,ZMC,TYC
 1000 CONTINUE
 2000 CONTINUE
      STOP
      END
      MASTER LAB
      COMMON/CFF/COF(19,4)
C          FORMATS
    1 FORMAT(19F4.0)
    2 FORMAT(5X,43HNUMERIC METHOD CANNOT BE USED FOR THIS CASE)
   10 FORMAT(8F10.0)
   11 FORMAT(2E11.4)
   12 FORMAT(5X,5HCASE ,I2)
   16 FORMAT(4F10.0,I10)
   30 FORMAT(5X,4HAPB=,F7.5,2X,2HG=,F4.2,2X,2HW=,F3.0,2X,3HAL=,F8.6,2X,2
     1HM=,F4.2,2X,2HN=,F4.2,2X,4HPSI=,F8.6,2X,3HMU=,F4.2)
   31 FORMAT(5X,3HRR=,F7.5,2X,3HRW=,F5.3,2X,4HPOK=,E13.6,2X,2HE=,E13.6,2
     1X,3HKA=,I2)
   32 FORMAT(5X,4HT3A=,E13.6,2X,3HTY=,E13.6,2X,3HMY=,E13.6,2X,3HMZ=,E13.
     16,2X,3HFW=,E13.6,2X,4HPLT=,E13.6)
   33 FORMAT(5X,3HCA=,F8.6,2X,3HEA=,F9.6,2X,3HUA=,F9.6,2X,3HTA=,F9.6,2X,
     14HFXA=,F6.4,2X,4HFYA=,F6.4,2X,4HMZA=,F7.4,2X,6HFY*UM=,F9.6)
  166 FORMAT(3E20.6)
  200 FORMAT(1H1)
  201 FORMAT(20X,6HINPUTS)
  202 FORMAT(/)
~~201 F/."A;R20JV6HIX?';;[~~
  400 FORMAT(20X,6HOUTPUT)
      IT=1
      READ(1,1)((COF(I,J),I=1,19)J=1,4)
      READ(1,11)POK,E
      READ(1,10)RR,RW,AL
      RR=RR/12.
      RW=RW/12.
      AL=AL/57.3
      SLA=SIN(AL)
      CLA=COS(AL)
```

```
      PI=3.141593
      WRITE(2,200)
      READ(1,16)APBA,GA,AM,AN,KA
      RA=(1./(.5*APBA))/12.
      APBA=APBA*12.
      W=59.
      UM=.4
      DO 100 JKB=1,4
      UM=UM+.1
      T3A=W/CLA
      PSI=-.005
      DO 100 JKC=1,24
      PSI=PSI+.0005
      WRITE(2,166)T3A
      DO 61 J=1,20
      ABA=.75*PI*T3A*POK/APBA
      ABA=ABA*ABA
      ABA=ABA**.3333333
      ABA=AM*AN*ABA
      CA=SQRT(ABA)
      UA=-RA*PSI/(CLA*UM*CA)
      EA=0.
      TA=+RA*SLA*(1./RR+1./RW)/UM
      TV=TA
      GK=GA
      IFA=1
      CALL NUMERIC(GK,KA,TV,UA,EA,FXA,FYA,ZMA,IFA,IT)
      IF(IFA.EQ.2) GO TO 99
   64 CONTINUE
      T3A2=T3A
      TES=(CLA+UM*FYA*SLA)
      IF(TES.LE.0.) GO TO 63
      T3A=-W/(CLA+UM*FYA*SLA)
      GO TO 62
   63 T3A=-W*100.
   62 CONTINUE
      WRITE(2,166)T3A
      DIFF=ABS(T3A2-T3A)
      IF(DIFF.LE..5) GO TO 65
   61 CONTINUE
   65 CONTINUE
      TY=T3A*(UM*FYA*CLA-SLA)
      YM=-UM*T3A*CA*ZMA*SLA
      ZM=UM*T3A*CA*ZMA*CLA
      FW=TY/W
      WRITE(2,201)
      WRITE(2,30)APBA,GA,W,AL,AM,AN,PSI,UM
      WRITE(2,31)RR,RW,POK,E,KA
      WRITE(2,400)
      FYUM=UM*FYA
      PLT=PSI/((-T3A)**.3333333)
      WRITE(2,33)CA,EA,UA,TA,FXA,FYA,ZMA,FYUM
      WRITE(2,32)T3A,TY,YM,ZM,FW,PLT
      ~~.I:ER2V33[CAVEAV*AV:AVFJAVFKAV$"AVFK[~~
      WRITE(2,202)
      GO TO 100
   99 WRITE(2,2)
  100 CONTINUE
      STOP
```

APPENDIX 6

Coordinate Geometry

1. Plane through 3 given points

Assume equation of plane given by $ax + by + cz + d = 0$ and this passes through points (x_1, y_1, z_1), (x_2, y_2, z_2), (x_3, y_3, z_3)

Then
$$ax_1 + by_1 + cz_1 + d = 0 \quad (1)$$
$$ax_2 + by_2 + cz_2 + d = 0 \quad (2)$$
$$ax_3 + by_3 + cz_3 + d = 0 \quad (3)$$

or
$$x_1 + (b/a)y_1 + (c/a)z_1 + (d/a) = 0 \quad (4)$$
$$x_2 + (b/a)y_2 + (c/a)z_2 + (d/a) = 0 \quad (5)$$
$$x_3 + (b/a)y_3 + (c/a)z_3 + (d/a) = 0 \quad (6)$$

if $e = (b/a)$, $f = (c/a)$, $g = (d/a)$, then from equation 4

$$g = -x_1 - e\,y_1 - f\,z_1 \quad (7)$$

from equations 5 and 7

$$f = \frac{(x_2 - x_1) + e(y_2 - y_1)}{(z_1 - z_2)} \quad (8)$$

Substituting for g and f from equations 7 and 8, into equation 6 and rearranging

$$e = \frac{(x_1 - x_3)(z_1 - z_2) + (x_2 - x_1)(z_1 - z_3)}{(y_3 - y_1)(z_1 - z_2) + (z_3 - z_1)(y_2 - y_1)} \quad (9)$$

equation of plane is

$$x + ey + fz + g = 0 \quad (10)$$

2. Angle between 2 Planes

If the equations of the planes are

$$\left.\begin{aligned} x + ey + fz + g &= 0 \\ \text{and}\quad x + e'y + f'z + g' &= 0 \end{aligned}\right\} \quad (11)$$

Then angle between planes

$$= \cos^{-1}\left\{ \frac{\pm (1 + ee' + ff')}{\sqrt{(1 + e^2 + f^2)(1 + e'^2 + f'^2)}} \right\}$$

(In the case of contact between rail and wheel, the equation of a plane through the rail has the equation

$$x_t = K$$

∴ angle between planes

$$= \cos^{-1}\left\{ \frac{1}{\sqrt{1 + e^2 + f^2}} \right\} \quad)$$

APPENDIX 7

Longitudinal Creep, Lateral Creep and Spin on Roller Rig

(Lower wheel is denoted by suffix 'R')

Assume contact point on lower wheel is originally at the point

$$\underset{\sim}{r}_R = (0, 0, -r_R)$$

and the angular velocity at this point is

$$\underset{\sim}{\omega}_R = (0, \dot{\Phi}_R, 0)$$

where $\dot{\Phi}_R$ is the angular velocity of the lower wheel.

When the upper wheel is yawed through an angle ψ relative to the lower wheel, the contact point on the lower wheel moves forward and laterally by small amounts x_R and y_R respectively, relative to the original contact point so that the new position vector becomes $\underset{\sim}{r}_R = (x_R, y_R, -r_R)$.

When one wheel is yawed relative to the other wheel, the tangent plane, in plan view, between the surfaces, rotates through an angle α where

$$\alpha < \psi$$

and the transformation matrix is

$$\begin{bmatrix} 1 & \alpha & 0 \\ -\alpha & 1 & 0 \\ 0 & 0 & 1 \end{bmatrix}$$

If λ is the cone angle of the upper wheel, i.e. the angle between the tangent plane and the horizontal, then the contact point can be defined in axes in the plane of, and normal to, the contact area using the transformation matrix

$$\begin{bmatrix} 1 & 0 & 0 \\ 0 & \cos\lambda & \sin\lambda \\ 0 & -\sin\lambda & \cos\lambda \end{bmatrix}$$

Combining these transformation matrices they become

$$\begin{bmatrix} 1 & \alpha & 0 \\ -\alpha\cos\lambda & \cos\lambda & \sin\lambda \\ \alpha\sin\lambda & -\sin\lambda & \cos\lambda \end{bmatrix}$$

(The axes systems for the upper and lower wheels are shown in Fig. A7.1)

Thus, the position vector becomes

$$\underset{\sim}{r}_R = \left(x_R + \alpha y_R, -x_R\alpha\cos\lambda + y_R\cos\lambda - r_R\sin\lambda, x_R\alpha\sin\lambda - y_R\sin\lambda - r_R\cos\lambda\right)$$

and the angular velocity vector

$$\underset{\sim}{\omega}_R = \left(\alpha\dot{\Phi}_R, \dot{\Phi}_R\cos\lambda, -\dot{\Phi}_R\sin\lambda\right)$$

The velocity vector is given by $(\underset{\sim}{r}_R \wedge \underset{\sim}{\omega}_R)$

so that

$$(\underset{\sim}{r}_R \wedge \underset{\sim}{\omega}_R)_1 = -\dot{\Phi}_R\sin\lambda\left(y_R\cos\lambda - r_R\sin\lambda - x_R\alpha\cos\lambda\right) - \dot{\Phi}_R\cos\lambda\left(x_R\alpha\sin\lambda - y_R\sin\lambda - r_R\cos\lambda\right) \quad (1)$$

and

$$(\underset{\sim}{r}_R \wedge \underset{\sim}{\omega}_R)_3 = \dot{\Phi}_R\cos\lambda\left(x_R + \alpha y_R\right) - \alpha\dot{\Phi}_R\left(y_R\cos\lambda - r_R\sin\lambda - x_R\alpha\cos\lambda\right) \quad (2)$$

But α and y_R are small quantities so that $\alpha y_R \simeq 0$

Therefore $(\underset{\sim}{r}_R \wedge \underset{\sim}{\omega}_R)_3 = x_R\dot{\Phi}_R\cos\lambda + \alpha\dot{\Phi}_R r_R\sin\lambda \quad (3)$

Assuming $(\underset{\sim}{r}_R \wedge \underset{\sim}{\omega}_R)_3 = 0$

Then $x_R = -\alpha r_R\tan\lambda \quad (4)$

and $(\underset{\sim}{r}_R \wedge \underset{\sim}{\omega}_R)_2 = -\dot{\Phi}_R\sin\lambda(x_R + \alpha y_R) - \alpha\dot{\Phi}_R(x_R\alpha\sin\lambda - y_R\sin\lambda - r_R\cos\lambda)$

$$= -x_R\dot{\Phi}_R\sin\lambda + r_R\alpha\dot{\Phi}_R\cos\lambda$$

$$= \alpha r_R\tan\lambda\,\dot{\Phi}_R\sin\lambda + r_R\alpha\dot{\Phi}_R\cos\lambda$$

$$= \frac{\alpha r_R\dot{\Phi}_R}{\cos\lambda} \quad (5)$$

FIG. A7.1 Axes System for Upper & Lower Wheels

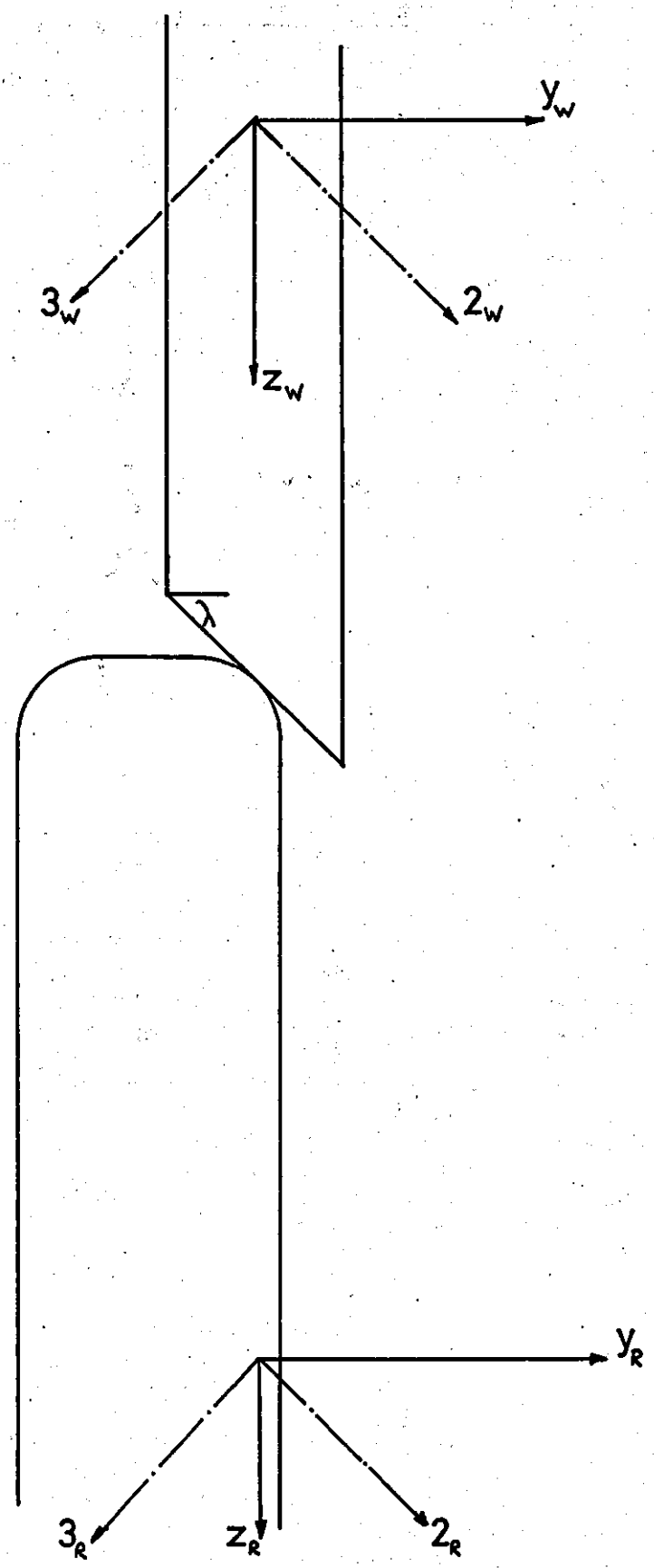

If the upper wheel is denoted by suffix 'W' then a similar set of equations may be derived for the contact point on this wheel.

If $\underset{\sim}{r}_W = (x_W, y_W, r_W)$

and $\underset{\sim}{\omega}_W = (0, \dot{\Phi}_W, 0)$

Assuming the contact point on the upper wheel is rotated through an angle $(-\beta)$ (see Fig. A8.1) then the transformation matrix becomes

$$\begin{bmatrix} 1 & -\beta & 0 \\ \beta\cos\lambda & \cos\lambda & \sin\lambda \\ -\beta\sin\lambda & -\sin\lambda & \cos\lambda \end{bmatrix}$$

Therefore the position vector is:

$$\underset{\sim}{r}_W = \left(x_w - y_w\beta,\ x_w\beta\cos\lambda + y_w\cos\lambda + r_w\sin\lambda,\ -\beta x_w\sin\lambda - y_w\sin\lambda + r_w\cos\lambda\right)$$

and the angular velocity vector becomes:

$$\underset{\sim}{\omega}_W = \left(-\beta\dot{\Phi}_W,\ \dot{\Phi}_W\cos\lambda,\ -\dot{\Phi}_W\sin\lambda\right)$$

The velocity vector is given by $(\ \underset{\sim}{r}_W \wedge \underset{\sim}{\omega}_W\ )$

so that

$$\begin{aligned}(\ \underset{\sim}{r}_W \wedge \underset{\sim}{\omega}_W\ )_1 &= -\dot{\Phi}_W\sin\lambda\left(x_w\beta\cos\lambda + y_w\cos\lambda + r_w\sin\lambda\right) \\ &\quad -\dot{\Phi}_W\cos\lambda\left(r_w\cos\lambda - \beta x_w\sin\lambda - y_w\sin\lambda\right) \\ &= -\dot{\Phi}_W r_W \qquad (6)\end{aligned}$$

$$(\ \underset{\sim}{r}_W \wedge \underset{\sim}{\omega}_W\ )_3 = \dot{\Phi}_W\cos\lambda\left(x_w - y_w\beta\right) + \beta\dot{\Phi}_W\left(r_w\sin\lambda\right)$$

Since y_W and β are small quantities $\quad y_W\beta \doteq 0$

and assuming $(\ \underset{\sim}{r}_W \wedge \underset{\sim}{\omega}_W\ )_3 = 0$

Then $\qquad x_W = -\beta r_w\tan\lambda \qquad (7)$

$$(\underset{\sim}{r}_R \wedge \underset{\sim}{\omega}_W)_2 = -\dot{\Phi}_W \sin\lambda\, x_W + \beta \dot{\Phi}_W r_W \cos\lambda$$

$$= \dot{\Phi}_W \sin\lambda . \beta . r_W . \tan\lambda + \beta \dot{\Phi}_W r_W \cos\lambda$$

$$= \frac{\beta r_W \dot{\Phi}_W}{\cos\lambda} \qquad (8)$$

Now $x_R = x_W$

From equations 4 and 7

$$-\alpha . r_R . \tan\lambda = -\beta . r_W . \tan\lambda$$

Therefore $$\alpha . r_R = \beta . r_W \qquad (9)$$

This result is obvious from the geometry of the system and can be seen in Fig. A8.1.

If the <u>longitudinal creep</u> is defined as

$$\gamma_1 = \frac{(\underset{\sim}{r}_W \wedge \underset{\sim}{\omega}_W)_1 - (\underset{\sim}{r}_R \wedge \underset{\sim}{\omega}_R)_1}{|V|}$$

where $$|V| = \left| \tfrac{1}{2} \left((\underset{\sim}{r}_W \wedge \underset{\sim}{\omega}_W)_1 + (\underset{\sim}{r}_R \wedge \underset{\sim}{\omega}_R) \right) \right|$$

i.e. $$\gamma_1 = \frac{-\dot{\Phi}_W r_W - \dot{\Phi}_R r_R}{\left| \tfrac{1}{2} (-\dot{\Phi}_W r_W + \dot{\Phi}_R r_R) \right|}$$

Thus the condition for zero longitudinal creep is

$$-\dot{\Phi}_W r_W - \dot{\Phi}_R r_R = 0$$

or $$\dot{\Phi}_W r_W = -\dot{\Phi}_R r_R \qquad (10)$$

The <u>lateral creep</u> is defined as

$$\gamma_2 = \frac{(\underset{\sim}{r}_W \wedge \underset{\sim}{\omega}_W)_2 - (\underset{\sim}{r}_R \wedge \underset{\sim}{\omega}_R)_2}{|V|}$$

$$= \frac{\dfrac{\beta r_W \dot{\Phi}_W}{\cos\lambda} - \dfrac{\alpha r_R \dot{\Phi}_R}{\cos\lambda}}{|V|}$$

$$= \frac{(-\beta \dot{\Phi}_R r_R - \alpha r_R \dot{\Phi}_R)}{|V| \cos\lambda}$$

$$= \frac{-\dot{\Phi}_R r_R (\alpha + \beta)}{|V| \cos\lambda} \qquad (11)$$

It is shown in Appendix 8 that the yaw angle $\psi = \alpha + \beta$

Therefore $$\gamma_2 = \frac{-\dot{\Phi}_R r_R \psi}{|V| \cos\lambda} \qquad (12)$$

(It can be seen from this expression that γ_2 depends on the direction of rotation of the wheel)

The <u>spin</u> is defined as

$$\omega_3 = \frac{\underset{\sim}{\omega}_{W3} - \underset{\sim}{\omega}_{R3}}{|V|}$$

$$= \frac{-\dot{\Phi}_W \sin\lambda + \dot{\Phi}_R \sin\lambda}{|V|}$$

$$= \frac{\left(\frac{\dot{\Phi}_R r_R}{r_W} + \dot{\Phi}_R\right) \sin\lambda}{|V|}$$

$$= \frac{\dot{\Phi}_R}{\dot{\Phi}_R r_R} \left(\frac{r_R}{r_W} + 1\right) \sin\lambda$$

$$= \left(\frac{1}{r_W} + \frac{1}{r_R}\right) \sin\lambda \qquad (13)$$

(The spin ω_3 does not depend on the rotation of the wheel)

APPENDIX 8

Angle of yaw, ψ, of upper wheel relative to lower wheel

Assume ψ = angle of yaw of upper wheel relative to lower wheel.

α = angle of rotation of contact point on lower wheel.

β = angle of rotation of contact point on upper wheel.

Since both upper and lower wheels are bodies of revolution, in plan view they can be represented by circles which roll around each other, as shown in Fig. A8.1

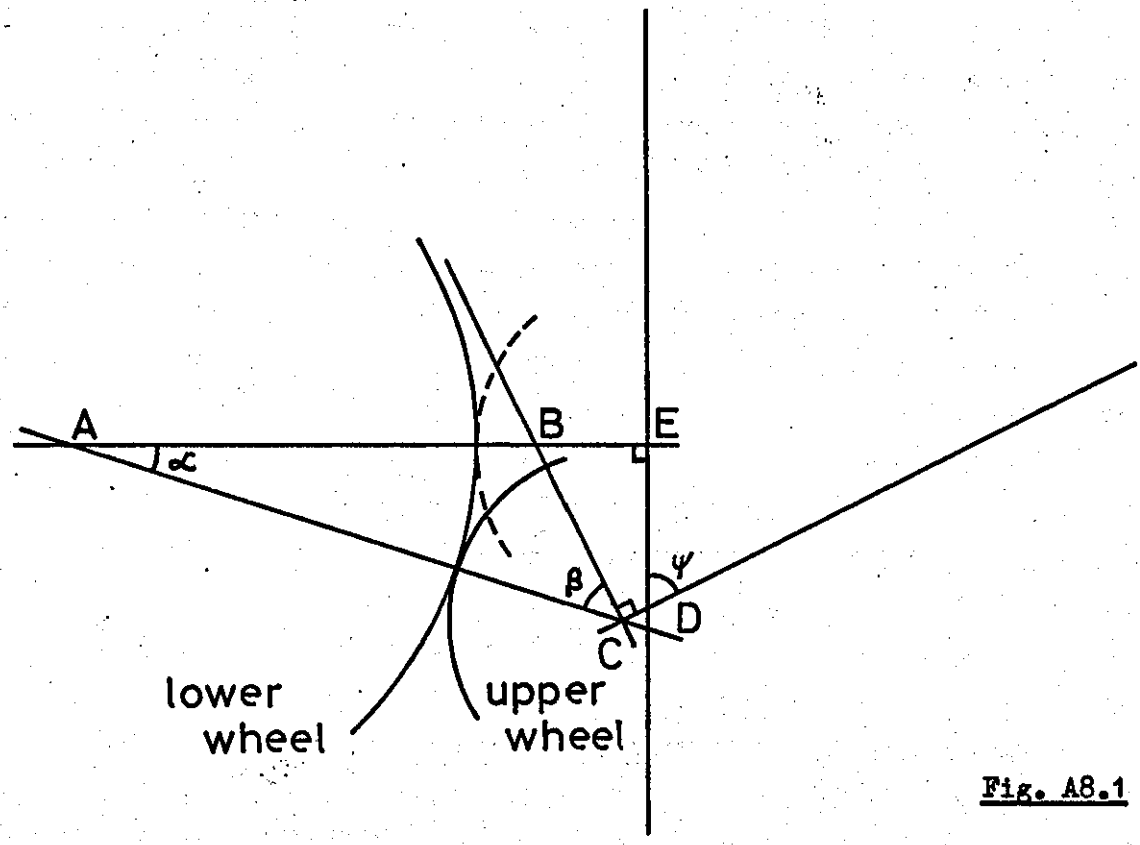

Fig. A8.1

From Fig. A8.1

$$\widehat{ABC} = 180^\circ - (\alpha + \beta)$$

$$\widehat{EBC} = \alpha + \beta$$

$$\widehat{EDC} = 180^\circ - \psi$$

$$\widehat{EBC} + \widehat{EDC} = 180^\circ$$

$$\alpha + \beta + 180^\circ - \psi = 180^\circ$$

$$\psi = \alpha + \beta$$

APPENDIX 9

Contact Ellipse Semi-Axes a, b

Assume $R_x^{\pm}$, $R_y^{\pm}$ are the principal radii of curvature at the point of contact between two bodies of revolution, where + refers to the lower body and - to the upper body. These are considered +ve if the centre of curvature lies within the body. It may be noted that for the body of revolution shown in Fig. A9.1, the principal radii are given by R_1 and $(R_2 / \cos\alpha)$

If, ψ = angle between planes containing R_x^+ and R_x^-, then constants A and B may be defined as:

$$A + B = \frac{1}{2}\left(\frac{1}{R_x^+} + \frac{1}{R_x^-} + \frac{1}{R_y^+} + \frac{1}{R_y^-}\right) \tag{1}$$

and $$B - A = \frac{1}{2}\left[\left(\frac{1}{R_x^+} - \frac{1}{R_y^+}\right)^2 + \left(\frac{1}{R_x^-} - \frac{1}{R_y^-}\right)^2 + 2\left(\frac{1}{R_x^+} - \frac{1}{R_y^+}\right)\left(\frac{1}{R_x^-} - \frac{1}{R_y^-}\right)\cos 2\psi\right]^{\frac{1}{2}} \tag{2}$$

and $$\cos\theta = \frac{B - A}{A + B} \tag{3}$$

The semiaxes of the contact ellipse a and b are given by

$$a = m\sqrt[3]{\frac{3\pi}{4} \cdot \frac{N(k_1 + k_2)}{(A+B)}} \tag{4}$$

and $$b = n\sqrt[3]{\frac{3\pi}{4} \cdot \frac{N(k_1 + k_2)}{(A+B)}} \tag{5}$$

where m and n are functions of θ and are plotted in Fig. A9.2

$$k_1 = \frac{1 - \sigma_1^2}{\pi E_1} \qquad \text{and} \qquad k_2 = \frac{1 - \sigma_2^2}{\pi E_2}$$

(k_1 & k_2 are equal, if the elastic constants of both bodies are the same).

N = normal force

It may be noted that (a/b) = (m/n), and therefore does not depend on the normal force whereas the actual values of a and b do.

FIG. A 9.1 Principal Radii of Body of Revolution

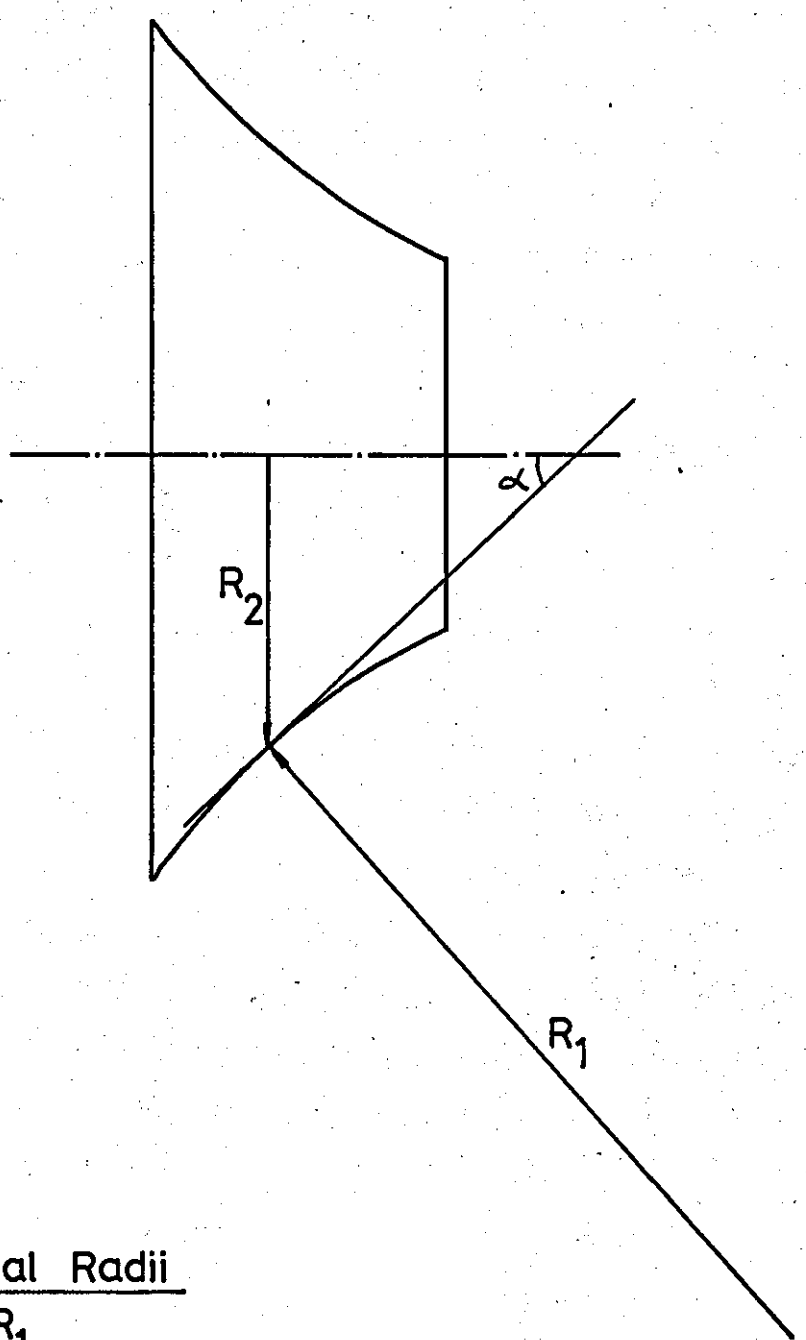

Principal Radii	
R_1	
$\left(\frac{R_2}{\cos\alpha}\right)$	

FIG. A9·2 Contact Ellipse Constants m, n, g, E v θ

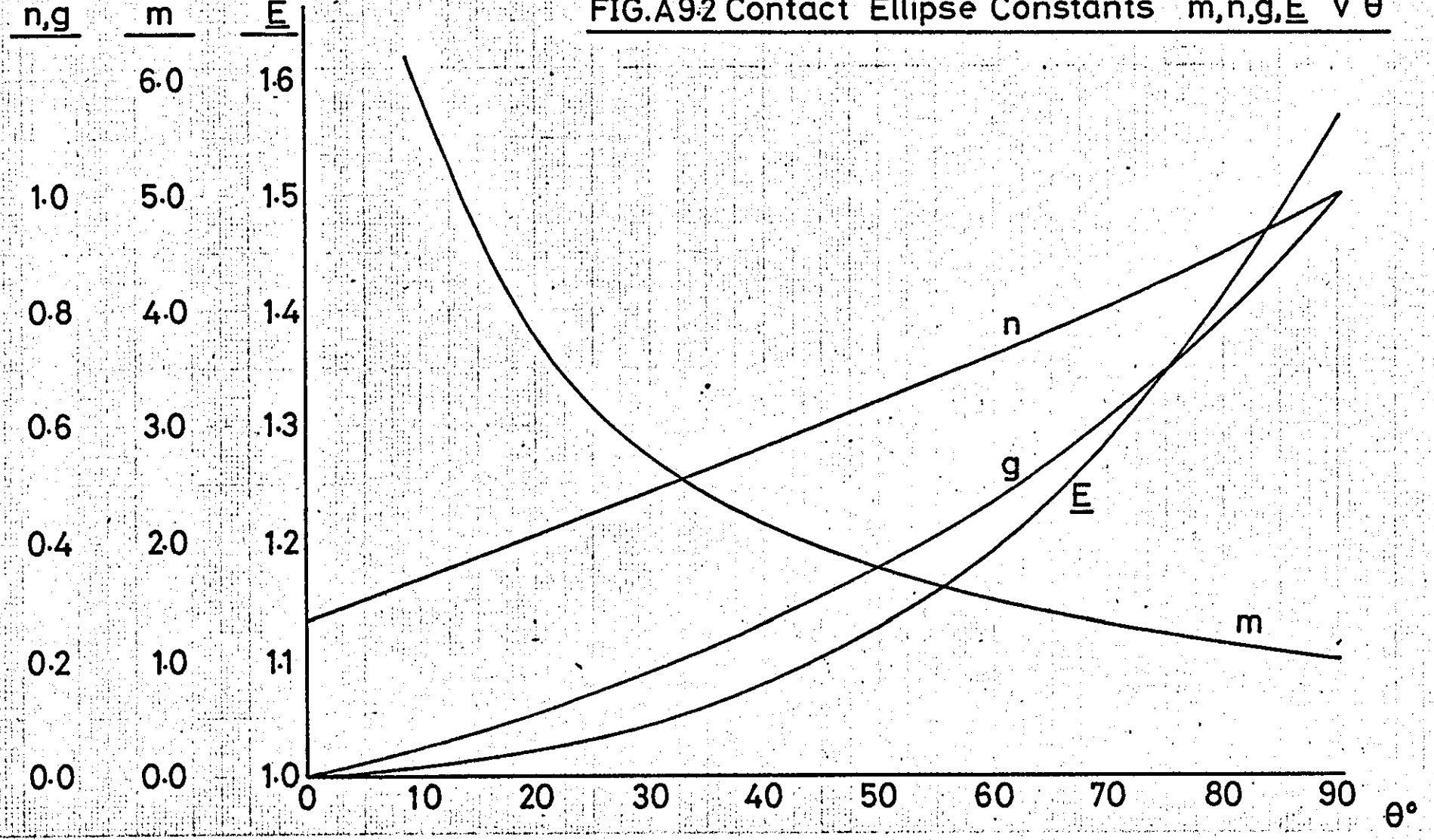

Small Yaw Angle Approximation

If the angle ψ is small then the expressions for the constants may be written as:

$$A = \frac{1}{2}\left(\frac{1}{R_x^+} + \frac{1}{R_x^-}\right) \quad (6)$$

and $$B = \frac{1}{2}\left(\frac{1}{R_y^+} + \frac{1}{R_y^-}\right) \quad (7)$$

A term ρ, called the characteristic length of the bodies is defined as

$$\frac{1}{\rho} = \frac{A+B}{2} = \frac{1}{4}\left(\frac{1}{R_x^+} + \frac{1}{R_x^-} + \frac{1}{R_y^+} + \frac{1}{R_y^-}\right) \quad (8)$$

and $$\cos\theta = \frac{\left|\frac{1}{R_x^+} + \frac{1}{R_x^-} - \frac{1}{R_y^+} - \frac{1}{R_y^-}\right|}{\left(\frac{1}{R_x^+} + \frac{1}{R_x^-} + \frac{1}{R_y^+} + \frac{1}{R_y^-}\right)} \quad (9)$$

g = min. (a/b, b/a) is plotted in Fig. A9.2 as a function of θ

If $A \geqslant B$ then $a \leqslant b$

and if $A \leqslant B$ then $b \leqslant a$

This gives the ~~slope~~ shape of the contact ellipse. The actual size of the contact ellipse also depends on the normal load and it may be shown that

$$(A+B) = \frac{3N(1-\sigma)E}{2\pi G c^3 \sqrt{g}} \text{ or } c = \sqrt[3]{\frac{3N(1-\sigma)E\rho}{4\pi G \sqrt{g}}} \quad (10)$$

where $c = \sqrt{ab}$

E = complete elliptic integral of the 2nd kind, plotted in Fig. A9.2 as a function of θ.

G = Modulus of Rigidity

The size of the contact ellipse can be calculated using equation 10.

The area of contact = πab

The average pressure = $\frac{N}{\pi ab}$

The maximum contact pressure = $\frac{1.5N}{\pi ab}$

APPENDIX 10

Experimental Data Sheet

Date: 10.8.72.

Radius of lower wheel: $\frac{1}{4}$" (6.35 mm)

Cone angle of upper wheel: 49°

Rolling radius of lower wheel: 5.875" (149.2 mm)

Rolling radius of upper wheel: 5.313" (135 mm)

Vertical load (W): 59 lb. (262 N)

Speed of lower wheel: 165 revs/min.

Clinometer static setting: 0° 17

Distance from pivot to contact point: 31.75" (805 mm)

DTI readings with slits of light in line for different wheel positions (static): .2437, .2411, .2398, .2478, .2466, .2520, .2345, .2511, .2356, .2505, .2333

Average value = 0.2433

+ve Rotation

ψ DTI (ins.)	ψ (rad.)	F_{DTI} (mm) Load Ring	F (kN)	μf_2	Clino. (min.)
.21	- .00104	.132	.091	.576	26
.22	- .00072	.147	.101	.533	23
.23	- .00041	.152	.105	.516	23
.24	- .00009	.163	.110	.492	23
.25	.00022	.183	.124	.440	23
.26	.00054	.203	.137	.393	23
.27	.00085	.229	.151	.345	23
.28	.00117	.256	.169	.291	23
.29	.00148	.305	.200	.206	22
.30	.0018	.351	.228	.141	22
.31	.00211	.406	.265	.066	22
.32	.00243	.470	.307	- .008	22
.33	.00274	.559	.365	- .092	22
.34	.00306	.612	.401	- .136	22
.35	.00337	.666	.436	- .175	22
.36	.00369	.757	.497	- .234	22
.37	.0040	.813	.534	- .265	22
.38	.00431	.874	.574	- .295	22
.39	.00463	.975	.641	- .339	22

-ve Rotation

ψ DTI (ins.)	ψ (rad.)	F_{DTI} (mm)	F (kN)	μf_2	Clino.
.21	- .00104	.307	.201	.204	23
.22	- .00072	.264	.174	.275	23
.23	- .00041	.231	.154	.337	22
.24	- .00009	.205	.138	.391	23
.25	.00022	.185	.125	.437	23
.26	.00054	.163	.111	.490	23
.27	.00085	.147	.101	.531	22

APPENDIX 11

Roll Effects on Experimental Rig

Test 1: Deflection of Vertical Supports

A load was applied to the vertical supports and the deflection measured with a dialtest indicator. The results are shown in Fig. A11.1 where the deflection is plotted versus load.

Test 2: Effect of Built-in Roll Moment

A series of tests were carried out on the rig using the lower wheel with the 101.5 mm radius (a) and the 49° upper wheel (d). The lateral load was applied in three different positions, firstly in a horizontal line with the contact point, secondly 6.4 mm below the contact point and thirdly 6.4 mm above the contact point. In eachcase the lateral load required to lift the wheel off its supports was measured for various yaw angles, together with the angle of roll on the clinometer. W = 396 N in each case. The results are plotted in Fig. A11.2 where it can be seen that when the wire is offset there are obvious changes in roll angle as the lateral load is increased. The effects of these changes can be seen in Fig. A11.3 where (μf_2) is plotted against $(\psi / N^{\frac{1}{3}})$ for the measured forces. The change in slope of the results is due to the induced rolling moments.

Test 3: Measurement of Lateral Displacement

A dialtest indicator was fixed in a horizontal position in order to measure lateral displacement of the upper wheel. It was positioned just above the contact point against the flat portion of the wheel. The same wheels were used as in the previous test, i.e. 101.5 mm radius lower wheel with the 49° upper wheel. Tests were carried out with two different vertical loads, W = 396 N and W = 129 N, both with the lateral load applied in a horizontal line with the

FIG. A11·1 Deflection of Vertical Supports

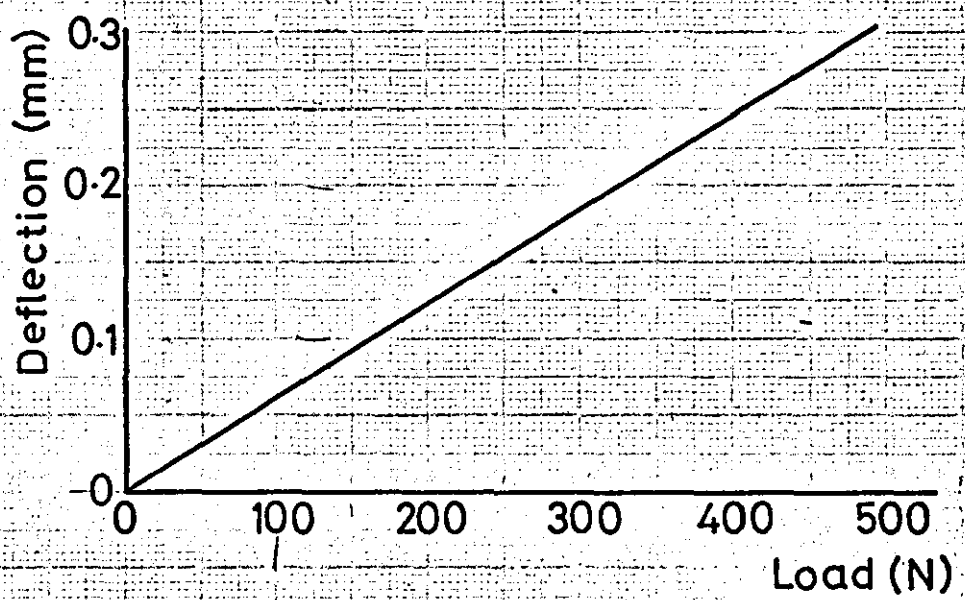

FIG. A11·2 Effect of Rolling Moment on Roll Angle and Lateral Force

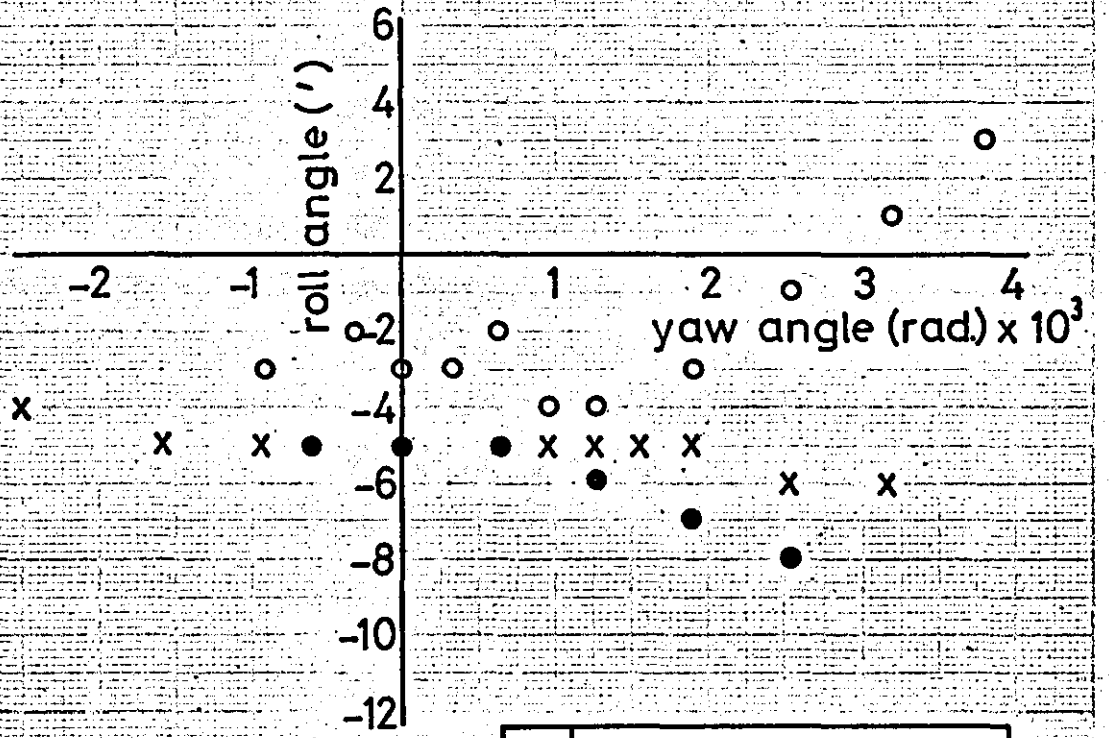

●	Wire Up 6·4mm
x	Wire Horizontal
o	Wire Down 6·4mm

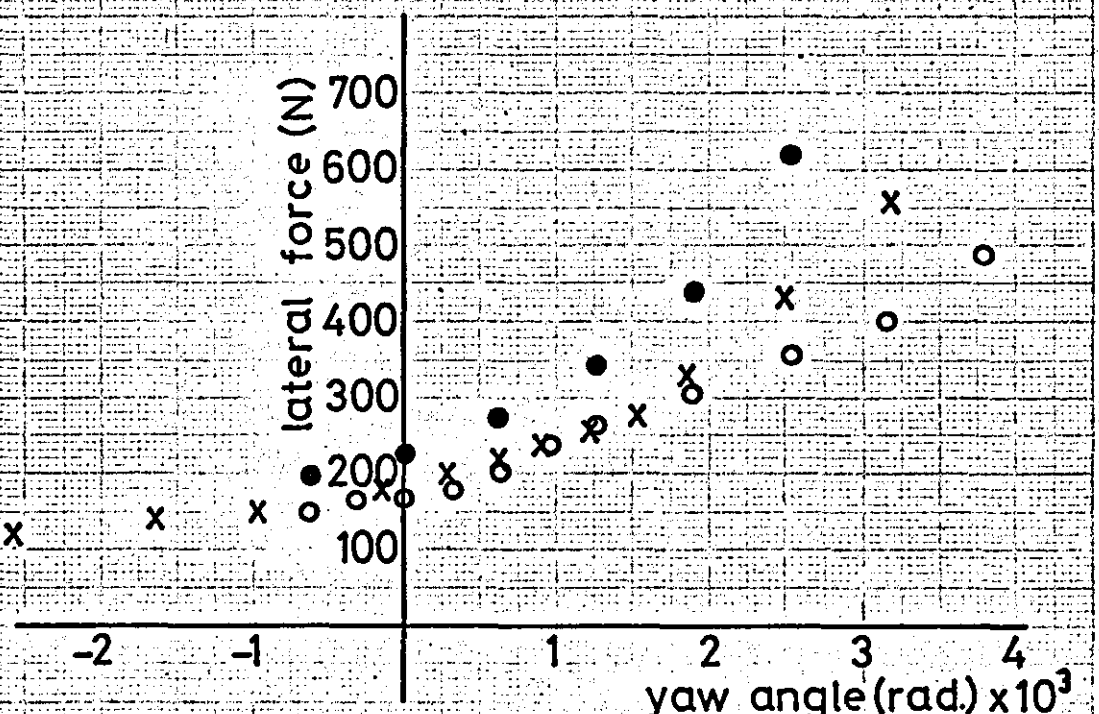

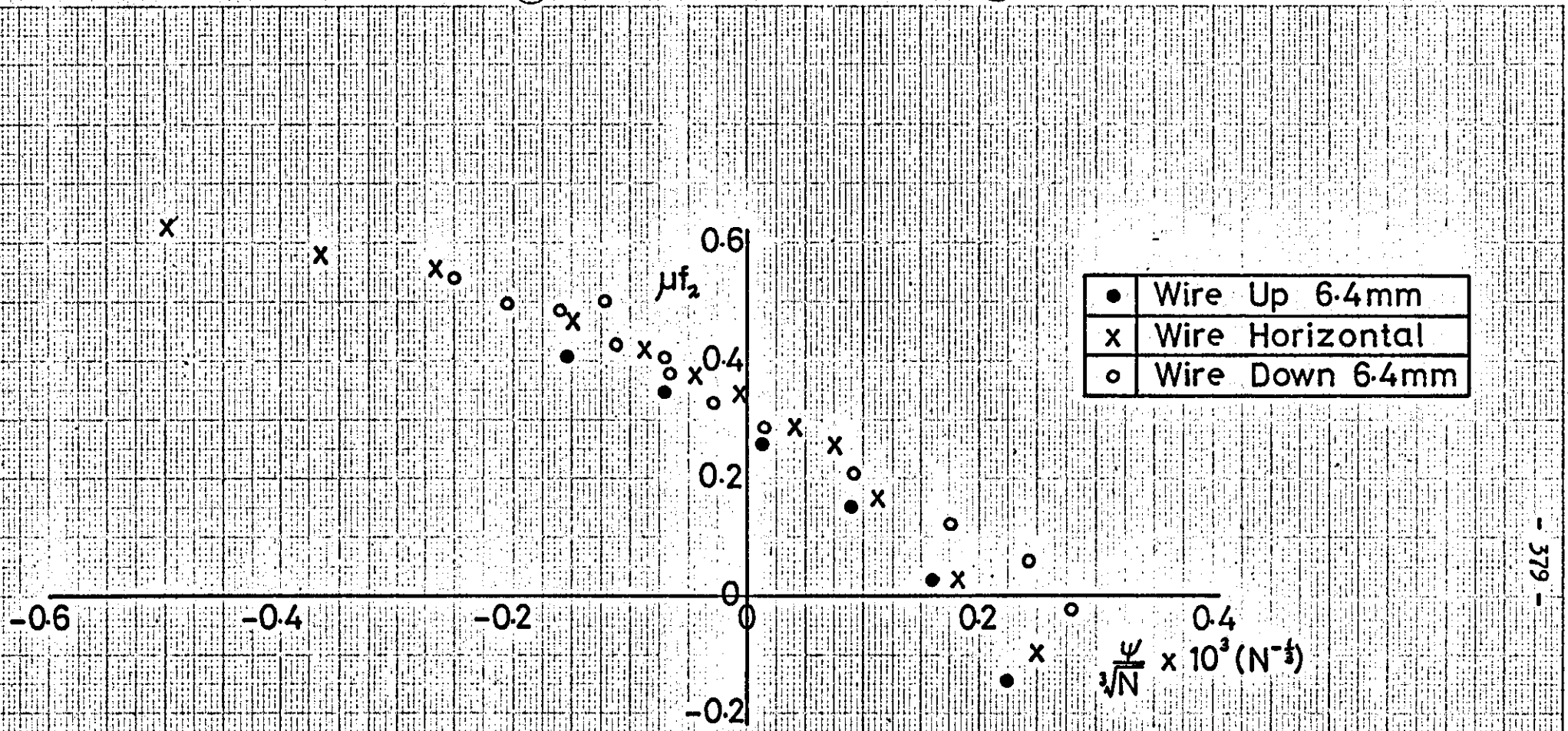

FIG. A11·3 Effect of Rolling Moment on Lateral Force Parameter

contact point. The wheel was set at various yaw angles, and the 'static' displacement on the DTI and the 'static' roll angle were both measured. The wheels were then rotated and the lateral force increased until the upper wheel just lifted off its supports, whereupon the DTI and clinometer were again read together with the lateral load.

The results of these tests are shown in Fig. A11.4 for the 396 N load and in Fig. A11.5 for the 129 N load. They show up several interesting points mentioned in the discussion of results, Section 8.6.

(1) Both figures show the change in lateral displacement from the 'static' to 'dynamic' positions and in both cases the upper wheel is displaced to the left as the lateral load is increased. Accompanying this lateral displacement is a roll angle which is -ve.

(2) It can be seen that the roll angles are practically constant throughout the range of yaw angles, for both 'static' and 'dynamic' positions. The 'dynamic' roll angle is different for the 129 N case from the 396 N case because the rolling moment due to the counterbalance weight is different in each case.

(3) It can be seen in both Fig. A11.4 and Fig. A11.5 that as the yaw angle and therefore the lateral load is increased, the upper wheel is displaced slightly, effectively changing the zero yaw position. This effect is very much less than the zero shift from 'static' to 'dynamic' position and is less than 0.25 mm for the complete range of yaw angles, but it does show that for very small roll angle changes, the lateral shift in the plane of the contact point is significant.

Fig. A11.6 is a plot of (μf_2) v $(\psi / N^{\frac{1}{3}})$ for the two sets of results, while Fig. A11.7 shows the results modified to take into account the zero shift due to roll. It can be seen that the slope of the results at larger loads, changes slightly when the roll correction is applied.

FIG. A11·4 Roll Angle, Lateral Displacement, Lateral Force v Yaw Angle (W=396N)

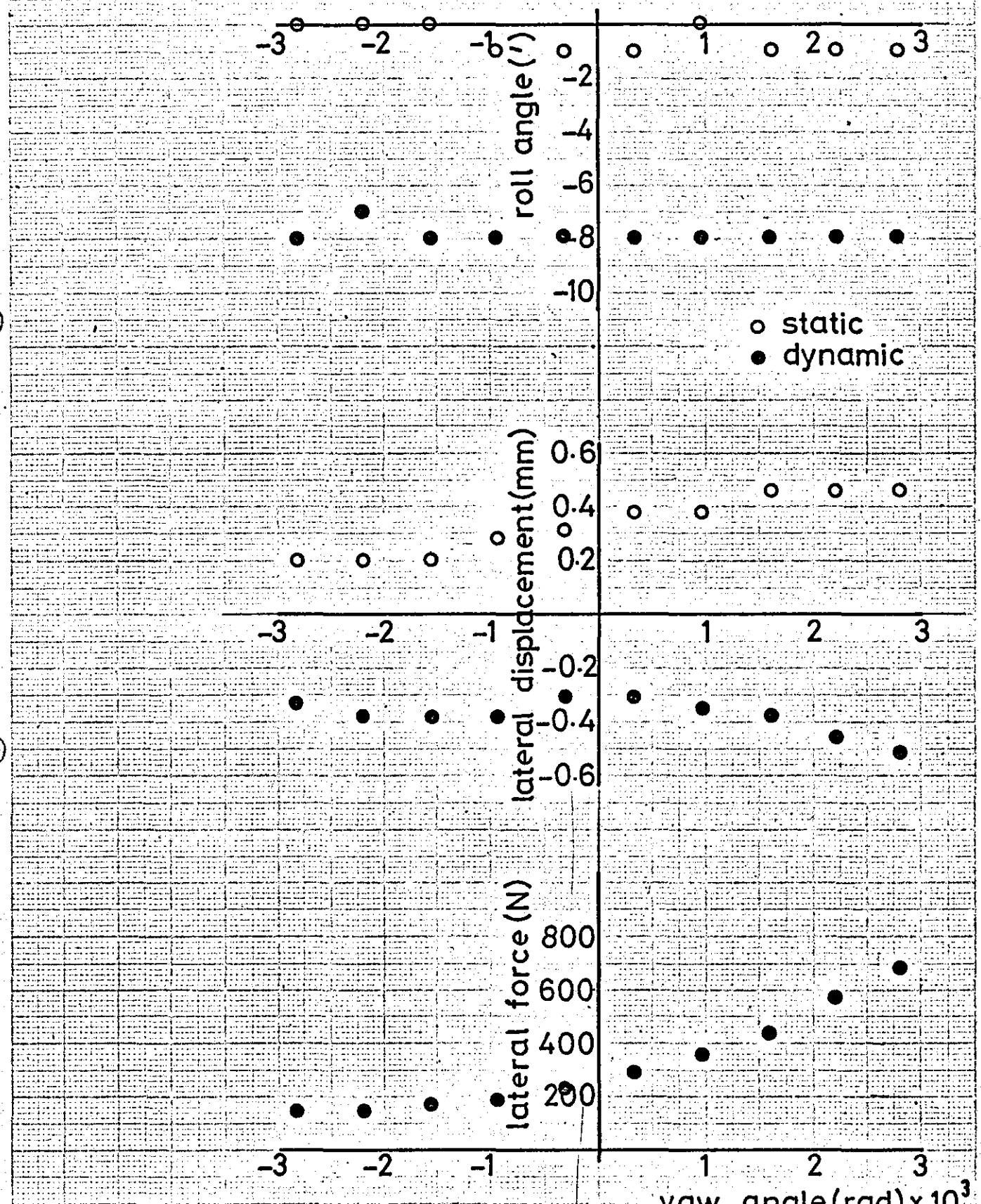

FIG. A11·5 Roll Angle, Lateral Displacement, Lateral Force v Yaw Angle (W=129N)

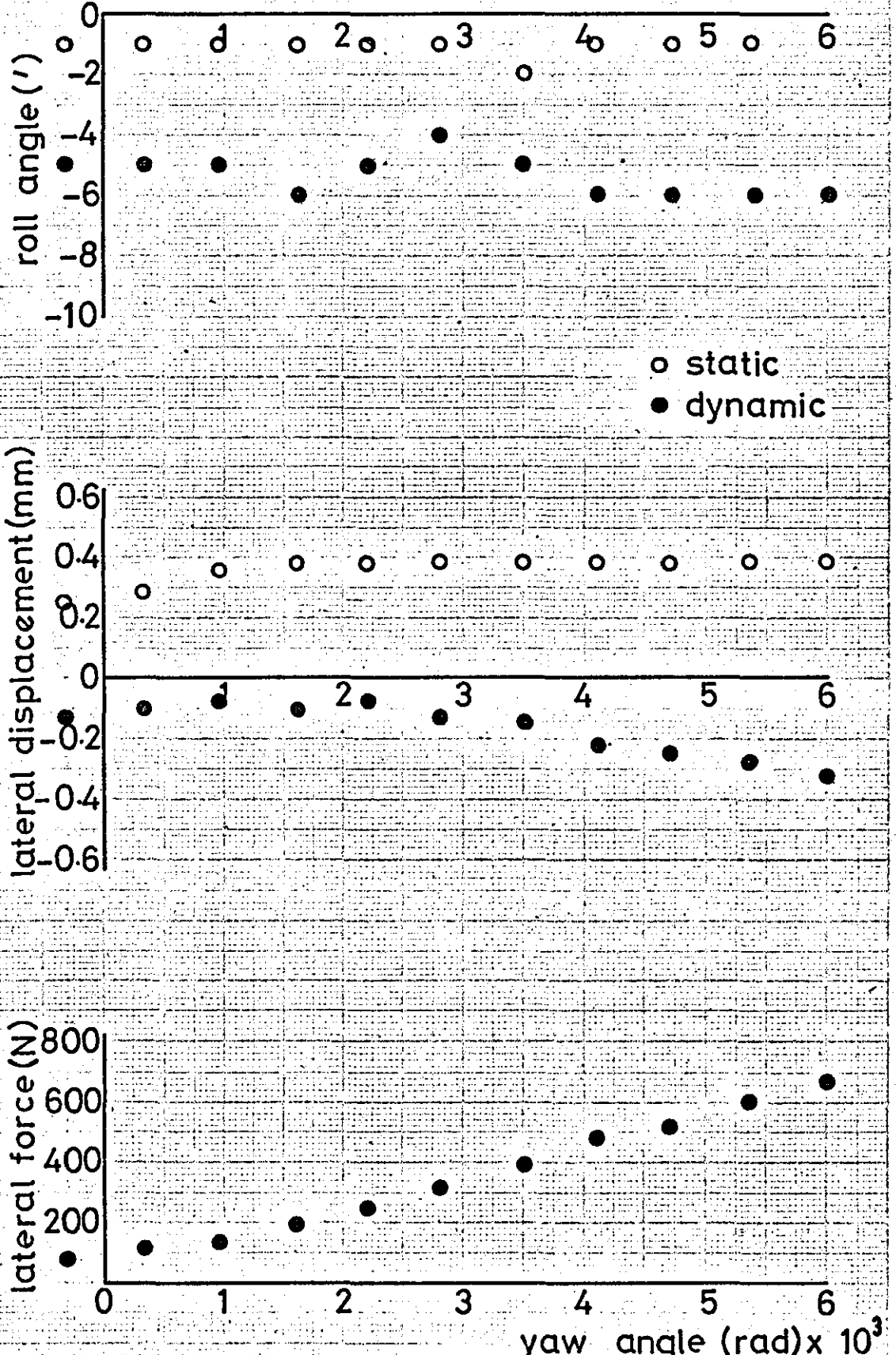

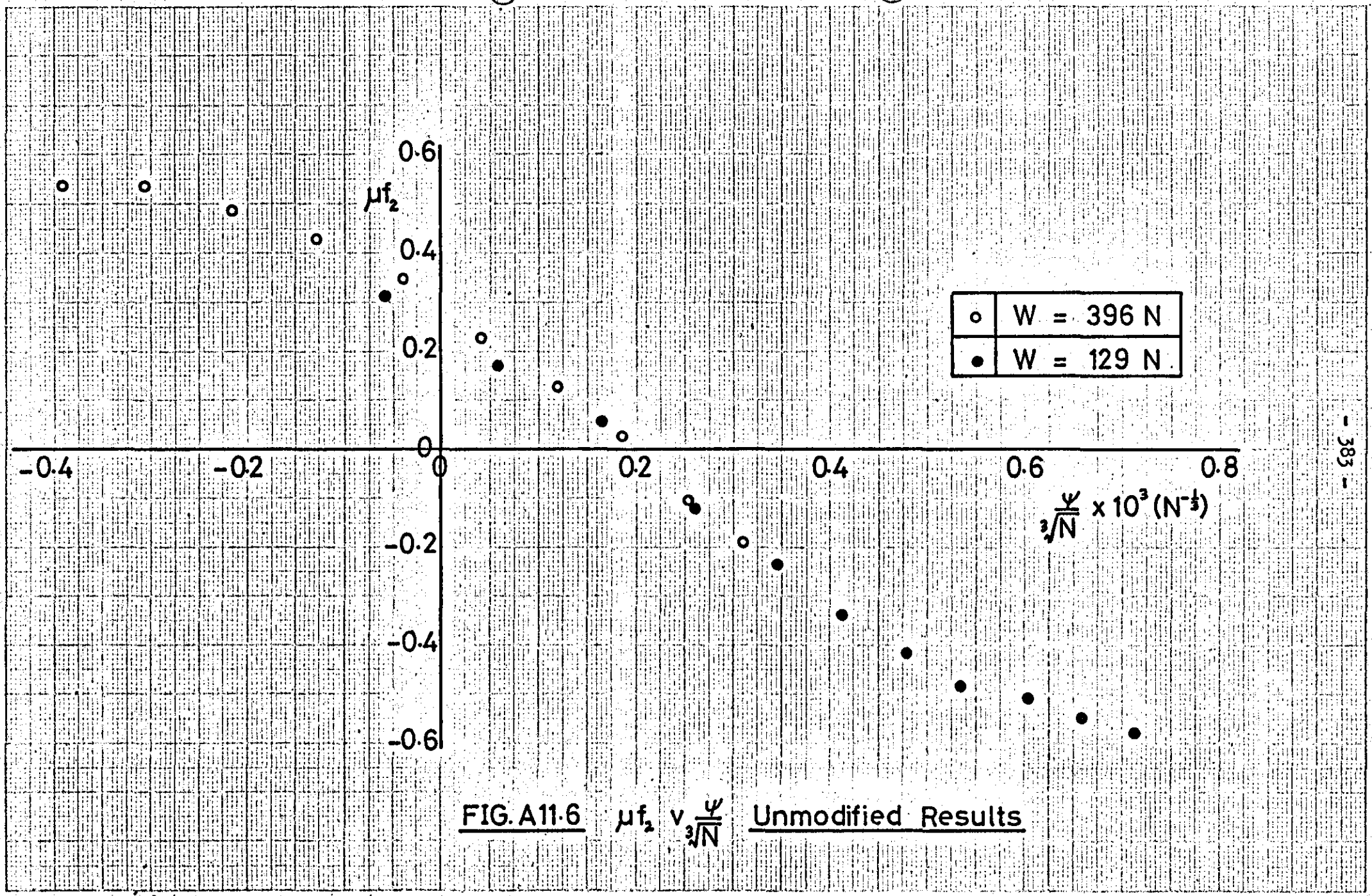

FIG. A11·6 μf_2 v $\frac{\Psi}{\sqrt[3]{N}}$ Unmodified Results

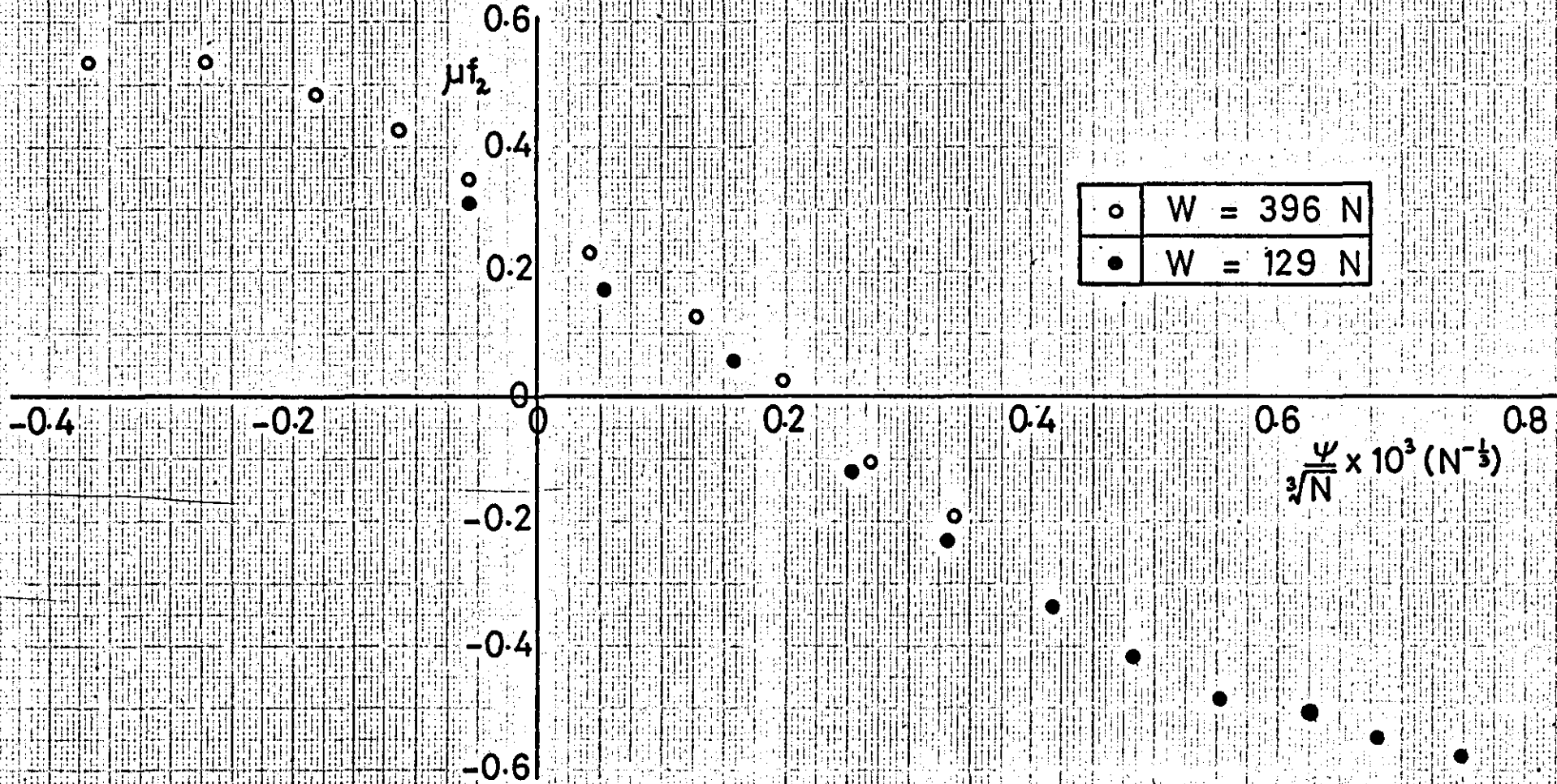

FIG. A11·7 μf_2 v $\frac{\Psi}{\sqrt[3]{N}}$ Roll Modified Results